EMERGING THERAPEUTIC TARGETS IN BRAIN CANCER

EDITED BY: Terrance Johns, David Nathanson and Pim French
PUBLISHED IN: Frontiers in Oncology and Frontiers in Neurology

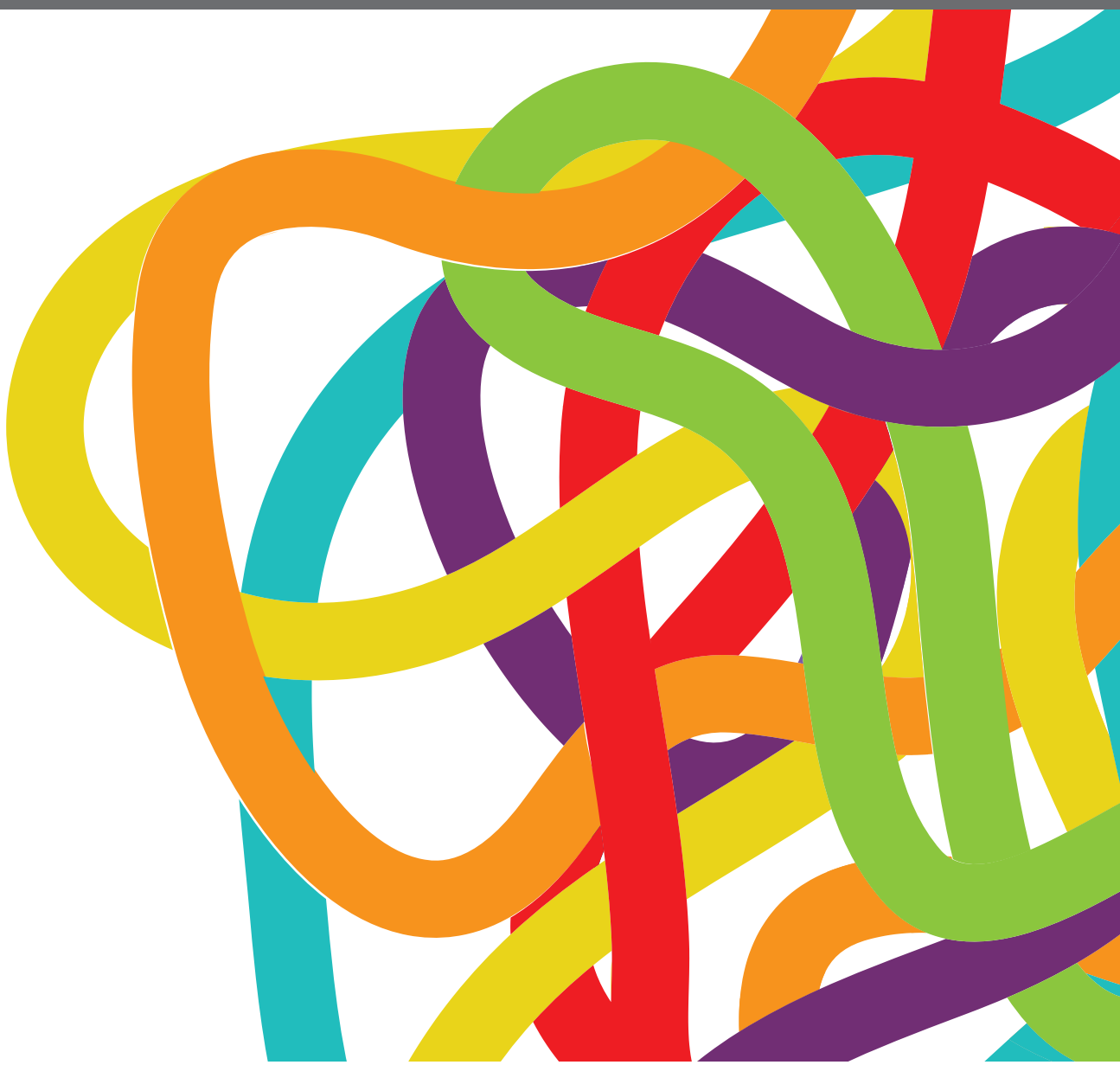

frontiers Research Topics

Frontiers eBook Copyright Statement

The copyright in the text of individual articles in this eBook is the property of their respective authors or their respective institutions or funders. The copyright in graphics and images within each article may be subject to copyright of other parties. In both cases this is subject to a license granted to Frontiers.

The compilation of articles constituting this eBook is the property of Frontiers.

Each article within this eBook, and the eBook itself, are published under the most recent version of the Creative Commons CC-BY licence. The version current at the date of publication of this eBook is CC-BY 4.0. If the CC-BY licence is updated, the licence granted by Frontiers is automatically updated to the new version.

When exercising any right under the CC-BY licence, Frontiers must be attributed as the original publisher of the article or eBook, as applicable.

Authors have the responsibility of ensuring that any graphics or other materials which are the property of others may be included in the CC-BY licence, but this should be checked before relying on the CC-BY licence to reproduce those materials. Any copyright notices relating to those materials must be complied with.

Copyright and source acknowledgement notices may not be removed and must be displayed in any copy, derivative work or partial copy which includes the elements in question.

All copyright, and all rights therein, are protected by national and international copyright laws. The above represents a summary only. For further information please read Frontiers' Conditions for Website Use and Copyright Statement, and the applicable CC-BY licence.

ISSN 1664-8714
ISBN 978-2-88976-221-7
DOI 10.3389/978-2-88976-221-7

About Frontiers

Frontiers is more than just an open-access publisher of scholarly articles: it is a pioneering approach to the world of academia, radically improving the way scholarly research is managed. The grand vision of Frontiers is a world where all people have an equal opportunity to seek, share and generate knowledge. Frontiers provides immediate and permanent online open access to all its publications, but this alone is not enough to realize our grand goals.

Frontiers Journal Series

The Frontiers Journal Series is a multi-tier and interdisciplinary set of open-access, online journals, promising a paradigm shift from the current review, selection and dissemination processes in academic publishing. All Frontiers journals are driven by researchers for researchers; therefore, they constitute a service to the scholarly community. At the same time, the Frontiers Journal Series operates on a revolutionary invention, the tiered publishing system, initially addressing specific communities of scholars, and gradually climbing up to broader public understanding, thus serving the interests of the lay society, too.

Dedication to Quality

Each Frontiers article is a landmark of the highest quality, thanks to genuinely collaborative interactions between authors and review editors, who include some of the world's best academicians. Research must be certified by peers before entering a stream of knowledge that may eventually reach the public - and shape society; therefore, Frontiers only applies the most rigorous and unbiased reviews.
Frontiers revolutionizes research publishing by freely delivering the most outstanding research, evaluated with no bias from both the academic and social point of view. By applying the most advanced information technologies, Frontiers is catapulting scholarly publishing into a new generation.

What are Frontiers Research Topics?

Frontiers Research Topics are very popular trademarks of the Frontiers Journals Series: they are collections of at least ten articles, all centered on a particular subject. With their unique mix of varied contributions from Original Research to Review Articles, Frontiers Research Topics unify the most influential researchers, the latest key findings and historical advances in a hot research area! Find out more on how to host your own Frontiers Research Topic or contribute to one as an author by contacting the Frontiers Editorial Office: frontiersin.org/about/contact

EMERGING THERAPEUTIC TARGETS IN BRAIN CANCER

Topic Editors:
Terrance Johns, University of Western Australia, Australia
David Nathanson, University of California, Los Angeles, United States
Pim French, Erasmus University Medical Center, Netherlands

Citation: Johns, T., Nathanson, D., French, P., eds. (2022). Emerging Therapeutic Targets in Brain Cancer. Lausanne: Frontiers Media SA.
doi: 10.3389/978-2-88976-221-7

Table of Contents

frontiers in Oncology

ORIGINAL RESEARCH
published: 19 April 2021
doi: 10.3389/fonc.2021.654350

Integrated Analysis Reveals Prognostic Value and Immune Correlates of CD86 Expression in Lower Grade Glioma

Huaide Qiu[1,2†], Wei Tian[3†], Yikang He[2,4†], Jiahui Li[2], Chuan He[1], Yongqiang Li[2], Ning Liu[3] and Jianan Li[2*]*

[1] Department of Rehabilitation Medicine, Jiangsu Shengze Hospital Affiliated to Nanjing Medical University, Suzhou, China, [2] Center of Rehabilitation Medicine, The First Affiliated Hospital of Nanjing Medical University, Nanjing, China, [3] Department of Neurosurgery, The First Affiliated Hospital of Nanjing Medical University, Nanjing, China, [4] Department of Rehabilitation Medicine, Zhongda Hospital, School of Medicine, Southeast University, Nanjing, China

OPEN ACCESS

Edited by:
David Nathanson, UCLA David Geffen School of Medicine, United States

Reviewed by:
RongJun Cui, Mudanjiang Medical University, China
Feng Xu, Shantou University, China

***Correspondence:**
Ning Liu
liuning0853@126.com
Jianan Li
lijianan@njmu.edu.cn

[†]These authors have contributed equally to this work

Specialty section:
This article was submitted to Neuro-Oncology and Neurosurgical Oncology, a section of the journal Frontiers in Oncology

Received: *16 January 2021*
Accepted: *29 March 2021*
Published: *19 April 2021*

Citation:
Qiu H, Tian W, He Y, Li J, He C, Li Y, Liu N and Li J (2021) Integrated Analysis Reveals Prognostic Value and Immune Correlates of CD86 Expression in Lower Grade Glioma. Front. Oncol. 11:654350. doi: 10.3389/fonc.2021.654350

Background: CD86 has great potential to be a new target of immunotherapy by regulating cancer immune response. However, it remains unclear whether CD86 is a friend or foe in lower-grade glioma (LGG).

Methods: The prognostic value of CD86 expression in pan-cancer was analyzed using Cox regression and Kaplan-Meier analysis with data from the cancer genome atlas (TCGA). Cancer types where CD86 showed prognostic value in overall survival and disease-specific survival were identified for further analyses. The Chinese Glioma Genome Atlas (CGGA) dataset were utilized for external validation. Quantitative real-time PCR (qRT-PCR), Western blot (WB), and Immunohistochemistry (IHC) were conducted for further validation using surgical samples from Jiangsu Province hospital. The correlations between CD86 expression and tumor immunity were analyzed using the Estimation of Stromal and Immune cells in Malignant Tumours using Expression data (ESTIMATE) algorithm, Tumor IMmune Estimation Resource (TIMER) database, and expressions of immune checkpoint molecules. Gene Set Enrichment Analysis (GSEA) was performed using *clusterprofiler* r package to reveal potential pathways.

Results: Pan-cancer survival analysis established CD86 expression as an unfavorable prognostic factor in tumor progression and survival for LGG. CD86 expression between Grade-II and Grade-III LGG was validated using qRT-PCR and WB. Additionally, CD86 expression in LGG with unmethylated O(6)-methylguanine-DNA-methyltransferase (MGMT) promoter was significantly higher than those with methylated MGMT ($P<0.05$), while in LGG with codeletion of 1p/19q it was significantly downregulated as opposed to those with non-codeletion ($P<2.2*10-16$). IHC staining validated that CD86 expression was correlated with MGMT status and X1p/19q subtypes, which was independent of tumor grade. Multivariate regression validated that CD86 expression acts as an unfavorable prognostic factor independent of clinicopathological factors in overall

survival of LGG patients. Analysis of tumor immunity and GSEA revealed pivotal role of CD86 in immune response for LGG.

Conclusions: Integrated analysis shows that CD86 is an unfavorable prognostic biomarker in LGG patients. Targeting CD86 may become a novel approach for immunotherapy of LGG.

Keywords: pan-cancer analysis, CD86, immune microenvironment, lower-grade glioma, prognosis

INTRODUCTION

Cancer cells escape surveillance of human immune system partly by activating immune checkpoint pathways, which leads to suppressed anti-cancer immune responses of the host (1, 2). To reactivate immune response against cancers, immune checkpoint inhibitors (ICIs) were developed and rose to be a revolution for cancer treatment (3). ICIs reinvigorate anti-cancer response by reactivating immune cells, and as a result enable clearance of cancer cells (4, 5). But well-established ICIs, including blockades targeting CTLA-4 and PD-1/PDL-1, only apply to a subset of cancer patients due to heterogeneous gene expressions and microenvironment across various cancer types (6), and as such novel therapeutic targets need to be considered (7, 8).

CD86 (B7–2), an immunoglobulin-like protein on antigen presenting cells (APCs), works in parallel with the CD80 (B7–1) as a natural ligand for CD28 and CTLA-4 (9). CD86 promotes T-cell proliferation, function and survival by interacting with CD28 as a co-stimulator, while in activated T cells it interacts with CTLA-4 and acts as a suppressor (10, 11). In this bidirectional way, the interplay of CD86 with CD28 and CTLA-4 are of great importance for immune responses against autoimmunity (12) and cancers (13). Notably, CD86 has shown higher affinity for binding to CTLA-4 than that to CD28 (14), indicating the significance of CD86 in immunotherapeutic strategies based on CTLA-4 blockades, which have shown promising effects in treating solid tumors like melanoma (15) and mesothelioma (16) in clinical trials. Besides, CD86 expression was observed to be associated with unfavorable prognosis in myeloma (17) and leukemia (18). Due to the fact that CD86 may serve as a key regulator in cancer immune response *via* T-cell-mediated mechanisms, it has great potential to be a new target of immunotherapy. However, it remains unclear whether CD86 is a friend or foe in pan-cancer given its dual-edge role in regulating immune response.

In this study, we comprehensively analyzed the prognostic value of CD86 expression in pan-cancer, and found that CD86 acts as an unfavorable factor in the progression and prognosis of lower-grade glioma (LGG). External validation was conducted using surgical samples in our hospital and data from the Chinese Glioma Genome Atlas (CGGA) dataset. To predict survival probability of individual patient with CD86 expression and clinical features, a nomogram was developed and validated in both the cancer genome atlas (TCGA) and the CGGA datasets. Further, we explored the correlations between CD86 expression and tumor immunity of LGG samples, and Gene Set Enrichment Analysis (GSEA) was performed to reveal potential pathways.

MATERIALS AND METHODS

Acquisition of Data and Ethics Approval

Normalized RNA Sequencing data with Fragments Per Kilobase of transcript per Million mapped reads (FPKM) in 33 different cancer types were downloaded from UCSC Xena (https://xena.ucsc.edu/), while clinical information was accessed using TCGAbiolinks R package on July 1st, 2020. Data for the validation cohort was accessed from the CGGA database (http://www.cgga.org.cn/), which was updated on June 14, 2020. Experimental validation was conducted using surgical samples from department of neurosurgery, the first affiliated hospital of Nanjing Medical University, also known as Jiangsu Province people's hospital (JSPH). The web-lab validation was approved by the Institutional Review Board and the Ethics Committee of JSPH (No: 2020-SRFA-167), and all patients provided informed consent.

Statistical Analysis

Survival analysis was performed using Cox regression analysis and Kaplan-Meier method, where Cox P-values and log-rank P-values were calculated. Between-group comparisons were conducted using Wilcoxon test (comparison between 2 groups) or Kruskal-Wallis test (comparison among 3 or more groups) (19). Spearman correlation was applied to determine significant correlations. Data were analyzed and visualized using R software 3.6.2, and P-value<0.05 was considered as statistically significant.

Survival Analysis of CD86 Expression in Pan-Cancer

Survival analysis was conducted to estimate the prognostic value of CD86 expression on overall survival (OS) and disease-specific survival (DSS) in pan-cancer. In Cox regression analysis, Cox P-values and hazard ratios (HRs) with 95% confidence intervals (CI) were calculated; whereas, log-rank P-values and HRs with 95%CI were calculated in Kaplan-Meier method. Cancer types where CD86 expression showed prognostic value in OS and DSS were identified for further analyses.

Correlations Between CD86 Expression and Tumor Progression

In the identified cancer types, the correlations between CD86 expression and tumor grade or stage were analyzed to explore the role of CD86 in tumor progression. The comparison of CD86 expression levels among different tumor stages/grades were explored. To investigate whether CD86 expression has independent prognostic value in overall survival, multivariate Cox regression was conducted to adjust the effect of

demographic variables and tumor grade/stage. Exploration of cancer types for which CD86 expression showed prognostic value in tumor progression as well as in OS lead to the identification of LGG. CD86 expression profiles among different histological and molecular subtypes stratified by tumor grade of LGG were investigated.

MRNA Extraction and qRT-PCR in JSPH LGG Samples

To further validate the results, 24 surgical samples of LGG (12 grade-II and 12 grade-III) were collected from JSPH and stored in liquid nitrogen. Total RNA was isolated from LGG samples using TRIzol reagent (Invitrogen, USA) according to the manufacturer's instructions. Subsequently, quantitative real-time PCR (qRT-PCR) was employed to detect the expression levels of CD86 mRNA (forward: 5'-CTTTGCTTCTCT GCTGCTGT-3' and reverse: 5'-GGCCATCACAAAGAGAA TGTTAC-3') with an ABI StepOnePlus system (Applied Biosystems) and TaqMan-based qRT-PCR assays. The primers for CD86 mRNA PCR were purchased from Guangzhou RiboBio (Guangzhou, China). β-Actin mRNA (forward: 5'-CACCC GCGAGTACAACCTTC-3' and reverse: 5'-CCCATACCCA CCATCACACC-3') levels were measured for normalization. Data were analyzed using the $2^{-\Delta\Delta Ct}$ method with each test performed in triplicate.

Immunohistochemical Analysis

The tissues for immunohistochemical analysis were fixed by formalin and embedded in paraffin. After being dewaxed in xylene and antigen retrieval, slides were incubated with Anti-CD86 antibody (ab243887, 1:200, Abcam, USA) overnight at 4°C, and then incubated with a Goat Anti-Rabbit IgG H&L antibody (1:50, Beyotime, China) at room temperature for 1 h, followed by incubation with ABC-peroxidase reagent for 1h, washed with PBS, stained with 3, 3-diaminobenzidine (30 mg dissolved in 100 mL Tris-buffer containing 0.03% H_2O_2) for 5 min, and rinsed in water before counterstained with hematoxylin. Each stained slide was individually reviewed and scored by two independent neuropathologists. Negative controls without primary antibody were included in all experiments to ensure the quality of the staining.

Western Blot (WB) Analysis

Total protein was extracted from tissues using RIPA buffer (KenGEN, China), where protein concentrations were quantified with a BCA Protein Assay Kit (KenGEN, China). Protein was subjected to 10% SDS-PAGE and transferred to PVDF membranes (Millipore, USA). After being blocked with 5% non-fat milk for 2 h, the membranes were incubated overnight at 4°C with primary antibodies against CD86 (ab243887, 1:1000, Abcam, USA), followed by incubation with an HRP-conjugated secondary antibody (1: 3000, YIFEIXUE BIO TECH, China). β-Actin was used as the control (1:1,000, Beyotime, China).

Validation of Prognostic Value of CD86 Expression in CGGA

The prognostic value of CD86 expression in the identified cancer was then validated in the CGGA LGG cohort (n=420). The Kaplan-Meier method was conducted to evaluate the prognostic value of CD86, which was further examined using univariate and multivariate Cox regression. Demographic information (age and gender), cancer type (primary/recurrent), tumor grade, and CD86 expression were incorporated in the regression analyses. If P values were unanimously less than 0.05 in both univariate and multivariate regressions, then CD86 expression was considered as an independent prognostic factor in overall survival of LGG.

Development and Validation of a Nomogram

Using TCGA dataset, CD86 expression and clinical information, including gender, age, tumor grade, cancer type (primary or recurrent), chemotherapy (Yes or No), radiotherapy (Yes or No), and molecular subtypes was employed in univariate and multivariate Cox regressions to identify independent prognostic factors. Subsequently, a nomogram with independent prognostic factors was formulated and validated using the receiver operator characteristic (ROC) analysis and calibration at multiple time-points (20). Validation the nomogram was carried out in both TCGA and the CGGA datasets. Area under curves (AUCs) were calculated to evaluate the discrimination of the nomogram with AUC>0.7 being acceptable and AUC>0.8 being excellent (21, 22). Calibration was performed to compare the predicted probability and the actual observation, indicating the predicative accuracy of the nomogram.

Exploration of CD86-Related Tumor Immunity and Gene Set Enrichment Analysis

Correlation analyses were conducted between CD86 expression and tumor immunity evaluated by tumor purity, immune cells, and immune checkpoint molecules to explore the potential mechanisms whereby CD86 affects prognosis. Tumor purity was measured by stromal score (SS) and immune score (IS), as calculated with the Estimation of Stromal and Immune cells in Malignant Tumours using Expression data (ESTIMATE) algorithm (23). The relationships between CD86 expression and immune cells were analyzed using Tumor IMmune Estimation Resource (TIMER) database (https://cistrome.shinyapps.io/timer/), an online web server that extracted data from gene expression profiles and calculated the abundance of tumor-infiltrating immune cells (24, 25), which was correlated to CD86 expression level with the purity-corrected partial Spearman method (25). Additionally, the association between CD86 expression and immune checkpoint molecules were delineated using Spearman correlation analysis. Correlation coefficients >0.7 were considered as strong correlation, while those falls in the range from 0.4 to 0.7 were interpretated as

moderate correlation and values less than 0.4 as weak correlation (26). GSEA was performed using *clusterProfiler* r package (27) to identify the enriched terms in Gene Ontology (GO) and Kyoto Encyclopedia of Genes and Genomes (KEGG).

RESULTS

Pan-Cancer Survival Analysis of CD86 Expression Identified Three Cancer Types

The schematic workflow of the study is presented in **Figure 1**, where the body image was downloaded from Gene Expression Profiling Interactive Analysis (GEPIA) (http://gepia.cancer-pku.cn/) (28). Survival Analysis of CD86 expression in pan-cancer was conducted to identify relevant cancer types. In Cox regression analysis, the results revealed that CD86 expression was significantly associated with survival rates in five cancer types, i.e., cervical squamous cell carcinoma and endocervical adenocarcinoma (CESC), LGG, skin cutaneous melanoma (SKCM), thymoma (THYM) and uveal melanoma (UVM) (**Figure 2**). Survival analysis on OS showed protective effects of CD86 expression in CESC (HR = 0.702, 95%CI [0.527, 0.935], Cox P = 0.016) and SKCM (HR= 0.710, 95%CI [0.623, 0.809], Cox P < 0.001), while unfavorable effects were demonstrated in LGG (HR= 1.490, 95%CI [1.227,1.810], Cox P < 0.001), THYM (HR = 3.099, 95%CI [1.400, 6.861], Cox P = 0.005) and UVM (HR = 2.318, 95%CI [1.313, 4.092], Cox P = 0.004) (**Figure 2A**). The results on DSS were in line with the OS analysis, showing similar effect of CD86 expression in the five cancer types: CESC (HR = 0.611, 95%CI [0.436, 0.856], Cox P = 0.004), LGG (HR = 1.555, 95%CI [1.261, 1.917], Cox P < 0.001), SKCM (HR = 0.696, 95%CI [0.604, 0.803], Cox P < 0.001), THYM (HR = 3.603, 95% CI [1.082, 11.993], Cox P = 0.037) and UVM (HR = 2.112, 95%CI [1.160, 3.845], Cox P = 0.014) (**Figure 2B**).

Using Kaplan-Meier method, we also conducted pan-cancer survival analysis of CD86 expression. CD86 was observed to be prognostic in four cancer types (**Figure 3A**), i.e., LGG (HR = 1.5, 95%CI [1.2, 1.8], log-rank P < 0.001) (**Figure 3B**), SKCM (HR = 0.71, 95%CI [0.62, 0.81], log-rank P < 0.001) (**Figure 3C**), UVM (HR = 2.3, 95%CI [1.3, 4.1], log-rank P < 0.001) (**Figure 3D**) and Testicular Germ Cell Tumor (TGCT; HR = 3.9, 95%CI [1, 15], log-rank P = 0.022) (**Figure 3E**). Similarly, CD86 expression demonstrated to be prognostic on DSS in four cancer types: LGG (HR = 2.3, 95%CI [1.3, 4.1], log-rank P < 0.001) (**Figure 3F**), SKCM (HR = 2.3, 95%CI [1.3, 4.1], log-rank P < 0.001) (**Figure 3G**), UVM (HR = 2.3, 95%CI [1.3, 4.1], log-rank P < 0.001) (**Figure 3H**), and CESC (HR = 2.3, 95%CI [1.3, 4.1], log-rank P = 0.013) (**Figure 3I**). The intersection of survival analysis with OS and DSS highlighted three cancer types (LGG, SKCM, and UVM), which indicated that CD86 expression has prognostic value in these three cancer types.

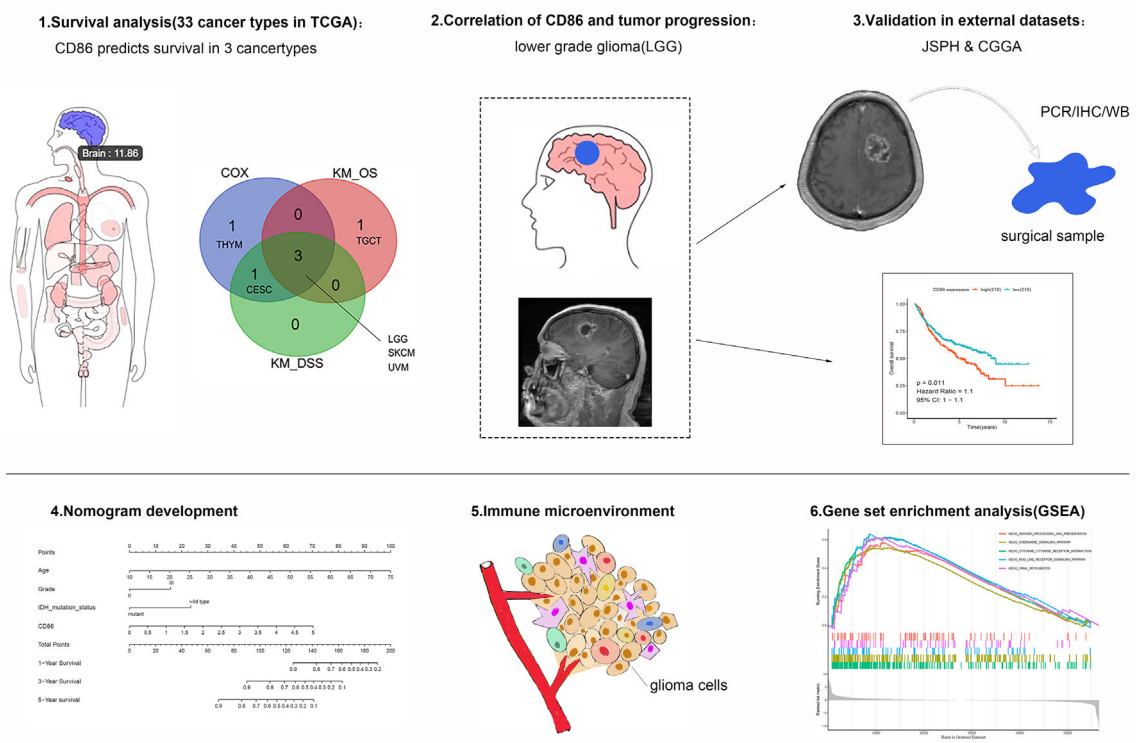

FIGURE 1 | Schematic flowchart of the study process. The top left panel indicates that CD86 expression level of the brain is 11.86 [expression= Log_2(TPM + 1)].

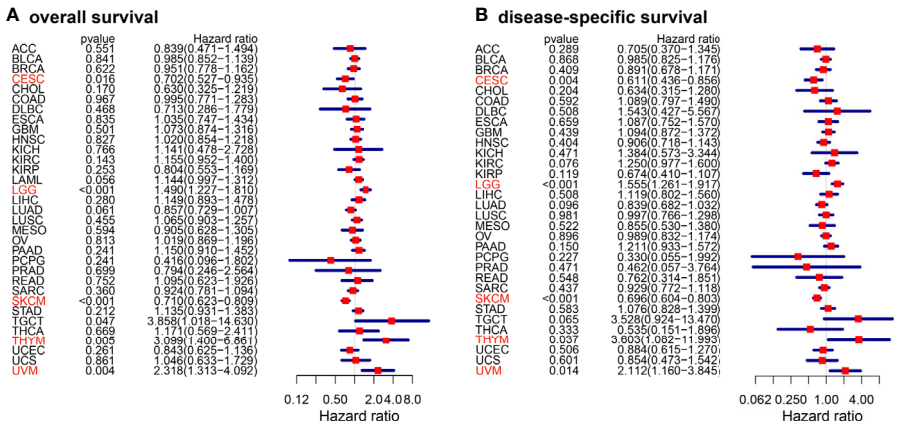

FIGURE 2 | Forest plots of cox regression analysis with CD86 expressions in different cancer types. **(A)** Overall survival (OS). **(B)** Disease-specific survival (DSS). Cancer types with statistically significant prognostic value of CD86 in both OS and DSS are highlighted in red.

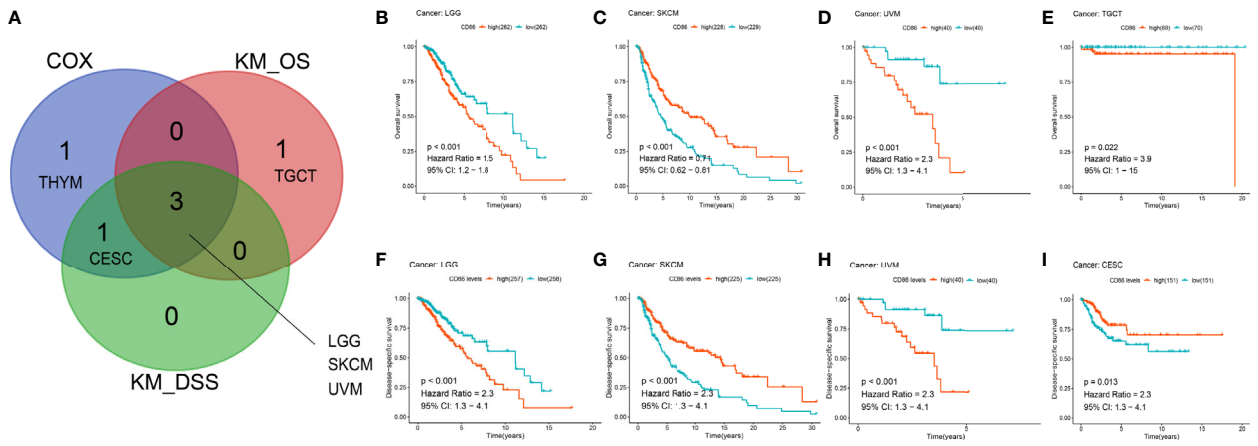

FIGURE 3 | Kaplan-Meier analysis with CD86 expressions in different cancer types. **(A)** The Venn diagram of the identified cancer types in cox regression analysis and Kaplan-Meier method. **(B–E)** Kaplan-Meier survival curve showing the prognostic value of CD86 on OS in LGG **(B)**, SKCM **(C)**, UVM **(D)**, TGCT **(E)**. **(F–I)** Kaplan-Meier survival curve showing the prognostic value of CD86 on DSS in LGG **(F)**, SKCM **(G)**, UVM **(H)**, CESC **(I)**.

CD86 Expression Was Correlated With Tumor Progression and Worse OS in LGG

We investigated the correlations between CD86 expression and tumor progression in the identified cancer types: SKCM, UVM and LGG. Although CD86 expression was significantly altered among different tumor stages in SKCM (**Figure 4A**), no independent prognostic value in OS was observed (**Figure 4B**). In contrast, there was no significant correlation between CD86 expression and tumor stage of UVM (**Figure 4C**), neither was independent prognostic value of CD86 for UVM (**Figure 4D**). Higher CD86 expression was present in Grade-III LGG as compared to Grade-II (p=0.025), indicating a carcinogenetic effect of CD86 in LGG (**Figure 4E**). The multivariate regression analysis showed an independent prognostic value of CD86 in LGG on OS (HR = 1.678, 95%CI [1.308, 2.152], Cox P < 0.001) after variables including age, gender, and tumor grade were adjusted (**Figure 4F**). Consistent with bioinformatic analysis, *in vitro* experiments with 24 surgical samples of LGG using qRT-PCR (**Figure 4G**) and WB analysis (**Figure 4H**) indicated that CD86 expression in Grade-III LGG was significantly higher than that in Grade-II. Thus, CD86 was observed to be an unfavorable prognostic factor in tumor progression, OS, and DSS for LGG.

CD86 Expression Was Correlated With Histological and Molecular Subtypes of LGG

CD86 expression profiles among histological and molecular subtypes stratified by tumor grade in LGG were examined. Significantly higher expression of CD86 was observed in

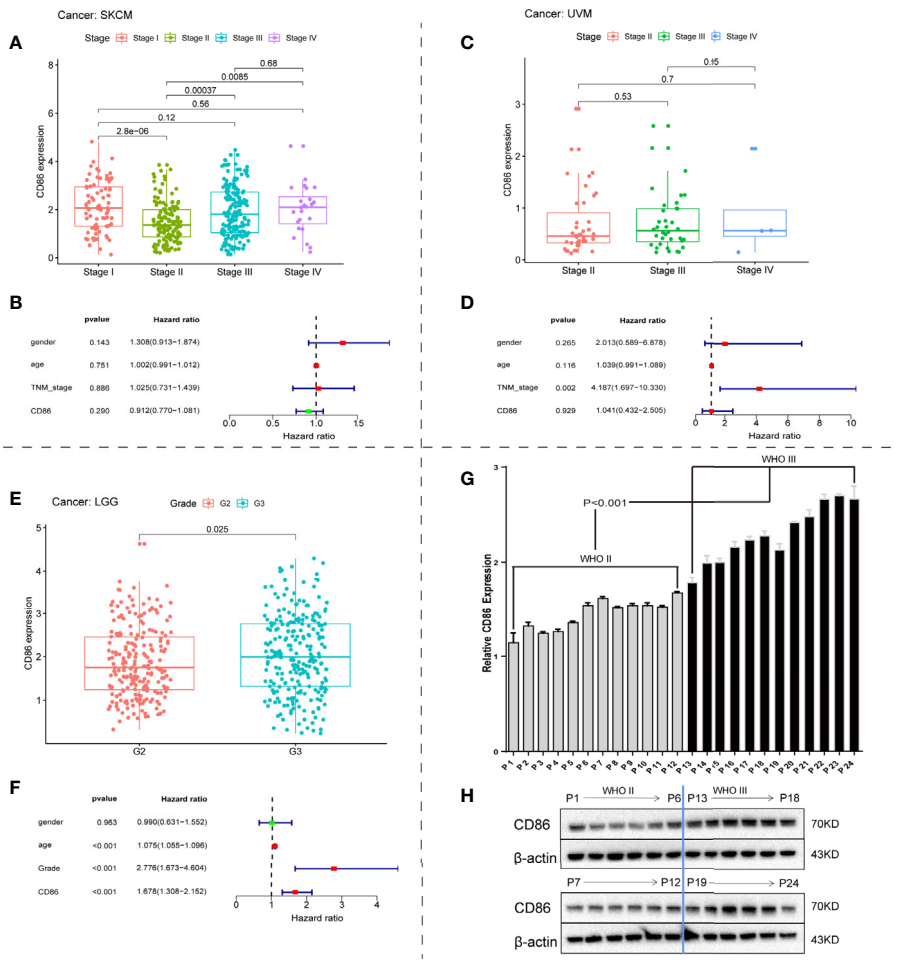

FIGURE 4 | Correlations between CD86 expression and tumor progression. CD86 expression in different stages of SKCM **(A)** and UVM **(C)**. Multivariate regression analysis of CD86 expression, age, gender, and tumor stage for OS in SKCM **(B)** and UVM **(D)**. **(E)** CD86 expression between different grades of LGG. **(F)** Multivariate regression analysis of CD86 expression, age, gender, and tumor grade for OS in LGG. **(G)** CD86 mRNA expression evaluated by qRT-PCR in different grades of LGG. **(H)** CD86 protein expression evaluated by WB in different grades of LGG.

Grade-III astrocytoma as compared with oligoastrocytoma and oligodendroglioma of the same grade, while oligodendroglioma presented lower CD86 expression as opposed to oligoastrocytoma ($P<1.4*10^{-14}$) (**Figure 5A**). Grade-II glioma showed the same trend between histological types, with no statistical difference detected in CD86 expressions between astrocytoma and oligoastrocytoma (**Figure 5A**). Besides, CD86 expression in MGMT-unmethylated LGG (Grade-II & Grade-III) was significantly higher than those with methylated MGMT ($P<0.05$) (**Figure 5B**). As shown in **Figure 5C**, markedly higher CD86 expressions were demonstrated in Grade-III glioma with wild-type (WT) isocitrate dehydrogenase (IDH) compared with IDH mutant ($P<0.001$), while no between-group significance was observed in Grade-II glioma. CD86 in LGG with codeletion of 1p/19q was significantly downregulated as opposed to those with non-codeletion ($P<2.2*10^{-16}$) (**Figure 5D**). Immunohistochemistry (IHC) staining validated that CD86 expression was correlated with MGMT status and X1p/19q subtypes (**Figure 5E**), which is independent of tumor grade. IHC staining for 24 cases with LGG can be accessed in **Supplementary File S1**.

CD86 Was an Unfavorable Prognostic Factor in CGGA LGG Patients

The prognostic performance of CD86 expression in LGG was validated in CGGA to determine whether the prognostic value of CD86 was independent of datasets. Kaplan-Meier analysis showed that CD86 expression was significantly correlated with survival rates in LGG (HR = 1.1, 95%CI [1, 1.1], log-rank P = 0.011) (**Figure 6A**), primary LGG (HR = 1.1, 95%CI [1, 1.2], log-rank P < 0.001) (**Figure 6B**), and recurrent LGG (HR = 1, 95%CI [0.96, 1.1], log-rank P = 0.05) (**Figure 6C**). The results of univariate and multivariate regression validated that CD86 acts as an unfavorable prognostic factor independent of clinicodemographic factors in overall survival of LGG patients (**Figure 6D, E**).

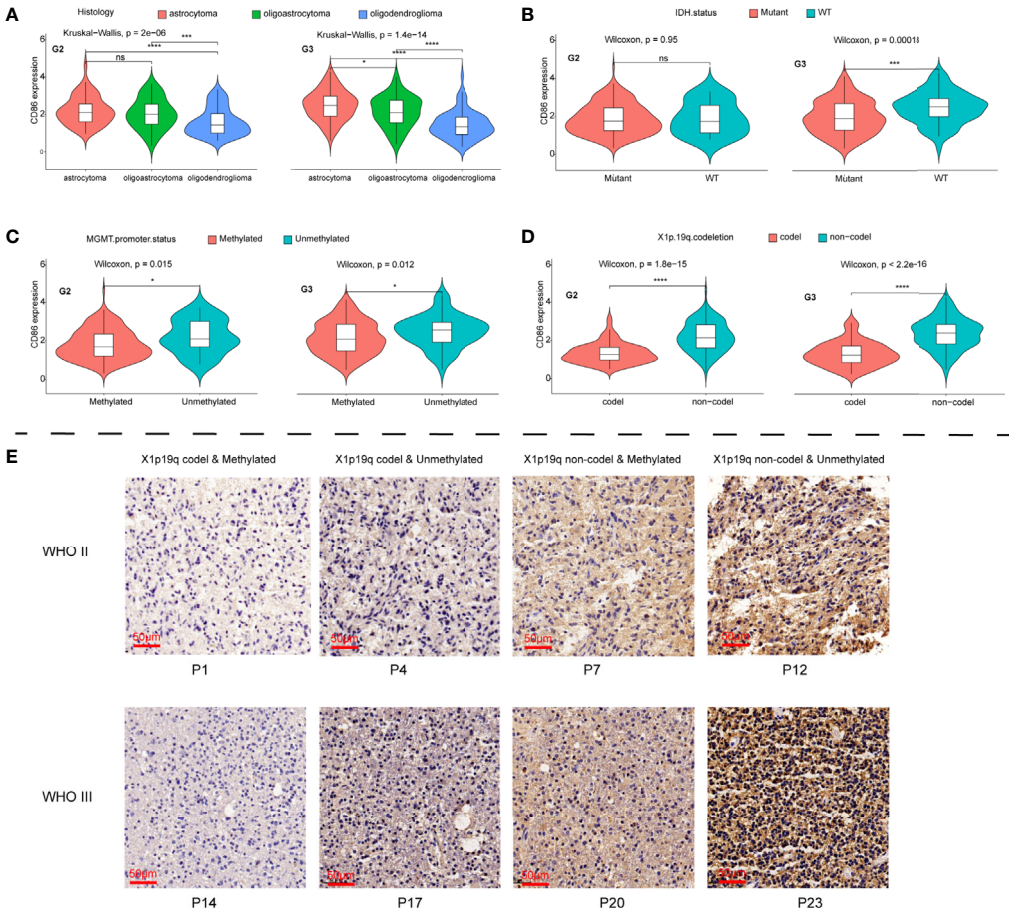

FIGURE 5 | Comparisons of CD86 expression with different histological/molecular subtypes of LGG stratified by tumor grade. **(A)** CD86 expression in astrocytoma, oligoastrocytoma and oligodendroglioma. **(B)** CD86 expression in IDH mutant and WT of LGG. **(C)** CD86 expression in MGMT-methylated LGG versus unmethylated type. **(D)** CD86 expression in LGG with X1p/19q codeletion versus non-codeletion. **(E)** IHC staining of CD86 among different molecular subtypes regarding status on MGMT methylation and X1p/19q codeletion. *p<0.05 **p<0.01, ***p<0.001, ****p<0.0001, ns: not significant.

Development and Validation of a Nomogram

Univariate Cox regression revealed prognostic values of CD86 expression, age, tumor grade, as well as molecular subtypes including IDH mutation status, X1p/19q codeletion, and MGMT methylation (**Figure 7A**); whereas, multivariate Cox regression showed independent prognostic roles of CD86 expression, age, tumor grade, and IDH mutation status in overall survival of LGG (**Figure 7B**). A nomogram with these independent factors was formulated to predict an individualized probability of survival (**Figure 7C**). The ROC curve analysis of the nomogram in TCGA dataset showed acceptable to excellent accuracy in classification with 1-year AUC of 0.904, 3-year AUC of 0.801, 5-year AUC of 0.794 (**Figure 7D**). Additionally, ROC analysis in the CGGA dataset validated the classification performance with 1-year AUC of 0.665, 3-year AUC of 0.726, 5-year AUC of 0.728 (**Figure 7E**). Moreover, calibration revealed adequate prediction accuracy of the nomogram at multiple timepoints in TCGA (**Figure 7F**) and CGGA (**Figure 7G**).

CD86 Expression Was Correlated With Tumor Immunity and Implicated in Immune-Related Pathways

As shown in **Figures 8A**, **B**, SS and IS were both significantly correlated with CD86 expression (r>0.7, $P<2.2*10^{-16}$), indicating CD86 could serve as a biomarker in tumor purity. Spearman correlation analysis demonstrated strong correlations of CD86 expression with CD4+ cells (**Figure 8E**), macrophage (**Figure 8F**), neutrophil (**Figure 8G**), as well as with dendritic cells (**Figure 8H**) using TIMER (r>0.7, P<0.0001). Moderate correlation was also observed between CD86 expression and B cells (**Figure 8C**), and there was weak correlation between CD86 expression and CD8+ cells (**Figure 8D**). Meanwhile, we found that CD86 expression correlated with multiple immune checkpoint molecules, including VSIR, HAVCR2, and PDCD1LG2 (PD-L2) (r>0.7, P<0.0001) (**Figure 8I**). Additionally, CD86 levels was associated with BTLA, CTLA4, CD274 (PD-L1), and PDCD1 (PD1) with moderate correlation (r>0.4, P<0.001) (**Figure 8I**).

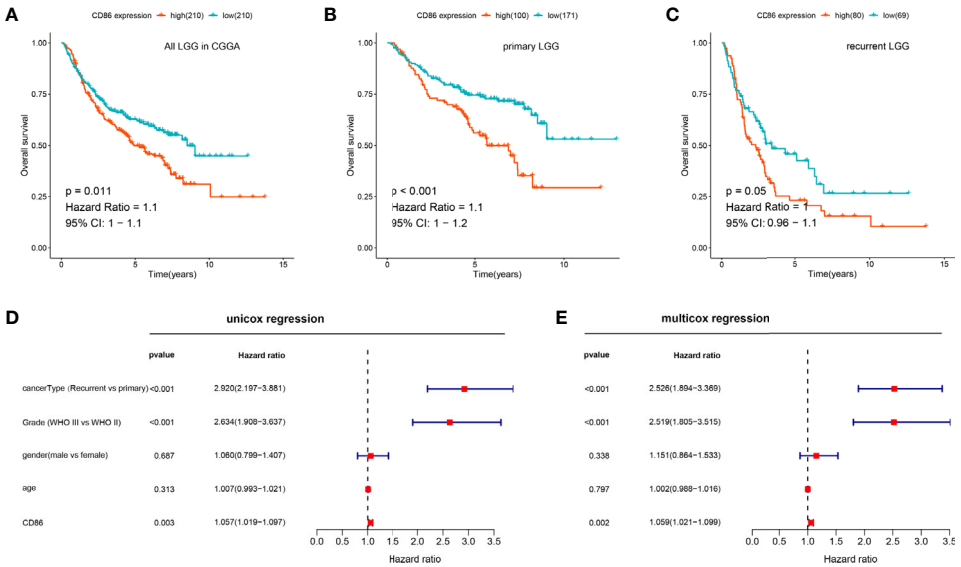

FIGURE 6 | Validation of the prognostic value of CD86 for LGG in CGGA. **(A)** Kaplan-Meier analysis of CD86 expression and OS in all LGG. **(B)** Kaplan-Meier analysis of CD86 expression and OS in primary LGG. **(C)** Kaplan-Meier analysis of CD86 expression and OS in recurrent LGG. **(D)** Univariate Cox regression of CD86 expression, LGG cancer type (primary or recurrent), grade, gender and age. **(E)** Multivariate Cox regression using the same variables.

Subsequently, GSEA was conducted to explore the underlying mechanisms whereby CD86 expression may alter prognosis in LGG. The results of GO analysis showed that CD86 was significantly enriched in adaptive immune response based on somatic recombination of immune receptors, coagulation, leukocyte cell-cell adhesion, and lymphocyte mediated immunity (**Figure 8J**). In KEGG analysis, CD86 was significantly enriched in antigen processing and presentation, chemokine signaling pathway, and cytokine-cytokine receptor interaction (**Figure 8K**).

DISCUSSION

In the present study, pan-cancer survival analyses revealed prognostic values of CD86 expression in three cancer types, i.e., LGG, SKCM and UVM. CD86 demonstrated to be an unfavorable factor independent of clinicodemographic variables in tumor progression and prognosis for LGG, which was validated by qRT-PCR and WB in LGG samples, as well as a real-world cohort in CGGA. Additionally, data from TCGA showed CD86 expression was associated with aggressive molecular subtypes of LGG, and IHC staining of surgical samples confirmed these associations. To predict an individualized probability of survival, a nomogram was developed with TCGA dataset, showing adequate classification performance and predictive accuracy in TCGA as well as the CGGA dataset. To explore potential mechanisms by which CD86 acts as an unfavorable prognostic factor in LGG, analysis of tumor immunity and GSEA revealed pivotal role of CD86 in immune response for LGG.

Although CD86 has been reported to be associated with poor prognosis in chronic lymphocytic leukemia (9), myeloma (29), and overall glioma (30), there was no report of its prognostic value in LGG and melanoma. As shown in the present study, CD86 expression level was significantly correlated with worse survival and it was upregulated as the tumor grade increases in LGG. Besides, univariate and multivariate Cox regression validated the independent prognostic value of CD86. Further, analysis of the correlations between CD86 expression and molecular subtypes of LGG indicated that CD86 expression was significantly higher in MGMT-unmethylated type and LGG with non-codeletion of 1p/19q. Low MGMT unmethylation has been established to be associated with poor survival of glioma according to previous studies (31–33), while IDH mutant with 1p/19q codeletion has been observed to have better therapeutic response and clinical outcomes compared to those with non-codeletion (34–36). Therefore, CD86 may alter the malignant processes of LGG by interacting with pathways related to MGMT status and 1p/19q codeletion, which could be relevant to treatment decisions for LGG patients.

Further, we formulated a nomogram to guide clinical practice in an individualized manner, and its predictive performance was validated across different datasets. Although many previous studies have adopted nomogram models in predicting overall survival of LGG patients, most of them (37–39) suffered from a lack of external validation. Our study, on the other hand, offered solid external validation with ROC analysis and calibration plot and the nomogram demonstrated

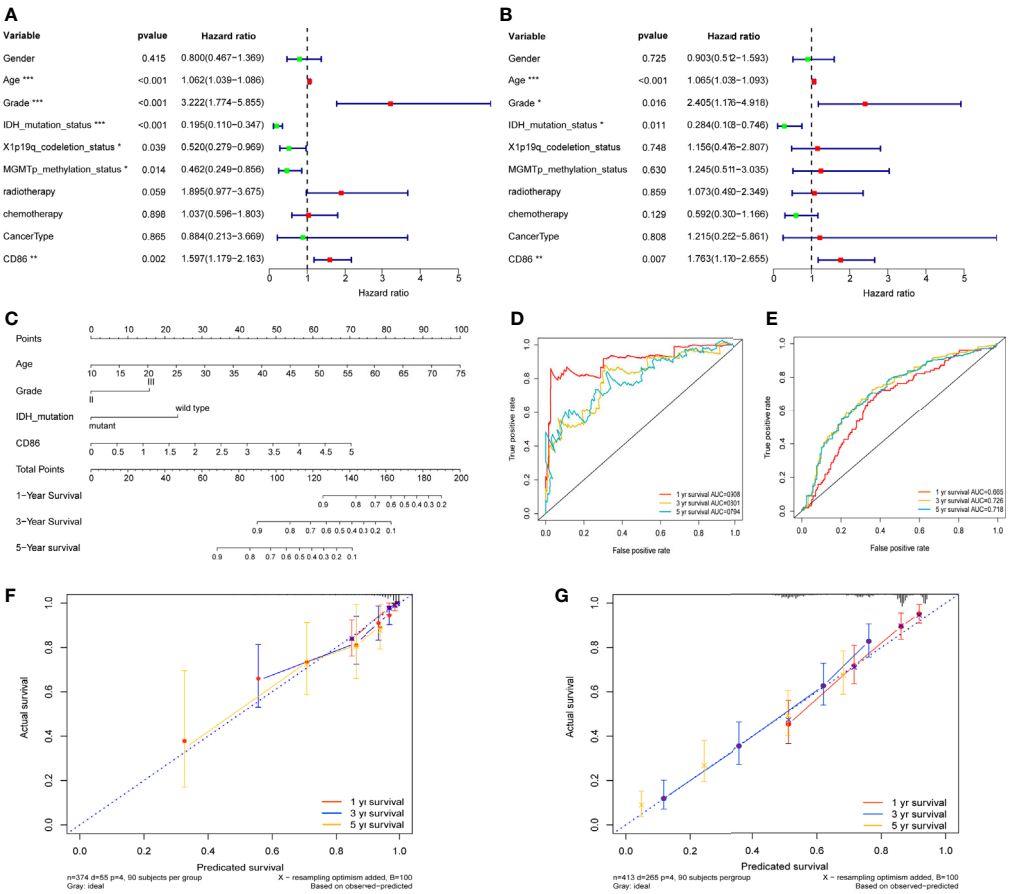

FIGURE 7 | Development and validation of a Nomogram. Univariate Cox regression **(A)** and Multivariate Cox regression **(B)** with CD86 expression, demographic and clinicopathological factors; Red dots represent risk factor (HRs>1), while green dots represent protective factor (HRs<1). *P<0.05, **P<0.01, ***P<0.001. **(C)** Nomogram with independent prognostic factors. ROC curve analysis at 1 year, 3years, and 5 years using TCGA dataset **(D)** and the CGGA dataset **(E)**. Calibration plot at 1 year, 3years, and 5 years in TCGA **(F)** and the CGGA **(G)**.

to be clinically relevant, discriminant and accurate in predicting survival outcomes.

To further investigate on the mechanisms, the correlations between CD86 expression and immunity were comprehensively explored. The results indicated that CD86 expression was significantly associated with TME, which has been identified as a key factor in tumor progression and therapeutic response (40, 41). Specifically, we found strong correlations of CD86 expression with immune infiltration of CD4+ cells, macrophage, neutrophil and dendritic cells. These results were consistent with previous studies (38, 42) indicating higher levels of immune cell infiltration may contribute to worse prognosis of LGG. Additionally, CD86 levels demonstrated strong correlations with multiple immune checkpoint molecules, including VSIR, HAVCR2, and PDCD1LG2 (PD-L2). Although there was no report of VSIR and HAVCR2 in LGG, PD-L2 was observed to be an unfavorable prognosticator in tumor progression and prognosis for LGG patients (43). Likewise, CD86 could be a prognostic biomarker and serves as a potential therapeutic target for LGG patients.

To our best knowledge, this article presents the first report on the prognostic value of CD86 expression in pan-cancer. CD86 expression demonstrated to be an unfavorable prognostic factor in survival and tumor progression for LGG patients, thereby serving as potential target of immunotherapy. However, a cause-effect relationship of CD86 expression with prognosis could not be established in the present study. Further investigations about downstream mechanisms arewfi 2 needed, while potential pathways shown in GSEA suggested possible directions.

CONCLUSION

In summary, CD86 expression is associated with tumor progression and prognosis for LGG patients, where its prognostic value was observed to be independent of clinical features. Besides, CD86 expression was correlated with levels of tumor-infiltrated immune cells and expressions of immune

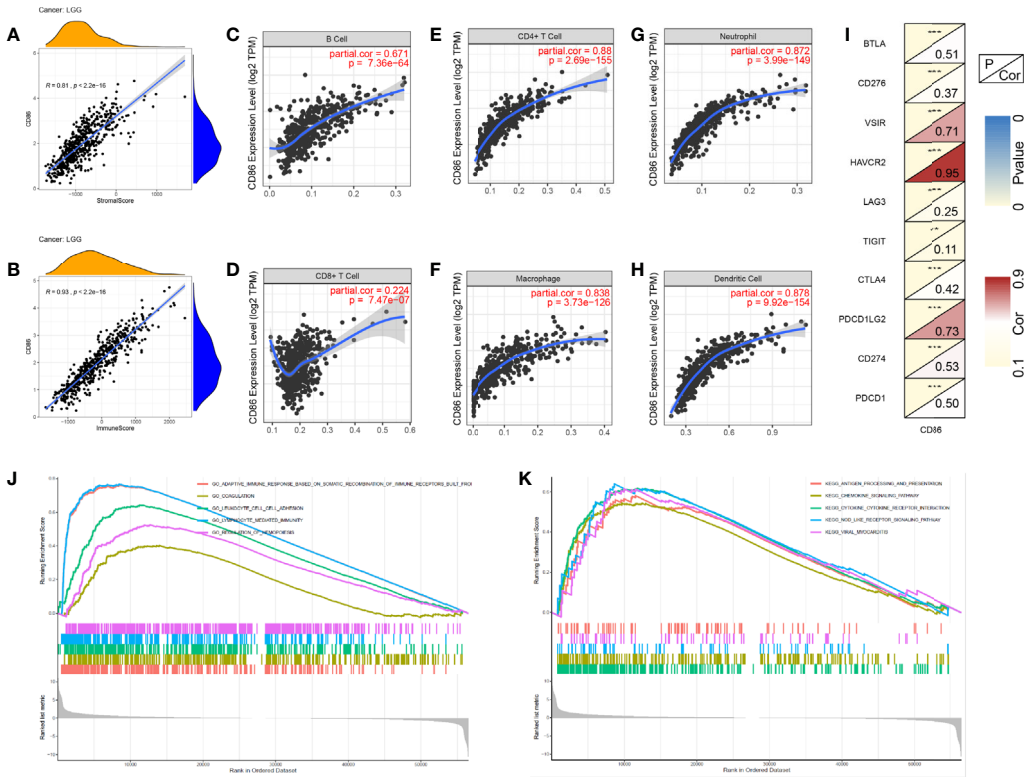

FIGURE 8 | Exploration of CD86-related tumor immunity and GSEA. **(A)** Correlations between CD86 expression and Stromal Score. **(B)** Correlations between CD86 expression and Immune Score. Correlations between CD86 expression and different immune cells: B cell **(C)**, CD8 T cell **(D)**, CD4 T cell **(E)**, macrophage **(F)**, neutrophil **(G)**, and dendritic cell **(H)**. **(I)** Correlations between CD86 expression and different immune checkpoint molecules. **(J)** GSEA of GO terms. **(K)** GSEA in KEGG pathway. **p<0.01, ***p<0.001.

checkpoint molecules. CD86 could be a novel biomarker in the prognosis and treatment of LGG.

DATA AVAILABILITY STATEMENT

Publicly available datasets were analyzed in this study. This data can be found here: [https://xena.ucsc.edu/, http://www.cgga.org.cn/].

ETHICS STATEMENT

The studies involving human participants were reviewed and approved by the Institutional Review Board and the Ethics Committee of JSPH (No: 2020-SRFA-167). The patients/participants provided their written informed consent to participate in this study.

AUTHOR CONTRIBUTIONS

HQ: Conceptualization, Data curation, Formal analysis, Roles/Writing - original draft, Writing - review & editing. WT: Lab investigation and Methodology. YH: Roles/Writing - original draft, Writing - review & editing. JHL, CH, and YL: Writing and revision of the draft. NL, and JNL: Funding acquisition, Methodology, Project administration, Resources, Supervision.

FUNDING

This study was funded by The Introduced Project of Suzhou Clinical Medical Expert Team (SZYJTD201725), the Nanjing Municipal Science and Technology Bureau (No. 2019060002), the Postgraduate Research & Practice Innovation Program of Jiangsu Province(SJCX20_0478), and Key Project of Jiangsu Provincial Department of Science and Technology (BE2017007-5).

SUPPLEMENTARY MATERIAL

The Supplementary Material for this article can be found online at: https://www.frontiersin.org/articles/10.3389/fonc.2021.654350/full#supplementary-material

Supplementary File S1 | IHC staining of CD86 for 24 cases with LGG.

REFERENCES

1. Darvin P, Toor SM, Nair VS, Elkord E. Immune checkpoint inhibitors: recent progress and potential biomarkers. *Exp Mol Med* (2018) 50(12):1–11. doi: 10.1038/s12276-018-0191-1
2. Hegde PS, Karanikas V, Evers S. The Where, the When, and the How of Immune Monitoring for Cancer Immunotherapies in the Era of Checkpoint Inhibition. *Clin Cancer Res* (2016) 22(8):1865–74. doi: 10.1158/1078-0432.CCR-15-1507
3. Demaria O, Cornen S, Daëron M, Morel Y, Medzhitov R, Vivier E. Harnessing innate immunity in cancer therapy. *Nature* (2019) 574 (7776):45–56. doi: 10.1038/s41586-019-1593-5
4. Topalian SL, Taube JM, Anders RA, Pardoll DM. Mechanism-driven biomarkers to guide immune checkpoint blockade in cancer therapy. *Nat Rev Cancer* (2016) 16(5):275–87. doi: 10.1038/nrc.2016.36
5. O'Donnell JS, Teng MWL, Smyth MJ. Cancer immunoediting and resistance to T cell-based immunotherapy. *Nat Rev Clin Oncol* (2019) 16(3):151–67. doi: 10.1038/s41571-018-0142-8
6. Topalian SL, Drake CG, Pardoll DM. Immune checkpoint blockade: a common denominator approach to cancer therapy. *Cancer Cell* (2015) 27 (4):450–61. doi: 10.1016/j.ccell.2015.03.001
7. Li B, Chan HL, Chen P. Immune Checkpoint Inhibitors: Basics and Challenges. *Curr Med Chem* (2019) 26(17):3009–25. doi: 10.2174/0929867324666170804143706
8. Qin S, Xu L, Yi M, Yu S, Wu K, Luo S. Novel immune checkpoint targets: moving beyond PD-1 and CTLA-4. *Mol Cancer* (2019) 18(1):155. doi: 10.1186/s12943-019-1091-2
9. Takács F, Tolnai-Kriston C, Hernádfői M, Szabó O, Szalóki G, Szepesi Á, et al. The Effect of CD86 Expression on the Proliferation and the Survival of CLL Cells. *Pathol Oncol Res* (2019) 25(2):647–52. doi: 10.1007/s12253-018-0512-7
10. Brzostek J, Gascoigne NR, Rybakin V. Cell Type-Specific Regulation of Immunological Synapse Dynamics by B7 Ligand Recognition. *Front Immunol* (2016) 7:24. doi: 10.3389/fimmu.2016.00024
11. Chen R, Ganesan A, Okoye I, Arutyunova E, Elahi S, Lemieux MJ, et al. Targeting B7-1 in immunotherapy. *Med Res Rev* (2020) 40(2):654–82. doi: 10.1002/med.21632
12. Keir ME, Sharpe AH. The B7/CD28 costimulatory family in autoimmunity. *Immunol Rev* (2005) 204:128–43. doi: 10.1111/j.0105-2896.2005.00242.x
13. Leach DR, Krummel MF, Allison JP. Enhancement of antitumor immunity by CTLA-4 blockade. *Science* (1996) 271(5256):1734–6. doi: 10.1126/science.271.5256.1734
14. Schwartz JC, Zhang X, Fedorov AA, Nathenson SG, Almo SC. Structural basis for co-stimulation by the human CTLA-4/B7-2 complex. *Nature* (2001) 410 (6828):604–8. doi: 10.1038/35069112
15. Hodi FS, O'Day SJ, McDermott DF, Weber RW, Sosman JA, Haanen JB, et al. Improved survival with ipilimumab in patients with metastatic melanoma. *N Engl J Med* (2010) 363(8):711–23 doi: 10.1056/NEJMoa1003466.
16. Calabrò L, Morra A, Fonsatti E, Cutaia O, Amato G, Giannarell D, et al. Tremelimumab for patients with chemotherapy-resistant advanced malignant mesothelioma: an open-label, single-arm, phase 2 trial. *Lancet Oncol* (2013) 14 (11):1104–11. doi: 10.1016/S1470-2045(13)70381-4
17. Pope B, Brown RD, Gibson J, Yuen E, Joshua D. B7-2-positive myeloma: incidence, clinical characteristics, prognostic significance, and implications for tumor immunotherapy. *Blood* (2000) 96(4):1274–9. doi: 10.1182/blood.V96.4.1274
18. Maeda A, Yamamoto K, Yamashita K, Asagoe K, Nohgawa M, Kita K, et al. The expression of co-stimulatory molecules and their relationship to the prognosis of human acute myeloid leukaemia: poor prognosis of B7-2-positive leukaemia. *Br J Haematol* (1998) 102(5):1257–62. doi: 10.1046/j.1365-2141.1998.00901.x
19. Xu F, Chen JX, Yang XB, Hong XB, Li ZX, Lin L, et al. Analysis of Lung Adenocarcinoma Subtypes Based on Immune Signatures Identifies Clinical Implications for Cancer Therapy. *Mol Ther Oncolytics* (2020) 17:241–9. doi: 10.1016/j.omto.2020.03.021
20. Xu F, He L, Zhan X, Chen J, Xu H, Huang X, et al. DNA methylation-based lung adenocarcinoma subtypes can predict prognosis, recurrence, and immunotherapeutic implications. *Aging (Albany NY)* (2020) 12(24):25275–93. doi: 10.18632/aging.104129
21. Ranson WA, Neifert SN, Cheung ZB, Mikhail CM, Caridi JM, Cho SK. Predicting in-hospital complications after anterior cervical discectomy and fusion: a comparison of the Elixhauser and Charlson comorbidity indices. *World Neurosurg* (2020) 134:e487–96. doi: 10.1016/j.wneu.2019.10.102
22. Conoscenti C, Rotigliano E, Cama M, Caraballo-Arias NA, Lombardo L, Agnesi V. Exploring the effect of absence selection on landslide susceptibility models: a case study in Sicily, Italy. *Geomorphology* (2016) 261:222–35. doi: 10.1016/j.geomorph.2016.03.006
23. Yoshihara K, Shahmoradgoli M, Martínez E, Vegesna R, Kim H, Torres-Garcia W, et al. Inferring tumour purity and stromal and immune cell admixture from expression data. *Nat Commun* (2013) 4:2612. doi: 10.1038/ncomms3612
24. Li B, Severson E, Pignon JC, Zhao H, Li T, Novak J, et al. Comprehensive analyses of tumor immunity: implications for cancer immunotherapy. *Genome Biol* (2016) 17(1):174. doi: 10.1186/s13059-016-1028-7
25. Li T, Fan J, Wang B, Traugh N, Chen Q, Liu JS, et al. TIMER: A Web Server for Comprehensive Analysis of Tumor-Infiltrating Immune Cells. *Cancer Res* (2017) 77(21):e108–10. doi: 10.1158/0008-5472.CAN-17-0307
26. Schober P, Boer C, Schwarte LA. Correlation Coefficients: Appropriate Use and Interpretation. *Anesth Analg* (2018) 126(5):1763–8. doi: 10.1213/ANE.0000000000002864
27. Yu G, Wang LG, Han Y, He QY. clusterProfiler: an R package for comparing biological themes among gene clusters. *Omics: J Integr Biol* (2012) 16(5):284–7. doi: 10.1089/omi.2011.0118
28. Tang Z, Li C, Kang B, Gao G, Li C, Zhang Z. GEPIA: a web server for cancer and normal gene expression profiling and interactive analyses. *Nucleic Acids Res* (2017) 45(W1):W98–102. doi: 10.1093/nar/gkx247
29. Brown R, Kabani K, Favaloro J, Yang S, Ho PJ, Gibson J, et al. CD86+ or HLA-G+ can be transferred via trogocytosis from myeloma cells to T cells and are associated with poor prognosis. *Blood* (2012) 120(10):2055–63. doi: 10.1182/blood-2012-03-416792
30. Qiu H, Li Y, Cheng S, Li J, He C, Li J. A Prognostic Microenvironment-Related Immune Signature via ESTIMATE (PROMISE Model) Predicts Overall Survival of Patients With Glioma. *Front Oncol* (2020) 10:580263. doi: 10.3389/fonc.2020.580263
31. Chamberlain MC. Prognostic or predictive value of MGMT promoter methylation in gliomas depends on IDH1 mutation. *Neurology* (2014) 82 (23):2147–8. doi: 10.1212/01.wnl.0000451452.30826.6b
32. Karschnia P, Teske N, Dorostkar MM, Siller S, Weller J, Baehring JM, et al. Extent and prognostic value of MGMT promotor methylation in glioma WHO grade II. *Sci Rep* (2020) 10(1):19758. doi: 10.1038/s41598-020-76312-x
33. van den Bent MJ, Dubbink HJ, Sanson M, van der Lee-Haarloo CR, Hegi M, Jeuken JW, et al. MGMT promoter methylation is prognostic but not predictive for outcome to adjuvant PCV chemotherapy in anaplastic oligodendroglial tumors: a report from EORTC Brain Tumor Group Study 26951. *J Clin Oncol* (2009) 27(35):5881–6. doi: 10.1200/JCO.2009.24.1034
34. Brat DJ, Verhaak RG, Aldape KD, Yung WK, Salama SR, Cooper LA, et al. Comprehensive, Integrative Genomic Analysis of Diffuse Lower-Grade Gliomas. *N Engl J Med* (2015) 372(26):2481–98. doi: 10.1056/NEJMoa1402121
35. van den Bent MJ, Brandes AA, Taphoorn MJ, Kros JM, Kouwenhoven MC, Delattre JY, et al. Adjuvant procarbazine, lomustine, and vincristine chemotherapy in newly diagnosed anaplastic oligodendroglioma: long-term follow-up of EORTC brain tumor group study 26951. *J Clin Oncol* (2013) 31 (3):344–50. doi: 10.1200/JCO.2012.43.2229
36. Chamberlain MC, Born D. Prognostic significance of relative 1p/19q codeletion in oligodendroglial tumors. *J Neurooncol* (2015) 125(2):249–51. doi: 10.1007/s11060-015-1906-y
37. Tu Z, Wu L, Wang P, Hu Q, Tao C, Li K, et al. N6-Methylandenosine-Related lncRNAs Are Potential Biomarkers for Predicting the Overall Survival of Lower-Grade Glioma Patients. *Front Cell Dev Biol* (2020) 8:642. doi: 10.3389/fcell.2020.00642
38. Yin W, Jiang X, Tan J, Xin Z, Zhou Q, Zhan C, et al. Development and Validation of a Tumor Mutation Burden-Related Immune Prognostic Model for Lower-Grade Glioma. *Front Oncol* (2020) 10:1409. doi: 10.3389/fonc.2020.01409
39. Wang Y, Wang Z, Zhao B, Chen W, Wang Y, Ma W. Development of a nomogram for prognostic prediction of lower-grade glioma based on alternative splicing signatures. *Cancer Med* (2020) 9(24):9266–81. doi: 10.1002/cam4.3530

40. Yin Q, Han T, Fang B, Zhang G, Zhang C, Roberts ER, et al. K27-linked ubiquitination of BRAF by ITCH engages cytokine response to maintain MEK-ERK signaling. *Nat Commun* (2019) 10(1):1870. doi: 10.1038/s41467-019-09844-0
41. Kondratova M, Czerwinska U, Sompairac N, Amigorena SD, Soumelis V, Barillot E, et al. A multiscale signalling network map of innate immune response in cancer reveals cell heterogeneity signatures. *Nat Commun* (2019) 10(1):4808. doi: 10.1038/s41467-019-12270-x
42. Lin S, Xu H, Zhang A, Ni Y, Xu Y, Meng T, et al. Prognosis Analysis and Validation of m(6)A Signature and Tumor Immune Microenvironment in Glioma. *Front Oncol* (2020) 10:541401. doi: 10.3389/fonc.2020.541401
43. Wang ZL, Li GZ, Wang QW, Bao ZS, Wang Z, Zhang CB, et al. PD-L2 expression is correlated with the molecular and clinical features of glioma, and acts as an unfavorable prognostic factor. *Oncoimmunology* (2019) 8(2): e1541535. doi: 10.1080/2162402X.2018.1541535

Conflict of Interest: The authors declare that the research was conducted in the absence of any commercial or financial relationships that could be construed as a potential conflict of interest.

Copyright © 2021 Qiu, Tian, He, Li, He, Li, Liu and Li. This is an open-access article distributed under the terms of the Creative Commons Attribution License (CC BY). The use, distribution or reproduction in other forums is permitted, provided the original author(s) and the copyright owner(s) are credited and that the original publication in this journal is cited, in accordance with accepted academic practice. No use, distribution or reproduction is permitted which does not comply with these terms.

frontiers in Oncology

ORIGINAL RESEARCH
published: 29 April 2021
doi: 10.3389/fonc.2021.672928

Glioma-Associated Stromal Cells Stimulate Glioma Malignancy by Regulating the Tumor Immune Microenvironment

Xiangming Cai[1†], Feng Yuan[2,3†], Junhao Zhu[4], Jin Yang[3], Chao Tang[3], Zixiang Cong[2,3] and Chiyuan Ma[1,2,3,4]*

[1] School of Medicine, Southeast University, Nanjing, China, [2] School of Medicine, Nanjing University, Nanjing, China, [3] Department of Neurosurgery, Jinling Hospital, Nanjing, China, [4] School of Medicine, Nanjing Medical University, Nanjing, China

OPEN ACCESS

Edited by:
Terrance Johns,
University of Western Australia,
Australia

Reviewed by:
Simon Hanft,
Westchester Medical Center,
United States
Michael Edward Ivan,
University of Miami Health System,
United States

***Correspondence:**
Chiyuan Ma
machiyuan_nju@126.com

[†]These authors have contributed equally to this work and share first authorship

Specialty section:
This article was submitted to Neuro-Oncology and Neurosurgical Oncology, a section of the journal Frontiers in Oncology

Received: 26 February 2021
Accepted: 12 April 2021
Published: 29 April 2021

Citation:
Cai X, Yuan F, Zhu J, Yang J, Tang C, Cong Z and Ma C (2021) Glioma-Associated Stromal Cells Stimulate Glioma Malignancy by Regulating the Tumor Immune Microenvironment. Front. Oncol. 11:672928. doi: 10.3389/fonc.2021.672928

Background: The glioma-associated stromal cell (GASC) is a recently identified type of cell in the glioma microenvironment and may be a prognostic marker for glioma. However, the potential mechanisms of GASCs in the glioma microenvironment remain largely unknown. In this work, we aimed to explore the mechanisms of GASCs in gliomas, particularly in high-grade gliomas (HGG).

Methods: We used glioma datasets from The Cancer Genome Atlas (TCGA) and the Chinese Glioma Genome Atlas (CGGA). We utilized the Single-sample Gene Set Enrichment Analysis (ssGSEA) algorithm to discriminate between patients with high or low GASC composition. The xCELL and CIBERSORT algorithms were used to analyze the composition of stromal cells and immune cells. Risk score and a nomogram model were constructed for prognostic prediction of glioma.

Results: We observed for the first time that the levels of M2 macrophages and immune checkpoints (PD-1, PD-L1, PD-L2, TIM3, Galectin-9, CTLA-4, CD80, CD86, CD155, and CIITA) were significantly higher in the high GASC group and showed positive correlation with the GASC score in all glioma population and the HGG population. Copy number variations of DR3 and CIITA were higher in the high-GASC group. THY1, one of the GASC markers, exhibited lower methylation in the high GASC group. The constructed risk score was an independent predictor of glioma prognostics. Finally, a credible nomogram based on the risk score was established.

Conclusions: GASCs stimulate glioma malignancy through the M2 macrophage, and are associated with the level of immune checkpoints in the glioma microenvironment. The methylation of THY1 could be used as prognostic indicator and treatment target for glioma. However, further studies are required to verify these findings.

Keywords: glioma, glioma-associated stromal cell, immune check points, M2 macrophages, tumor microenvironment

INTRODUCTION

Glioma is the most common primary malignant tumor of the central nervous system, and it generally has a poor prognosis. The World Health Organization (WHO) classified gliomas into grades I-IV, with grades III and IV indicating high-grade gliomas (HGG) (1). The current treatments for HGG involve tumor resection, radiotherapy (RT), and temozolomide (TMZ), but this strategy has not yielded optimal effects (2).

Immunotherapy has been extensively studied for human malignant tumors in the past few years (3). However, due to the "immune-cold" phenotype and inner complexity of glioma (4), only a minority of glioma patients benefit from immune checkpoint (ICP) inhibitors (5). Researchers are deepening our understanding of the complex interactions between glioma and the immune system and trying to maximize the effectiveness of immunotherapy for glioma (6).

The glioma-associated stromal cell (GASC) is a recently identified important stromal cell in the glioma microenvironment, with potential value for prognostic prediction and therapeutic perspectives (7). The available evidence indicates that GASCs facilitate angiogenesis, invasion, and tumor growth (7). However, the potential mechanisms of GASCs remain largely unknown.

We aimed to identify the underlying mechanisms of GASCs in a glioma microenvironment, particularly in HGG. **Figure 1** illustrates the workflow of the study.

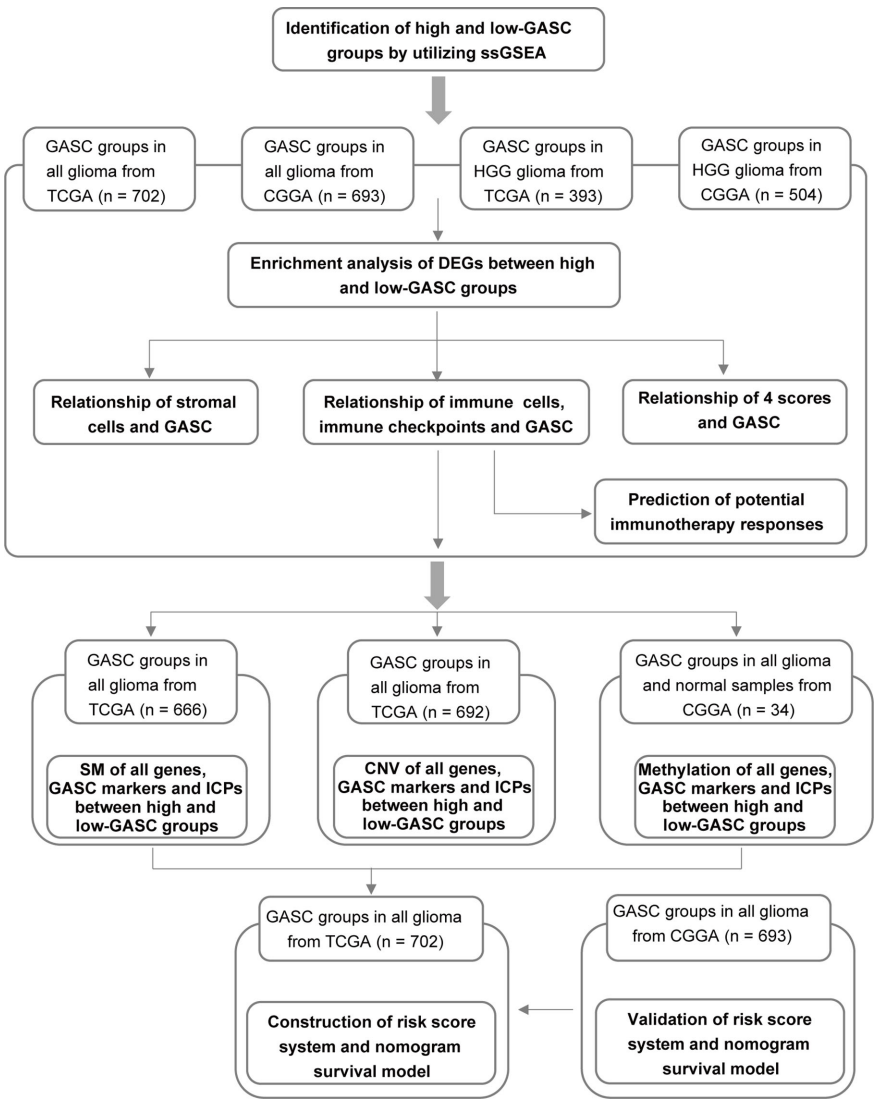

FIGURE 1 | Flow diagram of this investigation. HGG, high-grade glioma; DEGs, differentially expressed genes; 4 scores, stemness, mesenchymal-EMT, tumorigenic cytokine, and angiogenic activity scores; SM, somatic mutations; CNV, copy number variations; ICPs, immune checkpoints.

MATERIALS AND METHODS

Glioma Datasets

The Cancer Genome Atlas (TCGA, https://portal.gdc.cancer.gov/) and Chinese Glioma Genome Atlas (CGGA, www.cgga.org.cn/) are public databases. The mRNA sequencing data and clinical information data for 702 glioma samples from TCGA and 693 glioma samples from CGGA were downloaded. Among these samples, 393 samples from TCGA and 504 samples from CGGA were high-grade glioma (HGG). The somatic mutation data for 666 glioma samples from TCGA were downloaded. The copy number variation data for 692 samples from TCGA were downloaded from the UCSC Xena Project database (http://xena.ucsc.edu/). For methylation analysis, the methylation data for 34 samples from CGGA and mRNA sequencing data for 325 samples were downloaded from CGGA.

ssGSEA Analysis

A gene set of GASC markers (**Table S1**) was obtained from Clavreul et al. (7). Enrichment scores for GASCs were separately calculated for each sample with the Single-sample Gene Set Enrichment Analysis (ssGSEA) algorithm. We also used the ssGSEA algorithm to calculate the stemness score (8), mesenchymal-epithelial-to-mesenchymal transition (EMT) score (9), tumorigenic cytokine score (10) and angiogenic activity score (11) based on the corresponding gene sets (**Table S1**). The "GSVA" R package (version 1.34.0) was applied to conduct an ssGSEA analysis.

Principle Component Analysis (PCA)

PCA was used to show the differentiation of high- and low-GASC groups and was visualized with the "ggfortify" R package (version 0.4.11).

Differential Analysis of Expressed Gene

We used Morpheus (https://software.broadinstitute.org/morpheus) to identify significantly differentially expressed genes (DEGs) between the high- and low-GASC groups. $P < 0.05$ and $|\log2 \text{ FC (fold-change)}| \geq 1$ were selected as the cutoff values for statistically significant DEGs. A heatmap of DEG expression was produced by the "pheatmap" R package (version 1.0.12).

Functional Annotation

To reveal the probable biofunctions and signaling pathways that were correlated with the DEGs, we performed Gene Ontology (GO) annotations enrichment analysis, Kyoto Encyclopedia of Genes and Genomes (KEGG) pathway analysis and enrichment analysis, and Gene Set Enrichment Analysis (GSEA) using the "clusterProfiler" (12) package (version 3.14.3) in R. Adjusted $p < 0.05$ was selected as the cutoff criterion.

xCELL Analysis and Cell Type Identification by Estimating Relative Subsets of RNA Transcripts (CIBERSORT) Analysis

xCell is an R package (version 1.1.0) that estimates the comprehensive levels of 64 cell types, which include 14 stromal cells. CIBERSORT can accurately quantify the abundance scores of 22 types of immune cells for each sample. We applied xCELL and CIBERSORT to separately calculate the abundance scores for stromal cells and immune cells in glioma samples.

Analysis of Somatic Mutations and Copy Number Variations

The somatic mutations of glioma samples from TCGA were calculated and visualized by the "Maftools" R package (version 2.2.10) (13). The copy number variations were visualized by the "ComplexHeatmap" R package (version 2.2.0).

Prediction of the Immunotherapy Response

The Tumor Immune Dysfunction and Exclusion (TIDE) algorithm (14) was employed to predict the clinical response of immune checkpoint inhibitors for each glioma sample.

Construction of Prognostic Model

The glioma datasets from TCGA and CGGA were used separately as a training dataset and validation dataset during the construction of the prognostic model. In the filtering process, least absolute shrinkage and selection operator (LASSO) regression analysis was applied to filter input parameters with $p < 0.05$. The input parameters included GASC score, GASC markers, immune checkpoints, stemness score, mesenchymal-EMT score, tumorigenic cytokine score, angiogenic activity score, stromal cell scores, and immune cell scores. Then, multivariate Cox regression analysis was conducted, and the risk score for glioma was computed *via* this formula: risk = score $\sum_{i=1}^{n} \beta_i \times X_i$. X_i indicates the input parameter of multivariate regression analysis, and β_i represents the coefficient of X_i. Risk score and clinicopathological features were used to construct a prognostic model with uni- and multivariate Cox regression analysis. A nomogram was built to show the prognostic model. Receiver operating characteristic (ROC) curve analysis was conducted to evaluate the effect of the prognostic model in the training and validation datasets. "glmnet" (version 4.1), "rms" (version 6.1.0), and "timeROC" (version 0.4) R packages were used for the construction of prognostic model.

Statistical Analysis

All statistical analyses were performed utilizing R software (version 3.5.1), and statistical significance was set at $p < 0.05$. Comparisons between 2 continuous variables were evaluated by Student's *t*-test and one-way ANOVA with ≥ 3 variables. Boxplots and bar charts were utilized to display these comparisons using the "ggplot" R package (version 3.3.3). The chi-square test or Fisher's exact test were used for comparisons of categorized variables. The Kaplan-Meier approach was conducted for survival analysis, and the log-rank test was used to compare the overall survival (OS). Spearman correlation analysis was applied to evaluate two continuous variables, and the data were visualized with "ggplot" and "corrgram" (version 1.13) R packages. Univariate Cox regression was applied to identify potential predictors of survival, and the data were displayed with "forestplot" (version 1.10.1) R package.

RESULTS

Identification of High- and Low-GASC Groups With ssGSEA

To analyze the potential mechanisms of GASCs in the glioma microenvironment, we obtained mRNA sequencing data for 702 samples from TCGA and 693 samples from CGGA, and then calculated the GASC score for each sample using the ssGSEA algorithm (**Figure 1**). Samples from TCGA and CGGA were classified separately into high- or low-GASC groups according to the median of the GASC score. Information for the high- and low-GASC groups is shown in **Figures 2A, B** and **Table 1**. Separate classification was also performed for 393 HGG samples from TCGA and 504 HGG from CGGA into high- and low-

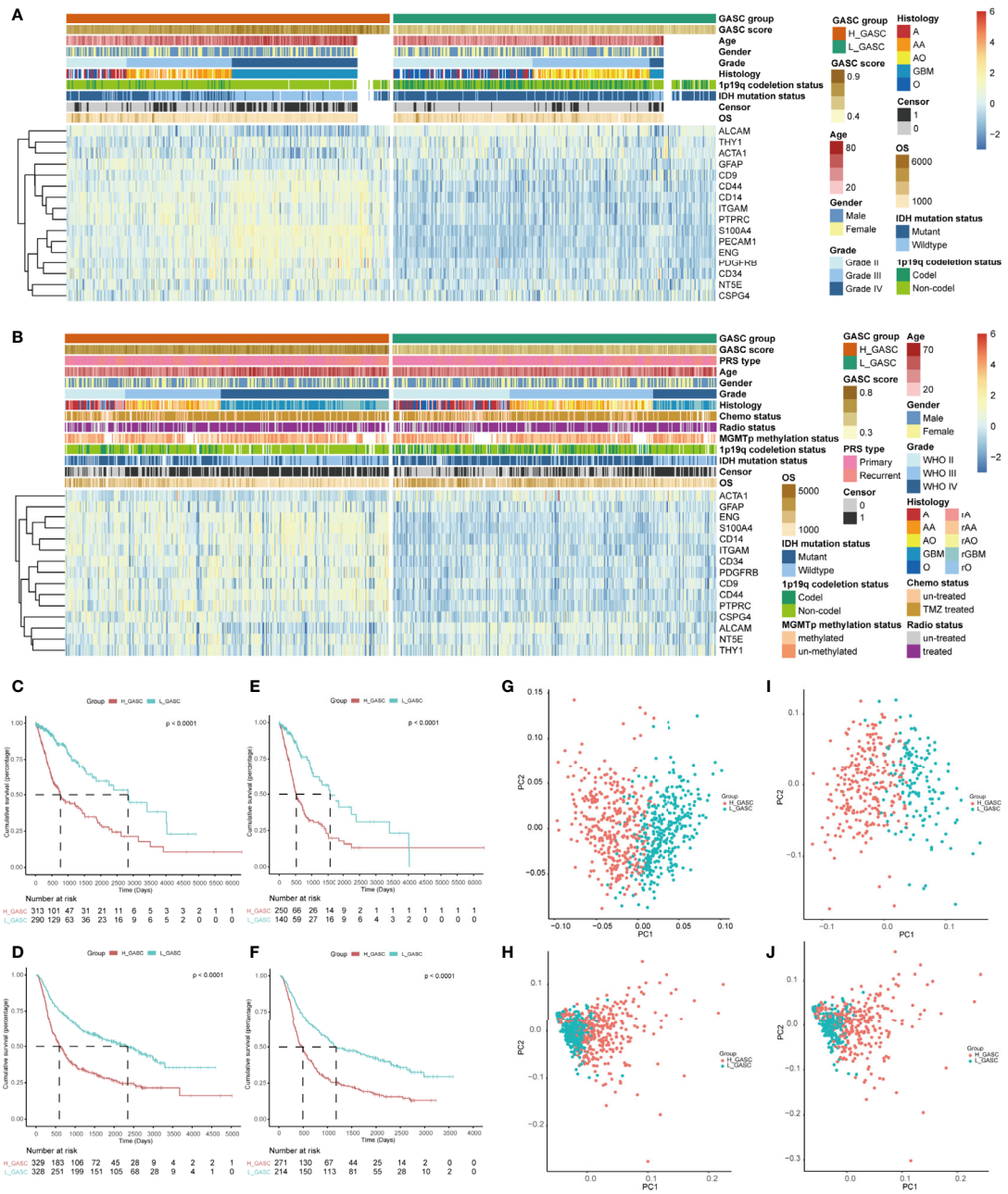

FIGURE 2 | Identification of high- and low-GASC groups. **(A, B)** Heatmap of GASC markers in all glioma population (**A** for TCGA and **B** for CGGA). **(C–F)** Kaplan-Meier overall survival (OS) curves for samples in high- and low-GASC groups from all glioma population (**C** for TCGA and **D** for CGGA) and high-grade glioma population (**E** for TCGA and **F** for CGGA). **(G–J)** Principal component analysis of high- and low-GASC groups from all glioma population (**G** for TCGA and **H** for CGGA) and high-grade glioma population (**I** for TCGA and **J** for CGGA).

GASC groups using the same method. K-M curves were drawn, and the results revealed that a higher GASC score was associated with worse OS in all glioma population and the HGG population ($p < 0.0001$; **Figures 2C–F**). PCA showed robust differences in the expression portraits of the GASC markers between the high- and low-GASC groups (**Figures 2G–J**).

Enrichment Analysis of DEGs Between the High- and Low-GASC Groups

DEGs between the high- and low-GASC groups were identified with the Morpheus webtool (**Figure S1**). Functional enrichment revealed a significant association between DEGs and immune-related terms. Biological process (BP) terms enriched in the GO analysis included "lymphocyte chemotaxis" and "neutrophil activation" in all glioma population (**Figures 3A, D** and **Table S2**) and the HGG population (**Figures 4A, D** and **Table S2**). The "JAK-STAT signaling pathway" and "IL-17 signaling pathway" were enriched in the KEGG analysis in all glioma population (**Figures 3B, E** and **Table S3**) and the HGG population (**Figures 4B, E** and **Table S3**). GSEA analysis revealed immune-related terms such as "Antigen processing and presentation" and "PD-L1 expression and PD-1 checkpoint pathway" in all glioma population (**Figures 3C, F** and **Table S6**) and the HGG population (**Figures 4C, F** and **Table S6**).

Correlation of Stemness, Mesenchymal-EMT, Tumorigenic Cytokine, and Angiogenic Activity Scores With GASCs

To explore the potential mechanisms of GASCs in glioma, we also calculated stemness, mesenchymal-EMT, tumorigenic cytokine, and angiogenic activity scores for each glioma sample using the ssGSEA algorithm (**Table S1**). The results showed that mesenchymal-EMT, tumorigenic cytokine, and angiogenic activity scores were significantly higher in the high-GASC group (**Figure 5A**), and were positively correlated with the GASC score in all glioma population (**Figures 5B, C**) and the HGG population (**Figures 5D, E**).

TABLE 1 | Correlations between GASC groups and clinical characteristics in glioma patients.

Characteristic	TCGA			CGGA		
	H_GASC	L_GASC	*p*-value	H_GASC	L_GASC	*p*-value
All cases	351	351		346	347	
Age (yeas)	51.11 ± 15.89	43.25 ± 13.54	<0.001*	45.06 ± 13.30	41.51 ± 11.15	0.003*
Gender			0.126			0.792
Female	123	132		149	146	
Male	193	161		197	201	
Grade			<0.001*			<0.001*
Grade II	65	151		64	124	
Grade III	114	127		102	153	
Grade IV	137	15		180	69	
Histology			<0.001*			<0.001*
A + rA	28	27		46	73	
AA + rAA	69	45		70	82	
AO + rAO	21	66		25	57	
GBM + rGBM	137	15		180	69	
O + rO	20	97		17	43	
PRS type						0.006*
Primary				193	229	
Recurrent				153	118	
1p19q codeletion status			<0.001*			<0.001*
Codel	28	141		44	101	
Non-codel	301	194		267	211	
IDH mutation status			<0.001*			<0.001*
Mutant	139	289		134	222	
Wildtype	187	47		190	96	
MGMTp methylation status						0.696
methylated				158	157	
un-methylated				110	117	
Radiotherapy status						0.219
treated				259	251	
un-treated				61	75	
Chemotherapy status						0.013
TMZ treated				257	229	
un-treated				67	94	

*A, astrocytoma; O, oligodendroglioma; AA, anaplastic astrocytoma; AO, anaplastic oligodendroglioma; GBM, glioblastoma; r, recurrence; PRS type, primary-recurrent-secondary type; TMZ, temozolomide; *p < 0.05.*

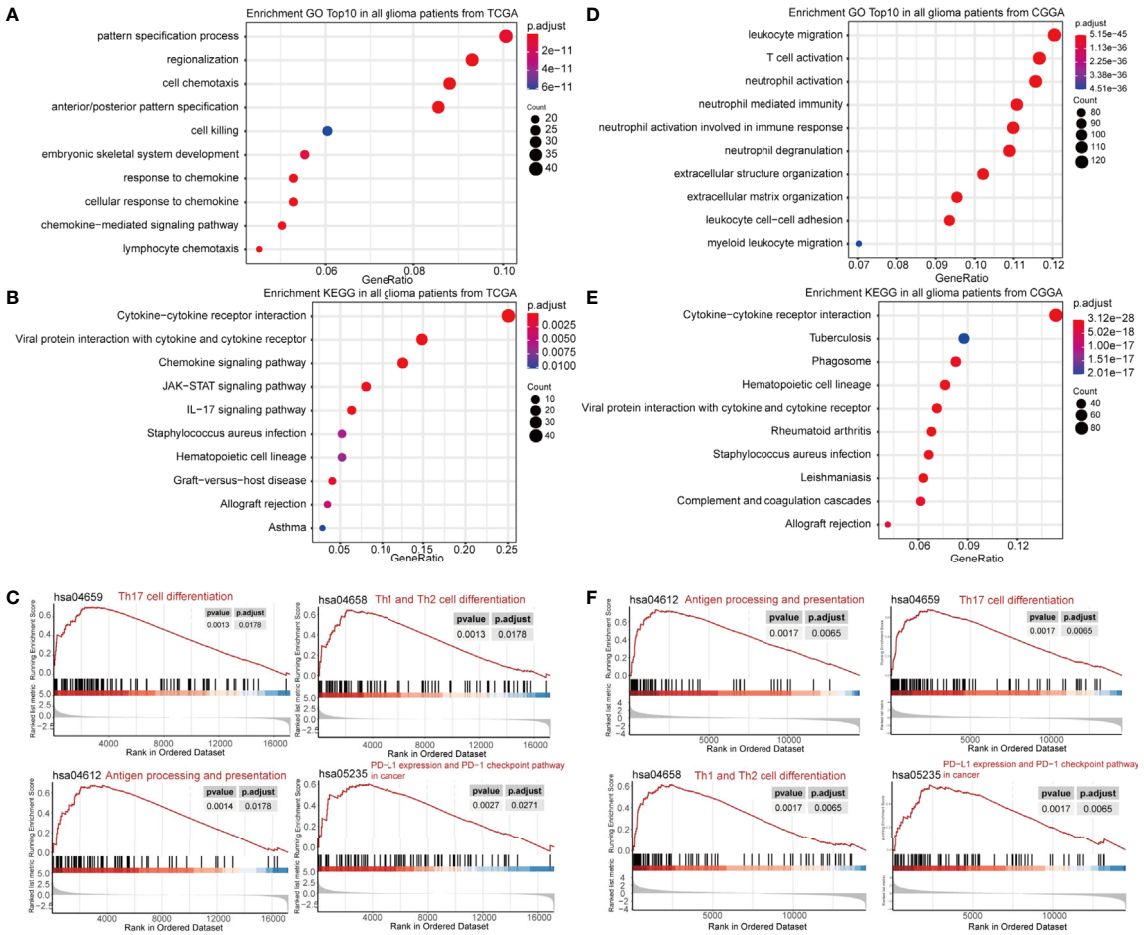

FIGURE 3 | Functional annotation of upregulated DEGs between the high- and low-GASC groups from all glioma population. **(A, B)** GO analysis **(A)** and KEGG pathway analysis **(B)** of up-regulated DEGs from TCGA data. **(C)** GSEA analysis of genes from TCGA data. **(D, E)** GO analysis **(D)** and KEGG pathway analysis **(E)** of up-regulated DEGs from CGGA data. **(F)** GSEA analysis of genes from CGGA data.

Associations Between GASCs and Stromal Cells

To discover the relationship between GASCs and other stromal cells, we computed the levels of 14 stromal cells using the xCELL algorithm. Bar charts showed that endothelial cells, lymphatic endothelial cells, and microvascular endothelial cells were higher in the high-GASC group in all glioma population from the TCGA (**Figure 6A**) and CGGA (**Figure 6D**) databases. Univariate Cox regression revealed that the level of mesenchymal stem cells is a protective factor for glioma (**Figures 6B, E**). A coefficient matrix showed that the GASC score was positively correlated with the levels of endothelial cells, lymphatic endothelial cells, and microvascular endothelial cells (**Figures 6C, F**). Similar results were found in the HGG population (**Figure S3**).

Immune Landscape of the High- and Low-GASC Groups

Because some immune-related terms were enriched in the functional annotation analysis, we explored the relationship between GASCs and the immune microenvironment. The CIBERSORT algorithm computed the relative abundance of 22 types of immune cells, which are shown in **Figure 7**. Overall, the adaptive immunity was at a relatively lower level in the high-GASC group compared with that in the low-GASC group. Notably, the level of M2 macrophages was significantly higher in the high-GASC group (**Figures 8A, C**) and was positively correlated with GASC score (**Figure 9A**) in all glioma population. Univariate Cox regression also revealed that the level of M2 macrophages is a risk factor for glioma (**Figures 8B, D**). Similar results were found in the HGG population (**Figures 8E–H**, **9B**).

We also analyzed the correlation of GASCs and 14 important ICPs. As shown in **Figure 10**, the expression levels of most ICPs were statistically higher in the high-GASC group. The univariate Cox regression showed that the expression levels of PD-L2, TIM3, CD80, CD86, CD155, and CIITA were risk factors for glioma in all glioma population and the HGG population. Correlation analysis indicated strong positive correlations within ICPs. The GASC score was positively correlated with

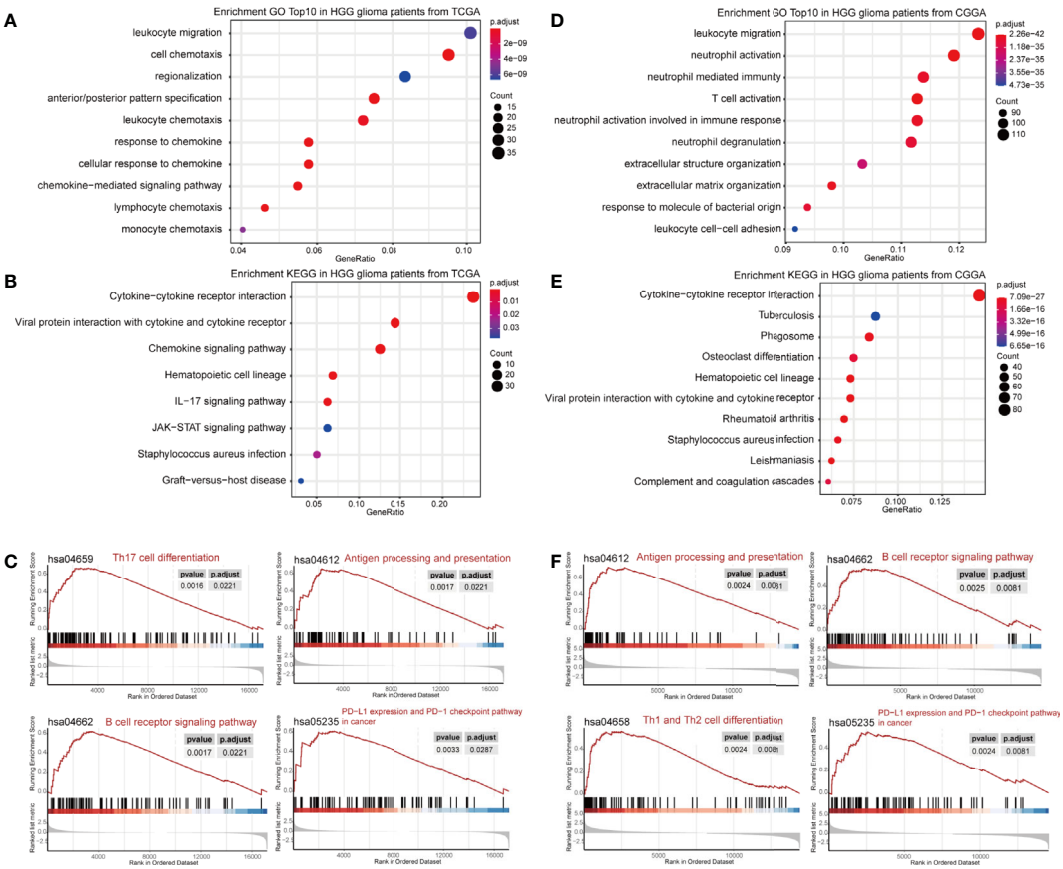

FIGURE 4 | Functional annotation of upregulated DEGs between the high- and low-GASC groups from the high-grade glioma population. **(A, B)** GO analysis **(A)** and KEGG pathway analysis **(B)** of up-regulated DEGs from TCGA data. **(C)** GSEA analysis of genes from TCGA data. **(D, E)** GO analysis **(D)** and KEGG pathway analysis **(E)** of up-regulated DEGs from CGGA data. **(F)** GSEA analysis of genes from CGGA data.

PD-1, PD-L1, PD-L2, TL1A, TIM3, Galactin-9, CTLA-4, CD80, CD86, CD155, LAG3, and CIITA in all glioma population and the HGG population (**Figure 9**).

Copy Number Variations (CNVs) in DR3 and CIITA Indicated Worse OS

We also downloaded the somatic mutation and CNV data for glioma to analyze the difference in genomic alterations between the high- and low-GASC groups in all glioma population. The 20 genes with the greatest amounts of somatic mutations and CNVs are shown in **Figure S4**. We also compared the somatic mutations and CNVs of GASC markers between the high- and low-GASC groups (**Figure S5**), but found no significant difference in genomic alterations. However, in the comparison of somatic mutations and CNVs of ICPs between the high- and low-GASC groups (**Figure S6**), the results showed that the CNVs of DR3 and CIITA were significantly higher in the high-GASC group (**Figure S6E**). Survival analysis indicated that the CNVs of DR3 and CIITA significantly decreased the OS of glioma patients (**Figures S6F, G**).

Higher THY1 and CD80 Methylation Indicated Better OS

In the search for a possible treatment target for glioma, we conducted methylation analysis of GASC markers and ICPs. Because there was not a satisfactory match between samples with methylation data in the CGGA database and samples in the CGGA_693 mRNA dataset, we also downloaded the CGGA_325 mRNA dataset and separated these samples into high- and low-GASC groups with the previously mentioned method. Overall, 26 glioma samples (6 in the high-GASC group and 20 in the low-GASC group) and 8 normal samples with methylation data were included.

The GASC markers indicated that the methylation levels of THY1, CD9, CD14, CD44, ITGAM, and ACTA1 were significantly different among the high-GASC, low-GASC, and normal groups (**Figure 11A** and **Figure S7**). Then, we divided the glioma samples into high- and low-methylation groups according to the median of the gene methylation level. Survival analysis indicated that statistical difference was only observed between high- and low-THY1 methylation groups (p = 0.018; **Figure 11B**). High THY1

A

Characteristic	TCGA			CGGA		
	H_GASC	L_GASC	p-value	H_GASC	L_GASC	p-value
Stemness score	0.45 ± 0.06	0.45 ± 0.06	0.401	0.37 ± 0.06	0.35 ± 0.07	<0.001*
Mesenchymal-EMT score	0.39 ± 0.04	0.36 ± 0.03	<0.001*	0.30 ± 0.05	0.26 ± 0.05	<0.001*
Tumorigenic cytokine score	-0.10 ± 0.08	-0.16 ± 0.07	<0.001*	0.07 ± 0.11	-0.04 ± 0.08	<0.001*
Angiogenic activity score	0.37 ± 0.02	0.33 ± 0.02	<0.001*	0.38 ± 0.03	0.36 ± 0.03	<0.001*

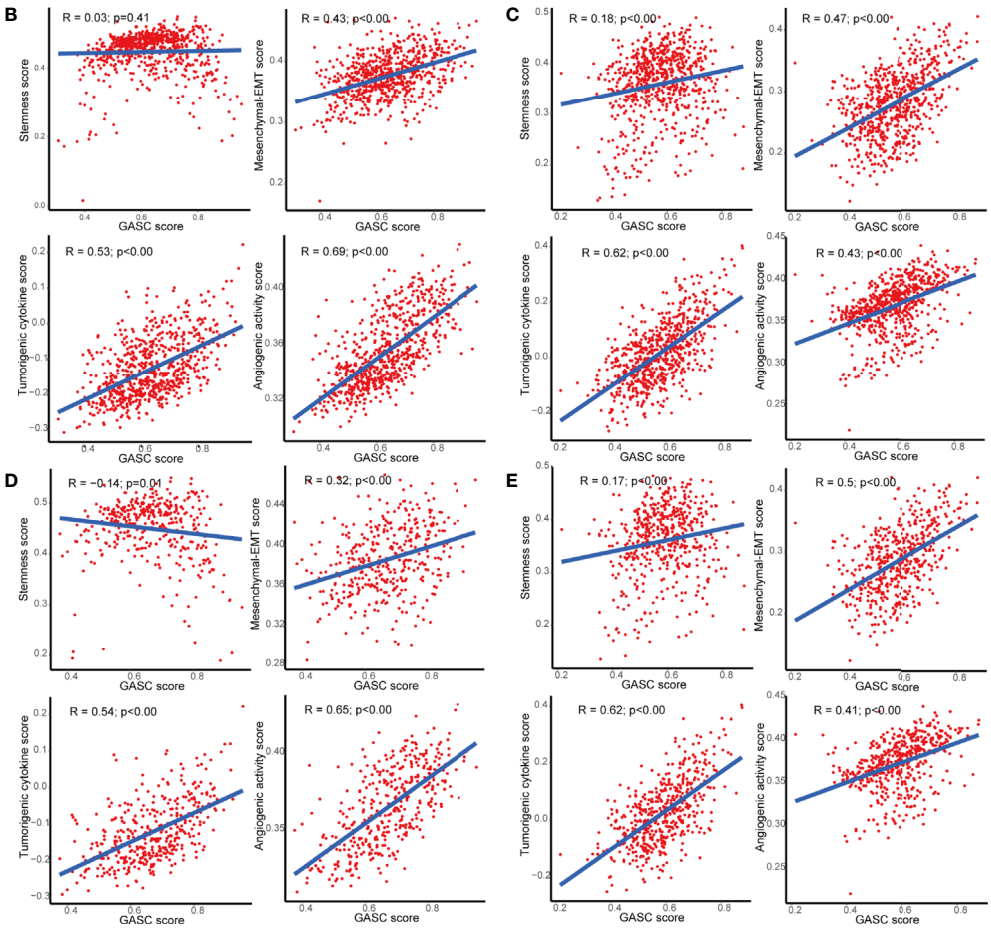

FIGURE 5 | Correlations between GASCs and Stemness, Mesenchymal-EMT, Tumorigenic cytokine, and Angiogenic activity scores. **(A)** Correlations between GASC groups and stemness, mesenchymal-EMT, tumorigenic cytokine and angiogenic activity scores. **(B–E)** Scatterplot of GASC score and 4 scores in all glioma population (**B** for TCGA and **C** for CGGA) and high-grade glioma population (**D** for TCGA and **E** for CGGA). *Statistical significance.

methylation suggested greater patient OS. In the methylation analysis of ICPs, significant differences were detected in Galactin-9, CD80, CD155, and LAG3 (**Figure 11C** and **Figure S8**). However, only high- and low-CD80 methylation groups showed statistical difference in the survival analysis ($p = 0.031$; **Figure 11D**), and high CD80 methylation indicated better OS.

Predicted Potential Immunotherapy Responses Between the High- and Low-GASC Groups

The TIDE webtool was applied to predict the likelihood of immune response for each sample. The results showed that in all glioma population, the low-GASC group (56%, 197/351 in TCGA; 40%, 138/347 in CGGA) was more likely to respond to immunotherapy than the high-GASC group (40%, 141/351 in TCGA; 29%, 102/346 in CGGA). However, in the HGG population, difference was found only in the TCGA dataset (high-GASC vs. low-GASC: 31% vs. 44%; **Figures S9A–E**).

In order to further analyze the immune infiltration between the responder and no responder groups, we compared the levels of immune cells between these two groups. The results showed that in all glioma population, the responder group had lower "T cells CD8" and "Macrophages M0" and higher "Mast cells activated" (**Figures S9F, G**). For the HGG population, "T cells CD8" was lower in the responder group, and "Mast cells activated" was higher in the responder group (**Figures S9H, I**).

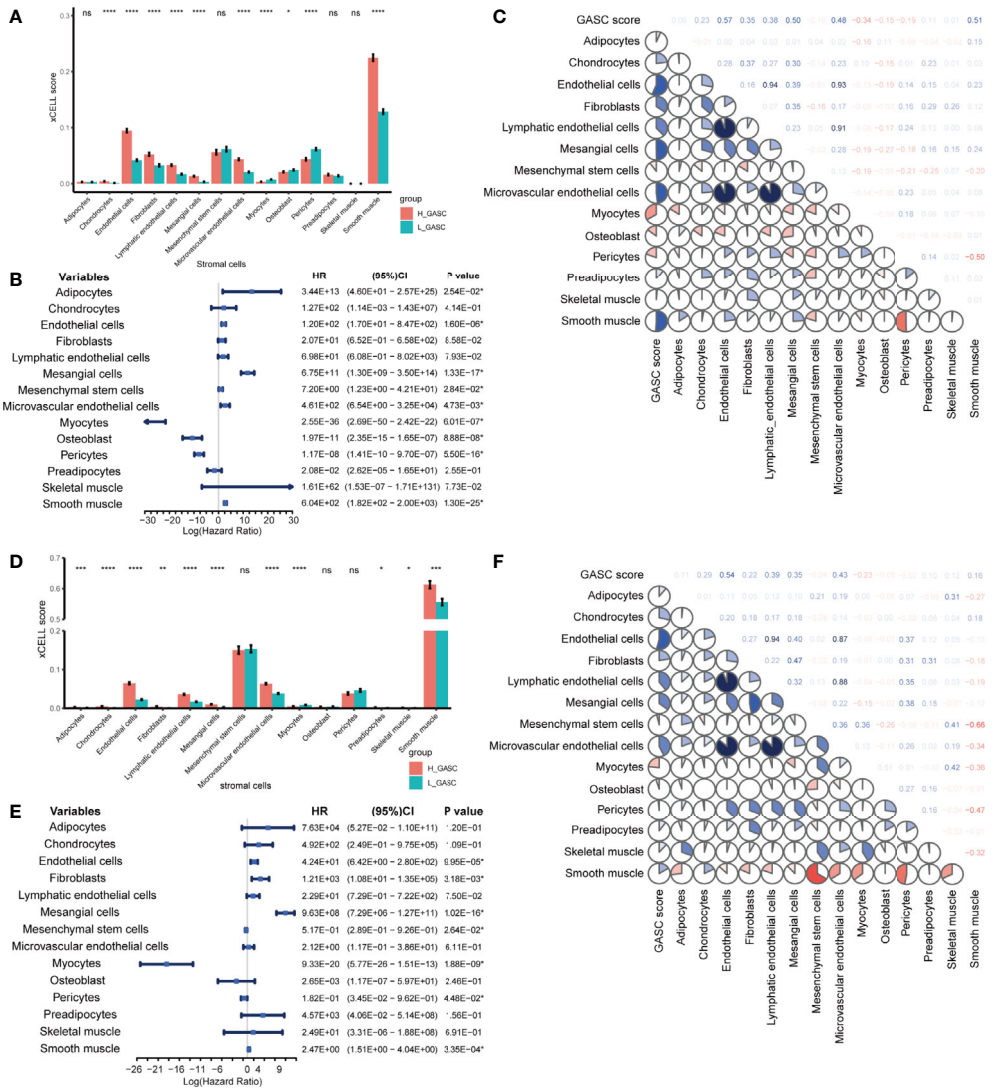

FIGURE 6 | Associations between GASCs and stromal cells in all glioma population. **(A, D)** Bar charts illustrating the differences of xCELL scores between high- and low-GASC groups (**A** for TCGA and **D** for CGGA). ns: $p > 0.05$, $^{*}p \leq 0.05$, $^{**}p \leq 0.01$, $^{***}p \leq 0.001$, $^{****}p \leq 0.0001$. **(B, E)** Forest plots of univariate Cox regression analysis of stromal cells (**B** for TCGA and **E** for CGGA). **(C, F)** Correlograms of GASC score and stromal cells intercorrelation (**C** for TCGA and **F** for CGGA).

Construction of a Risk Score System and Establishment and Validation of a Nomogram Survival Model

The mRNA sequencing data from TCGA (702 samples) was used as training dataset, and the data from CGGA (693 samples) was set as an independent validation dataset. For the training dataset, GASC score, GASC markers, immune checkpoints, stemness score, mesenchymal-EMT score, tumorigenic cytokine score, angiogenic activity score, stromal cell scores, and immune cell scores were filtered using LASSO regression with the "glmnet" R package. The change in trajectory of each variable was plotted in **Figure 12A**. We utilized 10-fold cross-validation to construct the model, and **Figure 12B** shows the confidence interval under each lambda. When lambda equaled 0.03431609, the model reached the optimal value, and 19 variables were selected for the next analysis. In the multivariable Cox regression analysis, the number of variables was reduced to 9, and the final 9-variable signature formula was: Risk score = 0.20 × CSPG4 – 0.30 × ALCAM + 35.16 × Adipocytes – 11.11 × Osteoblast – 7.05 × Pericytes – 2.50 × Plasma cells + 0.22 × CD274 + 0.16 × CD80 + 13.45 × angiogenesis. The risk score was calculated for each sample in the training and validation datasets. Thus, we divided samples into high- and low-risk groups according to the median risk score. Survival analysis revealed that in the training dataset, glioma patients in high-risk group have worse OS ($p < 0.0001$; **Figure 12C**), which was also confirmed in the validation dataset ($p < 0.0001$; **Figure 12D**).

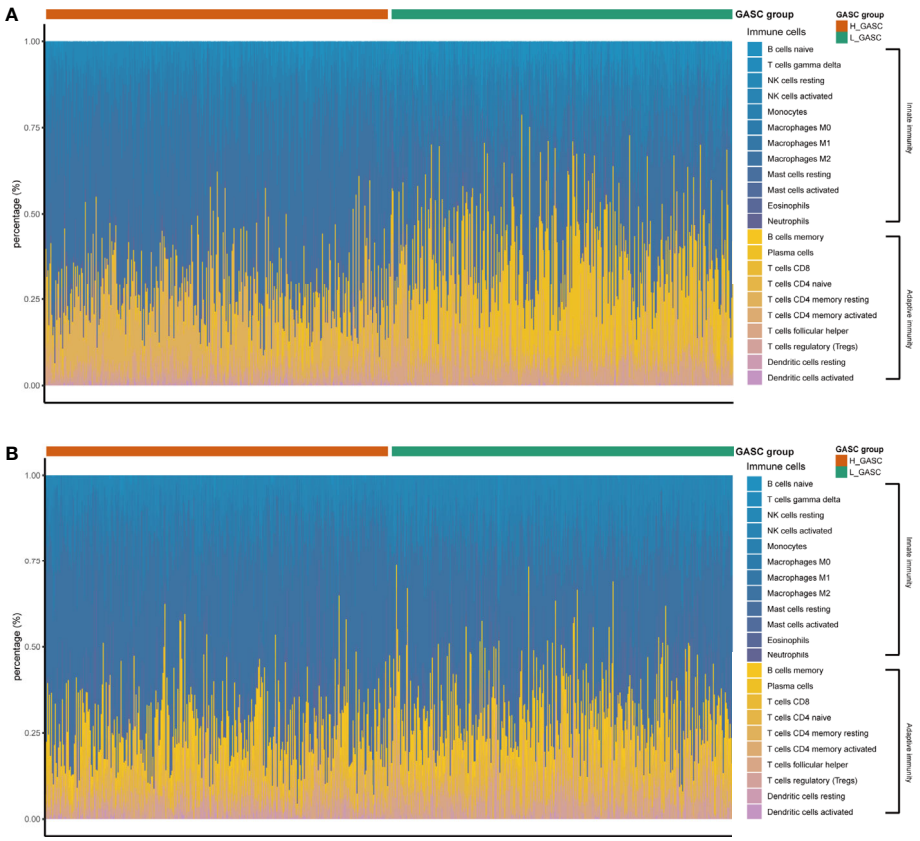

FIGURE 7 | The relative abundances of the 22 types of immune cells. **(A)** Results from TCAG data. **(B)** Results from CGGA data.

Then, we constructed a nomogram model to predict the prognosis of glioma, which included the risk score and clinicopathologic features. The uni- and multivariate Cox regression analysis (**Figure 12E**) indicated that risk score was an independent predictor for glioma prognostics. We finally included four features (age, WHO grade, isocitrate dehydrogenase (IDH) mutation status, and risk score) in the nomogram model (**Figure 12F**). Time-dependent ROC analysis further indicated that the area under the curve (AUC) for 1-, 3-, and 5-year OS were 0.902, 0.948, and 0.911, respectively, in the training dataset (**Figure 12G**). These AUCs were better compared with IDH mutation status, which is a traditional indicator, and were 0.842, 0.862, and 0.813 at the 1-, 3-, and 5-year marks (**Figure 12I**). Similar results were obtained in the validation datasets (**Figures 12H, J**).

DISCUSSION

The GASC is a recently identified particular type of cell in the glioma microenvironment, with various names, e.g., glioma-associated human MSCs (GA-hMSCs) (7). The phenotypic and functional properties of GASCs are similar to those of cancer-associated fibroblasts and mesenchymal stem cells. The mechanism of GASCs in the glioma microenvironment is still largely unknown. In this work, we explored the potential mechanisms of GASCs in the glioma microenvironment, and discovered that GASCs may upregulate the level of M2 macrophages and ICPs. We also found that the CNVs of DR3 and CIITA were higher in the high-GASC group, and the methylation level of THY1 was lower in the high-GASC group, which could be a potential treatment target for glioma, particularly in HGG.

The tumor microenvironment determines the invasiveness of glioma. The EMT regulates this invasive state of glioma, particularly in HGG (9). Studies reported that GASCs drive cell invasion through HA synthase-2 (HAS2) induction (15), the UCA1/miR-182/PFKFB2 axis (16), the C5a/p38/ZEB1 axis (17) and CCL2/JAK1/MLC2 signaling (18). In the current work, we also discovered that the GASC score was positively correlated with the mesenchymal-EMT score in all glioma population and the HGG population (**Figure 5**). Terms from functional annotation include adhesion-related terms (**Tables S2**, **S6**), e.g., "Cell adhesion molecules".

In the current study, we found a strong correlation between the GASC score and tumorigenic cytokine score, indicating the tumor-supporting function of GASCs. Studies reported that GASCs have tumor-promoting effects *in vitro* and *in vivo* (19–21).

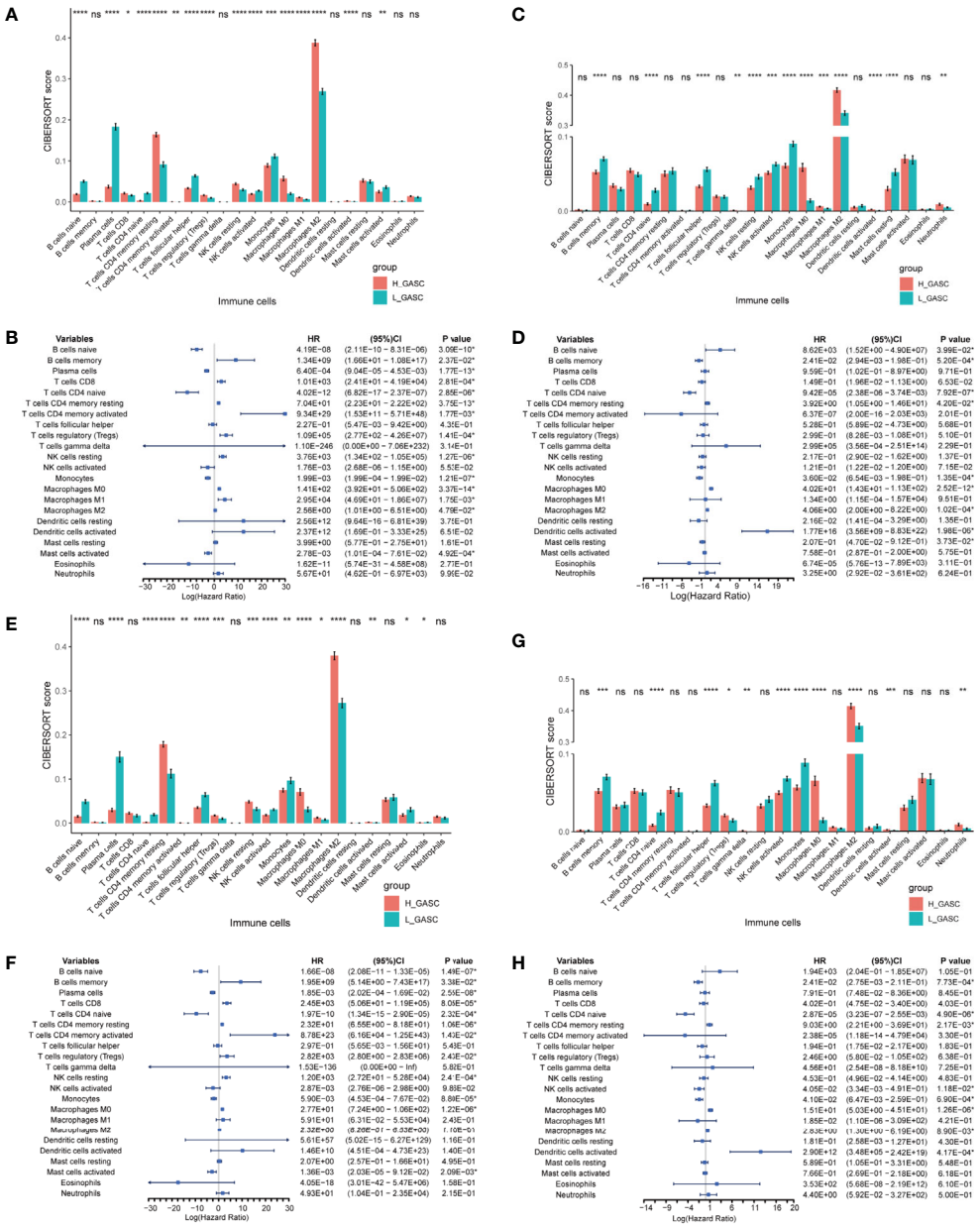

FIGURE 8 | Associations between GASCs and immune cells. **(A, C, E, G)** Bar charts illustrating the differences in CIBERSORT scores between high- and low-GASC groups in all glioma population (**A** for TCGA and **C** for CGGA) and high-grade glioma population (**E** for TCGA and **G** for CGGA). **(B, D, F, H)** Forest plots of univariate Cox regression analysis of immune cells in all glioma population (**B** for TCGA and **D** for CGGA) and high-grade glioma population (**F** for TCGA and **H** for CGGA). ns: $p \geq 0.05$, *$p \leq 0.05$, **$p \leq 0.01$, ***$p \leq 0.001$, ****$p \leq 0.0001$

Additionally, Figueroa et al. also suggested that the tumor-supporting role of GASCs is mediated by the exosomal delivery of specific oncogenic miRNAs (21).

Although GASCs infiltrate into the glioma stroma, they are predominantly located around blood vessels (22), particularly abnormal vessels (23). Previous studies indicated that GASCs increase the angiogenesis of glioma (24, 25). Zhang et al. suggested that CD90^{low} (THY1) GASCs stimulate angiogenesis *via* vascular endothelial cells (25). In the current work, we detected a high correlation between the GASC score and the angiogenesis score (**Figure 5**) in all glioma population and the HGG population. We also found that in addition to endothelial cells, the GASC score also was positively correlated with microvascular endothelial cells (**Figures 6** and **Figure S3**). The levels of endothelial cells and microvascular endothelial cells were higher in the high-GASC group (**Figures 6** and **Figure S3**).

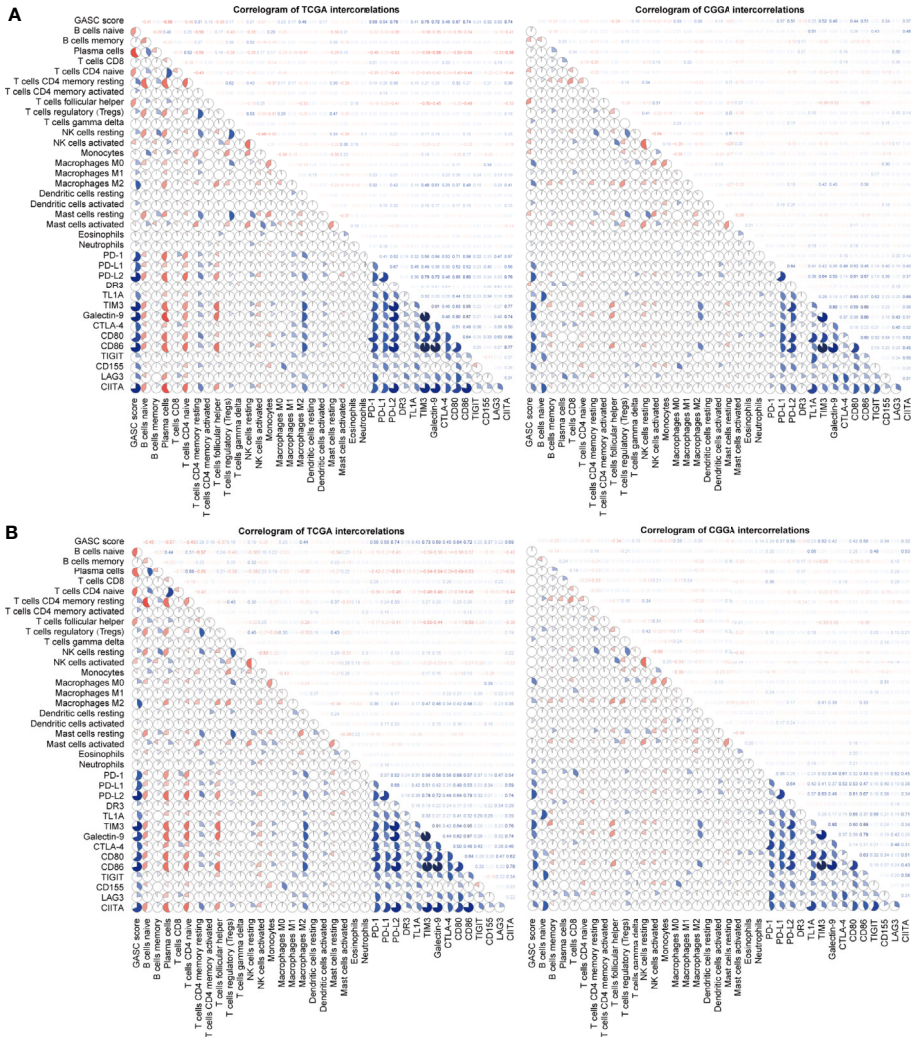

FIGURE 9 | Correlogram of GASC score, immune cells, and expression of ICP intercorrelation. **(A)** Correlogram of data in all glioma population. **(B)** Correlogram of data in high-grade glioma population.

These results indicated that GASCs may promote angiogenesis of glioma by stimulating the growth of both blood vessels and microvessels, which requires further verification.

Tumor-associated macrophages (TAMs) play an emerging role in glioma progression and are found in high proportions in the immune landscape of malignant glioma (26, 27). There are continuous phenotypes in the activation state of TAMs, in which M1 and M2 represent two extreme phenotypes (28). M2 has an anti-inflammatory phenotype, which leads to downregulation of immune responses, and thus prevents tissue damage and supports healing processes (27). In this work, our results suggest for the first time that GASCs are highly correlated with M2 macrophages in the glioma microenvironment. Based on our results, the level of M2 macrophages in the high-GASC group is statistically higher than that in the low-GASC group in all glioma population and the HGG population ($p \leq 0.0001$; **Figure 8**). We also found high correlation coefficients between GASC scores and M2 macrophages in all glioma population (R = 0.46 (TCGA); R = 0.30 (CGGA); **Figure 9A**) and the HGG population (R = 0.44 (TCGA); R = 0.26 (CGGA); **Figure 9B**). These results indicated that TAMs may be phenotypically polarized to M2 macrophages by GASCs, which may further depress the immunity of the microenvironment and stimulate malignant progression of glioma. Conversely, the M2 macrophages may also upregulate the level of GASCs and further increase the malignant properties of glioma, e.g., invasion and angiogenesis.

Immune checkpoint blockade is the most developed immunotherapy in clinical use (4), but its efficiency still remains doubtful. We analyzed the expression levels of 14 important ICPs and found that the expression levels of most ICPs were higher in the high-GASC group. Although this result

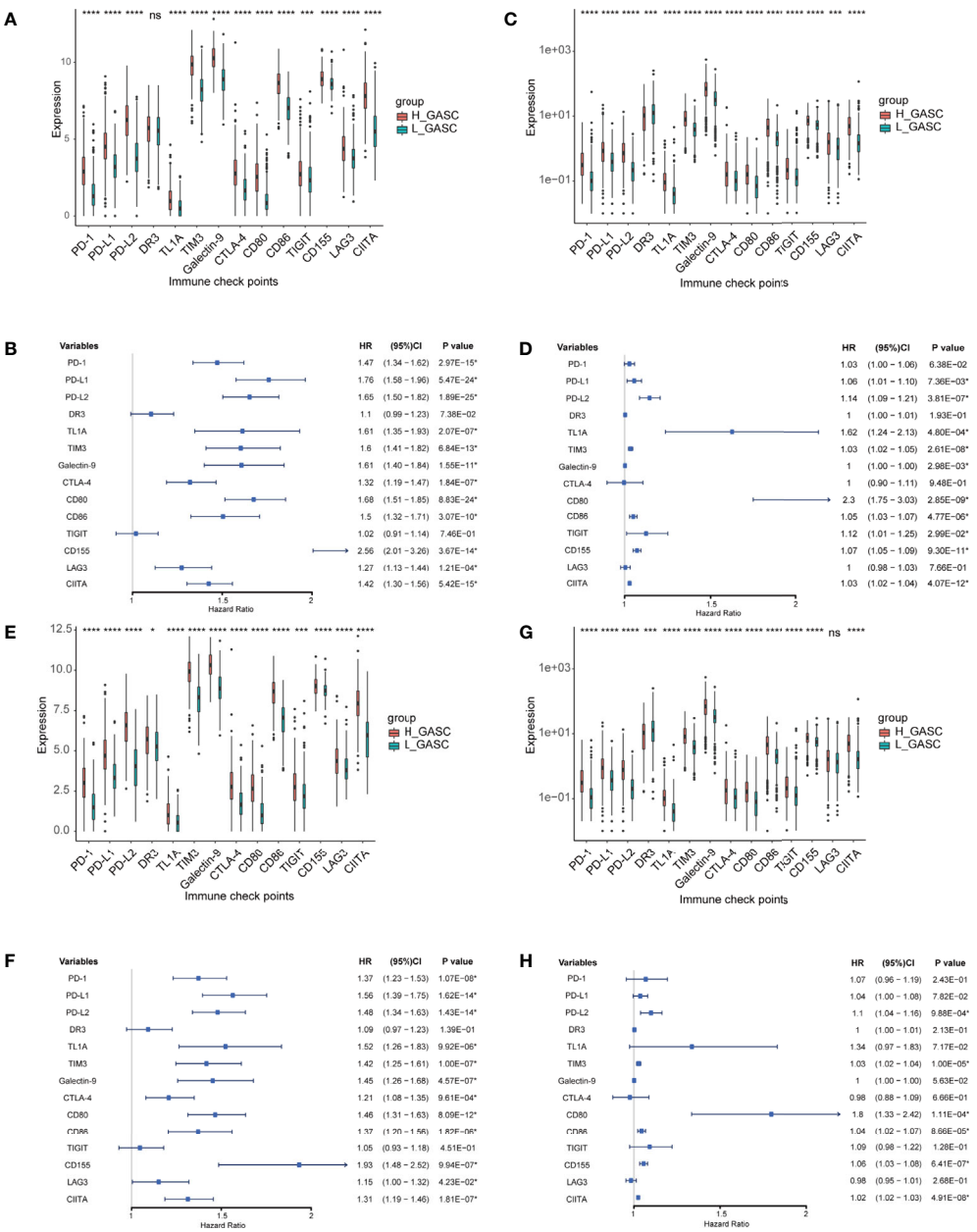

FIGURE 10 | Associations between GASCs and expression of ICPs. **(A, C, E, G)** Bar charts illustrating the differences of ICP' expressions between high- and low-GASC groups in all glioma population (**A** for TCGA and **C** for CGGA) and high-grade glioma population (**E** for TCGA and **G** for CGGA). **(B, D, F, H)** Forest plots of univariate Cox regression analysis of ICP' expressions in all glioma population (**B** for TCGA and **D** for CGGA) and high-grade glioma population (**F** for TCGA and **H** for CGGA). ns: $p > 0.05$, *$p \leq 0.05$, ***$p \leq 0.001$, ****$p \leq 0.0001$

suggested that the high-GASC group may have a more optimal immunotherapy response, the results from the TIDE prediction were puzzling because they showed a contrary tendency (**Figure S9**). These contradictory results reflect the inner complexity of glioma, and in response to this, further high-quality studies of immunotherapy in glioma are required.

McDonald et al. reported that deletion of DR3 (Tumor Necrosis Factor Receptor Superfamily Members 25, TNFRSF25) was found in oligodendroglioma (29). The results from Qian et al.'s work suggested that suppression of CIITA (class II transactivator) downregulates the expression of MHC class II molecules in glioma (30). In the current study, we discovered

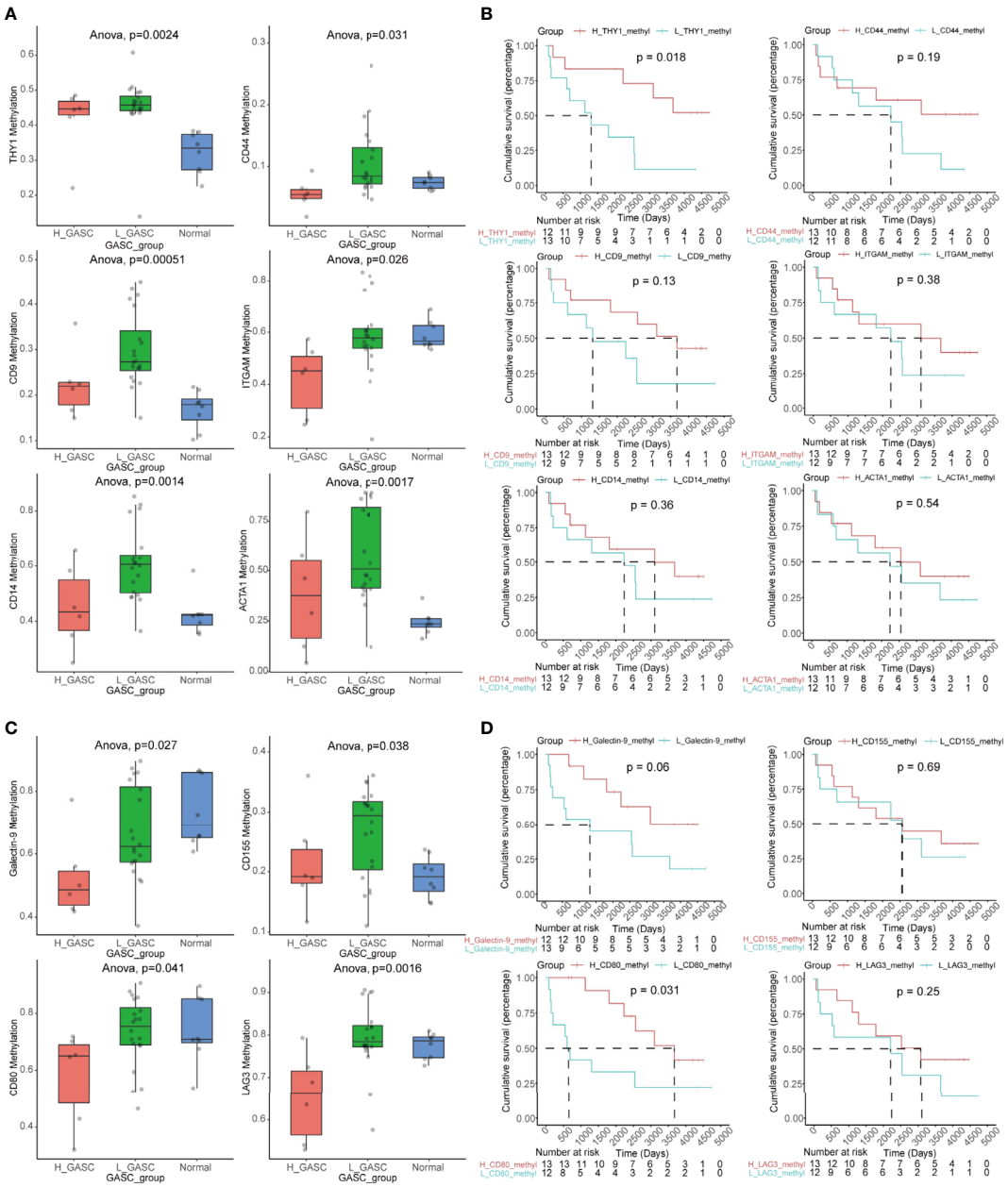

FIGURE 11 | Methylation analysis of GASC markers and ICPs. **(A)** Box plots illustrating the differences in THY1, CD9, CD14, CD44, ITGAM and ACTA1 methylation levels across high-GASC, low-GASC and normal groups. **(B)** Kaplan-Meier overall survival (OS) curves for samples in high- and low-methylation groups of THY1, CD9, CD14, CD44, ITGAM and ACTA1. **(C)** Box plots illustrating the differences in Galectin-9, CD80, CD155 and LAG3 methylation levels across high-GASC, low-GASC and normal groups. **(D)** Kaplan-Meier OS curves for samples in high- and low-methylation groups of Galectin-9, CD80, CD155 and LAG3.

that the CNVs of DR3 ($P < 0.001$) and CIITA ($p = 0.015$) were significantly higher in the high-GASC group (**Figure S6E**). The glioma patients with amplified/deleted DR3 or amplified CIITA had worse OS compared with wild-type glioma patients (**Figures S6F, G**). These results indicate that the CNVs of DR3 and CIITA may be potential prognostic indicators for glioma, and further studies are expected to verify their efficiency.

THY1 (CD90) is a surrogate marker for a variety of stem cells, including glioblastoma stem cells (GSC) (31) and GASC (7). Svensson et al. detected $CD90^-$ and $CD90^+$ GASC subpopulations by cell sorting and discovered that the $CD90^-$ subpopulation exhibited greater tumor vascularization and immunosuppression activity than the $CD90^+$ subpopulation (32). Zhang et al. further investigated these two subpopulations. They found that $CD90^{high}$

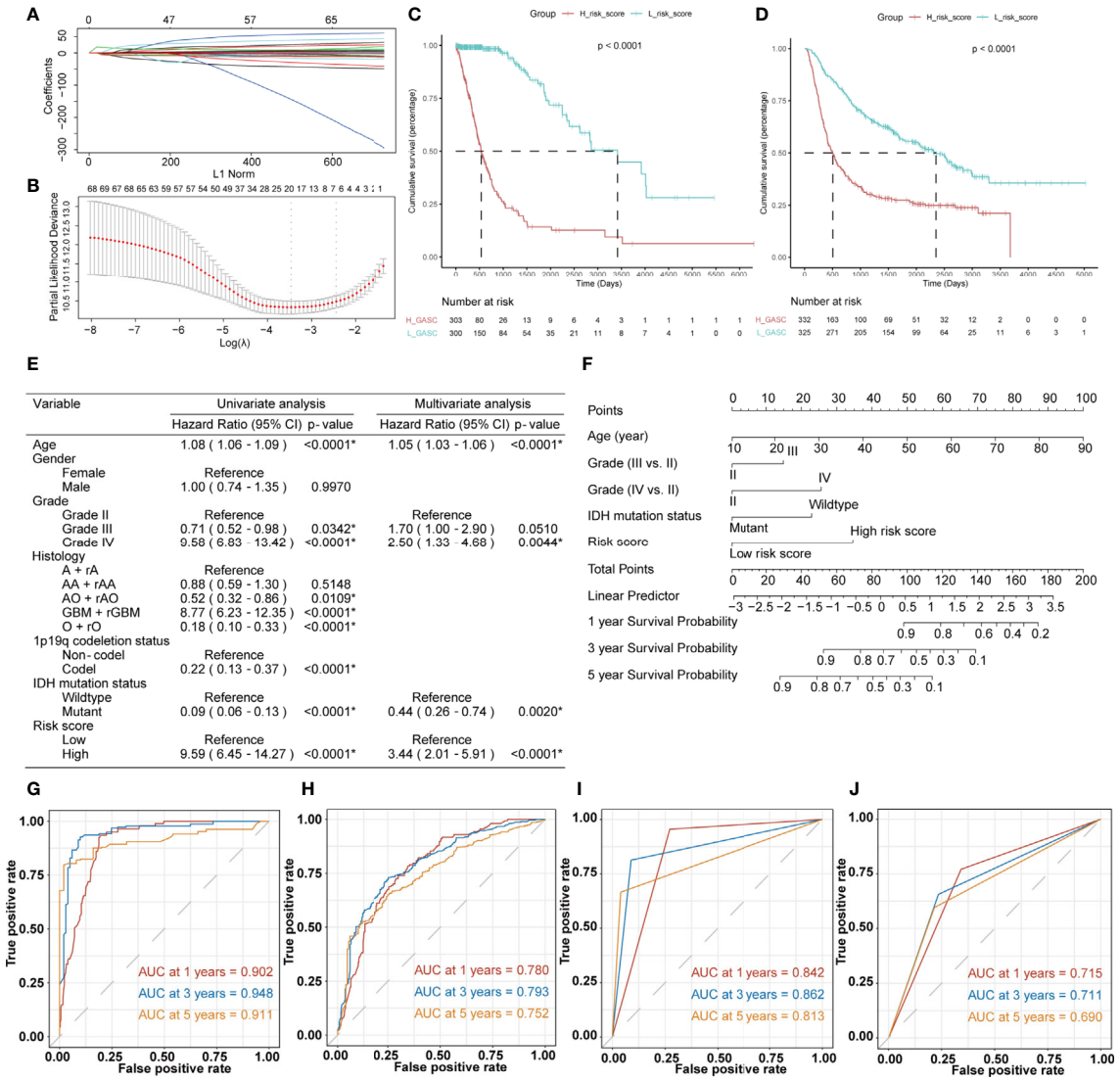

Variable	Univariate analysis		Multivariate analysis	
	Hazard Ratio (95% CI)	p- value	Hazard Ratio (95% CI)	p- value
Age	1.08 (1.06 - 1.09)	<0.0001*	1.05 (1.03 - 1.06)	<0.0001*
Gender				
Female	Reference			
Male	1.00 (0.74 - 1.35)	0.9970		
Grade				
Grade II	Reference		Reference	
Grade III	0.71 (0.52 - 0.98)	0.0342*	1.70 (1.00 - 2.90)	0.0510
Grade IV	9.58 (6.83 - 13.42)	<0.0001*	2.50 (1.33 - 4.68)	0.0044*
Histology				
A + rA	Reference			
AA + rAA	0.88 (0.59 - 1.30)	0.5148		
AO + rAO	0.52 (0.32 - 0.86)	0.0109*		
GBM + rGBM	8.77 (6.23 - 12.35)	<0.0001*		
O + rO	0.18 (0.10 - 0.33)	<0.0001*		
1p19q codeletion status				
Non- codel	Reference			
Codel	0.22 (0.13 - 0.37)	<0.0001*		
IDH mutation status				
Wildtype	Reference		Reference	
Mutant	0.09 (0.06 - 0.13)	<0.0001*	0.44 (0.26 - 0.74)	0.0020*
Risk score				
Low	Reference		Reference	
High	9.59 (6.45 - 14.27)	<0.0001*	3.44 (2.01 - 5.91)	<0.0001*

FIGURE 12 | Construction of the risk score system and establishment and validation of the nomogram survival model. **(A, B)** LASSO Cox regression analysis of training dataset. **(C, D)** Kaplan-Meier overall survival (OS) curves for samples in high- and low-risk score groups (**C** for training dataset and **D** for validation dataset). **(E)** Uni- and multi-variate Cox regression analysis for prognostic model. *Statistical significance. **(F)** The nomogram for predicting 1-, 3-, or 5-year OS. **(G, H)** Time-dependent ROC curves of the nomogram prediction on the 1-, 3-, and 5-year survival rates (**G** for training dataset and **H** for validation dataset). **(I, J)** Time-dependent ROC curves of the IDH mutation status prediction on the 1-, 3-, and 5-year survival rates (**I** for training dataset and **J** for validation dataset).

GASCs drove glioma progression *via* increasing proliferation, migration, and adhesion. However, $CD90^{low}$ GASCs contributed to glioma progression through the stimulation of vascular formation *via* vascular endothelial cells (25). In the current work, we discovered that the methylation levels were different among high-GASC, low-GASC, and normal groups (**Figure 11A**), and the high THY1 methylation group had better OS compared with the low THY1 methylation group (p = 0.018; **Figure 11B**). These results suggested for the first time that the methylation of THY1 could be a potential prognostic indicator of glioma as well as a treatment target.

To create a comprehensive risk score, we included the following features, produced from mRNA sequencing data, in the filtering process: GASC score, stemness score, mesenchymal-EMT score, tumorigenic cytokine score, angiogenic activity score, stromal cell scores, and immune cell scores. The results showed that the risk score could be used to differentiate patients with high or low risk (**Figures 12C, D**), and the risk score was an independent prognostic indicator for glioma (**Figure 12E**). The validation results from the CGGA validation dataset verified the robustness of our nomogram model (**Figure 12H**). We also compared the efficiency of the nomogram model with a traditional prognostic indicator, IDH mutation status. The AUCs for the nomogram model were better than those for IDH mutation status in the training dataset (**Figures 12G, I**)

and the validation dataset (**Figures 12H, J**). To verify the credibility of this nomogram model, further high-quality clinical studies are required.

There are limitations in our study. First, because of a lack of public mRNA resources with proportions of GASCs, stromal cells, and immune cells, we selected the ssGEAS algorithm to compute these data, because it has been widely used with proven reliability. Second, because this is a retrospective study, the efficiency of our risk score and nomogram model needs to be verified in further high-quality prospective cohorts. In addition, our predicted results for immunotherapy response were contradictory with the expression level of ICPs. Glioma, particularly HGG, is characterized by remarkably high tumor heterogeneity and an "immune-cold" phenotype, denoting an immunosuppressive microenvironment. The GASC is an important cell type in the microenvironment and might influence immunotherapy responses. Based on previous research, the overexpression of some ICPs on malignant cells may increase the anti-tumor immune responses (33). Nevertheless, although our data suggested that higher ICP expression occurs in the high-GASC group, TIME prediction revealed worse immunotherapy responses in the high-GASC group. This contradiction may result from the inner complexity of the glioma microenvironment. Further prospective clinical trials to test immunotherapy for glioma with the GASC proportion data are required to produce a reliable conclusion regarding the relationship between GASCs and immunotherapy responses.

CONCLUSION

We found potential mechanisms of GASCs in the glioma microenvironment, particularly HGG, and we also discovered that GASCs are positively correlated with the level of M2 macrophages and ICPs. The methylation of THY1 decreased in the high-GASC group, which could be a prognostic indicator and treatment target for glioma. We also developed a prognostic nomogram for glioma. Further studies to verify these findings and the performance of our model with large prospective cohorts are warranted.

DATA AVAILABILITY STATEMENT

Publicly available datasets were analyzed in this study. This data can be found here: TCGA database (https://portal.gdc.cancer.gov/) and CGGA database (www.cgga.org.cn/).

AUTHOR CONTRIBUTIONS

CM conceived and designed the investigation. XC and FY analyzed the data and drafted the manuscript. JZ, JY, CT, and ZC conducted statistical analyses. All authors contributed to the article and approved the submitted version.

ACKNOWLEDGMENTS

Special thanks to Sheng Zhao for his support.

SUPPLEMENTARY MATERIAL

The Supplementary Material for this article can be found online at: https://www.frontiersin.org/articles/10.3389/fonc.2021.672928/full#supplementary-material

Supplementary Figure 1 | Differential analysis of expressed genes. **(A, B)** Heatmap of DEGs in all glioma population (**A** for TCGA and **B** for CGGA). **(C, D)** Heatmap of DEGs in high-grade glioma population (**C** for TCGA and **D** for CGGA).

Supplementary Figure 2 | Functional annotation of downregulated DEGs between the high- and low-GASC groups. **(A, B)** GO analysis **(A)** and KEGG pathway analysis (**B**) of down-regulated DEGs in all glioma population from TCGA data. **(C, D)** GO analysis **(C)** and KEGG pathway analysis **(D)** of down-regulated DEGs in all glioma population from CGGA data. **(E, F)** GO analysis (**E**) and KEGG pathway analysis **(F)** of down-regulated DEGs in high-grade glioma population from TCGA data. **(G, H)** GO analysis **(G)** and KEGG pathway analysis **(H)** of down-regulated DEGs in high-grade glioma population from CGGA data.

Supplementary Figure 3 | Associations between GASCs and stromal cells in the high-grade glioma population. **(A, D)** Bar chart illustrating the differences in xCELL scores between high- and low-GASC groups (**A** for TCGA and **D** for CGGA). ns: $p > 0.05$, $^{*}p \le 0.05$, $^{**}p \le 0.01$, $^{***}p \le 0.001$, $^{****}p \le 0.0001$. **(B,E)** Forest plot of univariate Cox regression analysis of stromal cells (**B** for TCGA and **E** for CGGA). **(C,F)** Correlogram of GASC score and stromal cells intercorrelation (**C** for TCGA and **F** for CGGA).

Supplementary Figure 4 | Comparison of genomic alterations between the high- and low-GASC groups in the TCGA dataset. **(A, B)** Differential copy number variation analysis between high- **(A)** and low- **(B)** GASC groups. **(C, D)** Differential somatic mutation analysis between high- **(C)** and low- **(D)** GASC groups.

Supplementary Figure 5 | Comparison of genomic alterations of GASC markers between the high- and low-GASC groups in the TCGA dataset. **(A, B)** Differential copy number variation analysis between high- **(A)** and low- **(B)** GASC groups. **(C, D)** Differential somatic mutation analysis between high- **(C)** and low- **(D)** GASC groups. **(E)** Correlations between GASC groups and somatic mutation of GASC markers.

Supplementary Figure 6 | Comparison of genomic alterations of ICPs between the high- and low-GASC groups in the TCGA dataset. **(A, B)** Differential copy number variation analysis between high- **(A)** and low- (**B**) GASC groups. **(C, D)** Differential somatic mutation analysis between high- **(C)** and low- (**D**) GASC groups. **(E)** Correlations between GASC groups and somatic mutation of ICPs. **(F,G)** Kaplan-Meier overall survival (OS) curves for samples of amplified, deleted and wildtype DR3 groups **(F)** and CIITA groups **(G)**.

Supplementary Figure 7 | Methylation analysis of GASC markers. **(A)** Box plots illustrating the differences in CD34, ALCAM, CSPG4, ENG, GFAP, S100A4, NT5E, PDGFRB, PECAM1 and PTPRC methylation levels across high-GASC, low-GASC and normal groups.

Supplementary Figure 8 | Methylation analysis of immune checkpoints. **(A)** Box plots illustrating the differences in PD-1, PD-L1, PD-L2, DR3, TL1A, CTLA-4, CD86, TIM3 and CIITA methylation levels across high-GASC, low-GASC and normal groups.

Supplementary Figure 9 | Predicted potential immunotherapy responses between the high- and low-GASC groups. **(A–D)** Predicted potential

immunotherapy responses of samples from all glioma population (**A** for TCGA and **B** for CGGA) and high-grade glioma population (**C** for TCGA and **D** for CGGA). **(E)** Correlation of GASC and Predicted immunotherapy responses. **(F–I)** Bar chart illustrating the differences in immune cell scores between responder and no responder groups in all glioma population (**F** for TCGA and **G** for CGGA) and high-grade glioma population (**H** for TCGA and **I** for CGGA).

REFERENCES

1. Louis DN, Ohgaki H, Wiestler OD, Cavenee WK, Burger PC, Jouvet A, et al. The 2007 WHO Classification of Tumours of the Central Nervous System. *Acta Neuropathol* (2007) 114:97–109. doi: 10.1007/s00401-007-0243-4
2. Liu S, Zhao Q, Shi W, Zheng Z, Liu Z, Meng L, et al. Advances in Radiotherapy and Comprehensive Treatment of High-Grade Glioma: Immunotherapy and Tumor-Treating Fields. *J Cancer* (2021) 12:1094–104. doi: 10.7150/jca.51107
3. Hegde PS, Chen DS. Top 10 Challenges in Cancer Immunotherapy. *Immunity* (2020) 52:17–35. doi: 10.1016/j.immuni.2019.12.011
4. Qi Y, Liu B, Sun Q, Xiong X, Chen Q. Immune Checkpoint Targeted Therapy in Glioma: Status and Hopes. *Front Immunol* (2020) 11:578877. doi: 10.3389/fimmu.2020.578877
5. Luo H, Tao C, Wang P, Li J, Huang K, Zhu X. Development of a Prognostic Index Based on Immunogenomic Landscape Analysis in Glioma. *Immun Inflammation Dis* (2021) 1–13. doi: 10.1002/iid3.407
6. Sonabend AM, Stupp R, Lee-Chang C, Okada H. Glioma Immunoediting, a Driver of Tumor Evolution, and the Next Battle for Immunotherapy. *Oncotarget* (2021) 12:8–9. doi: 10.18632/oncotarget.27865
7. Clavreul A, Menei P. Mesenchymal Stromal-Like Cells in the Glioma Microenvironment: What are These Cells? *Cancers (Basel)* (2020) 12 (9):2628. doi: 10.3390/cancers12092628
8. Ma Q, Long W, Xing C, Chu J, Luo M, Wang HY, et al. Cancer Stem Cells and Immunosuppressive Microenvironment in Glioma. *Front Immunol* (2018) 9:2924. doi: 10.3389/fimmu.2018.02924
9. Iser IC, Pereira MB, Lenz G, Wink MR. The Epithelial-to-Mesenchymal Transition-Like Process in Glioblastoma: An Updated Systematic Review and In Silico Investigation. *Med Res Rev* (2017) 37:271–313. doi: 10.1002/med.21408
10. Sheu BC, Chang WC, Cheng CY, Lin HH, Chang DY, Huang SC. Cytokine Regulation Networks in the Cancer Microenvironment. *Front Biosci* (2008) 13:6255–68. doi: 10.2741/3152
11. Chang HY, Sneddon JB, Alizadeh AA, Sood R, West RB, Montgomery K, et al. Gene Expression Signature of Fibroblast Serum Response Predicts Human Cancer Progression: Similarities Between Tumors and Wounds. *PloS Biol* (2004) 2:E7. doi: 10.1371/journal.pbio.0020007
12. Yu G, Wang LG, Han Y, He QY. clusterProfiler: An R Package for Comparing Biological Themes Among Gene Clusters. *OMICS* (2012) 16:284–7. doi: 10.1089/omi.2011.0118
13. Mayakonda A, Lin DC, Assenov Y, Plass C, Koeffler HP. Maftools: Efficient and Comprehensive Analysis of Somatic Variants in Cancer. *Genome Res* (2018) 28:1747–56. doi: 10.1101/gr.239244.118
14. Fu J, Li K, Zhang W, Wan C, Zhang J, Jiang P, et al. Large-Scale Public Data Reuse to Model Immunotherapy Response and Resistance. *Genome Med* (2020) 12:21. doi: 10.1186/s13073-020-0721-z
15. Lim EJ, Suh Y, Yoo KC, Lee JH, Kim IG, Kim MJ, et al. Tumor-Associated Mesenchymal Stem-Like Cells Provide Extracellular Signaling Cue for Invasiveness of Glioblastoma Cells. *Oncotarget* (2017) 8:1438–48. doi: 10.18632/oncotarget.13638
16. He Z, You C, Zhao D. Long non-Coding RNA Uca1/miR-182/PFKFB2 Axis Modulates Glioblastoma-Associated Stromal Cells-Mediated Glycolysis and Invasion of Glioma Cells. *Biochem Biophys Res Commun* (2018) 500:569–76. doi: 10.1016/j.bbrc.2018.04.091
17. Lim E-J, Kim S, Oh Y, Suh Y, Kaushik N, Lee J-H, et al. Corrigendum to: Crosstalk Between GBM Cells and Mesenchymal Stemlike Cells Promotes the Invasiveness of GBM Through the C5a/p38/ZEB1 Axis. *Neuro-Oncology* (2020) 22:1229. doi: 10.1093/neuonc/noaa125
18. Lim EJ, Suh Y, Kim S, Kang SG, Lee SJ. Force-Mediated Proinvasive Matrix Remodeling Driven by Tumor-Associated Mesenchymal Stem-Like Cells in Glioblastoma. *BMB Rep* (2018) 51:182–7. doi: 10.5483/bmbrep.2018.51.4.185
19. Behnan J, Isakson P, Joel M, Cilio C, Langmoen IA, Vik-Mo EO, et al. Recruited Brain Tumor-Derived Mesenchymal Stem Cells Contribute to Brain Tumor Progression. *Stem Cells* (2014) 32:1110–23. doi: 10.1002/stem.1614
20. Hossain A, Gumin J, Gao F, Figueroa J, Shinojima N, Takezaki T, et al. Mesenchymal Stem Cells Isolated From Human Gliomas Increase Proliferation and Maintain Stemness of Glioma Stem Cells Through the IL-6/gp130/STAT3 Pathway. *Stem Cells* (2015) 33:2400–15. doi: 10.1002/stem.2053
21. Figueroa J, Phillips LM, Shahar T, Hossain A, Gumin J, Kim H, et al. Exosomes From Glioma-Associated Mesenchymal Stem Cells Increase the Tumorigenicity of Glioma Stem-Like Cells Via Transfer of Mir-1587. *Cancer Res* (2017) 77:5808–19. doi: 10.1158/0008-5472.CAN-16-2524
22. Kim SM, Kang SG, Park NR, Mok HS, Huh YM, Lee SJ, et al. Presence of Glioma Stroma Mesenchymal Stem Cells in a Murine Orthotopic Glioma Model. *Childs Nerv Syst* (2011) 27:911–22. doi: 10.1007/s00381-011-1396-y
23. Trylcova J, Busek P, Smetana K Jr., Balaziova E, Dvorankova B, Mifkova A, et al. Effect of Cancer-Associated Fibroblasts on the Migration of Glioma Cells In Vitro. *Tumour Biol* (2015) 36:5873–9. doi: 10.1007/s13277-015-3259-8
24. Clavreul A, Guette C, Faguer R, Tétaud C, Boissard A, Lemaire L, et al. Glioblastoma-Associated Stromal Cells (Gascs) From Histologically Normal Surgical Margins Have a Myofibroblast Phenotype and Angiogenic Properties. *J Pathol* (2014) 233:74–88. doi: 10.1002/path.4332
25. Zhang Q, Yi D-Y, Xue B-Z, Wen W-W, Lu Y-P, Abdelmaksou A, et al. CD90 Determined Two Subpopulations of Glioma-Associated Mesenchymal Stem Cells With Different Roles in Tumour Progression. *Cell Death Disease* (2018) 9:1101. doi: 10.1038/s41419-018-1140-6
26. Akins EA, Aghi MK, Kumar S. Incorporating Tumor-Associated Macrophages Into Engineered Models of Glioma. *iScience* (2020) 23:101770–. doi: 10.1016/j.isci.2020.101770
27. Roesch S, Rapp C, Dettling S, Herold-Mende C. When Immune Cells Turn Bad-Tumor-Associated Microglia/Macrophages in Glioma. *Int J Mol Sci* (2018) 19:436. doi: 10.3390/ijms19020436
28. Murray PJ. Macrophage Polarization. *Annu Rev Physiol* (2017) 79:541–66. doi: 10.1146/annurev-physiol-022516-034339
29. McDonald JM, Dunmire V, Taylor E, Sawaya R, Bruner J, Fuller GN, et al. Attenuated Expression of DFFB is a Hallmark of Oligodendrogliomas With 1p-Allelic Loss. *Mol Cancer* (2005) 4:35. doi: 10.1186/1476-4598-4-35
30. Qian J, Luo F, Yang J, Liu J, Liu R, Wang L, et al. Tlr2 Promotes Glioma Immune Evasion by Downregulating Mhc Class Ii Molecules in Microglia. *Cancer Immunol Res* (2018) 6:1220–33. doi: 10.1158/2326-6066.Cir-18-0020
31. Avril T, Etcheverry A, Pineau R, Obacz J, Jegou G, Jouan F, et al. Cd90 Expression Controls Migration and Predicts Dasatinib Response in Glioblastoma. *Clin Cancer Res* (2017) 23:7360–74. doi: 10.1158/1078-0432.Ccr-17-1549
32. Svensson A, Ramos-Moreno T, Eberstål S, Scheding S, Bengzon J. Identification of Two Distinct Mesenchymal Stromal Cell Populations in Human Malignant Glioma. *J Neurooncol* (2017) 131:245–54. doi: 10.1007/s11060-016-2302-y
33. Yearley JH, Gibson C, Yu N, Moon C, Murphy E, Juco J, et al. Pd-L2 Expression in Human Tumors: Relevance to Anti-PD-1 Therapy in Cancer. *Clin Cancer Res* (2017) 23:3158–67. doi: 10.1158/1078-0432.Ccr-16-1761

Conflict of Interest: The authors declare that the research was conducted in the absence of any commercial or financial relationships that could be construed as a potential conflict of interest.

Copyright © 2021 Cai, Yuan, Zhu, Yang, Tang, Cong and Ma. This is an open-access article distributed under the terms of the Creative Commons Attribution License (CC BY). The use, distribution or reproduction in other forums is permitted, provided the original author(s) and the copyright owner(s) are credited and that the original publication in this journal is cited, in accordance with accepted academic practice. No use, distribution or reproduction is permitted which does not comply with these terms.

frontiers in Oncology

ORIGINAL RESEARCH
published: 17 May 2021
doi: 10.3389/fonc.2021.671144

miR-1258 Attenuates Tumorigenesis Through Targeting E2F1 to Inhibit *PCNA* and *MMP2* Transcription in Glioblastoma

Hongkun Qin[1†], Yanping Gui[1†], Rong Ma[2], Heng Zhang[1], Yabing Guo[1], Yuting Ye[1], Jia Li[1], Li Zhao[1] and Yajing Wang[3*]*

[1] Pathology and Patient Derived Xenograft Efficacy Evaluation Center, School of Basic Medicine and Clinical Pharmacy, China Pharmaceutical University, Nanjing, China, [2] Department of Anesthesiology, The First Affiliated Hospital, Nanjing Medical University, Nanjing, China, [3] Department of Physiology, School of Basic Medicine and Clinical Pharmacy, China Pharmaceutical University, Nanjing, China

OPEN ACCESS

Edited by:
Pim French,
Erasmus University Medical Center, Netherlands

Reviewed by:
Pietro Luigi Poliani, University of Brescia, Italy
Alessia Pellerino, University Hospital of the City of Health and Science of Turin, Italy

***Correspondence:**
Yajing Wang
cpuwyj@cpu.edu.cn
Li Zhao
zhaoli@cpu.edu.cn

[†]These authors have contributed equally to this work and share first authorship

Specialty section:
This article was submitted to Neuro-Oncology and Neurosurgical Oncology, a section of the journal Frontiers in Oncology

Received: 23 February 2021
Accepted: 06 April 2021
Published: 17 May 2021

Citation:
Qin H, Gui Y, Ma R, Zhang H, Guo Y, Ye Y, Li J, Zhao L and Wang Y (2021) miR-1258 Attenuates Tumorigenesis Through Targeting E2F1 to Inhibit PCNA and MMP2 Transcription in Glioblastoma. Front. Oncol. 11:671144. doi: 10.3389/fonc.2021.671144

MicroRNAs are a group of endogenous small non-coding RNAs commonly dysregulated in tumorigenesis, including glioblastoma (GBM), the most malignant brain tumor with rapid proliferation, diffuse invasion, and therapeutic resistance. Accumulating evidence has manifested that miR-1258 exerts an inhibitory role in many human cancers. However, the expression pattern of miR-1258 and its potential function in GBM tumorigenesis remain unclear. In this study, we reported that miR-1258 expression decreased with the ascending pathological grade of glioma, which indicated an unfavorable prognosis of patients. Functional assays revealed an inhibitory effect of miR-1258 on malignant proliferation, therapeutic resistance, migration, and invasion of GBM *in vitro*. Moreover, xenograft models also suggested a repression effect of miR-1258 on gliomagenesis. Mechanistically, miR-1258 directly targeted E2F1 in 3'-untranslated regions and attenuated E2F1-mediated downstream gene *PCNA* and *MMP2* transcriptions. Furthermore, restoration of E2F1 expression in GBM cells effectively rescued the tumor-suppressive effect of miR-1258. Our studies illustrated that miR-1258 functioned as a tumor suppressor in GBM by directly targeting E2F1, subsequently inhibiting *PCNA* and *MMP2* transcriptions, which contributed to new potential targets for GBM therapy and other E2F1-driven cancers.

Keywords: miR-1258, glioblastoma, E2F1, temozolomide, transcriptional regulation, tumorigenesis

Abbreviations: miRNA, microRNA; GBM, glioblastoma; 3'-UTR, 3'-untranslated regions; NHA, normal human astrocytes; DMEM, Dulbecco's modified Eagle's medium; FBS, fetal bovine serum; LGG, low-grade glioma; NBT, normal brain tissue; CGGA, The Chinese Glioma Genome Atlas; TCGA, The Cancer Genome Atlas; miR-1258, miR-1258 mimic; NC, negative control; EV, empty vector; PCR, polymerase chain reaction; qRT-PCR, quantitative real-time polymerase chain reaction; Wt, wild-type; Mut, mutant; ChIP, chromatin immunoprecipitation; TMZ, temozolomide; BCNU, carmustine.

INTRODUCTION

Glioblastoma (GBM) is the most common and lethal form of glioma with high aggressiveness and low survival rate. Currently, the treatment of GBM typically consists of surgical resection, postsurgical radiotherapy, and chemotherapy. Despite those advanced therapeutic strategies, the median survival time of GBM patients is only 12–16 months, and the 5-year survival rate is less than 5% (1). Therefore, there is an urgent need to understand the molecular mechanisms and pathogenesis underlying GBM progression, which is essential to improve current therapeutic strategies for GBM.

MicroRNAs (miRNAs) are endogenous small non-coding RNAs with 20~24 nucleotides, regulating various biological processes, including cell proliferation, apoptosis, and invasion. miRNAs bind to the complementary sites in 3'-untranslated regions (3'-UTRs) of the target mRNA sequences to inhibit their translations (2). Emerging evidence has revealed that miRNAs' aberrant expression is associated with the carcinogenesis and progression of GBM (3). In recent years, some attention has been paid to the roles of miR-1258 in human cancers. miR-1258 exerts an inhibitory role in hepatocellular carcinoma metastasis *via* targeting Smad2/3 (4). miR-1258 was reported to inhibit osteosarcoma cell proliferation by targeting AKT3 (5). Besides, miR-1258 directly targets E2F8 to regulate cell cycles and inhibit cell proliferation in colorectal cancer (6). However, its clinical relevance and molecular mechanisms in GBM are unknown.

In this study, we identified that miR-1258 expression decreased obviously in glioma patient tissue samples, comparing with normal brain tissue. Its aberrant low expression negatively correlated with the grade of glioma and indicated an unfavorable prognosis of GBM patients. Inversely, the upregulation of miR-1258 inhibited gliomagenesis *in vitro* and *in vivo*. Mechanistically, miR-1258 played a suppressive role in GBM cells by directly targeting *E2F1* mRNA 3'-UTR sequence to inhibit the E2F1-mediated downstream transcriptions of *PCNA* and *MMP2*. Our study suggested that miR-1258 might represent a promising therapeutic target in GBM.

MATERIALS AND METHODS

Cell Lines and Primary GBM Cells Culture

Human GBM U87, U251, A172, normal human astrocytes (NHA), and 293T cell lines were obtained from the Cell Bank of the Chinese Academy of Sciences (Shanghai, China). Cell lines were authenticated using short tandem repeat profiling. The GBM cell lines and 293T cells were cultured in Dulbecco's modified Eagle's medium (DMEM; Gibco, USA) with 10% fetal bovine serum (FBS). NHA cells were cultured in DMEM/F-12 medium (Gibco, USA) with L-glutamine and 5% FBS. Patient-derived primary GBM cells GBM666 were freshly isolated from a surgical-resected GBM specimen. Briefly, tissues mechanically minced in prechilled DMEM/F-12 medium and digested with 2 U/mL of Dispase II (Thermofisher, USA), 0.5 mg/mL of Collagenase IV (Sigma, USA), and 10 U/mL of DNase I (Yeasen, Shanghai, China) at 37°C for 60 min. Ammonium–chloride–potassium lysing buffer was used to lyse red blood cells. After being digested, the cells were washed and passed through a 100 μm cell strainer. Finally, cells were cultured in DMEM/F-12 medium with L-glutamine, 20 ng/mL of basic fibroblast growth factor (bFGF; Thermofisher, USA), 20 ng/mL of Epidermal growth factor (EGF; Thermofisher, USA), and 15% FBS. All cells were cultured at 37°C in a humidified atmosphere with 5% CO_2.

Patients and Specimens

Five low-grade glioma (LGG), 28 GBM, and 5 normal brain tissue (NBT) samples between 2016 and 2020 were obtained from the Department of Neurosurgery, First Affiliated Hospital of Nanjing Medical University. Written informed consent for using the samples for this study was obtained from the patients or their family members. This research was approved by the Ethics Committee of China Pharmaceutical University.

Public Datasets Collection

Gliomas with microarray miRNA expression data were downloaded from the Chinese Glioma Genome Atlas (CGGA) microarray database. Glioma gene expression data were downloaded from The Cancer Genome Atlas (TCGA) microarray databases. Data for miRNA-target interaction prediction were obtained from TargetScan, miRTP, miRDB, miRmap, and RNA22 databases. JASPAR and PROMO databases were used to analyze the possible promoter region and identify putative transcription factor binding sites. Data for immunohistochemical analysis were downloaded from the Human Protein Atlas database.

Cell Transfection

miR-1258 mimic (miR-1258) and human miRNA negative control (miR-NC) were purchased from GenePharma (Shanghai, China). The E2F1 overexpression vector pEnter-E2F1 (E2F1) and pEnter empty vector (EV) were purchased from Vigenebio (Shandong, China). Cells were transfected with miRNAs or vectors using Lipofectamine 2000 (Invitrogen, USA) according to the manufacturer's protocols.

For establishing stable miR-1258 expressing U251 cell line, the full-length coding region and miRNA flanking sequence of miR-1258 were cloned from human genomic DNA by PCR. The PCR product was transferred into the pLVX-Puro vector and packaged in 293T cells. U251 cells were transfected with the miR-NC and miR-1258 lentiviruses, and stable cell lines were selected using puromycin at 2.5 μg/mL for 7 days.

Cell Proliferation Assays

Cell proliferation assays were performed using the CCK-8 assays (Dojindo, Japan). After transfection, cells were plated in 96-well plates at a density of 2×10^3 cells per well. For drug response screening assay, transfected GBM cells were treated with different concentrations of temozolomide (TMZ, TCI, Japan) or carmustine (BCNU, Aladdin, China) for 48 h. At the indicated time points, the activity of cells was measured at OD 450 nm using SpectraMax 190 plate reader (Molecular Devices, USA).

Colony Formation Assays

After transfection, cells were seeded in a 6-well plate at a density of 2×10^3 cells per well and cultured for 7 days. The resulting colonies were washed three times with PBS and fixed with 4% formaldehyde for 15 min, finally stained with 0.5% crystal violet (Sigma, USA) for 20 min.

Flow Cytometry Analysis

For detecting cell apoptosis, a total of 1×10^5 transfected cells were seeded in a 6-well plate and treated with 500 μM TMZ for 48 h. Then pretreated cells were harvested, washed three times with prechilled PBS solution, and resuspended in a single cell suspension. The cell apoptosis analysis was performed with the Annexin V-FITC and PI Apoptosis Detection Kit (Miltenyi, Germany) according to the manufacturer's instructions. Flow cytometric analysis was performed using MACSQuant Analyzer 10 (Miltenyi, Germany) and analyzed by Flowjo (Tree Star, USA).

Morphological Analysis

Transfected cells were treated with 500 μM TMZ for 72 h. Then cells were viewed under an inverted microscope (Leica, Germany) at 200× magnification for morphological comparison.

Cell Migration and Invasion Experiments

For the wound healing scratch assays, a uniform wound was made by scratching with a 200 μL pipette tip when the transfected cells reached 90% confluence in 12-well plates. Cells were maintained in a serum-free culture medium after being washed three times with PBS. After 24 h, each well was photographed under an inverted microscope (Leica, Germany) at 100× magnification. The cells protruding from the border of the scratches were counted to calculate the wound recovery rate.

For the Transwell assays, Transwell inserts (Corning, USA) were pre-coated with 20 μg/μL of Matrigel (BD Biosciences, USA), then placed in a 24-well plate. Transfected cells were resuspended at a density of 3×10^4/ml in serum-free culture medium and transferred to the upper chambers. In parallel, culture medium containing 10% FBS was added to the lower chamber of each well. After incubation for 24 h, cells on the inner membrane of the upper chamber were removed with cotton swabs. Invading cells were fixed with 4% paraformaldehyde for 15 min and then stained with 0.5% crystal violet for 20 min. Three fields of invading cells in each well were captured randomly and counted under an inverted microscope (Leica, Germany) at 100× magnification.

Protein Preparation and Western Blot

Total proteins were prepared using prechilled RIPA buffer (Thermo Fisher, USA) with proteinase inhibitor cocktail (Thermo Fisher, USA). For separating nuclear and cytoplasmic proteins, cells were harvested and lysed in nuclear and cytoplasmic extraction reagents (Keygentec, China) according to the manufacturer's protocols. The proteins were subjected to western blot using antibodies against E2F1 (1:1000, Cell Signaling, USA), N-cadherin (1:1000, Proteintech, USA), MMP2 (1:1000, Proteintech, USA), MMP9 (1:1000, Proteintech, USA), Snail1 (1:1000, ABclonal, China), GAPDH (1:5000, Proteintech, USA), Lamin A/C (1:1000, Proteintech, USA). Relative expression levels were normalized to endogenous loading control using ImageJ software (National Institutes of Health, USA).

RNA Extraction and Polymerase Chain Reaction (PCR)

The total RNA of cells and clinical tissues was extracted using TRIzol (Invitrogen, USA) according to the manufacturer's instructions. One microgram of total RNA was used as a template for cDNA synthesis using a HiScript III 1st Strand cDNA Synthesis Kit (Vazyme, China). Quantitative real-time polymerase chain reaction (qRT-PCR) was performed on triplicate samples in a reaction mix of SYBR Green (Vazyme, China) with a QuantStudio 3 Real-Time PCR System (Applied Biosystems, USA). Quantification of the miR-1258 was performed with a stem-loop real-time PCR miRNA kit (Vazyme, China). The levels of mRNA were normalized to GAPDH. The levels of miR-1258 were normalized to U6 small nuclear RNA. The expressions of the indicated genes were normalized to the endogenous reference control by using the $2^{-\Delta\Delta Ct}$ method. Sequences of the primers used for qRT-PCR in this study are listed in **Supplementary Table S1**.

Immunofluorescence

For immunofluorescence staining, transfected cells were fixed with 4% formaldehyde, permeabilized with 0.3% Triton X-100, and then blocked with 3% BSA for 1 hour at room temperature. After the incubation, cells were probed with E2F1 primary antibody (1:400, Cell Signaling, USA). For γ-H2A.X immunofluorescence staining, transfected cells were treated with 500 μM TMZ for 4 h, followed by fixed with 4% formaldehyde, permeabilized with 0.3% Triton X-100, and then blocked with 3% BSA for 1 hour at room temperature. After the incubation, cells were probed with Phospho-Histone H2A.X (Ser139) primary antibody (1:400, Cell Signaling, USA). After overnight incubation at 4°C, the cells were washed three times with PBS and incubated with Alexa Fluor 488-labeled Goat Anti-Rabbit IgG H&L antibodies (1:500, Abcam, USA) for 1 h at room temperature. The nuclei were stained with DAPI (Keygentec, China) and visualized with a Zeiss LSM 800 laser scanning confocal microscope (ZEISS, Germany). The γ-H2A.X foci were determined using ImageJ software (National Institutes of Health, USA).

Dual-Luciferase Reporter Assays

Wild-type (Wt) or mutant (Mut) 3'-UTR segments of the *E2F1* gene were cloned into pmirGLO Dual-Luciferase miRNA Target Expression Vector (Promega, USA) (pmirGLO-E2F1). U251 and GBM666 cells were co-transfected with either Wt or Mut pmirGLO-E2F1 and miR-1258 or miR-NC overnight and incubated in fresh complete medium for an additional 36 h after transfection. Next, cells were harvested, and luciferase activity was measured using the Dual-Luciferase Reporter Assay Kit (Promega, USA) and normalized to Renilla luciferase activity.

Wt or Mut promoter sequences of *PCNA* and *MMP2* gene were cloned into pGL3-basic Luciferase Reporter Vector

(Promega, USA) (pGL3-PCNA and pGL3-MMP2). U251 and GBM666 cells were co-transfected with either Wt or Mut pGL3-PCNA or pGL3-MMP2 plasmid, and pEnter-E2F1 or empty pEnter vector, together with pRL-TK Vector (Promega, USA) overnight, and incubated in fresh complete medium for an additional 36 h after transfection. Next, cells were harvested, and luciferase activity was measured using the Dual-Luciferase Reporter Assay Kit (Promega, USA) and normalized to Renilla luciferase activity.

Immunohistochemistry

For immunohistochemical analysis, sections were deparaffinized and rehydrated through a descending alcohol series, followed by antigens retrieval, and endogenous peroxidase activity blocking. The sections were then incubated with primary antibodies against E2F1 (1:200, Cell Signaling, USA), PCNA (1:1000 Proteintech, USA), and MMP2 (1:400 Proteintech, USA) following by visualized with a two-step process and a DAB staining kit (ZSGB-BIO, China). Finally, slides were counterstained with hematoxylin, dehydrated, and mounted. The quantification of Immunohistochemistry staining was measured by positive-stained tumor cells. The proportion of positive-stained tumor cells was graded as follows: 1, 0%–25% positive tumor cells; 2, 25%–50% positive tumor cells; 3, 50%–75% positive tumor cells; and 4, 75% or greater positive tumor cells.

Chromatin Immunoprecipitation (ChIP)

ChIP assays were performed with a ChIP kit (Beyotime, China) according to the manufacturer's instructions. In brief, U251 and GBM666 cells were fixed, lysed, and sonicated. The cell lysates were clarified and precleared with Protein A/G agarose beads and salmon sperm DNA and incubated with the anti-E2F1 antibody (1:100, Cell Signaling, USA) or control rabbit IgG (1:100, Bioss, China). The immunocomplexes were sequentially washed with low-salt wash buffer, high salt wash buffer, TE buffer, and elution buffer. The eluted DNA–protein complexes were decrosslinked, purified with a DNA purification kit (Tiangen, China) according to the manufacturer's instructions, and then subjected to PCR analysis with 3% agarose gel electrophoresis. Primer sequences are shown in **Supplementary Table S2**.

Subcutaneous Xenograft Model

Six-week-old female athymic BALB/c nude mice were purchased from Cavans Laboratory Animals Ltd. (Changzhou, China). U251 cells stably expressing miR-1258 or miR-NC were subdivided into the miR-1258 group and miR-NC group. For establishing the subcutaneous GBM model, a total of 2×10^6 U251 cells were implanted bilaterally in the axillary, respectively, per mouse. After 7 days of subcutaneous implantation, tumor volumes were measured by the formula ($V = 0.5 \times \text{width}^2 \times \text{length}$, mm^3) every 2 days until the tumor volume reached 1200 mm^3. The mice were sacrificed, and subcutaneous xenografts were removed, photographed, embedded in paraffin, and sectioned for immunohistochemistry assays. All procedures were approved by the Committee on the Ethics of Animal Experiments of China Pharmaceutical University.

Statistical Analysis

Each experiment was repeated at least three times to ensure the reliability of the results. All data were represented by mean ± standard deviation. Significant differences between the groups were estimated by Student's t-test or one-way analysis of variance. The Kaplan-Meier curves were used to describe the survival, and the log-rank test was applied for assessing statistical significance between groups. The relationships between miR-1258 or E2F1 expression and the clinicopathological characteristics were analyzed by using the χ^2 test. Pearson's correlation analysis was used to assess correlations between two variables. A value of $p < 0.05$ was considered statistically significant. All statistical analyses were performed using GraphPad 8.0 (GraphPad Software, USA).

RESULTS

miR-1258 Expression Decreases With Ascending Pathological Grade of Glioma and Correlates With Poor Prognosis in GBM

To investigate the role of miR-1258 in the progression of GBM, we first analyzed clinical glioma data derived from the CGGA database. Kaplan-Meier's survival analysis revealed that patients with high miR-1258 expression had a much better overall survival rate than those with low miR-1258 expression levels in all glioma patients ($p = 0.0199$, n=171, **Figure 1A**). Moreover, the expression profiles in glioma tissues illustrated that miR-1258 expression was significantly lower in the IV grade glioma than that in the II grade and III grade gliomas ($p < 0.01$, **Figure 1B**). Besides, the analysis of correlations between miR-1258 expression level and clinicopathological characteristics revealed that low miR-1258 expression was notably associated with WHO grade ($p < 0.001$), histology ($p < 0.001$), and IDH status ($p = 0.008$) (**Supplementary Table S3**). qRT-PCR was carried out to evaluate the miR-1258 expressions in 5 LGG, 28 GBM, and 5 NBT clinical samples. miR-1258 levels in NBT were significantly higher than those in glioma specimens ($p < 0.001$). Its expression decreased with the ascending pathological grade of glioma ($p < 0.05$, **Figure 1C**). Furthermore, we found that miR-1258 expressions were downregulated in GBM cell lines and patient-derived GBM cells compared to NHAs by qRT-PCR, which is highly consistent with our above clinical sample analysis data ($p < 0.05$, **Figure 1D**). These results suggested that low expressions of miR-1258 proposed an unfavorable prognosis in glioma patients, and miR-1258 played an essential role in the progression of GBM.

Upregulation of miR-1258 Expression Attenuates the Malignant Biological Behavior of GBM Cells

Since miR-1258 played a vital role in the progression of GBM, we next investigated the effects of miR-1258 on GBM cell proliferation, therapeutic resistance, migration, and invasion. U251 and GBM666 cells were transfected with miR-NC or miR-1258, and transfection efficiency was determined by qRT-PCR. The results confirmed that miR-1258 expressions were significantly increased in the miR-1258 group after 48 h of transfection compared to that in the miR-NC

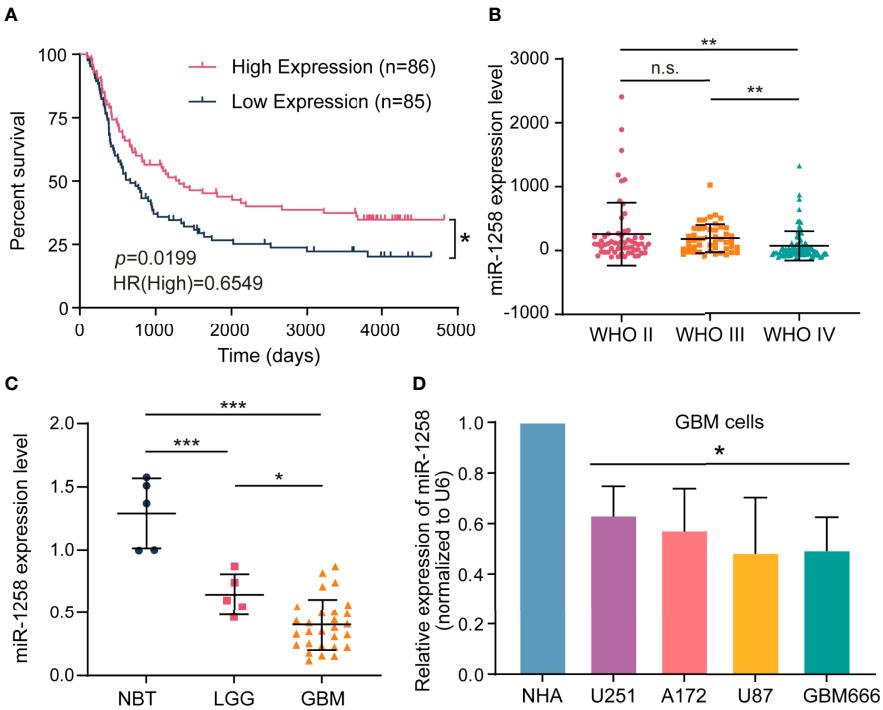

FIGURE 1 | Low expressions of miR-1258 propose an unfavorable prognosis in glioma patients. **(A)** The Kaplan–Meier curve of overall survival with log-rank test stratified by the miR-1258 level (high and low expression divided by the median expression level) in all grades of gliomas in the CGGA database; $*p < 0.05$ between indicated groups. **(B)** Relative miR-1258 expressions in WHO II, WHO III and WHO IV glioma patients were calculated using the CGGA database; $**p < 0.01$, n.s., no significance between indicated groups. **(C)** The expressions of miR-1258 in 5 NBT, 5 LGG, and 28 GBM tissues were analyzed by qRT-PCR, $*p < 0.05$, $***p < 0.001$ between indicated groups. **(D)** miR-1258 expressions were detected in normal human astrocytes (NHA), three GBM cell lines (U251, A172, U87), and GBM666 primary GBM cells by qRT-PCR, $*p < 0.05$ when compared to NHA.

group ($p < 0.001$, **Supplementary Figure S1A**). Next, CCK-8 and colony formation assays showed that the upregulation of miR-1258 attenuated the proliferation of GBM cells ($p < 0.001$, **Figures 2A, B**). Interestingly, the upregulation of miR-1258 did not affect the apoptotic ratios of GBM cells without chemical treatment ($p > 0.05$, **Supplementary Figure S1B**). Considering that TMZ is the first-line chemotherapy regent for GBM (7), the role of miR-1258 on TMZ sensitivity of GBM cells was further investigated. Exposed to 500μM TMZ for 48 h, the flow cytometry analysis showed that miR-1258 overexpression made GBM cells more sensitive to TMZ therapy ($p < 0.001$, **Figure 2C**). The half-maximal inhibitory concentration (IC_{50}) of TMZ in U251 and GBM666 cells for 48 h also indicated that miR-1258 made GBM cells become more sensitive (**Supplementary Figure S1C**). TMZ can induce DNA double-strand breaks which phosphorylate histone H2A.X at serine139 site, producing γ-H2A.X foci those are a hallmark of DNA double-strand breaks and are markedly enhanced in apoptotic cells (8). Exposed to 500μM for 4 h, the immunofluorescent analysis of γ-H2A.X foci results also illustrated that miR-1258 significantly enhanced γ-H2A.X foci formation in GBM cells induced by TMZ ($p < 0.001$, **Supplementary Figure S1D**). Finally, the results of the morphological assays showed that the cellular morphology of 500 μM TMZ-treated miR-1258 overexpressing GBM cells were damaged as compared with the miR-NC transfected GBM cells (**Supplementary Figure S1E**) at 72h. BCNU is another FDA-approved alkylating agent for the treatment of brain tumors (9). We also investigated miR-1258 on BCNU sensitivity of GBM cells, and the IC_{50} for 48 h results showed that miR-1258 overexpression also made GBM cells more sensitized to BCNU (**Supplementary Figure S1C**).

Subsequently, wound healing scratch assays identified that the migratory abilities of miR-1258 overexpressing GBM cells were significantly inhibited ($p < 0.001$, **Figure 2D**). Transwell assays also revealed that miR-1258 upregulation notably blocked the invasive abilities of GBM cells ($p < 0.001$, **Figure 2E**). Meanwhile, western blot results showed that the expressions of major migration and invasion proteins (N-cadherin, MMP2, MMP9, and Snail1) were significantly downregulated by miR-1258 in both U251 and GBM666 cells ($p < 0.05$, **Figure 2F**). In conclusion, these data indicated that miR-1258 attenuated the proliferation, migration, and invasion of GBM cells and potentiates the validity of TMZ and BCNU on GBM cells *in vitro*.

miR-1258 Directly Targets *E2F1* mRNA in 3'-UTR

As mentioned previously, miRNAs are endogenous non-coding RNAs composed of 20-24 nucleotides and exert their functions by binding to the 3'-UTRs of downstream target genes. To uncover the molecular mechanisms of miR-1258 mediating anti-gliomagenesis effects, we intersected five prediction databases,

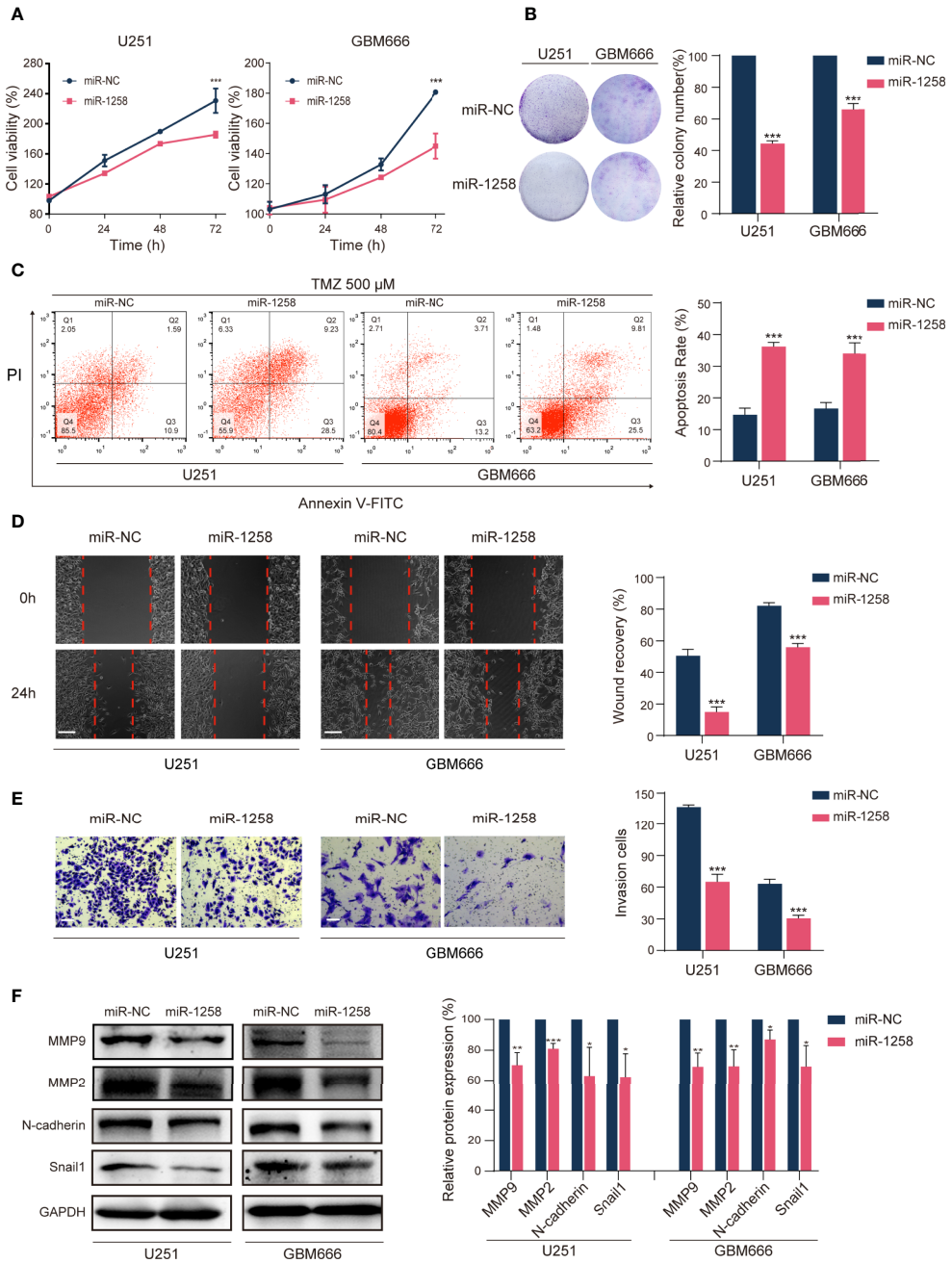

FIGURE 2 | miR-1258 overexpression attenuates GBM cell tumorigenesis *in vitro*. **(A)** CCK-8 assays detected reduced proliferation rates of U251 and GBM666 cells transfected with miR-1258 mimic after 24, 48, and 72 h; ***$p < 0.001$ at indicated time points, when compared to miR-NC group. **(B)** Colony formation detected reduced long-term cell viability of miR-1258 transfected GBM cells. ***$p < 0.001$ when compared to miR-NC group. **(C)** GBM cells were transfected with miR-1258 or miR-NC for 24 h, followed by treatment with 500 μM TMZ for 48 h, and increased apoptosis ratios were determined in miR-1258 group by flow cytometry; ***$p < 0.001$ when compared to miR-NC group. **(D)** Decreased migration abilities of miR-1258 transfected GBM cells were detected by wound healing scratch assays; ***$p < 0.001$ when compared to miR-NC group. Scale bar = 100 μm. **(E)** Matrigel invasion assays revealed the inhibitory role of miR-1258 overexpression on GBM cell invasion; ***$p < 0.001$ when compared to miR-NC group. Scale bar = 100 μm. **(F)** Expressions of major migration and invasion proteins were downregulated in miR-1258 transfected GBM cells detected by western blot assays; *$p < 0.05$, **$p < 0.01$, ***$p < 0.001$ when compared to miR-NC group. Representative images were shown and analyzed as mean ± SD from three independent experiments.

including TargetScan, miRTP, miRDB, RNA22, and miRmap, and focused that *E2F1* could be one of the potential target genes of miR-1258 (**Figure 3A** and **Supplementary Table S4**).

E2F1 is a critical activator of the E2 promoter binding factor family, which controls protein expression at G1/S transition by activating related genes such as EZH2, MYC, CDK4 (10, 11).

Abnormal activation of E2F1 has been studied in various tumor types in recent years. It is widely accepted that *E2F1* is an important transcription factor, which regulates cell proliferation, migration, and invasion (12–15). Meanwhile, next-generation sequencing and bioinformatics analysis have demonstrated that E2F1 is highly expressed in GBM (16). In **Figure 3B**, western blot experiments revealed that miR-1258 overexpression significantly reduced E2F1 expression in GBM cells ($p < 0.01$).

Next, Dual-Luciferase reporter assays were executed to confirm the miR-1258-binding sites in the 3'-UTR of *E2F1* mRNA. The 3'-UTR of *E2F1* exists two putative miR-1258 binding sites (position 1 995-1002, position 2 1207-1213) (**Figure 3C**). So, pmirGLO vectors containing wild-type or mutant *E2F1* 3'-UTR segments were constructed. We mutated these two binding sites individually (Mut1 and Mut2) as well as combined (Mut1+2) (**Figure 3D**). As shown in **Figure 3E**, miR-1258 significantly reduced the luciferase activity of wild-type (Wt) *E2F1* 3'-UTR in GBM cells ($p < 0.01$). The luciferase activity was also reduced in Mut2 *E2F1* 3'-UTR ($p < 0.05$), but no significant change in Mut1 and Mut1+2 ($p > 0.05$). Our results suggested that miR-1258 mainly target *E2F1* 3'-UTR in position 1 (995–1002).

Next, we measured the expression of E2F1 in different GBM cell lines by western blot. The results consistently illustrated that E2F1 expressions were higher in GBM cells than that in normal cells ($p < 0.05$, **Figure 3F**). The TCGA microarray databases illustrated that the expression levels of E2F1 increased with ascending pathological grade of glioma ($p < 0.001$, **Figure 3G**). Besides, the immunohistochemistry results of clinical GBM samples and the Human Protein Atlas database showed that E2F1 expression levels were much higher than those in NBT and LGG samples (**Figure 3H**).

We also tested the E2F1 protein expression in clinical GBM samples using western blot; same as the results of immunohistochemistry, we noticed that the expression of E2F1 was significantly higher in the glioma when compared to NBT, and increased with ascending pathological grade of glioma ($p < 0.05$, **Supplementary Figure S2A**). In addition, the analysis of correlations between E2F1 expression level and clinicopathological characteristics revealed high E2F1 expression was notably associated with age ($p < 0.001$), WHO grade ($p < 0.001$), histology ($p < 0.001$), IDH status ($p < 0.001$), 1p/19q codeletion ($p = 0.004$), *MGMT* Promoter Methylation ($p < 0.001$) and transcriptome subtype ($p < 0.001$) (**Supplementary Table S5**).

Finally, we analyzed the correlation between miR-1258 and E2F1 in the GBM samples. Pearson's correlation analysis of our clinical GBM samples suggested that E2F1 protein expression levels were significantly negatively correlated with corresponding miR-1258 levels (n=20, $r = -0.4581$, $p = 0.0422$, **Figure 3I**). Taken together, we suggested that miR-1258 downregulated E2F1 level by directly targeting its 3'-UTR in GBM cells.

E2F1 Is One of the Functional Targets of miR-1258 in GBM

It was concluded that E2F1 was a direct target of miR-1258, and overexpression of miR-1258 minimized various malignant biological behaviors of GBM cells above. We further verified whether E2F1 is a functional target of miR-1258. E2F1 expression vector or empty vector with either miR-1258 or miR-NC were co-transfected into U251 and GBM666 cells. Both CCK-8 and colony formation assays demonstrated that the restoration of E2F1 expression partly antagonized the anti-proliferation effects of miR-1258 (miR-1258+E2F1 vs. miR-1258 +EV $p < 0.001$, **Figures 4A, B**). Flow cytometry analysis also showed that the restoration of E2F1 expression antagonized the efficacy of TMZ and reduced the pro-apoptosis effect of miR-1258 (miR-1258+E2F1 vs. miR-1258+EV $p < 0.001$, **Figure 4C**). Simultaneously, the IC_{50} of TMZ in U251 and GBM666 cells indicated that E2F1 made GBM cells become less sensitive and effectively rescued the inhibitory effect of miR-1258 (**Supplementary Figure S3A**). In the immunofluorescent analysis of γ-H2A.X foci, E2F1 enhancement modulated the TMZ-induced γ-H2A.X foci formation, which was elicited by the overexpression of miR-1258 in GBM cells (miR-1258+E2F1 vs. miR-1258+EV $p < 0.01$, **Supplementary Figure S3B**). In line with our previous results, with the distinct cellular morphology change, the restoration of E2F1 reduced the efficacy of TMZ and counteracted the inhibitory effect of miR-1258 (**Supplementary Figure S3C**).

Meanwhile, we also found that the restoration of E2F1 expression significantly promoted the migration and invasion abilities of miR-1258-expression GBM cells (miR-1258+E2F1 vs. miR-1258+EV $p < 0.05$, **Figures 4D-F**). These results showed that overexpression of E2F1 partly attenuated the anti-tumorgenesis effects of miR-1258 on malignant biological behaviors of GBM cells, indicating that E2F1 was a crucial functional target of miR-1258.

miR-1258 Attenuates E2F1-Mediated Gliomagenesis by Downregulating Transcription of *PCNA* and *MMP2*

All results above suggested that miR-1258 might exert inhibitory effects *via* E2F1 transcriptional regulation. Western blot results showed that miR-1258 overexpression significantly inhibited E2F1 expressions in both cytoplasm and nuclear in U251 and GBM666 cells ($p < 0.05$, **Figure 5A**). Moreover, immunofluorescence assays also demonstrated a similar tendency (**Figure 5B**).

It is widely recognized that PCNA and MMP2 widely participate in gliomagenesis (17–20). Spearman's rank correlation analysis of the TCGA GBM database also revealed positive correlations between *E2F1* and *PCNA* or *MMP2* mRNA transcript levels (n=669, r =0.5488, $p < 0.001$ in *E2F1-PCNA*, n = 156, $r = 0.1722$, $p < 0.001$ in *E2F1-MMP2*, **Figure 5C**). qRT-PCR assays showed that exogenously expressed miR-1258 significantly reduced *PCNA* and *MMP2* mRNA expression in GBM cells, and the restoration of E2F1 effectively rescued the inhibitory effect of miR-1258 (miR-1258+E2F1 vs. miR-1258+EV $p < 0.05$, **Figure 5D**).

We next analyzed the promoter regions of *PCNA* and *MMP2* using JASPAR and PROMO databases and identified E2F1 binding sequences. To further support our findings, Dual-Luciferase reporter assays were executed to confirm the E2F1

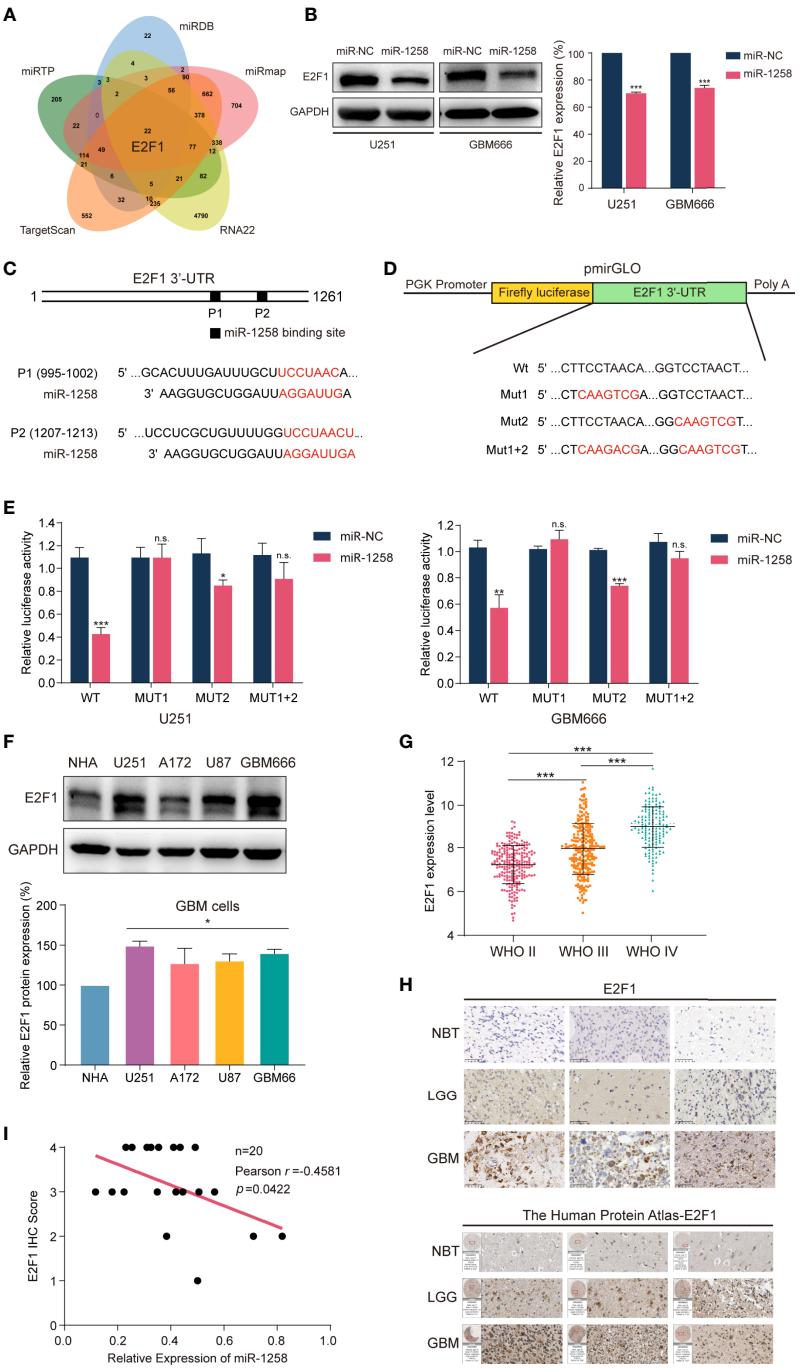

FIGURE 3 | miR-1258 directly targets E2F1 in 3'-UTR and negatively regulates its expression. **(A)** The Venn diagram demonstrated that miR-1258 targeted *E2F1* mRNA intersecting five prediction databases: TargetScan, miRTP, miRDB, RNA22, and miRmap. **(B)** The decreased expressions of E2F1 protein were detected by western blot in U251 and GBM666 cells transfected with miR-1258; ***$p < 0.001$ when compared to miR-NC group. **(C)** Algorithms predicted two miR-1258 target sequences in the *E2F1* mRNA 3'-UTR. **(D)** The schematic diagram illustrated the construction of WT and Mut 3'-UTR sequences in pmirGLO Dual-Luciferase miRNA target expression vector. **(E)** Dual-Luciferase reporter assays were used to assess GBM cells transfected with luciferase vectors carrying WT or Mut 3'-UTR of *E2F1*, in response to miR-1258 or miR-NC; *$p < 0.05$, **$p < 0.01$, ***$p < 0.001$, n.s., no significance between miR-1258 and miR-NC group. **(F)** E2F1 expressions were detected by western blot in normal human astrocytes (NHA), three GBM cell lines (U251, A172, U87), and GBM666 primary GBM cells; *$p < 0.05$ when compared to NHA. **(G)** Relative expression data of E2F1 in 226 WHO II cases, 244 WHO III cases, and 150 WHO IV cases were analyzed using the TCGA database; ***$p < 0.001$ between indicated groups. **(H)** E2F1 protein expressions were determined by immunohistochemistry in NBT, LGG and GBM samples; Scale bar = 50 μm. The expressions of E2F1 were also analyzed using the Human Protein Atlas database. **(I)** The correlations between E2F1 protein expression levels and relative miR-1258 expression levels in 20 GBM samples were analyzed by Pearson's correlation analysis; $r = -0.4581$, $p = 0.0422$.

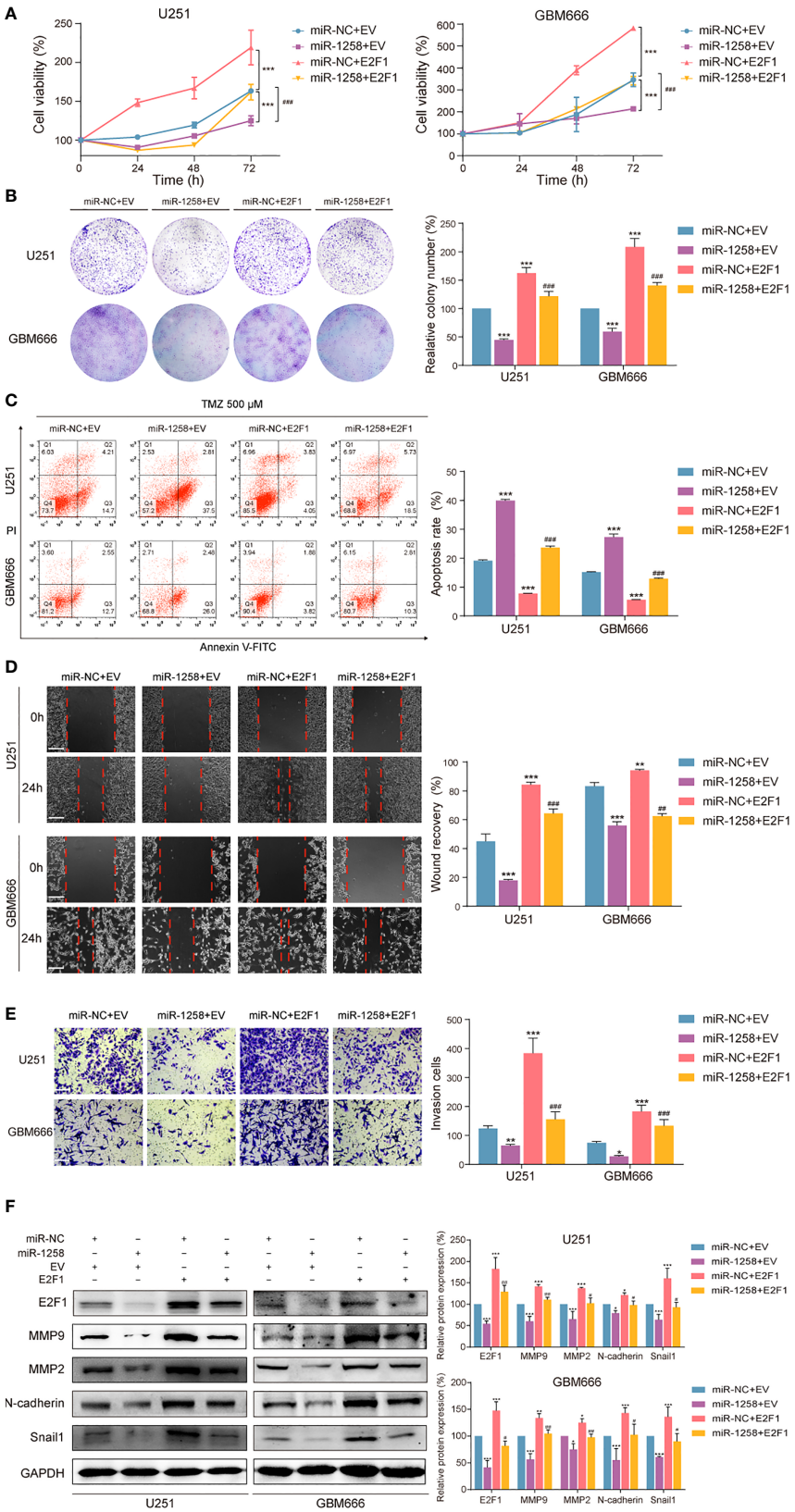

FIGURE 4 | Continued

FIGURE 4 | Restoration of E2F1 abrogates the inhibitory effects of miR-1258 on GBM cell proliferation, therapeutic resistance, migration, and invasion. **(A)** The viability of miR-1258 transfected U251 and GBM666 cells were rescued by E2F1 assessed by the CCK-8 assay; $^{***}p < 0.001$ versus the miR-NC+EV group. $^{###}p < 0.001$, versus the miR-1258+EV group. **(B)** Colony formation assays demonstrated the long-term cell viability of miR-1258 transfected GBM cells were rescued by E2F1; $^{***}p < 0.001$ versus the miR-NC+EV group. $^{###}p < 0.001$, versus the miR-1258+EV group. **(C)** After 24 h co-transfection, GBM cells were treated with 500 μM TMZ for 48 h, and then counteracted apoptosis ratios were determined in miR-1258+E2F1 group by flow cytometry; $^{***}p < 0.001$ versus the miR-NC +EV group. $^{###}p < 0.001$, versus the miR-1258+EV group. **(D)** The migration abilities of miR-1258 transfected GBM cells were rescued by E2F1 assessed by wound healing scratch assays; $^{**}p < 0.01$, $^{***}p < 0.001$ versus the miR-NC+EV group. $^{##}p < 0.01$, $^{###}p < 0.001$ versus the miR-1258+EV group. Scale bar = 100 μm. **(E)** Matrigel invasion assays revealed the rescue impact of restoration of E2F1 on GBM cells invasion; $^{*}p < 0.05$, $^{**}p < 0.01$ and $^{***}p < 0.001$ versus the miR-NC+EV group. $^{###}p < 0.001$ versus the miR-1258+EV group. Scale bar = 100 μm. **(F)** Expressions of migration and invasion proteins were restored by E2F1 detected by western blot in GBM cells after co-transfection; $^{*}p < 0.05$, $^{**}p < 0.01$ and $^{***}p < 0.001$ versus the miR-NC+EV group. $^{#}p < 0.05$, $^{##}p < 0.01$ and $^{###}p < 0.001$ versus the miR-1258+EV group.

binding sites in the promoter regions of *PCNA* and *MMP2* genes. pGL3-Basic vectors containing wild-type or mutant *PCNA* and *MMP2* promoter sequences were constructed (**Figure 5E**). E2F1 significantly upregulated the luciferase activities of wild-type (Wt) *PCNA* and *MMP2* promoter sequences in GBM cells ($p < 0.05$). However, there was no significant change in luciferase activity in mutation vectors ($p > 0.05$, **Figure 5F**). We confirmed that E2F1 was mainly binding to the *PCNA* promoter at position -1956~-1945 and binding to the *MMP2* promoter at position -1033~-1026, respectively. Finally, ChIP assays further showed E2F1 enriched in both *PCNA* and *MMP2* promoter regions (**Figure 5G**). These results identified that miR-1258 could partly eliminate E2F1-mediated malignant biological behaviors in GBM *via* transcriptional regulation of its downstream effectors *PCNA* and *MMP2*.

miR-1258 Overexpression Attenuates GBM Tumorigenesis and Invasion Phenotype *In Vivo*

Considering the significant inhibitory effects of miR-1258 on GBM cells *in vitro*, we further investigate the anti-tumorgenesis effects of miR-1258 in a subcutaneous xenograft GBM model. Results manifested that the growth of subcutaneous tumors was significantly inhibited by miR-1258 overexpression ($p < 0.01$, **Figures 6A–C**). Moreover, immunohistochemistry suggested that the miR-1258 overexpressing group had lower expressions of E2F1, PCNA, and MMP2 (**Figure 6D**), consistent with our results *in vitro*. The animal experiment results confirmed that miR-1258 exerted an inhibitory effect on gliomagenesis by repressing E2F1 expression.

DISCUSSION

The existing therapeutic approach to GBM consists of surgical resection followed by concurrent radiotherapy and chemotherapy. Though those approach has improved survival, almost GBM patients still succumb. Effective treatment options for GBM are not well established (21). Elucidating the molecular basis of GBM progression could contribute to novel therapies to block GBM progression.

Accumulating evidence has indicated that abnormal expression of miRNAs is closely associated with the tumorigenesis of human cancers (22–24), which can serve as molecular biomarkers for diagnosis, prognosis, and treatment for GBM (25). Similarly, our results first reported that miR-1258 expression decreased with the ascending pathological grade of glioma in both the CGGA database and clinical samples. Notably, patients with high miR-1258 expression had much better overall survival, which suggested miR-1258 function as a potential diagnostic and prognostic biomarker for glioma patients, especially the GBM patients. In previous studies, miR-1258 has been demonstrated an inhibitory role in many cancer types (4, 5, 26). Here, we also noticed that miR-1258 acted as a tumor-suppressive miRNA on GBM proliferation, therapeutic resistance, migration, and invasion *in vitro* and *in vivo* by functional experiments. The expression of miRNAs in serum is stable (27), and peripheral blood is easy to collect from patients. miR-1258 may therefore be a potential tumor marker and help the development of valuable tools for early diagnosis of gliomas in clinical practice for neuro-oncologists and pathologists. Interestingly, we found that miR-1258 affected the apoptotic rate of GBM cells when TMZ existed. As listed in **Supplementary Table S4**, we also found that *PARP3*, *ABCG1* and *BCL2* were potential targets of miR-1258, whose expression could be downregulated by miR-1258. Recently studies have revealed that combining PARP3 inhibitors with TMZ can potentiate the validity of TMZ in SW620 cell subcutaneous xenograft models (28). ABCG1 has been demonstrated highly expressed in GBM (29, 30). As a member of the ATP-binding cassette transporters, ABCG1 induces drug resistance in many cancers, including hepatocellular carcinoma and osteosarcoma (31, 32), so we speculated that ABCG1 may also participate in TMZ resistance in GBM. BCL-2, one of the most common anti-apoptotic proteins, encoded by the *BCL2* gene, has been widely reported to involve in TMZ resistance (33, 34). Hence, further study on the participation and the effect of miR-1258 on TMZ sensitivity is warranted.

E2F1, as a member of the E2F family, is an essential transcription factor, which involves in the regulation of multiple biological processes of cancers, including cell cycle, programmed cell death, DNA damage, and self-renew of cells (35, 36). Activation of E2F1 can also initiate the target genes transcription to maintain the progression of the cell cycles and induce the progression of anti-apoptosis and cell invasion in cancers (15, 37). Abnormal overexpression of E2F1 has also been reported in glioma (16, 38). Interestingly, there has been increasing attention that miRNAs post-transcriptionally regulate E2F1 expression, including miR-205-5p, miR-342-3p, miR-93, and miR-598 (39–41). To better comprehend the tumor-suppressive function of miR-1258 mechanistically, we identified E2F1 as one of the direct and functional targets for miR-1258 in GBM. Dual-Luciferase reporter assays demonstrated miR-1258 directly binding to *E2F1* 3'-UTR,

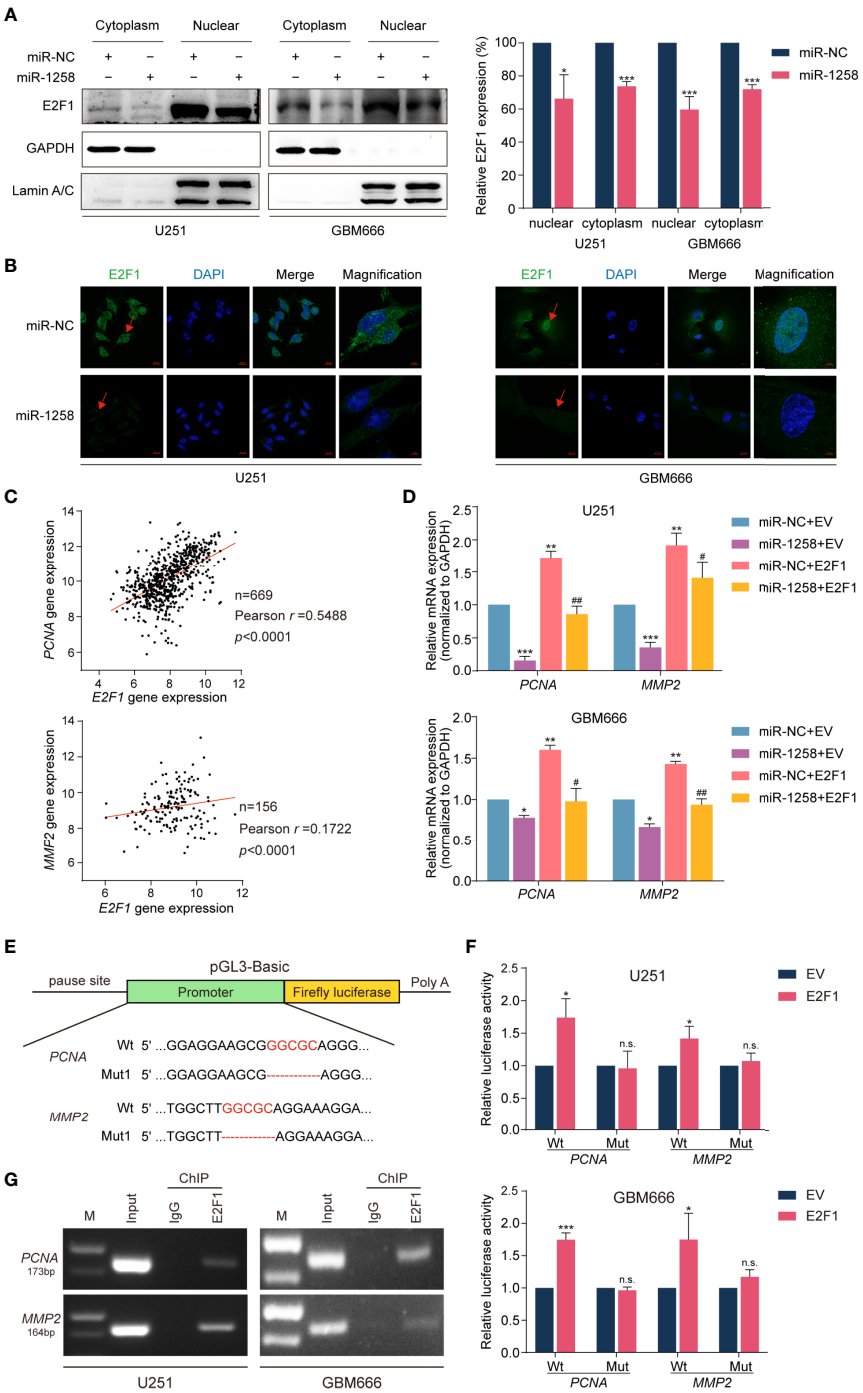

FIGURE 5 | miR-1258 exerts inhibitory effects *via* transcriptional regulation of *PCNA* and *MMP2* by E2F1. **(A)** The decreased expressions of E2F1 in U251 and GBM66 cells transfected with miR-1258 in cytoplasmic and nuclear fraction were detected by western blot; $^{*}p < 0.05$, $^{***}p < 0.001$ when compared to miR-NC group. **(B)** Immunofluorescence assays were applied to analyze GBM cells transfected with miR-1258 or miR-NC. Cell nuclei were stained by DAPI. Red arrows showed the nuclear expression of E2F1. Scale bar = 20 μm. In magnification, Scale bar = 5 μm. **(C)** The correlations between *E2F1* gene expression and *PCNA*, *MMP2* levels in the TCGA database were analyzed by Pearson's correlation analysis; $r = 0.5488$, $p < 0.0001$ in *E2F1-PCNA*, $r = 0.1722$, $p < 0.0001$ in *E2F1-MMP2*. **(D)** The mRNA expressions of *PCNA* and *MMP2* in miR-1258 transfected GBM cells were restored by E2F1 using the qRT-PCR assay; $^{*}p < 0.05$, $^{**}p < 0.01$, $^{***}p < 0.001$ versus the miR-NC+EV group. $^{\#}p < 0.05$, $^{\#\#}p < 0.01$, versus the miR-1258+EV group. **(E)** The schematic diagram illustrated the construction of *PCNA* and *MMP2* WT and Mut promoter sequences in the pGL3-Basic vector. **(F)** Dual-Luciferase reporter assays were used to assess GBM cells transfected with luciferase vectors carrying WT or Mut promoter sequences of *PCNA* and *MMP2* upon transfection of an E2F1 expression vector or EV; $^{*}p < 0.05$, $^{***}p < 0.001$, n.s., no significance between E2F1 and EV group. **(G)** ChIP assays were used to analyze the enrichment of E2F1 on the *PCNA* and *MMP2* promoter region in GBM cells.

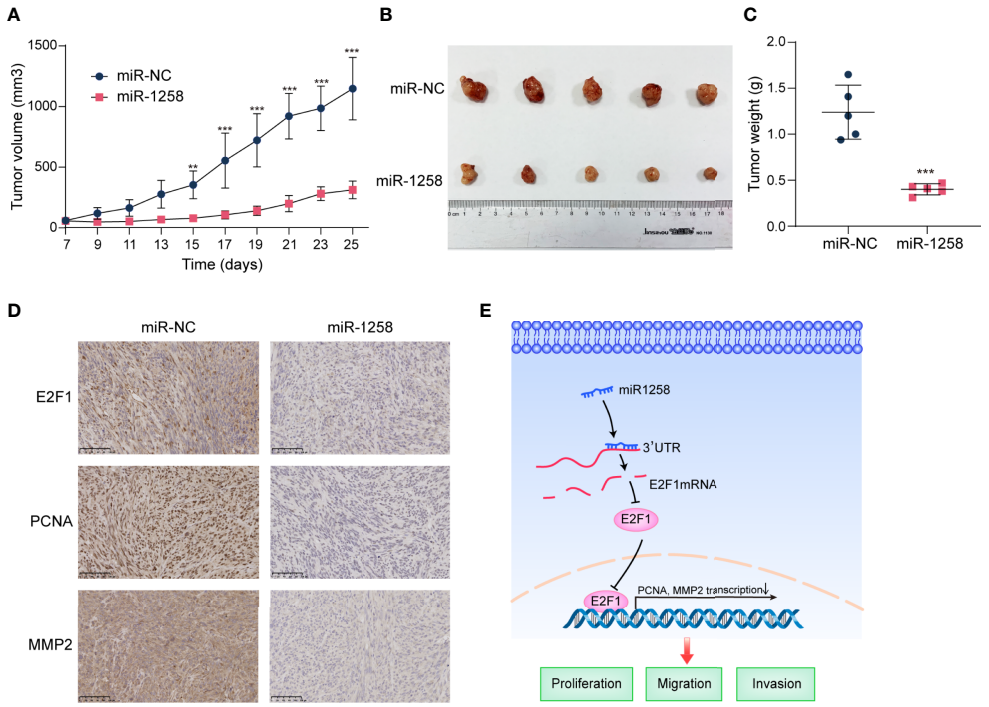

FIGURE 6 | miR-1258 decreases tumorigenicity and invasion characteristics in xenograft model. **(A)** Stable-transfected U251 cells with miR-1258 mimic or miR-NC were implanted bilaterally in the axillary, respectively, per mouse. The volumes of subcutaneous xenografts were measured from day 7 to day 25 every 2 days (V=0.5×width2×length, units: mm3, n=5); $^{**}p < 0.01$, $^{***}p < 0.001$ at indicated time points, when compared to miR-NC group. **(B)** Respective images of subcutaneous xenografts were shown. **(C)** The tumor weights were decreased in miR-1258 group; $^{***}p < 0.001$ between indicated groups. **(D)** The expressions of E2F1, PCNA, and MMP2 significantly diminished in miR-1258 group detected by immunohistochemical analysis. Representative images were shown; Scale bar, 100 μm. **(E)** The mechanistic scheme illustrated that miR-1258 attenuates tumorigenesis through targeting E2F1 to inhibit *PCNA* and *MMP2* transcription in glioblastoma.

thereby inhibiting E2F1 expression, consistent with our results that E2F1 expressed highly in GBM tissues as well as GBM cell lines. By contrast, the restoration of E2F1 reversed GBM cell proliferation inhibition, therapeutic resistance, migration, and invasion mediated by enhanced expression of miR-1258. Our study results indicated that the miR-1258/E2F1 axis represented a critical regulation mechanism underlying the molecular pathogenesis of GBM. Very recently, Peng X et al. has reported that miR-1258 overexpression inhibits cell proliferation, invasion and migration by targeting the E2F1 and altering AKT and P53 signal pathway in cervical cancer (42), which also highlights a wide regulatory network of miR-1258/E2F1 axis in cancers.

PCNA, which encodes proliferating cell nuclear antigen, is an essential factor in DNA replication and many other cancer cell processes, especially in cell proliferation (43). Matrix metalloproteinase 2, an enzyme encoded by the *MMP2* gene, is involved in degrading type IV collagen. It is widely recognized that matrix metalloproteinase-2 mediated basement membrane degradation is positively linked with the migration, invasion, and metastasis of cancers (44). Only a few studies have reported that E2F1 stimulates transcription of the *PCNA* and *MMP2* (45, 46). However, the transcriptional regulations of E2F1 on *PCNA* and *MMP2* genes in GBM remain unclear. In this study, we demonstrated that E2F1 directly bound to the promoter regions of *PCNA* and *MMP2* to regulate their transcriptional activity, facilitating the expression of these gliomagenesis genes, finally attenuating the inhibitory effects of miR-1258 on cell proliferation, therapeutic resistance, migration, and invasion in GBM cells. These findings also indicated that E2F1 exerted a crucial role in the malignant behavior of GBM and could serve as a potential diagnostic marker and therapeutic target in GBM. However, it is still unclear whether E2F1 participates in the regulation of other downstream effectors in gliomagenesis. Hence, this issue deserves to be clarified.

Our findings collectively highlighted the novel evidence of a crucial link between miR-1258 and the tumorigenesis of human GBM. miR-1258 played an inhibitory role in the progression of GBM and functioned as a tumor suppressor by down-regulating E2F1 expression and attenuated E2F1-mediated downstream gene *PCNA* and *MMP2* transcriptions (**Figure 6E**). To date, miRNA-based therapies are still in the initial stages (25). Our novel findings establish the role of miR-1258 as a potential diagnostic marker and a therapeutic target in GBM.

DATA AVAILABILITY STATEMENT

The original contributions presented in the study are included in the article/**Supplementary Material**. Further inquiries can be directed to the corresponding authors.

ETHICS STATEMENT

The studies involving human participants were reviewed and approved by Ethics Committee of China Pharmaceutical University. The patients/participants provided their written informed consent to participate in this study. The animal study was reviewed and approved by Ethics Committee of China Pharmaceutical University.

AUTHOR CONTRIBUTIONS

LZ and YW conceived and supervised the research. HQ and YanG designed, performed all the experiments, and interpreted data. RM provided clinical samples. HZ and YaG helped conduct animal experiments. YY and JL helped conduct immunohistochemistry experiments. HQ wrote the manuscript. HQ, LZ, and YW revised the manuscript. All authors contributed to the article and approved the submitted version.

FUNDING

This study was supported by the National Natural Science Foundation of China (No. 81773774 and No. 81872903), the "Double First-Class" University project of China Pharmaceutical University (CPU2018GY03 and CPU2018GY37), and the Postgraduate Research & Practice Innovation Program of Jiangsu Province (KYCX20-0656).

ACKNOWLEDGMENTS

We acknowledge the Cellular and Molecular Biology Center of China Pharmaceutical University for the use of instrumentation facilities.

SUPPLEMENTARY MATERIAL

The Supplementary Material for this article can be found online at: https://www.frontiersin.org/articles/10.3389/fonc.2021.671144/full#supplementary-material

REFERENCES

1. Tan A, Ashley D, López G, Malinzak M, Friedman H, Khasraw M. Management of Glioblastoma: State of the Art and Future Directions. *CA: Cancer J Clin* (2020) 70:299–312. doi: 10.3322/caac.21613
2. Goodall GJ, Wickramasinghe VO. RNA in cancer. *Nat Rev Cancer* (2021) 21:22–36. doi: 10.1038/s41568-020-00306-0
3. Rynkeviciene R, Simiene J, Strainiene E, Stankevicius V, Usinskiene J, Miseikyte Kaubriene E, et al. Non-Coding RNAs in Glioma. *Cancers* (2018) 11:17. doi: 10.3390/cancers11010017
4. Huang W, Tian X, Bi S, Zhang S, He T, Song L, et al. The β-Catenin/TCF-4-LINC01278-miR-1258-Smad2/3 Axis Promotes Hepatocellular Carcinoma Metastasis. *Oncogene* (2020) 39:4538–50. doi: 10.1038/s41388-020-1307-3
5. Liu W, Zhou Z, Zhang Q, Rong Y, Li L, Luo Y, et al. Overexpression of miR-1258 Inhibits Cell Proliferation by Targeting AKT3 in Osteosarcoma. *Biochem Biophys Res Commun* (2019) 510:479–86. doi: 10.1016/j.bbrc.2019.01.139
6. Zhang Z, Li J, Huang Y, Peng W, Qian W, Gu J, et al. Upregulated miR-1258 Regulates Cell Cycle and Inhibits Cell Proliferation by Directly Targeting E2F8 in CRC. *Cell Proliferation* (2018) 51:e12505. doi: 10.1111/cpr.12505
7. Bell E, Pugh S, McElroy J, Gilbert M, Mehta M, Klimowicz A, et al. Molecular-Based Recursive Partitioning Analysis Model for Glioblastoma in the Temozolomide Era: A Correlative Analysis Based on NRG Oncology RTOG 0525. *JAMA Oncol* (2017) 3:784–92. doi: 10.1001/jamaoncol.2016.6020
8. Kaina B. Temozolomide in Glioblastoma Therapy: Role of Apoptosis, Senescence and Autophagy. Comment on Strobel et al., Temozolomide and Other Alkylating Agents in Glioblastoma Therapy. *Biomedicines* 2019, 7, 69. *Biomedicines* (2019) 7(4):90. doi: 10.3390/biomedicines7040090
9. Westphal M, Hilt DC, Bortey E, Delavault P, Olivares R, Warnke PC, et al. A Phase 3 Trial of Local Chemotherapy With Biodegradable Carmustine (BCNU) Wafers (Gliadel Wafers) in Patients With Primary Malignant Glioma. *Neuro Oncol* (2003) 5:79–88. doi: 10.1093/neuonc/5.2.79
10. Lee S, Roh Y, Kim S, Lee J, Seol S, Lee H, et al. Activation of EZH2 and SUZ12 Regulated by E2F1 Predicts the Disease Progression and Aggressive Characteristics of Bladder Cancer. *Clin Cancer Res an Off J Am Assoc Cancer Res* (2015) 21:5391–403. doi: 10.1158/1078-0432.Ccr-14-2680
11. Poppy Roworth A, Ghari F, La Thangue NB. To Live or Let Die – Complexity Within the E2F1 Pathway. *Mol Cell Oncol* (2015) 2:e970480. doi: 10.4161/23723548.2014.970480
12. Polager S, Ginsberg D. p53 and E2f: partners in life and death. *Nat Rev Cancer* (2009) 9:738–48. doi: 10.1038/nrc2718
13. Biswas A, Johnson D. Transcriptional and Nontranscriptional Functions of E2F1 in Response to DNA Damage. *Cancer Res* (2012) 72:13–7. doi: 10.1158/0008-5472.Can-11-2196
14. Engelmann D, Pützer B. The Dark Side of E2F1: in Transit Beyond Apoptosis. *Cancer Res* (2012) 72:571–5. doi: 10.1158/0008-5472.Can-11-2575
15. Emanuele M, Enrico T, Mouery R, Wasserman D, Nachum S, Tzur A. Complex Cartography: Regulation of E2F Transcription Factors by Cyclin F and Ubiquitin. *Trends Cell Biol* (2020) 30:640–52. doi: 10.1016/j.tcb.2020.05.002
16. He J, Zhao Y, Zhao E, Wang X, Dong Z, Chen Y, et al. Cancer-Testis Specific Gene OIP5: A Downstream Gene of E2F1 That Promotes Tumorigenesis and Metastasis in Glioblastoma by Stabilizing E2F1 Signaling. *Neuro-oncology* (2018) 20:1173–84. doi: 10.1093/neuonc/noy037
17. Karamitopoulou E, Perentes E, Melachrinou M, Maraziotis T. Proliferating Cell Nuclear Antigen Immunoreactivity in Human Central Nervous System Neoplasms. *Acta Neuropathol* (1993) 85:316–22. doi: 10.1007/bf00227728
18. Tan P, Li Z, Cai W, Lu J, Xie F, Weng Y. [Expression of nm23 and Proliferating Cell Nuclear Antigen (PCNA) in Human Brain Gliomas and Their Significance]. *Ai Zheng = Aizheng = Chin J Cancer* (2003) 22:1077–80. doi: 10.3321/j.issn:1000-467X.2003.10.016
19. Du R, Petritsch C, Lu K, Liu P, Haller A, Ganss R, et al. Matrix Metalloproteinase-2 Regulates Vascular Patterning and Growth Affecting Tumor Cell Survival and Invasion in GBM. *Neuro-oncology* (2008) 10:254–64. doi: 10.1215/15228517-2008-001
20. Ramachandran R, Sørensen M, Aaberg-Jessen C, Hermansen S, Kristensen B. Expression and Prognostic Impact of Matrix Metalloproteinase-2 (MMP-2) in Astrocytomas. *PloS One* (2017) 12:e0172234. doi: 10.1371/journal.pone.0172234
21. Delgado-Martín B, Medina M. Advances in the Knowledge of the Molecular Biology of Glioblastoma and Its Impact in Patient Diagnosis, Stratification, and Treatment. *Adv Sci (Weinheim Baden-Wurttemberg Germany)* (2020) 7:1902971. doi: 10.1002/advs.201902971
22. Dragomir M, Kopetz S, Ajani J, Calin G. Non-Coding RNAs in GI Cancers: From Cancer Hallmarks to Clinical Utility. *Gut* (2020) 69:748–63. doi: 10.1136/gutjnl-2019-318279
23. Wallace J, O'Connell R. MicroRNAs and Acute Myeloid Leukemia: Therapeutic Implications and Emerging Concepts. *Blood* (2017) 130:1290–301. doi: 10.1182/blood-2016-10-697698
24. Wong C, Tsang F, Ng I. Non-Coding RNAs in Hepatocellular Carcinoma: Molecular Functions and Pathological Implications. *Nat Rev Gastroenterol Hepatol* (2018) 15:137–51. doi: 10.1038/nrgastro.2017.169

25. Pottoo FH, Javed MN, Rahman JU, Abu-Izneid T, Khan FA. Targeted Delivery of miRNA Based Therapeuticals in the Clinical Management of Glioblastoma Multiforme. *Semin Cancer Biol* (2021) 69:391–8. doi: 10.1016/j.semcancer.2020.04.001
26. Wang L, Kumar S, Calin G, Li Z, Chim C. Frequent Methylation of the Tumour Suppressor miR-1258 Targeting PDL1: Implication in Multiple Myeloma-Specific Cytotoxicity and Prognostification. *Br J Haematol* (2020) 190:249–61. doi: 10.1111/bjh.16517
27. Chen X, Ba Y, Ma L, Cai X, Yin Y, Wang K, et al. Characterization of microRNAs in Serum: A Novel Class of Biomarkers for Diagnosis of Cancer and Other Diseases. *Cell Res* (2008) 18:997–1006. doi: 10.1038/cr.2008.282
28. Oplustil O'Connor L, Rulten SL, Cranston AN, Odedra R, Brown H, Jaspers JE, et al. The PARP Inhibitor AZD2461 Provides Insights Into the Role of PARP3 Inhibition for Both Synthetic Lethality and Tolerability With Chemotherapy in Preclinical Models. *Cancer Res* (2016) 76:6084–94. doi: 10.1158/0008-5472.Can-15-3240
29. Chen YH, Cimino PJ, Luo J, Dahiya S, Gutmann DH. ABCG1 Maintains High-Grade Glioma Survival In Vitro and In Vivo. *Oncotarget* (2016) 7:23416–24. doi: 10.18632/oncotarget.8030
30. Dréan A, Rosenberg S, Lejeune FX, Goli L, Nadaradjane AA, Guehennec J, et al. ATP binding cassette (ABC) transporters: expression and clinical value in glioblastoma. *J Neurooncol* (2018) 138:479–86. doi: 10.1007/s11060-018-2819-3
31. Liao X, Song G, Xu Z, Bu Y, Chang F, Jia F, et al. Oxaliplatin Resistance is Enhanced by Saracatinib Via Upregulation Wnt-ABCG1 Signaling in Hepatocellular Carcinoma. *BMC Cancer* (2020) 20:31. doi: 10.1186/s12885-019-6480-9
32. Roundhill EA, Jabri S, Burchill SA. ABCG1 and Pgp Identify Drug Resistant, Self-Renewing Osteosarcoma Cells. *Cancer Lett* (2019) 453:142–57. doi: 10.1016/j.canlet.2019.03.011
33. Zhang X, Yu J, Zhao C, Ren H, Yuan Z, Zhang B, et al. MiR-181b-5p Modulates Chemosensitivity of Glioma Cells to Temozolomide by Targeting Bcl-2. *Biomed Pharmacother = Biomed Pharmacother* (2019) 109:2192–202. doi: 10.1016/j.biopha.2018.11.074
34. Han J, Chen Q. MiR-16 Modulate Temozolomide Resistance by Regulating BCL-2 in Human Glioma Cells. *Int J Clin Exp Pathol* (2015) 8:12698–707.
35. La Thangue N. The Yin and Yang of E2F-1: Balancing Life and Death. *Nat Cell Biol* (2003) 5:587–9. doi: 10.1038/ncb0703-587
36. Bell L, Ryan K. Life and Death Decisions by E2F-1. *Cell Death Differ* (2004) 11:137–42. doi: 10.1038/sj.cdd.4401324
37. Zheng X, Huang M, Xing L, Yang R, Wang X, Jiang R, et al. The circRNA circSEPT9 Mediated by E2F1 and EIF4A3 Facilitates the Carcinogenesis and Development of Triple-Negative Breast Cancer. *Mol Cancer* (2020) 19:73. doi: 10.1186/s12943-020-01183-9
38. Zhi T, Jiang K, Xu X, Yu T, Zhou F, Wang Y, et al. ECT2/PSMD14/PTTG1 Axis Promotes the Proliferation of Glioma Through Stabilizing E2F1. *Neuro-oncology* (2019) 21:462–73. doi: 10.1093/neuonc/noy207
39. Bao C, Chen J, Chen D, Lu Y, Lou W, Ding B, et al. MiR-93 Suppresses Tumorigenesis and Enhances Chemosensitivity of Breast Cancer Via Dual Targeting E2F1 and CCND1. *Cell Death Dis* (2020) 11:618. doi: 10.1038/s41419-020-02855-6
40. Lai X, Gupta S, Schmitz U, Marquardt S, Knoll S, Spitschak A, et al. MiR-205-5p and miR-342-3p Cooperate in the Repression of the E2F1 Transcription Factor in the Context of Anticancer Chemotherapy Resistance. *Theranostics* (2018) 8:1106–20. doi: 10.7150/thno.19904
41. Liu F, Zhang Q, Liang Y. MicroRNA-598 Acts as an Inhibitor in Retinoblastoma Through Targeting E2F1 and Regulating AKT Pathway. *J Cell Biochem* (2020) 121:2294–302. doi: 10.1002/jcb.29453
42. Peng X, Zhang Y, Gao J, Cai C. MiR-1258 Promotes the Apoptosis of Cervical Cancer Cells by Regulating the E2F1/P53 Signaling Pathway. *Exp Mol Pathol* (2020) 114:104368. doi: 10.1016/j.yexmp.2020.104368
43. Hall P, Levison D, Woods A, Yu C, Kellock D, Watkins J, et al. Proliferating Cell Nuclear Antigen (PCNA) Immunolocalization in Paraffin Sections: An Index of Cell Proliferation With Evidence of Deregulated Expression in Some Neoplasms. *J Pathol* (1990) 162:285–94. doi: 10.1002/path.1711620403
44. Gilkes DM, Semenza GL, Wirtz D. Hypoxia and the Extracellular Matrix: Drivers of Tumour Metastasis. *Nat Rev Cancer* (2014) 14:430–9. doi: 10.1038/nrc3726
45. Li Y, Wang L, Lu C. An E2F site in the 5'-promoter region contributes to serum-dependent up-regulation of the human proliferating cell nuclear antigen gene. *FEBS Lett* (2003) 544:112–8. doi: 10.1016/s0014-5793(03)00485-x
46. Johnson J, Pillai S, Chellappan S. Abstract 268: Differential Regulation of MMP Promoters by E2F Transcription Factors: Potential Role of c-MYC and Id1. *Cancer Res* (2011) 71:268–8. doi: 10.1158/1538-7445.Am2011-268

Conflict of Interest: The authors declare that the research was conducted in the absence of any commercial or financial relationships that could be construed as a potential conflict of interest.

Copyright © 2021 Qin, Gui, Ma, Zhang, Guo, Ye, Li, Zhao and Wang. This is an open-access article distributed under the terms of the Creative Commons Attribution License (CC BY). The use, distribution or reproduction in other forums is permitted, provided the original author(s) and the copyright owner(s) are credited and that the original publication in this journal is cited, in accordance with accepted academic practice. No use, distribution or reproduction is permitted which does not comply with these terms.

frontiers in Oncology

ORIGINAL RESEARCH
published: 25 May 2021
doi: 10.3389/fonc.2021.668090

Expression Profiling of Glioblastoma Cell Lines Reveals Novel Extracellular Matrix-Receptor Genes Correlated With the Responsiveness of Glioma Patients to Ionizing Radiation

*Rodolfo Bortolozo Serafim[1,2,3], Patrick da Silva[1], Cibele Cardoso[2,3], Luis Fernando Macedo Di Cristofaro[1], Renato Petitto Netto[1], Rodrigo de Almeida[1], Geovana Navegante[1], Camila Baldin Storti[2,3], Juliana Ferreira de Sousa[4], Felipe Canto de Souza[2,3], Rodrigo Panepucci[2,3], Cristiano Gallina Moreira[1], Larissa Siqueira Penna[1], Wilson Araujo Silva Jr[2,3] and Valeria Valente[1,2,3]**

[1] School of Pharmaceutical Sciences, São Paulo State University (UNESP), Araraquara, Brazil, [2] Center for Cell-Based Therapy (CTC), Regional Blood Center of Ribeirão Preto, Ribeirão Preto, Brazil, [3] Department of Genetics, Ribeirão Preto Medical School, University of São Paulo (USP), Ribeirão Preto, Brazil, [4] Radiation Oncology Branch, National Cancer Institute, National Institutes of Health (NIH), Bethesda, MD, United States

Glioblastoma (GBM) is the most lethal and frequent type of brain tumor, leading patients to death in approximately 14 months after diagnosis. GBM treatment consists in surgical removal followed by radio and chemotherapy. However, tumors commonly relapse and the treatment promotes only a slight increase in patient survival. Thus, uncovering the cellular mechanisms involved in GBM resistance is of utmost interest, and the use of cell lines has been shown to be an extremely important tool. In this work, the exploration of RNAseq data from different GBM cell lines revealed different expression signatures, distinctly correlated with the behavior of GBM cell lines regarding proliferation indexes and radio-resistance. U87MG and U138MG cells, which presented expressively reduced proliferation and increased radio-resistance, showed a particular expression signature encompassing enrichment in many extracellular matrix (ECM) and receptor genes. Contrasting, U251MG and T98G cells, that presented higher proliferation and sensibility to radiation, exhibited distinct signatures revealing consistent enrichments for DNA repair processes and although several genes from the ECM-receptor pathway showed up-regulation, enrichments for this pathway were not detected. The ECM-receptor is a master regulatory pathway that is known to impact several cellular processes including: survival, proliferation, migration, invasion, and DNA damage signaling and repair, corroborating the associations we found. Furthermore, searches to The Cancer Genome Atlas (TCGA) repository revealed prognostic correlations with glioma patients for the majority of genes highlighted in the signatures and led to the identification of 31 ECM-receptor genes individually correlated with radiation responsiveness. Interestingly,

OPEN ACCESS

Edited by:
David Nathanson,
UCLA David Geffen School of Medicine, United States

Reviewed by:
Chao Zhang, Qilu Hospital of Shandong University, China
Sara Pedron, University of Illinois at Urbana-Champaign, United States
Elvira V. Grigorieva, Institute of Molecular Biology and Biophysics (RAS), Russia

***Correspondence:**
Valeria Valente
valeria.valente@unesp.br

Specialty section:
This article was submitted to Neuro-Oncology and Neurosurgical Oncology, a section of the journal Frontiers in Oncology

Received: 15 February 2021
Accepted: 30 April 2021
Published: 25 May 2021

Citation:
Serafim RB, da Silva P, Cardoso C, Di Cristofaro LFM, Netto RP, de Almeida R, Navegante G, Storti CB, de Sousa JF, de Souza FC, Panepucci R, Moreira CG, Penna LS, Silva WA Jr and Valente V (2021) Expression Profiling of Glioblastoma Cell Lines Reveals Novel Extracellular Matrix-Receptor Genes Correlated With the Responsiveness of Glioma Patients to Ionizing Radiation. Front. Oncol. 11:668090. doi: 10.3389/fonc.2021.668090

we observed an association between the number of upregulated genes and survivability greater than 5 years after diagnosis, where almost all the patients that presented 21 or more upregulated genes were deceased before 5 years. Altogether our findings suggest the clinical relevance of ECM-receptor genes signature found here for radiotherapy decision and as biomarkers of glioma prognosis.

Keywords: glioblastoma, GBM cell lines, expression profiling, extracellular matrix, ECM-receptors, radioresistance

INTRODUCTION

Glioblastoma (GBM) is the most common and aggressive primary brain tumor in adults. The current protocols for treating GBM involve surgical resection followed by chemotherapy and radiotherapy, but the rate of patient survival is only 14 months (1). The poor prognosis accrues mainly from the resistance of GBM cells against chemical and radiotherapeutic agents, along with the abrupt increase in proliferation acquired during tumor progression. The extensive interaction of tumor cells with the extracellular matrix (ECM) favors invasiveness and brain infiltration, preventing the cure even after extensive surgical resection (2). In face of this scenario, standard treatment does not restrain recurrences and about 80% of relapses are located at the resection margin, which is the site predominantly affected by higher doses of radiation (3). Also, GBM resistance is notably correlated with the high percentage of cancer stem cells (CSC) population usually found in these tumors (4). CSC responds to genotoxic agents in an adaptive manner and usually survives inside the therapeutic environment, quickly regenerating the tumor after treatment cessation and supporting relapses in a few months (5). Thus, a better understanding of tumor cells' response to irradiation is crucial for the comprehension of GBM aggressiveness.

The accelerated proliferation of GBM cells also drives the pronounced complexity of these tumors that typically encompasses a huge genetic diversity along with a heterogeneous microenvironment. The presence of hypoxic and hyper-perfused regions, redox gradients and different pro-inflammatory cytokines sustain a dynamic environment, promoting both the proliferative and infiltrative phenotypes (6). Also, a diversity of ECM proteins interacts with tumor and stromal cells and plays a central role in cellular communication, supplying growth factor production, migration and invasion (7, 8). The ECM is usually remodeled in tumor tissues and promotes desmoplasia, which is characterized by an increase in total levels of fibrillar collagen, fibronectin, proteoglycans, and tenascin C. These changes have been associated with tumor *stiffening*, which is a more rigid and resistant state that acquires at least 1.5-fold higher resistance to mechanical stress than the surrounding normal tissue. The *stiffening* state can promote epithelial to mesenchymal transition (EMT) that is also correlated with drug resistance and it is hypothesized to contribute to transformation of cancer cells in CSC (9).

Irradiation, the major therapeutic approach used to handle GBM, also produces important changes in the tumor microenvironment that may support resistance, proliferation and recurrence, such as: increased oxidative stress, hypoxia, neuroinflammation, altered expression of adhesion molecules, senescence induction and neo-angiogenesis. The high levels of radiation-induced reactive oxygen species (ROS) promote the remodeling of collagen and proteoglycans, activation of cellular proteases and changes in the cytoskeleton, contributing to development of senescent phenotypes (6). Metabolic changes also occur in tumor microenvironments in response to radiation-induced oxidative stress, such as increased production of antioxidant peptides and hypoxia generation. Radiation-induced stabilization/activation of HIF-1 (Hypoxia Inducible Factor 1) triggers protective processes by regulating downstream target genes that can stimulate immunosuppressive and anti-apoptotic responses (10). Another important aspect is the radiation-induced bystander effect, such as mitochondrial dysfunction, production of persistent or irreparable DNA damage, DDR (DNA damage response) activation, irreversible cell cycle arrest, and also the cellular senescence (6). Furthermore, GBM cells were reported to be able to constitutively activate senescence by blocking cyclin-dependent kinase inhibitors, for example p16 and p21 (11), which favors the release of pro-inflammatory signaling molecules and proteolytic enzymes (12).

Thus, the exposure of GBM to radiation can affect the composition of the ECM, altering the tumor proliferation and infiltration capabilities. These phenotypes are supported by the overexpression of diverse ECM proteins, including structural components (brevican, vitronectin, tenascin C, hyaluronin, lysyl oxidase), degradation enzymes (Matrix metalloproteinases) (13) and glioma-matrix interactors (ICAM-1, DDR-1, Integrins) (14, 15). Altogether, these data disclose that the relationship between tumor cells and the ECM supports the particularly infiltrative phenotype of GBM that is strongly correlated with radioresistance (16). As radiotherapy remains a primary treatment modality for gliomas, it is of great interest to better understand the acquisition of radioresistance of glioma cells and the targets to modify their tolerance to radiation. Different GBM cell lineages, such as U87MG, T98G, U251MG, are frequently used in studies of radioresistance (17–20). From clonogenic survival assays, the T98G cell line showed higher radioresistance when compared to the U87MG lineage, consistent with the lower levels of ATM kinase in U87MG cells (18). Differently, another study showed that U87MG presents higher resistance against irradiation (IR) than T98G cells and, in both cell lines, the radioresistance profile was correlated with mTOR/AKT activity, which is an important pathway not only for cell survival but also for the maintenance of astrocytic characteristics (20). It was also demonstrated that U87MG cells

are more radioresistant than the U251MG lineage. This behavior was associated with the cell cycle dynamics, which was prevalent in G1/S phases for U87MG and in G2/M for U251MG cells, and with the expression of the APE1 (Human Apurinic Endonuclease 1), an enzyme involved in base excision repair (19). Thus, although several studies have investigated radioresistance of GBM cell lines, the literature is divergent and a comprehensive analysis of gene expression profiling associated with cells' response to IR is still missing. These data would be of great importance since they will permit a wider understanding of the genetic heterogeneity of these cell lines and the molecular basis of the resistant phenotype of GBM cells.

In this work we have explored gene expression profiles of different GBM cell lines that present distinct phenotypes regarding radiation sensibility, aiming the identification of genetic characteristics correlated with radiation responsiveness. Using RNAseq data from five different GBM cell lines, we identified distinct profiles of deregulated genes in radioresistant *versus* sensitive cells. The ECM-cell interaction pathway was predominantly altered in irradiation-resistant cells (U87MG and U138MG), while the DNA damage response/DNA repair pathways were preferentially altered in irradiation-sensitive cells (T98G and U251MG). Consistently, T98G and U251MG cell lines presented the highest proliferation ratios, which is associated with replicative stress and is known to promote constitutive activation of DNA damage signaling. Among the genes positive or negatively associated with radioresistance, integrins were noteworthy. Furthermore, two integrins remarkably overexpressed in IR-resistant cells, integrin-α5 (ITGA5) and integrin-β1 (ITGB1), were validated by western blot and were also induced after IR treatment, confirming their enrollment in IR responsiveness. Importantly, we have also found 31 genes of the ECM-receptor interaction pathway, out of 83, correlated with poor responsiveness of patients to radiation treatment. Altogether, these data provide additional support to the enrollment of ECM-deregulation in the acquisition of IR-resistance and endorse the suitability of these cell lines for studies aiming the characterization of the genetic basis of radioresistant and/or proliferative phenotypes of GBM cells.

METHODS

Cell lines, Culture Conditions, and Treatment With Ionizing Radiation

The U87MG, U138MG, U251MG, and T98G cell lines were obtained from the American Type Culture Collection in 2010. U343MG cells were obtained from the laboratory of Prof. Carlos Gilberto Carlotti Junior, FMRP-USP, also in 2010. The ACBRI-371 non-tumor astrocytes were obtained from Cell Systems and gently provided by professor Elza Tiemi Sakamoto Hojo (FFCLRP-USP). Cells were grown in Dulbecco's Modified Eagle Medium (DMEM, Thermo Fisher Scientific) supplemented with 10% fetal bovine serum (Thermo Fisher Scientific) and incubated at 37°C and 5% CO_2. The cells were analyzed monthly by immunofluorescence after DNA staining for Mycoplasma detection. Cell line authentication was performed using STR profiling with the GenePrint® 10 System (Promega) following fabricant's instructions. Authentication was done and validated the identity of U87MG and T98G cell lines in 2017, and the majority of experiments were conducted in the following 6 months. Cells were treated with ionizing radiation at a dose exposure rate of 10 Gy (X-ray irradiator RS-2000, Rad Source) three times every 48 hours for cytotoxicity assay and at a single dose of 10 Gy for apoptosis/cell death and western blot analysis. To choose the radiation regimen, we carried out several previous experiments (data not shown) using the MTT essay to identify a radiation dose that was able to increase cell death ratios and was not excessively toxic for the cell lines studied here.

Cytotoxicity Assay, Cell Death Analysis, and Growth Curve

The cytotoxicity assay was carried out using the MTT (3- (4,5-dimethylthiazol-2-yl) -2,5-diphenyltetrazolium bromide) method. 500 cells were seeded in 96-well plates, grown for 24 hours and then irradiated three times every 48 hours. The MTT assay was performed 48 hours after the third irradiation treatment. The medium was removed and exchanged for 100 µL of fresh culture medium to cytotoxicity evaluation. Then, 10 µl of 12 mM MTT (3- (4,5-dimethylthiazol-2-yl) -2,5-diphenyltetrazolium bromide) was added over 3 hours at 37°C and 5% CO_2. After incubation, the crystals were diluted with isopropanol and read on plate reader at 570 nm. The data were analyzed by One-way ANOVA test. Differences were considered significant when $p < 0.05$. Apoptosis and effective cell death were measured using annexin V and propidium iodide staining. $8x10^4$ cells were seeded in 12 well plates, grown for 24 hours and irradiated. 48 hours after IR treatment, the cells were harvested, incubated with annexin V for 15 minutes and propidium iodide was added to a final concentration of 2 ng/µL. The cell suspension was immediately analyzed in a flow cytometer (FACSCanto, BD Biosciences). The data showed the average of three independent experiments. The results were analyzed by Kruskal–Wallis test (analysis of variance, ANOVA). Differences were considered significant when $p < 0.05$. For the growth curve, $1x10^3$ cells were seeded in 96 well plates and DNA content evaluated every 24 hours for 6 days. At each analysis point, the culture medium from each well was withdrawn, washed with PBS 1x, and fixed with 70% ethanol for 10 minutes. After, the DNA of the cells was stained with 0.05% crystal violet solution for 15 minutes. Next, the cells were washed and 10% acetic acid solution was added for 30 minutes to read on plate reader at 570 nm. The data were analyzed by Two-way ANOVA test. Differences were considered significant when $p < 0.05$. The statistical significance was represented by *$p<0.05$, **$p<0.001$ and ***$p<0.0001$. Graphs were plotted with GraphPad Prism 4.0 software.

RNA Extraction and Quantitative RT-PCR

RNA extraction was performed with RNeasy RNA extraction Kit (Qiagen) following the manufacturer's instructions.

RNA concentration and purity were determined in the spectrophotometer at 260–280 nm. The RNA was treated with DNAse I (Invitrogen) in the presence of an RNAse inhibitor (RNAseOUT; Invitrogen). Then, cDNA synthesis was performed using the High Capacity Kit (Applied Biosystems), also following the manufacturer's instructions. qPCR reactions were performed in the 7500 RealTime PCR System (Applied Biosystems) using Power SYBR Green PCR Master Mix (Applied Biosystems), according to manufacturer's recommendations. As previously described, HPRT was used as the control of constitutive expression. The calculations of relative expression were based on the $2^{-\Delta\Delta CT}$ equation (21). Statistical analyzes were performed with the One-way ANOVA test, using the GraphPad Prism 4.0 software.

SDS-Polyacrylamide Gel Electrophoresis and Western Blot

Protein samples were separated by electrophoresis in SDS-polyacrylamide gel (6%) and transferred to nitrocellulose membrane. The membrane was blocked with a TBST buffer (1X TBS, 0.25% Tween-20) containing 5% skimmed milk at room temperature for 60 minutes under stirring. The primary antibodies used were: anti-ITGA5 (Cell Signaling, #98204) at dilution 1:1000, anti-ITGB1 (Cell Signaling, #4706) at dilution 1:1000, anti-tubulin (ABCAM, ab7291) at dilution 1:10000, anti-phospho-AKT (Cell Signaling, #4060) at dilution 1:2000, anti-AKT (Cell Signaling, #4691) at dilution 1:1000 and anti-GAPDH (Cell Signaling, #5174) at dilution 1:1000. Images were captured by ChemiDoc™ Imaging System from Bio-Rad.

Pathway Enrichment and Patient Survival Curves

In order to identify cellular pathways enriched in treatment-resistant *versus* to sensitive GBM cells, we analyzed RNA sequencing data from different GBM cell lines that was previously generated in our laboratory (PRJNA631805). Genes presenting padj ≤ 0,0001 and log fold change > 2 in U87MG and/or U138MG cells (radio-resistant) compared to T98G and/or U251MG cells (radio-sensitive) were considered as differentially expressed. The list obtained for each comparison (**Supplementary Table 1**) was subjected to pathway analysis by KEGG through the website www.webgestalt.org (**Supplementary Table 2**). Pathway enrichment graphs were plotted with GraphPad Prism 4.0 software. For a refined understanding of expression variations among the genes included in enriched pathways, gene expression fold-changes of each GBM cell line relative to non-tumor astrocytes (ACBRI-371) were calculated and illustrated as heatmaps. Thus, gene expression levels in the different GBM cells were estimated considering ACBRI-371 cells as a reference.

We used the data available in The Cancer Genome Atlas (TCGA) database (https://www.synapse.org/#!Synapse:syn2812961) for survival analysis (**Supplementary Table 3**). To access the differences in survival based on ECM genes expression, we choose the best cutoff in expression value of each gene by calculating receiver operating characteristic (ROC) (22) curves for death incidence by time. Survival curves were plotted by the Kaplan-Meier method and compared by the log-rank test. Differences were considered significant when $p < 0.05$. Graphs were plotted with GraphPad Prism 4.0 software.

RESULTS

IR-Resistant GBM Cell Lines Show Higher Expression of ECM Genes and the Interacting Receptors

Here we profiled the sensitivity of different GBM cells to ionizing radiation (IR) in order to search for correlations between cell behavior and global gene expression patterns. The panel of cell lines analyzed included U87MG, U138MG, U251MG, U343MG and T98G, which show distinct proliferation indexes. U343MG and T98G cell lines proliferated significantly faster when compared to U87MG or U138MG, showing nearly 3.5 and 5-fold increment in cell number after six days of growing. U251MG exhibited intermediate proliferation rates, significantly differing only from T98G cells that showed 2-fold increment after six days of growing (**Figure 1A**). Cell viability was initially evaluated after three rounds of IR exposure, at a dose of 10 Gy in intervals of 48 hours. Two days after the last treatment, U251MG and T98G cultures showed only 5% and 15% of viable cells respectively, while U87MG and U138MG revealed approximately 40% of viability (**Figure 1B**). These data suggested that U87MG and U138MG cells present higher resistance against IR. However, this experiment does not inform if IR was causing cytotoxicity or a cytostatic disturb in the affected cells. To investigate each of these options were occurring, we evaluated apoptosis and cell death indexes after one round of IR exposure. Again, U87MG and U138MG cells did not exhibit any significant increment in apoptosis or cell death, while T98G and U251MG cultures presented increase only in effective cell death levels, showing 30% and 40% of dead cells, respectively (**Figure 1C**).

To better understand the molecular mechanisms underlying the competence of these cells in handling genotoxic insults and replicative stress, we further examined global transcriptional profiles available in our laboratory (23). RNAseq analysis revealed a collection of genes differentially expressed in each cell line analyzed when comparing resistant *versus* sensitive cells (**Supplementary Table 1**). Interestingly, IR-resistant cells presented higher expression levels of several ECM components and their related receptors (**Figure 2** and **Supplementary Table 2**). These pathways did not appear enriched when we evaluate the genes increased in radiation sensitive cell lines (**Supplementary Figure 1**). **Figure 3A** shows the relative expression levels of the ECM-receptor interaction genes that significantly varied among GBM cell lines, using non-tumor astrocytes as a reference. Although each cell line revealed a particular set of altered genes, we also observed that the resistant cells (U87MG+U138MG) share several overexpressed genes belonging to the ECM-receptor pathway, indicating promising radio-resistance biomarkers (**Supplementary Table 2**). Additionally, resistant cells usually

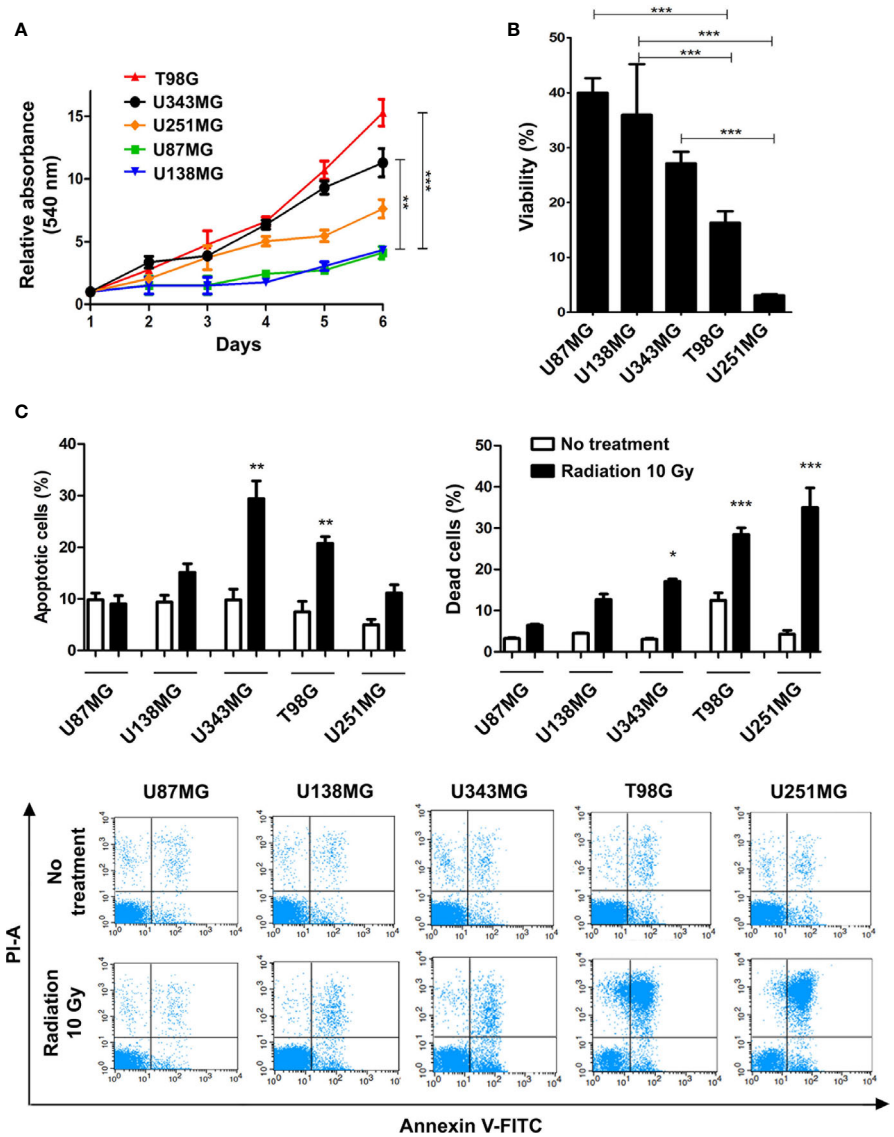

FIGURE 1 | Proliferation and ionizing radiation resistance analysis in GBM cell lines. **(A)** Proliferation assay of T98G, U343MG, U251MG, U87MG, and U138MG. **(B)** Cytotoxicity assay of GBM cells after radiation treatment. **(C)** Quantification of apoptosis and cell death of GBM cells after irradiation are shown in the upper graphics and representative images of flow cytometry experiments are presented in the lower panel. Error bars represent the SEM of 3 independent experiments. Graphs were plotted with GraphPad Prism 4.0 software. *p < 0.05, **p < 0.001, and ***p < 0.0001.

show overexpression of both, receptors and their ligands simultaneously, while in sensitive cells the overexpression is found only in either receptor or ligand (**Supplementary Table 4** and **Supplementary Figure 2**). These data suggested that the downstream PI3K signaling pathway would not be effectively activated in IR-sensitive cells. Alterations observed in the heatmap of **Figure 3A** were validated by qPCR for a set of five genes arbitrarily selected, namely: ITGA3, ITGA5, ITGA8, LAMB1 and LAMA2. The expression levels of ITGA3 and ITGA5 were significantly higher in U87MG and U138MG cells, ITGA8 and LAMB1 were increased in T98G, and U138MG showed higher levels of LAMA2 (**Supplementary Figure 3**), confirming RNAseq analysis consistency. Two genes presenting increased levels in the resistant cells, ITGA5 and ITGB1, were also examined by western blot (**Figure 3B**) and protein overexpression was confirmed. Since ITGB1 and ITGA5 have been previously described as key players in the acquisition of radioresistance by GBM cells (24–27), we can presume a strength confidence in the correlation between the set of genes identified in our study with IR resistance. Once ITGA5/ITGB1 were also described as responsive to IR, we evaluated their expression levels after IR-treatment. **Figure 3C** shows that both analyzed receptors presented increased protein amounts between 24 and 48 hours after treatment, confirming the requirement of these proteins for radiation

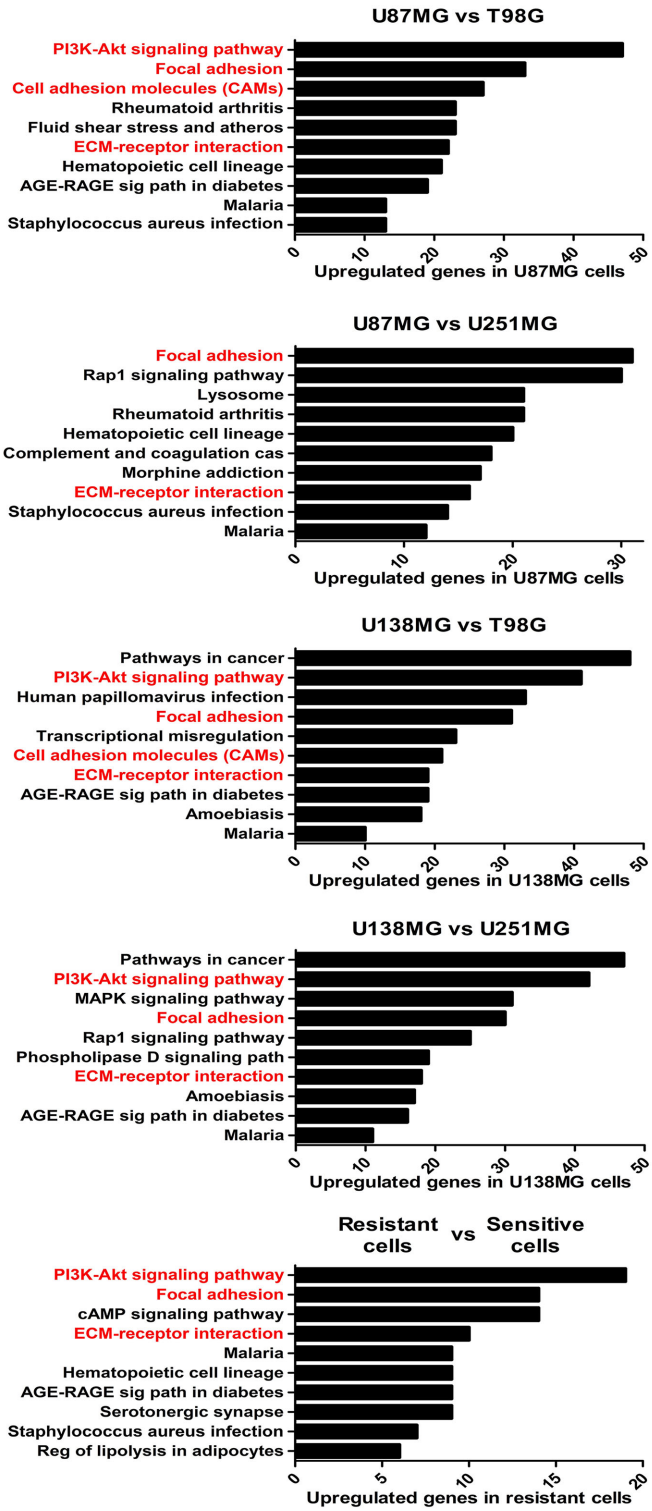

FIGURE 2 | The enriched KEGG pathways in treatment-resistant cells in comparison to sensitive cells. All genes with padj ≤ 0,0001 and log fold change > 2 in U87MG and/or U138MG cells compared to T98G and/or U251MG cells were subjected to pathway analysis by KEGG. The pathways related to cell-extracellular matrix interaction were highlighted in red. A False Discovery Rate (FDR) ≤ 0.05 was used as a threshold to select significant pathways. Graphs were plotted with GraphPad Prism 4.0 software.

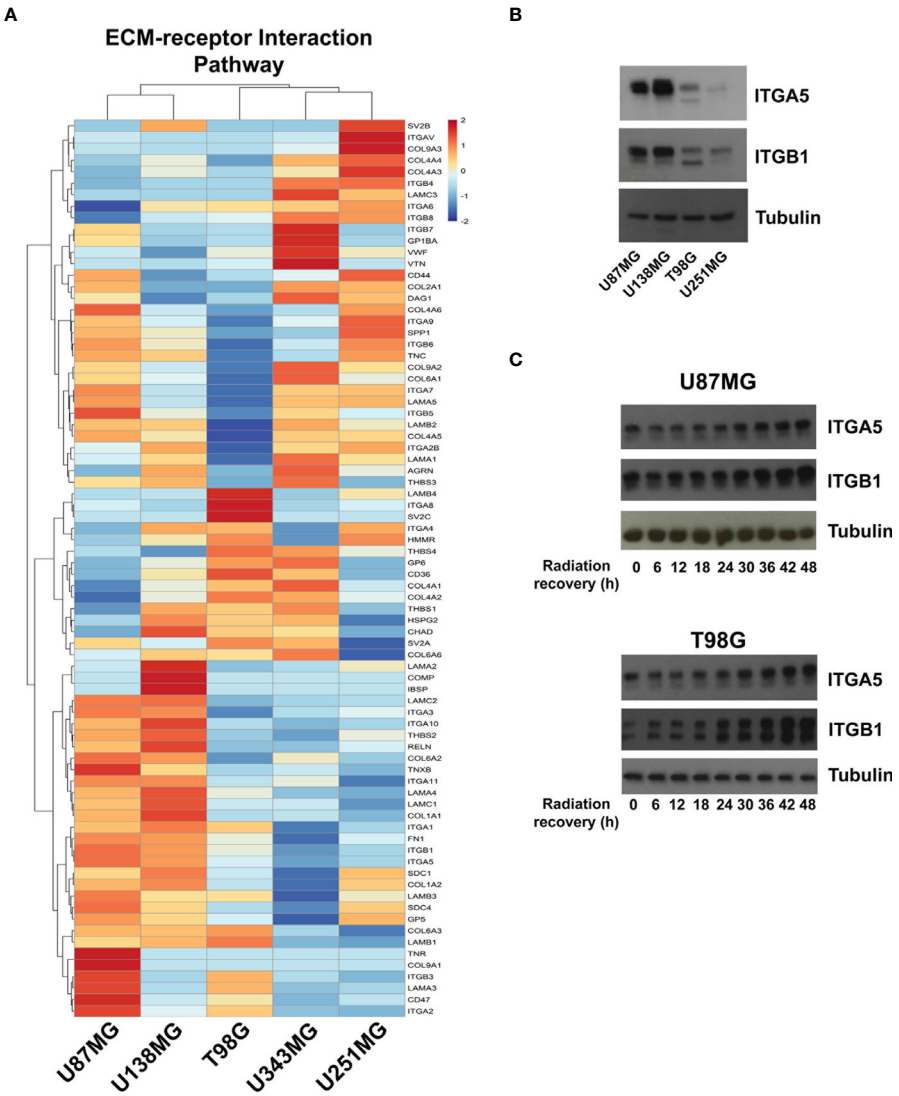

FIGURE 3 | Expression profile of the ECM-receptor interaction genes in GBM cell lines. **(A)** Heatmap of the relative expression of genes enriched in the ECM-receptor interaction pathway, estimated expression in each GBM cell line relative to non-tumor astrocytes (ACBRI-371) are shown. **(B)** Western blot validating ITGA5 and ITGB1 expression in U87MG, U138MG, T98G, and U251MG cell lines. **(C)** Protein samples were collected 0, 6, 12, 18, 24, 30, 36, 42, and 48h after irradiation treatment with 10 Gy and the ITGA5 and ITGB1 protein levels assessed by western blot. The two bands detected for these integrins correspond to the precursor (upper band) and mature (lower band) forms of the protein, and variations are commonly observed depending on the cell line analyzed.

responsiveness. Therefore, the endogenous high levels observed in resistant cells and the additional induction promoted by IR, corroborate they indeed play an important role in cellular response to IR, and support that all genes identified here are potentially enrolled in radioresistance acquisition by GBM cells.

Several ECM genes are able to activate the PI3K signaling pathway as a survival mechanism. Thus, we evaluated whether AKT inhibition would sensitize U87MG and U138MG cells to radiation. We observed that AKT levels did not vary between the evaluated cell lines (**Supplementary Figures 4A, B**), however, U87MG and U251MG cells showed higher ratios of AKT phosphorylation at the position S473 (**Supplementary Figure 4B**). Thus, to assess the effects of AKT inhibition in IR resistance, cells were treated with the potent pan-AKT kinase inhibitor GSK690693, for 4 hours followed by irradiation with a dose of 10 Gy. After 48 hours, we observed that the AKT inhibitor was able to increase IR-sensibility of T98G cells at all concentrations evaluated, of U251MG cells at 20 and 30 μM and of U138MG cells only at 30 μM. Although T98G and U251MG showed higher amounts of dead cells when receiving radiation combined with the inhibitor, we did not see any increase in cell death levels for U87MG and a only slight increase for U138MG in the highest concentration of the inhibitor. This result suggested that AKT is not essential for the elevated resistance presented by U87MG and U138MG cell lines. Once other kinases, such as AMPK and DAPK3, might also be affected by

the pan-inhibitor we utilized, we could speculate that these kinases, likewise, do not favor sensitization of the resistant GBM cell lines. However, the effect of the combined treatment was shown to be more effective in U251MG cells, indicating that cell lines with reduced amount of upregulated ECM genes are more dependent on the PI3K pathway. Altogether, these data suggest that the set of 31 ECM-receptor genes we found overexpressed in the resistant cell lines activates an extensive pro-survival signaling network that work collectively to sustain IR-resistance in GBM cells.

Alterations in DNA Repair Pathways Are Enriched in the GBM Cell Lines Presenting Higher Proliferation

We also investigated if alterations in the expression of DNA repair genes exhibit any association with resistance to ionizing radiation. Actually, we did not observe correlations between variations in the expression of DNA repair genes and IR resistance among the different cell lines analyzed. Also, we observed that these pathways, mainly the Mismatch Repair (MMR) and the Homologous Recombination (HR) pathways, are enriched in cells that showed higher proliferative potential (**Figure 4** and **Supplementary Figure 5**). To confirm the association between DNA repair genes expression and proliferation activity in GBM samples, we searched for correlations between the expression of MKI67, and MMR and HR genes, using the TCGA (The Cancer Genome Atlas) data. We observed that 64.7% and 46.8% of the genes from the MMR and HR pathways show a meaningful Spearman correlation with MKI67 (>0.5), which is comparable with the correlation exhibited by 75.8% of the genes belonging to the DNA replication machinery. Although we did not observe enrichment for genes of the Nucleotide Excision Repair (NER), Base Excision Repair (BER), and Non-Homologous End-Joining (NHEJ) repair pathways in the more proliferative cell lines, these pathways also showed association with MKI67, but at lesser extent, of 37.5%, 29.4% and 21.4%, respectively (**Supplementary Table 5**). These data indicated a tougher association of DNA

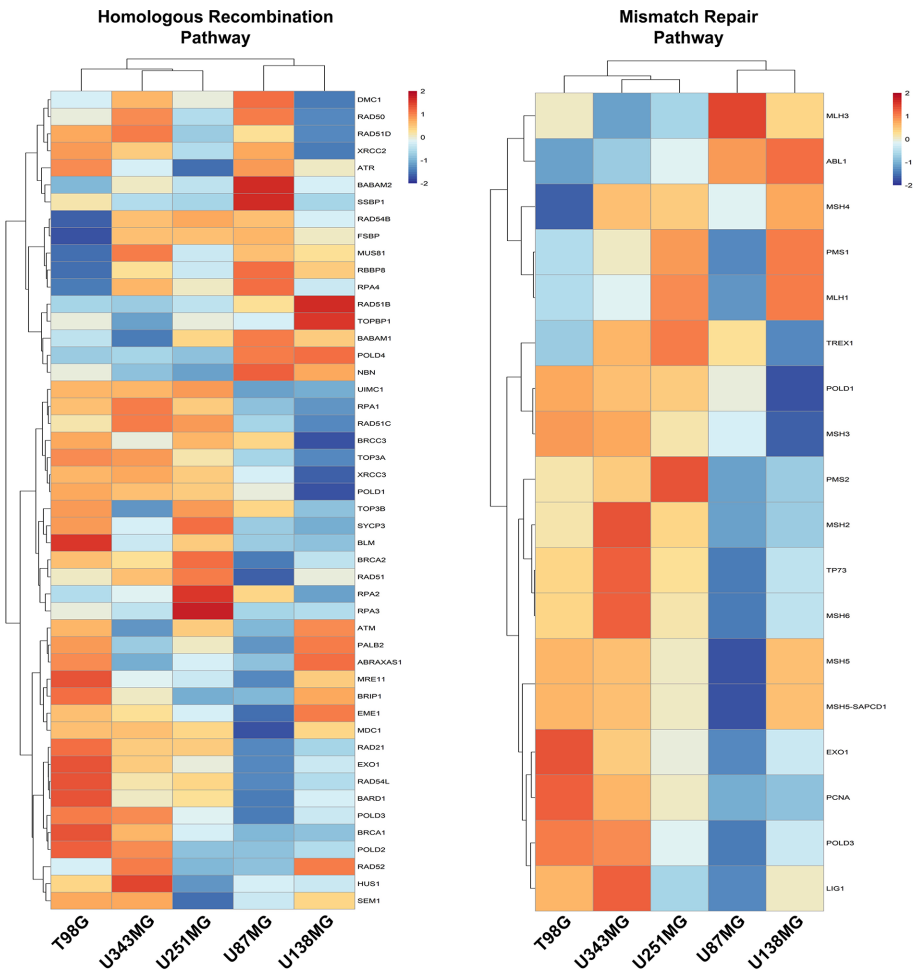

FIGURE 4 | Homologous Recombination and Mismatch Repair pathways are enriched in proliferative GBM cell lines. Heatmaps representative of the expression of genes from the Homologous Recombination and Mismatch Repair pathways were generated with the data from each GBM cell line relative to non-tumor astrocytes (ACBRI-371).

repair alterations with the proliferative activity than with the radio-resistance.

ECM-Receptor Signature Derived From IR-Resistant Cells Correlate With Radiation Responsiveness of LGG Patients

Next, we seek to understand if the high levels of the ECM-receptor genes were correlated with IR response of lower-grade glioma (LGG) patients from the TCGA database, for which RNAseq data and clinical information were publicly accessible. We have chosen the LGG cohort due to availability of gene expression data and treatment protocols for the majority of samples characterized, whereas for the GBM cohort, treatment regimens are missing for many cases. For this analysis, we separated the patients into 4 groups: i) untreated patients whose tumors expressed low-levels of the analyzed gene; ii) untreated patients whose tumors expressed high-levels of the analyzed gene; iii) irradiated patients whose tumors expressed low-levels of the analyzed gene; iv) irradiated patients whose tumors expressed high-levels of the analyzed gene. Initially, the ROC (Receiver Operating Characteristic) curve was constructed to define the threshold between low and high levels of expression for each target gene (**Supplementary Table 6**). Then, the survival of patients with low or high expression was evaluated. We observed that the increased expression of 31 ECM-receptor genes was correlated with worse prognosis in irradiated patients (**Figure 5**). Importantly, patients selected for radiation treatment show an intrinsic poorer survival prognosis than patients not selected for treatment (**Supplementary Figure 6**), but inside the group of irradiated patients we indeed detected significant differences. In addition, we did not observe changes in survival among non-irradiated patients. These data revealed that individuals with low expression of ECM-receptor genes presented improved response to IR, showing significantly increased survival when compared to patients with high expression of the ECM-receptor signature. We also found 7 genes for which augmented expression is associated with patients' prognosis, regardless they were treated or not with IR (**Supplementary Figure 7**).

Finally, we evaluated if the progressive accumulation of up-regulated genes would impact the resistance of tumors to irradiation. For this, we defined six categories with an increasing number of altered genes, from up to 5 until 30, and evaluated the survival of patients, submitted to IR treatment, belonging to each class. We observed that among patients who survived for more than 5 years after diagnosis, 54% showed up to 10 overexpressed genes from the signature identified, 43% had up to 20, and only 2% exhibited more than 21 overexpressed genes (**Figure 6A**). However, among patients who died before 5 years of diagnosis, 5% showed up to 10 overexpressed genes, 52% revealed up to 20 up-regulated genes and 41% exhibited from 21 to 30 increased genes (**Figure 6A**). Kaplan-meier curves illustrate the survival of patients included in each category (**Figure 6B**). These data revealed that the number of genes from the ECM-receptor signature is a strong predictor of the response to radiotherapy, and suggests that patients displaying more than 20 overexpressed genes do not benefit from treatment.

DISCUSSION

Although radiotherapy is the main choice among the available treatments for GBM, it is known that this type of therapy induces high levels of genomic instability and considerable alterations in tumor microenvironment. An important consequence of RT is the remodeling of the extracellular matrix, promoting upregulation of several ECM proteins, such as: structural components, ligand-receptors, proteases and regulators of tumor cells adaptation. Altogether, these alterations culminate in increased survival, proliferation, migration, invasion and angiogenesis, supporting the prominent aggressiveness and the frequent recurrences of GBM (6). In this study, we evaluated irradiation-induced cell death levels and observed that the GBM cells with lower proliferation levels, U87MG and U138MG, are more resistant to ionizing radiation (IR) and present many overexpressed genes associated with the ECM-receptor interaction pathway. According to our observations, it has been shown that GBM cells are able to remodel the associated ECM by promoting coordinated alterations in cell adhesion, which were mediated mainly by molecules such as integrins and cadherins, and cell detachment, caused by ECM degrading proteases (28). On the other hand, cells with higher proliferation ratios, such as T98G and U251MG, were more sensitive to IR and presented upregulation of several genes involved in DNA damage response, whose expression was also positively correlated with MKI67. The phenotype observed in the radiosensitive cell lines might be explained by the elevated cellular proliferation, which leads to replicative stress and induces genomic instability, promoting constitutive activation of the DNA damage signaling (29). Thus, the additional stress exogenously promoted by irradiation could potentiate the intrinsic replicative stress of these cells, intensifying cell death ratios. Among the cell lines utilized in our work, U87MG and U251MG were widely used in former studies for intracranial xenograft implants and showed the capability of inducing highly invasive tumors, containing nuclear atypia, hypercellularity, pleomorphism, and angiogenesis (30). However, cell proliferation indexes from tumors generated by these two cell lines were not evaluated in a comparable manner. It was also demonstrated that transcriptional profiles are drastically modified when *in vivo* models are used (31). This phenomenon implicates that cell behavior and the associated expression patterns might be divergent from that observed in the 2D culture model explored here. However, the clinical relevance of the genes identified in our study as biomarkers of IR-responsiveness was corroborated by the correlation between their expression levels and the response of glioma patients to radiotherapy.

Within the ECM-receptor interaction pathway, integrins are noteworthy. Integrins have been shown to play important roles

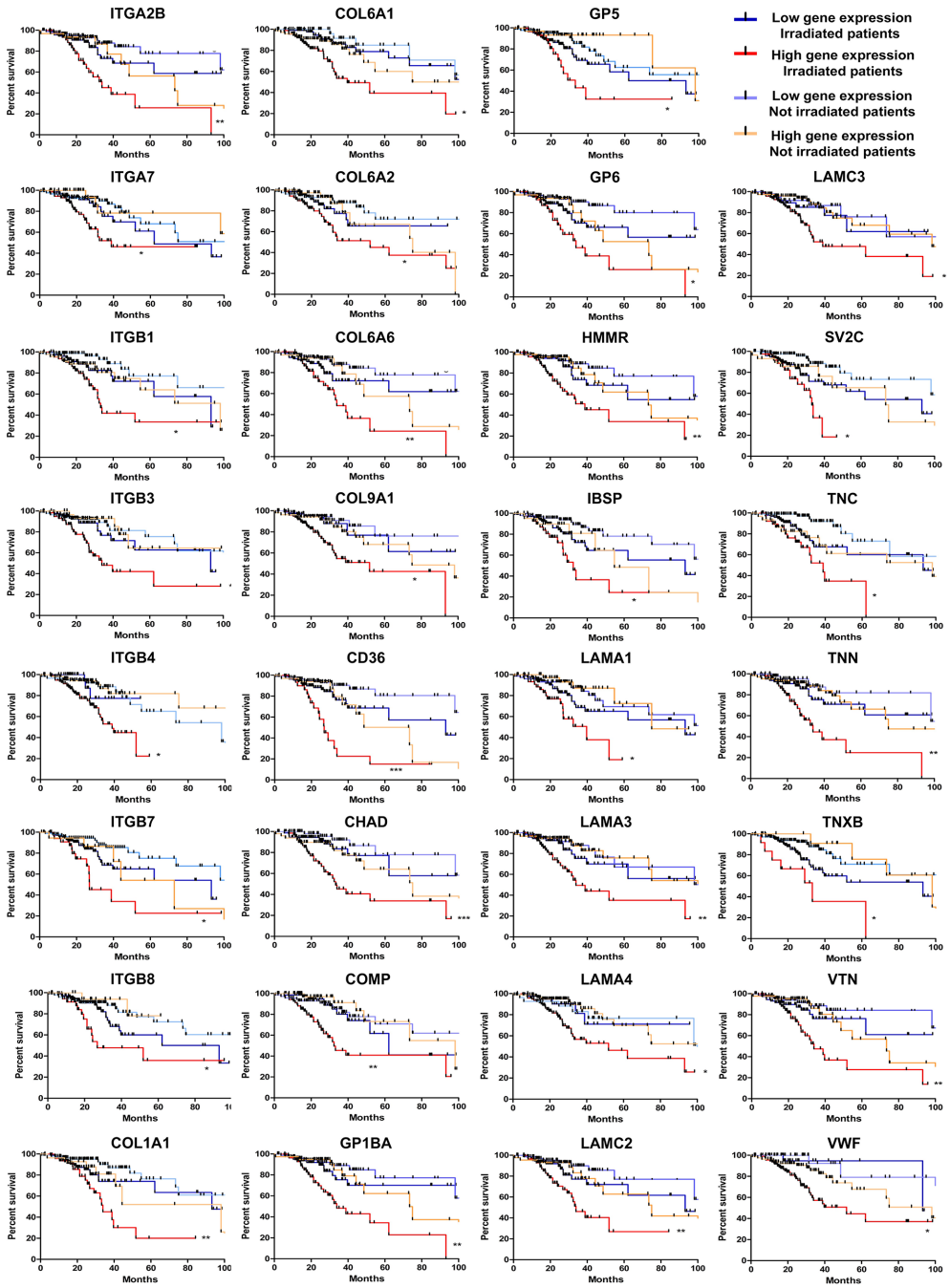

FIGURE 5 | High levels of 31 ECM-receptor interaction transcripts are correlated with poor survival prognosis of radiation-treated patients. Kaplan Meier survival curves for LGG patients according to expression levels of the ECM-receptor interaction genes in the tumors. Patients were divided into four groups: i) untreated patients whose tumors expressed low levels of the analyzed gene; ii) untreated patients whose tumors expressed high levels of the analyzed gene; iii) irradiated patients whose tumors expressed low levels of the analyzed gene; iv) irradiated patients whose tumors expressed high levels of the analyzed gene. *$p < 0.05$, **$p < 0.001$, and ***$p < 0.0001$. The P-values were obtained from a log-rank test. Graphs were plotted with GraphPad Prism 4.0 software.

in tumor microenvironment, being involved in the control of cell survival, proliferation, migration and invasion, since they activate pathways like FAK (focal adhesion kinase) and PI3K/AKT (phosphoinositide 3-kinase/protein kinase B) (7). According to our data, deregulation in integrin signaling were formerly associated with cancer (32). Several integrin subunits are overexpressed during astrocytoma progression and showed competence to promote invasion, angiogenesis, and radioresistance (33). Among the molecular subtypes of GBM, mesenchymal tumors are considered the most invasive and

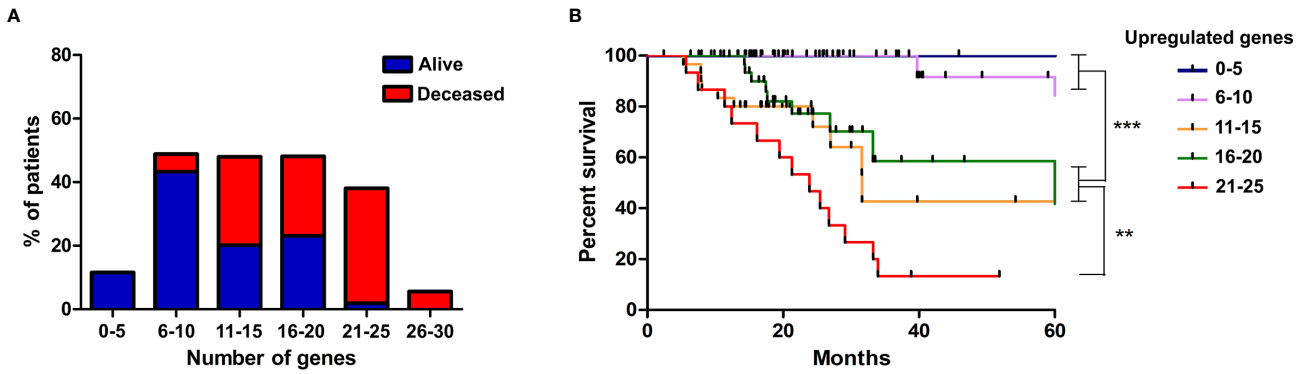

FIGURE 6 | The progressive accumulation of up-regulated ECM-receptor interaction genes impacts the resistance of tumors to irradiation. **(A)** The number of genes with expression above the threshold defined by the ROC curve was evaluated in each patient submitted to IR treatment and six categories, with an increasing number of altered genes, were defined. The percentage of alive or deceased patients included in each category is indicated. **(B)** Kaplan Meier survival curves for LGG patients according to the categories described in **(A)**. Graphs were plotted with GraphPad Prism 4.0 software.

angiogenic (34, 35). Coincidentally, this subtype demonstrated global overexpression of integrins compared to others (33), highlighting integrins as attractive therapeutic targets for mesenchymal GBMs.

Curiously, distinct integrins were altered in either sensitive or resistant cell lines, such as ITGA6, ITGA8, ITGAV, ITGB4 and ITGB8 overexpressed in the sensitive cells, and ITGA3, ITGA5, ITGA10, ITGA11, ITGB1 and ITGB7 increased in the resistant cell lines. Considering the set of integrins upregulated in radioresistant cell lines, ITGB1, ITGA5 and ITGA3 were previously reported as associated with IR resistance. ITGB1 stabilizes RAD51 thus, favoring DNA double strand breaks repair by homologous recombination. This is enabled by the reduction of proteasome-mediated RAD51 degradation *via* RING-1 (24). Additionally, ITGB1 physically interacts with EGFR and increases *in vitro* resistance of GBM cells to IR in an AKT phosphorylation dependent manner, and has been related to worse prognosis of GBM patients (25). When dimerized with ITGA5, ITGB1 also promotes greater resistance of GBM cells by regulating the levels of the anti-apoptotic proteins Survivin and PEA-15 (26). Here we also demonstrated that ITGB1 and ITGA5 protein levels were gradually upregulated when we treated GBM cell lines with ionizing radiation, indicating that these proteins are IR-responsive. Accordingly, it has been shown that GBM cells present ITGB1 upregulation after irradiation, as well as radiosensitization when ITGB1 was silenced (27). In addition, radiation-induced upregulation of ITGB1 has been demonstrated *in vitro* and *in vivo* in prostate cancer cells (36), as well as upregulation of ITGA5 on colorectal tumor cells after X-ray irradiation (37). Furthermore, the mRNA expression of the genes comprising the CD151-ITGA3-ITGB1 complex is correlated to lower survival rates in GBM patients probably as a consequence of the synergistic effect with the EGF/EGFR pathway, which gives GBM cells greater motility and invasion (38). Since several ECM components activate the PI3K/AKT pathway, we also decided to investigate whether radioresistance is a consequence of this activation. However, after inhibiting AKT and simultaneously irradiating the resistant cell lines, we did not observe considerable sensitization, thus indicating that the ECM-receptor genes found as overexpressed do not depend solely on AKT signaling to promote radioresistance in the cell lines here studied and that other pathways might be involved. Regarding the integrins upregulated in sensitive cells, we observed higher amounts of ITGA6, which is able to regulate CHK1 and cdc25 levels in primary cultures of GBM neurospheres and is therefore important for the ATR signaling (39). In addition, ITGA6 was reported to induce the expression of the ZEB1 transcription factor and, consequently, the FGFR1 proliferation inducer (target of the ZEB1/YAP1 complex) (39). Thus, it could be suggested that ITGA6 might have a role in reducing the replicative stress of highly proliferative cells.

Additionally, we have also found that 31 genes of the ECM-receptor interaction pathway, out of 83, correlated with poor responsiveness of patients to radiation treatment. Supporting our findings, some of the genes contained in this signature were previously described as correlated to radioresistance. COL1A1, ITGB4 and VTN have been associated with radioresistance in different types of cancer, such as nasopharyngeal carcinoma, esophageal squamous cell carcinoma and head and neck cancer (40–42). Furthermore, although not correlating to response to irradiation, recent studies have shown that COL1A1, ITGA7, ITGB3, ITGB4, HMMR and IBSP upregulation confer low survival rate to glioma patients (43–48). Importantly, we have shown that the majority of patients with up to 10 simultaneously upregulated genes survive more than 5 years, while for most of the patients with more than 10 upregulated genes the prognosis is remarkably worse, with an overall survival lower than 5 years. It is also relevant to emphasize that radioresistant cells usually presented receptors and the respective ligands simultaneously upregulated, differently from the sensitive cell lines that eventually showed upregulation of either the receptor or the corresponding ligand. Thus, our results indicated that the upregulation of at least 21 ECM-receptor interaction genes is

important for the acquisition of a radioresistant phenotype, mostly when both receptor and ligand are included.

In conclusion, our results corroborate with recent studies that have shown the ECM-receptor interaction pathway as an important driver of glioma radioresistance. More importantly, we identified for the first time, new markers of the ECM pathway correlated with GBM IR-resistance, namely: ITGA2B, ITGA7, ITGB4, ITGB7, COL1A1, COL6A1, COL6A2, COL6A6, COL9A1, CD36, CHAD, COMP, GP1BA, GP5, GP6, HMMR, IBSP, LAMA1, LAMA3, LAMA4, LAMC2, LAMC3, SV2C, TNC, TNN, TNXB, VTN and VWF. Notably, the genes identified as correlated with IR responsiveness in individual cell lines were validated in clinical data as biomarkers of patient response to radiotherapy. Additionally, the cell lines studied here proved to be useful models for functional experiments involving mechanistic investigations regarding IR resistance and proliferation capacity, once they can be explored as representative of different adaptive states of tumor cells. This group of genes could also be explored for screening patients who would benefit from radiotherapy and, moreover, represent promising targets for the development of adjuvant therapies that will possibly improve the outcome of patients with highly radioresistant gliomas.

DATA AVAILABILITY STATEMENT

The original contributions presented in the study are included in the article **Supplementary Material**. Further inquiries can be directed to the corresponding author.

AUTHOR CONTRIBUTIONS

Investigation, RS, PS, CC, LM, RN, RA, GN, CS, JS, and FS. Conceptualization, RS and VV. Formal Analysis, RS. Writing – original draft, RS, RA, GN, LP, and VV. Writing – Review and Editing, VV. Supervision and Resources, RP, CM, WS, and VV. Funding Acquisition, WS and VV. All authors contributed to the article and approved the submitted version.

FUNDING

This work was supported by Fundação de Amparo à Pesquisa do Estado de São Paulo (FAPESP) (grants #2013/13465-1 and #2018/05018-9 to VV and grant #2013/08135-2 to WS), and by the Programa de Apoio ao Desenvolvimento Científico from the Faculty of Pharmaceutical Sciences of Araraquara (PADC). This study was also financed in part by the Coordenação de Aperfeiçoamento de Pessoal de Nível Superior – Brasil (CAPES) - Finance Code 001. RS received a post-doctoral fellowship from CAPES (#88887.369191/2019-00). CAPES also supported LM, GN, and CS; CNPq (Conselho Nacional de Desenvolvimento Científico e Tecnológico) supported CC and RN; and FAPESP supported PS (#2016/12744-2 and #2018/22799-4) and RA (#2017/15208-7 and #2019/24335-8).

ACKNOWLEDGMENTS

The authors thank Silvia Regina Andrade Nascimento for laboratory technical assistance, and Leandro Federiche Borges and Alexandre Colello Bruno for the support with cell irradiation procedures.

SUPPLEMENTARY MATERIAL

The Supplementary Material for this article can be found online at: https://www.frontiersin.org/articles/10.3389/fonc.2021.668090/full#supplementary-material

Supplementary Figure 1 | The enriched KEGG pathways in treatment-sensitive cells in comparison to resistant cells. All genes with padj ≤ 0,0001 and log fold change > 2 in T98G and/or U251MG cells compared to U87MG and/or U138MG cells were subjected to pathway analysis by KEGG. The pathways related to cell-extracellular matrix interaction were highlighted in red. A False Discovery Rate (FDR) ≤ 0.05 was used as a threshold to select significant pathways. Graphs were plotted with GraphPad Prism 4.0 software.

Supplementary Figure 2 | Interaction map of de-regulated genes from the ECM-receptor pathway according to KEGG analysis. Genes shown in red are upregulated in each indicated cell line, whereas genes shown in black did not present expression alteration. The figure was adapted from KEGG analysis result.

Supplementary Figure 3 | qPCR validation of the RNAseq data. The expression of the ITGA3, ITGA5, ITGA8, LAMB1 and LAMA2 genes was evaluated in U87MG, U138MG, T98G and U251MG cells by qPCR. The relative expression of target mRNAs was normalized by HPRT. The non-tumor astrocytes ACBRI371 cells were used as reference for relative expression calculations. Graphs were plotted with GraphPad Prism 4.0 software. *p < 0.05, **p < 0.001, and ***p < 0.0001.

Supplementary Figure 4 | AKT inhibition sensitizes U251MG cells to ionizing radiation. **(A)** The RNAseq data was used to obtain the number of reads per AKT1, AKT2 and AKT3 transcripts in U87MG, U138MG, T98G and U251MG cells. **(B)** AKT expression level and its phosphorylation ratio in U87MG, U138MG, T98G and U251MG cells. **(C)** Analysis of cell death after AKT inhibition and treatment with ionizing radiation. U87MG, U138MG, T98G and U251MG cells were treated with GSK690693 for 4 hours and irradiated with 10 Gy. Graphs were plotted with GraphPad Prism 4.0 software. **p < 0.001, and ***p < 0.0001.

Supplementary Figure 5 | Nucleotide Excision Repair, Base Excision Repair and Non-homologous End-joining pathways in GBM cell lines. Heatmap of Nucleotide Excision Repair, Base Excision Repair and Non-homologous End-joining genes in U87MG, U138MG, T98G, U251MG and U343MG cells.

Supplementary Figure 6 | Patients selected for treatment with ionizing radiation have worse survival prognosis. Kaplan Meier survival curves for LGG patients treated or not treated with ionizing radiation. **p < 0.001. The P-value was obtained from a log-rank test. Graphs were plotted with GraphPad Prism 4.0 software.

Supplementary Figure 7 | High levels of 7 ECM-receptor interaction transcripts are correlated with poor survival prognosis in radiation-treated and non-treated patients. Kaplan Meier survival curves for LGG patients according to the ECM-receptor interaction genes expression levels in the tumors. Patients were divided into four groups: i) untreated patients whose tumors expressed low levels of the analyzed gene; ii) untreated patients whose tumors expressed high levels of the analyzed gene; iii) irradiated patients whose tumors expressed low levels of the

analyzed gene; iv) irradiated patients whose tumors expressed high levels of the analyzed gene. *P < 0.05, **p < 0.001, and ***p < 0.0001. The P-values were obtained from a log-rank test. Graphs were plotted with GraphPad Prism 4.0 software.

Supplementary Table 1 | Genes identified as differentially expressed in the comparisons between IR-resistant and sensitive cells. All genes with padj ≤ 0.0001 and log fold change > 2 were selected as differentially expressed in each indicated comparison.

Supplementary Table 2 | Enriched KEGG pathways in each comparison of IR-resistant *versus* sensitive cells. All genes with padj ≤ 0.0001 and log fold change > 2 or < -2 of each comparison were subjected to pathway analysis by KEGG.

Supplementary Table 3 | Clinical and expression data of LGG patients used in survival analysis. The clinical data of patients from the lower-grade glioma cohort and expression levels of the selected ECM-receptor interaction genes were downloaded from The Cancer Genome Atlas (TCGA) database (https://www.synapse.org/#!Synapse:syn2812961) and used for survival analysis.

Supplementary Table 4 | Number of receptors, ligands and pair of ligand-receptors upregulated in each GBM cell line. The receptors and ligands were considered upregulated when padj ≤ 0.0001 and log fold change > 2.

Supplementary Table 5 | Correlation between de-regulated genes from different categories and MKI67 expression. Data were obtained from the cbioportal.org website. Spearman's Correlation > 0.5 was used as a threshold.

Supplementary Table 6 | Values of expression threshold determined as adequate to define high and low expression of each gene utilized in the survival analysis. The receiver-operating characteristic (ROC) curves for death incidence by time were used to determine the expression cutoff.

REFERENCES

1. Brandes AA, Tosoni A, Franceschi E, Reni M, Gatta G, Vecht C. Glioblastoma in Adults. *Crit Rev Oncol Hematol* (2008) 67(2):139–52. doi: 10.1016/j.critrevonc.2008.02.005
2. Manini I, Caponnetto F, Bartolini A, Ius T, Mariuzzi L, Di LC, et al. Role of Microenvironment in Glioma Invasion: What We Learned From In Vitro Models. *Int J Mol Sci* (2018) 19(1):147. doi: 10.3390/ijms19010147
3. Stupp R, Hegi ME, Gilbert MR, Chakravarti A. Chemoradiotherapy in Malignant Glioma: Standard of Care and Future Directions. *J Clin Oncol* (2007) 25(26):4127–36. doi: 10.1200/JCO.2007.11.8554
4. Zeppernick F, Ahmadi R, Campos B, Dictus C, Helmke BM, Becker N, et al. Stem Cell Marker CD133 Affects Clinical Outcome in Glioma Patients. *Clin Cancer Res* (2008) 14(1):123–9. doi: 10.1158/1078-0432.CCR-07-0932
5. Liau BB, Sievers C, Donohue LK, Gillespie SM, Flavahan WA, Miller TE, et al. Adaptive Chromatin Remodeling Drives Glioblastoma Stem Cell Plasticity and Drug Tolerance. *Cell Stem Cell* (2017) 20(2):233–46.e7. doi: 10.1016/j.stem.2016.11.003
6. Gupta K, Burns TC. Radiation-Induced Alterations in the Recurrent Glioblastoma Microenvironment: Therapeutic Implications. *Front Oncol* (2018) 8(NOV):1–11. doi: 10.3389/fonc.2018.00503
7. Ellert-Miklaszewska A, Poleszak K, Pasierbinska M, Kaminska B. Integrin Signaling in Glioma Pathogenesis: From Biology to Therapy. *Int J Mol Sci* (2020) 21(3):888. doi: 10.3390/ijms21030888
8. Virga J, Szivos L, Hortobágyi T, Chalsaraei MK, Zahuczky G, Steiner L, et al. Extracellular Matrix Differences in Glioblastoma Patients With Different Prognoses. *Oncol Lett* (2019) 17(1):797–806. doi: 10.3892/ol.2018.9649
9. Gkretsi V, Stylianopoulos T. Cell Adhesion and Matrix Stiffness: Coordinating Cancer Cell Invasion and Metastasis. *Front Oncol* (2018) 8 (MAY):145. doi: 10.3389/fonc.2018.00145
10. Kim YH, Yoo KC, Cui YH, Uddin N, Lim EJ, Kim MJ, et al. Radiation Promotes Malignant Progression of Glioma Cells Through HIF-1alpha Stabilization. *Cancer Lett* (2014) 354(1):132–41. doi: 10.1016/j.canlet.2014.07.048
11. Stein GH, Drullinger LF, Soulard A, Dulić V. Differential Roles for Cyclin-Dependent Kinase Inhibitors p21 and p16 in the Mechanisms of Senescence and Differentiation in Human Fibroblasts. *Mol Cell Biol* (1999) 19(3):2109–17. doi: 10.1128/MCB.19.3.2109
12. Jeon HY, Kim JK, Ham SW, Oh SY, Kim J, Park JB, et al. Irradiation Induces Glioblastoma Cell Senescence and Senescence-Associated Secretory Phenotype. *Tumor Biol* (2016) 37(5):5857–67. doi: 10.1007/s13277-015-4439-2
13. Park CM, Park MJ, Kwak HJ, Lee HC, Kim MS, Lee SH, et al. Ionizing Radiation Enhances Matrix Metalloproteinase-2 Secretion and Invasion of Glioma Cells Through Src/Epidermal Growth Factor Receptor-Mediated p38/Akt and Phosphatidylinositol 3-Kinase/Akt Signaling Pathways. *Cancer Res* (2006) 66(17):8511–9. doi: 10.1158/0008-5472.CAN-05-4340
14. Kesanakurti D, Chetty C, Rajasekhar Maddirela D, Gujrati M, Rao JS. Essential Role of Cooperative NF-κb and Stat3 Recruitment to ICAM-1 Intronic Consensus Elements in the Regulation of Radiation-Induced Invasion and Migration in Glioma. *Oncogene* (2013) 32(43):5144–55. doi: 10.1038/onc.2012.546
15. Wild-Bode C, Weller M, Rimner A, Dichgans J, Wick W. Sublethal Irradiation Promotes Migration and Invasiveness of Glioma Cells: Implications for Radiotherapy of Human Glioblastoma. *Cancer Res* (2001) 61(6):2744–50.
16. Ulrich TA, De Juan Pardo EM, Kumar S. The Mechanical Rigidity of the Extracellular Matrix Regulates the Structure, Motility, and Proliferation of Glioma Cells. *Cancer Res* (2009) 69(10):4167–74. doi: 10.1158/0008-5472.CAN-08-4859
17. Yao KC, Komata T, Kondo Y, Kanzawa T, Kondo S, Germano IM. Molecular Response of Human Glioblastoma Multiforme Cells to Ionizing Radiation: Cell Cycle Arrest, Modulation of the Expression of Cyclin-Dependent Kinase Inhibitors, and Autophagy. *J Neurosurg* (2003) 98(2):378–84. doi: 10.3171/jns.2003.98.2.0378
18. Roy K, Wang L, Makrigiorgos GM, Price BD. Methylation of the ATM Promoter in Glioma Cells Alters Ionizing Radiation Sensitivity. *Biochem Biophys Res Commun* (2006) 344(3):821–6. doi: 10.1016/j.bbrc.2006.03.222
19. Naidu MD, Mason JM, Pica RV, Hua F, Peña LA. Radiation Resistance in Glioma Cells Determined by DNA Damage Repair Activity of Ape1/Ref-1. *J Radiat Res* (2010) 51(4):393–404. doi: 10.1269/jrr.09077
20. Anandharaj A, Cinghu S, Park WY. Rapamycin-Mediated mTOR Inhibition Attenuates Survivin and Sensitizes Glioblastoma Cells to Radiation Therapy. *Acta Biochim Biophys Sin (Shanghai)* (2011) 43(4):292–300. doi: 10.1093/abbs/gmr012
21. Livak KJ, Schmittgen TD. Analysis of Relative Gene Expression Data Using Real-Time Quantitative PCR and the 2-ΔΔCT Method. *Methods* (2001) 25 (4):402–8. doi: 10.1006/meth.2001.1262
22. Heagerty PJ, Lumley T, Pepe MS. Time-Dependent ROC Curves for Censored Survival Data and a Diagnostic Marker. *Biometrics* (2000) 56(2):337–44. doi: 10.1111/j.0006-341X.2000.00337.x
23. de Sousa JF, da Silva P, Serafim RB, Nociti RP, Moreira CG, Silva WA, et al. RNA Sequencing Data of Different Grade Astrocytoma Cell Lines. *Data Br* (2021) 34:106643. doi: 10.1016/j.dib.2020.106643
24. Ahmed KM, Pandita RK, Singh K, Hunt CR. β1-Integrin Impacts Rad51 Stability and DNA Double-Strand Break Repair by Homologous Recombination. *Mol Cell Biol* (2018) 38(9):1–17. doi: 10.1128/MCB.00672-17
25. Petrás M, Lajtos T, Friedlander E, Klekner Á, Pintye É, Feuerstein BG, et al. Molecular Interactions of ErbB1 (EGFR) and Integrin-β1 in Astrocytoma Frozen Sections Predict Clinical Outcome and Correlate With Akt-Mediated In Vitro Radioresistance. *Neuro Oncol* (2013) 15(8):1027–40. doi: 10.1093/neuonc/not046
26. Renner G, Janouskova H, Noulet F, Koenig V, Guerin E, Bär S, et al. Integrin α5β1 and p53 Convergent Pathways in the Control of Anti-Apoptotic Proteins PEA-15 and Survivin in High-Grade Glioma. *Cell Death Differ* (2016) 23(4):640–53. doi: 10.1038/cdd.2015.131
27. Cordes N, Hansmeier B, Beinke C, Meineke V, Van Beuningen D. Irradiation Differentially Affects Substratum-Dependent Survival, Adhesion, and Invasion of Glioblastoma Cell Lines. *Br J Cancer* (2003) 89(11):2122–32. doi: 10.1038/sj.bjc.6601429

28. Cuddapah VA, Robel S, Watkins S, Sontheimer H. A Neurocentric Perspective on Glioma Invasion. *Nat Publ Gr [Internet]* (2014) 15(7):455–65. doi: 10.1038/nrn3765
29. Bartkova J, Hamerlik P, Stockhausen MT, Ehrmann J, Hlobilkova A, Laursen H, et al. Replication Stress and Oxidative Damage Contribute to Aberrant Constitutive Activation of DNA Damage Signalling in Human Gliomas. *Oncogene [Internet]* (2010) 29(36):5095–102. doi: 10.1038/onc.2010.249
30. Candolfi M, Curtin JF, Nichols WS, Muhammad AG, King GD, Pluhar GE, et al. Intracranial Glioblastoma Models in Preclinical Neuro-Oncology : Neuropathological Characterization and Tumor Progression. *J Neurooncol* (2007) 85:133–48. doi: 10.1007/s11060-007-9400-9
31. Camphausen K, Purow B, Sproull M, Scott T, Ozawa T, Deen DF, et al. Influence of In Vivo Growth on Human Glioma Cell Line Gene Expression;: Convergent Profiles Under Orthotopic Conditions. *PNAS* (2005) 102 (23):8287–92. doi: 10.1073/pnas.0502887102
32. Desgrosellier JS, Cheresh DA. Integrins in Cancer: Biological Implications and Therapeutic Opportunities. *Nat Rev Cancer [Internet]* (2010) 10(12):890. doi: 10.1038/nrc2965
33. Malric L, Monferran S, Gilhodes J, Boyrie S, Dahan P, Skuli N, et al. Interest of Integrins Targeting in Glioblastoma According to Tumor Heterogeneity and Cancer Stem Cell Paradigm: An Update. *Oncotarget* (2017) 8(49):86947–68. doi: 10.18632/oncotarget.20372
34. Xie Q, Mittal S, Berens ME. Targeting Adaptive Glioblastoma: An Overview of Proliferation and Invasion. *Neuro Oncol* (2014) 16(12):1575–84. doi: 10.1093/neuonc/nou147
35. Behnan J, Finocchiaro G, Hanna G. The Landscape of the Mesenchymal Signature in Brain Tumours. *Brain* (2019) 142(4):847–66. doi: 10.1093/brain/awz044
36. Eke I, Makinde AY, Aryankalayil MJ, Reedy JL, Citrin DE, Chopra S, et al. Long-Term Tumor Adaptation After Radiotherapy: Therapeutic Implications for Targeting Integrins in Prostate Cancer. *Mol Cancer Res* (2018) 16:1855–65. doi: 10.1158/1541-7786.MCR-18-0232
37. Meineke V, Gilbertz K, Schilperoort K, Cordes N, Sendler A, Moede T, et al. Ionizing Radiation Modulates Cell Surface Integrin Expression and Adhesion of COLO- 320 Cells to Collagen and Fibronectin In Vitro. *Strahlentherapie und Onkol* (2002) 12):709–14. doi: 10.1007/s00066-002-0993-9
38. Zhou P, Erfani S, Liu Z, Jia C, Chen Y, Xu B, et al. Cd151-α3β1 Integrin Complexes Are Prognostic Markers of Glioblastoma and Cooperate With EGFR to Drive Tumor Cell Motility and Invasion. *Oncotarget* (2015) 6 (30):29675–93. doi: 10.18632/oncotarget.4896
39. Kowalski-Chauvel A, Modesto A, Gouaze-andersson V, Baricault L, Gilhodes J, Delmas C, et al. Alpha-6 Integrin Promotes Radioresistance of Glioblastoma by Modulating DNA Damage Response and the Transcription Factor Zeb1. *Cell Death Dis [Internet]* (2018) 9(9):872. doi: 10.1038/s41419-018-0853-x
40. Wei F, Tang L, He Y, Wu Y, Shi L, Xiong F, et al. BPIFB1 (LPLUNC1) Inhibits Radioresistance in Nasopharyngeal Carcinoma by Inhibiting VTN Expression. *Cell Death Dis* (2018) 9(4):432. doi: 10.1038/s41419-018-0409-0
41. Yang L, Zhang X, Hou Q, Huang M, Zhang H, Jiang Z, et al. Single-Cell RNA-seq of Esophageal Squamous Cell Carcinoma Cell Line With Fractionated Irradiation Reveals Radioresistant Gene Expression Patterns. *BMC Genomics* (2019) 20(1):1–11. doi: 10.1186/s12864-019-5970-0
42. You GR, Cheng AJ, Lee LY, Huang YC, Liu H, Chen YJ, et al. Prognostic Signature Associated With Radioresistance in Head and Neck Cancer Via Transcriptomic and Bioinformatic Analyses. *BMC Cancer* (2019) 19(1):1–11. doi: 10.1186/s12885-018-5243-3
43. Haas TL, Sciuto MR, Brunetto L, Valvo C, Signore M, Fiori ME, et al. Integrin α7 Is a Functional Marker and Potential Therapeutic Target in Glioblastoma. *Cell Stem Cell* (2017) 21(1):35–50.e9. doi: 10.1016/j.stem.2017.04.009
44. Stangeland B, Mughal AA, Grieg Z, Sandberg CJ, Langmoen IA. Combined Expressional Analysis, Bioinformatics and Targeted Proteomics Identify New Potential Therapeutic Targets in Glioblastoma Stem Cells. *Oncotarget* (2015) 6(28):26192–215. doi: 10.18632/oncotarget.4613
45. Schittenhelm J, Klein A, Tatagiba MS, Meyermann R, Fend F, Simon L. Comparing the Expression of Integrins αvβ3, αvβ 5, αvβ6, αvβ8, Fibronectin and Fibrinogen in Human Brain Metastases and Their Corresponding Primary Tumors. *Int J Clin Exp Pathol* (2013) 6(12):2719–32.
46. Balbous A, Cortes U, Guilloteau K, Villalva C, Flamant S, Gaillard A, et al. A Mesenchymal Glioma Stem Cell Profile Is Related to Clinical Outcome. *Oncogenesis* (2014) 3(October 2013):1–10. doi: 10.1038/oncsis.2014.5
47. Hu Y, Ylivinkka I, Chen P, Li L, Hautaniemi S, Nyman TA, et al. Netrin-4 Promotes Glioblastoma Cell Proliferation Through Integrin β4 Signaling. *Neoplasia* (2012) 14(3):219–27. doi: 10.1593/neo.111396
48. Xu T, Qin R, Zhou J, Yan Y, Lu Y, Zhang X, et al. High Bone Sialoprotein (Bsp) Expression Correlates With Increased Tumor Grade and Predicts a Poorer Prognosis of High-Grade Glioma Patients. *PloS One* (2012) 7(10): e48415. doi: 10.1371/journal.pone.0048415

Conflict of Interest: The authors declare that the research was conducted in the absence of any commercial or financial relationships that could be construed as a potential conflict of interest.

Copyright © 2021 Serafim, da Silva, Cardoso, Di Cristofaro, Netto, de Almeida, Navegante, Storti, de Sousa, de Souza, Panepucci, Moreira, Penna, Silva and Valente. This is an open-access article distributed under the terms of the Creative Commons Attribution License (CC BY). The use, distribution or reproduction in other forums is permitted, provided the original author(s) and the copyright owner(s) are credited and that the original publication in this journal is cited, in accordance with accepted academic practice. No use, distribution or reproduction is permitted which does not comply with these terms.

frontiers in Oncology

ORIGINAL RESEARCH
published: 27 May 2021
doi: 10.3389/fonc.2021.640910

Molecular and Clinical Characterization of UBE2S in Glioma as a Biomarker for Poor Prognosis and Resistance to Chemo-Radiotherapy

Li Hu[1†], Xingbo Cheng[1†], Zev Binder[2], Zhibin Han[1], Yibo Yin[1], Donald M. O'Rourke[2], Sida Wang[1], Yumeng Feng[1], Changjiang Weng[3], Anhua Wu[4] and Zhiguo Lin[1]*

[1] Department of Neurosurgery, The First Affiliated Hospital of Harbin Medical University, Harbin, China, [2] Department of Neurosurgery, Perelman School of Medicine at the University of Pennsylvania, Philadelphia, PA, United States, [3] State Key Laboratory of Veterinary Biotechnology, Harbin Veterinary Research Institute of Chinese Academy of Agricultural Sciences, Harbin, China, [4] Department of Neurosurgery, The First Hospital of China Medical University, Shenyang, China

OPEN ACCESS

Edited by:
Terrance Johns,
University of Western Australia,
Australia

Reviewed by:
Roger Leng,
University of Alberta, Canada
Jason Cain,
Hudson Institute of Medical Research,
Australia

***Correspondence:**
Zhiguo Lin
linzhgu@sina.com

[†]These authors have contributed equally to this work and share first authorship

Specialty section:
This article was submitted to Neuro-Oncology and Neurosurgical Oncology, a section of the journal Frontiers in Oncology

Received: 12 December 2020
Accepted: 07 May 2021
Published: 27 May 2021

Citation:
Hu L, Cheng X, Binder Z, Han Z, Yin Y, O'Rourke DM, Wang S, Feng Y, Weng C, Wu A and Lin Z (2021) Molecular and Clinical Characterization of UBE2S in Glioma as a Biomarker for Poor Prognosis and Resistance to Chemo-Radiotherapy. Front. Oncol. 11:640910. doi: 10.3389/fonc.2021.640910

Glioblastoma is the most common and lethal brain cancer globally. Clinically, this cancer has heterogenous molecular and clinical characteristics. Studies have shown that UBE2S is highly expressed in many cancers. But its expression profile in glioma, and the correlation with clinical outcomes is unknown. RNA sequencing data of glioma samples was downloaded from the Chinese Glioma Genome Atlas and The Cancer Genome Atlas. A total of 114 cases of glioma tissue samples (WHO grades II-IV) were used to conduct protein expression assays. The molecular and biological characteristics of UBE2S, and its prognostic value were analyzed. The results showed that high UBE2S expression was associated with a higher grade of glioma and PTEN mutations. In addition, UBE2S affected the degree of malignancy of glioma and the development of chemo-radiotherapy resistance. It was also found to be an independent predictor of worse survival of LGG patients. Furthermore, we identified five UBE2S ubiquitination sites and found that UBE2S was associated with Akt phosphorylation in malignant glioblastoma. The results also revealed that UBE2S expression was negatively correlated with 1p19q loss and IDH1 mutation; positively correlated with epidermal growth factor receptor amplification and PTEN mutation. This study demonstrates that UBE2S expression strongly correlates with glioma malignancy and resistance to chemo-radiotherapy. It is also a crucial biomarker of poor prognosis.

Keywords: glioblastoma multiform, UBE2S, PTEN, pAkt, chemo-radiotherapy, prognosis

Abbreviations: GBM, Glioblastoma multiform; TMZ, temozolomide; CGGA, Chinese Glioma Genome Atlas; TCGA, The Cancer Genome Atlas; VEGF, Vascular Endothelial Growth Factor; EMT, Epithelial Mesenchymal Transition; FAK, Focal Adhesion Kinase; CCRT, Computerized Controlled Radiation Therapy; GO, Gene ontology; KEGG, Kyoto encyclopedia of genes and genomes; OS, overall survival; LGG, Low-grade glioma; IR, ionizing radiation.

INTRODUCTION

GBM is the most common primary malignant brain tumor in adults (1). Despite advances in comprehensive therapy, such as development of neurosurgical resection, adjuvant radiotherapy, and alkylating agent temozolomide (TMZ) chemotherapy, GBM patients are characterized by poor prognosis and the 5-year survival rate is below 10%. The median overall survival is 12 to 15 months following primary diagnosis (2, 3), due to aggressiveness of the tumor, resistance to treatments, and recurrence over time (4). Advances in gene technology have enabled identification of molecular signatures for classification of glioma in recent years. Previous studies report that a complicated molecular network of signaling pathways is implicated in mediating malignancy of glioma (5). Therefore, exploring such therapeutic targets that are capable of regulating multiple molecules or signaling pathways in progression of glioma and TMZ resistance are beneficial for improving glioma treatment. Recent studies explored the role of genetic mutations in glioma, however, it is not clear which mutation is significantly associated with specific characteristics of glioma. Classification based only on histopathology does not effectively describe all the malignant features of GBMs, mainly their responses to treatments. For example, some GBMs are mainly sensitive to radio-chemotherapy whereas others are resistant to radiotherapy and chemotherapy. Notably, GBMs are aggressive and are characterized by early recurrence, whereas others progress slowly for prolonged period (6, 7). Molecular parameters are now considered for GBMs classification due to these limitations in traditional classification methods.

UBE2S, a 24 kDa ubiquitin-conjugating enzyme, is highly expressed in most human cancers, including breast cancer, colon tumors, and ovarian cancer (8–11), compared with normal tissues, implying that it is involved in oncogenesis. Moreover, UBE2S is highly expressed in hepatocellular carcinoma (HCC), where it interacts with TRIM28 and enhances ubiquitination of p27, thus promoting HCC progression (12). UBE2S associates with and targets pVHL for ubiquitin-mediated proteolysis, thus stabilizing HIF-1α. Furthermore, overexpression of UBE2S promotes proliferation, invasion and metastasis through pVHL-HIF pathway (9). UBE2S knockdown results in reduction in FAK phosphorylation at Tyr397, thus inhibiting signal level for cell migration and invasion (13). Akt1 phosphorylates UBE2S and enhances its stability, and knockdown of UBE2S expression inhibits NHEJ-mediated DNA repair, however, this activity has not been validated using clinical data.

Large scale meta-analysis of cancer microarray data show that UBE2S is a commonly activated gene in multiple cancers. However, its expression in glioma tissues and the potential correlation between UBE2S and clinical outcome in patients with glioma have not been explored. The aim of this study was to explore expression levels of UBE2S in glioma, and to explore the relationship between UBE2S expression and prognosis of glioma, and chemo-radiotherapy resistance.

MATERIALS AND METHODS

Clinical Data and Tumor Specimen Selection

A retrospective cohort of 114 glioma patients was included in the present study. Glioma samples were obtained from open-craniotomy surgery performed at the First Affiliated Hospital of Harbin Medical University. Inclusion criteria were as follows: primary diagnosis of glioma between 2008 and 2016 and no previous diagnosis of carcinoma. Patients who had received neoadjuvant treatment before primary surgery were excluded. Normal brain specimens (n = 5) were obtained from patients with severe brain injury who underwent partial normal brain resection and decompression. Histopathological analysis (according to the WHO classification) were performed by two independent neuropathologists, and a consensus was reached in all cases. Ethical approval for carrying out this study was obtained from the Committees for the Ethical Review of Research at the First Affiliated Hospital of Harbin Medical University, Harbin, China. Informed consent was obtained from each participant before participation in this study. mRNA expression microarray data and related clinical information for glioma samples were retrieved from The Cancer Genome Atlas and Chinese Glioma Genome Atlas databases.

Cell lines, Antibodies, and Reagents

Glioma cell lines were obtained from Helen Diller Cancer Center of the University of California, San Francisco (UCSF). UBE2S-specific shRNA (5'-GGGCTCTCTTCCTCCTTCCAC-3') and control shRNA (5'-TTCTCCGAACGTGTCACGT-3') oligonucleotides were established. Knockdown of endogenous UBE2S expressions in U87 and U251 cells was performed using lentivirus-expressing shRNA as described previously (14). Rabbit anti-GAPDH and anti-Ki67 polyclonal antibodies were purchased from Proteintech Group (Proteintech Group, Chicago, IL). Rabbit anti-HA and anti-Flag polyclonal antibodies were purchased from Sigma-Aldrich (St. Louis, MO). Rabbit anti-pAkt S473, and anti-PTEN polyclonal antibodies were purchased from Abcam (Cambridge, MA, USA). Anti-Flag M2 magnetic Beads were purchased from Sigma-Aldrich (St. Louis, MO), whereas MK-2206 was purchased from Selleck Chemicals (Houston, TX, USA).

Immunohistochemistry

Paraffin-embedded sections (4μm) of excised specimens were immunostained for determination of UBE2S protein level. Staining was performed using the streptavidin-biotin peroxidase complex method, following the manufacturer's instructions (Dako, Denmark). Negative and positive controls were included in the immunohistochemistry procedure. Immunohistochemical staining score standard: positive rate of UBE2S staining more than 10% was considered as positive group. UBE2S staining of glioma was divided into positive group and negative group based on this criterion (15). All immunostained sections were reviewed by two investigators who were blinded to the treatments and the immunostained images were acquired using an Olympus inverted microscope.

Immunoprecipitation and Immunoblotting

Tissue were harvested for total protein extraction. Protein concentration was determined using Bradford method. For immunoprecipitation, lysates were incubated with anti-Flag M2 magnetic beads overnight at 4°C. Immunoprecipitants were then subjected to electrophoresis. For western blot analysis, equal amounts of protein were loaded and separated by SDS-PAGE. Gels were equilibrated in transfer buffer (50 mM Tris, 40 mM glycine, 0.375% SDS and 20% methanol) and transferred to a PVDF membrane (Millipore, USA) through electrophoresis. The membrane was blocked with 5% skim milk in TBST buffer (20 mM Tris-HCl, pH 7.4, 150 mM NaCl and 0.1% Tween20) and incubated over night at 4°C with specific primary antibodies. The membrane was then washed with TBST, and incubated with horseradish peroxidase conjugated secondary antibodies (Invitrogen, USA) for 1 h (16).

Gene Ontology (GO) and Kyoto Encyclopedia of Genes and Genomes (KEGG) Analysis

To identify the biological processes and KEGG signaling pathways related to UBE2S expression in glioma, GO enrichment analysis and KEGG pathway analysis were performed using clusterProfler to explore the biological significance and key pathways associated with UBE2S of differentially expressed genes (DEGs) (criteria: p-value < 0.05, significantly enriched). Fisher's exact test was used to identify significant GO terms and pathways.

Apoptosis Assays by Annexin V-FITC/PI Double Staining

U87 or U251 cells were seeded in 6-well plates at a density of 1×10^5 cells/well. After treatment with 6MV X-Ray (10Gy), cells were collected and stained using an Annexin V-FITC/PI Apoptosis Detection kit according to the manufacturer's instructions (no. C1062, Beyotime, Nanjing, China). Cells were then analyzed using a flow cytometer (Beckhman Coulter Inc, Brea, CA, USA).

Statistical Analysis

Overall survival analysis was performed using Log-rank test. Cox regression analysis was performed using the survival package in R software. Statistical differences among groups were determined by one-way analysis of variance (ANOVA) followed by Newman-Keuls test for multiple comparisons. In those experiments where experimental values were normalized to controls, statistical difference compared with the controls was calculated using Kruskal-Wallis test or Wilcoxon test. Correlations between UBE2S expression and various clinicopathological characteristics were assessed by $\chi 2$-tests. SPSS 17.0, Prism5 and R software (version 3.3.2) were used for statistical analysis. $p<0.05$ was considered as statistically significant. Significance was set at *$p<0.05$, **$p<0.01$ or ***$p<0.001$.

RESULTS

UBE2S Expression Is Associated With Glioma Grades

Expression pattern of UBE2S across grades and subtypes defined by expression clusters by the TCGA work-group were explored (17). In the TCGA cohort, UBE2S expression increased with increasing grade of glioma with the highest expression level in WHO Grade IV ($p < 0.0001$, **Figure 1A**). Similar findings were obtained with the CGGA cohort (**Figure 1B**) which showed that UBE2S expression was highly correlated with the malignancy of glioma. Analysis based on the TCGA subtype classification system showed that the Proneural subtype had the highest UBE2S expression level whereas the mesenchymal subtype had the lowest UBE2S expression in TCGA cohort (**Figure 1C**). In the CGGA cohort, UBE2S expression was up-regulated in Classical subtypes (**Figure 1D**).

UBE2S-Related Genomic Alterations and Biological Processes

IDH1 mutation status is a clinically effective molecular marker in glioma (18). Glioma patients were divided into IDH1 mutation group and IDH1 wild-type group and the association between UBE2S expression level and the IDH1 status was determined. In the TCGA cohort, UBE2S expression level was significantly higher in the IDH1 wild-type group compared with expression level in the IDH1 mutation group of LGG patients (**Figure 2A**). However, no statistical significance was detected between the two groups of GBM patients. Further analysis of the relationship between UBE2S expression level and PTEN status showed that UBE2S expression level was significantly higher in PTEN mutation group compared with the expression level in the PTEN wild-type group of LGG patients (**Figure 2B**). However, no statistical significance was observed between the two groups of GBM patients (**Figure 2B**). Glioma patients were grouped into TP53 wild-type group and TP53 mutation group, and analysis showed no significant difference in UBE2S expression between the two groups (**Figure 2C**). Analysis of the relationship between UBE2S expression level and EGFR status, showed that UBE2S expression was significantly higher in EGFR mutation group compared with the level in EGFR wild-type group of LGG patients (**Figure 2D**). However, no statistical significance was observed between the two groups in GBM patients (**Figure 2D**). These findings show that UBE2S has a PTEN mutant, EGFR mutant and IDH1 wild-type preference in LGG patients.

To explore the biological features of glioma associated with different UBE2S expression, Pearson correlation analyses were performed to determine the correlation between UBE2S expression and other genes in CGGA sequencing dataset. A total of 283 genes were correlated with UBE2S mRNA expression in the CGGA RNAseq dataset ($|R| \geq 0.6$, $p \leq 0.01$, **Figure 3A**). Further analysis on the oncogenic features of UBE2S showed that the genomic or transcriptional alterations associated with the origin or progression of glioma correlated with degrees of UBE2S expression level (**Figures 3A, B**). Selected glioma genes with high and low UBE2S expression level were separately derived from the TCGA RNA-sequencing database and a heatmap for enrichment scores was generated using the "pheatmap" package in R. IDH1-mutant lower grade glioma had significantly lower levels of UBE2S expression compared with the wild-type (**Figure 3A**). Co-deletion of 1p19q, which is an indicator of optimistic outcome, was mainly observed in glioma with lower UBE2S

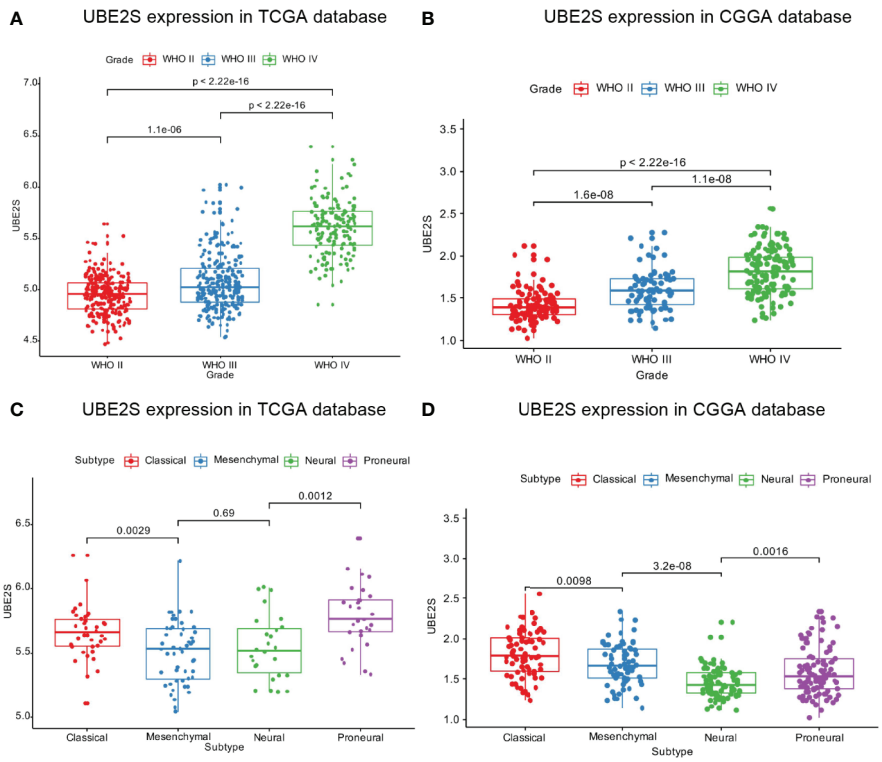

FIGURE 1 | UBE2S was significantly upregulated in glioblastoma. **(A, B)** UBE2S expression level was significantly high in glioblastoma (WHO IV) samples in TCGA and CGGA data set. **(C, D)** UBE2S expression pattern in different molecular subtypes in TCGA and CGGA data set. P is based on Kruskal-Wallis test.

expression level. The incidence of malignant factor, EGFR amplification and PTEN mutation, was significantly higher in glioma samples with higher expression levels of UBE2S compared with those with low expression levels. On the other hand, TP53 mutation showed no association with UBE2S expression. Similar findings were observed in the TCGA cohort (**Figure 3B**) whereby UBE2S expression was significantly correlated with the key molecular characteristics of glioma.

The correlated genes were used for functional annotation analysis and were ranked by p value in increasing order. Analysis showed that UBE2S related genes were mainly involved in normal biological processes, such as ATPase activity, microtubule binding, tubulin binding, catalytic activity, acting on DNA, helicase activity in molecular function (**Figure S1A**); organelle fission, nuclear division, chromosome segregation, mitotic nuclear division, nuclear chromosome segregation in biological processes term (**Figure S1B**); chromosomal region, spindle, condensed chromosome, chromosome centromeric region in cell component (**Figure S1C**). Furthermore, KEGG pathways analyses were performed for comprehensive analysis of critical pathways related to UBE2S (**Figure S1D**). The most vital pathways of UBE2S included cell cycle, spliceosome, DNA replication, progesterone-mediated oocyte maturation, oocyte meiosis, cellular senescence, mismatch repair, nucleotide excision repair, base excision repair and fanconi anemia pathway (**Figure S1D**).

Correlation Between UBE2S, Glioma Malignancy, and Chemo-Radiotherapy Resistance

To validate the RNA-based results, protein levels of UBE2S were determined by IHC in an independent cohort of human glioma (n = 114) and normal brain tissue (n = 5) from The First Affiliated Hospital of Harbin Medical University (Harbin, China). We found that UBE2S expression level was higher in grades III-IV glioma tumors (malignant glioma) compared with non-glioma brain tissue specimens or in grade II glioma tumors (**Figure 4**). These findings show that UBE2S protein expression was positively correlated with malignancy of glioma.

Baseline clinical characteristics of patients included in this study are shown in **Table 1**. Out of 114 glioma specimens 58 (51%) showed significant UBE2S expression. In addition, 61 out of the 114 patients (54%) responded poorly to neoadjuvant radio- or chemotherapy. Notably, samples from 53 out of the 61 poor responders (87%) showed positive staining for UBE2S. Further analysis showed that patients with positive staining for UBE2S were significantly associated with resistance to neoadjuvant therapy ($p < 0.001$). Subsequently, the correlation between UBE2S expression and chemo-radiotherapy sensitivity was determined using a Cox proportional hazards regression model. Univariate analysis showed a statistically significant correlation between chemo-radiotherapy sensitivity and

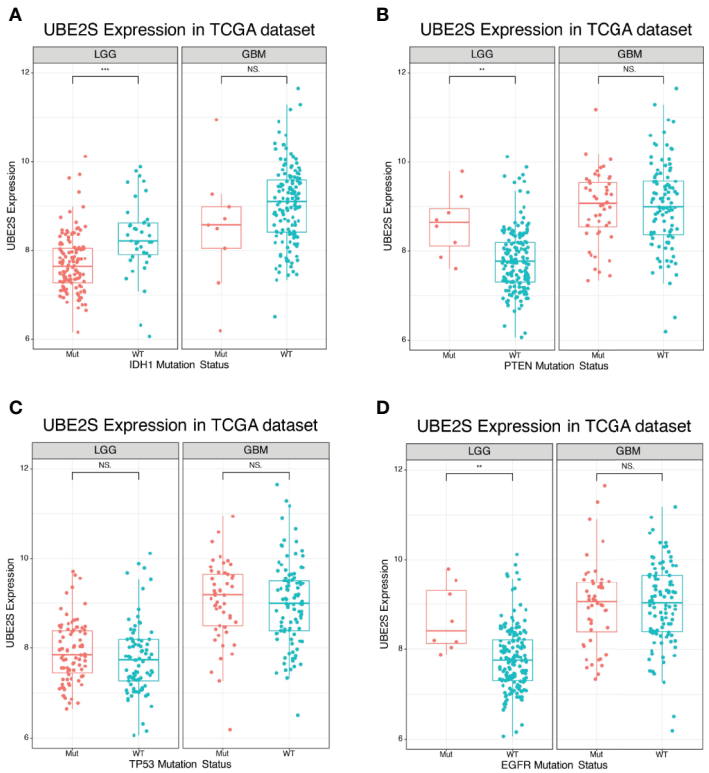

FIGURE 2 | Expression of UBE2S in glioma of different mutation types. **(A)** UBE2S was significantly upregulated in IDH1 wild-type LGG glioma in TCGA data set compared with the mutants. **(B)** UBE2S was significantly upregulated in PTEN mutation LGG glioma in TCGA data set compared with the wild-type. **(C)** UBE2S expression was not significantly different between TP53 mutation and TP53 wild-type LGG/GBM glioma in TCGA data set. **(D)** UBE2S was significantly upregulated in EGFR mutation LGG glioma in TCGA data set. Wilcoxon test was used to determine statistical difference. ***P < 0.001, **P < 0.01, NS represents non-significant.

expression levels of UBE2S ($p < 0.001$; hazard ratio HR = 0.016) (**Table S1**). Multivariate analysis further showed that expression level of UBE2S was an independent and significant predictor of chemo-radiotherapy sensitivity ($p < 0.001$; hazard ratio HR = 0.012) (**Table S1**).

In summary, these findings show that UBE2S is highly expressed in grades III-IV glioma and the high expression level of UBE2S is correlated with glioma malignancy and chemo-radiotherapy resistance.

UBE2S Is Associated With Worse Survival for Glioma Patients

Kaplan Meier survival curve was used to determine the prognostic value of UBE2S expression in the overall survival (OS) of glioma. In the TCGA cohort (n = 691), High UBE2S expression (> median value) was associated with poor prognosis whereas a low expression level of UBE2S was associated with good prognosis in LGG patients ($p < 0.001$, **Figures S2A, B**). However, UBE2S expression level was not associated with prognosis of GBM patients ($p = 0.9157$) in the TCGA cohort. In the CGGA cohort, high UBE2S expression level (> median value) was significantly associated with worse prognosis compared with low expression of UBE2S in LGG patients ($p < 0.001$), whereas this association was not observed in GBM patients (n = 325, $p = 0.3924$, **Figures S2C, D**). These findings show that high UBE2S expression was statistically correlated with shorter OS in LGG patients.

UBE2S Acts Synergistically With Akt Phosphorylation in Promoting Glioblastoma Malignancy

Abnormal expression of UBE2S in glioma prompted us to explore the clinical relevance of PI3K/Akt/UBE2S oncogenic synergy. Akt1 physically interacts with UBE2S and phosphorylates UBE2S at Thr152 in glioma cells, which is important for stabilization of UBE2S (14). To further validate this finding using clinical data, phosphorylation of Akt1 (S473, named pAkt) and UBE2S expression in 114 specimens were determined by immunohistochemistry (IHC) (**Figure 5A**). Percentage of UBE2S-expressing tumors (i.e., UBE2S+ pAkt- and UBE2S+ pAkt+) in grade III-IV tumors was significantly higher compared with that in grade II tumors (83.34% versus 9.26%; **Figure 5B** and **Table 2**). Significantly higher Akt phosphorylation positive specimens (UBE2S- pAkt+ and UBE2S+ pAkt+) were observed in grade III-IV group compared with grade II group (78.34% versus 16.67% in Grade II). Notably,

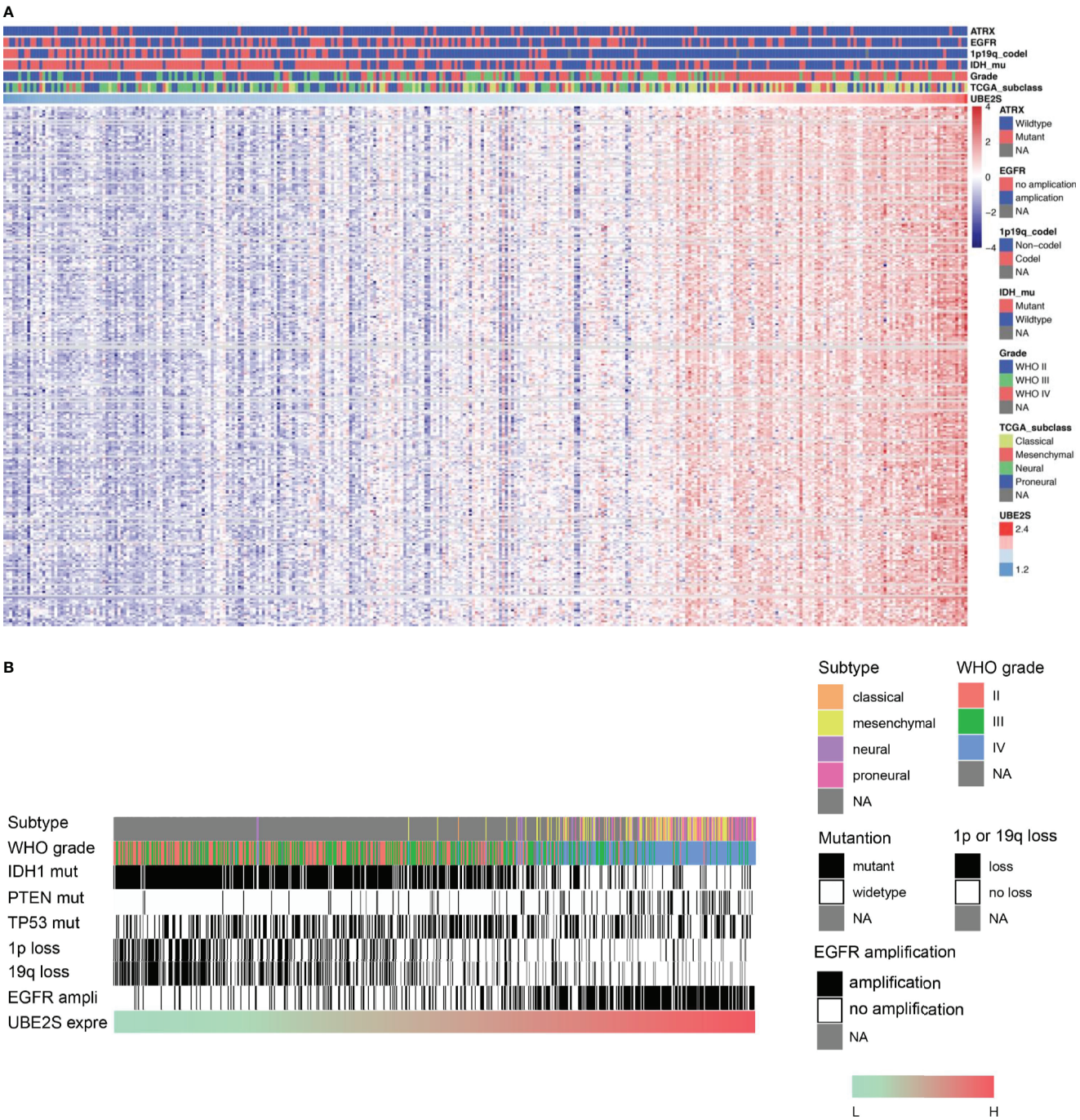

FIGURE 3 | Correlations between UBE2S expression level with the classical genomic or transcriptional alterations in glioma. **(A)** Correlations between UBE2S expression level and the classical genomic or transcriptional alterations in whole grade glioma in CGGA data set. **(B)** Correlations of UBE2S expression level and the classical genomic or transcriptional alterations in whole grade glioma in TCGA data set. Pearson correlation analyses were used.

a significant correlation was observed between UBE2S and phosphorylation of Akt1 (i.e. UBE2S+ pAkt+) and a worse pathological grade in Grade III-IV group compared with grade II group (Grade III-IV, 66.67%; Grade II, 5.56%; $p < 0.001$).

In summary, these findings show that high UBE2S expression and active Akt1 are associated with adverse tumor characteristics. Therefore, PTEN-Akt1 pathways may positively regulate UBE2S function in glioma tissue by enhancing its stability.

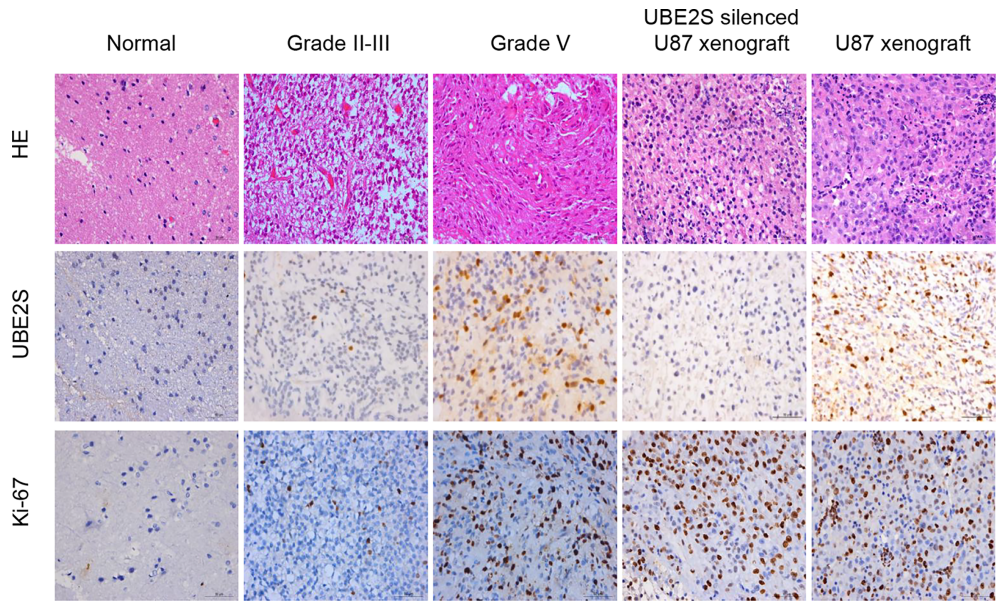

FIGURE 4 | UBE2S was highly expressed in glioma tissue specimens. Representative images of hematoxylin/eosin (HE) staining showing UBE2S and Ki-67 immunoreactivity from the tissue. Tumor xenograft obtained from U87 cells was stained with anti-UBE2S monoclonal antibody and used as positive control (PC). Normal tissue and tumor xenograft from UBE2S-silenced U87 cells were stained with anti-UBE2S monoclonal antibody and used as negative control (NC) (×400). Scale bar: 50 μm.

TABLE 1 | Clinicopathological characteristics of glioma patients for immunohistochemical investigation.

Characteristic	IHC-UBE2S (-) N (%)	IHC-UBE2S (+) N (%)	P value
Age			0.078
< 40	18 (50.0)	18 (50.0)	
40-60	35 (54.7)	29 (45.3)	
> 60	3 (21.4)	11 (78.6)	
Sex			0.869
Female	25 (50.0)	25 (50.0)	
Male	31 (48.4)	33 (51.6)	
Tumor stage			0.000
I-II	42 (77.8)	12 (22.2)	
III-IV	14 (23.3)	46 (76.7)	
Seizure			0.596
Absent	37 (47.4)	41 (52.6)	
Present	19 (52.8)	17 (47.2)	
IICP			0.194
Absent	27 (56.2)	21 (43.8)	
Present	29 (43.9)	37 (56.1)	
Cystic degeneration			0.562
Absent	45 (50.6)	44 (49.4)	
Present	11 (44.0)	14 (56.0)	
MTD			0.412
< 5 cm	37 (52.1)	34 (47.9)	
≥ 5 cm	19 (44.2)	24 (55.8)	
Chemoradiotherapy sensitivity			0.000
No	8 (13.1)	53 (86.9)	
Yes	48 (90.6)	5 (9.4)	

Mapping of Critical Lysine Residues for UBE2S Function

UBE2S is an unstable protein, and its degradation is dependent on a proteasome pathway, however, ubiquitination sites on this protein have not been explored. To explore UBE2S ubiquitination sites, U87 cells were transfected with Flag-UBE2S and the immunoprecipitated Flag-UBE2S was analyzed by mass spectrometry. Analysis showed that five lysine residues at position 18, 82, 117, 197 and 198 were ubiquitinated (**Figure 6A**). We hypothesized that these lysine

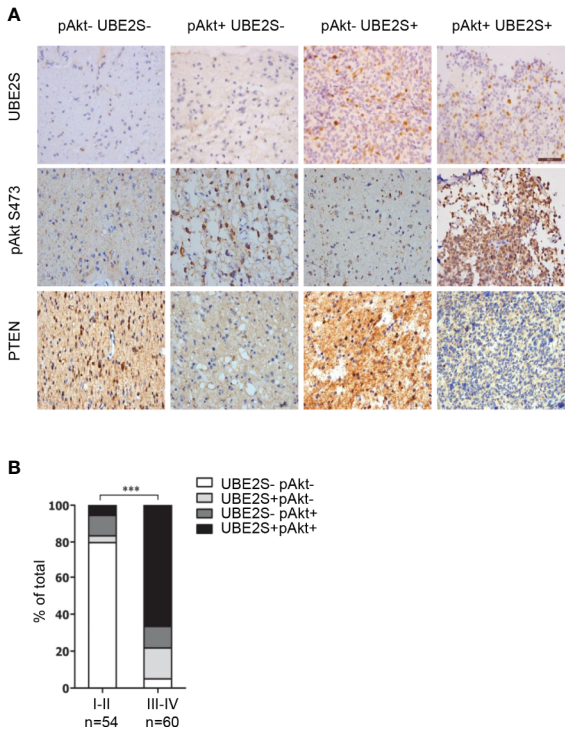

FIGURE 5 | Association of UBE2S expression and activation of Akt pathway in glioma clinical samples. **(A)** Representative IHC staining for UBE2S, pAkt and PTEN on adjacent sections of formalin-fixed paraffin-embedded human glioma specimens. Scale bar: 50 μm. **(B)** Summary of the IHC assessment of UBE2S expression and Akt phosphorylation (pAkt) status in 114 human glioma patients. ***P < 0.001, based on $\chi 2$-test.

ubiquitination sites may be required for UBE2S degradation in the nascent protein. The lysine residues were mutated to individually to arginine residues (K18R, K82R, K117R, K197R, and K198R), or as a group (named as UBE2S-5KR). The mutants were co-transfected with HA-Ubiquitin (HA-Ub) in U87 cells and ubiquitination of the mutants was analyzed by Western blot. UBE2S-5KR was less ubiquitinated compared with other individually mutants (**Figure 6B**). UBE2S-5KR was more stable in cycloheximide (CHX) treated cells compared with wild type UBE2S in U87 cells (**Figure 6C**).

Knockdown of UBE2S Expression Increases GBM Sensitivity to Radiotherapy

To explore the biological significance of UBE2S in radiotherapy resistance in glioma, U87 and U251 cells were exposed to 6MV X-ray and then the apoptosis rate was determined by flow cytometry. Knockdown of UBE2S expression increased sensitivity of U87 and U251 cells to IR-mediated apoptosis (**Figures 7A–D**). To explore the role of UBE2S in radiotherapy resistance, UBE2S expression was rescued in UBE2S knockdown cells. Cells transfected with Flag-tagged UBE2S showed significant decrease in apoptosis rate compared with the rate in the UBE2S knockdown group. Akt1 inhibitor MK-2206 reduces expression of UBE2S by reducing ubiquitination of UBE2S (14). To further explore the role of UBE2S in radiotherapy resistance, radiotherapy sensitivity of MK-2206 pre-treated glioma cells was determined by assaying apoptosis rate. MK-2206 pre-treated glioma cells were more sensitivity to IR compared with the control glioma cells (**Figures S3A–S3D**). In addition, MK-2206 pre-treated cells transfected with a plasmid expressing UBE2S-5KR effectively rescued apoptosis in these cells (**Figures S3B, 3D**). This finding shows that UBE2S overexpression is associated with radiotherapy resistance.

DISCUSSION

Glioma is the most common and most malignant intracranial tumor. It is characterized by high relapse rate and high mortality in adults. Despite advances in standard-of-care treatment, including surgical resection followed by radiotherapy and chemotherapy, the median overall survival of glioma patients has not significantly improved. Therefore, new therapeutic approaches are urgently needed.

UBE2S expression has been reported in various human cancers (8, 11, 15, 19), however its role in glioma is not known. In this work, 2 large datasets of glioma patients from the TCGA and the CGGA databases, as well as the clinical data from 114 glioma patients were used to perform a comprehensive analysis on the role of UBE2S on glioma. Analysis showed that UBE2S expression level was significantly up-regulated with increase in tumor grade in both TCGA and CGGA data set. The difference in UBE2S expression in molecular subtypes between TCGA and CGGA data set can be attributed to the different composition of patients in the two datasets. These results were further validated by IHC analysis, which showed high expression levels of protein in the GBM tissue compared with the level in the nonmalignant tissue. In this study, the expression level was positively correlated with the clinical stage of glioma, which is consistent with previous findings on correlation of UBE2S expression level with tumor grades in other types of tumors. These findings show that UBE2S expression level was significantly correlated with malignancy.

TABLE 2 | Association of UBE2S and pAkt immunoreactivity with glioma.

Group	No. of specimens	Immunoreactivity			
		UBE2S- pAkt-	UBE2S+ pAkt-	UBE2S- pAkt+	UBE2S+ pAkt+
Grade I-II	n=54	43 (79.63%)	2 (3.70%)	6 (11.11%)	3 (5.56%)
Grade III-IV	n=60	3 (5%)	10 (16.67%)	7 (11.67%)	40(66.67%)
Total	n=114	46 (40.35%)	12 (10.53%)	13 (11.40%)	43 (37.72%)

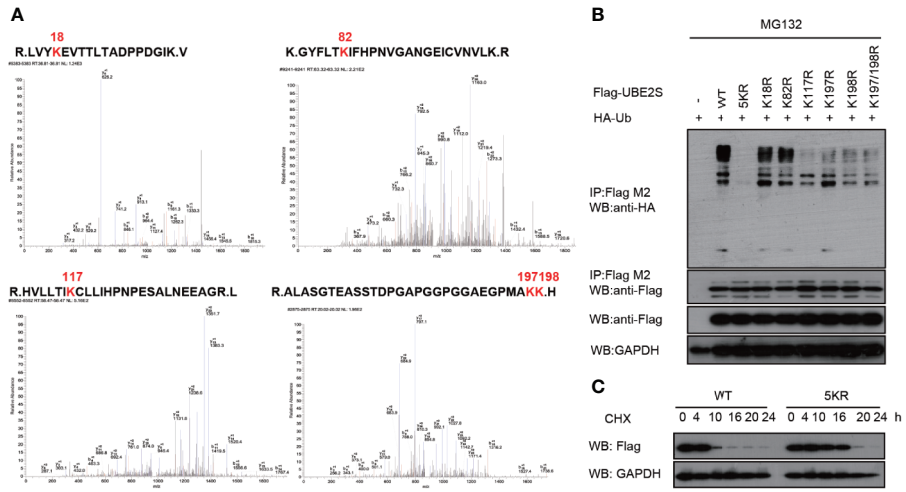

FIGURE 6 | Validation of ubiquitination sites of UBE2S. **(A)** Identification of ubiquitination sites of UBE2S by *Mass Spectrometry*. **(B)** U87 cells were transfected with indicated plasmids and treated with 100 nM CHX for four hours before harvest. Representative pictures of whole-cell lysates and immunoprecipitants as analyzed by Western blotting using the indicated antibodies. Experiments were performed in triplicates. **(C)** U87 cells were transfected with indicated plasmids and treated with 100 nM CHX at different times as indicated. Representative pictures of UBE2S protein levels as analyzed by Western blotting. Experiments were performed in triplicates.

To explore the mechanism of action of UBE2S in participation of the above signaling pathways in glioma, association between UBE2S and the molecular genetic features of glioma in different grades was determined. Analysis showed that UBE2S expression was positively associated with PTEN-mutation and EGFR amplification and negatively associated to IDH1-mutation and co-deletion of 1p19q in whole grade glioma (**Figure 3**). In addition, UBE2S expression was positively correlated with PTEN-mutation and EGFR amplification, but negatively correlated with IDH1-mutation in LGG samples retrieved from TCGA dataset (**Figure 2**). However, no significant correlation was observed for GBM, which can be attributed to the heterogeneity of high-grade glioma. The positively correlated PTEN-mutation was also identified by IHC analysis, and its monoallelic mutations are mainly detected in glioblastoma (20). The mutation rate of PTEN was 30% - 40% in GBM, and these findings have had a significant impact on management of PTEN mutant subtypes of glioma. Moreover, studies report that EGFR amplification promotes invasion, proliferation and resistance to radiotherapy and chemotherapy in GBM (21–23). The negatively related IDH1-mutation in LGG and co-deletion of 1p19q in whole grade glioma, have been previously associated with prolonged PFS and OS in patients after treatment (24). Similarly, the findings of this study show that higher UBE2S expression level is correlated with a significantly poor overall survival in LGG. Uni- and multi-variate cox regression analysis showed that UBE2S was an independent prognostic marker for clinical outcome. Therefore, UBE2S is a vital biomarker for predicting prognosis of glioma.

UBE2S is involved in multiple processes and mediates development and progression of malignant tumors. Previous studies report that, UBE2S stabilizes hypoxia-inducible factor 1α (HIF-1α) by mediating proteosomal degradation of von Hippel-Lindau (VHL), and affects expression of Vascular Endothelial Growth Factor (VEGF) and induction of Epithelial Mesenchymal Transition (EMT) thus promoting cell proliferation, invasion and metastasis through pVHL-HIF pathway (9, 25, 26). Moreover, UBE2S knockdown reduces Tyr397 phosphorylation of Focal Adhesion Kinase (FAK) thus suppressing multiple signals for cell proliferation, migration, and invasion (13).

Pathway enrichment analyses showed that UBE2S is implicated in multiple biological processes, including G1/S transition of mitotic cell cycle, DNA replication, cell proliferation and DNA repair. These results established the critical character of UBE2S in tumor development. and Notably, these findings are consistent with existing findings on the major physiological function of UBE2S in elongation of K11 ubiquitin chains initiated by Anaphase-Promoting Complex (APC/C) and by promotion of degradation of APC/C substrates during mitosis and promoting mitotic exit (27).

In addition to contribution to tumor proliferation, UBE2S plays important roles in DNA repair. Radiotherapy with latest proton and carbon ion irradiation and chemotherapy with TMZ for GBM are associated with single and double-strand DNA breaks (28, 29). Therefore, key factors participating in DNA damage repair mechanism may be associated with chemo-radiotherapy resistance. Previous studies report that UBE2S knockdown increases sensitivity of cervical cancer HeLa cells to etoposide and doxorubicin. In addition, UBE2S knockdown increased chemosensitivity to topotecan, however, the mechanism is not known (8, 30). Furthermore, overexpression of UBE2S is significantly associated with poor response to neoadjuvant Computerized Controlled Radiation Therapy (CCRT) (30). In our previous study, UBE2S was associated with NHEJ-mediated DNA damage repair (14). Knockdown of UBE2S increases sensitivity of

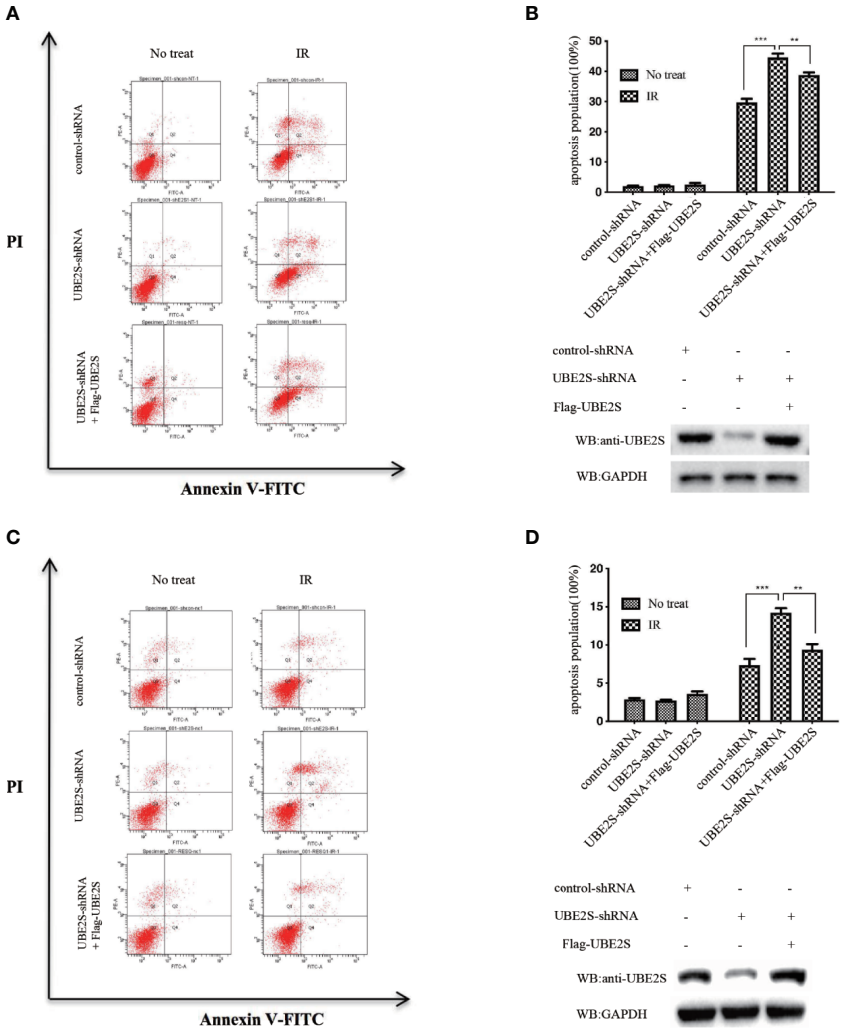

FIGURE 7 | Knockdown of UBE2S expression increases sensitivity of U87 and U251 cells to IR-induced apoptosis. **(A)** Indicated cells were treated with IR, and apoptotic cells were analyzed using FACS. **(B)** The upper panel shows the graphical representation of FACS analysis in **(A)**. Results are derived from three independent experiments and presented as mean ± SEM. ***P < 0.001, **P < 0.01. The lower panel shows the protein expression levels as indicated. **(C)** Indicated cells were treated with IR, and apoptotic cells were analyzed using FACS. **(D)** The upper panel shows the graphical representation of the FACS analysis in **(C)**. Means represent three independent experiments. Error bars indicate SEM. ***P < 0.001, **P < 0.01. The lower panel shows the protein expression levels as indicated. Statistical differences were determined by ANOVA.

glioma cells to IR. Notably, rescue of UBE2S expression did not completely restore apoptosis inhibited by UBE2S knockdown, implying that additional molecular mechanisms are involved. Therefore, further studies should explore the mechanisms by which UBE2S promotes the apoptosis phenotype of glioma.

The unstable characteristic of UBE2S provide a basis for further exploration of its role in different tumors. Our previous study reported that increased stabilization of UBE2S occurs after phosphorylation by Akt1. Therefore, MK-2206, an Akt1 inhibitor, was used to explore the role of UBE2S in radiotherapy resistance. MK-2206 pre-treated glioma cells, which exhibited low UBE2S expression levels, were more sensitive to IR. However, re-expressed UBE2S-5KR, a stable mutant of UBE2S, effectively rescued apoptosis. Therefore, UBE2S is an effective predictor of chemo-radiotherapy sensitivity and MK-2206 may be used to reverse radiotherapy resistance by targeting UBE2S.

CONCLUSIONS

In summary, the findings of this study show that higher levels of UBE2S are associated with a greater tumor burden, poor response to neoadjuvant therapy, and worse overall survival for LGG patients. This study shows the potential significance of UBE2S expression in diagnosis and prognosis of glioma and further explored the function of this protein in glioma. However, further studies are needed to

confirm these results. The underlying mechanism provides a basis for UBE2S as a new molecular target for prevention and treatment of glioma. UBE2S is therefore a potential novel biomarker and therapeutic target for the treatment of human glioma.

DATA AVAILABILITY STATEMENT

The original contributions presented in the study are included in the article/**Supplementary Material**. Further inquiries can be directed to the corresponding author.

ETHICS STATEMENT

The studies involving human participants were reviewed and approved by The Committees for the Ethical Review of Research at the First Affiliated Hospital of Harbin Medical University, Harbin, China. Written informed consent to participate in this study was provided by the participants' legal guardian/next of kin. The animal study was reviewed and approved by The Committees for the Ethical Review of Research at the First Affiliated Hospital of Harbin Medical University, Harbin, China.

AUTHOR CONTRIBUTIONS

LH and XC performed all experiments, prepared figures and drafted the manuscript. LH, ZH, YY, SW, and YF participated in data analysis and interpretation of results. LH, CW, AW, and ZL designed the study and participated in data analysis. ZB and DR gave many valuable comments on the draft, and also polished it. All authors contributed to the article and approved the submitted version.

FUNDING

This work was supported by National Natural Science Foundation of China (No. 81772678, 81802755, 81472360 and U20A20383), The China Postdoctoral Science Foundation (No. 2018M630372), Heilongjiang Postdoctoral Fund (No. LBH-Z17166), and Liaoning Science and Technology Plan Projects (No. 2011225034 to AW).

ACKNOWLEDGMENTS

We thank the staff members of The Cancer Genome Atlas for their involvement in the cBioPortal for Cancer Genomics Program.

SUPPLEMENTARY MATERIAL

The Supplementary Material for this article can be found online at: https://www.frontiersin.org/articles/10.3389/fonc.2021.640910/full#supplementary-material

REFERENCES

1. Shergalis A, Bankhead A3rd, Luesakul U, Muangsin N, Neamati N. Current Challenges and Opportunities in Treating Glioblastoma. *Pharmacol Rev* (2018) 70:412–45. doi: 10.1124/pr.117.014944
2. Ohba S and Hirose Y. Current and Future Drug Treatments for Glioblastomas. *Curr Med Chem* (2016) 23:4309–16. doi: 10.2174/0929867323666161014132907
3. Veliz I, Loo Y, Castillo O, Karachaliou N, Nigro O and Rosell R. Advances and Challenges in the Molecular Biology and Treatment of Glioblastoma-is There Any Hope for the Future? *Ann Transl Med* (2015) 3:7. doi: 10.3978/j.issn.2305-5839.2014.10.06
4. Qazi MA, Vora P, Venugopal C, Sidhu SS, Moffat J, Swanton C, et al. Intratumoral Heterogeneity: Pathways to Treatment Resistance and Relapse in Human Glioblastoma. *Ann Oncol* (2017) 28:1448–56. doi: 10.1093/annonc/mdx169
5. Abe S, Watabe H, Takaseki S, Aihara M and Yoshitomi T. The Effects of Prostaglandin Analogues on Intracellular Ca2+ in Ciliary Arteries of Wild-Type and Prostanoid Receptor-Deficient Mice. *J Ocul Pharmacol Ther* (2013) 29:55–60. doi: 10.1089/jop.2011.0197
6. Sugimoto K, Ideguchi M, Kimura T, Kajiwara K, Imoto H, Sadahiro H, et al. Epithelioid/Rhabdoid Glioblastoma: A Highly Aggressive Subtype of Glioblastoma. *Brain Tumor Pathol* (2016) 33:137–46. doi: 10.1007/s10014-015-0243-3
7. Fatai AA, Gamieldien J. A 35-Gene Signature Discriminates Between Rapidly- and Slowly-Progressing Glioblastoma Multiforme and Predicts Survival in Known Subtypes of the Cancer. *BMC Cancer* (2018) 18:377. doi: 10.1186/s12885-018-4103-5
8. Tedesco D, Zhang J, Trinht L, Lalehzadeh G, Meisner R, Yamaguchi KD, et al. The Ubiquitin-Conjugating Enzyme E2-EPF is Overexpressed in Primary Breast Cancer and Modulates Sensitivity to Topoisomerase Ii Inhibition. *Neoplasia* (2007) 9:601–13. doi: 10.1593/neo.07385
9. Jung CR, Hwang KS, Yoo J, Cho WK, Kim JM, Kim WH, et al. E2-Epf UCP Targets pVHL for Degradation and Associates With Tumor Growth and Metastasis. *Nat Med* (2006) 12:809–16. doi: 10.1038/nm1440
10. Welsh JB, Zarrinkar PP, Sapinoso LM, Kern SG, Behling CA, Monk BJ, et al. Analysis of Gene Expression Profiles in Normal and Neoplastic Ovarian Tissue Samples Identifies Candidate Molecular Markers of Epithelial Ovarian Cancer. *Proc Natl Acad Sci USA* (2001) 98:1176–81. doi: 10.1073/pnas.98.3.1176
11. Wagner KW, Sapinoso LM, El-Rifai W, Frierson HF, Butz N, Mestan J, et al. Overexpression, Genomic Amplification and Therapeutic Potential of Inhibiting the UbcH10 Ubiquitin Conjugase in Human Carcinomas of Diverse Anatomic Origin. *Oncogene* (2004) 23:6621–9. doi: 10.1038/sj.onc.1207861
12. Zhang RY, Liu ZK, Wei D, Yong YL, Lin P, Li H, et al. UBE2S Interacting With TRIM28 in the Nucleus Accelerates Cell Cycle by Ubiquitination of p27 to Promote Hepatocellular Carcinoma Development. *Signal Transduct Target Ther* (2021) 6:64. doi: 10.1038/s41392-020-00432-z
13. Ayesha AK, Hyodo T, Asano E, Sato N, Mansour MA, Ito S, et al. UBE2S is Associated With Malignant Characteristics of Breast Cancer Cells. *Tumour* (2016) 37:763–72. doi: 10.1007/s13277-015-3863-7
14. Hu L, Li X, Liu Q, Xu J, Ge H, Wang Z, et al. UBE2S, a Novel Substrate of Akt1, Associates With Ku70 and Regulates DNA Repair and Glioblastoma Multiforme Resistance to Chemotherapy. *Oncogene* (2017) 36:1145–56. doi: 10.1038/onc.2016.281
15. Chen MF, Lee KD, Lu MS, Chen CC, Hsieh MJ, Liu YH, et al. The Predictive Role of E2-EPF Ubiquitin Carrier Protein in Esophageal Squamous Cell Carcinoma. *J Mol Med* (2009) 87:307–20. doi: 10.1007/s00109-008-0430-3
16. Hu L, Li L-L, Lin Z-G, Jiang Z-C, Li H-X, Zhao S-G, et al. Blockage of Potassium Channel Inhibits Proliferation of Glioma Cells Via Increasing Reactive Oxygen Species. *Oncol Res Featuring Preclinical Clin Cancer Ther* (2014) 22:57–65. doi: 10.3727/096504014x14098532393518

17. Brennan CW, Verhaak RG, McKenna A, Campos B, Noushmehr H, Salama SR, et al. The Somatic Genomic Landscape of Glioblastoma. *Cell* (2013) 155:462–77. doi: 10.1016/j.cell.2013.09.034
18. Eckel-Passow JE, Lachance DH, Molinaro AM, Walsh KM, Decker PA, Sicotte H, et al. Glioma Groups Based on 1p/19q, IDH, and TERT Promoter Mutations in Tumors. *New Engl J Med* (2015) 372:2499–508. doi: 10.1056/NEJMoa1407279
19. Roos FC, Evans AJ, Brenner W, Wondergem B, Klomp J, Heir P, et al. Deregulation of E2-EPF Ubiquitin Carrier Protein in Papillary Renal Cell Carcinoma. *Am J Pathol* (2011) 178:853–60. doi: 10.1016/j.ajpath.2010.10.033
20. Benitez JA, Ma J, D'Antonio M, Boyer A, Camargo MF, Zanca C, et al. PTEN Regulates Glioblastoma Oncogenesis Through Chromatin-Associated Complexes of DAXX and Histone H3.3. *Nat Commun* (2017) 8:15223. doi: 10.1038/ncomms15223
21. Mazzoleni S, Politi LS, Pala M, Cominelli M, Franzin A, Sergi Sergi L, et al. Epidermal Growth Factor Receptor Expression Identifies Functionally and Molecularly Distinct Tumor-Initiating Cells in Human Glioblastoma Multiforme and is Required for Gliomagenesis. *Cancer Res* (2010) 70:7500–13. doi: 10.1158/0008-5472.CAN-10-2353
22. Hatanpaa KJ, Burma S, Zhao D and Habib AA. Epidermal Growth Factor Receptor in Glioma: Signal Transduction, Neuropathology, Imaging, and Radioresistance. *Neoplasia* (2010) 12:675–84. doi: 10.1593/neo.10688
23. Chakravarti A, Chakladar A, Delaney MA, Latham DE, Loeffler JS. The Epidermal Growth Factor Receptor Pathway Mediates Resistance to Sequential Administration of Radiation and Chemotherapy in Primary Human Glioblastoma Cells in a RAS-dependent Manner. *Cancer Res* (2002) 62:4307–15.
24. Hartmann C, Hentschel B, Tatagiba M, Schramm J, Schnell O, Seidel C, et al. Molecular Markers in Low-Grade Gliomas: Predictive or Prognostic? *Clin Cancer Res* (2011) 17:4588–99. doi: 10.1158/1078-0432.CCR-10-3194
25. Pugh CW and Ratcliffe PJ. Regulation of Angiogenesis by Hypoxia: Role of the HIF System. *Nat Med* (2003) 9:677–84. doi: 10.1038/nm0603-677
26. Gal A, Sjoblom T, Fedorova L, Imreh S, Beug H and Moustakas A. Sustained TGF Beta Exposure Suppresses Smad and non-Smad Signalling in Mammary Epithelial Cells, Leading to EMT and Inhibition of Growth Arrest and Apoptosis. *Oncogene* (2008) 27:1218–30. doi: 10.1038/sj.onc.1210741
27. Williamson A, Wickliffe KE, Mellone BG, Song L, Karpen GH and Rape M. Identification of a Physiological E2 Module for the Human Anaphase-Promoting Complex. *Proc Natl Acad Sci USA* (2009) 106:18213–8. doi: 10.1073/pnas.0907887106
28. Chiblak S, Tang Z, Campos B, Gal Z, Unterberg A, Debus J, et al. Radiosensitivity of Patient-Derived Glioma Stem Cell 3-Dimensional Cultures to Photon, Proton, and Carbon Irradiation. *Int J Radiat Oncol Biol Phys* (2016) 95:112–9. doi: 10.1016/j.ijrobp.2015.06.015
29. Jiapaer S, Furuta T, Tanaka S, Kitabayashi T and Nakada M. Potential Strategies Overcoming the Temozolomide Resistance for Glioblastoma. *Neurol Med Chir (Tokyo)* (2018) 58:405–21. doi: 10.2176/nmc.ra.2018-0141
30. Liang J, Nishi H, Bian ML, Higuma C, Sasaki T, Ito H, et al. The Ubiquitin-Conjugating Enzyme E2-EPF is Overexpressed in Cervical Cancer and Associates With Tumor Growth. *Oncol Rep* (2012) 28:1519–25. doi: 10.3892/or.2012.1949

Conflict of Interest: The authors declare that the research was conducted in the absence of any commercial or financial relationships that could be construed as a potential conflict of interest.

Copyright © 2021 Hu, Cheng, Binder, Han, Yin, O'Rourke, Wang, Feng, Weng, Wu and Lin. This is an open-access article distributed under the terms of the Creative Commons Attribution License (CC BY). The use, distribution or reproduction in other forums is permitted, provided the original author(s) and the copyright owner(s) are credited and that the original publication in this journal is cited, in accordance with accepted academic practice. No use, distribution or reproduction is permitted which does not comply with these terms.

frontiers in Oncology

REVIEW
published: 16 June 2021
doi: 10.3389/fonc.2021.696402

Targeting Immunometabolism in Glioblastoma

*Aditya A. Mohan, William H. Tomaszewski, Aden P. Haskell-Mendoza, Kelly M. Hotchkiss, Kirit Singh, Jessica L. Reedy, Peter E. Fecci, John H. Sampson and Mustafa Khasraw**

Preston Robert Tisch Brain Tumor Center at Duke, Department of Neurosurgery, Duke University Medical Center, Durham, NC, United States

We have only recently begun to understand how cancer metabolism affects antitumor responses and immunotherapy outcomes. Certain immunometabolic targets have been actively pursued in other tumor types, however, glioblastoma research has been slow to exploit the therapeutic vulnerabilities of immunometabolism. In this review, we highlight the pathways that are most relevant to glioblastoma and focus on how these immunometabolic pathways influence tumor growth and immune suppression. We discuss hypoxia, glycolysis, tryptophan metabolism, arginine metabolism, 2-Hydroxyglutarate (2HG) metabolism, adenosine metabolism, and altered phospholipid metabolism, in order to provide an analysis and overview of the field of glioblastoma immunometabolism.

Keywords: glioblastoma, immunotherapy, metabolism, immunometabolism, tryptophan, arginine, 2HG, adenosine

OPEN ACCESS

Edited by:
Terrance Johns, University of Western Australia, Australia

Reviewed by:
Lukas Bunse, German Cancer Research Center (DKFZ), Germany
Serena Pellegatta, Fondazione Istituto Neurologio Carlo Besta (IRCCS), Italy

***Correspondence:**
Mustafa Khasraw
mustafa.khasraw@duke.edu

Specialty section:
This article was submitted to Neuro-Oncology and Neurosurgical Oncology, a section of the journal Frontiers in Oncology

Received: *16 April 2021*
Accepted: *26 May 2021*
Published: *16 June 2021*

Citation:
Mohan AA, Tomaszewski WH, Haskell-Mendoza AP, Hotchkiss KM, Singh K, Reedy JL, Fecci PE, Sampson JH and Khasraw M (2021) Targeting Immunometabolism in Glioblastoma. Front. Oncol. 11:696402. doi: 10.3389/fonc.2021.696402

INTRODUCTION

Advances in immunotherapies have revolutionized cancer care, yet unfortunately, they have been largely unsuccessful in managing glioblastoma. One of the primary obstacles in treating glioblastoma with immunotherapy has been overcoming the heterogeneous and immunosuppressive tumor microenvironment (TME) that is, at least in part, regulated by tumor metabolism. Since 1927, when Otto Warburg et al. first described tumor's preferential use of glycolysis to generate adenosine triphosphate (ATP) (1), there has been a burgeoning interest in understanding tumor metabolism and how it influences tumor growth. However, it is only recently that our understanding of tumor metabolism has extended beyond the confines of the tumor cell membrane and that we have begun to understand how tumor metabolism affects noncancerous cells such as tumor-infiltrating immune cells.

While glioblastoma cells are metabolically distinct from noncancerous tissue in the brain, certain metabolic similarities exist between glioblastoma and proliferating immune cells. These similarities include an upregulation of glucose utilization, glycolysis, fatty acid oxidization, amino acid metabolism, and nucleotide synthesis. As such, glioblastoma cells can induce immunosuppression by outcompeting immune cells for critical nutrients. In addition to contending with immune cells for metabolites, certain glioblastoma cells can also avail distinctive metabolic pathways to produce unique metabolites such as 2-Hydroxyglutarate (2HG) and extracellular adenosine, which can directly suppress the immune system. While there are multiple mechanisms by which tumors can alter their metabolism and influence the immune

system, we have utilized large-scale omics analysis to selectively highlight pathways that are critical to glioblastoma pathogenesis (2–5).

In this review, we outline how altered metabolic pathways in glioblastoma contribute to immunosuppression and discuss approaches to target these phenomena, in order to improve future immunotherapy outcomes.

HYPOXIA

Hypoxia is a key feature of tumor growth and describes a condition in which the oxygen demand within an organism, cell, or tissue exceeds the available supply, typically described as < 10 mmHg O_2 (6). Hypoxia is frequently found in solid tumors, including glioblastoma, due to rapid tumor growth, ultimately outstripping vascular supply and therefore, preventing O_2 diffusion (6, 7). In gliomas, these hypoxic changes can be visualized on MR imaging, with high grade lesions displaying prominent ring-shaped contrast-enhancement with a hypointense center. Histological analysis of these regions often reveals highly anaplastic cells surrounding a necrotic tumor core, termed pseudopalisading necrosis (7, 8). The most important transcription factors in the cellular response to low pO_2 are the hypoxia-inducible factors (HIFs). HIF-mediated signaling plays a role in vasculogenesis, tumor and cancer stem-like cell proliferation, and immunosuppression within the tumor microenvironment (TME). This family consists of a constitutively expressed β subunit (HIF1β), and at least three tightly regulated α subunits, HIF1α, HIF2α, and HIF3α. In normoxic conditions, the heterodimeric protein's α subunit is rapidly degraded by the proteasome. Hypoxic conditions stabilize the α subunit and allow it to translocate to the nucleus, dimerize with the β subunit and induce transcription of hypoxia response genes (6, 7). In glioblastoma, it has been demonstrated that cells in the perivascular niche and necrotic areas upregulate the expression of HIF2α, and that this expression colocalizes with the stem cell markers CD133 and Olig2 (9, 10). Hypoxia increases growth and proliferation of glioma cells and glioma stem-cells, and strongly induces HIF2α, as well as stem genes. Ectopic expression of non-degradable HIF2α induced a stem-like phenotype in glioma cells and enhanced tumorigenicity *in vivo* (11). Hypoxia induced by the antibody bevacizumab that targets the vascular endothelial growth factor (VEGF), has also been shown to induce autophagy-related genes, resulting in a resistance mechanism to anti-VEGF therapy that could be abrogated by autophagy inhibition (12). In the past two decades, many basic investigations focusing on targeting hypoxia to increase the efficacy of VEGF inhibition were initiated, including inhibiting autophagy with chloroquine, or attempting to prevent HIF1α synthesis with mTOR inhibitors such as temsirolimus and everolimus (13).

Hypoxic changes in the glioma microenvironment may also modulate key immune effector molecules (**Figure 1**). Hypoxia has been further shown to induce T cell exhaustion through mitochondrial fragmentation and decreased oxidative phosphorylation, among other mechanisms (14). Furthermore, under hypoxic conditions, glioma cells secrete interleukins IL-6 and IL-8, which serve as autocrine proliferative signals and localize to perinecrotic regions with many pseudopalisading glioblastoma cells (15, 16). IL-6 signaling also plays a role in maintaining the tumor stem cell niche and stimulating angiogenesis (15, 17). Finally, IL-6 has been shown to induce upregulation of the programmed death-ligand 1 (PD-L1) on tumor-infiltrating and circulating myeloid cells (18). Additionally, glioma cells and proliferating endothelial cells in the hypoxic perivascular niche respond to HIF1α and VEGF signaling by upregulation of the chemokine receptor CXCR4, allowing for increased migration (19).

A small-molecule HIF2α inhibitor PT2385, which was later improved to the second-generation inhibitor PT2977 (now

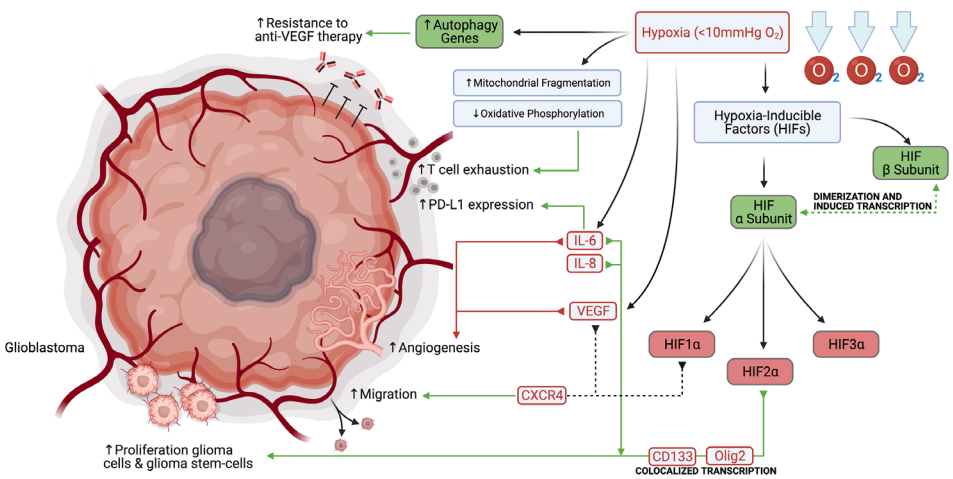

FIGURE 1 | Hypoxia promotes glioblastoma and glioblastoma stem-cell proliferation, migration, angiogenesis, PD-L1 expression, and resistance to anti-VEGF therapy.

known as 'MK-6482'), has also been shown to block the transcription of HIF2α-responsive genes, including *VEGFA*, *CCND1* and the glucose transporter–encoding gene *SLC2A1*, and both molecules demonstrated on-target antitumor activity in mouse xenograft models of renal cell cancer (20). PT2385 showed promising preliminary promising activity in early phase development. This is also studied in glioblastoma and in a combination study with nivolumab (21). MK-6482 is nearly identical to PT2385, but with a more favourable pharmacokinetic profile and is also undergoing evaluation in early phase trials (20).

GLYCOLYSIS

Glycolysis is the primary metabolic pathway that provides energy and involves the breakdown of glucose to form the high energy molecules ATP and NADH. The brain is an energy demanding organ with about 25% of the body's glucose consumption being devoted to brain function (22). Despite the brain's high energy demand, it has relatively low levels of glucose when compared to plasma (23). Glucose transporter 1 (GLUT1) is responsible for shuttling glucose into the brain, as well as driving it into cells (24). Neurons, oligodendrocytes, astrocytes, and tumor cells are especially dependent on glucose for survival and energy production (25, 26). Neurons additionally express Glucose transporter 3 (GLUT3), which is five-fold more efficient at transporting glucose than GLUT1 (24). The PI3k-Akt-mTOR pathway is primarily responsible for fulfilling the energy demands of transformed cells, neurons, and glia (27, 28).

Aerobic glycolysis (Warburg's effect) is a hallmark of cancer and is a process through which cancer cells produce lactate after undergoing glucose-mediated oxidative phosphorylation (29). Like other tumors, glioblastoma highly expresses GLUT1 and its energy demands are greater than that of normal brain cells (30, 31). Transformed, neuronal, and glial cells have high energy demands in a low glucose environment, and act as a sink that depletes glucose which limits immune cell anti-tumor effector functions. Gliomas can further recruit and maintain immunosuppressive immune populations such as pro-tumor mononuclear phagocytes which also undergo glycolysis and deplete available glucose, among other nutrients including L-arginine and L-cysteine, from the tumor microenvironment (32, 33). Blockage of the Akt-mTOR pathway *via* administration of Akt inhibitors in low glucose environments has been shown to inhibit growth of glioma cells (34). Additionally, high expression of a glycolysis related gene signature was associated with cancer progression, adhesion, proliferation, angiogenesis, and drug resistance, further demonstrating the important role of glycolysis in glioblastoma (35).

Immune cells, and in particular effector T cells, are dependent on glycolysis to support their proliferation and effector functions (36) (**Figure 2**). TCR signaling in T cells results in PI3k-Akt-mTOR signaling, which further increases glucose requirements (37). Low glucose availability is a known driver of the exhaustion phenotype in T cells (38). Recent research suggests that exhausted T cells exist on a continuum from a precursor exhausted state, that are responsive to checkpoint blockade, to a terminally exhausted state, which are refractory to checkpoint blockade therapy (39). Precursor exhausted T cells have been shown to have reduced expression of glycolysis related genes in relation to naïve and effector T cells (40). Interestingly the PD1/PDL1 receptor ligand pair has divergent functions in T cells and the tumor. Ligation of PD1 on T cells reduces glucose uptake, where increased expression of PDL1 on tumor cells improves tumor glycolysis (41–43). Reinforcing exhaustion in T cells *via*

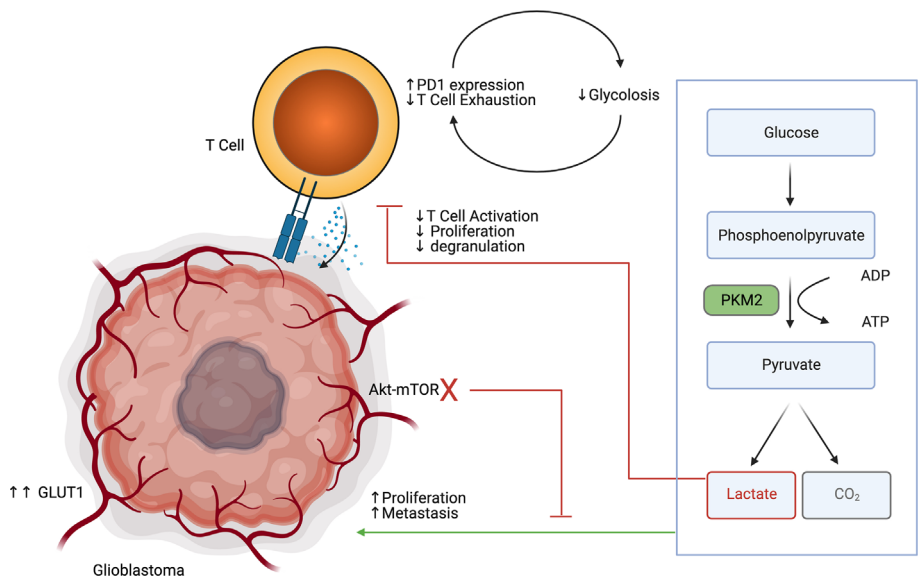

FIGURE 2 | Glioblastoma glycolysis drives tumor progression while inhibiting T cell glycolysis, activation, proliferation and degranulation.

inhibitory signals and reducing glucose uptake is a synergistic way that the tumor cells maintain the immunosuppressive microenvironment. Furthermore, lactate accumulation in the glioblastoma TME is in of itself a potent immunosuppressive agent. Lactate has been shown to polarize macrophages towards an M2 phenotype, impair lymphocyte proliferation, activation, and degranulation (44). Broad pharmaceutical inhibition of glycolysis may not result in a net anti-tumor effect, as it has pro-tumor effects in glioma cells, but is also important for anti-tumor effects in T cells. Drugs that disrupt glycolysis preferentially in the tumor or bolster glucose uptake specifically in T cells would be attractive methods of leveraging metabolism to provide an anti-tumor effect.

TRYPTOPHAN METABOLISM

The tryptophan catabolism is among the most characterized immunometabolic pathways in glioblastoma since it contributes to both tumor progression and immune evasion. Tryptophan, the least abundant amino acid, can be incorporated into proteins, modified to produce serotonin, or metabolized to produce kynurenines (Kyn). Briefly, tryptophan is metabolized by indoleamine 2,3-dioxygenase (IDO)1/2 and tryptophan 2,3-dioxygenase (TDO), another important enzyme of the kynurenine pathway, to produce N-formyl kynurenine, which is converted to kynurenine by arylformamidase (AFMID). Kynurenine is further metabolized through various pathways to produce metabolites including kynurenic acid, anthranilic acid, 3-hydroxykynurenine, xanthurenic acid, quinolinic acid, picolinic acid, and nicotinamide-adenine-mononucleotide (45). Although difficult to control each of these metabolites' pathways individually, it has been possible to inhibit their production through upstream IDO1/2 and TDO inhibition. IDO1/2 expression are typically found in peripheral tissues, while TDO expression is associated with hepatic tryptophan metabolism. Although recent evidence suggests that there may be value in specifically targeting TDO in the context of glioblastoma, tryptophan metabolism in glioblastoma has primarily been explored in the setting of IDO1/2.

Kynurenines and quinolinic acid have been previously described to be able to drive neoplastic proliferation through Wnt/β-catenin signaling (46). Kynurenines further influence tumorigenesis in glioblastoma by modulating DNA repair enzyme, polymerase kappa, thereby preventing DNA damage and allowing genomic instability to propagate leading to tumor heterogeneity (47). Kynurenines and quinolinic acid may also promote cell proliferation in a fibroblast growth factor-1 (FGF-1) dependent manner (48). Lastly, nicotinamide-adenine-mononucleotide can be converted to NAD+, which confers tumor cells' resistance to oxidative stress. Although the mechanism remains largely unclear, IDO expression may play a role in tumor angiogenesis and metastasis through control of IFNg and IL-6 (49). Mondal et al. found that *in vivo* IDO inhibition reduced metastasis and neovascularization (50). In patients with glioblastoma, IDO expression was strongly associated with shortened overall survival (51).

IDO1/2 mediated depletion of tryptophan was initially thought of as an ancient innate immune mechanism to prevent the growth of microorganisms while reducing inflammation and autoimmunity in areas such as the brain (52). In fact, IDO1/2 expression is significantly increased in inflammatory tissues due to IFNg, TGF-β, and PGE2 signaling to potently inhibit active inflammation (**Figure 3**). Wainwright et al. were among the first to demonstrate that glioblastoma cells significantly upregulated

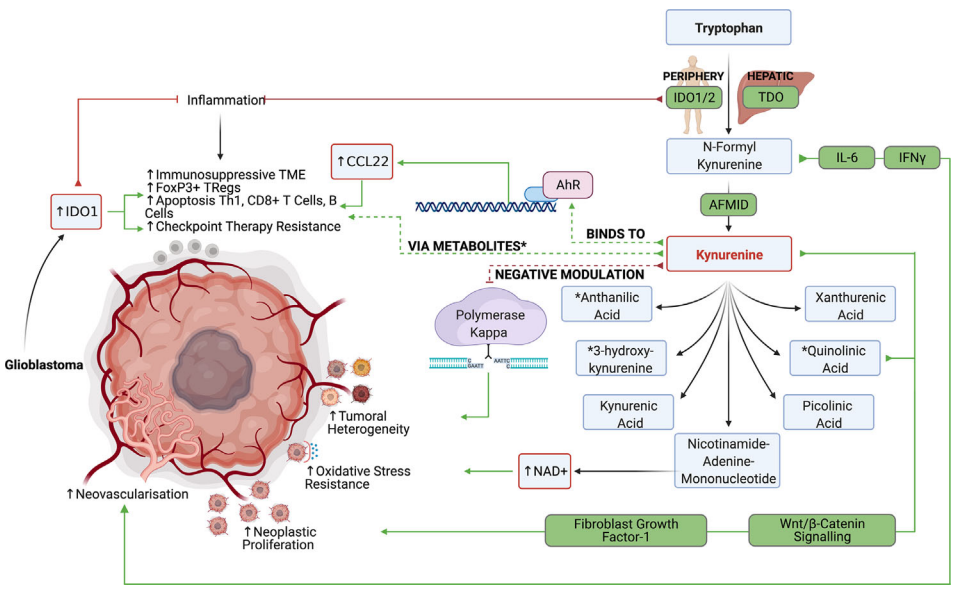

FIGURE 3 | The IDO1/2 and TDO pathway allow the production of various tryptophan metabolites, which suppress anti-glioblastoma lymphocyte responses while promoting tumor growth.

the expression of IDO1 and suggested that IDO1 may also contribute to tumor progression by promoting an immunosuppressive phenotype (53).

In both clinical studies and preclinical murine glioma models, tumors with high expression levels of IDO1 were infiltrated with more FoxP3+ regulatory T cells (53). It has been suggested that tryptophan metabolism can induce Treg differentiation based on the kynurenines' ability to bind to cytosolic ligand-activated transcription factor AhR (54). Kynurenine-driven AhR activation also induces the production of CCL22 to recruit Tregs into the glioblastoma TME (55). In addition to inducing suppressive T cell populations, tryptophan metabolism may blunt antitumor CD4 and CD8 responses through various mechanisms. Opitz et al. found that TDO derived kynurenines reduced the proliferation of both CD4+ and CD8+ T cells and reduced LCA+ CD8+ T cell infiltration in human gliomas with high TDO expression (56). Furthermore, depletion of tryptophan in the TME leads to an accumulation of unbound tryptophan–tRNA in T cells which activates the GCN2 mediated stress response and inhibits RNA transcription and protein synthesis in T cells leading to cell cycle arrest and apoptosis (57). Although currently contested, some evidence suggests that tryptophan deprivation may also inhibit the mTOR pathway in T cells to inhibit effector T cell functions. Additionally, metabolites like quinolinic acid, 3-hydoxyanthranilic acid, and 3-hydroxykynurenine have been shown to induce apoptosis in Th1 helper cells, CD8+ Effector T cells, B cells, while sparing immunosuppressive Th2 helper cells.

IDO inhibitors such as 1-L-MT, IDO-IN-2, Navoximod (GDC-0919), IDO-IN-1, Linrodostat, coptisine chloride, PF-06840003, and TDO inhibitors such as 680C91 have recently been developed (58). While IDO inhibitors such as navoximod did not improve antitumor responses in preclinical glioblastoma models, Kesarwani et al. found that navoximod synergistically improved antitumor responses when combined with RT and immune checkpoint blockade (59). Hanihara et al. and Li et al. similarly found that while 1-L-MT did not improve antitumor immunity on its own, 1-L-MT significantly synergized with temozolomide administration and radiation therapy (60, 61). Wainwright et al. found that IDO inhibitors particularly synergized with PD1 and CTLA4 blockade in the mice (62, 63). Interestingly, advanced age is associated with an increase of brain IDO expression and this is not reversed by IDO enzyme inhibitor treatment (64). It remains to be seen if targeting IDO will translate into clinical benefit in cancer and in gliomas.

ARGININE METABOLISM

Arginine is yet another amino acid substrate that is actively metabolized by tumor cell to promote tumor progression and immunosuppression. L-arginine is critical in the urea cycle and is a modulator of immune function and tumor metabolism. L-arginine is utilized as a substrate for both Arginase 1 (ARG1) and cytokine inducible nitric oxide synthase (iNOS). ARG1 converts L-arginine to urea and ornithine, which is further utilized in the urea cycle. iNOS converts L-arginine to citrulline and nitric oxide (NO), which is important for directing anti-tumor functions in immune cells (65).

Depletion of arginine has been identified as a successful treatment strategy in cancers that are deficient in aspects of arginine metabolism and are reliant on exogenous sources (**Figure 4**). This approach has been successful in Leukemia, where transformed cells were found to be deficient in asparagine synthase and were not capable of producing asparagine. This left the tumors vulnerable to treatment with L-asparaginase which depleted asparagine (66). Similarly the function arginosuccinate synthase 1 (ASS1) is defective in some tumors, which makes them dependent on exogenous arginine (66). In glioblastoma, there seems to be an abundance of arginine transporters, which is evidenced by a notable accumulation of byproducts of arginine metabolism (67, 68). This suggests that arginine metabolism is functional, and may be sensitive to targeted depletion. A recent study that utilized a pegylated recombinant human ARG1, depleted arginine, and induced cytotoxicity in glioma cells (69). Similarly, selective iNOS inhibitors 1400W and S-MIU have recently been shown to reduce tumor growth in a EGFRvIII mutant overexpressing U87 glioblastoma model (70). How arginine fosters immunosuppression in the TME is also an area of research that seeks to elucidate the tumor promoting effects of arginine metabolism.

Macrophages are a large component of the TME, constituting up to 30% of the tumor by weight (71, 72), and the divergent functions of arginine metabolism are best appreciated in this immune cell subset. Macrophages are a highly plastic cell type, which can adopt either pro- or anti-tumor function depending on their environmental cues. Macrophage polarization has traditionally been thought of to exist on a continuum from M1 to M2 phenotypes which confer inflammatory/anti-tumor phenotypes and repair/pro-tumor phenotypes, respectively. Recent research suggests that the M1-M2 dichotomy is likely an oversimplification (73), which is underscored by the numerous reports that tumor associated macrophages (TAMs) in glioblastoma express a mixture of M1 and M2 related genes (74, 75). TAMs which primarily metabolize arginine *via* iNOS are considered more anti-tumor. iNOS dependent anti-tumor TAMs skew the TME towards cytotoxicity through stimulating Th1 responses *via* secretion of CXCL9 and CXCL10, inducing cytotoxic CD8s through TNFα and IL1β, and direct killing of tumor cells through nitric oxide (NO) and Reactive Oxygen Species (ROS). Conversely TAMs which metabolize arginine primarily through ARG1 are thought to have more pro-tumor activity. ARG1 dependent pro-tumor TAMs stimulate angiogenesis through VEGF and IL6, promote invasion and proliferation *via* TGFβ and STAT3, and support immunosuppression through IL-10 and TGFβ (65). TAMs in glioblastoma are considered to be pro-tumor overall, and their accumulation correlates with worse prognostic outcomes (76). Due to the highly plastic nature of TAMs and their abundance in the glioblastoma TME, they are an attractive target for repolarization from a pro-tumor to an anti-tumor phenotype.

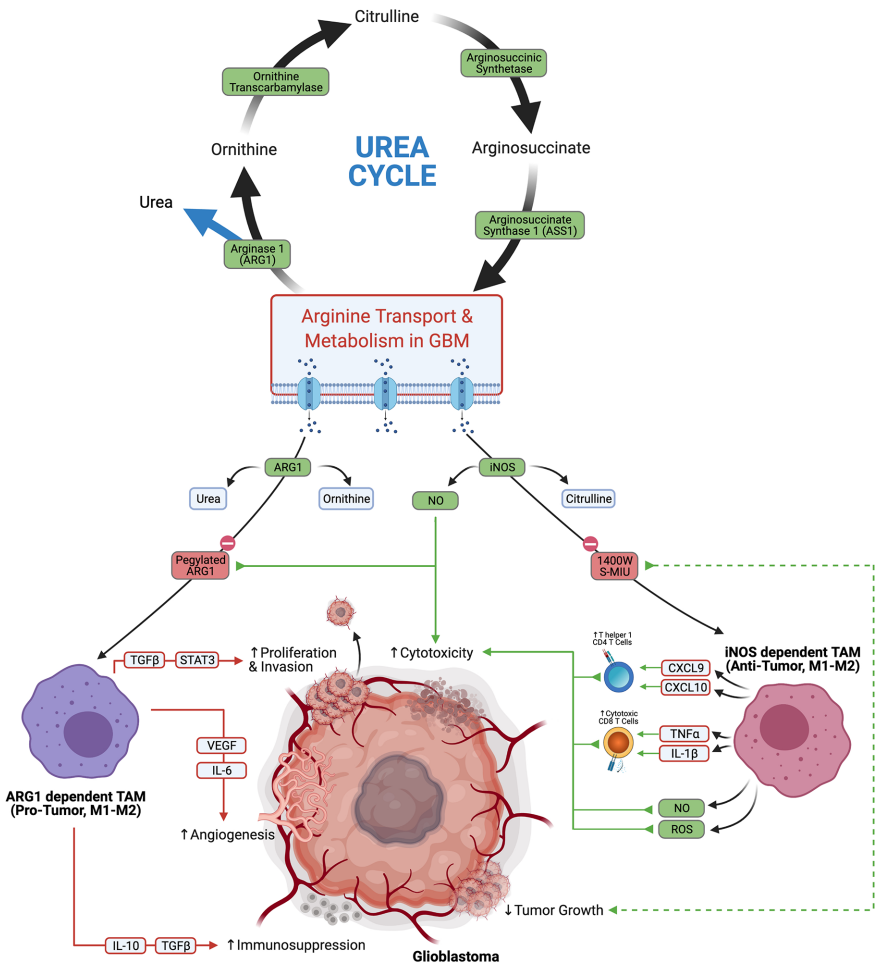

FIGURE 4 | Glioblastoma arginine metabolism *via* iNOS or Arg1 polarizes the tumor associated macrophages towards anti-tumor tumor or pro-tumor phenotypes, respectively.

Finding ways to selectively shift arginine metabolism in TAMs towards iNOS presents an interesting treatment modality that could potentially skew a large portion of the TME to an overall anti-tumor effect.

2-HYDROXYGLUTARATE METABOLISM

2HG production represents a unique immune-metabolomic pathway found in many cancer cells, including low-grade gliomas and secondary glioblastoma. Within low-grade gliomas and secondary glioblastoma, 2HG is often produced due to mutations in the catalytic domains of isocitrate dehydrogenase isoform 1 (IDH1) and isocitrate dehydrogenase isoform 2 (IDH2). The most common mutations in IDH1 include R132H, R132C, R132L, R132S, and R100Q, while the most common mutations in IDH2 include R140Q, R140G, R140W, R140L, R172K, R172G, R172M, R172Q, R172T, R172S (77). While IDH1 is found in the cytoplasm of cells, IDH2 is found in the mitochondrial matrix. Despite their differences in cellular sub-localization, both wildtype IDH1 and wildtype IDH2 catalyze the decarboxylation of isocitrate using $NADP^+$ and Mg^{2+} as cofactors and produce α-Ketoglutaric acid and CO_2 (78). Wildtype IDH1 and wildtype IDH2 are normally also able to catalyze the reverse reaction by reducing α-Ketoglutaric acid into isocitrate using NADPH as a cofactor. α-Ketoglutaric acid also acts as a substrate for an alternative reduction reaction that incompletely reduces α-Ketoglutaric acid into 2-Hydroxyglutarate instead of isocitrate in an NADPH driven manner. Somatic missense mutations of arginine in IDH1 and IDH2 lead to impaired oxidative carboxylation and favor the incomplete reduction of α-Ketoglutaric acid into 2-Hydroxyglutarate (79). While 2HG is produced by other enzymes including hydroxyacid-oxoacid transhydrogenase (80), human phosphoglycerate dehydrogenase (81), lactate dehydrogenase (82), and l-malate dehydrogenase (83), it is believed that IDH1/2 mutations are almost exclusively what drive 2HG overaccumulation in low-grade glioma and

secondary glioblastoma. In grade II/III gliomas carrying IDH1/2 mutations, 2HG concentrations have been found between 1 and ~30 m*M* (77). The overaccumulation of 2HG can both promote gliomagenesis while inhibiting anti-tumor immunity.

The oncogenic process can be mediated through epigenetic regulation, 2HG, inhibition of DNA repair enzymes, promotion of autophagy, and promotion of invasiveness. 2HG exerts control over cellular epigenetics by favoring the hypermethylation of various genes by inhibiting α-Ketoglutaric acid-dependent dioxygenases such as Tet methylcytosine dioxygenases (TETs) (84). Koivunen et al. demonstrated that TET2, in particular, was inhibited by 2HG (85). TET2 inhibition was demonstrated to decrease tumor cell differentiation and promote tumorigenesis in the setting of glioblastoma by Garcia et al. (86) Perhaps most notably, 2HG was shown to increase methylation of histone lysines and c-Myc binding at the promoter of the telomerase reverse transcriptase (TERT) gene encouraging tumor transformation and immortalization (87). 2HG was also shown by Chen et al. to inhibit the AlkB family of DNA repair enzymes such as ALKBH2 and ALKBH3 (88). 2HG further promotes autophagy and cell survival by indirectly controlling mTORC1 and mTORC2 signaling. 2HG does this by activity inhibiting KDM4A, which allows DEPTOR to activate the mTORC1/2 pathway (78). 2HG may also have a role in destabilizing the basement membrane of glioblastoma cells through the inhibition of collagen stabilizing enzymes such as PLOD1, PLOD3, P4HA1, and PHA3 (79). In addition to IDH1/2 mutations helping produce 2HG, these mutations also favor the consumption of NADPH instead of their production. The depletion of NADPH helps induce cellular dysregulation and impairs cellular defense against reactive oxygen species (77).

While 2HG has been shown to influence tumor growth, 2HG has also been demonstrated to modulate anti-tumor immunity (**Figure 5**). Bunse et al. demonstrated that 2HG produced by tumors can be transported into immune cells *via* SLC13A3, which generally impairs immune function (89). Within T cells, 2HG was shown to inhibit T cell activity by inhibiting enzymes such as ornithine decarboxylase, transcription factors such as NF-κB p65, and the NFAT pathway through NFATC1 (89). It was demonstrated that T-cells treated with 2HG producing astrocytes demonstrated decreased production of IFN-γ and IL-2 upon activation (89). 2HG also directly inhibits T cell activation by inhibiting the steps that lead to calcium influx, such as early ATP-dependent TCR signaling events, c-Jun N-terminal kinase (JNK), and PLC-γ1(Y783) phosphorylation (89). Of note, the effect of 2HG on the suppression of T-cell activation was most prominent in CD4+ T cells. 2HG was also found by Kohanbasch *et al.* to reduce the expression of STAT1 in DC cells, thereby inhibiting the secretion of CXCL10 in the glioblastoma TME (90). This represents yet another mechanism by which 2HG may suppress T cell activity. Interestingly, IDH1/2 mutant tumors are generally infiltrated by T cells expressing less PD-1 than those T cells found in IDH1/2 wildtype tumors (89). This may be due to 2HG inhibiting NFAT translocation, which is necessary for inducing PD-1 expression. IDH1/2 mutant tumors are also generally infiltrated by less immunosuppressive M2 Macrophages (91). Amankulor et al. suggest that the decreased immunosuppressive cell infiltration in IDH1/2 mutant tumors

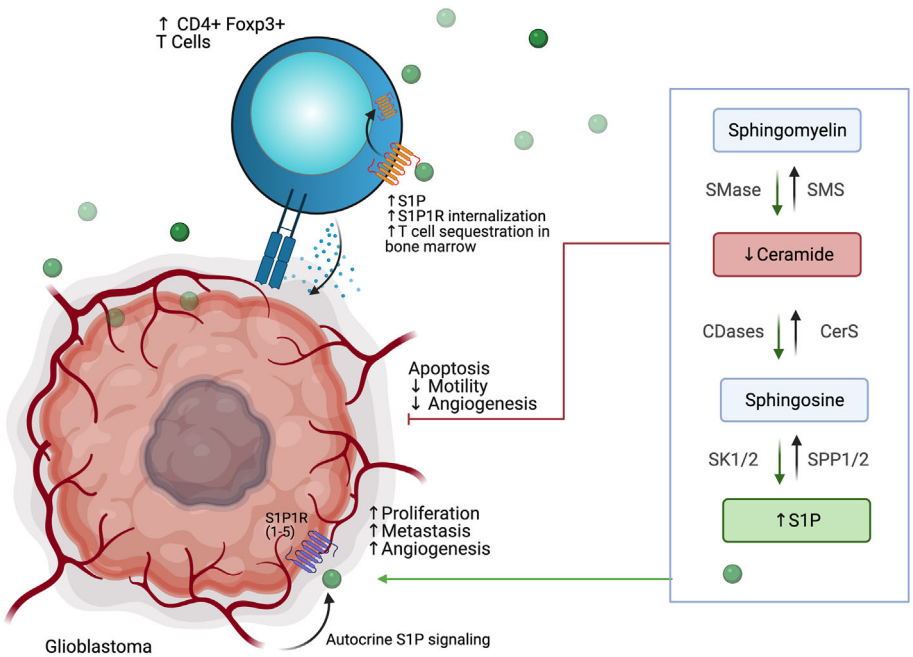

FIGURE 5 | 2 HG produced by IDH1/2 mutant secondary glioblastoma promotes tumor survival while impairing T cell activation and degranulation.

may play a role in controlling the growth of secondary glioblastoma (92).

Given the immunometabolic importance of IDH1/2 mutations, IDH mutation-specific inhibitors have been developed. IDH1 mutations have been targeted through molecules such as Ivosidenib, BAY-1436032, and AG-5198 (93). IDH2 mutations have been targeted through molecules such as Enasidenib, AGI-6780, and GI-6780 (93). IDH1 and IDH2 mutations have been co-targeted though molecules such as AG-881, which is currently being evaluated in the phase 3 INDIGO trial (NCT04164901) in patients with residual or recurrent Grade 2 glioma with an IDH1 or IDH2 mutation (93). Since IDH mutations may help anti-tumor immunity by decreasing PD1 expression and decreasing immunosuppressive cell infiltration, there may rationale to combine IDH mutation inhibitors with other immunostimulatory therapies such as checkpoint blockade. Bunse et al. demonstrated that BAY1436032 and PD-1 therapy increased overall survival in a murine IDH1 R132H model (89). Similarly, Kadiyala et al. found that 2HG inhibition, IR treatment, temozolomide, and anti-PDL1 administration led to complete tumor regression in 60% of mice bearing IDH1 mutant gliomas (94). In addition to small molecule inhibition, Platten et al. recently demonstrated that the IDH1 R132H mutant pathway could also be targeted by a peptide vaccine approach in newly diagnosed gliomas (95). While IDH inhibitors and vaccines represent one of the remarkable success stories in low grade IDH mutated gliomas, they are unfortunately not a therapeutic option in IDH wild type glioblastoma.

ADENOSINE METABOLISM

In normal physiology, adenosine and ATP are found in the cytosol of tissues, while these metabolites' extracellular levels are rarely observable (96). In certain pathologies such as gliomagenesis, intracellular adenosine can be secreted *via* bidirectional equilibrating nucleoside transporters (97), and ATP is released extracellularly *via* plasma membrane disruption or ATP efflux induced by hypoxia or inflammation and mediated by ABC transporters, anion channels, connexins, pannexins, and receptors like P2X7R (98). Once in the extracellular environment, ATP is degraded by enzymes such as CD73 and CD39 to produce adenosine. While the CD73 and CD39 mediated pathway of adenosine production are the most relevant to glioblastoma, extracellular adenosine may also be generated *via* ecto-phosphodiesterase/pyrophosphatase family proteins, nicotinamide adenine dinucleotide glycohydrolases, prostatic acid phosphatase, and alkaline phosphatase (99, 100). Extracellular adenosine is regulated either by cellular uptake or extracellular adenosine deaminase enzymes. The extracellular adenosine that remains can signal through high-affinity A2a and low-affinity A2b receptors expressed on tumors, tumor-associated cells, and immune cells. Blocking this adenosine signaling represents an intriguing target to modulating anti-tumor responses.

The adenosine metabolism pathway is of particular importance in glioblastoma and low-grade gliomas. Ott et al. recently found that in patients with gliomas, the A2aR/CD73/CD39 pathway was most frequently expressed (101). In the hypoxic glioblastoma TME setting, there is an increased expression of HIF1a in tumor tissue leading to increased expression of CD39 and CD73 on tumor cells, immune cells, stromal cells, and endothelial cell, leading to increased extracellular adenosine. This extracellular adenosine can signal through adenosine receptors to improve tumor survival, stimulate tumor cell proliferation, and induce tumor cell invasion and angiogenesis. Adenosine can improve tumor cell survival through the AKT and ERK pathways, inhibiting caspase pathway activation, upregulation of Bcl2 family antiapoptotic genes and downregulation of P53 (102, 103). Adenosine has been shown to induce tumor cell proliferation through various pathways including but not limited to AKT, ERK, JNK, and P38, ERa, and upregulation of cyclin proteins (104–106). Adenosine has been shown to increase the expression of matrix metalloproteases (MMPs) and FXYD5, which disrupt the tumor's ECM and drive invasiveness by reducing cell adhesion, respectively (107). Lastly, adenosine signaling can help drive angiogenesis by inducing increased VEGF, IL8, angiopoietin 2, and erythropoietin (100).

In addition to regulating tumor growth, adenosine signaling has a multifaceted role in controlling anti-tumor immunity (**Figure 6**). While extracellular ATP functions as danger associated molecular pattern (DAMP) that can stimulate both innate and adaptive immunity, extracellular adenosine serves to dampen the immune system (108). Within T cells, adenosine signaling through receptors such as A2aR inhibits MAP kinase, protein kinase C, NFkB, and NFAT pathways and inhibit proximal TCR signaling (109, 110). T cells treated with adenosine demonstrated decreased IL-2, TNFa, and INFg production, decreased CD28 expression, and increased expression of PD1, CTLA4, and LAG3 (108, 111, 112). Adenosine signaling was also shown to help generate Tregs by increasing the expression of FoxP3 in CD4 T cells (113). These Tregs were found to upregulate CD39 and CD73, creating a positive feedback loop in the TME (113). Adenosine signaling similarly blunted NK cell target cell killing, proliferation, and the production of IFNg and TNFa (114–116). DC cells treated with adenosine exhibited decreased expression of TNFa and IL12 while increasing their expression of immunosuppressive factors including IL-5, IL-6, IL-10, TGFβ, arginase, and IDO, and PD-L2 (117, 118). In macrophages, adenosine signaling *via* A2aR and A2bR were shown to induce M2 polarization (119) and blunted the secretion of neutrophil chemoattractants (111). Adenosine signaling also directly impaired neutrophil function finding their ability to adhere, degranulate, phagocytose, and produce TNFa and superoxide (120).

Sitkovsky et al. were one of the first to demonstrate enhanced anti-tumor immunity in A2aR knockout mice and demonstrated that A2aR could be inhibited using pharmacologic blockade (121, 122). In preclinical models, the immunosuppressive effect of adenosine signaling has been

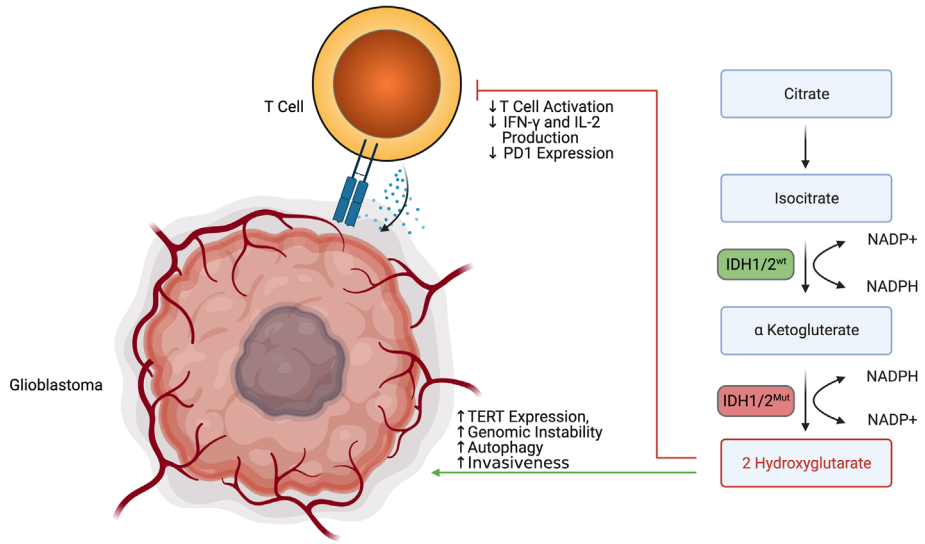

FIGURE 6 | Glioblastoma cells control the amount of extracellular adenosine in the glioblastoma immune microenvironment and use adenosine to decrease T cell degranulation and increase T cell exhaustion.

blunted using anti-CD73 and anti-CD39 blockade (123). In multiple murine tumor models, A2aR inhibition synergized with anti-PD1, anti-TIM3, and anti-CTLA4 antibodies to improve survival and reduce tumor metastasis (124–126). Inhibitors of this pathway such as Istradefylline, SCH-442416, Preladenant, BAY-545, Ciforadenant (CPI-444), Imaradenant (AZD4635), SCH58261, AB928 and AB680 have emerged and many of them are in clinical development (123). Targeting the adenosine signaling pathway in glioblastoma remains an active area of research.

ALTERED PHOSPHOLIPID METABOLISM

Sphingolipids are important structural components of the cell membrane that play a role in membrane fluidity and integrity. Many sphingolipids are also highly bioactive and play roles in a variety of cellular processes. Sphingosine, the first discovered sphingolipid, is induced by cellular stressors, including chemotherapy and radiation, and functions in cytoskeletal reorganization, cell cycle regulation, senescence and apoptosis. Since then, many other sphingomyelins have been identified, including ceramide, a molecule involved in regulation of apoptosis and is believed to be the central hub of sphingolipid metabolism, as well as sphingosine-1-phosphate, or S1P, which has roles in promoting survival, migration, and inflammation (127, 128).

Sphingolipid synthesis occurs *de novo via* condensation of serine and palmitate to 3-keto-dyhydrosphingosine, which *via* several intermediate steps involving ceramide synthases (CERS1-6) is converted to ceramide, a molecule well-identified as a pro-apoptotic signal (128, 129). Ceramide consists of an 18-carbon sphingosine long-chain base that contains an amide-linkage to a fatty acyl chain of variable carbon number; synthesis by CERS1-6 is the rate-limiting step of *de novo* ceramide synthesis and each enzyme is responsible for ceramides of specific fatty acyl chain length. Ceramides can also be synthesized *via* salvage following breakdown of complex sphingolipids such as sphingomyelins, *via* the subcellularly-localized sphingomyelinases (acid, neutral, and alkaline SMases), and cerebrosides, *via* glucosylceramidase and galactosylceramidase. Ceramide breakdown *via* ceramidases leads to sphingosine formation, which may be recycled or phosphorylated by the sphingosine kinases SK1 and Sk2 to form S1P. S1P is a ligand for the five G-protein coupled receptors S1PR1-5 and is normally rapidly metabolized *via* S1P phosphatase (SGPP) and S1P lyase 1 (SPL). Activation of S1PRs results in cellular proliferation and further production of S1P to promote cell motility and survival. This tight linkage of interconnected pathways for the rapid synthesis and breakdown of ceramide (pro-apoptotic) and S1P (pro-survival) has given rise to the "sphingolipid rheostat" model, in which the balance of these two biomolecules plays an important and potentially targetable role in normal cellular function and oncogenesis (127–131).

Derangement of the sphingolipid rheostat is implicated in the pathogenesis of glioblastoma (**Figure 7**). Analysis of human glioma tissue revealed significantly lower ceramide levels in high grade tumors relative lower grade tumors, and relative to peritumoral brain tissue (132). This difference was most dramatic for the C18 ceramide. Likewise, S1P levels in glioma tissues were higher than in normal gray matter; glioma stem-like cells have also been shown to secrete S1P as an autocrine, resulting in proliferation and increased expression stemness markers (132, 133). Taken together, this S1P/

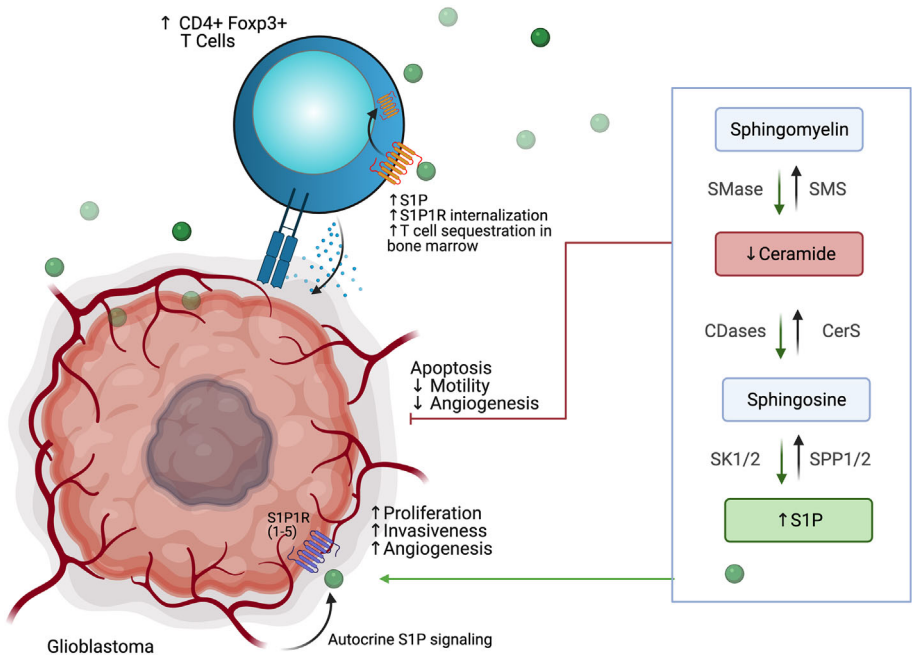

FIGURE 7 | Glioblastoma cells use altered phospholipid metabolism to induce tumor proliferation, invasiveness, and angiogenesis while sequestering T cell populations away from the tumor microenvironment.

ceramide shift represents a common, targetable feature of malignancy even with regard for the heterogeneity displayed within and between glioblastomas. In gliomas, this shift is likely due to multiple alterations in sphingolipid synthesis, including increased expression of SK1 (134–136), deletion of chromosomal regions containing SPL (137), and downregulation of S1P phosphatase 2 (138), resulting in increased S1P levels; as well as inhibition of ceramide synthase (139) and increased expression of ceramidases (134). The activity of SMases in glioblastoma is still being elucidated, but it has been shown that acid SMase may sensitize glioma cells to chemotherapy and radiation by increasing metabolism of sphingomyelin to ceramide and consequent apoptosis in the context of p53-deficiency; conversely, neutral SMase may be involved in increasing ceramide production in p53-wildtype cells (129). Increased understanding of the proapoptotic role of SMases in glioblastoma may yield new therapeutic targets.

Interactions of glioblastoma with surrounding neuronal, glial, and immune cells in the TME are continuing to be appreciated. As discussed above, S1P plays an autocrine role in gliomas, and has been shown to be constitutively secreted in rodent glioma cells and human glioblastoma cell lines, likely due to SK1 activity (134, 140, 141). Increased SK1 activity, in turn, has been shown to be induced by microenvironmental IL-1 and HIF-2α activity (142, 143). S1P is also capable of acting as a chemoattractant for innate and adaptive immune cells (144, 145). Increased glioblastoma-derived S1P may thus promote formation of TAMs. TAMs, in turn, may also contribute S1P to the TME and increase SK1 activity (130). TAMs also produce NO, which has been shown to decrease acid SMase activity in glioma cells, resulting in therapeutic resistance (146). Despite the breakdown of the blood-brain barrier (BBB) in glioblastoma, there is often a paucity of T-cells in the TME or within the tumor (so-called tumor-infiltrating lymphocytes, or TILs). Those cells that are present are often the CD4+ CD25+ FoxP3+ population of immunosuppressive regulatory T-cells, termed T_{regs} (147). In addition to their role in apoptosis, global alterations of SMase expression modulate differentiation of T cell populations, with acid SMase activation linked to increased numbers of CD4+ Th1 and Th17 cells, while mice deficient in acid SMase exhibit increased T_{regs} (148, 149). Recently, it has been shown that glioblastomas may cause sequestration of T cells in bone marrow *via* T-cell internalization of S1PR1, and enforced expression of S1PR1 in combination with T-cell activation *via* 4-1BB agonism can increase survival *in vivo* (144). 4-1BB agonism has also been shown to rescue the poor efficacy of PD-1 blockade in glioblastoma *in vivo*; translation of these results to clinical trials is greatly anticipated (150). Blockade of S1PR1 is commonly employed using the sphingosine analog fingolimod to reduce immune trafficking in multiple sclerosis; fingolimod may also inhibit ceramide synthases, SK1, and SPL and was proposed as a possible therapeutic for glioblastoma (144, 151). A small trial of fingolimod was initiated with the aim of assessing whether sequestration of lymphocytes *via* S1PR1 antagonism could reduce post-chemoradiation lymphopenia in glioblastoma patients, but

results have not yet been published (NCT02490930). Interestingly, Baeyens et al. recently found that monocytes in the lymph node may also produce S1P and influence T cell differentiation and T cell residence time in the lymph node (152). Their work suggests an alternative mechanism by which drugs that target S1P signaling can influence the glioblastoma TME and immune populations.

Additionally, an emerging mediator of aberrant phospholipid metabolism in glioblastoma is polymerase I and transcript release factor (PTRF), also known as Cavin1. PTRF was originally discovered to be involved in dissociation of RNA polymerase I-rRNA-DNA ternary complexes during transcription (153, 154). Through its colocalization with caveolin1 (Cav1) on the plasma membrane, it has been subsequently identified as essential for the formation of caveolae, cell-membrane infoldings that are 50-100 nm in diameter and function in cell signaling, lipid metabolism, and endocytosis (155, 156). Indeed, mutations in PTRF cause congenital generalized lipodystrophies in humans, providing further evidence for its role in lipid metabolism (157, 158). PTRF has also been shown to play a role in oncogenesis, as reduced PTRF expression in prostate and lung cancer is associated with progressive disease (45).

There is increasing evidence of a role for PTRF in the growth and progression of glioblastoma. PTRF has been shown to be upregulated in chemoresistant glioma cells and in human tumor tissues, with increasing PTRF expression correlating glioma grade and with tumor recurrence (155, 159). Huang et al. showed that EGFRvIII, an EGFR mutant with constitutively active tyrosine kinase activity present in ~25% of glioblastoma patients, drove PTRF upregulation (159). Blockade of PI3K and AKT reduced PTRF expression, showing a role for PTRF in EGFR-driven gliomagenesis even in the absence of the EGFRvIII mutation. This overexpression of PTRF in gliomas results in increased secretion of exosomes, cell growth, and aberrant methylation (159).

Interestingly, *in silico* analyses have suggested that PTRF expression is negatively correlated with the presence of cytotoxic lymphocytes intratumorally (160). Yi et al. recently showed that overexpression of PTRF in primary glioblastoma cells results in accumulation of lysophosphatidylcholine (LPC) species and decreased phosphatidylcholine (PC), resulting in increased membrane fluidity, endocytosis, and levels of the protein cytoplasmic phospholipase A2 (cPLA2), which provides fatty acids for mitochondrial fatty acid oxidation. *In vivo*, PTRF overexpression resulted in increased tumor growth and shorter survival. The authors found that intratumoral interferon gamma (IFN-γ) and granzyme B (GzmB) were decreased, with decreased numbers of CD8+ TILs, providing evidence for the role of abnormal phospholipid synthesis in glioblastoma immunosuppression. Strikingly, inhibition of cPLA2 restored IFN-γ and GzmB levels and resulted in increased TIL accumulation (161). Future investigations of cPLA2 in combination with existing immune activating therapies such as checkpoint blockade or CAR-T cells are warranted.

DISCUSSION

Several metabolic pathways are implicated in maintaining immunosuppression and glioblastoma outgrowth in the TME. These aspects have the potential to be exploited therapeutically but also for the development of diagnostic tools, including imaging tools such as MR spectroscopy for 2HG (162), hyperpolarized [1-13C] lactate (163), intratumoral acidity using pH-weighted amine chemical exchange saturation transfer (CEST) MRI (164) and amino acid PET tracers like 18F-fluoroethyltyrosine (FET) (165).

Targeting metabolic pathways has potential for conditioning the TME to become more responsive to frontline immunotherapies that have succeeded in more immunogenic cancers, as well as providing the opportunity to expand the limited treatment modalities that are currently approved. As experimental tools mature, our ability to better appreciate the heterogeneity between and within tumors advances. Many of the pathways mentioned have attracted study in more immunogenic cancers while preclinical data is sparse for glioblastoma models.

While there are a number of ongoing clinical trials exploring glioblastoma immunotherapies from the perspective of checkpoint blockade, there are relatively fewer trials pursuing immunometabolism modulation. For example, despite the extensive characterization of pathways like adenosine metabolism, glioblastoma research has yet to pursue A2aR inhibitors in the clinic. While the tryptophan metabolism pathway is by far the most clinically explored in IDH1 wildtype glioblastoma with 2 studies completed (NCT02052648, NCT02502708) and two studies recruiting (NCT04047706, NCT04049669), other pathways have unfortunately been less pursued. With the exception of one study pursuing arginine metabolism (NCT04587830) many of the other pathways analyzed in this review have not yet been explored in the clinic.

Metabolic mechanisms in glioma, and their interactions with the TME, and immune cells are helpful to develop precision medicine approaches. The presence of infiltrating immune cells in the TME presents a challenge but also a potential for therapeutic targets. Effector CD8+ T-cells express high levels of co-stimulatory and co-inhibitory molecules with a preferential accumulation of regulatory T cells (Tregs) in CNS tumors (166). The immunosuppressive environment of brain tumors has been highlighted in gliomas and other CNS tumors (144). Tregs play an essential role in ameliorating auto-immunity, but in the setting of brain TME, their anti-inflammatory activity creates a more permissive environment for tumor progression (167).

While targeting the IDH metabolic pathway with IDH inhibitors, and also more recently the IDH antigen, has demonstrated encouraging preliminary results in IDH mutated gliomas (95), glioblastoma or IDH wild type gliomas lack a uniformly expressed tumor specific antigen and are highly heterogenous. Research focus on targeting the metabolism in IDH wildtype glioblastoma, investigation of the role of metabolic pathways in glioblastoma, developing an appreciation for their differing activities across tumor types, and an increased willingness to explore these pathways in glioblastoma without

first waiting for exploration in other tumors, should allow for selective and targeted treatment options and should inspire hope to treat patients with glioblastoma with immunotherapy.

CONCLUSIONS

The field of immunometabolism represents a unique opportunity with emerging data supporting further research to fully understand mechanisms of resistance and to find potential synergy between immunometabolic pathways as well as other immunotherapy modalities. In addition to the pathways outlined, there remain other unknown metabolic aspects to discover to improve available therapies for patients with glioblastoma.

AUTHOR CONTRIBUTIONS

MK, AM, and JR conceived of and designed the work. AM, MK, WT, and AH-M drafted, and subsequently all authors revised the manuscript. KH and KS developed the figures, which were revised with input from all authors. All authors contributed to the article and approved the submitted version.

REFERENCES

1. Warburg O, Wind F, Negelein E. The Metabolism of Tumors in the Body. *J Gen Physiol* (1927) 8:519–30. doi: 10.1085/jgp.8.6.519
2. Heiland DH, Worner J, Gerrit Haaker J, Delev D, Pompe N, Mercas B, et al. The Integrative Metabolomic-Transcriptomic Landscape of Glioblastome Multiforme. *Oncotarget* (2017) 8:49178–90. doi: 10.18632/oncotarget.16544
3. Gadaleta F, Bessonov K, Van Steen K. Integration of Gene Expression and Methylation to Unravel Biological Networks in Glioblastoma Patients. *Genet Epidemiol* (2017) 41:136–44. doi: 10.1002/gepi.22028
4. Kesarwani P, Prabhu A, Kant S, Chinnaiyan P. Metabolic Remodeling Contributes Towards an Immune-Suppressive Phenotype in Glioblastoma. *Cancer Immunol Immunother* (2019) 68:1107–20. doi: 10.1007/s00262-019-02347-3
5. Dentro SC, Leshchiner I, Haase K, Tarabichi M, Wintersinger J, Deshwar AG, et al. Characterizing Genetic Intra-Tumor Heterogeneity Across 2,658 Human Cancer Genomes. *bioRxiv* (2020) 312041. doi: 10.1101/312041
6. Jawhari S, Ratinaud MH, Verdier M. Glioblastoma, Hypoxia and Autophagy: A Survival-Prone 'Menage-a-Trois'. *Cell Death Dis* (2016) 7: e2434. doi: 10.1038/cddis.2016.318
7. Monteiro AR, Hill R, Pilkington GJ, Madureira PA. The Role of Hypoxia in Glioblastoma Invasion. *Cells* (2017) 6(4):45. doi: 10.3390/cells6040045
8. Rong Y, Durden DL, Van Meir EG, Brat DJ. 'Pseudopalisading' Necrosis in Glioblastoma: A Familiar Morphologic Feature That Links Vascular Pathology, Hypoxia, and Angiogenesis. *J Neuropathol Exp Neurol* (2006) 65:529–39. doi: 10.1097/00005072-200606000-00001
9. Seidel S, Garvalov BK, Wirta V, von Stechow L, Schanzer A, Meletis K, et al. A Hypoxic Niche Regulates Glioblastoma Stem Cells Through Hypoxia Inducible Factor 2 Alpha. *Brain* (2010) 133:983–95. doi: 10.1093/brain/awq042
10. Li Z, Bao S, Wu Q, Wang H, Eyler C, Sathornsumetee S, et al. Hypoxia-Inducible Factors Regulate Tumorigenic Capacity of Glioma Stem Cells. *Cancer Cell* (2009) 15:501–13. doi: 10.1016/j.ccr.2009.03.018
11. Heddleston JM, Li Z, McLendon RE, Hjelmeland AB, Rich JN. The Hypoxic Microenvironment Maintains Glioblastoma Stem Cells and Promotes Reprogramming Towards a Cancer Stem Cell Phenotype. *Cell Cycle* (2009) 8:3274–84. doi: 10.4161/cc.8.20.9701
12. Hu YL, DeLay M, Jahangiri A, Molinaro AM, Rose SD, Carbonell WS, et al. Hypoxia-Induced Autophagy Promotes Tumor Cell Survival and Adaptation to Antiangiogenic Treatment in Glioblastoma. *Cancer Res* (2012) 72:1773–83. doi: 10.1158/0008-5472.CAN-11-3831
13. Rapisarda A, Melillo G. Overcoming Disappointing Results With Antiangiogenic Therapy by Targeting Hypoxia. *Nat Rev Clin Oncol* (2012) 9:378–90. doi: 10.1038/nrclinonc.2012.64
14. Liu YN, Yang JF, Huang DJ, Ni HH, Zhang CX, Zhang L, et al. Hypoxia Induces Mitochondrial Defect That Promotes T Cell Exhaustion in Tumor Microenvironment Through MYC-Regulated Pathways. *Front Immunol* (2020) 11:1906. doi: 10.3389/fimmu.2020.01906
15. Brat DJ, Bellail AC, Van Meir EG. The Role of Interleukin-8 and its Receptors in Gliomagenesis and Tumoral Angiogenesis. *Neuro Oncol* (2005) 7:122–33. doi: 10.1215/S1152851704001061
16. Rolhion C, Penault-Llorca F, Kemeny JL, Lemaire JJ, Jullien C, Labit-Bouvier C, et al. Interleukin-6 Overexpression as a Marker of Malignancy in Human Gliomas. *J Neurosurg* (2001) 94:97–101. doi: 10.3171/jns.2001.94.1.0097
17. Ma J, Benitez JA, Li J, Miki S, Ponte de Albuquerque C, Galatro T, et al. Inhibition of Nuclear PTEN Tyrosine Phosphorylation Enhances Glioma Radiation Sensitivity Through Attenuated DNA Repair. *Cancer Cell* (2019) 35:504–18.e507. doi: 10.1016/j.ccell.2019.01.020
18. Lamano JB, Lamano JB, Li YD, DiDomenico JD, Choy W, Veliceasa D, et al. Glioblastoma-Derived IL6 Induces Immunosuppressive Peripheral Myeloid Cell PD-L1 and Promotes Tumor Growth. *Clin Cancer Res* (2019) 25:3643–57. doi: 10.1158/1078-0432.CCR-18-2402
19. Zagzag D, Lukyanov Y, Lan L, Ali MA, Esencay M, Mendez O, et al. Hypoxia-Inducible Factor 1 and VEGF Upregulate CXCR4 in Glioblastoma: Implications for Angiogenesis and Glioma Cell Invasion. *Lab Invest* (2006) 86:1221–32. doi: 10.1038/labinvest.3700482
20. Choueiri TK, Kaelin WG. Targeting the HIF2–VEGF Axis in Renal Cell Carcinoma. *Nat Med* (2020) 26:1519–30. doi: 10.1038/s41591-020-1093-z
21. Strowd RE, Ellingson BM, Wen PY, Ahluwalia MS, Piotrowski AF, Desai AS, et al. Safety and Activity of a First-in-Class Oral HIF2-alpha Inhibitor, PT2385, in Patients With First Recurrent Glioblastoma (GBM). *J Clin Oncol* (2019) 37:2027–7. doi: 10.1200/JCO.2019.37.15_suppl.2027
22. Mergenthaler P, Lindauer U, Dienel GA, Meisel A. Sugar for the Brain: The Role of Glucose in Physiological and Pathological Brain Function. *Trends Neurosci* (2013) 36:587–97. doi: 10.1016/j.tins.2013.07.001
23. Flavahan WA, Wu Q, Hitomi M, Rahim N, Kim Y, Sloan AE, et al. Brain Tumor Initiating Cells Adapt to Restricted Nutrition Through Preferential Glucose Uptake. *Nat Neurosci* (2013) 16:1373–82. doi: 10.1038/nn.3510
24. Vannucci SJ, Maher F, Simpson IA. Glucose Transporter Proteins in Brain: Delivery of Glucose to Neurons and Glia. *Glia* (1997) 21:2–21. doi: 10.1002/(SICI)1098-1136(199709)21:1<2::AID-GLIA2>3.0.CO;2-C
25. Vaughn AE, Deshmukh M. Glucose Metabolism Inhibits Apoptosis in Neurons and Cancer Cells by Redox Inactivation of Cytochrome C. *Nat Cell Biol* (2008) 10:1477–83. doi: 10.1038/ncb1807
26. Amaral AI, Hadera MG, Tavares JM, Kotter MR, Sonnewald U. Characterization of Glucose-Related Metabolic Pathways in Differentiated Rat Oligodendrocyte Lineage Cells. *Glia* (2016) 64:21–34. doi: 10.1002/glia.22900
27. Agostini M, Romeo F, Inoue S, Niklison-Chirou MV, Elia AJ, Dinsdale D, et al. Metabolic Reprogramming During Neuronal Differentiation. *Cell Death Differ* (2016) 23:1502–14. doi: 10.1038/cdd.2016.36
28. Masui K, Tanaka K, Akhavan D, Babic I, Gini B, Matsutani T, et al. mTOR Complex 2 Controls Glycolytic Metabolism in Glioblastoma Through FoxO Acetylation and Upregulation of c-Myc. *Cell Metab* (2013) 18:726–39. doi: 10.1016/j.cmet.2013.09.013
29. Ganapathy-Kanniappan S, Geschwind JF. Tumor Glycolysis as a Target for Cancer Therapy: Progress and Prospects. *Mol Cancer* (2013) 12:152. doi: 10.1186/1476-4598-12-152
30. Guo H, Nan Y, Zhen Y, Zhang Y, Guo L, Yu K, et al. miRNA-451 Inhibits Glioma Cell Proliferation and Invasion by Downregulating Glucose Transporter 1. *Tumour Biol* (2016) 37:13751–61. doi: 10.1007/s13277-016-5219-3

31. Spence AM, Muzi M, Graham MM, O'Sullivan F, Link JM, Lewellen TK, et al. 2-[18f]Fluoro-2-Deoxyglucose and Glucose Uptake in Malignant Gliomas Before and After Radiotherapy. Correlation with Outcome. *Clin Cancer Res* (2002) 8:971–9.
32. Won WJ, Deshane JS, Leavenworth JW, Oliva CR, Griguer CE. Metabolic and Functional Reprogramming of Myeloid-Derived Suppressor Cells and Their Therapeutic Control in Glioblastoma. *Cell Stress* (2019) 3:47–65. doi: 10.15698/cst2019.02.176
33. Raber P, Ochoa AC, Rodriguez PC. Metabolism of L-arginine by Myeloid-Derived Suppressor Cells in Cancer: Mechanisms of T Cell Suppression and Therapeutic Perspectives. *Immunol Invest* (2012) 41:614–34. doi: 10.3109/08820139.2012.680634
34. Hou X, Liu Y, Liu H, Chen X, Liu M, Che H, et al. PERK Silence Inhibits Glioma Cell Growth Under Low Glucose Stress by Blockage of p-AKT and Subsequent HK2's Mitochondria Translocation. *Sci Rep* (2015) 5:9065. doi: 10.1038/srep09065
35. Zhang C, Wang M, Ji F, Peng Y, Wang B, Zhao J, et al. A Novel Glucose Metabolism-Related Gene Signature for Overall Survival Prediction in Patients With Glioblastoma. *BioMed Res Int* (2021) 2021:8872977–8872977. doi: 10.1155/2021/8872977
36. Ho PC, Bihuniak JD, Macintyre AN, Staron M, Liu X, Amezquita R, et al. Phosphoenolpyruvate Is a Metabolic Checkpoint of Anti-Tumor T Cell Responses. *Cell* (2015) 162:1217–28. doi: 10.1016/j.cell.2015.08.012
37. Siska PJ, Rathmell JC. T Cell Metabolic Fitness in Antitumor Immunity. *Trends Immunol* (2015) 36:257–64. doi: 10.1016/j.it.2015.02.007
38. Siska PJ, van der Windt GJ, Kishton RJ, Cohen S, Eisner W, MacIver NJ, et al. Suppression of Glut1 and Glucose Metabolism by Decreased Akt/mTORC1 Signaling Drives T Cell Impairment in B Cell Leukemia. *J Immunol (Baltimore Md 1950)* (2016) 197:2532–40. doi: 10.4049/jimmunol.1502464
39. Kallies A, Zehn D, Utzschneider DT. Precursor Exhausted T Cells: Key to Successful Immunotherapy? *Nat Rev Immunol* (2020) 20:128–36. doi: 10.1038/s41577-019-0223-7
40. Bengsch B, Johnson AL, Kurachi M, Odorizzi PM, Pauken KE, Attanasio J, et al. Bioenergetic Insufficiencies Due to Metabolic Alterations Regulated by the Inhibitory Receptor PD-1 Are an Early Driver of CD8(+) T Cell Exhaustion. *Immunity* (2016) 45:358–73. doi: 10.1016/j.immuni.2016.07.008
41. Patsoukis N, Bardhan K, Chatterjee P, Sari D, Liu B, Bell LN, et al. PD-1 Alters T-Cell Metabolic Reprogramming by Inhibiting Glycolysis and Promoting Lipolysis and Fatty Acid Oxidation. *Nat Commun* (2015) 6:6692. doi: 10.1038/ncomms7692
42. Chang CH, Qiu J, O'Sullivan D, Buck MD, Noguchi T, Curtis JD, et al. Metabolic Competition in the Tumor Microenvironment Is a Driver of Cancer Progression. *Cell* (2015) 162:1229–41. doi: 10.1016/j.cell.2015.08.016
43. Parsa AT, Waldron JS, Panner A, Crane CA, Parney IF, Barry JJ, et al. Loss of Tumor Suppressor PTEN Function Increases B7-H1 Expression and Immunoresistance in Glioma. *Nat Med* (2007) 13:84–8. doi: 10.1038/nm1517
44. de la Cruz-Lopez KG, Castro-Munoz LJ, Reyes-Hernandez DO, Garcia-Carranca A, Manzo-Merino J. Lactate in the Regulation of Tumor Microenvironment and Therapeutic Approaches. *Front Oncol* (2019) 9:1143. doi: 10.3389/fonc.2019.01143
45. Badawy AA. Kynurenine Pathway of Tryptophan Metabolism: Regulatory and Functional Aspects. *Int J Tryptophan Res* (2017) 10:1178646917691938. doi: 10.1177/1178646917691938
46. Thaker AI, Rao MS, Bishnupuri KS, Kerr TA, Foster L, Marinshaw JM, et al. IDO1 Metabolites Activate Beta-Catenin Signaling to Promote Cancer Cell Proliferation and Colon Tumorigenesis in Mice. *Gastroenterology* (2013) 145:416–25.e411-414. doi: 10.1053/j.gastro.2013.05.002
47. Bostian AC, Eoff RL. Aberrant Kynurenine Signaling Modulates DNA Replication Stress Factors and Promotes Genomic Instability in Gliomas. *Chem Res Toxicol* (2016) 29:1369–80. doi: 10.1021/acs.chemrestox.6b00255
48. Di Serio C, Cozzi A, Angeli I, Doria L, Micucci I, Pellerito S, et al. Kynurenic Acid Inhibits the Release of the Neurotrophic Fibroblast Growth Factor (FGF)-1 and Enhances Proliferation of Glia Cells, In Vitro. *Cell Mol Neurobiol* (2005) 25:981–93. doi: 10.1007/s10571-005-8469-y
49. Munn DH, Mellor AL. Indoleamine 2,3 Dioxygenase and Metabolic Control of Immune Responses. *Trends Immunol* (2013) 34:137–43. doi: 10.1016/j.it.2012.10.001
50. Mondal A, Smith C, DuHadaway JB, Sutanto-Ward E, Prendergast GC, Bravo-Nuevo A, et al. IDO1 Is an Integral Mediator of Inflammatory Neovascularization. *EBioMedicine* (2016) 14:74–82. doi: 10.1016/j.ebiom.2016.11.013
51. Mitsuka K, Kawataki T, Satoh E, Asahara T, Horikoshi T, Kinouchi H. Expression of Indoleamine 2,3-Dioxygenase and Correlation With Pathological Malignancy in Gliomas. *Neurosurgery* (2013) 72:1031–1038; discussion 1038-1039. doi: 10.1227/NEU.0b013e31828cf945
52. Yuasa HJ, Ball HJ, Ho YF, Austin CJ, Whittington CM, Belov K, et al. Characterization and Evolution of Vertebrate Indoleamine 2, 3-Dioxygenases IDOs From Monotremes and Marsupials. *Comp Biochem Physiol B Biochem Mol Biol* (2009) 153(2):137–44. doi: 10.1016/j.cbpb.2009.02.002
53. Wainwright DA, Balyasnikova IV, Chang AL, Ahmed AU, Moon KS, Auffinger B, et al. IDO Expression in Brain Tumors Increases the Recruitment of Regulatory T Cells and Negatively Impacts Survival. *Clin Cancer Res* (2012) 18:6110–21. doi: 10.1158/1078-0432.CCR-12-2130
54. Vogel CF, Goth SR, Dong B, Pessah IN, Matsumura F. Aryl Hydrocarbon Receptor Signaling Mediates Expression of Indoleamine 2,3-Dioxygenase. *Biochem Biophys Res Commun* (2008) 375:331–5. doi: 10.1016/j.bbrc.2008.07.156
55. Wainwright DA, Dey M, Chang A, Lesniak MS. Targeting Tregs in Malignant Brain Cancer: Overcoming IDO. *Front Immunol* (2013) 4:116. doi: 10.3389/fimmu.2013.00116
56. Opitz CA, Litzenburger UM, Sahm F, Ott M, Tritschler I, Trump S, et al. An Endogenous Tumour-Promoting Ligand of the Human Aryl Hydrocarbon Receptor. *Nature* (2011) 478:197–203. doi: 10.1038/nature10491
57. Munn DH, Sharma MD, Baban B, Harding HP, Zhang Y, Ron D, et al. GCN2 Kinase in T Cells Mediates Proliferative Arrest and Anergy Induction in Response to Indoleamine 2,3-Dioxygenase. *Immunity* (2005) 22:633–42. doi: 10.1016/j.immuni.2005.03.013
58. Prendergast GC, Malachowski WJ, Mondal A, Scherle P, Muller AJ. Indoleamine 2,3-Dioxygenase and Its Therapeutic Inhibition in Cancer. *Int Rev Cell Mol Biol* (2018) 336:175–203. doi: 10.1016/bs.ircmb.2017.07.004
59. Kesarwani P, Prabhu A, Kant S, Kumar P, Graham SF, Buelow KL, et al. Tryptophan Metabolism Contributes to Radiation-Induced Immune Checkpoint Reactivation in Glioblastoma. *Clin Cancer Res* (2018) 24:3632–43. doi: 10.1158/1078-0432.CCR-18-0041
60. Hanihara M, Kawataki T, Oh-Oka K, Mitsuka K, Nakao A, Kinouchi H. Synergistic Antitumor Effect With Indoleamine 2,3-Dioxygenase Inhibition and Temozolomide in a Murine Glioma Model. *J Neurosurg* (2016) 124:1594–601. doi: 10.3171/2015.5.JNS141901
61. Li M, Bolduc AR, Hoda MN, Gamble DN, Dolisca SB, Bolduc AK, et al. The Indoleamine 2,3-Dioxygenase Pathway Controls Complement-Dependent Enhancement of Chemo-Radiation Therapy Against Murine Glioblastoma. *J Immunother Cancer* (2014) 2:21. doi: 10.1186/2051-1426-2-21
62. Correction: Durable Therapeutic Efficacy Utilizing Combinatorial Blockade Against IDO, CTLA-4, and PD-L1 in Mice With Brain Tumors. *Clin Cancer Res* (2015) 21:662. doi: 10.1158/1078-0432.CCR-14-3211
63. Wainwright DA, Chang AL, Dey M, Balyasnikova IV, Kim CK, Tobias A, et al. Durable Therapeutic Efficacy Utilizing Combinatorial Blockade Against IDO, CTLA-4, and PD-L1 in Mice With Brain Tumors. *Clin Cancer Res* (2014) 20:5290–301. doi: 10.1158/1078-0432.CCR-14-0514
64. Ladomersky E, Zhai L, Lauing KL, Bell A, Xu J, Kocherginsky M, et al. Advanced Age Increases Immunosuppression in the Brain and Decreases Immunotherapeutic Efficacy in Subjects With Glioblastoma. *Clin Cancer Res* (2020) 26:5232–45. doi: 10.1158/1078-0432.ccr-19-3874
65. Rath M, Müller I, Kropf P, Closs EI, Munder M. Metabolism Via Arginase or Nitric Oxide Synthase: Two Competing Arginine Pathways in Macrophages. *Front Immunol* (2014) 5:532. doi: 10.3389/fimmu.2014.00532
66. Phillips MM, Sheaff MT, Szlosarek PW. Targeting Arginine-Dependent Cancers With Arginine-Degrading Enzymes: Opportunities and Challenges. *Cancer Res Treat* (2013) 45:251–62. doi: 10.4143/crt.2013.45.4.251
67. Kobayashi K, Ohnishi A, Promsuk J, Shimizu S, Kanai Y, Shiokawa Y, et al. Enhanced Tumor Growth Elicited by L-Type Amino Acid Transporter 1 in Human Malignant Glioma Cells. *Neurosurgery* (2008) 62:493–503; discussion 503-494. doi: 10.1227/01.neu.0000316018.51292.19
68. Chinnaiyan P, Kensicki E, Bloom G, Prabhu A, Sarcar B, Kahali S, et al. The Metabolomic Signature of Malignant Glioma Reflects Accelerated Anabolic

Metabolism. *Cancer Res* (2012) 72:5878–88. doi: 10.1158/0008-5472.Can-12-1572-t
69. Khoury O, Ghazale N, Stone E, El-Sibai M, Frankel AE, Abi-Habib RJ. Human Recombinant Arginase I (Co)-PEG5000 [HuArgI (Co)-PEG5000]-induced Arginine Depletion Is Selectively Cytotoxic to Human Glioblastoma Cells. *J Neurooncol* (2015) 122:75–85. doi: 10.1007/s11060-014-1698-5
70. Jahani-Asl A, Bonni A. iNOS: A Potential Therapeutic Target for Malignant Glioma. *Curr Mol Med* (2013) 13:1241–9. doi: 10.2174/1566524011313080002
71. Morantz RA, Wood GW, Foster M, Clark M, Gollahon K. Macrophages in Experimental and Human Brain Tumors. Part 2: Studies of the Macrophage Content of Human Brain Tumors. *J Neurosurg* (1979) 50:305–11. doi: 10.3171/jns.1979.50.3.0305
72. Rossi ML, Hughes JT, Esiri MM, Coakham HB, Brownell DB. Immunohistological Study of Mononuclear Cell Infiltrate in Malignant Gliomas. *Acta Neuropathol* (1987) 74:269–77. doi: 10.1007/bf00688191
73. Ginhoux F, Schultze JL, Murray PJ, Ochando J, Biswas SK. New Insights Into the Multidimensional Concept of Macrophage Ontogeny, Activation and Function. *Nat Immunol* (2016) 17:34–40. doi: 10.1038/ni.3324
74. Müller S, Kohanbash G, Liu SJ, Alvarado B, Carrera D, Bhaduri A, et al. Single-Cell Profiling of Human Gliomas Reveals Macrophage Ontogeny as a Basis for Regional Differences in Macrophage Activation in the Tumor Microenvironment. *Genome Biol* (2017) 18:234–4. doi: 10.1186/s13059-017-1362-4
75. Chen Z, Hambardzumyan D. Immune Microenvironment in Glioblastoma Subtypes. *Front Immunol* (2018) 9:1004. doi: 10.3389/fimmu.2018.01004
76. Hambardzumyan D, Gutmann DH, Kettenmann H. The Role of Microglia and Macrophages in Glioma Maintenance and Progression. *Nat Neurosci* (2016) 19:20–7. doi: 10.1038/nn.4185
77. Cairns RA, Mak TW. Oncogenic Isocitrate Dehydrogenase Mutations: Mechanisms, Models, and Clinical Opportunities. *Cancer Discov* (2013) 3:730–41. doi: 10.1158/2159-8290.CD-13-0083
78. Jezek P. 2-Hydroxyglutarate in Cancer Cells. *Antioxid Redox Signal* (2020) 33:903–26. doi: 10.1089/ars.2019.7902
79. Gagné LM, Boulay K, Topisirovic I, Huot ME, Mallette FA. Oncogenic Activities of IDH1/2 Mutations: From Epigenetics to Cellular Signaling. *Trends Cell Biol* (2017) 27:738–52. doi: 10.1016/j.tcb.2017.06.002
80. Struys EA, Verhoeven NM, Ten Brink HJ, Wickenhagen WV, Gibson KM, Jakobs C. Kinetic Characterization of Human Hydroxyacid-Oxoacid Transhydrogenase: Relevance to D-2-Hydroxyglutaric and Gamma-Hydroxybutyric Acidurias. *J Inherit Metab Dis* (2005) 28:921–30. doi: 10.1007/s10545-005-0114-x
81. Fan J, Teng X, Liu L, Mattaini KR, Looper RE, Vander Heiden MG, et al. Human Phosphoglycerate Dehydrogenase Produces the Oncometabolite D-2-Hydroxyglutarate. *ACS Chem Biol* (2015) 10:510–6. doi: 10.1021/cb500683c
82. Intlekofer AM, Dematteo RG, Venneti S, Finley LW, Lu C, Judkins AR, et al. Hypoxia Induces Production of L-2-Hydroxyglutarate. *Cell Metab* (2015) 22:304–11. doi: 10.1016/j.cmet.2015.06.023
83. Rzem R, Vincent MF, Van Schaftingen E, Veiga-da-Cunha M. L-2-Hydroxyglutaric Aciduria, a Defect of Metabolite Repair. *J Inherit Metab Dis* (2007) 30:681–9. doi: 10.1007/s10545-007-0487-0
84. Dang L, Su SM. Isocitrate Dehydrogenase Mutation and (R)-2-Hydroxyglutarate: From Basic Discovery to Therapeutics Development. *Annu Rev Biochem* (2017) 86:305–31. doi: 10.1146/annurev-biochem-061516-044732
85. Koivunen P, Lee S, Duncan CG, Lopez G, Lu G, Ramkissoon S, et al. Transformation by the (R)-Enantiomer of 2-Hydroxyglutarate Linked to EGLN Activation. *Nature* (2012) 483:484–8. doi: 10.1038/nature10898
86. Garcia MG, Carella A, Urdinguio RG, Bayon GF, Lopez V, Tejedor JR, et al. Epigenetic Dysregulation of TET2 in Human Glioblastoma. *Oncotarget* (2018) 9:25922–34. doi: 10.18632/oncotarget.25406
87. Ohka F, Ito M, Ranjit M, Senga T, Motomura A, Motomura K, et al. Quantitative Metabolome Analysis Profiles Activation of Glutaminolysis in Glioma With IDH1 Mutation. *Tumour Biol* (2014) 35:5911–20. doi: 10.1007/s13277-014-1784-5
88. Chen F, Bian K, Tang Q, Fedeles BI, Singh V, Humulock ZT, et al. Oncometabolites D- and L-2-Hydroxyglutarate Inhibit the AlkB Family DNA Repair Enzymes Under Physiological Conditions. *Chem Res Toxicol* (2017) 30:1102–10. doi: 10.1021/acs.chemrestox.7b00009
89. Bunse L, Pusch S, Bunse T, Sahm F, Sanghvi K, Friedrich M, et al. Suppression of Antitumor T Cell Immunity by the Oncometabolite (R)-2-Hydroxyglutarate. *Nat Med* (2018) 24:1192–203. doi: 10.1038/s41591-018-0095-6
90. Kohanbash G, Carrera DA, Shrivastav S, Ahn BJ, Jahan N, Mazor T, et al. Isocitrate Dehydrogenase Mutations Suppress STAT1 and CD8+ T Cell Accumulation in Gliomas. *J Clin Invest* (2017) 127:1425–37. doi: 10.1172/JCI90644
91. Komohara Y, Ohnishi K, Kuratsu J, Takeya M. Possible Involvement of the M2 Anti-Inflammatory Macrophage Phenotype in Growth of Human Gliomas. *J Pathol* (2008) 216:15–24. doi: 10.1002/path.2370
92. Amankulor NM, Kim Y, Arora S, Kargl J, Szulzewsky F, Hanke M, et al. Mutant IDH1 Regulates the Tumor-Associated Immune System in Gliomas. *Genes Dev* (2017) 31:774–86. doi: 10.1101/gad.294991.116
93. Golub D, Iyengar N, Dogra S, Wong T, Bready D, Tang K, et al. Mutant Isocitrate Dehydrogenase Inhibitors as Targeted Cancer Therapeutics. *Front Oncol* (2019) 9:417. doi: 10.3389/fonc.2019.00417
94. Kadiyala P, Carney SV, Gauss JC, Garcia-Fabiani MB, Haase S, Alghamri MS, et al. Inhibition of 2-Hydroxyglutarate Elicits Metabolic Reprogramming and Mutant IDH1 Glioma Immunity in Mice. *J Clin Invest* (2021) 131(4):e139542. doi: 10.1172/JCI139542
95. Platten M, Bunse L, Wick A, Bunse T, Le Cornet L, Harting I, et al. A Vaccine Targeting Mutant IDH1 in Newly Diagnosed Glioma. *Nature* (2021) 592:463–8. doi: 10.1038/s41586-021-03363-z
96. Falzoni S, Donvito G, Di Virgilio F. Detecting Adenosine Triphosphate in the Pericellular Space. *Interface Focus* (2013) 3:20120101. doi: 10.1098/rsfs.2012.0101
97. Pastor-Anglada M, Perez-Torras S. Who Is Who in Adenosine Transport. *Front Pharmacol* (2018) 9:627. doi: 10.3389/fphar.2018.00627
98. Sabirov RZ, Okada Y. ATP Release Via Anion Channels. *Purinergic Signal* (2005) 1:311–28. doi: 10.1007/s11302-005-1557-0
99. Zimmermann H, Zebisch M, Strater N. Cellular Function and Molecular Structure of Ecto-Nucleotidases. *Purinergic Signal* (2012) 8:437–502. doi: 10.1007/s11302-012-9309-4
100. Vigano S, Alatzoglou D, Irving M, Menetrier-Caux C, Caux C, Romero P, et al. Targeting Adenosine in Cancer Immunotherapy to Enhance T-Cell Function. *Front Immunol* (2019) 10:925. doi: 10.3389/fimmu.2019.00925
101. Ott M, Tomaszowski KH, Marisetty A, Kong LY, Wei J, Duna M, et al. Profiling of Patients With Glioma Reveals the Dominant Immunosuppressive Axis Is Refractory to Immune Function Restoration. *JCI Insight* (2020) 5(17):e134386. doi: 10.1172/jci.insight.134386
102. Merighi S, Benini A, Mirandola P, Gessi S, Varani K, Leung E, et al. Hypoxia Inhibits Paclitaxel-Induced Apoptosis Through Adenosine-Mediated Phosphorylation of Bad in Glioblastoma Cells. *Mol Pharmacol* (2007) 72:162–72. doi: 10.1124/mol.106.031849
103. Kim H, Kang JW, Lee S, Choi WJ, Jeong LS, Yang Y, et al. A3 Adenosine Receptor Antagonist, Truncated Thio-Cl-IB-MECA, Induces Apoptosis in T24 Human Bladder Cancer Cells. *Anticancer Res* (2010) 30:2823–30.
104. Gessi S, Bencivenni S, Battistello E, Vincenzi F, Colotta V, Catarzi D, et al. Inhibition of A2A Adenosine Receptor Signaling in Cancer Cells Proliferation by the Novel Antagonist TP455. *Front Pharmacol* (2017) 8:888. doi: 10.3389/fphar.2017.00888
105. Lin Z, Yin P, Reierstad S, O'Halloran M, Coon VJ, Pearson EK, et al. Adenosine A1 Receptor, a Target and Regulator of Estrogen Receptoralpha Action, Mediates the Proliferative Effects of Estradiol in Breast Cancer. *Oncogene* (2010) 29:1114–22. doi: 10.1038/onc.2009.409
106. Zhou Y, Chu X, Deng F, Tong L, Tong G, Yi Y, et al. The Adenosine A2b Receptor Promotes Tumor Progression of Bladder Urothelial Carcinoma by Enhancing MAPK Signaling Pathway. *Oncotarget* (2017) 8:48755–68. doi: 10.18632/oncotarget.17835
107. Mittal D, Sinha D, Barkauskas D, Young A, Kalimutho M, Stannard K, et al. Adenosine 2B Receptor Expression on Cancer Cells Promotes Metastasis. *Cancer Res* (2016) 76:4372–82. doi: 10.1158/0008-5472.CAN-16-0544
108. Allard B, Longhi MS, Robson SC, Stagg J. The Ectonucleotidases CD39 and CD73: Novel Checkpoint Inhibitor Targets. *Immunol Rev* (2017) 276:121–44. doi: 10.1111/imr.12528
109. Linnemann C, Schildberg FA, Schurich A, Diehl L, Hegenbarth SI, Endl E, et al. Adenosine Regulates CD8 T-Cell Priming by Inhibition of Membrane-Proximal T-Cell Receptor Signalling. *Immunology* (2009) 128:e728–737. doi: 10.1111/j.1365-2567.2009.03075.x

110. Jimenez JL, Punzon C, Navarro J, Munoz-Fernandez MA, Fresno M. Phosphodiesterase 4 Inhibitors Prevent Cytokine Secretion by T Lymphocytes by Inhibiting Nuclear Factor-KappaB and Nuclear Factor of Activated T Cells Activation. *J Pharmacol Exp Ther* (2001) 299:753–9.
111. Cekic C, Linden J. Purinergic Regulation of the Immune System. *Nat Rev Immunol* (2016) 16:177–92. doi: 10.1038/nri.2016.4
112. Allard D, Turcotte M, Stagg J. Targeting A2 Adenosine Receptors in Cancer. *Immunol Cell Biol* (2017) 95:333–9. doi: 10.1038/icb.2017.8
113. Deaglio S, Dwyer KM, Gao W, Friedman D, Usheva A, Erat A, et al. Adenosine Generation Catalyzed by CD39 and CD73 Expressed on Regulatory T Cells Mediates Immune Suppression. *J Exp Med* (2007) 204:1257–65. doi: 10.1084/jem.20062512
114. Hatfield SM, Kjaergaard J, Lukashev D, Schreiber TH, Belikoff B, Abbott R, et al. Immunological Mechanisms of the Antitumor Effects of Supplemental Oxygenation. *Sci Transl Med* (2015) 7:277ra230. doi: 10.1126/scitranslmed.aaa1260
115. Miller JS, Cervenka T, Lund J, Okazaki IJ, Moss J. Purine Metabolites Suppress Proliferation of Human NK Cells Through a Lineage-Specific Purine Receptor. *J Immunol (Baltimore Md 1950)* (1999) 162:7376–82.
116. Beavis PA, Divisekera U, Paget C, Chow MT, John LB, Devaud C, et al. Blockade of A2A Receptors Potently Suppresses the Metastasis of CD73+ Tumors. *Proc Natl Acad Sci U S A* (2013) 110:14711–6. doi: 10.1073/pnas.1308209110
117. Milo R, Jorgensen P, Moran U, Weber G, Springer M. BioNumbers–the Database of Key Numbers in Molecular and Cell Biology. *Nucleic Acids Res* (2010) 38:D750–3. doi: 10.1093/nar/gkp889
118. Li L, Huang L, Ye H, Song SP, Bajwa A, Lee SJ, et al. Dendritic Cells Tolerized With Adenosine A(2)AR Agonist Attenuate Acute Kidney Injury. *J Clin Invest* (2012) 122:3931–42. doi: 10.1172/JCI63170
119. Csoka B, Selmeczy Z, Koscso B, Nemeth ZH, Pacher P, Murray PJ, et al. Adenosine Promotes Alternative Macrophage Activation Via A2A and A2B Receptors. *FASEB J* (2012) 26:376–86. doi: 10.1096/fj.11-190934
120. Yago T, Tsukamoto H, Liu Z, Wang Y, Thompson LF, McEver RP. Multi-Inhibitory Effects of A2A Adenosine Receptor Signaling on Neutrophil Adhesion Under Flow. *J Immunol (Baltimore Md 1950)* (2015) 195:3880–9. doi: 10.4049/jimmunol.1500775
121. Ohta A, Gorelik E, Prasad SJ, Ronchese F, Lukashev D, Wong MK, et al. A2A Adenosine Receptor Protects Tumors From Antitumor T Cells. *Proc Natl Acad Sci U S A* (2006) 103:13132–7. doi: 10.1073/pnas.0605251103
122. Ohta A, Sitkovsky M. Role of G-Protein-Coupled Adenosine Receptors in Downregulation of Inflammation and Protection From Tissue Damage. *Nature* (2001) 414:916–20. doi: 10.1038/414916a
123. Leone RD, Emens LA. Targeting Adenosine for Cancer Immunotherapy. *J Immunother Cancer* (2018) 6:57. doi: 10.1186/s40425-018-0360-8
124. Beavis PA, Milenkovski N, Henderson MA, John LB, Allard B, Loi S, et al. Adenosine Receptor 2A Blockade Increases the Efficacy of Anti-PD-1 Through Enhanced Antitumor T-Cell Responses. *Cancer Immunol Res* (2015) 3:506–17. doi: 10.1158/2326-6066.CIR-14-0211
125. Mittal D, Young A, Stannard K, Yong M, Teng MW, Allard B, et al. Antimetastatic Effects of Blocking PD-1 and the Adenosine A2A Receptor. *Cancer Res* (2014) 74:3652–8. doi: 10.1158/0008-5472.CAN-14-0957
126. Iannone R, Miele L, Maiolino P, Pinto A, Morello S. Adenosine Limits the Therapeutic Effectiveness of Anti-CTLA4 mAb in a Mouse Melanoma Model. *Am J Cancer Res* (2014) 4:172–81.
127. Ogretmen B. Sphingolipid Metabolism in Cancer Signalling and Therapy. *Nat Rev Cancer* (2018) 18:33–50. doi: 10.1038/nrc.2017.96
128. Hannun YA, Obeid LM. Principles of Bioactive Lipid Signalling: Lessons From Sphingolipids. *Nat Rev Mol Cell Biol* (2008) 9:139–50. doi: 10.1038/nrm2329
129. Hawkins CC, Ali T, Ramanadham S, Hjelmeland AB. Sphingolipid Metabolism in Glioblastoma and Metastatic Brain Tumors: A Review of Sphingomyelinases and Sphingosine-1-Phosphate. *Biomolecules* (2020) 10 (10):1357. doi: 10.3390/biom10101357
130. Riboni L, Abdel Hadi L, Navone SE, Guarnaccia L, Campanella R, Marfia G. Sphingosine-1-Phosphate in the Tumor Microenvironment: A Signaling Hub Regulating Cancer Hallmarks. *Cells* (2020) 9(2):337. doi: 10.3390/cells9020337
131. Tea MN, Poonnoose SI, Pitson SM. Targeting the Sphingolipid System as a Therapeutic Direction for Glioblastoma. *Cancers (Basel)* (2020) 12(1):111. doi: 10.3390/cancers12010111
132. Riboni L, Campanella R, Bassi R, Villani R, Gaini SM, Martinelli-Boneschi F, et al. Ceramide Levels are Inversely Associated With Malignant Progression of Human Glial Tumors. *Glia* (2002) 39:105–13. doi: 10.1002/glia.10087
133. Marfia G, Campanella R, Navone SE, Di Vito C, Riccitelli E, Hadi LA, et al. Autocrine/Paracrine Sphingosine-1-Phosphate Fuels Proliferative and Stemness Qualities of Glioblastoma Stem Cells. *Glia* (2014) 62:1968–81. doi: 10.1002/glia.22718
134. Abuhusain HJ, Matin A, Qiao Q, Shen H, Kain N, Day BW, et al. A Metabolic Shift Favoring Sphingosine 1-Phosphate at the Expense of Ceramide Controls Glioblastoma Angiogenesis. *J Biol Chem* (2013) 288:37355–64. doi: 10.1074/jbc.M113.494740
135. Li J, Guan HY, Gong LY, Song LB, Zhang N, Wu J, et al. Clinical Significance of Sphingosine Kinase-1 Expression in Human Astrocytomas Progression and Overall Patient Survival. *Clin Cancer Res* (2008) 14:6996–7003. doi: 10.1158/1078-0432.CCR-08-0754
136. Van Brocklyn JR, Jackson CA, Pearl DK, Kotur MS, Snyder PJ, Prior TW. Sphingosine Kinase-1 Expression Correlates With Poor Survival of Patients With Glioblastoma Multiforme: Roles of Sphingosine Kinase Isoforms in Growth of Glioblastoma Cell Lines. *J Neuropathol Exp Neurol* (2005) 64:695–705. doi: 10.1097/01.jnen.0000175329.59092.2c
137. Steck PA, Ligon AH, Cheong P, Yung WK, Pershouse MA. Two Tumor Suppressive Loci on Chromosome 10 Involved in Human Glioblastomas. *Genes Chromosomes Cancer* (1995) 12:255–61. doi: 10.1002/gcc.2870120404
138. Ogawa C, Kihara A, Gokoh M, Igarashi Y. Identification and Characterization of a Novel Human Sphingosine-1-Phosphate Phosphohydrolase, hSPP2. *J Biol Chem* (2003) 278:1268–72. doi: 10.1074/jbc.M209514200
139. Jensen SA, Calvert AE, Volpert G, Kouri FM, Hurley LA, Luciano JP, et al. Bcl2L13 Is a Ceramide Synthase Inhibitor in Glioblastoma. *Proc Natl Acad Sci U S A* (2014) 111:5682–7. doi: 10.1073/pnas.1316700111
140. Riccitelli E, Giussani P, Di Vito C, Condomitti G, Tringali C, Caroli M, et al. Extracellular Sphingosine-1-Phosphate: A Novel Actor in Human Glioblastoma Stem Cell Survival. *PloS One* (2013) 8:e68229. doi: 10.1371/journal.pone.0068229
141. Edsall LC, Cuvillier O, Twitty S, Spiegel S, Milstien S. Sphingosine Kinase Expression Regulates Apoptosis and Caspase Activation in PC12 Cells. *J Neurochem* (2001) 76:1573–84. doi: 10.1046/j.1471-4159.2001.00164.x
142. Bouquerel P, Gstalder C, Muller D, Laurent J, Brizuela L, Sabbadini RA, et al. Essential Role for SphK1/S1P Signaling to Regulate Hypoxia-Inducible Factor 2alpha Expression and Activity in Cancer. *Oncogenesis* (2016) 5: e209. doi: 10.1038/oncsis.2016.13
143. Paugh BS, Bryan L, Paugh SW, Wilczynska KM, Alvarez SM, Singh SK, et al. Interleukin-1 Regulates the Expression of Sphingosine Kinase 1 in Glioblastoma Cells. *J Biol Chem* (2009) 284:3408–17. doi: 10.1074/jbc.M807170200
144. Chongsathidkiet P, Jackson C, Koyama S, Loebel F, Cui X, Farber SH, et al. Sequestration of T Cells in Bone Marrow in the Setting of Glioblastoma and Other Intracranial Tumors. *Nat Med* (2018) 24:1459–68. doi: 10.1038/s41591-018-0135-2
145. Gude DR, Alvarez SE, Paugh SW, Mitra P, Yu J, Griffiths R, et al. Apoptosis Induces Expression of Sphingosine Kinase 1 to Release Sphingosine-1-Phosphate as a "Come-and-Get-Me" Signal. *FASEB J* (2008) 22:2629–38. doi: 10.1096/fj.08-107169
146. Perrotta C, Cervia D, Di Renzo I, Moscheni C, Bassi MT, Campana L, et al. Nitric Oxide Generated by Tumor-Associated Macrophages Is Responsible for Cancer Resistance to Cisplatin and Correlated With Syntaxin 4 and Acid Sphingomyelinase Inhibition. *Front Immunol* (2018) 9:1186. doi: 10.3389/fimmu.2018.01186
147. Fecci PE, Mitchell DA, Whitesides JF, Xie W, Friedman AH, Archer GE, et al. Increased Regulatory T-Cell Fraction Amidst a Diminished CD4 Compartment Explains Cellular Immune Defects in Patients With Malignant Glioma. *Cancer Res* (2006) 66:3294–302. doi: 10.1158/0008-5472.CAN-05-3773
148. Bai A, Guo Y. Acid Sphingomyelinase Mediates Human CD4(+) T-Cell Signaling: Potential Roles in T-Cell Responses and Diseases. *Cell Death Dis* (2017) 8:e2963. doi: 10.1038/cddis.2017.360
149. Zhou Y, Salker MS, Walker B, Munzer P, Borst O, Gawaz M, et al. Acid Sphingomyelinase (ASM) Is a Negative Regulator of Regulatory T Cell (Treg) Development. *Cell Physiol Biochem* (2016) 39:985–95. doi: 10.1159/000447806

150. Woroniecka KI, Rhodin KE, Dechant C, Cui X, Chongsathidkiet P, Wilkinson D, et al. 4-1BB Agonism Averts TIL Exhaustion and Licenses PD-1 Blockade in Glioblastoma and Other Intracranial Cancers. *Clin Cancer Res* (2020) 26:1349–58. doi: 10.1158/1078-0432.CCR-19-1068
151. Pitman MR, Woodcock JM, Lopez AF, Pitson SM. Molecular Targets of FTY720 (Fingolimod). *Curr Mol Med* (2012) 12:1207–19. doi: 10.2174/156652412803833599
152. Baeyens A, Bracero S, Chaluvadi VS, Khodadadi-Jamayran A, Cammer M, Schwab SR, et al. Monocyte-Derived S1P in the Lymph Node Regulates Immune Responses. *Nature* (2021) 592:290–5. doi: 10.1038/s41586-021-03227-6
153. Jansa P, Mason SW, Hoffmann-Rohrer U, Grummt I. Cloning and Functional Characterization of PTRF, a Novel Protein Which Induces Dissociation of Paused Ternary Transcription Complexes. *EMBO J* (1998) 17:2855–64. doi: 10.1093/emboj/17.10.2855
154. Mason SW, Sander EE, Grummt I. Identification of a Transcript Release Activity Acting on Ternary Transcription Complexes Containing Murine RNA Polymerase I. *EMBO J* (1997) 16:163–72. doi: 10.1093/emboj/16.1.163
155. Wang X, Liu T, Bai Y, Liao H, Qiu S, Chang Z, et al. Polymerase I and Transcript Release Factor Acts as an Essential Modulator of Glioblastoma Chemoresistance. *PloS One* (2014) 9:e93439. doi: 10.1371/journal.pone.0093439
156. Hill MM, Bastiani M, Luetterforst R, Kirkham M, Kirkham A, Nixon SJ, et al. PTRF-Cavin, a Conserved Cytoplasmic Protein Required for Caveola Formation and Function. *Cell* (2008) 132:113–24. doi: 10.1016/j.cell.2007.11.042
157. Patni N, Garg A. Congenital Generalized Lipodystrophies–New Insights Into Metabolic Dysfunction. *Nat Rev Endocrinol* (2015) 11:522–34. doi: 10.1038/nrendo.2015.123
158. Hayashi YK, Matsuda C, Ogawa M, Goto K, Tominaga K, Mitsuhashi S, et al. Human PTRF Mutations Cause Secondary Deficiency of Caveolins Resulting in Muscular Dystrophy With Generalized Lipodystrophy. *J Clin Invest* (2009) 119:2623–33. doi: 10.1172/JCI38660
159. Huang K, Fang C, Yi K, Liu X, Qi H, Tan Y, et al. The Role of PTRF/Cavin1 as a Biomarker in Both Glioma and Serum Exosomes. *Theranostics* (2018) 8:1540–57. doi: 10.7150/thno.22952
160. Guo Q, Guan GF, Cheng W, Zou CY, Zhu C, Cheng P, et al. Integrated Profiling Identifies Caveolae-Associated Protein 1 as a Prognostic Biomarker of Malignancy in Glioblastoma Patients. *CNS Neurosci Ther* (2019) 25:343–54. doi: 10.1111/cns.13072
161. Yi K, Zhan Q, Wang Q, Tan Y, Fang C, Wang Y, et al. PTRF/Cavin-1 Remodels Phospholipid Metabolism to Promote Tumor Proliferation and Suppress Immune Responses in Glioblastoma by Stabilizing cPLA2. *Neuro Oncol* (2021) 23:387–99. doi: 10.1093/neuonc/noaa255
162. Chen W, Peng Y, Jiang X, Zhao J, Zhao H, Zhu Y. Isomers Identification of 2-Hydroxyglutarate Acid Disodium Salt (2HG) by Terahertz Time-Domain Spectroscopy. *Sci Rep* (2017) 7:12166. doi: 10.1038/s41598-017-11527-z
163. Chaumeil MM, Radoul M, Najac C, Eriksson P, Viswanath P, Blough MD, et al. Hyperpolarized (13)C MR Imaging Detects No Lactate Production in Mutant IDH1 Gliomas: Implications for Diagnosis and Response Monitoring. *NeuroImage Clin* (2016) 12:180–9. doi: 10.1016/j.nicl.2016.06.018
164. Wang Y-L, Yao J, Chakhoyan A, Raymond C, Salamon N, Liau LM, et al. Association Between Tumor Acidity and Hypervascularity in Human Gliomas Using pH-weighted Amine Chemical Exchange Saturation Transfer Echo-Planar Imaging and Dynamic Susceptibility Contrast Perfusion MRI at 3T. *Am J Neuroradiol* (2019) 40:979–86. doi: 10.3174/ajnr.A6063
165. Hayes AR, Jayamanne D, Hsiao E, Schembri GP, Bailey DL, Roach PJ, et al. Utilizing 18F-Fluoroethyltyrosine (FET) Positron Emission Tomography (PET) to Define Suspected Nonenhancing Tumor for Radiation Therapy Planning of Glioblastoma. *Pract Radiat Oncol* (2018) 8:230–8. doi: 10.1016/j.prro.2018.01.006
166. Friebel E, Kapolou K, Unger S, Núñez NG, Utz S, Rushing EJ, et al. Single-Cell Mapping of Human Brain Cancer Reveals Tumor-Specific Instruction of Tissue-Invading Leukocytes. *Cell* (2020) 181:1626–42.e1620. doi: 10.1016/j.cell.2020.04.055
167. Chaudhary B, Elkord E. Regulatory T Cells in the Tumor Microenvironment and Cancer Progression: Role and Therapeutic Targeting. *Vaccines* (2016) 4:28. doi: 10.3390/vaccines4030028

Conflict of Interest: PF reports consulting for Monteris Medical. JS has an equity interest in Istari Oncology, which has licensed intellectual property from Duke related to the use of poliovirus and D2C7 in the treatment of glioblastoma. JS is an inventor on patents related to PEP-CMV DC vaccine with tetanus, as well as poliovirus vaccine and D2C7 in the treatment of glioblastoma. JS has an equity interest in Annias Immunotherapeutics, which has licensed intellectual property from Duke related to the use of the pepCMV vaccine in the treatment of glioblastoma. MK reports advisory roles for Janssen, AbbVie, and Jackson Laboratory for Genomic Medicine, and research funding from AbbVie, Bristol-Myers Squibb, and Specialized Therapeutics.

The remaining authors declare that the research was conducted in the absence of any commercial or financial relationships that could be construed as a potential conflict of interest.

Copyright © 2021 Mohan, Tomaszewski, Haskell-Mendoza, Hotchkiss, Singh, Reedy, Fecci, Sampson and Khasraw. This is an open-access article distributed under the terms of the Creative Commons Attribution License (CC BY). The use, distribution or reproduction in other forums is permitted, provided the original author(s) and the copyright owner(s) are credited and that the original publication in this journal is cited, in accordance with accepted academic practice. No use, distribution or reproduction is permitted which does not comply with these terms.

frontiers in Oncology

ORIGINAL RESEARCH
published: 21 July 2021
doi: 10.3389/fonc.2021.648023

Combination Treatment of CI-994 With Etoposide Potentiates Anticancer Effects Through a Topoisomerase II-Dependent Mechanism in Atypical Teratoid/Rhabdoid Tumor (AT/RT)

Hee Yeon Kim[1,2†], *Seung Ah Choi*[1,2†], *Eun Jung Koh*[1,2], *Kyung Hyun Kim*[1,2], *Ji Hoon Phi*[1,2], *Ji Yeoun Lee*[1,2,3] *and Seung-Ki Kim*[1,2*]

[1] Division of Pediatric Neurosurgery, Pediatric Clinical Neuroscience Center, Seoul National University Children's Hospital, Seoul, South Korea, [2] Department of Neurosurgery, Seoul National University Hospital, Seoul National University College of Medicine, Seoul, South Korea, [3] Department of Anatomy, Seoul National University College of Medicine, Seoul, South Korea

OPEN ACCESS

Edited by:
David Nathanson,
UCLA David Geffen School of Medicine, United States

Reviewed by:
Carsten Friedrich,
Klinikum Oldenburg AöR, Germany
Jeffrey Rubens,
Johns Hopkins University, United States

***Correspondence:**
Seung-Ki Kim
nsthomas@snu.ac.kr

[†]These authors have contributed equally to this work

Specialty section:
This article was submitted to Neuro-Oncology and Neurosurgical Oncology, a section of the journal Frontiers in Oncology

Received: 31 December 2020
Accepted: 21 June 2021
Published: 21 July 2021

Citation:
Kim HY, Choi SA, Koh EJ, Kim KH, Phi JH, Lee JY and Kim S-K (2021) Combination Treatment of CI-994 With Etoposide Potentiates Anticancer Effects Through a Topoisomerase II-Dependent Mechanism in Atypical Teratoid/Rhabdoid Tumor (AT/RT). Front. Oncol. 11:648023. doi: 10.3389/fonc.2021.648023

Purpose: Atypical teratoid/rhabdoid tumor (AT/RT) is arising typically in young children and is associated with a dismal prognosis which there is currently no curative chemotherapeutic regimen. Based on previous studies showing high histone deacetylase 1 (HDAC1) expression in AT/RT, the HDAC1 inhibitor CI-994 was used as a novel treatment strategy in this study. We assessed the anticancer effects of CI-994 and conventional drugs (etoposide, cisplatin or 4-HC) in AT/RT cells.

Methods: AT/RT patient-derived primary cultured cells and cell lines were prepared. HDAC1 was estimated by real-time quantitative polymerase chain reaction (RT-qPCR). The interaction of the drugs was analyzed using isobologram analysis. Cell viability, apoptosis, HDAC enzyme activity and western blot assays were carried out.

Results: HDAC1 was overexpressed in AT/RT compared to medulloblastoma. The combination index (CI) of CI-994 with etoposide revealed a synergistic effect in all AT/RT cells, but no synergistic effect was observed between CI-994 and cisplatin or 4-HC. CI-994 effectively reduced not only Class I HDAC gene expression but also HDAC enzyme activity. The combination treatment of CI-994 with etoposide significantly increased apoptosis compared to the single treatment. The enhanced effect of apoptosis by this combination treatment is related to a signaling pathway which decreases topoisomerase (Topo) II and increases histone H3 acetylation (Ac-H3).

Conclusion: We demonstrate that the combination treatment of CI-994 with etoposide exerts a synergistic anticancer effect against AT/RT by significantly inducing apoptosis through Topo II and Ac-H3 regulation.

Clinical Relevance: This combination treatment might be considered a viable therapeutic strategy for AT/RT patients.

Keywords: atypical teratoid/rhabdoid tumor, combination treatment, HDAC1 inhibition, synergism, topoisomerase II

INTRODUCTION

Atypical teratoid/rhabdoid tumor (AT/RT) is one of the most malignant pediatric brain tumors that typically arises in infants younger than 3 years old (1). Maximal safe resection followed by multimodal therapy is recommended as the standard treatment. However, the prognosis of patients with AT/RT is still poor (2, 3). The difficulty of gross total resection, incomplete efficacy of intensive chemotherapy and limitation of radiotherapy for young patients highlight the urgency of developing novel therapeutic strategies (3).

AT/RT is characterized by biallelic loss-of-function alterations in *SMARCB1*, which encodes the hSNF5/BAF47/INI1 subunit of the SWI/SNF chromatin remodeling complex (3, 4). Previous in-depth molecular studies explained the observed clinical heterogeneity but relatively unaltered genome of AT/RT by noting substantial heterogeneity in epigenetic profiles (2, 3). The Toronto group (5) and German group (6) recently classified AT/RT into 3 molecular subgroups based on its epigenetic profiles from two different perspectives. Studies targeting the mechanisms of epigenetic regulation in AT/RT treatment have been extensively conducted, leading to successful use of histone deacetylase (HDAC) inhibitors such as trichostatin A, SAHA, and SNDX-275 (7). It also suggested that a specific class of HDAC inhibitors may be more effective for certain molecular classes of AT/RT (5).

HDAC regulates the expression of genes and proteins involved in both cancer initiation and progression (8), and high expression levels of several HDACs are associated with poor prognosis of cancer patients (9). Additionally, HDACs have been found to regulate cancer cell functions, including DNA damage, cell death and differentiation (10). Therefore, the anticancer effects of HDAC inhibitors have been evaluated in various cancers (11).

HDAC1, which is a Class I HDAC, has been reported to play important roles in epigenetic regulation for tumor progression and is significantly overexpressed in many cancers (10, 12), including AT/RT (13, 14). Importantly, HDAC1 is highly expressed in AT/RT tissues compared to normal cerebellum and CNS non-cerebellum (15). As a drug that can inhibit HDAC1, CI-994 (Tacedinaline, N-acetyldinaline) is an oral compound that is also a selective Class I HDAC inhibitor (16). CI-994 has been verified to exhibit significant anticancer activity against a broad spectrum of human cancers *in vitro* (17) and *in vivo* (16).

Many preclinical and clinical studies have examined rational combinations of HDAC inhibitors with many current therapies for the treatment of hematological and solid tumor malignancies (18). Notably, CI-994 was investigated in combination with other anticancer drugs in phase I/II clinical trials for solid tumors (19). Therefore, the potential benefits that CI-994 might confer in the treatment of AT/RT led us to investigate the combination treatment of CI-994 with conventional anticancer drugs.

In this study, we evaluated the combination treatments of CI-994 with three different conventional chemotherapeutic agents (etoposide, cisplatin, or ifosfamide) commonly used in two protocols for the treatment of AT/RT (2). As etoposide showed the most potent synergistic effect with CI-994, we investigated the potential signaling pathway affected by this combination that leads to its anticancer effects.

MATERIALS AND METHODS

Patients and Samples

Brain tumor tissues (**Table 1**) were collected from patients diagnosed with AT/RT (N=13) and MBL (N=13) who underwent initial surgery at the Seoul National University Children's Hospital. The Institutional Review Board (IRB) of the Seoul National University Hospital (SNUH) approved the study protocol (IRB approval No. 1707-095-878). The pathological diagnosis of AT/RT was made histologically and confirmed by

TABLE 1 | Patient information.

Sample	Gender	Age	Location	M stage	Subtypes
SNU.AT/RT-1	M	13m	Lt. CPA	M3	MYC
SNU.AT/RT-2	M	18m	Vermis	M3	TYR/MYC
SNU.AT/RT-3	F	32m	Rt. CPA	M0	MYC
SNU.AT/RT-4	M	17m	Vermis	M0	SHH
SNU.AT/RT-5	M	20m	Lt. LV	M3	TYR/MYC
SNU.AT/RT-6	F	2	Lt. cbll	M0	TYR/MYC
SNU.AT/RT-7	F	2m	Rt. cbll	M0	TYR/MYC
SNU.AT/RT-8	M	11m	Lt. LV	M3	TYR/MYC
SNU.AT/RT-9	F	2m	Rt. cbll	M3	TYR/MYC
SNU.AT/RT-10	M	10m	4V	M0	TYR
SNU.AT/RT-11	M	28m	Rt. parietal	M0	undefined
SNU.AT/RT-12	F	14m	Rt. CPA	M3	undefined
SNU.AT/RT-13	M	23m	Rt. LV	M0	undefined
SNU.MBL-1	M	3	4V	M3	Group3
SNU.MBL-2	F	3	4V	M2	Group3
SNU.MBL-3	M	8	4V	M0	WNT
SNU.MBL-4	F	7	4V	M0	WNT
SNU.MBL-5	F	31m	4V	M3	Group4
SNU.MBL-6	M	7	4V	M0	Group4
SNU.MBL-7	M	7	4V	M1	Group4
SNU.MBL-8	F	17m	4V	M0	SHH
SNU.MBL-9	M	9m	Lt. cbll	M0	SHH
SNU.MBL-10	M	8	Rt. cbll	M0	SHH
SNU.MBL-11	F	4	4V	M0	undefined
SNU.MBL-12	F	15	Rt. CPA	M0	undefined
SNU.MBL-13	M	11	4V	M0	undefined

MB, medulloblastoma; AT/RT, atypical teratoid/rhabdoid tumor; M, male; F, female; m, month; Rt, right; Lt, left; V, ventricle; cbll, cerebellum; LV, lateral ventricle.

the lack of INI-1/SMARCB1 protein expression. The AT/RT subgroup was determined by immunohistochemistry staining of tissues (6). The molecular groups of medulloblastoma were analyzed by NanoString nCounter (20).

Real-Time Quantitative Polymerase Chain Reaction (RT-qPCR)

Total RNA was isolated using the miRNeasy Mini Kit (Qiagen, Hilden, Germany), and cDNA was synthesized using the EcoDry Premix kit (Clontech, Mountain View, CA) (21). RT-qPCR assay was performed by a TaqMan assay on an ABI 7500 system (Applied Biosystems, Foster City, CA) using TaqMan probes for HDAC1, HDAC2, HDAC3, HDAC8, and GAPDH. The relative expression levels in each sample were calculated and quantified by using the $2^{-\Delta\Delta CT}$ method. The value of each control sample was set to one and was used to calculate the fold change in target gene expression. GAPDH was utilized to normalize the gene expression results.

Immunohistochemistry (IHC)

The expression of HDAC1 protein within tissues were verified by IHC as previously described (6). A total of 8 cases of tissue (4 cases in medulloblastoma and 4 cases in AT/RT) used to verify HDAC1 protein expression. Of these, 3 cases of each group were newly obtained, and 1 case of each group was included in the previous RT-qPCR analysis. Briefly, the sections were incubated with primary antibodies, HDAC1 (1:1000, Abcam, Cambridge, MA), for 32 min at 37°C, and a secondary antibody for 20 min at 37°C. The stained sections were detected using the Ventana ChromoMap Kit (Ventana Medical Systems) and discovered using XT automated IHC strainer (Ventana Medical Systems, Oro Valley, AZ).

Cell Culture

AT/RT primary cells were cultured as previously described (21). The cell lines of AT/RT (BT12 and BT 16) and MBL (UW228 and MED8A) were provided from Dr. Peter Houghton (Nationwide Children's Hospital) and Dr. Young Shin Ra (Asan Medical Center, Seoul, Korea), respectively. The human neural stem cell HB1.F3 was used as a normal control. All cells were cultured in Dulbecco's modified Eagle's medium (DMEM; Welgene, Seoul, Korea) containing 10% fetal bovine serum and 1% antibiotic-antimycotics and incubated at 37°C in a 5% CO_2 atmosphere.

Drugs

CI-994, etoposide, and cisplatin were purchased from Selleckchem (Houston, TX). We used the activated form of ifosfamide, 4-hydroperoxycyclophosphamide (4-HC), from Cayman (Ann Arbor, MI). The drugs were dissolved in dimethyl sulfoxide (DMSO) to generate 10 mM stock solutions and diluted to the indicated concentrations with culture medium before the experiments.

Cell Viability Assays

The median inhibitory concentration (IC_{50}) was determined in AT/RT cells. The cells (4×10^3) were cultured in 96-well plates and exposed to various concentrations of the drugs (0-100 μM). Cells treated with 0.1% DMSO were used as a control. Cell viability was measured using the EZ-cytox kit (Daeil Lab Service, Seoul, Korea) after drug treatment for 72 h. The percentage of cell viability of the treated cells was measured relative to that of the control cells. Cell growth curves were drawn, and the IC_{50} was calculated by nonlinear regression analysis using Prism software (La Jolla, CA).

Isobologram Analysis

To evaluate the dose-responses of the CI-994-based combination treatments, an isobologram was drawn for each drug combination based on 5 constant ratios: 0.25× IC_{50}, 0.5× IC_{50}, IC_{50}, 2× IC_{50}, and 4× IC_{50} (22). The synergy, additivity or antagonism was calculated on the basis of the multiple drug effect equation and quantified by the combination index (CI) and fraction affected (Fa) according to the Chou-Talalay algorithm utilizing CompuSyn software (Paramus, NJ, www.combosyn.com) (22, 23). The CI values indicate synergistic (CI < 1), additive (CI = 1) or antagonistic effects (CI > 1). The Fa levels of 50% (Fa = 0.5), 70% (Fa = 0.7), and 80% (Fa = 0.8) inhibition were created to study the dose-dependent interaction of the drug combinations. Fa < 0.5 was regarded as irrelevant because a large fraction of the cell population showed proliferation and reduced growth inhibition.

HDAC Enzyme Activity Analysis

HDAC enzyme activity was assessed by an HDAC enzyme activity kit (Biovision, Mountain View, CA) (23). After 72 h of drug treatment, proteins (50 μg) extracted from the cells was mixed with the assay substrate and incubated at 37°C for 1 h. The reaction was stopped by adding 10 μl of lysine developer and incubated for an additional 30 min at 37°C. Test samples were measured by a fluorimeter (Molecular Devices, Sunnyvale, CA) at 405 nm.

Apoptosis Analysis

Apoptosis was evaluated by the Annexin V-Fluorescein isothiocyanate (FITC)/propidium iodide (PI) binding assay kit (BD Biosciences, Franklin Lakes, NJ) according to the manufacturer's instructions. After drug treatment for 48 h, the cells (1×10^6 cells/ml) were harvested, stained with Annexin V and PI in the dark for 15 min, subjected to FACSCanto (BD), and analyzed by FlowJo software.

Western Blot

Total proteins were extracted using radioimmunoprecipitation (RIPA) lysis buffer. Western blotting was performed using the iBlot system (Invitrogen) as previously described (23). The following primary antibodies were used: topoisomerase II (Topo II, 1:5000, Abcam), acetylated histone H3 (Ac-H3, 1:2000, Abcam), γ-H2AX (1:5000, Abcam), cleaved Parp (1:1000, Cell Signaling Technology, Danvers, MA), active Caspase-3 (cleaved Caspase-3, 1:100, Millipore, MA), Survivin (1:5000, Abcam), NF-κB (1:500, Abcam), C-Myc (1:10000, Abcam) and β-actin (1:5000, Sigma-Aldrich, St. Louis, MO). The blots were visualized by enhanced chemiluminescence (ECL, Invitrogen) with X-ray film. The band intensities were quantified using ImageJ software and normalized to β-actin.

Statistical Analysis

All the values were calculated as the mean ± SD or expressed as the percentage ± SD of the controls. Multiple group comparisons were performed by 1-way ANOVA. Differences between 2 groups were determined using a 2-tailed Student's *t*-test and Mann-Whitney test. GraphPad Prism v7.0 software was used for all the statistical analyses. All the analyses were repeated at least three times, and differences were considered statistically significant at $p < 0.05$.

RESULTS

Overexpression of HDAC1 in AT/RT

We first evaluated the mRNA expression levels of HDAC1 in AT/RT tissues and cells. Compared with MBL tissues, AT/RT tissues exhibited increased HDAC1 mRNA expression (2.19-fold, $p < 0.05$, **Figure 1A**) and protein expression (**Figures 1C, D**). In addition, we confirmed that there was no significant change in HDAC1 mRNA expression depending on the MYC subgroup (*p*= NS, **Supplementary Figure S1**). HDAC1 was more highly expressed in all AT/RT cells than in MBL cells (6-fold $p < 0.05$, **Figure 1B**).

Determination of IC_{50} Values

The prerequisite for confirming a synergistic effect is to determine the potency of each drug and the slopes of their concentration response curves. Therefore, we investigated the IC_{50} values of each drug in primary cultured AT/RT cells (SNU.AT/RT-9 and SNU.AT/RT-10) and AT/RT cell lines (BT12 and BT16). Increasing concentrations of each drug significantly reduced the viability of all AT/RT cells in a dose-dependent manner (**Figure 2**). The IC_{50} values ranged from 7.5 ± 0.2 to 65.0 ± 22.0 μM for CI-994, 4.9 ± 2.4 to 13.4 ± 4.3 μM for etoposide, 1.0 ± 0.05 to 56.1 ± 7.5 μM for cisplatin, and 5.3 ± 0.2 to 57.4 ± 5.0 μM for 4-HC in AT/RT cells (**Table 2**). The IC_{50} values of HB.F3 cells were 48.1 ± 26.6 μM for CI-994, 16.3 ± 5.2 μM for etoposide, 62.8 ± 3.8 μM for cisplatin, and 25.7 ± 11.1 μM for 4-HC. Compared to AT/RT cells, HB.F3 cells were more resistant to etoposide and cisplatin.

Synergistic Effect of the Combination Treatment of CI-994 With Etoposide Against AT/RT

To determine the drug interaction of CI-994 with conventional chemotherapeutic agents, we calculated the fraction affected (Fa)

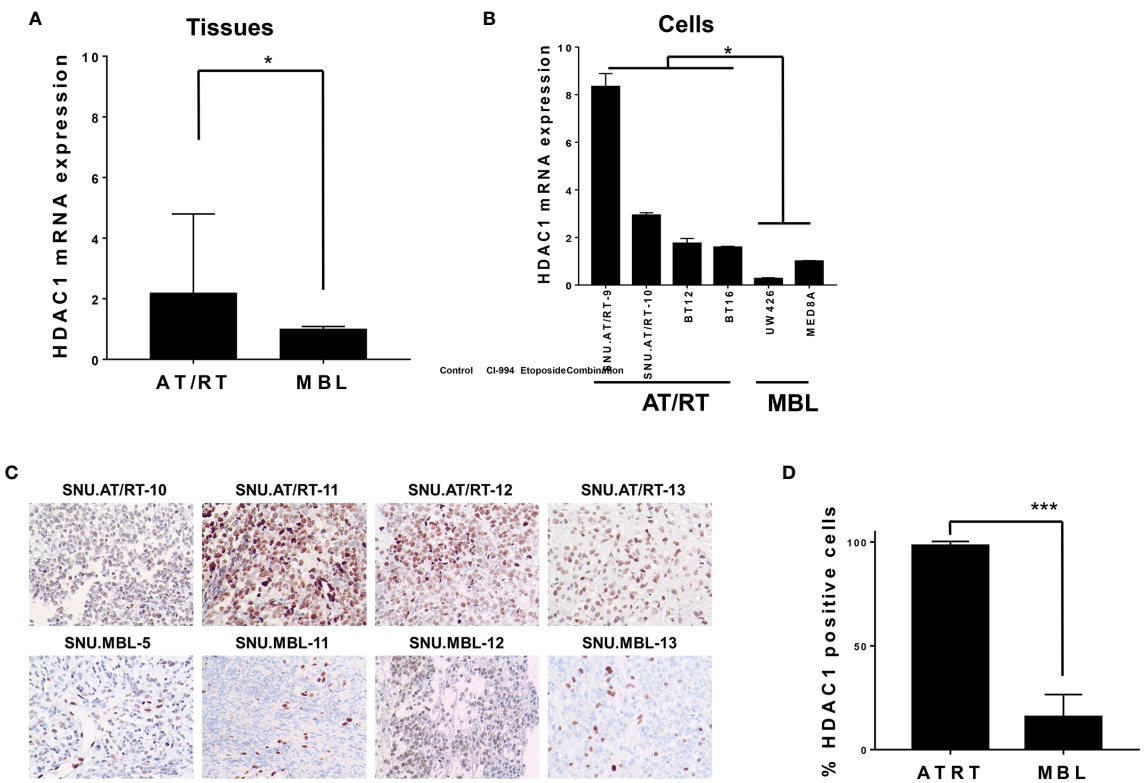

FIGURE 1 | HDAC1 expression in AT/RT samples compared to MBL samples. **(A)** The quantitative polymerase chain reaction (qPCR) showed that HDAC1 mRNA expression in AT/RT tissues was 2.19 ($p = 0.027$) folds higher than in MB tissues. **(B)** HDAC1 mRNA level was tested in 3 AT/RT primary cultured cells(SNU.AT/RT-5, SNU.AT/RT-9, SNU.AT/RT-10) and each established AT/RT (BT12, BT16) and MB (UW426, MED8A) cell lines. HDAC1 is significantly overexpressed in AT/RT samples compared to the lowest expression level in UW426, one of MB cell lines. **(C)** IHC results show significantly higher HDAC1 protein expression in AT/RT compared to medulloblastoma. **(D)** The graph shows the percentage of HDAC1 positive cells in IHC ($p < 0.0001$). *$p < 0.05$, ***$p < 0.0001$.

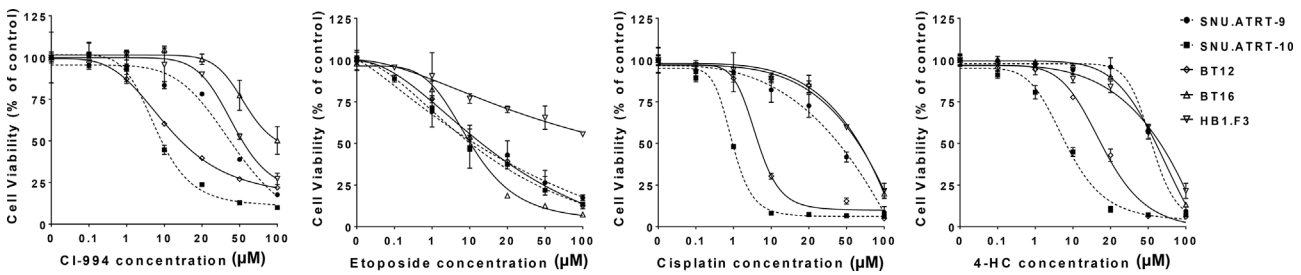

FIGURE 2 | Single treatment in AT/RT cells. The viability of AT/RT cells against selected drugs (CI-994, etoposide, cisplatin, or 4-HC) was assessed by estimating their IC50.

TABLE 2 | IC_{50} of each drug in AT/RT cell lines.

Cell lines	CI-994	Etoposide	Cisplatin	4-HC*
SNU.AT/RT-9	40.4 ± 10.4μM	13.4 ± 4.3μM	25.1 ± 4.1μM	56.5 ± 16.8μM
SNU.AT/RT-10	7.5 ± 0.2μM	9.9 ± 0.4μM	1.0 ± 0.05μM	5.3 ± 0.2μM
BT12	36.1 ± 1.5μM	9.2 ± 0.7μM	4.7 ± 1.1μM	15.7 ± 0.3μM
BT16	65.0 ± 22.0μM	4.9 ± 2.4μM	56.1 ± 7.5μM	57.4 ± 5.0μM
HB1.F3**	48.1 ± 26.6μM	16.3 ± 5.2μM	62.8 ± 3.8μM	25.7 ± 11.1μM

*Activated form of ifosfamide, **Neural stem cells.*

and combination index (CI) values. The effect of the combination treatment of CI-994 with etoposide in all AT/RT cells was interpreted as synergistic: 0.3-0.54 in SNU.AT/RT-9 cells, 0.09-0.13 in SNU.AT/RT-10 cells, 0.5-0.8 in BT12 cells and 0.32-0.49 in BT16 cells (**Figure 3A** and **Supplementary Table S1**). The combination treatment of CI-994 with cisplatin or 4-HC did not exert synergistic effects in some cells (**Figures 3B, C**). In particular, antagonism was observed in SNU.AT/RT-10 cells with the combination treatment of CI-994 with cisplatin (**Supplementary Table S2**) and in SNU.AT/RT-10 cells and BT12 cells with the combination treatment of CI-994 with 4-HC (**Supplementary Table S3**). Therefore, etoposide was chosen as the drug to be combined with CI-994.

At the optimal concentration of the combination treatment of CI-994 with etoposide, dose-response plots and Fa-CI were generated to the confirm drug interaction. The combination dose-response curves of all the AT/RT cells treated with CI-994 and etoposide shifted to the left, which indicated synergism by lowering the IC_{50} equivalent (**Figure 4A**). The Fa-CI plot showed all points to be under the horizontal line, which equaled 1 of the CI value at all concentrations. In the case of BT16 cells, all the points were closer to the bottom line than the points of the other AT/RT cells. The data points below the line of additivity indicate synergism (**Figure 4B**). The viability of cells exposed to the combination treatment of CI-994 with etoposide was significantly reduced by approximately 1.95- to 4.8-fold compared to that of cells exposed to the single treatment in all AT/RT cells ($p < 0.0001$, **Figure 4C**).

Inhibition of HDAC1 mRNA Expression by CI-994

To confirm whether CI-994 effectively inhibits the mRNA expression of Class I HDAC, we performed RT-qPCR. As expected, HDAC1 expression was significantly decreased by CI-994 treatment alone and by the combination treatment compared to the control treatment in all AT/RT cells (**Figure 5A** and **Supplementary Table S4**). Etoposide single treatment did not affect HDAC1 mRNA expression. We also examined the mRNA expression of HDAC2, HDAC3 and HDAC8, which was significantly decreased by the CI-994 single treatment and combination treatment. In some AT/RT cells, HDAC2, HDAC3 or HDAC8 expression was reduced by etoposide single treatment.

Decreased Activity of HDAC Following Combination Treatment of CI-994 With Etoposide

The inhibitory effect of the combination treatment of CI-994 with etoposide on HDAC activity was evaluated. Compared to the control treatment, the CI-994 single treatment and combination treatment effectively decreased the enzyme activities in all AT/RT cells (**Figure 5B** and **Supplementary Table S5**). Interestingly, the etoposide single treatment slightly suppressed HDAC enzyme activity in SNU.AT/RT-10 cells, BT12 cells, and BT16 cells, but not in SNU.AT/RT-9 cells.

Enhanced Apoptosis Following Combination Treatment With CI-994 and Etoposide

To confirm whether the synergistic anticancer effect of the combination treatment of CI-994 with etoposide is associated with apoptosis, we analyzed the proportion of apoptotic cells by Annexin V-FITC/PI binding assay. The percentage of apoptotic cells was significantly increased in all AT/RT cells treated with CI-994, etoposide and the combination. Importantly, the combination treatment induced more early apoptosis than CI-

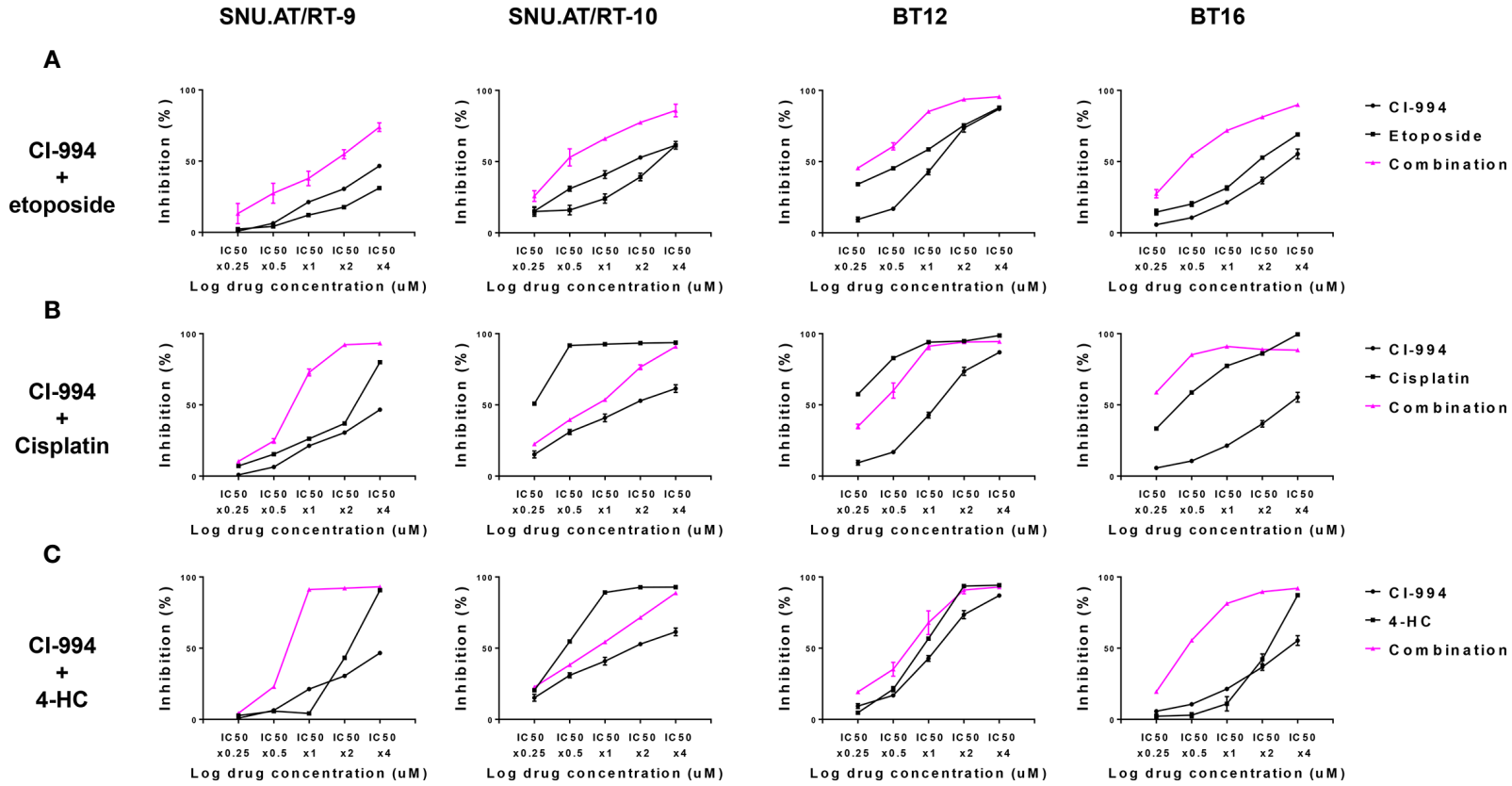

FIGURE 3 | Comparative evaluation of the combination effect of CI-994 with conventional anticancer drugs. Curve shift analysis of CI-994 with conventional drugs (etoposide, cisplatin and 4-HC) in AT/RT cells shows that the degree of left shift represented the amount of synergism associated with the indicated drug combination. Single treatment: Black lines, Combination treatment: Pink lines. **(A)** In response to the combination treatment of CI-994 with etoposide, synergistic effects were observed and inhibited the growth potential of all AT/RT cells in a dose-dependent manner. **(B, C)** The combination treatment of CI-994 with cisplatin or 4 HC exerted cell type-specific effects. Synergistic effects were observed in the cells treated with the combination of CI-994 with cisplatin only for SNU.AT/RT-9 cells and in cells treated with the combination of CI-994 with 4-HC for SNU.AT/RT-9 cells and BT-16 cells.

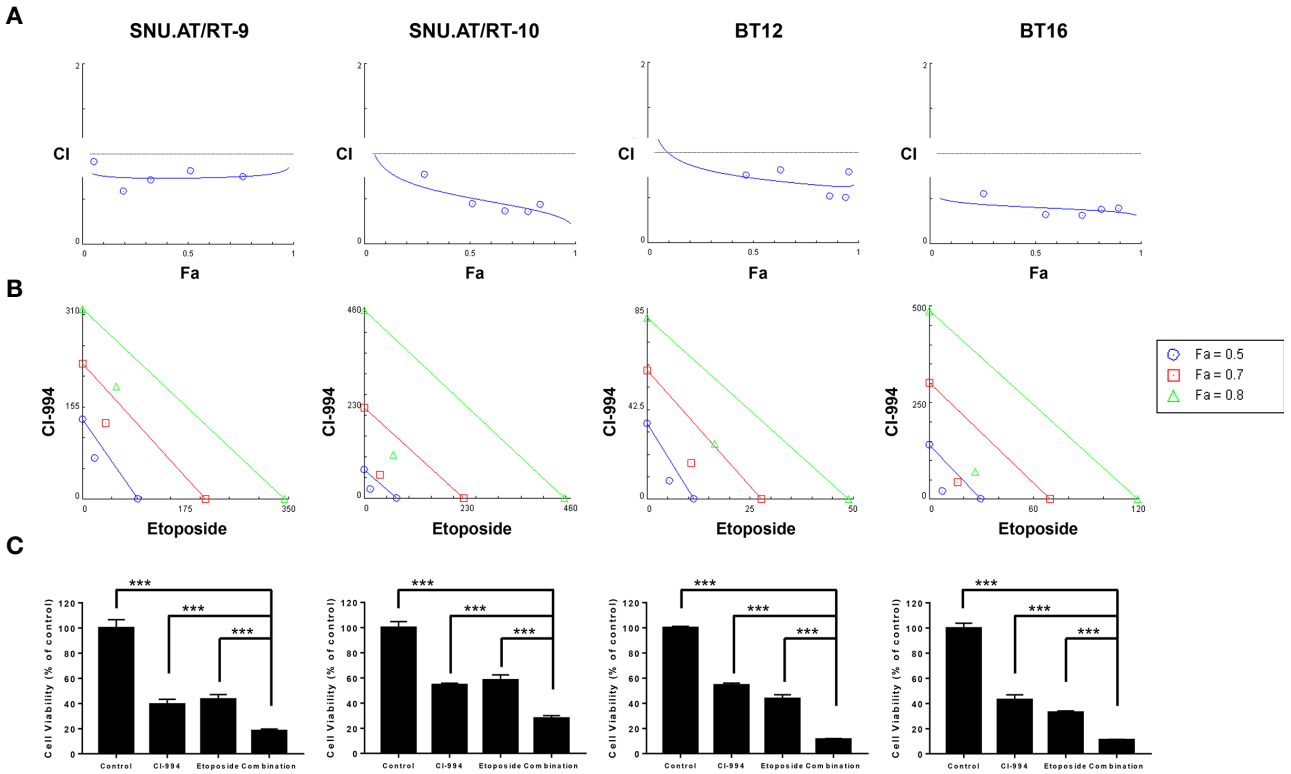

FIGURE 4 | Synergistic effect of the combination treatment of CI-994 with etoposide in atypical teratoid/rhabdoid tumor (AT/RT) cells. Fraction affected *vs.* combination index (Fa-CI) plot was calculated for the combination of CI-994 with etoposide using an isobologram. **(A)** Dose-response curve shows that if the combination points (blue lines) lie below the gray line, there is a synergistic effect. Low CI values with increased Fa values suggest better compatibility and high synergism between CI-994 and etoposide. Graphs show a synergistic effect in all AT/RT cells. **(B)** The blue, red and green lines represent the theoretical additive line and the 0.5, 0.7 and 0.8 values, respectively. The synergy between CI-994 and etoposide increases as the calculated values approach the origin. In all AT/RT cells, synergism was observed at concentrations with Fa 0.5, Fa 0.7 and Fa 0.8 points. **(C)** Combination treatment of CI-994 with etoposide was significantly more effective than single treatment in all AT/RT cells. ***$p < 0.0001$.

994 or etoposide single treatment in all AT/RT cells (**Figures 6A, B** and **Supplementary Table S6**).

Decreased Topoisomerase II Expression and Increased Histone H3 Acetylation Following Combination Treatment With CI-994 and Etoposide

To investigate the molecular mechanisms associated with the synergistic anticancer effect of the combination treatment of CI-994 with etoposide on AT/RT cells, we explored the signaling pathways associated with DNA damage induced by Topo II and H3 acetylation (Ac-H3). In the majority of AT/RT cells, compared with the control and single treatments, the combination treatment led to decreased protein expression of Topo II and increased expression of Ac-H3, γ-H2AX, cleaved Parp, and cleaved Caspase-3 (**Figure 7** and **Supplementary Figure S2**). Survivin was decreased in response to the single and combination treatment in most AT/RT cells; however, in BT16 cells, Survivin expression was increased in response to the etoposide single treatment. Since CI-994 increased Ac-H3 expression, Ac-H3 expression may induce the expression of the DNA damage-related protein γ-H2AX and initiation of early apoptosis, which increases the levels of cleaved Parp and Caspase-3. We also confirmed changes in the expression of NF-κB and C-Myc after drug treatment. The combination treatment of CI-994 and etoposide did not show any difference in the expression of NF-κB (**Supplementary Figure S3A**) but C-Myc (**Supplementary Figure S3B**) was effectively decreased in all AT/RT cells. On the other hand, the etoposide single treatment did not affect Ac-H3 expression but increased γ-H2AX expression. These data suggested that the combination treatment enhanced DNA breakdown by decreasing Topo II expression and increasing Ac-H3 expression, which potentiated apoptosis (**Figure 8**).

DISCUSSION

Our study demonstrated the synergistic anticancer effect of the combination treatment of CI-994 with etoposide on AT/RT. The underlying mechanism of action was thought to occur through enhanced apoptosis due to decreased expression of Topo II and increased expression of Ac-H3.

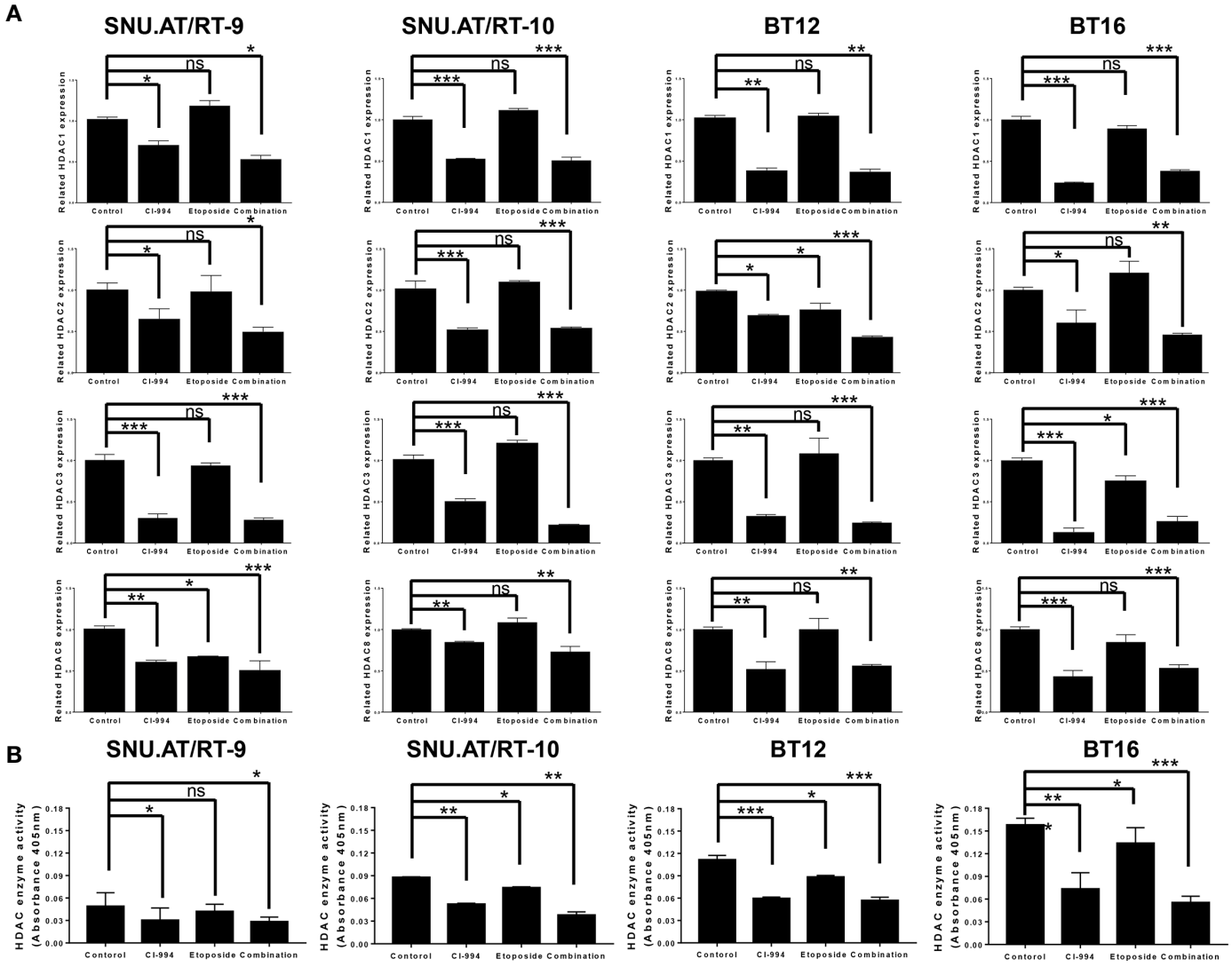

FIGURE 5 | Class I histone deacetylase (HDAC) mRNA expression and HDAC enzyme activity following combination treatment of CI-994 with etoposide. **(A)** Class I HDAC expression was measured by RT-qPCR in AT/RT cells. Class I HDAC mRNA expression was significantly reduced by CI-994 treatment in all AT/RT cells. HDAC1 mRNA expression was not affected by etoposide single treatment in all AT/RT cells, but HDAC 2, 3, and 8 expression tended to decrease in some cells. **(B)** HDAC enzyme activities were significantly reduced by the CI-994 treatment and combination treatment. Even etoposide single treatment led to a slight decrease in SNU.AT/RT-10 cells, BT12 cells, and BT16 cells, but not in SNU.AT/RT-9. *$p < 0.05$, **$p < 0.001$, ***$p < 0.0001$, ns, not significant.

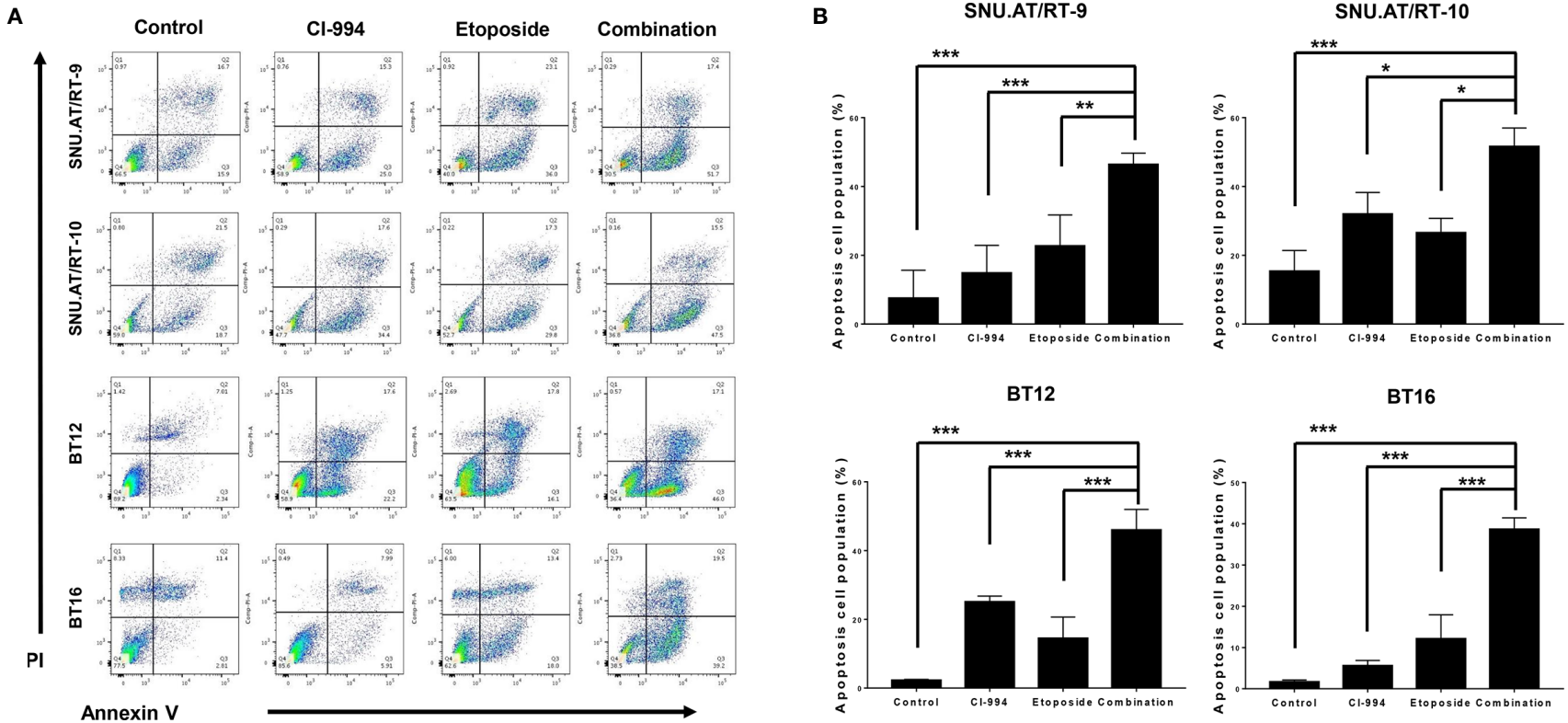

FIGURE 6 | Effect of the combination treatment of CI-994 with etoposide on apoptosis in AT/RT cells. **(A)** Apoptosis in AT/RT cells was analyzed by Annexin V-FITC/propidium iodide assay and flow cytometry. **(B)** Percentages of apoptotic cells are presented on graphs. Combination of CI-994 with etoposide more considerably induced apoptosis in all AT/RT cells than the single treatment. *$p < 0.05$, **$p < 0.001$, ***$p < 0.0001$.

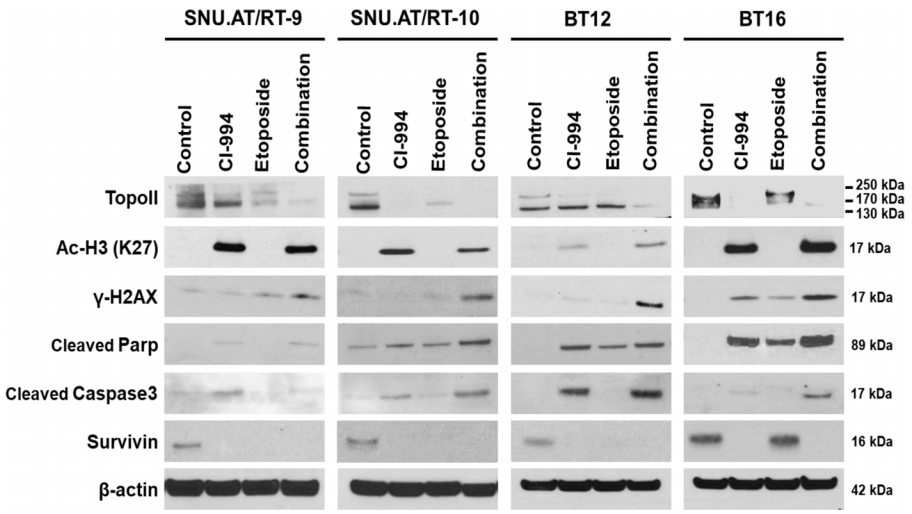

FIGURE 7 | Protein expression involved in the synergistic effect of the combination treatment of CI-994 with etoposide. Western blot analysis shows the levels of topoisomerase (Topo) II, histone 3 acetylation (Ac-H3), γ-H2AX, cleaved Parp, cleaved Caspase-3 and Survivin in response to the combination treatment of CI-994 with etoposide.

The importance of HDAC-targeted therapeutics in various tumors (8, 24) has led to the extended use of specific HDAC inhibitors in pediatric brain tumors, including AT/RT (14). Previous studies showing HDAC1 overexpression in AT/RT (13) and verification in our samples provided rationale for the use of HDAC1 inhibitors. Since there are no commercially available inhibitors that regulate only HDAC1, we used CI-994, which is a relatively selective HDAC1 inhibitor (25, 26). It would be difficult to target and selectively regulate only HDAC1 because HDAC1, 2, 3 and 8, which are Class I HDACs, interact with each other (27). This limitation highlights the importance of intensive research on the development of HDAC single isoform inhibitors. This is one of the limitations of our study and remains a challenge to be addressed.

The three molecular subgroups of AT/RT are well known, and this should be taken into account as different subgroups may induce different drug sensitivities (28). The subgroups of AT/RT cells we used in this study were different (SNU.AT/RT-9: TYR/MYC, SNU.AT/RT-10: TYR, BT12: TYR, BT16: controversial). It should be kept in mind that the sensitivity of the drug may vary depending on the subgroup.

The penetration of CI-994 through the blood-brain barrier (BBB) is low (permeability surface area products BBB: 12.7 ± 0.1 μL/min/g brain) (29). Therefore, delivery strategies *via* intratumoral (30), intracisternal (31) and intranasal (32) injections may be required to bypass the BBB.

Many preclinical studies have suggested that the combination treatment of HDAC inhibitors with conventional chemotherapeutics safely shows synergistic effects even at lower concentrations (18). Recent studies have suggested that the use of HDAC inhibitors may be beneficial for the treatment of children with AT/RT as part of multimodal therapies (14). Although CI-994 is a potential anticancer drug, it is associated with dose-dependent toxicity and side effects, including thrombocytopenia and neutropenia (19, 26). Therefore, we investigated the drug interactions between CI-994 and conventional anticancer drugs (etoposide, cisplatin and 4-HC) that are commonly used for the treatment of AT/RT patients (23). We used isobologram analysis to determine which anticancer drugs have synergistic effects when combined with CI-994. Among the three combinations, the combination treatment of CI-994 with etoposide exerted the strongest effect in a dose-dependent manner. Despite the molecular heterogeneity of AT/RT tumors, isobologram analysis of the combination treatment of CI-994 with etoposide showed consistent responses in all AT/RT cells. On the other hand, the combination of CI-994 with cisplatin or 4-HC revealed antagonism in at least one combination ratio in AT/RT cells, and the response of each cell was inconsistent. For these reasons, we conducted this study focusing on the combination treatment of CI-994 with etoposide.

Next, we determined whether CI-994 efficiently inhibits Class I HDAC gene expression and enzyme activities in AT/RT cells. The inhibitory effect of the combination treatment of CI-994 with etoposide was relatively similar to the effect of CI-994 alone. As a result, there might be other regulatory factors that could cause the synergistic effect of the combination treatment. We speculated that two target molecules modify each other's activity, thus generating the observed synergy. Previous studies have suggested that acetylation seems to influence the efficacy of etoposide, as both HDAC and histone acetyltransferase (HAT) activities increase the efficacy of etoposide (33). There is further evidence that HDAC1/2 complexes with Topo II modify each other's activity *in vitro* and *in vivo* (34). Topo II-associated HDAC activity was reduced by a specific HDAC inhibitor, and the combination treatment could increase cytotoxicity (34). Etoposide induces apoptosis by inhibiting the Topo II cleavage

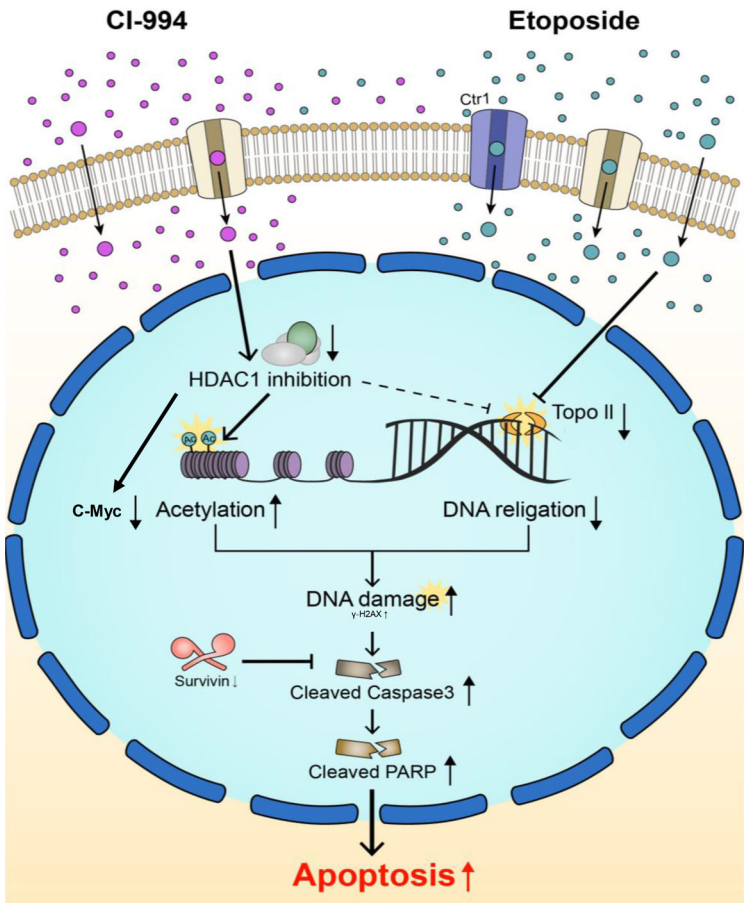

FIGURE 8 | Schematic diagram of two main targets of the combination treatment. Topo II and HDAC1 are known to interact with each other and modify each other's activity. CI-994 and etoposide can pass through cell membranes using transporters and/or passive diffusion. CI-994 enters the cell, inhibits HDAC1 enzyme activity and increases histone acetylation, therefore activating cleaved Parp. CI-994 also reduced C-Myc, which was more effective in combination treatment with etoposide. CI-994 can also increase γ–H2AX expression. Etoposide increases γ-H2AX expression, which not only increases cleaved Parp levels but also decreases Survivin levels. The action of each of these drugs through the regulation of Topo II and Ac-H3 synergistically increases cleaved Parp levels and cleaved Caspase-3 levels, leading to the apoptosis of AT/RT cells.

complexes, leading to the accumulation of DNA damage (33). In addition, CI-994 and other HDACi have shown to induce apoptosis through post-induction suppression of NF-κB or C-Myc-mediated transcription (35, 36). Taken together, we assumed that the synergistic interaction between CI-994 and etoposide is mediated through Topo II (37). Our results showed considerably decreased Topo II expression and increased Ac-H3 expression in response to the combination treatment, suggesting the possibility that apoptosis may be elevated by these signaling pathways. C-Myc may be involved in this signal pathways, not by NF-κB related signal pathway.

In summary, our results demonstrate that the combination treatment of CI-994 with etoposide exerts a synergistic anticancer effect by promoting apoptosis of AT/RT cells through the modulation of Topo II and Ac-H3 *in vitro*. Although the use of more selective HDAC1 inhibitors and the addition of animal experiments remain challenges, our results support the possibility that the combination treatment of CI-994 with etoposide deserves further attention as a therapeutic option for pediatric AT/RT.

DATA AVAILABILITY STATEMENT

The original contributions presented in the study are included in the article/**Supplementary Material**. Further inquiries can be directed to the corresponding author.

ETHICS STATEMENT

The studies involving human samples were reviewed and approved by the Institutional Review Board (IRB) of the Seoul National University Hospital (SNUH IRB approval No. 1707-095-878). The patients/participants provided their written informed consent to participate in this study.

AUTHOR CONTRIBUTIONS

S-KK supervised this study. SC designed the experiment. HK performed the experiment. SC and EK analyzed the data. SC and HK wrote the manuscript. JP, K-HK, SC and JL reviewed and edited the draft. All authors contributed to the article and approved the submitted version.

FUNDING

This work was supported by the National Research Foundation of Korea (NRF) grant funded by the Korean government (MSIT) (2019R1F1A1063068) and by grants from the National Cancer Center, Republic of Korea (NCC-1810861-1).

ACKNOWLEDGMENTS

We are grateful to Sung-hwan Bae for graphic illustration.

SUPPLEMENTARY MATERIAL

The Supplementary Material for this article can be found online at: https://www.frontiersin.org/articles/10.3389/fonc.2021.648023/full#supplementary-material

REFERENCES

1. Louis DN, Perry A, Reifenberger G, von Deimling A, Figarella-Branger D, Cavenee WK, et al. The 2016 World Health Organization Classification of Tumors of the Central Nervous System: A Summary. *Acta Neuropathol* (2016) 131(6):803–20. doi: 10.1007/s00401-016-1545-1
2. Biswas A, Kashyap L, Kakkar A, Sarkar C, Julka PK. Atypical Teratoid/Rhabdoid Tumors: Challenges and Search for Solutions. *Cancer Manag Res* (2016) 8:115–25. doi: 10.2147/CMAR.S83472
3. Richardson EA, Ho B, Huang A. Atypical Teratoid Rhabdoid Tumour: From Tumours to Therapies. *J Korean Neurosurg Soc* (2018) 61(3):302–11. doi: 10.3340/jkns.2018.0061
4. Versteege I, Sevenet N, Lange J, Rousseau-Merck MF, Ambros P, Handgretinger R, et al. Truncating Mutations of hSNF5/INI1 in Aggressive Paediatric Cancer. *Nature* (1998) 394(6689):203–6. doi: 10.1038/28212
5. Torchia J, Golbourn B, Feng S, Ho KC, Sin-Chan P, Vasiljevic A, et al. Integrated (Epi)-Genomic Analyses Identify Subgroup-Specific Therapeutic Targets in CNS Rhabdoid Tumors. *Cancer Cell* (2016) 30(6):891–908. doi: 10.1016/j.ccell.2016.11.003
6. Johann PD, Erkek S, Zapatka M, Kerl K, Buchhalter I, Hovestadt V, et al. Atypical Teratoid/Rhabdoid Tumors Are Comprised of Three Epigenetic Subgroups With Distinct Enhancer Landscapes. *Cancer Cell* (2016) 29 (3):379–93. doi: 10.1016/j.ccell.2016.02.001
7. Knipstein JA, Birks DK, Donson AM, Alimova I, Foreman NK, Vibhakar R. Histone Deacetylase Inhibition Decreases Proliferation and Potentiates the Effect of Ionizing Radiation in Atypical Teratoid/Rhabdoid Tumor Cells. *Neuro Oncol* (2012) 14(2):175–83. doi: 10.1093/neuonc/nor208
8. Eyupoglu IY, Savaskan NE. Epigenetics in Brain Tumors: HDACs Take Center Stage. *Curr Neuropharmacol* (2016) 14(1):48–54. doi: 10.2174/1570159X13666151030162457
9. Dembla V, Groisberg R, Hess K, Fu S, Wheler J, Hong DS, et al. Outcomes of Patients With Sarcoma Enrolled in Clinical Trials of Pazopanib Combined With Histone Deacetylase, Mtor, Her2, or MEK Inhibitors. *Sci Rep* (2017) 7 (1):15963. doi: 10.1038/s41598-017-13114-8
10. Eckschlager T, Plch J, Stiborova M, Hrabeta J. Histone Deacetylase Inhibitors as Anticancer Drugs. *Int J Mol Sci* (2017) 18(7):1414. doi: 10.3390/ijms18071414
11. Suraweera A, O'Byrne KJ, Richard DJ. Combination Therapy With Histone Deacetylase Inhibitors (Hdaci) for the Treatment of Cancer: Achieving the Full Therapeutic Potential of Hdaci. *Front Oncol* (2018) 8:92. doi: 10.3389/fonc.2018.00092
12. Duan H, Zhou K, Zhang Y, Yue P, Wang T, Li Y, et al. HDAC1 was Involved in Placental Breast Cancer Resistance Protein Regulation *In Vitro*: A Preliminary Study. *J Cell Mol Med* (2019) 23(8):5818–21. doi: 10.1111/jcmm.14414
13. Sredni ST, Halpern AL, Hamm CA, Bonaldo Mde F, Tomita T. Histone Deacetylases Expression in Atypical Teratoid Rhabdoid Tumors. *Childs Nerv Syst* (2013) 29(1):5–9. doi: 10.1007/s00381-012-1965-8
14. Perla A, Fratini L, Cardoso PS, Nor C, Brunetto AT, Brunetto AL, et al. Histone Deacetylase Inhibitors in Pediatric Brain Cancers: Biological Activities and Therapeutic Potential. *Front Cell Dev Biol* (2020) 8:546. doi: 10.3389/fcell.2020.00546
15. Kerl K, Ries D, Unland R, Borchert C, Moreno N, Hasselblatt M, et al. The Histone Deacetylase Inhibitor SAHA Acts in Synergism With Fenretinide and Doxorubicin to Control Growth of Rhabdoid Tumor Cells. *BMC Cancer* (2013) 13:286. doi: 10.1186/1471-2407-13-286
16. Thomas M, Clarhaut J, Tranoy-Opalinski I, Gesson JP, Roche J, Papot S. Synthesis and Biological Evaluation of Glucuronide Prodrugs of the Histone Deacetylase Inhibitor CI-994 for Application in Selective Cancer Chemotherapy. *Bioorg Med Chem* (2008) 16(17):8109–16. doi: 10.1016/j.bmc.2008.07.048
17. Loprevite M, Tiseo M, Grossi F, Scolaro T, Semino C, Pandolfi A, et al. *In Vitro* Study of CI-994, a Histone Deacetylase Inhibitor, in non-Small Cell Lung Cancer Cell Lines. *Oncol Res* (2005) 15(1):39–48. doi: 10.3727/096504005775082066
18. Thurn KT, Thomas S, Moore A, Munster PN. Rational Therapeutic Combinations With Histone Deacetylase Inhibitors for the Treatment of Cancer. *Future Oncol* (2011) 7(2):263–83. doi: 10.2217/fon.11.2
19. Pauer LR, Olivares J, Cunningham C, Williams A, Grove W, Kraker A, et al. Phase I Study of Oral CI-994 in Combination With Carboplatin and Paclitaxel in the Treatment of Patients With Advanced Solid Tumors. *Cancer Invest* (2004) 22(6):886–96. doi: 10.1081/CNV-200039852
20. Lee C, Lee J, Choi SA, Kim SK, Wang KC, Park SH, et al. M1 Macrophage Recruitment Correlates With Worse Outcome in SHH Medulloblastomas. *BMC Cancer* (2018) 18(1):535. doi: 10.1186/s12885-018-4457-8
21. Choi SA, Kim SK, Lee JY, Wang KC, Lee C, Phi JH. LIN28B Is Highly Expressed in Atypical Teratoid/Rhabdoid Tumor (at/RT) and Suppressed Through the Restoration of SMARCB1. *Cancer Cell Int* (2016) 16:32. doi: 10.1186/s12935-016-0307-4
22. Chou TC. Drug Combination Studies and Their Synergy Quantification Using the Chou-Talalay Method. *Cancer Res* (2010) 70(2):440–6. doi: 10.1158/0008-5472.CAN-09-1947
23. Jangra A, Choi SA, Yang J, Koh EJ, Phi JH, Lee JY, et al. Disulfiram Potentiates the Anticancer Effect of Cisplatin in Atypical Teratoid/Rhabdoid Tumors (at/RT). *Cancer Lett* (2020) 486:38–45. doi: 10.1016/j.canlet.2020.05.006
24. Li Y, Seto E. Hdacs and HDAC Inhibitors in Cancer Development and Therapy. *Cold Spring Harb Perspect Med* (2016) 6(10):48:38–45. doi: 10.1101/cshperspect.a026831
25. LoRusso PM, Demchik L, Foster B, Knight J, Bissery MC, Polin LM, et al. Preclinical Antitumor Activity of CI-994. *Invest New Drugs* (1996) 14(4):349–56. doi: 10.1007/BF00180810
26. Graziano MJ, Pilcher GD, Walsh KM, Kasali OB, Radulovic L. Preclinical Toxicity of a New Oral Anticancer Drug, CI-994 (Acetyldinaline), in Rats and Dogs. *Invest New Drugs* (1997) 15(4):295–310. doi: 10.1023/A:1005937502511
27. Livyatan I, Meshorer E. The HDAC Interaction Network. *Mol Syst Biol* (2013) 9:671. doi: 10.1038/msb.2013.33

28. Ho B, Johann PD, Grabovska Y, De Dieu Andrianteranagna MJ, Yao F, Fruhwald M, et al. Molecular Subgrouping of Atypical Teratoid/Rhabdoid Tumors-A Reinvestigation and Current Consensus. *Neuro Oncol* (2020) 22 (5):613–24. doi: 10.1093/neuonc/noz235
29. Seo YJ, Kang Y, Muench L, Reid A, Caesar S, Jean L, et al. Image-Guided Synthesis Reveals Potent Blood-Brain Barrier Permeable Histone Deacetylase Inhibitors. *ACS Chem Neurosci* (2014) 5(7):588–96. doi: 10.1021/cn500021p
30. Choi SA, Lee C, Kwak PA, Park CK, Wang KC, Phi JH, et al. Histone Deacetylase Inhibitor Panobinostat Potentiates the Anti-Cancer Effects of Mesenchymal Stem Cell-Based sTRAIL Gene Therapy Against Malignant Glioma. *Cancer Lett* (2019) 442:161–9. doi: 10.1016/j.canlet.2018.10.012
31. Choi SA, Kwak PA, Kim SK, Park SH, Lee JY, Wang KC, et al. *In Vivo* Bioluminescence Imaging for Leptomeningeal Dissemination of Medulloblastoma in Mouse Models. *BMC Cancer* (2016) 16(1):723. doi: 10.1186/s12885-016-2742-y
32. Yang SY, Choi SA, Lee JY, Park AK, Wang KC, Phi JH, et al. miR-192 Suppresses Leptomeningeal Dissemination of Medulloblastoma by Modulating Cell Proliferation and Anchoring Through the Regulation of DHFR, Integrins, and CD47. *Oncotarget* (2015) 6(41):43712–30. doi: 10.18632/oncotarget.6227
33. Montecucco A, Zanetta F, Biamonti G. Molecular Mechanisms of Etoposide. *EXCLI J* (2015) 14:95–108. doi: 10.18632/oncotarget.6227
34. Tsai SC, Valkov N, Yang WM, Gump J, Sullivan D, Seto E. Histone Deacetylase Interacts Directly With DNA Topoisomerase II. *Nat Genet* (2000) 26(3):349–53. doi: 10.1038/81671
35. Guo D, Hong D, Wang P, Wang J, Chen L, Zhao W, et al. Histone Deacetylase Inhibitor CI-994 Inhibits Osteoclastogenesis *Via* Suppressing NF-kappaB and the Downstream c-Fos/NFATc1 Signaling Pathways. *Eur J Pharmacol* (2019) 848:96–104. doi: 10.1016/j.ejphar.2019.01.021
36. Nebbioso A, Carafa V, Conte M, Tambaro FP, Abbondanza C, Martens J, et al. C-Myc Modulation and Acetylation Is a Key Hdac Inhibitor Target in Cancer. *Clin Cancer Res* (2017) 23(10):2542–55. doi: 10.1158/1078-0432.CCR-15-2388
37. Marchion DC, Bicaku E, Turner JG, Daud AI, Sullivan DM, Munster PN. Synergistic Interaction Between Histone Deacetylase and Topoisomerase II Inhibitors Is Mediated Through Topoisomerase Iiβ. *Clin Cancer Res* (2005) 11 (23):8467–75. doi: 10.1158/1078-0432.CCR-05-1073

Conflict of Interest: The authors declare that the research was conducted in the absence of any commercial or financial relationships that could be construed as a potential conflict of interest.

Copyright © 2021 Kim, Choi, Koh, Kim, Phi, Lee and Kim. This is an open-access article distributed under the terms of the Creative Commons Attribution License (CC BY). The use, distribution or reproduction in other forums is permitted, provided the original author(s) and the copyright owner(s) are credited and that the original publication in this journal is cited, in accordance with accepted academic practice. No use, distribution or reproduction is permitted which does not comply with these terms.

frontiers in Oncology

PERSPECTIVE
published: 22 July 2021
doi: 10.3389/fonc.2021.708017

Case Report: End-Stage Recurrent Glioblastoma Treated With a New Noninvasive Non-Contact Oncomagnetic Device

David S. Baskin[1,2,3]*, *Martyn A. Sharpe*[1,2], *Lisa Nguyen*[1,2] *and Santosh A. Helekar*[1,2,3]

[1] Kenneth R. Peak Brain and Pituitary Tumor Treatment Center, Department of Neurosurgery, Houston Methodist Neurological Institute, Houston, TX, United States, [2] Department of Neurosurgery, Houston Methodist Research Institute, Houston, TX, United States, [3] Department of Neurosurgery, Weill Cornell Medical College, New York, NY, United States

Alternating electric field therapy has been approved for glioblastoma (GBM). We have preclinical evidence for anticancer effects in GBM cell cultures and mouse xenografts with an oscillating magnetic field (OMF) generating device. Here we report OMF treatment of end-stage recurrent glioblastoma in a 53-year-old man who had undergone radical surgical excision and chemoradiotherapy, and experimental gene therapy for a left frontal tumor. He experienced tumor recurrence and progressive enlargement with leptomeningeal involvement. OMF for 5 weeks was well tolerated, with 31% reduction of contrast-enhanced tumor volume and reduction in abnormal T2-weighted Fluid-Attenuated Inversion Recovery volume. Tumor shrinkage appeared to correlate with treatment dose. These findings suggest a powerful new noninvasive therapy for glioblastoma.

Keywords: magnetic resonance imaging, contrast enhanced tumor, compassionate use treatment, radiation-type tumor necrosis 2, oscillating magnetic fields

OPEN ACCESS

Edited by:
David Nathanson, UCLA David Geffen School of Medicine, United States

Reviewed by:
Peter LaViolette, Medical College of Wisconsin, United States
Kenneth D. Swanson, Beth Israel Deaconess Medical Center and Harvard Medical School, United States

***Correspondence:**
David S. Baskin
dbaskin@houstonmethodist.org

Specialty section:
This article was submitted to Neuro-Oncology and Neurosurgical Oncology, a section of the journal Frontiers in Oncology

Received: *11 May 2021*
Accepted: *21 June 2021*
Published: *22 July 2021*

Citation:
Baskin DS, Sharpe MA, Nguyen L and Helekar SA (2021) Case Report: End-Stage Recurrent Glioblastoma Treated With a New Noninvasive Non-Contact Oncomagnetic Device. Front. Oncol. 11:708017. doi: 10.3389/fonc.2021.708017

INTRODUCTION

For glioblastoma (GBM), the most common malignant tumor of the brain in adults, treatment outcome remains dismal. In over 40 years median survival has only shown modest improvement (1), and standard of care treatment often has negative impact on quality of life (2). Treatment including radiation and chemotherapy takes a heavy toll. Frequently patients cannot tolerate the completion of the prescribed chemotherapy cycles. Thus, there is a great unmet need for a completely different therapeutic approach with better outcome and less toxicity.

A new FDA-approved treatment involving electric fields alternating at 200 kHz called Optune™ therapy is now available for recurrent GBM as monotherapy and in combination with temozolomide for newly diagnosed GBM (3, 4). It is also being tested in clinical trials for other cancers. Its hypothesized mechanism of action involves disruption of tubulin dimers, mitotic spindles, and cell division by electric field-induced dipole alignment and dielectrophoresis (5). It has a modest effect on survival, increasing median overall survival by 0.6 month in recurrent GBM (3), and in newly diagnosed GBM by 31% (4). Even this modest effect is encouraging for patients.

It has been shown that electromagnetic fields (EMF) produce anticancer effects *in vitro* (6, 7). We have conducted preclinical experiments with a new noninvasive wearable device known as an

Oncomagnetic device that generates oscillating magnetic fields (OMF) by rotating strong permanent magnets (8, 9). The OMF generating components (oncoscillators) of the device can be attached to a helmet and treatment with the device does not require shaving the head. Using the oncoscillators of the device and specially devised patterns of magnet rotations we have produced strong selective anticancer effects in patient derived GBM and xenografted mouse models without causing adverse effects on cultured normal cells and normal mice (10–12). The mechanism of action of OMF differs from Optune™ and involves disruption of the electron transport in the mitochondrial respiratory chain causing elevation of reactive oxygen species and caspase-dependent cancer cell death (10–12).

Here we report evidence of treatment response in the first patient to ever receive this therapy with an untreatable left frontal GBM, treated with a wearable Oncomagnetic device in an FDA-approved Expanded Access Program.

METHODS

Case Description

The patient is a 53-year-old man who first presented with altered mental status in May 2018. Imaging studies documented a large tumor in the left frontal lobe extending across the midline into the right frontal lobe, with diffuse and extensive infiltration through the corpus callosum. There was mass effect and severe edema. He was taken to the operating room on June 4, 2018, where he underwent left frontal craniotomy and radical excision of the tumor. The tumor was histopathologically confirmed as GBM. At the time of the surgery, the excision extended across the midline into the right frontal lobe. He was enrolled in a herpes simplex virus-thymidine kinase gene therapy program and received viral injection during surgery per protocol. In addition, per protocol, and as standard of care, he received concomitant radiation therapy and chemotherapy with temozolomide.

In August 2019, the patient presented with an area of contrast enhancement on MRI scan along the left ventricle. At first this was thought to be a treatment effect. This area progressively enlarged. Evaluations done before OMF treatment initiation on January 16, March 3, and April 15, 2020, demonstrated a clear recurrence. The tumor abutted the ventricle and there was evidence of leptomeningeal spread. The patient had already had radiation therapy and chemotherapy and the tumor was now progressing. The presence of leptomeningeal disease portends poor outcome, with median survival of 3.5 to 3.9 months (13).

Because of inadequacy of any standard of care options he was enrolled in an FDA-approved Expanded Access Program (EAP) for compassionate use treatment with the Oncomagnetic device. He signed an informed consent on April 15, 2020. The EAP study was carried out under a protocol approved by the Houston Methodist Research Institute Institutional Review Board.

Oncomagnetic Device

The Oncomagnetic device consists of 3 oncoscillators securely attached to an acrylonitrile butadiene styrene helmet and connected to a microprocessor-based electronic controller operated by a rechargeable battery (**Figure 1**). Further details regarding the device are given in the **Supplementary Appendix**. Based on a finite element model-based calculation of the spread of the field and the size and magnetization of the rotated diametrically magnetized neodymium magnets, we estimated that the combined effective field (at least 1 mT in strength) of the 3 oncoscillators covered the entire brain, including the upper part of the brain stem.

Oscillating Magnetic Field Treatment

The treatment consists of intermittent application of an OMF that needs to be generated by rotating permanent magnets in a

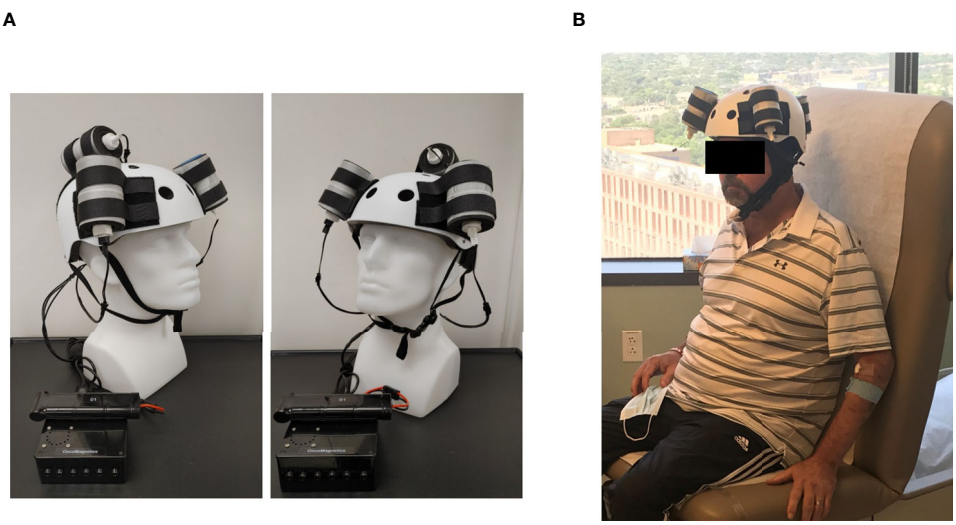

FIGURE 1 | Oncomagnetic Device. **(A)** Device helmet with 3 oncoscillators securely attached to it. The oncoscillators are connected to a controller box powered by a rechargeable battery. **(B)** The patient wearing the device helmet with three oncoscillators attached.

specific frequency profile and timing pattern to be effective. The patient received this treatment initially in the Peak Center clinic under the supervision of the treating physician and the Principal Investigator (DSB) of this study for the first 3 days. The dose was escalated over this period as follows. On the first day, the treatment was for 2 hours with a 5-min break between the first and the second hour. On the second and third days, it was increased to 2 and 3 2-hour sessions, respectively, with 1-hour breaks between the sessions. The patient's spouse was trained in the use and care of the device on these days. After this initial supervised phase, the treatment was continued at home unsupervised with the same regimen as on the third day, above. The spouse was instructed to maintain a daily log of the conduct and progress of treatment, and any observed treatment and adverse effects.

Clinical Evaluations and Neuroimaging

The patient was evaluated clinically by the treating physician on each of the 3 days that he received treatment in the clinic and 7, 16, 30 and 44 days after initiation of treatment. Magnetic Resonance Imaging (MRI) scans were done on Days 1, 3, 7, 16, 30 and 44. The Day 1 scan was done before initiation of treatment. All other scans were done after treatment initiation. The treatment was paused on Day 37 because of an unfortunate but unrelated severe closed head injury (CHI). MRI scans were done on a Siemens Magnetom Terra 7T scanner. MRI scans included T1 magnetization prepared rapid gradient echo scans with and without gadolinium contrast, and T2-weighted Fluid-Attenuated Inversion Recovery (FLAIR), T2-weighted Turbo Spin Echo, Diffusion Weighted Imaging, Susceptibility Weighted Imaging, proton Magnetic Resonance spectroscopy and Diffusion Tensor Imaging scans. Treatment effect on contrast-enhanced tumor (CET) was evaluated according to the response assessment in neuro-oncology (RANO) criteria for clinical trials (14). In addition, an automated software-based method developed in house was used to objectively calculate the CET volume (see below and **Supplementary Appendix**).

Data Analysis

Post-contrast T1 anatomical and T2-FLAIR MRI scans at each of the 6 time points were used to determine changes in contrast-enhanced tumor (CET) volume and non-enhanced tumor infiltration, respectively, before and after initiation of treatment. Information on image processing, data normalization and plotting are given in the **Supplementary Appendix**. Values obtained from pre-treatment clinical scans taken at 2 time points over 3 months before enrollment of the patient were also plotted on the same graph. Because this is a single patient case report, we could not perform any meaningful statistical analysis. However, to obtain a semi-quantitative assessment of the significance of the trend seen with treatment, we analyzed the changes in CET volume using Bayesian logic, given the observed increasing trend at two pre-treatment time points. Accordingly, we assumed that the chance of increase, decrease and no change in the rate of tumor growth was the same at each time point after treatment initiation to calculate the probability of a decrease at each post-treatment initiation time point.

RESULTS

The patient received OMF treatment with the Oncomagnetic device for 36 days. The treatment regimen was changed at various times during this period based on the caregiver reports and clinical findings, as described below.

Clinical Findings

After the initial 3 days of supervised treatment, the patient was seen again by the treating physician in the outpatient clinic on Day 7 from the start of treatment. Because of inattention at baseline, the patient was having difficulty with the length of treatment sessions. They were reduced to 2 hours/day Monday through Friday with Saturday and Sunday off. The Day 16 clinical examination revealed that he was tolerating the treatment sessions well, so they were increased to a total of 3 hours/day (in one-hour increments with 5 min breaks) Monday through Friday and the weekends off. On Day 30 visit, the patient reported headaches related to transient hypertension for which he was taking medication. The treating physician increased blood pressure medication (Valsartan) with improvement. The treatment was paused on Day 36 because of a closed head injury from a fall. Whether the fall was related to the treatment in any way is uncertain. It is worth noting, however, that the patient had experienced several falls before initiation of treatment. At the last follow-up on Day 44 the patient was admitted to the inpatient unit for evaluation of closed head injury and underwent detailed assessment. There were no serious adverse events reported during treatment. The patient's caregivers reported subjective improvement in speech and cognitive function.

MRI Findings

Evaluation of the T1 post-contrast clinical MRI scans obtained before initiation of treatment showed progression in accordance with the RANO criteria (**Figure 2A**). All scans acquired during treatment showed stable disease, according to these criteria (**Figure 2A**). To obtain an objective quantitative assessment of the CET volume we used an automated MATLAB software-based script. This analysis showed marked changes in CET volume with treatment. **Figure 2B** shows a plot of the CET volume as a function of time before and after initiation of treatment. It reveals that there was substantial growth of the tumor volume over the 3 months before the treatment. Within the first 3 days of treatment the trend is reversed with the volume steeply decreasing by ~10% on Day 7 and then less steeply by 31% on Day 30. Based on a Bayesian-type assessment of the probability of a decrease in CET volume at each post-treatment initiation time point, the decrease at Day 30 is statistically significant at $P = 0.036$. The treatment was paused on Day 37. After the pause we see another trend reversal and an increase in CET volume on Day 44.

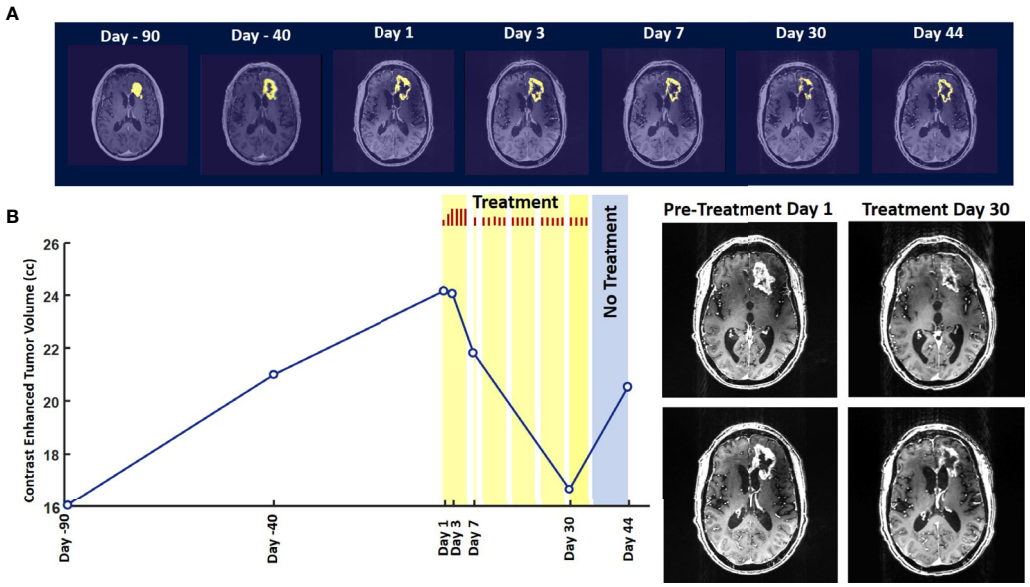

FIGURE 2 | Change in Contrast-Enhanced Tumor Volume. **(A)** T1-weighted axial post-contrast scans showing the contrast-enhanced tumor (CET) highlighted with an overlayed automated computer program-generated light-yellow mask at different time points **(B)** Left **–** A graph showing the change in CET volume over time. The treatment times and durations are shown as red bars and light-yellow highlights. The long pause in treatment is shown as a light-blue highlight. Right – T1-weighted axial post-contrast scans showing CET at two levels along the dorso-ventral axis at Day 1 before treatment and Day 30 of treatment.

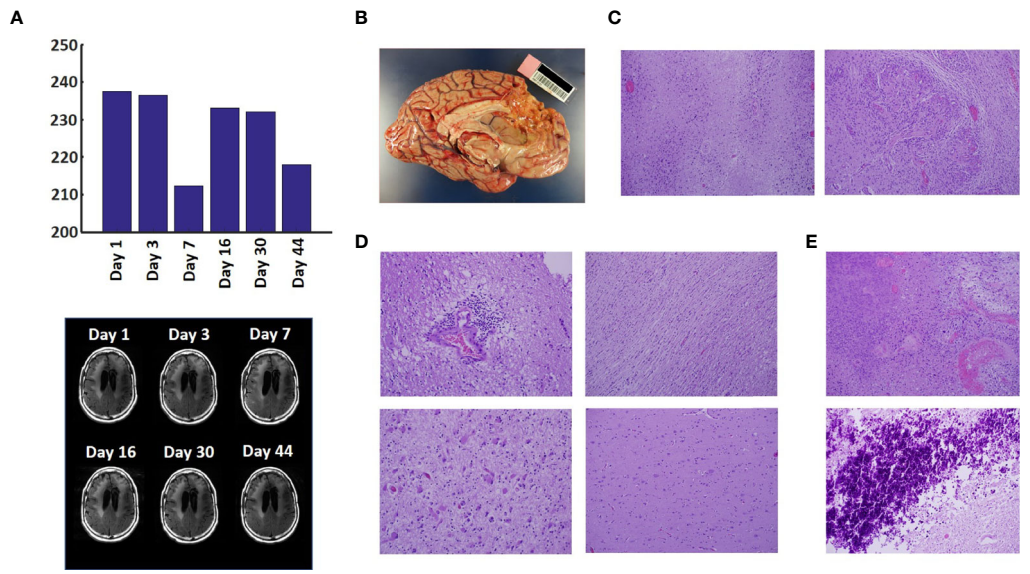

FIGURE 3 | Variation in Enhanced Intensity Volumes in T2-FLAIR MRI Scans and Autopsy Findings. **(A)** Top – Bar plots of the volumes of T2-FLAIR intensity enhancement in the whole brain at different time points. Overall, there was up to 11% decrease in T2 FLAIR volume over the course of treatment. Bottom – Representative T2-FLAIR images are shown. **(B)** Left hemisphere of the brain, examined grossly, showing no tumor mass. **(C)** Photomicrographs of the left cortex showing bland necrosis, residual tumor, and microvascular proliferation with thick-walled vessels. **(D)** Top left – Microscopic field of the left cingulate cortex showing a focus of rarefied, perivascular inflammation. Bottom left – Cortical field showing rarefied parenchyma and residual tumor cells, enlarged with treatment-type effect that can be seen in GBM. Top right – Micrographic field of the corpus callosum showing thinned, rarefied white matter tract. Bottom right – Field showing relatively uninvolved contralateral (right) cortex. **(E)** Top – Micrographic field in the left cortex showing infarct-like necrosis (left), tumor (right), and fibrin thrombus (lower right). Bottom – Left cortical field showing necrotic tissue with dystrophic calcification.

The T2-FLAIR data in **Figure 3A** show changes in enhanced intensity volume of 1 – 11% over time. The decreases in volume are greater after a 3-day pause in treatment on Day 7 and after an 8-day pause on Day 44. These decreases are likely due to reduction in treatment-related cerebral edema and/or reduction in non-contrast enhancing tumor infiltration. The patient died ~3 months after cessation of treatment from the CHI. A brain only autopsy showed a resection cavity in the left frontal lobe (6.0 x 5.0 x 3.5 cm) and recurrent/residual glioblastoma with associated treatment effect (see **Figures 3B–E**). Residual/recurrent high-grade glioma was present, including foci of densely cellular tumor, focal microvascular proliferation, and necrosis (**Figure 3C**). In addition, there was prominent treatment effect with pallor and rarefaction of white matter (**Figure 3D**), reactive astrocytosis, infarct-like necrosis (**Figure 3E**) and bizarre nuclear atypia within residual tumor cells. Additional features of treatment effect included dystrophic calcifications (**Figure 3E**).

DISCUSSION

The findings of this study indicate that Oncomagnetic device-based OMF therapy is well tolerated by a patient who has end-stage recurrent GBM with leptomeningeal involvement and has no other available effective treatment options. They also demonstrate a clinically significant reduction in CET volume with reductions in non-enhanced tumor volume and/or edema in T2-FLAIR scans. The temporal profile of changes in CET volume also suggests a correlation with the treatment dose and the presence or absence of treatment. When the treatment dose was higher (6 hours/day for 4 days) we see a tumor volume reduction rate of 2.32 cm^3/day. When it was lower (2 hours/day for 9 days and 3 hours/day for 18 days) the reduction is 1.03 cm^3/day. Moreover, when the treatment was paused for 8 days the decreasing trend reversed and the CET volume increased, instead. Assuming that the ~1.03 cm^3/day decreasing trend had continued until the treatment was paused, we can estimate that the CET volume grew at the rate of 1.26 cm^3/day during the pause. Despite the apparent correlation it is possible that the treatment response is independent of the short-term changes in the treatment dose.

To our knowledge, there is no report in the literature of a noninvasive treatment-related shrinkage of CET volume of GBM at a rate comparable to that seen in this study. One published report on Optune™ therapy has reported that the time course of change in tumor volume in MRI scans shows a ~15% reduction over ~3 months (15). Besides Optune™, the other type of treatment approved by the FDA and recommended as a standard in National Comprehensive Cancer Network guidelines for recurrent GBM is the anti-vascular endothelial growth factor (VEGF) monoclonal antibody, Bevacizumab (16, 17). Bevacizumab treatment response of reduction in tumor volume on MRI scans has been reported to be lower than is observed in the present study (18). Furthermore, while anti-VEGF drugs in general have mild toxicity profiles and two Phase II trials have shown anti-tumor efficacy (19, 20), a subsequent Phase III trial did not show a significant increase in overall survival (21–23).

CONCLUSION

Noninvasive Oncomagnetic device based OMF therapy appears to be a safe and efficacious new modality of treatment against GBM that potentially has many advantages over existing treatments. The present report has the limitation of the treatment being conducted in only a single patient so far. Extending it to more patients in research studies would provide additional information regarding safety and efficacy.

DATA AVAILABILITY STATEMENT

The original contributions presented in the study are included in the article/**Supplementary Material**. Further inquiries can be directed to the corresponding author.

ETHICS STATEMENT

The studies involving human participants were reviewed and approved by Houston Methodist Research Institute Institutional Review Board. The patient/participant provided their written informed consent to participate in this study. Written informed consent was obtained from the individual for the publication of any potentially identifiable images or data included in this article.

AUTHOR CONTRIBUTIONS

SH and DB designed the study and drafted the manuscript. SH designed the device used in the study, supervised its construction and testing and quantitively analyzed the imaging data. DB provided medical care to the study subject, supervised the delivery of device treatment, and conducted his clinical assessments. SH, MS, and DB designed the device treatment protocol and interpreted the findings. LN constructed and tested the device and provided device treatment to the study subject. All authors contributed to the article and approved the submitted version.

FUNDING

This work was supported by a grant from the Translational Research Initiative of the Houston Methodist Research Institute to SH and DB, and by Donna and Kenneth Peak, the Kenneth R. Peak Foundation, the John S. Dunn Foundation, the Taub Foundation, the Blanche Green Fund of the Pauline Sterne Wolff Memorial Foundation, the Kelly Kicking Cancer

Foundation, the Gary and Marlee Swarz Foundation, the Methodist Hospital Foundation, and the Veralan Foundation. The John S. Dunn Foundation also supports the Distinguished Professorship of MS.

ACKNOWLEDGMENTS

The authors thank the patient for graciously volunteering to be a research subject in this study and the rest of his family for supporting him. We appreciate the assistance of Dr. Matthew Cykowski, MD, Department of Pathology and Genomic Medicine, who provided pathologic description and images. We thank Blessy S. John and Alvin Saldon for aiding in device construction.

SUPPLEMENTARY MATERIAL

The Supplementary Material for this article can be found online at: https://www.frontiersin.org/articles/10.3389/fonc.2021.708017/full#supplementary-material

REFERENCES

1. Stupp R, Mason WP, van den Bent MJ, Weller M, Fisher B, Taphoorn MJ, et al. Radiotherapy Plus Concomitant and Adjuvant Temozolomide for Glioblastoma. *N Engl J Med* (2005) 352:987–96. doi: 10.1056/NEJMoa043330
2. Henriksson R, Asklund T, Poulsen HS. Impact of Therapy on Quality of Life, Neurocognitive Function and Their Correlates in Glioblastoma Multiforme: A Review. *J Neurooncol* (2011) 104:639–46. doi: 10.1007/s11060-011-0565-x
3. Stupp R, Wong ET, Kanner AA, Steinberg D, Engelhard H, Heidecke V, et al. NovoTTF-100A Versus Physician's Choice Chemotherapy in Recurrent Glioblastoma: A Randomised Phase III Trial of a Novel Treatment Modality. *Eur J Cancer* (2012) 48:2192–202. doi: 10.1016/j.ejca.2012.04.011
4. Stupp R, Taillibert S, Kanner A, Read W, Steinberg D, Lhermitte B, et al. Effect of Tumor-Treating Fields Plus Maintenance Temozolomide vs Maintenance Temozolomide Alone on Survival in Patients With Glioblastoma: A Randomized Clinical Trial. *JAMA* (2017) 318:2306–16. doi: 10.1001/jama.2017.18718
5. Tuszynski JA, Wenger C, Friesen DE, Preto J. An Overview of Sub-Cellular Mechanisms Involved in the Action of TTFields. *Int J Environ Res Public Health 13* (2016) 13:1–23. doi: 10.3390/ijerph13111128
6. Saliev T, Begimbetova D, Masoud AR, Matkarimov B. Biological Effects of non-Ionizing Electromagnetic Fields: Two Sides of a Coin. *Prog Biophys Mol Biol* (2019) 141:25–36. doi: 10.1016/j.pbiomolbio.2018.07.009
7. Jimenez H, Blackman C, Lesser G, Debinski W, Chan M, Sharma S, et al. Use of non-Ionizing Electromagnetic Fields for the Treatment of Cancer. *Front Biosci (Landmark Ed)* (2018) 23:284–97. doi: 10.2741/4591
8. Helekar SA, Convento S, Nguyen L, John BS, Patel A, Yau JM, et al. The Strength and Spread of the Electric Field Induced by Transcranial Rotating Permanent Magnet Stimulation in Comparison With Conventional Transcranial Magnetic Stimulation. *J Neurosci Methods* (2018) 309:153–60. doi: 10.1016/j.jneumeth.2018.09.002
9. Helekar SA, Voss HU. Transcranial Brain Stimulation With Rapidly Spinning High-Field Permanent Magnets. *IEEE Access* (2016) 4:2520–8. doi: 10.1109/ACCESS.2016.2568739
10. Helekar S, Sharpe M, Pichumani K, Ijare O, Nguyen L, Baskin D. CTNI-48. Novel Treatment of End Stage Recurrent Glioblastoma Treated With a Noninvasive Oncomagnetic Device Using Oscillating Magnetic Fields – a New and Powerful Noninvasive Therapy. *Neuro-Oncol* (2020) 22:ii53–3. doi: 10.1093/neuonc/noaa215.214
11. Helekar S, Hambarde S, Baskin D, Sharpe M. EXTH-13. Potent Anticancer Effects of a New Wearable Noninvasive Oncomagnetic Device: Cellular Mechanisms of Action. *Neuro-Oncol* (2020) 22:ii89–9. doi: 10.1093/neuonc/noaa215.367
12. Hambarde S, Sharpe M, Baskin D, Helekar S. CBIO-07. Cell Death Induced by an Oscillating Magnetic Field in Patient Derived Glioblastoma Cells is Mediated by Reactive Oxygen Species. *Neuro-Oncol* (2020) 22:ii17–7. doi: 10.1093/neuonc/noaa215.067
13. Andersen BM, Miranda C, Hatzoglou V, DeAngelis LM, Miller AM. Leptomeningeal Metastases in Glioma: The Memorial Sloan Kettering Cancer Center Experience. *Neurology* (2019) 92:e2483–91. doi: 10.1212/WNL.0000000000007529
14. Wen PY, Chang SM, Van den Bent MJ, Vogelbaum MA, Macdonald DR, Lee EQ. Response Assessment in Neuro-Oncology Clinical Trials. *J Clin Oncol* (2017) 35:2439–49. doi: 10.1200/JCO.2017.72.7511
15. Robins HI, Nguyen HN, Field A, Howard S, Salamat S, Deming DA. Molecular Evolution of a Glioblastoma Controlled With Tumor Treating Fields and Concomitant Temozolomide. *Front Oncol* (2018) 8:451. doi: 10.3389/fonc.2018.00451
16. Kreisl TN, Zhang W, Odia Y, Shih JH, Butman JA, Hammoud D, et al. A Phase II Trial of Single-Agent Bevacizumab in Patients With Recurrent Anaplastic Glioma. *Neuro Oncol* (2011) 13:1143–50. doi: 10.1093/neuonc/nor091
17. Friedman HS, Prados MD, Wen PY, Mikkelsen T, Schiff D, Abrey LE, et al. Bevacizumab Alone and in Combination With Irinotecan in Recurrent Glioblastoma. *J Clin Oncol* (2009) 27:4733–40. doi: 10.1200/JCO.2008.19.8721
18. Daniels D, Guez D, Last D, Hoffmann C, Nass D, Talianski A, et al. Early Biomarkers From Conventional and Delayed-Contrast Mri to Predict the Response to Bevacizumab in Recurrent High-Grade Gliomas. *AJNR Am J Neuroradiol* (2016) 37:2003–9. doi: 10.3174/ajnr.A4866
19. Vredenburgh JJ, Desjardins A, Herndon JE2nd, Marcello J, Reardon DA, Quinn JA, et al. Bevacizumab Plus Irinotecan in Recurrent Glioblastoma Multiforme. *J Clin Oncol* (2007) 25:4722–9. doi: 10.1200/JCO.2007.12.2440
20. Vredenburgh JJ, Desjardins A, Herndon JE2nd, Dowell JM, Reardon DA, Quinn JA, et al. Phase II Trial of Bevacizumab and Irinotecan in Recurrent Malignant Glioma. *Clin Cancer Res* (2007) 13:1253–9. doi: 10.1158/1078-0432.CCR-06-2309
21. Chinot OL, Wick W, Mason W, Henriksson R, Saran F, Nishikawa R, et al. Bevacizumab Plus Radiotherapy-Temozolomide for Newly Diagnosed Glioblastoma. *N Engl J Med* (2014) 370:709–22. doi: 10.1056/NEJMoa1308345
22. Wick W, Gorlia T, Bendszus M, Taphoorn M, Sahm F, Harting I, et al. Lomustine and Bevacizumab in Progressive Glioblastoma. *N Engl J Med* (2017) 377:1954–63. doi: 10.1056/NEJMoa1707358
23. Gilbert MR, Dignam JJ, Armstrong TS, Wefel JS, Blumenthal DT, Vogelbaum MA, et al. A Randomized Trial of Bevacizumab for Newly Diagnosed Glioblastoma. *N Engl J Med* (2014) 370:699–708. doi: 10.1056/NEJMoa1308573

Conflict of Interest: SH, MS, and DB are listed as inventors on a U.S. patent application filed by Houston Methodist Hospital for the device used in this report.

The remaining author declares that the research was conducted in the absence of any commercial or financial relationships that could be construed as a potential conflict of interest.

Copyright © 2021 Baskin, Sharpe, Nguyen and Helekar. This is an open-access article distributed under the terms of the Creative Commons Attribution License (CC BY). The use, distribution or reproduction in other forums is permitted, provided the original author(s) and the copyright owner(s) are credited and that the original publication in this journal is cited, in accordance with accepted academic practice. No use, distribution or reproduction is permitted which does not comply with these terms.

frontiers in Oncology

ORIGINAL RESEARCH
published: 30 July 2021
doi: 10.3389/fonc.2021.701500

Development and Validation of a Radiosensitivity Prediction Model for Lower Grade Glioma Based on Spike-and-Slab Lasso

Zixuan Du[1,2†], Shang Cai[3†], Derui Yan[1,2], Huijun Li[1,2], Xinyan Zhang[4], Wei Yang[5], Jianping Cao[5], Nengjun Yi[6] and Zaixiang Tang[1,2]*

[1] Department of Biostatistics, School of Public Health, Medical College of Soochow University, Suzhou, China, [2] Jiangsu Key Laboratory of Preventive and Translational Medicine for Geriatric Diseases, Medical College of Soochow University, Suzhou, China, [3] Department of Radiotherapy and Oncology, The Second Affiliated Hospital of Soochow University, Suzhou, China, [4] School of Data Science and Analytics, Kennesaw State University, Kennesaw, GA, United States, [5] State Key Laboratory of Radiation Medicine and Protection, School of Radiation Medicine and Protection, Collaborative Innovation Center of Radiation Medicine of Jiangsu Higher Education Institutions, Soochow University, Suzhou, China, [6] Department of Biostatistics, University of Alabama at Birmingham, Birmingham, AL, United States

OPEN ACCESS

Edited by:
David Nathanson, UCLA David Geffen School of Medicine, United States

Reviewed by:
David Akhavan, University of Kansas Medical Center, United States
Jing Xiao, Nantong University, China

***Correspondence:**
Zaixiang Tang
tangzx@suda.edu.cn

[†]These authors have contributed equally to this work

Specialty section:
This article was submitted to Neuro-Oncology and Neurosurgical Oncology, a section of the journal Frontiers in Oncology

Received: *28 April 2021*
Accepted: *16 July 2021*
Published: *30 July 2021*

Citation:
Du Z, Cai S, Yan D, Li H, Zhang X, Yang W, Cao J, Yi N and Tang Z (2021) Development and Validation of a Radiosensitivity Prediction Model for Lower Grade Glioma Based on Spike-and-Slab Lasso. Front. Oncol. 11:701500. doi: 10.3389/fonc.2021.701500

Background and Purpose: Lower grade glioma (LGG) is one of the leading causes of death world worldwide. We attempted to develop and validate a radiosensitivity model for predicting the survival of lower grade glioma by using spike-and-slab lasso Cox model.

Methods: In this research, differentially expressed genes based on tumor microenvironment was obtained to further analysis. Log-rank test was used to identify genes in patients who received radiotherapy and patients who did not receive radiotherapy, respectively. Then, spike-and-slab lasso was performed to select genes in patients who received radiotherapy. Finally, three genes (INA, LEPREL1 and PTCRA) were included in the model. A radiosensitivity-related risk score model was established based on overall rate of TCGA dataset in patients who received radiotherapy. The model was validated in TCGA dataset that PFS as endpoint and two CGGA datasets that OS as endpoint. A novel nomogram integrated risk score with age and tumor grade was developed to predict the OS of LGG patients.

Results: We developed and verified a radiosensitivity-related risk score model. The radiosensitivity-related risk score is served as an independent prognostic indicator. This radiosensitivity-related risk score model has prognostic prediction ability. Moreover, the nomogram integrated risk score with age and tumor grade was established to perform better for predicting 1, 3, 5-year survival rate.

Conclusions: This model can be used by clinicians and researchers to predict patient's survival rates and achieve personalized treatment of LGG.

Keywords: lower grade gliomas, radiosensitivity prediction model, radiosensitivity, spike-and-slab lasso, lasso

INTRODUCTION

Glioma is the most common malignant brain tumor in adults and one of the leading causes of death world worldwide. Age-adjusted incidence rates for all gliomas range from 4.67 to 5.73 per 100 000 persons (1). According to the Central Brain Tumor Registry of the United States reports, lower grade gliomas (LGG) consist of diffuse low grade and intermediate grade gliomas (World Health Organization grades II and III) (2). In 2016, presence/absence of isocitrate dehydrogenase (IDH) mutation and 1P/19Q codeletion were introduced to classify glioma based on histology and molecular characteristics by WHO (3). Surgical treatment, radiotherapy, chemotherapy, and a combination of radiotherapy and chemotherapy are the main options for the treatment of LGG. Among them, radiotherapy is the main constituent in the combined modality therapy, which has been shown to increase progression-free survival and improve overall survival for LGG patients (4).

However, heterogeneity in radiosensitivity exists among LGG patients. Large retrospective studies of LGG patients in the National Cancer Database (NCDB) have shown that radiotherapy is associated with improved survival outcomes in patients younger than 40 years of age, histological subtypes of astrocytomas, and early high-dose radiotherapy (5). It is desirable to determine radiosensitive LGG patients before incorporating radiotherapy as part of the combined modality therapy. Currently, radiosensitivity of LGG patients can be predicted by O6-methylguanine-DNA methyltransferase (MGMT) promoter methylation and 1p19q codeletion status (6). Moreover, IDH mutation and 1P/19Q codeletion were found to be associated with survival rate and can be used to predict the response to adjuvant therapy.

Even though, the radiosensitivity cannot be fully explained by existing biomarkers. A possible explanation could be provided by researching the tumor microenvironment (TME). TME plays a vital role in the occurrence, progression, and prognosis of tumors. Cancer cells, immune cells, blood vessels, fibroblasts, and other stromal cells make up the TME (7). TME and cancer therapy are complex interplay. Treatment targeted to the TME can increase the likelihood of a good prognosis for patients. Radiotherapy affects tumor blood vessels and immune cells in TME. Specifically, it causes radiation-induced inflammation through damage to endothelial cells and activates immunosuppressive pathways (8). Radiotherapy can shrink the local tumor, but it can also affect distant lesions due to the immunomodulatory effect initiated by the local tumor microenvironment (9). However, radiosensitivity based on TME in LGG has not been systematically discussed.

For LGG, Wen Yin et al. developed and validated an immune-related risk score system based on six hub genes to estimate the overall survival of LGG patients (10). An IDH1-associated immune prognostic signature includes four genes and a nomogram model was established for diffuse LGG (11). Considering the radiosensitivity of the tumor, Yi Cui et al. developed gene signatures by integrating radiosensitivity and immune gene signatures for predicting radiotherapy in breast cancer (12). A retrospective analysis validated 24-gene postoperative radiotherapy outcomes score in prostate cancer (13). But, up to now, a model for predicting the benefit of radiotherapy in LGG has not been established.

With the development of personalized oncology therapy, molecular biomarkers play an important role in the prognosis of LGG. To provide an optimal personalized treatment plan for LGG patients, it is important to find biomarkers and establish a radiosensitivity model based on the tumor microenvironment. Therefore, we attempted to develop and validate a radiosensitivity model for predicting the survival for LGG by using the spike-and-slab lasso Cox model. In summary, our study provided new insights into radiotherapy for LGG.

MATERIALS AND METHODS

Data Sources

We downloaded 515 LGG patients with clinical and 20503 gene expression datasets from a public database The Cancer Genome Atlas (TCGA, http://cancergenome.nih.gov/) by using the R package TCGA-Assembler (14). Survival information of 534 LGG patients was procured from UCSC Cancer Genomics Browser (https://xenabrowser.net/datapages/) (15). Overall survival (OS) and progression-free survival (PFS) as endpoints. We eliminated the samples without radiotherapy information (n=29) and removed patients with missing survival information (n=3). Considering each gene expression distribution, we also screened genes. The flowchart was summarized in **Figure 1**. Finally, after combining clinical information, RNAseq, and survival information, a final total of finally total of 474 patients with 14627 genes were obtained for the present study. We downloaded gene expression and clinical profiles of 443 LGG patients from CGGA693 dataset (16, 17) and 182 LGG patients from CGGA325 dataset (18, 19) as external validation datasets (http://www.cgga.org.cn/). The cleaned clinical data are summarized in **Supplementary Tables 1**, **2**.

Differential Expression Analysis and Functional Enrichment Analysis

The Estimation of Stromal and Immune cells in Malignant Tumor tissues using the Expression data (ESTIMATE) tool was used to evaluate the immune and stromal scores for each sample (20). We compared the survival rate between high-scores and low-scores based on the median of each score. Differentially expressed genes (DEGs) analysis was performed by using the *limma* package. The cut-off criteria were adjusted p-value by false discovery rate (FDR) <0.05 and log2 fold-change>1.5. Then, Gene Ontology (GO) and Kyoto Encyclopedia of Genes and Genomes (KEGG) were performed by using the R package clusterProfiler (21).

Spike-and-Slab Lasso and Lasso

The least absolute shrinkage and selection operator (Lasso) is the commonly used method to select variables. The lasso can select and shrink variables by using the form of the l_1-penalty (22). However, the lasso can include many irrelevant predictors and over-shrink large coefficients because of a single penalty.

The spike-and-slab formulation is the core ingredient that can identify promising models (23). Ročková and George developed

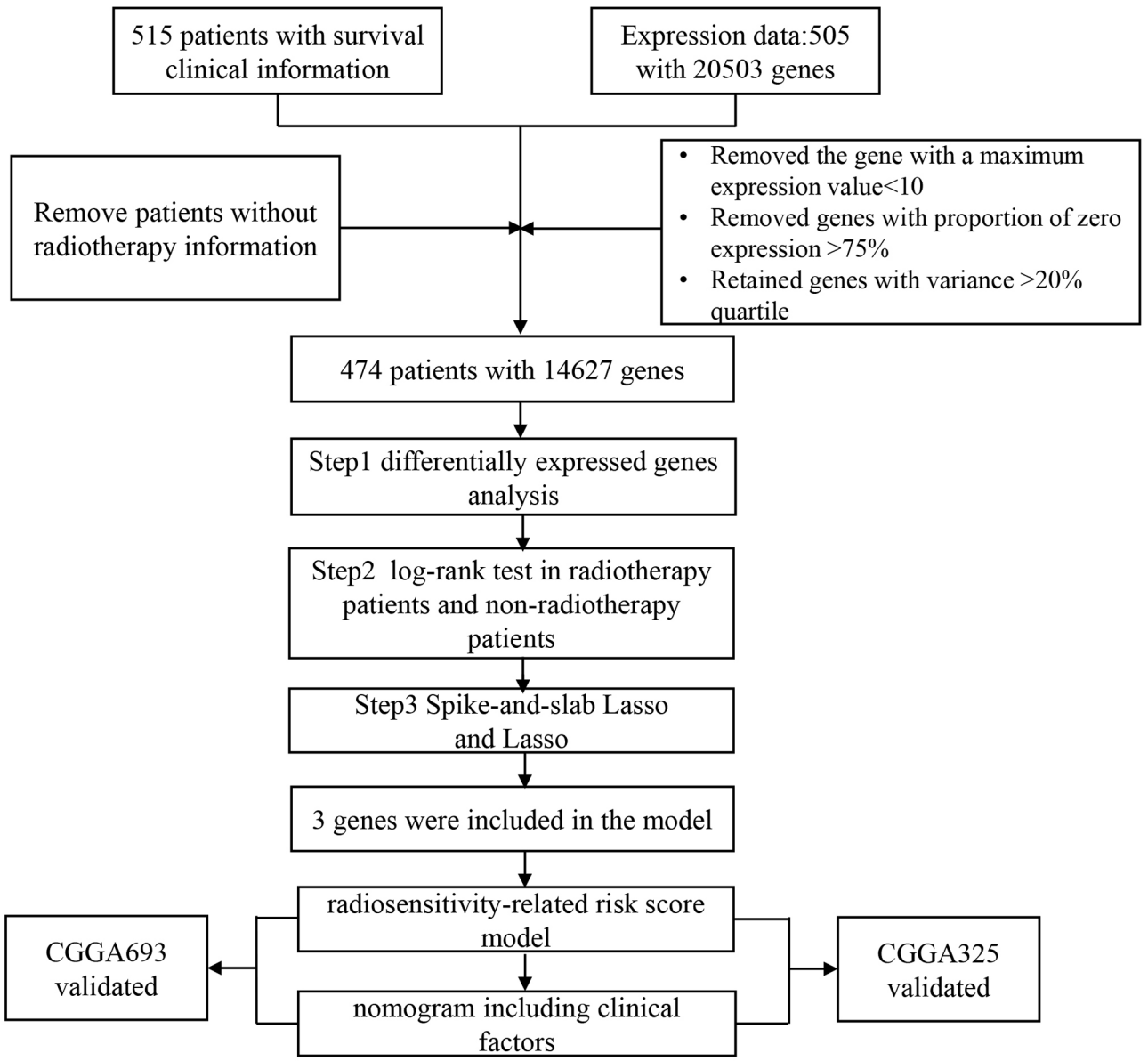

FIGURE 1 | The flow-chart of study design, patient selection and gene selection.

and applied spike-and-slab Lasso (sslasso) priors to select a variable. spike-and- slab Lasso has a two-point mixture of a Laplace spike distribution (s_0) and a Laplace slab (s_1). s_0 and s_1 are two scale parameters of the spike distribution and slab distribution respectively (24). Therefore, spike-and-slab Lasso has advantages in variable selection and parameter estimation. Recently, Tang et. extended the spike-and-slab lasso framework to generalized linear models and Cox survival models (25, 26). Lasso analysis was performed by using the "glmnet" R package. The model developed by spike-and-slab Lasso was implemented using R package BhGLM (Bayesian hierarchical generalized linear models) (https://github.com/nyiuab/BhGLM) (27).

Construction and Validation of Radiosensitivity-Related Risk Score

After obtaining the 491 DEGs based on tumor microenvironment, a log-rank test was performed to select genes in patients with radiotherapy and patients who did not receive radiotherapy. We obtained 111 genes for the next analysis. Spike-and-slab Lasso was used to identifying the best prognostic value of these genes. Finally, a radiosensitivity-related risk score was established utilizing spike-and-slab Lasso regression coefficients to multiply the expression values of genes in each patient. We used Kaplan-Meier survival analysis to evaluate the prognostic value of this risk score. Radiosensitive (RS) group and radioresistant (RR) group were

defined according to the difference in overall survival rate. The sensitivity and specificity of the model were evaluated by plotting time-dependent receiver operating characteristics (ROC). The radiosensitivity-related risk score was validated in TCGA dataset that PFS as endpoint and two CGGA datasets that OS as the endpoint.

Development and Validation of the Nomogram

Univariate and multivariate Cox regression analyses were performed to validate whether the risk score has an independent prediction factor. A nomogram to predict the 1-, 3-, and 5-years survival probability were developed according to the results of multivariate Cox analysis. The nomogram was validated in TCGA dataset that PFS as endpoint and two CGGA datasets that OS as the endpoint.

Analysis Method

All statistical analyses were performed by using the R (4.0.2). The Kaplan-Meier curves were employed to show survival curves. The log-rank test was used to filter radiosensitivity genes based on the tumor microenvironment. Time-dependent ROC curves were plotted by using "timeROC" R package. A nomogram was generated by using the "rms" R package. Infiltration levels for the RS and RR group were quantified by using the bioinformatics tool "CIBERSORT" R package (20). P-value of < 0.05 was considered to be statistically significant. All statistical tests were two-sided.

RESULTS

Differentially Expressed Genes Based on Tumor Microenvironment

To determine the gens of the TME, we calculated the Stromal score, Immune score and ESTIMATE score by using R package "ESTIMATE". Whole patients were classified into two group according to median score, respectively. As shown in **Supplementary Figure 1**, there was a significant difference between the low stromal-score group and the high stromal-score group (OS: p=0.043, PFS: p=0.025). For the immune-score group, the OS and PFS of the low immune-score group had significantly better than the high immune-score group (OS: p=0.0068, PFS: p=0.020). For the ESTIMATE score, the low ESTIMATE score group had the better OS and PFS than the high ESTIMATE score group (OS: p=0.029, PFS: p=0.039). We also plotted Volcano Plots (**Figure 2A**). Differentially expressed genes (DEGs) analysis between the high- and low-score groups were performed and 491 DEGs were obtained based on the TME(**Figure 2B**). Next, GO analysis demonstrated that the significant biological processes were T cell activation, leukocyte proliferation, and regulation of Tell cell activation (**Figure 2C**). In the KEGG pathway, there were pathways related to the TME, including PI3K-Akt signaling pathway, MAPK signaling pathway, B cell receptor signaling pathway, T cell receptor signaling pathway and PD-L1 expression and PD-1 checkpoint pathway in cancer (**Figure 2D**). These biological functions documented that the DEGs played an important role in TME-related biological procedures in LGG patients.

Construction of Sensitivity Prediction Model for Radiotherapy

After obtaining differentially expressed genes based on the tumor microenvironment, we performed a log-rank test to identify DEGs associated with radiosensitivity. Whole LGG patients were divided into the high- and low-expression level groups using the median gene expression level as a cutoff point. For radiotherapy patients, the patients in the high- and low-expression group have significant survival differences. However, there was no survival difference between the high- and low- expression level group for non-radiotherapy patients. Ultimately, we obtained 111 genes associated with OS based on TME.

To construct a radiosensitivity-related risk score in the TCGA cohort. Spike-and-slab Lasso was used to selecting genes. We fixed the slab scale s_1 to 1 and varied the spike scale s_0 over the grid of values: $0.0001+k\times0.002$, k = 0,1,2…,49, leading to 50 models. 10-fold cross-validation was performed to select an optimal model based on the deviance. The minimum value of deviance appears to be 924.330 when the spike scale s_0 is 0.0041 (**Figure 3A**). Therefore, we have chosen the prior scale (0.0041,1) for model fitting and prediction. Finally, three genes were included in the radiosensitivity-related risk score. They are INA (Alpha internexin), LEPREL1 (Leprecan-like 1) and PTCRA (Pre T-cell antigen receptor alpha). And the radiosensitivity-related risk score is the following: Risk score=-0.4442264*INA+0.2253638* LEPREL1+ 0.3067226*PTCRA. Each sample was calculated the radiosensitivity-related risk score. Using the median risk score, patients were divided into high- and low-risk groups. The low-risk group was defined as a radiosensitive group (RS), and the high-risk group was defined as a radioresistant group (RR). The Kaplan–Meier plots indicated that the RS group have a significantly better overall survival than the RR group in the patients who received radiotherapy (p<0.001, **Figure 3B**). There was no difference in overall survival between the RS group and RR group in patients does not receive radiotherapy (p=0.098, **Figure 3B**). Then, we further used ROC analysis to evaluate the predictive ability of radiosensitivity-related risk score model (1-year AUC:0.848 (0.749-0.948); 3-years AUC:0.794 (0.720-0.869); 5-years AUC:0.698 (0.604-0.792), **Figure 3C**).

We also fitted the model by the lasso approach and performed 10-fold cross-validation as a comparison. However, no genes were screened by using lasso (**Supplementary Figure 2**).

Validation of Radiosensitivity Model in Validation Sets

To validate the radiosensitivity-related risk score constructed in the TCGA cohort, we applied the risk score formula to PFS outcome in TCGA, CGGA693 and CGGA 325 datasets, respectively (**Figure 4**). Each patient has calculated the risk score and divided into RS group and RR group according to median risk score. The Kaplan–Meier analysis showed patients in RS group had a better prognosis while patients in RR group had unfavorable outcomes in radiotherapy patients (TCGA PFI:

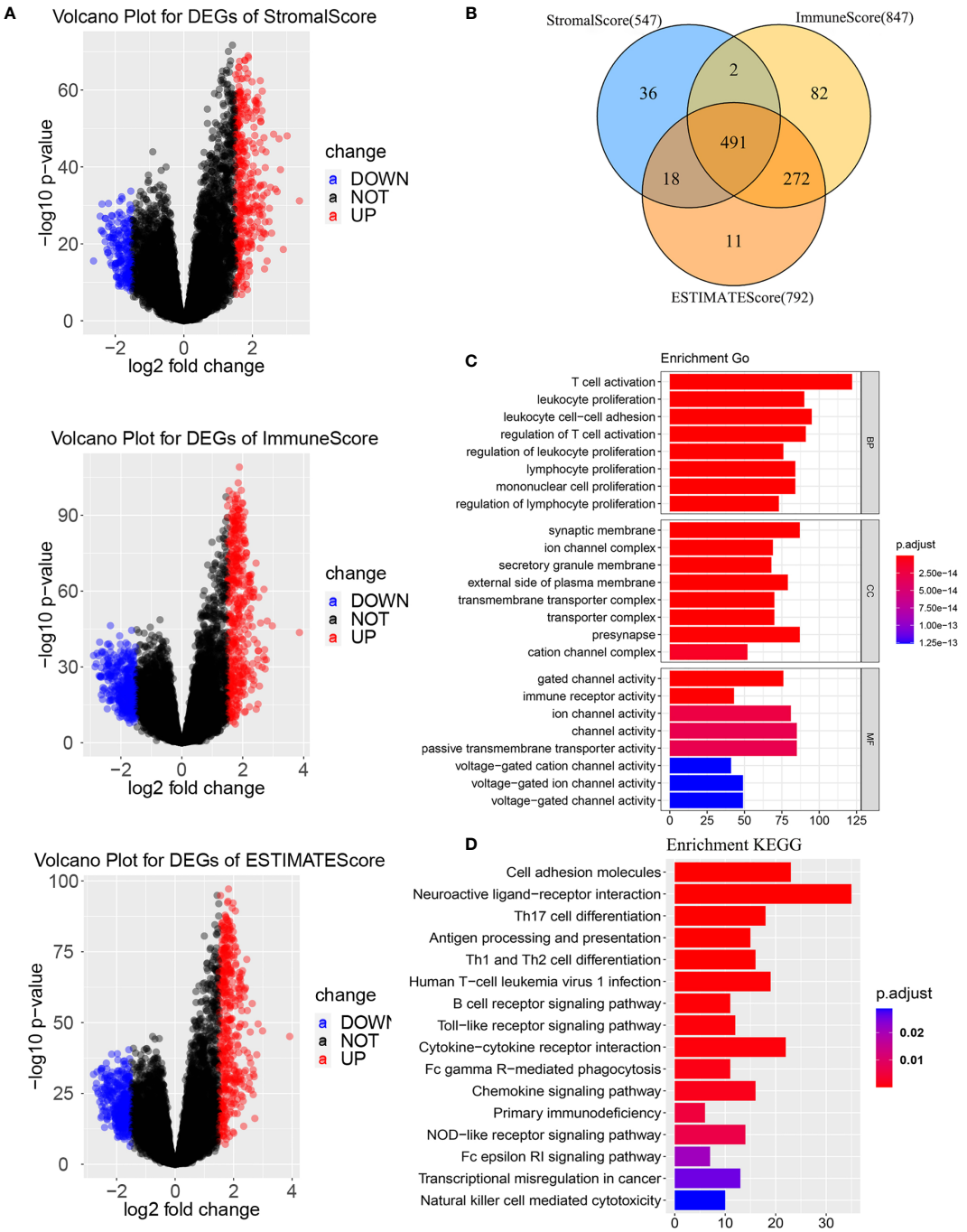

FIGURE 2 | Differentially expressed genes based on tumor microenvironment **(A)** Volcano Plots for DEGs. **(B)** Venn diagram. **(C)** GO enrichment analysis of the DEGs. **(D)** KEGG enrichment analysis of the DEGs. BP, biological process; MF, molecular function; CC, cellular component. GO, Gene Ontology; KEGG, Kyoto Encyclopedia of Genes and Genomes.

p<0.001, CGGA693: p<0.001, CGGA325: p<0.001 **Figures 4B, E, H**). ROC curve was used to evaluate the predictive accuracy for 1-, 3-, and 5-year survival. AUC values revealed the high predictive value of the radiosensitivity-related risk score for LGG patients. (TCGA PFI:1-year AUC:0.726 (0.652-0.800); 3-years AUC:0.670 (0.595-0.744); 5-years AUC:0.724(0.626-0.822). CGGA693:1-year AUC:0.641(0.530-0.752); 3-years AUC:0.645(0.576-0.715); 5-years AUC:0.630(0.559-0.701). CGGA325:1-year AUC:0.740 (0.609-0.871); 3-years AUC:0.774 (0.687-0.861); 5-years AUC:0.809 (0.733-0.884). **Figures 4C, F, I**).

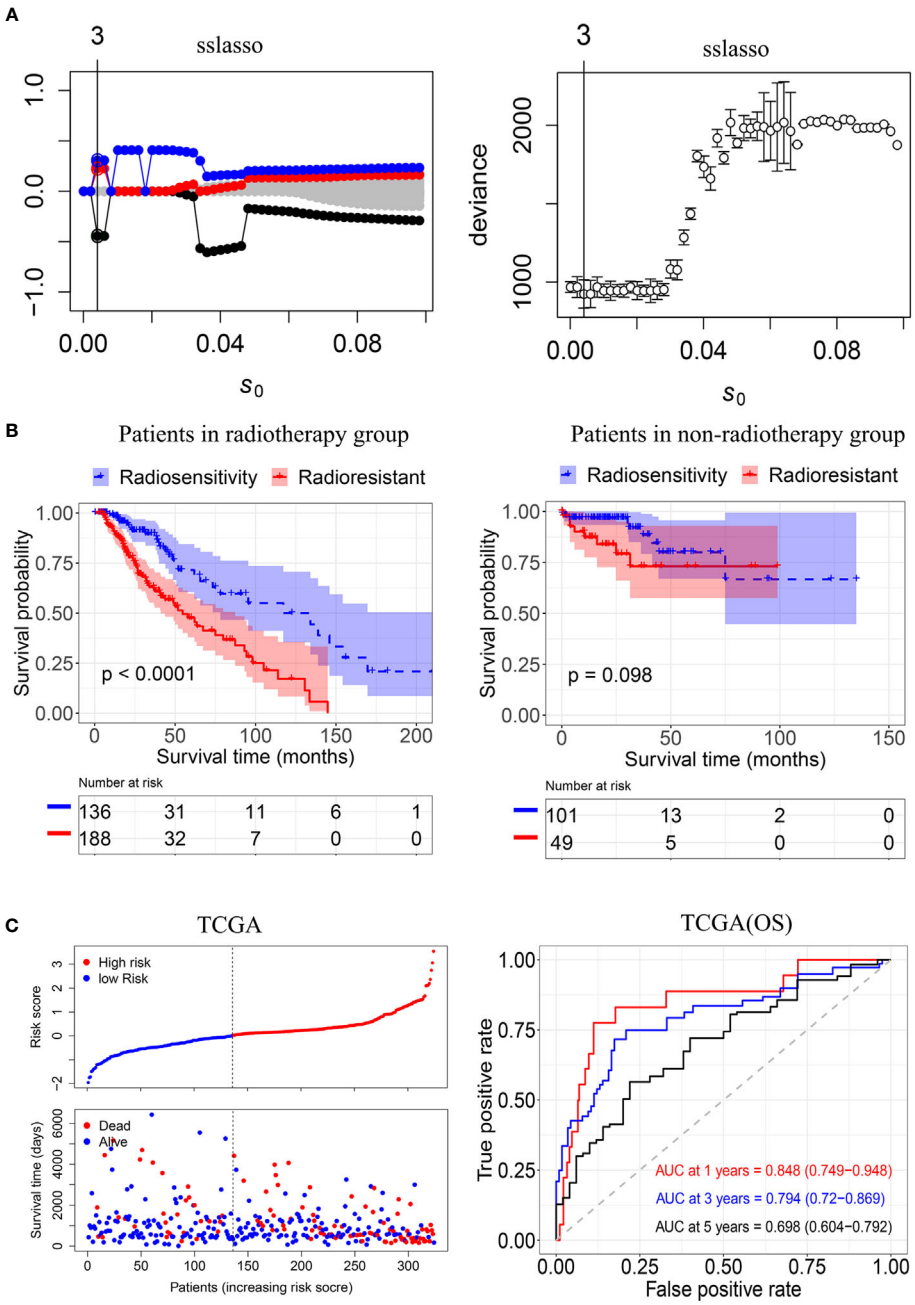

FIGURE 3 | Construction of the radiosensitivity-related risk score model. **(A)** The solution paths and partial log-likelihood profiles of the spike-and-slab model. **(B)** Kaplan–Meier curves for the RS group and RR group in patients with radiotherapy and patients did not receive radiotherapy. RR: radioresistant group. RS: radiosensitive group. **(C)** Risk scores distribution of each patient in the TCGA(OS) and time-dependent ROC curve analysis of the radiosensitivity-related risk score in the TCGA(OS). OS: Overall survival.

The Radiosensitivity-Related Risk Score Is an Independent Prognostic Indicator

Univariate and multivariate Cox regression was used to examine whether the radiosensitivity-related risk score was an independent prognostic factor. As demonstrated in **Supplementary Figure 3**. The univariate analysis showed that the age (HR:1.055, 95% CI:1.039-1.071, p<0.001), tumor grade (HR:2.630,95%CI:1.687-4.101, p=0.004) and risk score (HR:2.864, 95%CI:1.822-4.503, p<0.001) were significantly associated with OS. After adjusted clinical factors such as age, gender, tumor grade, race, IDH1, the multivariate Cox regression result showed that radiosensitivity-related risk score was an independent prognostic factor for LGG

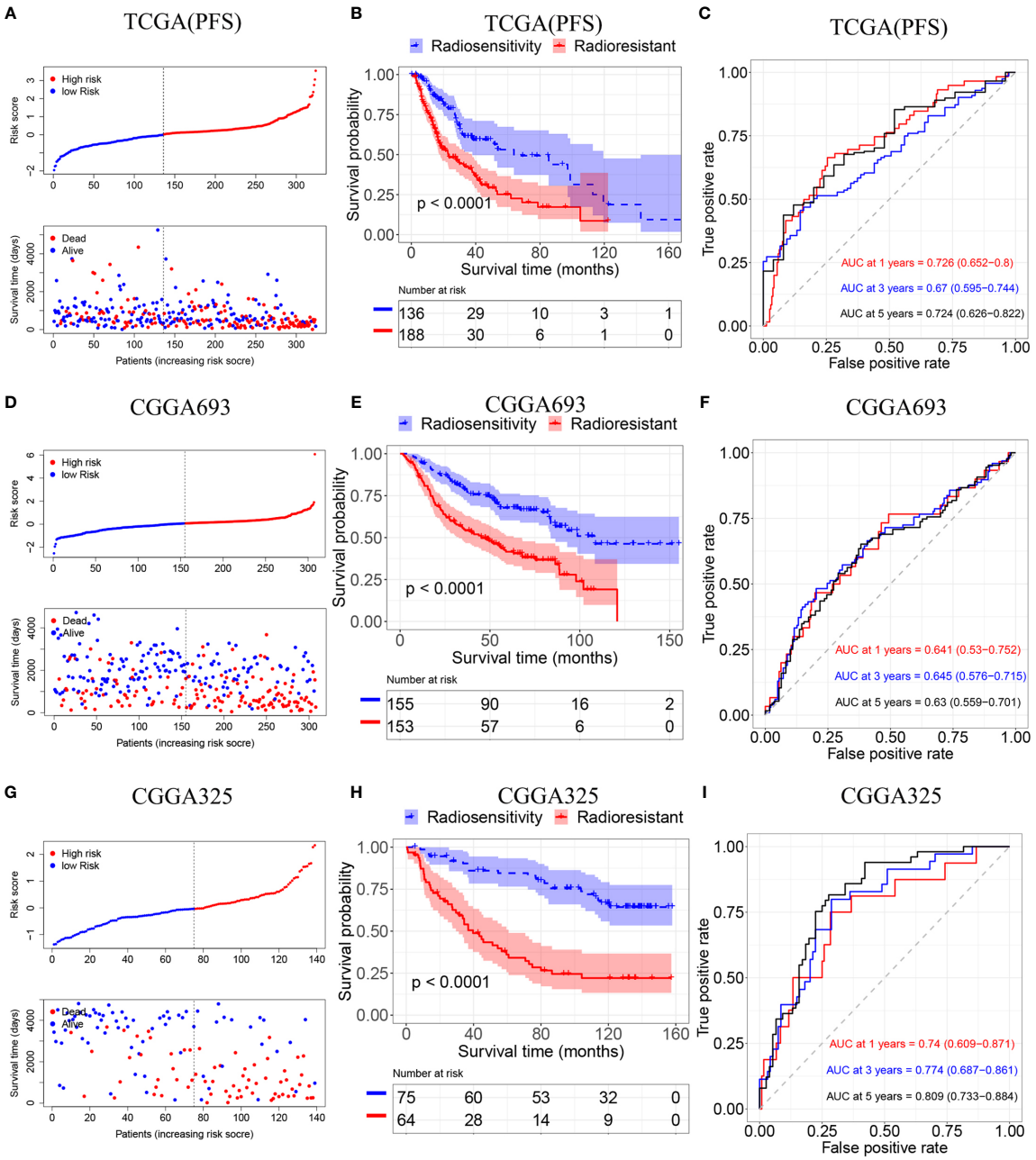

FIGURE 4 | Validation of the radiosensitivity-related risk score model. **(A)** Risk scores distribution of each patient in the TCGA(PFS). **(B)** Kaplan–Meier curves for the RS group and RR group in patients with radiotherapy from TCGA(PFS). **(C)**Time-dependent ROC curve analysis of the radiosensitivity-related risk score in the TCGA (PFS). **(D)** Risk scores distribution of each patient in the CGGA693. **(E)** Kaplan–Meier curves for the RS group and RR group in patients with radiotherapy from CGGA693. **(F)**Time-dependent ROC curve analysis of the radiosensitivity-related risk score in the CGGA693. **(G)** Risk scores distribution of each patient in the CGGA325. **(H)** Kaplan–Meier curves for the RS group and RR group in patients with radiotherapy from CGGA325. **(I)**Time-dependent ROC curve analysis of the radiosensitivity-related risk score in the CGGA325.

patients. When the OS as an endpoint, the HR was 3.657 (95% CI:2.171-6.160, p<0.001, **Figure 5A**). When the PFS as an endpoint, the HR was 2.522(HR: 2.522, 95%CI:1.627-3.908, p<0.001, **Figure 5B**). In CGGA datasets, we adjusted clinical factors such as age, gender, tumor grade, race, IDH2, and X1p19q2, the multivariate Cox regression results also demonstrated that radiosensitivity-related risk score was an independent prognostic factor for LGG (CGGA693: HR:1.726, 95%CI: 1.195-2.493, p=0.004. CGGA325: HR: 2.013, 95%CI: 1.096-3.696, p=0.028. **Figures 5C, D**).

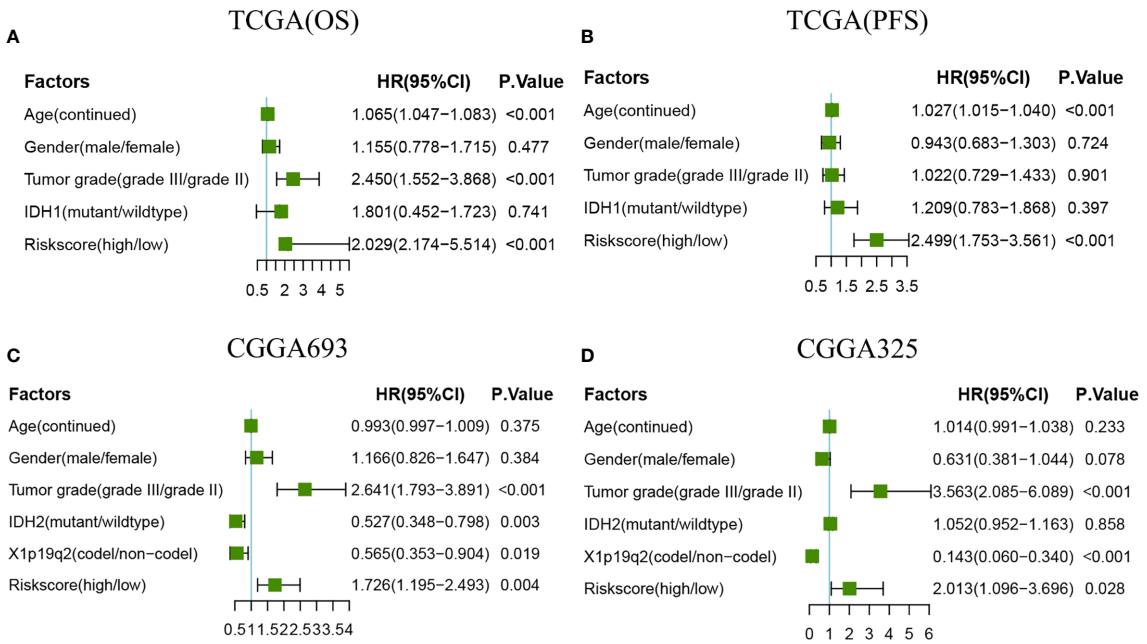

FIGURE 5 | Forest plots of multivariate Cox regression. **(A)** Forest plots of multivariate Cox regression in TCGA(OS). **(B)** Forest plots of multivariate Cox regression in TCGA(PFS). **(C)** Forest plots of multivariate Cox regression in CGGA693. **(D)** Forest plots of multivariate Cox regression in CGGA325.

Construction and Validation of Nomogram

The univariate and multivariate Cox regression analyses indicated that age, tumor grade, and risk score are correlated with OS. A nomogram containing two clinical factors (age and tumor grade) and risk score was developed to predict OS rate for LGG patients (**Figure 6A**). From the results of ROC analysis in **Figure 6B**, the AUCs of nomogram at 1-, 3-, 5-year was 0.902, 0.872, 0.815, respectively, which was higher than a model with a radiosensitivity-related risk score. **Figure 6C** demonstrated that the AUCs of nomogram at 1-, 3-, 5-year was 0.723, 0.660 and 0.745 for TCGA(PFS). We also used two CGGA datasets to verify a nomogram. **Figure 6D** demonstrated that the AUCs of nomogram at 1-, 3-, 5-year was 0.591(95%CI:0.485-0.697), 0.635 (95%CI:0.566-0.705) and 0.594 (95%CI:0.522-0.667) for CGGA693. **Figure 6E** demonstrated that the AUCs of nomogram at 1-, 3-, 5-year was 0.750 (95%CI:0.617-0.883), 0.775(95%CI:0.681-0.869) and 0.807 (95%CI:0.730-0.784) for CGGA325.The risk score for the prognostic model displayed superior predictive performance compared with the nomogram in the CGGA325.

Infiltration Levels for RS and RR Group

We performed infiltration levels for the RS group and RR group in LGG by employing the LM22 signature. In the process of plotting the heat map (**Figure 7A**), we removed zero abundance immune cells from more than half of the samples. Next, we estimated mean fractions of immune cells in the RS and RR group (**Figure 7B**). Tumor samples in the RS group shown more dendritic cells resting, T cells gamma delta and T cells CD4 naïve than the RR group. 15 tumor-infiltrating immune cells exhibit significantly different relative proportions between the RS and RR group **Figure 7C**.

DISCUSSION

Treatments of LGG include radiotherapy, chemotherapy and surgery. Fan Wu et. identified immune-related subtypes to select optimally patients suffering from LGG responsive to immunotherapy (28). A retrospective study suggested MRI feature that cyst formation on preoperative MR images was used to predict a favorable prognosis in patients with LGG (29). In a study of more than 1, 0000 people with LGG, researchers noted radiotherapy improved survival outcomes (5). However, the optimal radiotherapy for a particular patient based on individual symptoms and the risk of treatment-induced toxicity remains unclear. Advances have been made in biomarkers that predict response to treatment. Despite the beneficial effects of radiotherapy in LGG patients, this treatment has some significant side effects that should not be disregarded. Therefore, it is important to select biomarkers that can be used to screen radiosensitivity patients.

In this study, we obtained differentially expressed genes based on tumor microenvironment by calculating Stromal score, Immune Score and ESTIMATE Score. Then, we obtained DEGs and performed GO and KEGG. The log-rank test was used to identify genes associated in patients who received radiotherapy and patients who did not receive radiotherapy, respectively. Spike-and-slab Lasso was used to selecting genes. Finally, three genes (INA, LEPREL1, and PTCRA) are included in the model. A radiosensitivity-related risk score model was established based on the overall rate of TCGA dataset in patients who received radiotherapy. And we validated this model with TCGA dataset and two CGGA datasets. This radiosensitivity-related risk score model has prognostic prediction ability and is an independent prognostic indicator. A novel nomogram integrated risk score with age and tumor grade was

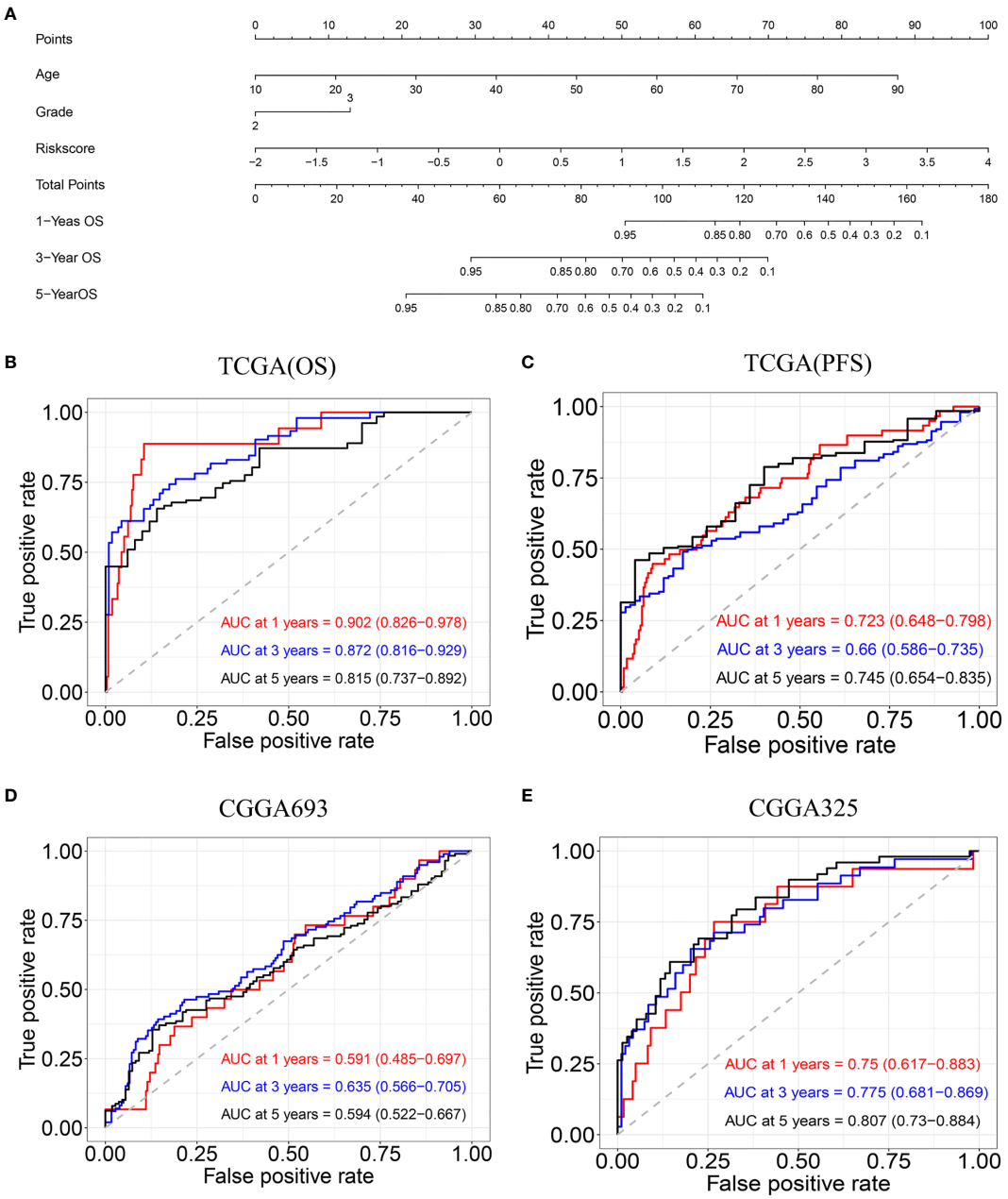

FIGURE 6 | Construction and validation of nomogram model. **(A)** Nomogram model for predicting the probability of 1-, 3-, and 5-year OS in LGG. **(B)** Time-dependent ROC curve analyses of the nomogram model in the TCGA(OS). **(C)** Time-dependent ROC curve analyses of the nomogram model in the TCGA(PFS). **(D)** Time-dependent ROC curve analyses of the nomogram model in the CGGA693. **(E)** Time-dependent ROC curve analyses of the nomogram model in the CGGA325.

developed to predict the OS of LGG patients. The nomogram was also validated in two CGGA datasets. According to the radiosensitivity-related risk score and nomogram, clinicians can able to identify a group of patients who are better benefit from radiotherapy and then can predict the 1-, 3-, and 5-years OS of LGG.

The three genes included in our radiosensitivity-related risk score model were INA, LEPREL1, and PTCRA. The INA gene encodes an intermediate filament involved in neurogenesis. α- is the fourth subunit of neurofilaments in the adult central nervous system (30). INA is overexpressed mostly in oligodendroglia phenotype gliomas and correlated with better PFS and OS (31). INA expression on immunohistochemistry in anaplastic gliomas showed a significant positive correlation with 1p/19q codeletion and can replace to some extent 1p/19q (32, 33). INA gene methylation is associated with the progression of colon adenoma (34)and gastroenteropancreatic neuroendocrine neoplasms (35). LEPREL1 similarity to the Leprecan family of proteoglycans and as a 3.4 kb transcript encoding an 80 kDa protein (36). Many pieces of

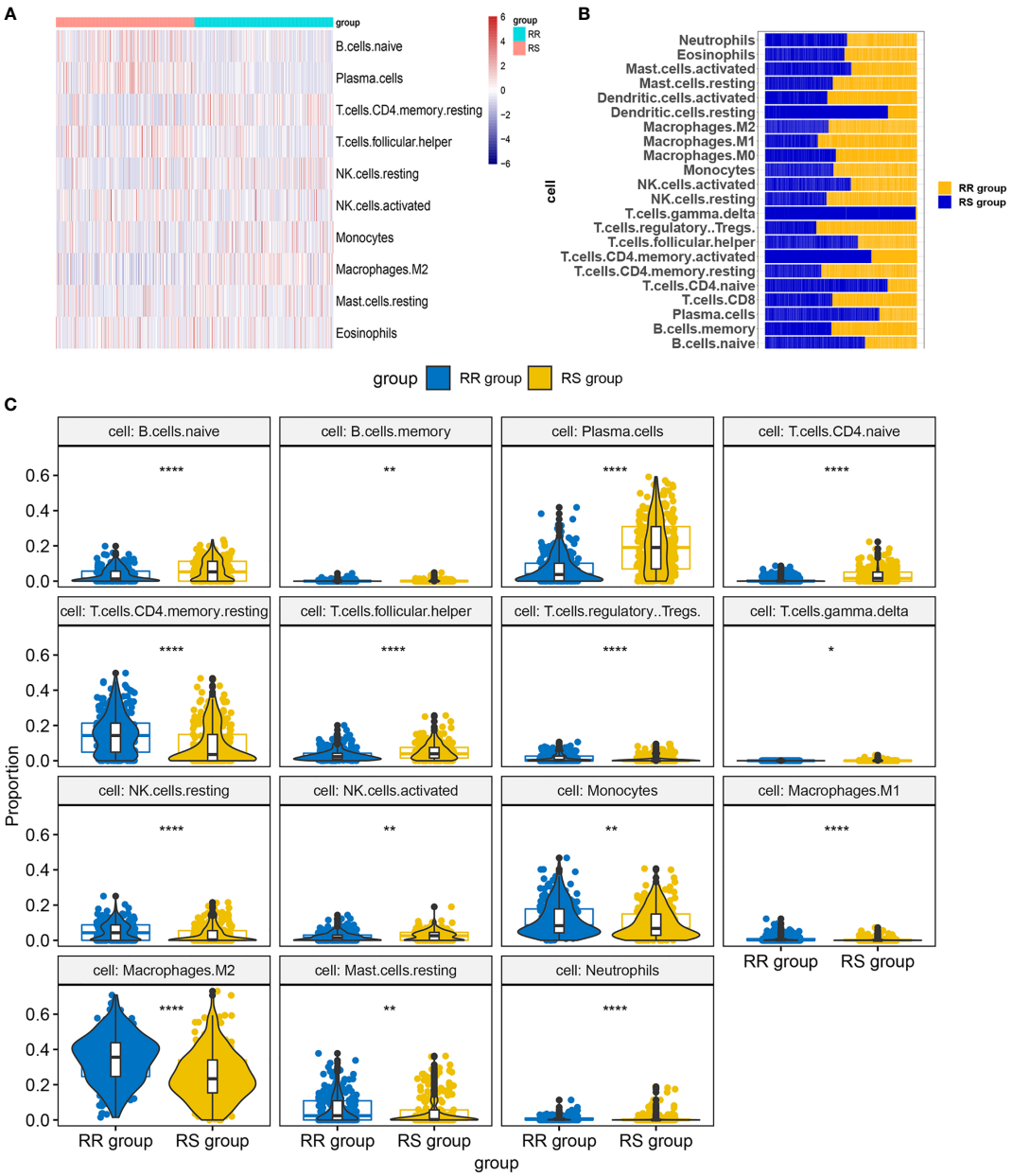

FIGURE 7 | Infiltration levels for RS and RR group. **(A)** Heat map of infiltration cells in RS and RR group. **(B)** Bar graphs of mean percentage of immune cells in RS and RR group. **(C)** Violin plots illustrating the relative proportions of the 15 TIICs exhibiting significantly different infiltrating degree in RS and RR group. RR, radioresistant group. RS, radiosensitive group. *p < 0.05, **p < 0.01, ***p < 0.001, ****p < 0.0001.

evidence shown that LEPREL1 was associated with ophthalmic diseases such as high myopia and lyens subluxation (37–39). For cancer, LEPREL1 may be a potential tumor suppressor gene by inhibiting HCC cell proliferation (40). LEPREL1 was methylation inactivation of tumor suppressor gene and involved in the pathogenesis of breast cancer (41). PTCRA participates in cancer-related signaling pathways. Research has shown that variation of PTCRA may be related to the prognosis of patients with chronic myelogenous leukemia (42). Unfortunately, we did not find a correlation between PTCRA gene and LGG.

There is growing evidence that the identification of prognostic factors is important for the optimal treatment of LGG patients. Han Sang Kim et al. used the NCI-60 cancer cell line to identify 31-gene signature of radiosensitivity from four different microarrays (43). This signature was verified in breast cancer (44), and low-grade glioma (45). Gene signatures have been successfully used in various cancer types to develop prognostic and predictive models that benefit patients. We developed a radiosensitivity-related risk score model to predict the benefit of radiotherapy in LGG. This study showed that in independent validation cohorts that radiosensitivity

patients had significant survival benefits from radiotherapy, whereas there was no difference between RS group and RR group in patients who did not receive radiotherapy. Two studies researched prediction of radiotherapy in prostate cancer (13)and breast cancer (12). They matched patients in the entire cohort and each biomarker-defined group, respectively. In prostate cancer, researchers compared the radiotherapy patients and no radiotherapy patients in high- and low-score. Recently, Xing Chen et al. developed and validated a six gene signature for breast cancer radiotherapy (46). In this article, they used the Kaplan-Meier curve to compare high- and low- score in radiotherapy group. In our study, the definition of radiosensitivity is that patients receiving radiotherapy, this subgroup patients obtained significantly more survival benefit than patients in another subgroup. Moreover, there were no differences between the two subgroups in patients who did not receive radiotherapy.

Selecting genes induced in the model plays an important role in establishing a prediction model. Researchers usually screen genes by using Cox regression analysis, Lasso Cox regression method, random forest algorithm and other methods. In our study, Spike-and-slab Lasso and Lasso were used to selecting genes. Results have shown that three genes were selected by using spike-and-slab Lasso. However, we were unable to screen for the gene with Lasso. Spike-and-slab Lasso can shrink many coefficients exactly to zero and select variables similar to the lasso. Spike-and-slab Lasso has the advantage of diminishing the estimation bias of Lasso by yielding weak shrinkage on important predictors and strong shrinkage on irrelevant predictors (25). The spike-and-slab Lasso method to select has been applied successfully in LGG real data. Our results demonstrated that advantages of spike-and-slab Lasso in screening variables compared with Lasso.

We developed and verified a radiosensitivity-related risk score model. Next, we performed ROC analysis to compare the predictive ability of a risk score model. We compared the radiosensitivity-related risk score model and nomogram, the results showed that the AUC of the nomogram was not significantly improved compared with a radiosensitivity-related risk score model.

Jun Su et al. constructed a prognostic risk score model (Model 1) based on eight TME-related genes using co-expression network analysis (WGCNA) and lasso (47). This model had potential value for predicting the sensitivity of LGG patients to radio- and chemotherapy. We both obtained the immune score and the stromal score by ESTIMATE algorithm. However, we obtained the TME related gene by using DEGs instead of WGCNA. We used the sslasso method to screen genes and developed the radiosensitivity prediction model in patients who received radiotherapy. Jun Su et al. constructed a prognostic risk score model in whole patients. Wen Jing Zeng et al. constructed a survival risk score system (Model 2) based identify prognostic genes associated with promoter methylation by using Cox proportional hazards regression analysis (48). This three-gene signature was validated in CGGA and performed stratified survival analysis. However. this model was not applied to radiosensitivity. Next, we compared these two models in patients who received radiotherapy and patients who not received radiotherapy. As shown in **Supplementary Figure 4**, Kaplan-Meier curves demonstrated that low-risk group had longer OS than high-risk group both in patients who underwent radiotherapy and patients who were not undergoing radiotherapy. Our model took into account not only people who received radiotherapy but also people who did not receive radiotherapy. Kaplan-Meier plots indicated that the RS group have a significantly better overall survival than the RR group in the patients who received radiotherapy ($p<0.001$, **Figure 3B**). There was no difference in overall survival between the RS group and RR group in patients does not receive radiotherapy ($p=0.098$, **Figure 3B**). Therefore, our model has better potential to identify RS and RR groups.

Our study provides new insights into the radiotherapy therapies for LGG. The main strength of this study is the method of selecting genes. We applied spike-and-slab Lasso to select genes different from Cox regression and Lasso. The radiosensitivity-related model can identify patients most likely to benefit from radiotherapy. However, a limitation of our study is that this is a retrospective study, and the models should be further confirmed by prospective studies.

In conclusion, the radiosensitivity-related score is an independent prognostic indicator. Patients with LGG can be divided into RS and RR groups. The patients in the RS group are more likely to benefit from radiotherapy. This model can be used by clinicians and researchers to predict patient's survival rates and achieve personalized treatment of LGG.

DATA AVAILABILITY STATEMENT

The original contributions presented in the study are included in the article/**Supplementary Material**. Further inquiries can be directed to the corresponding author.

AUTHOR CONTRIBUTIONS

Study conception and design: ZD, SC, NY, and ZT. Data collection and clean: ZD, DY, SC, WY, and XZ. Real data analysis and interpretation: ZD, HL, WY, NY, and JC. Drafting of the manuscript: ZD, HL, DY, JC, and XZ. All authors contributed to the article and approved the submitted version.

FUNDING

This work was supported in part by the National Natural Science Foundation of China (81773541), funded from the Priority Academic Program Development of Jiangsu Higher Education Institutions at Soochow University, the State Key Laboratory of Radiation Medicine and Protection (GZK1201919) to ZXT, National Natural Science Foundation of China (81872552, U1967220) to JPC. A project by the Second Affiliated Hospital of Soochow University (XKTJ-RC202007), Scientific Research Program for Young Talents of China National Nuclear Corporation (51003), Suzhou Science and Education Project (KJXW2017010), the Natural Science Foundation of Jiangsu Province (BK20180195), the National Natural Science Foundation of China (81902715) to SC The funding body did not play any roles in the design of the study and collection, analysis, and

interpretation of data and in writing the manuscript. This work was supported by the National Natural Science Foundation of China (31870844, 31570851) and A Project Funded by the Priority Academic Program Development of Jiangsu Higher Education Institutions (PAPD) to WY.

ACKNOWLEDGMENTS

We acknowledge the contributions of the TCGA and CGGA Research Network.

SUPPLEMENTARY MATERIAL

The Supplementary Material for this article can be found online at: https://www.frontiersin.org/articles/10.3389/fonc.2021.701500/full#supplementary-material

Supplementary Figure 1 | Survival curves plot for stromal score, immune score and ESTIMATE score.

Supplementary Figure 2 | Lasso Cox analysis.

Supplementary Figure 3 | Forest plots of univariate Cox regression. **(A)** Forest plots of univariate Cox regression in TCGA(OS). **(B)** Forest plots of univariate Cox regression in TCGA(PFS). **(C)** Forest plots of univariate Cox regression in CGGA693. **(D)** Forest plots of univariate Cox regression in CGGA325.

Supplementary Figure 4 | (A) Kaplan–Meier curves for the low riskscore group and high riskscore group in patients with radiotherapy and patients did not receive radiotherapy in model1. **(B)**Kaplan–Meier curves for the low riskscore group and high riskscore group in patients with radiotherapy and patients did not receive radiotherapy in model2.

Supplementary Table 1 | Basic patient characteristics in TCGA dataset.

Supplementary Table 2 | Basic patient characteristics in CGGA693 and CGGA325 datasets.

REFERENCES

1. Ostrom QT, Bauchet L, Davis FG, Deltour I, Fisher JL, Langer CE, et al. The Epidemiology of Glioma in Adults: A "State of the Science" Review. *Neuro Oncol* (2014) 16:896–913. doi: 10.1093/neuonc/nou087
2. Ostrom QT, Gittleman H, Farah P, Ondracek A, Chen Y, Wolinsky Y, et al. CBTRUS Statistical Report: Primary Brain and Central Nervous System Tumors Diagnosed in the United States in 2006-2010. *Neuro Oncol* (2013) 15 Suppl 2:ii1–56. doi: 10.1093/neuonc/not151
3. Wesseling P, Capper D. WHO 2016 Classification of Gliomas. *Neuropathol Appl Neurobiol* (2018) 44:139–50. doi: 10.1111/nan.12432
4. Wang TJC, Mehta MP. Low-Grade Glioma Radiotherapy Treatment and Trials. *Neurosurg Clin N Am* (2019) 30:111–8. doi: 10.1016/j.nec.2018.08.008
5. Nunna RS, Khalid S, Ryoo JS, Sethi A, Byrne RW, Mehta AI. Radiotherapy in Adult Low-Grade Glioma: Nationwide Trends in Treatment and Outcomes. *Clin Transl Oncol* (2020) 23(3):628–37. doi: 10.1007/s12094-020-02458-9
6. Chen R, Ravindra VM, Cohen AL, Jensen RL, Salzman KL, Prescot AP, et al. Molecular Features Assisting in Diagnosis, Surgery, and Treatment Decision Making in Low-Grade Gliomas. *Neurosurg Focus* (2015) 38:E2. doi: 10.3171/2015.1.FOCUS14745
7. Yang LV. Tumor Microenvironment and Metabolism. *Int J Mol Sci* (2017) 18 (12):2729. doi: 10.3390/ijms18122729
8. Jarosz-Biej M, Smolarczyk R, Cichon T, Kulach N. Tumor Microenvironment as A "Game Changer" in Cancer Radiotherapy. *Int J Mol Sci* (2019) 20 (13):3212. doi: 10.3390/ijms20133212
9. Ozpiskin OM, Zhang L, Li JJ. Immune Targets in the Tumor Microenvironment Treated by Radiotherapy. *Theranostics* (2019) 9:1215–31. doi: 10.7150/thno.32648
10. Yin W, Jiang X, Tan J, Xin Z, Zhou Q, Zhan C, et al. Development and Validation of a Tumor Mutation Burden-Related Immune Prognostic Model for Lower-Grade Glioma. *Front Oncol* (2020) 10:1409. doi: 10.3389/fonc.2020.01409
11. Deng X, Lin D, Chen B, Zhang X, Xu X, Yang Z, et al. Development and Validation of an IDH1-Associated Immune Prognostic Signature for Diffuse Lower-Grade Glioma. *Front Oncol* (2019) 9:1310. doi: 10.3389/fonc.2019.01310
12. Cui Y, Li B, Pollom EL, Horst KC, Li R. Integrating Radiosensitivity and Immune Gene Signatures for Predicting Benefit of Radiotherapy in Breast Cancer. *Clin Cancer Res* (2018) 24:4754–62. doi: 10.1158/1078-0432.CCR-18-0825
13. Zhao SG, Chang SL, Spratt DE, Erho N, Yu M, Ashab HA-D, et al. Development and Validation of a 24-Gene Predictor of Response to Postoperative Radiotherapy in Prostate Cancer: A Matched, Retrospective Analysis. *Lancet Oncol* (2016) 17:1612–20. doi: 10.1016/S1470-2045(16)30491-0
14. Zhu Y, Qiu P, Ji Y. TCGA-Assembler: Open-Source Software for Retrieving and Processing TCGA Data. *Nat Methods* (2014) 11:599–600. doi: 10.1038/nmeth.2956
15. Kuhn RM, Haussler D, Kent WJ. The UCSC Genome Browser and Associated Tools. *Brief Bioinform* (2013) 14:144–61. doi: 10.1093/bib/bbs038
16. Wang Y, Qian T, You G, Peng X, Chen C, You Y, et al. Localizing Seizure-Susceptible Brain Regions Associated With Low-Grade Gliomas Using Voxel-Based Lesion-Symptom Mapping. *Neuro Oncol* (2015) 17:282–8. doi: 10.1093/neuonc/nou130
17. Liu X, Li Y, Qian Z, Sun Z, Xu K, Wang K, et al. A Radiomic Signature as a non-Invasive Predictor of Progression-Free Survival in Patients With Lower-Grade Gliomas. *NeuroImage Clin* (2018) 20:1070–7. doi: 10.1016/j.nicl.2018.10.014
18. Bao ZS, Chen HM, Yang MY, Zhang CB, Yu K, Ye WL, et al. RNA-Seq of 272 Gliomas Revealed a Novel, Recurrent PTPRZ1-MET Fusion Transcript in Secondary Glioblastomas. *Genome Res* (2014) 24:1765–73. doi: 10.1101/gr.165126.113
19. Zhao Z, Meng F, Wang W, Wang Z, Zhang C, Jiang T. Comprehensive RNA-Seq Transcriptomic Profiling in the Malignant Progression of Gliomas. *Sci Data* (2017) 4:170024. doi: 10.1038/sdata.2017.24
20. Yoshihara K, Shahmoradgoli M, Martinez E, Vegesna R, Kim H, Torres-Garcia W, et al. Inferring Tumour Purity and Stromal and Immune Cell Admixture From Expression Data. *Nat Commun* (2013) 4:2612. doi: 10.1038/ncomms3612
21. Yu G, Wang LG, Han Y, He QY. Clusterprofiler: An R Package for Comparing Biological Themes Among Gene Clusters. *OMICS* (2012) 16:284–7. doi: 10.1089/omi.2011.0118
22. Tibshirani R. Regression Shrinkage and Selection *via* the Lasso: A Retrospective. *J R Stat Soc: Ser B (Stat Methodol)* (2011) 73:267–88. doi: 10.1111/j.1467-9868.2011.00771.x
23. Ročková V, George EI. EMVS: The EM Approach to Bayesian Variable Selection. *J Am Stat Assoc* (2014) 109:828–46. doi: 10.1080/01621459.2013.869223
24. Ročková V, George EI. *Bayesian Penalty Mixing: The Case of a Non-Separable Penalty*. Switzerland: Springer International Publishing (2016). doi: 10.1007/978-3-319-27099-9_11
25. Tang Z, Shen Y, Zhang X, Yi N. The Spike-And-Slab Lasso Generalized Linear Models for Prediction and Associated Genes Detection. *Genetics* (2017) 205:77–88. doi: 10.1534/genetics.116.192195
26. Tang Z, Shen Y, Zhang X, Yi N. The Spike-and-Slab Lasso Cox Model for Survival Prediction and Associated Genes Detection. *Bioinformatics* (2017) 33:2799–807. doi: 10.1093/bioinformatics/btx300
27. Yi N, Tang Z, Zhang X, Guo B. BhGLM: Bayesian Hierarchical GLMs and Survival Models, With Applications to Genomics and Epidemiology. *Bioinformatics* (2019) 35:1419–21. doi: 10.1093/bioinformatics/bty803
28. Wu F, Wang ZL, Wang KY, Li GZ, Chai RC, Liu YQ, et al. Classification of Diffuse Lower-Grade Glioma Based on Immunological Profiling. *Mol Oncol* (2020) 14:2081–95. doi: 10.1002/1878-0261.12707
29. Deng L, Shen L, Shen L, Zhao Z, Peng Y, Liu H, et al. Prognostic Value of Magnetic Resonance Imaging Features in Low-Grade Gliomas. *Biosci Rep* (2019) 39(6):BSR20190544. doi: 10.1042/BSR20190544
30. Yuan A, Rao MV, Veeranna, Nixon RA. Neurofilaments and Neurofilament Proteins in Health and Disease. *Cold Spring Harb Perspect Biol* (2017) 9(4): a018309. doi: 10.1101/cshperspect.a018309

31. Suh JH, Park CK, Park SH. Alpha Internexin Expression Related With Molecular Characteristics in Adult Glioblastoma and Oligodendroglioma. *J Korean Med Sci* (2013) 28:593–601. doi: 10.3346/jkms.2013.28.4.593
32. Figarella-Branger D, d.P. Maues A, Colin C, Bouvier C. Histomolecular Classification of Adult Diffuse Gliomas: The Diagnostic Value of Immunohistochemical Markers. *Rev Neurol* (2011) 167:683–90. doi: 10.1016/j.neurol.2011.07.006
33. Rajmohan KS, Sugur H, Shwetha SD, Pandey P, Santosh V. Alpha Internexin: A Surrogate Marker for 1p/19q Codeletion and Prognostic Marker in Anaplastic (WHO Grade III) Gliomas. *Neurol India* (2020) 68:832. doi: 10.4103/0028-3886.293453
34. Li Y, Bai L, Yu H, Cai D, Luo Y. Epigenetic Inactivation of α-Internexin Accelerates Microtubule Polymerization in Colorectal Cancer. *Cancer Res* (2020) 80:canres.1590.2020. doi: 10.1158/0008-5472.CAN-20-1590
35. Wang Y, Chen Y, Li X, Hu W, Zhang Y, Chen L, et al. Loss of Expression and Prognosis Value of Alpha-Internexin in Gastroenteropancreatic Neuroendocrine Neoplasm. *BMC Cancer* (2018) 18:691. doi: 10.1186/s12885-018-4449-8
36. Jarnum S, Kjellman C, Darabi A, Nilsson I, Edvardsen K, Aman P. LEPREL1, a Novel ER and Golgi Resident Member of the Leprecan Family. *Biochem Biophys Res Commun* (2004) 317:342–51. doi: 10.1016/j.bbrc.2004.03.060
37. Mordechai S, Gradstein L, Pasanen A, Ofir R, El Amour K, Levy J, et al. High Myopia Caused by a Mutation in LEPREL1, Encoding Prolyl 3-Hydroxylase 2. *Am J Hum Genet* (2011) 89:438–45. doi: 10.1016/j.ajhg.2011.08.003
38. Guo H, Tong P, Peng Y, Wang T, Liu Y, Chen J, et al. Homozygous Loss-of-Function Mutation of the LEPREL1 Gene Causes Severe non-Syndromic High Myopia With Early-Onset Cataract. *Clin Genet* (2014) 86:575–9. doi: 10.1111/cge.12309
39. Khan AO, Aldahmesh MA, Alsharif H, Alkuraya FS. Recessive Mutations in LEPREL1 Underlie a Recognizable Lens Subluxation Phenotype. *Ophthalmic Genet* (2015) 36:58–63. doi: 10.3109/13816810.2014.985847
40. Wang J, Xu X, Liu Z, Wei X, Zhuang R, Lu D, et al. LEPREL1 Expression in Human Hepatocellular Carcinoma and Its Suppressor Role on Cell Proliferation. *Gastroenterol Res Pract* (2013) 2013:109759. doi: 10.1155/2013/109759
41. Shah R, Smith P, Purdie C, Quinlan P, Baker L, Aman P, et al. The Prolyl 3-Hydroxylases P3H2 and P3H3 Are Novel Targets for Epigenetic Silencing in Breast Cancer. *Br J Cancer* (2009) 100:1687–96. doi: 10.1038/sj.bjc.6605042
42. Lavrov AV, Chelysheva EY, Smirnikhina SA, Shukhov OA, Turkina AG, Adilgereeva EP, et al. Frequent Variations in Cancer-Related Genes may Play Prognostic Role in Treatment of Patients With Chronic Myeloid Leukemia. *BMC Genet* (2016) 17 Suppl 1:14. doi: 10.1186/s12863-015-0308-7
43. Kim HS, Kim SC, Kim SJ, Park CH, Jeung HC, Kim YB, et al. Identification of a Radiosensitivity Signature Using Integrative Metaanalysis of Published Microarray Data for NCI-60 Cancer Cells. *BMC Genomics* (2012) 13:348. doi: 10.1186/1471-2164-13-348
44. Jang BS, Kim IA. A Radiosensitivity Gene Signature and PD-L1 Status Predict Clinical Outcome of Patients With Invasive Breast Carcinoma in The Cancer Genome Atlas (TCGA) Dataset. *Radiother Oncol* (2017) 124:403–10. doi: 10.1016/j.radonc.2017.05.009
45. Jang BS, Kim IA. A Radiosensitivity Gene Signature and PD-L1 Predict the Clinical Outcomes of Patients With Lower Grade Glioma in TCGA. *Radiother Oncol* (2018) 128:245–53. doi: 10.1016/j.radonc.2018.05.003
46. Chen X, Zheng J, Zhuo ML, Zhang A, You Z. A Six-Gene-Based Signature for Breast Cancer Radiotherapy Sensitivity Estimation. *Biosci Rep* (2020) 40(6): BSR20190544. doi: 10.1042/BSR20202376
47. Su J, Long W, Ma Q, Xiao K, Li Y, Xiao Q, et al. Identification of a Tumor Microenvironment-Related Eight-Gene Signature for Predicting Prognosis in Lower-Grade Gliomas. *Front Genet* (2019) 10:1143. doi: 10.3389/fgene.2019.01143
48. Zeng WJ, Yang YL, Liu ZZ, Wen ZP, Chen YH, Hu XL, et al. Integrative Analysis of DNA Methylation and Gene Expression Identify a Three-Gene Signature for Predicting Prognosis in Lower-Grade Gliomas. *Cell Physiol Biochem* (2018) 47:428–39. doi: 10.1159/000489954

Conflict of Interest: The authors declare that the research was conducted in the absence of any commercial or financial relationships that could be construed as a potential conflict of interest.

Publisher's Note: All claims expressed in this article are solely those of the authors and do not necessarily represent those of their affiliated organizations, or those of the publisher, the editors and the reviewers. Any product that may be evaluated in this article, or claim that may be made by its manufacturer, is not guaranteed or endorsed by the publisher.

Copyright © 2021 Du, Cai, Yan, Li, Zhang, Yang, Cao, Yi and Tang. This is an open-access article distributed under the terms of the Creative Commons Attribution License (CC BY). The use, distribution or reproduction in other forums is permitted, provided the original author(s) and the copyright owner(s) are credited and that the original publication in this journal is cited, in accordance with accepted academic practice. No use, distribution or reproduction is permitted which does not comply with these terms.

frontiers in Neurology

ORIGINAL RESEARCH
published: 09 August 2021
doi: 10.3389/fneur.2021.691378

The Relationship Between Peritumoral Brain Edema and the Expression of Vascular Endothelial Growth Factor in Vestibular Schwannoma

Hong-Hai You[1†], *Xiao-Yong Chen*[1†], *Jin-Yuan Chen*[2†], *Yue Bai*[2*] *and Fu-Xiang Chen*[1*]

[1] *Department of Neurosurgery, The First Affiliated Hospital of Fujian Medical University, Fuzhou, China,* [2] *Department of Ophthalmology, The First Affiliated Hospital of Fujian Medical University, Fuzhou, China*

OPEN ACCESS

Edited by:
David Nathanson, UCLA David Geffen School of Medicine, United States

Reviewed by:
Kamil Krystkiewicz, 10th Military Research Hospital and Polyclinic, Poland
Quan Cheng, Central South University, China

***Correspondence:**
Yue Bai
183730437@qq.com
Fu-Xiang Chen
chenfuxiang0404@126.com

These authors have contributed equally to this work and share first authorship

Specialty section:
This article was submitted to Neuro-Oncology and Neurosurgical Oncology, a section of the journal Frontiers in Neurology

Received: *06 April 2021*
Accepted: *04 June 2021*
Published: *09 August 2021*

Citation:
You H-H, Chen X-Y, Chen J-Y, Bai Y and Chen F-X (2021) The Relationship Between Peritumoral Brain Edema and the Expression of Vascular Endothelial Growth Factor in Vestibular Schwannoma. Front. Neurol. 12:691378. doi: 10.3389/fneur.2021.691378

Objective: This study aimed to explore the potential mechanism of peritumoral brain edema (PTBE) formation in vestibular schwannoma (VS) by detecting intra-tumoral vascular endothelial growth factor (VEGF) expression.

Methods: Between January 2018 and May 2021, 15 patients with PTBE and 25 patients without PTBE were included in the analysis. All patients enrolled in our study underwent surgery in our institution. Expression level of VEGF and microvessel density (MVD) between the two groups were analyzed. Edema index (EI) of each patient with PTBE was calculated.

Results: In the PTBE group, the average of EI was 1.53 ± 0.22. VEGF expression levels were significantly enhanced in the PTBE group compared with the non-PTBE group ($p < 0.001$). The expression level of VEGF in the PTBE group and non-PTBE group was 1.14 ± 0.21 and 0.52 ± 0.09, respectively. Similarly, there were significantly different amounts of MVD in the two groups ($p < 0.001$). The amount of MVD in the PTBE group and non-PTBE group was 11.33 ± 1.59 and 6.28 ± 1.77, respectively. Correlation analysis showed a highly significant positive correlation between VEGF and MVD ($r = 0.883$, $p < 0.001$) and VEGF and EI ($r = 0.876$, $p < 0.001$).

Conclusion: Our study confirmed the close relationship among VEGF expression, tumor angiogenesis, and formation of PTBE in VS patients. It may be possible to develop new effective therapies to attenuate PTBE in VS for alleviation of symptoms and reduction of postoperative complication.

Keywords: vestibular schwannoma, peritumoral brain edema, vascular endothelial growth factor, microvessel density, edema index

INTRODUCTION

Vestibular schwannoma (VS) is common benign tumor of the central nervous system accounting for 8.43% of the total (1), which is mainly located in the cerebellopontine angle. Peritumoral brain edema (PTBE) is a common sign of intracranial tumor but is less common in VS. Nevertheless, there are still a proportion of VS patients accompanied with PTBE, about 5–10% (1, 2). Severe PTBE

could cause suffering for patients and difficulties for surgeons, including aggravation of clinical symptoms, increase of surgical difficulties, and increase of postoperative complication risk.

Currently, the mechanism of PTBE formation is still unclear. Some scholars suggested that vascular endothelial growth factor (VEGF) played an important role in the process of PTBE formation in many intracranial tumors (3, 4). However, it is unknown whether VEGF plays a role in PTBE formation of VS. In our study, we aimed to explore the potential mechanism of PTBE formation in VS by detecting intra-tumoral VEGF expression.

MATERIALS AND METHODS

This study was performed at the First Affiliated Hospital of Fujian Medical University. All procedures were executed with the approval of the ethics committee of the First Affiliated Hospital of Fujian Medical University and the patients' written informed consent. Between January 2018 and May 2021, 180 patients with VS in our institution who were willing to receive surgical therapy were considered for inclusion. Before surgery, all patients underwent plain and enhanced magnetic resonance imaging (MRI) examination. Of this patient cohort, 15 patients with PTBE were included in the PTBE group. As a control, 25 patients without PTBE were randomly selected and assigned to the non-PTBE group. All tumor specimens from the patients in the PTBE group and the non-PTBE group were obtained for further analysis after surgery and confirmed as VS based on pathological assessment.

Calculation of Edema Index

The boundary of the VS was determined by contrast-enhanced T1-weighted imaging (**Figures 1A–C**). Using fluid-attenuated inversion-recovery (FLAIR) images (**Figure 1D**), we determined the boundary of PTBE. For each case in the PTBE group, three-dimensional reconstruction of the tumor with PTBE was performed to calculate the volume of tumor and edema based on neuronavigation workstation (iCranial v.3.0 stereotacxy; BrainLab, Munich, Germany) at our department (**Figure 1E**). The same approach was applied to calculate the volume of tumor in the non-PTBE group. The edema index (EI) was used to

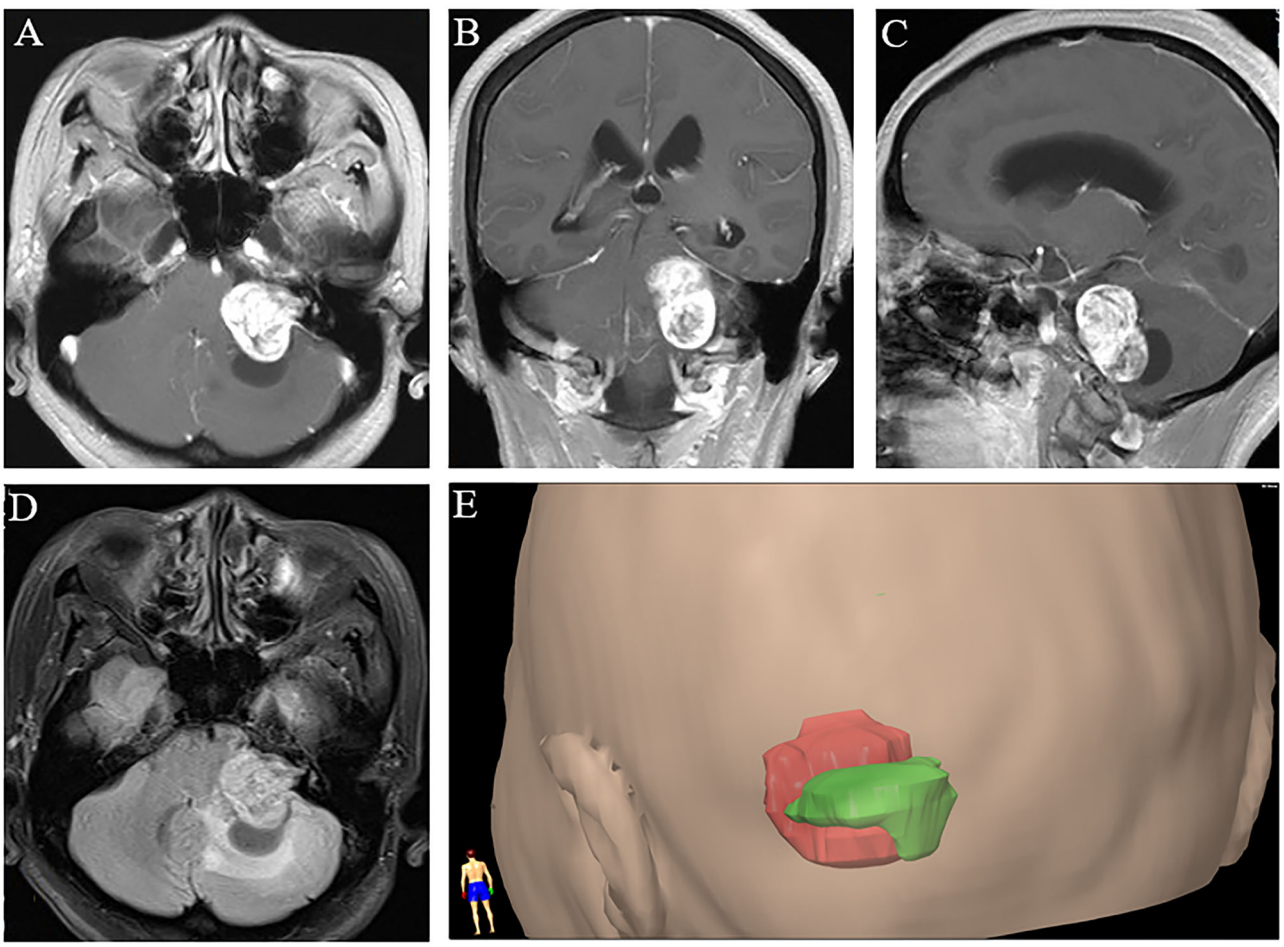

FIGURE 1 | Three-dimensional magnetic resonance imaging reconstruction of vestibular schwannoma with peritumoral brain edema. **(A–C)** Post-contrast axial, coronal, and sagittal T1-weighted images. **(D)** T2-weighted fluid-attenuated inversion-recovery image. **(E)** A representative image of three-dimensional reconstruction with tumor in red and peritumoral edema in green.

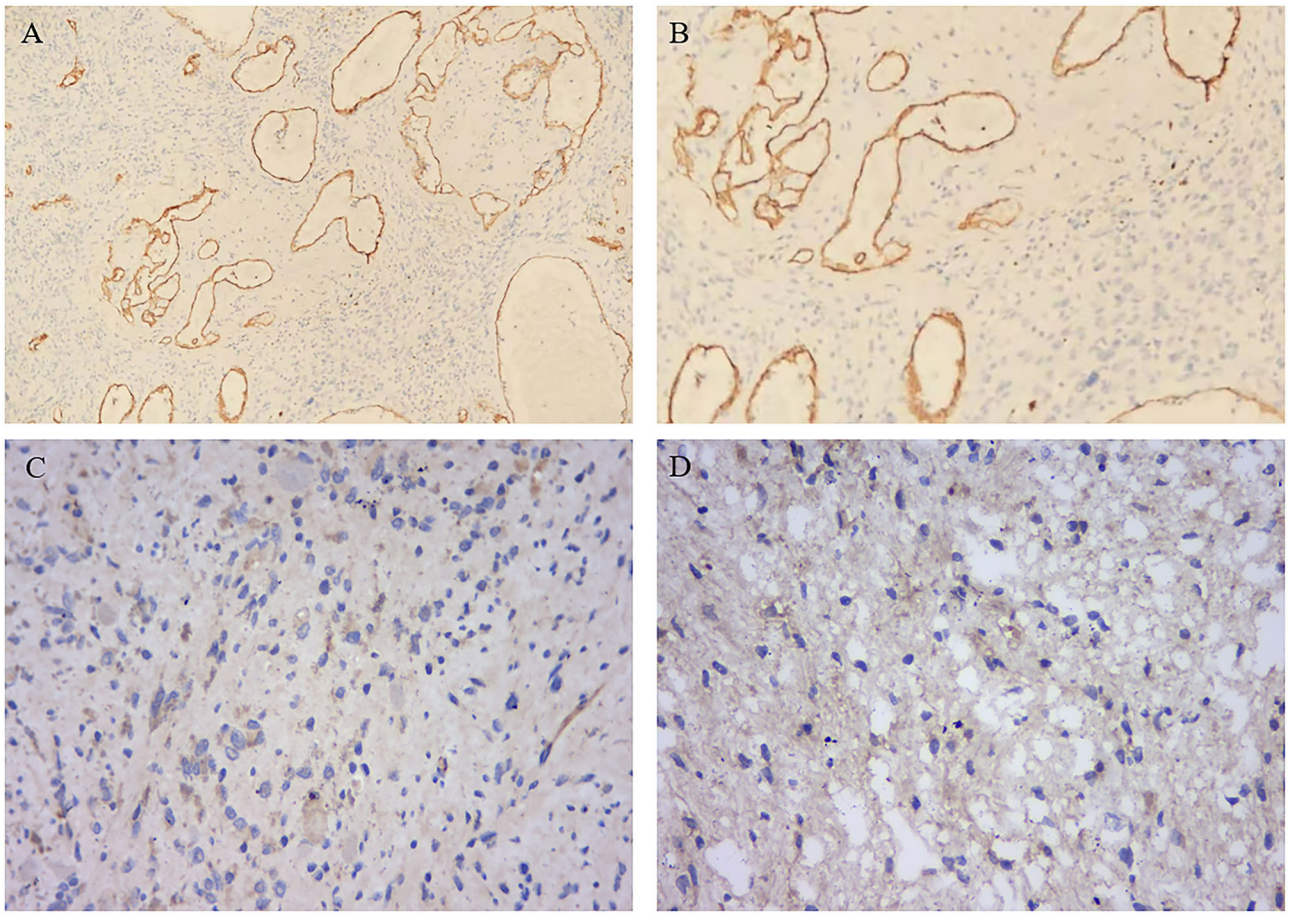

FIGURE 2 | Representative immunohistochemical staining of microvessel density and VEGF in PTBE group. **(A)** Low-magnification view of MVD. **(B)** High-magnification view of MVD. **(C)** Low-magnification view of VEGF staining. **(D)** High-magnification view of VEGF staining. MVD, microvessel density; VEGF, vascular endothelial growth factor; PTBE, peritumoral brain edema.

evaluate the severity of PTBE, which was defined as previously reported (5): (Vedema + Vtumor)/Vtumor. The degree of PTBE was graded as follows: 1, absence of edema; 1–1.5, mild; 1.5–3.0, moderate; and >3.0, severe.

Identification of Microvessel Density by CD34 Staining

By Weidner's criteria based on CD34 immunohistochemical staining (6), the microvessel density (MVD) was determined. First, the tissue sections were observed at low magnification (×100) to select the region of the highest neovascularization, which was also defined as "hot spot" (**Figure 2A**). Then, the number of microvessels of each "hot spot" was counted under a microscope at ×200 magnification (**Figure 2B**). The mean value of MVD in three randomly selected fields was finally calculated. Any single-stained endothelial cell or cluster of endothelial cells with or without vessel lumen, which was clearly separated from tumor cells, adjacent microvessels, and connective tissue, was recognized as a single, countable microvessel.

Immunohistochemical Staining of Vascular Endothelial Growth Factor

Surgically resected tumor specimens were fixed in 10% formaldehyde, and serial sections were prepared after paraffin embedding. Then, standard hematoxylin and eosin (H&E) staining and streptavidin–biotin peroxidase (SP) immunohistochemical technique were performed. Diaminobenzidine (DAB) was used as chromogen to perform SP detection for evaluating VEGF expression (**Figures 2C,D**). Based on the staining intensity, the VEGF expression was scored as previously described (grade 1, negative; grade 2, weak; grade 3, moderate; and grade 4, strong staining) (7), which corresponds to the percentage of stained tumor area at ×200 magnification (1, <5%; 2, 5–20%; 3, 21–50%; and 4, >50%).

Western Blotting Analysis

Western blotting detection kits, which were purchased from Wuhan ServiceBio Technology Co., Ltd. (Wuhan, China) were used in strict accordance with the manufacturer's recommendations. Briefly, total cell protein was extracted

TABLE 1 | Clinical data obtained for each of the 40 patients.

Case no.	Age (year)	Sex	Sample	Location	Peritumoral edema
1	56.5	M	Vestibular schwannoma	R	Yes
2	50.2	M	Vestibular schwannoma	L	Yes
3	56.6	M	Vestibular schwannoma	L	Yes
4	51.6	F	Vestibular schwannoma	L	Yes
5	75.8	F	Vestibular schwannoma	L	Yes
6	60.0	F	Vestibular schwannoma	L	Yes
7	56.6	F	Vestibular schwannoma	R	Yes
8	25.3	M	Vestibular schwannoma	L	Yes
9	43.2	M	Vestibular schwannoma	L	Yes
10	27.2	F	Vestibular schwannoma	L	Yes
11	53.2	M	Vestibular schwannoma	R	Yes
12	64.6	F	Vestibular schwannoma	R	Yes
13	33.3	M	Vestibular schwannoma	L	Yes
14	65.3	M	Vestibular schwannoma	R	Yes
15	38.4	F	Vestibular schwannoma	R	Yes
16	46.0	F	Vestibular schwannoma	R	No
17	53.9	F	Vestibular schwannoma	L	No
18	53.8	F	Vestibular schwannoma	L	No
19	43.5	M	Vestibular schwannoma	R	No
20	56.8	F	Vestibular schwannoma	R	No
21	71.6	F	Vestibular schwannoma	R	No
22	70.4	F	Vestibular schwannoma	L	No
23	24.8	M	Vestibular schwannoma	R	No
24	27.6	F	Vestibular schwannoma	L	No
25	57.8	F	Vestibular schwannoma	R	No
26	28.9	M	Vestibular schwannoma	L	No
27	61.9	F	Vestibular schwannoma	R	No
28	67.1	F	Vestibular schwannoma	R	No
29	26.4	M	Vestibular schwannoma	L	No
30	64.9	F	Vestibular schwannoma	L	No
31	46.1	F	Vestibular schwannoma	L	No
32	50.8	M	Vestibular schwannoma	L	No
33	42.5	F	Vestibular schwannoma	R	No
34	70.2	F	Vestibular schwannoma	L	No
35	70.8	M	Vestibular schwannoma	L	No
36	23.9	M	Vestibular schwannoma	L	No
37	29.2	F	Vestibular schwannoma	R	No
38	59.6	F	Vestibular schwannoma	R	No
39	62.1	M	Vestibular schwannoma	R	No
40	61.4	M	Vestibular schwannoma	L	No

M, male; F, female; R, right; L, left.

and measured by ultraviolet spectrophotometer. Samples were denatured by boiling for 5 min and then electrophoresed in 12% sodium dodecyl sulfate (SDS)–polyacrylamide gels. Proteins were transferred to NC membranes and blocked with 5% skimmed milk for 1 h at room temperature. The primary antibodies were diluted in TBST with 5% skimmed milk or 5% bovine serum albumin (BSA) and incubated overnight at 4°C. Membranes were washed by TBST for three times (5 min per time). The secondary antibodies (diluted 1:3,000 in TBST) were incubated at room temperature for 30 min. Then, they were re-washed by TBST for three times (5 min per time) and reacted to enhanced chemiluminescence (ECL) solution for 1–2 min. After that, the membranes were exposed, developed, and fixed on X-ray films for further scanning and archiving. The optical density values of the target band were analyzed by AlphaEaseFC software.

Statistical Analysis

All analyses were performed with SPSS version 22.0 (SPSS, Inc., Chicago, IL, USA). Continuous variables, presented as mean ± standard deviation or median (inter-quartile range), were analyzed by two-sample *t*-test or non-parametric test, respectively. Pearson's correlation analysis was adopted for determining correlation. A $p < 0.05$ was considered as statistically significant.

RESULTS

Clinical Parameters and Tumor Characteristics

As previously mentioned, we analyzed 40 cases for this study. The clinical data of all patients were complete and presented in **Table 1**. Overall, 17 were male and 23 were female with a median age of 53.9 (39.4–62.1) years. There were no statistical differences between the two groups in age ($p = 0.727$), sex ($p = 0.283$), and sample location ($p = 0.622$).

Tumor volume in the PTBE group was significantly larger than that in the non-PTBE group (17.23 ± 3.54 vs. 14.72 ± 3.47 cm^3, $p = 0.035$). In the PTBE group, mild edema was present around the lesions in eight cases, while seven cases presented with moderate edema. The maximum EI was 1.82, with an average value of 1.53 ± 0.22. Tumor volume was not statistically correlated with the severity of PTBE ($p = 0.619$).

Comparison of Vascular Endothelial Growth Factor Expression and Microvessel Density Among the Two Groups

Both groups revealed VEGF protein expression (**Figure 3A**). VEGF expression levels were significantly enhanced in the PTBE group compared with the non-PTBE group (**Figure 3B**, $p < 0.001$). The expression level of VEGF in the PTBE group and non-PTBE group was 1.14 ± 0.21 and 0.52 ± 0.09, respectively (**Table 2**). Similarly, there were significantly different amounts of MVD in the two groups (**Figure 3C**, $p < 0.001$), with the less amount in the non-PTBE group and the more amount in the PTBE group. The amount of MVD in the PTBE group and non-PTBE group was 11.33 ± 1.59 and 6.28 ± 1.77, respectively (**Table 2**).

Vascular Endothelial Growth Factor Expression Is Positively Correlated With Microvessel Density and Edema Index

In the PTBE group, all samples were positive staining for VEGF. Among them, five patients had a weak staining intensity of VEGF, and the number of patients with a moderate or strong staining intensity was 6 and 4, respectively. There was no significant difference of tumor volume in the patients with different staining

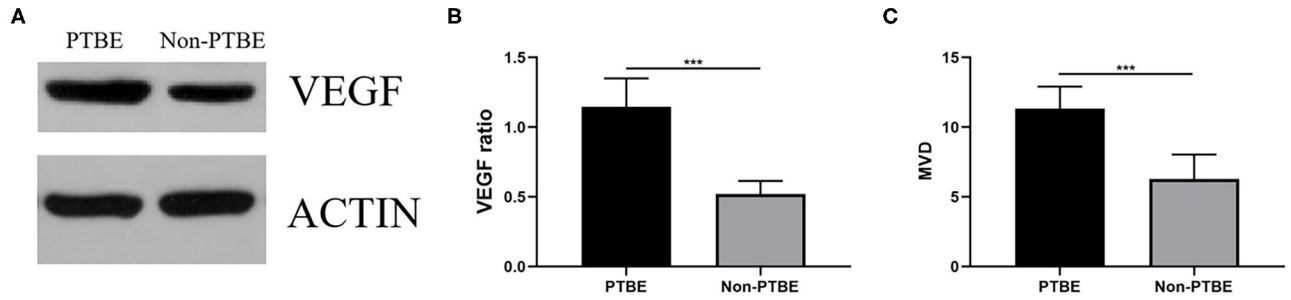

FIGURE 3 | The expression of VEGF and the amount of MVD. **(A)** The bands of VEGF in the two groups by Western blotting analysis. **(B)** Expression analysis showed that patients in the PTBE group had significantly higher expression level of VEGF than those of the non-PTBE group. **(C)** The amount of MVD in the PTBE group was significantly higher than that in the non-PTBE group. ***$p < 0.001$.

intensity ($p = 0.978$). The value of EI was significantly different in the three groups ($p = 0.001$). As displayed in **Figure 4**, correlation analysis revealed a highly significant positive correlation between VEGF and MVD ($r = 0.883$, $p < 0.001$); similarly, a highly positive correlation between VEGF and EI was confirmed ($r = 0.876$, $p < 0.001$).

TABLE 2 | Comparison of VEGF and MVD in the two groups.

Parameter	PTBE ($n = 15$)	Non-PTBE ($n = 25$)	p-value
VEGF	1.14 ± 0.21	0.52 ± 0.09	<0.001
MVD	11.33 ± 1.59	6.28 ± 1.77	<0.001

VEGF, vascular endothelial growth factor; MVD, microvessel density; PTBE, peritumoral brain edema.

DISCUSSION

The VS can directly compress the cerebellum, the brain stem, and peripheral nerves due to its location in the cerebellopontine angle. The VS on imaging can vary in size and present as a solid, cystic, or solid–cystic lesion. The incidence of VS combined with PTBE is low but not rare. Samii et al. reported 30 cases with PTBE in 605 patients with VS, showing that the incidence of PTBE in VS was only 5% (1), while another study reported a higher incidence of PTBE up to 37% (8). In recent years, with the remarkable development of surgical equipment and improvement of surgical technique, the safety and effectiveness of treatment for VS have substantially improved. Nevertheless, the surgical treatment of patients with VS remains a challenge especially in those with PTBE. The deleterious effects of PTBE are usually presented as a substantial increase in space-occupying effect of VS, including elevation of intracranial pressure and distortion of local structures, subsequently leading to a decrease of cerebral blood flow and a slowed metabolism of nearby cells. In addition, the occurrence of PTBE may contribute to the adherence of VS to the surrounding structures, resulting to the increase of surgical difficulty and postoperative complication rate (2). For example, a previous study reported that VS with PTBE had a worse short-term functional outcome and higher risk of bleeding after surgery (1). Therefore, PTBE in VS is correlated with the clinical course and prognosis of the disease.

Though the basic studies of PTBE in intracranial tumor has achieved promising results, the detailed mechanism of formation and action have not been elucidated so far. Research has suggested that PTBE belonged to vasogenic brain edema (9). Tumor growth and proliferation rely on the formation of its vascular network, which supplies oxygen and nutrients and removes metabolic waste. A high degree of vascularization could promote tumor growth and cause severe PTBE, which has been confirmed in astrocytomas (5). Thus, angiogenesis and anti-angiogenesis factors could regulate neovascularization of tumors and affect PTBE. VEGF is known to be an important angiogenic factor, which promotes the neovascularization and increases vascular permeability resulting in the promotion of tumor growth (10). In the early stages of neovascularization, VEGF modulates endothelial cell proliferation vascular dilation and vascular leakage. And in the later stages, VEGF regulates vessel maturation and stabilization. VEGF expression has confirmed its importance in the formation of PTBE in intracranial tumor, which is gradually becoming a research hot spot (10–13). Nassehi et al. revealed that the VEGF-A pathway may be essential for the formation of PTBE in meningiomas (13). However, there are few previous studies focusing on the association between VEGF and PTBE in VS.

The results of this study showed that tumor volume in the PTBE group was significantly larger than that in the non-PTBE group ($p = 0.035$) but not statistically correlated with the severity of PTBE ($p = 0.619$) and the staining intensity of VEGF ($p = 0.978$), while the value of EI was significantly different in the different grades of staining intensity of VEGF ($p = 0.001$). In addition, the value of MVD and expression of VEGF in PTBE group were significantly higher than those in non-PTBE group. Besides, VEGF expression were positively correlated with MVD and EI. MVD, as a standard measurement of angiogenesis, was widely considered as a prognostic indicator of intracranial tumors, and higher MVD was associated with worse outcome (14–16). The VS combined with PTBE often shows a rich blood supply in imaging examinations and higher volume of intraoperative blood loss. Though some normal tissues may

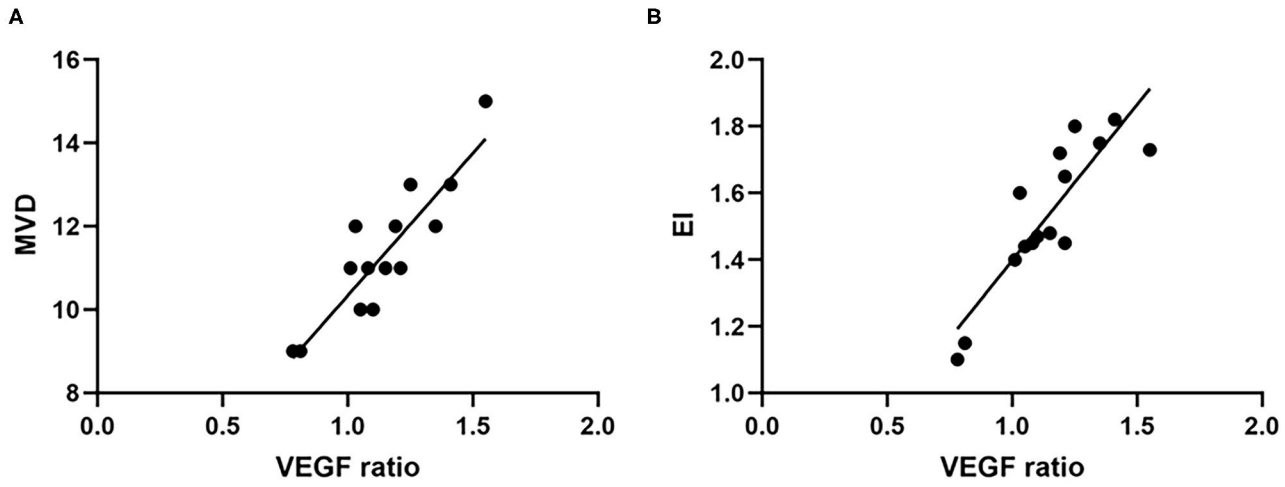

FIGURE 4 | The expression level of VEGF was positively correlated with MVD **(A)** and EI **(B)**. VEGF, vascular endothelial growth factor; MVD, microvessel density; EI, edema index.

produce VEGF, tumor cells present overexpression of VEGF *via* autocrine or paracrine effects. The increase of neovascularization secondary to overexpression of VEGF could promote the invasive potency of tumor toward the surrounding tissues. On the one hand, the results indicated that VS with PTBE may grow faster than that without PTBE, leading to a higher surgical difficulty; on the other hand, it is suggested that the differential expression of VEGF mainly affects severity of PTBE *via* its effects on vessels. Therefore, we believed that VEGF was an important factor of neovascularization in VS patients and was closely associated with PTBE formation. Without timely surgical resection, PTBE can be worse since more VEGF will be produced by the VS.

The VEGF, an endothelial-cell-specific mitogen, was first reported in guinea pig hepatocarcinoma in 1983 (17) and first isolated from pituitary follicular cells in 1989 (18). As a polyfunctional molecule, VEGF is 1,000 times more potent to induce vascular permeability, tumor neovascularization, and PTBE than histamine (19). VEGF is produced and secreted by tumors, acting specifically on endothelial cells to promote vascular endothelial cell proliferation and induce angiogenesis, on the one hand, and increasing vessel permeability to allow the extravasation and deposition of fibrinogen on the other (20). Specifically, VEGF could downregulate the expression of tight junction proteins, leading to increased formation of fenestra and cleft between vascular endothelial cells. Also, it could enhance the vesiculo-vacuolar formation within endothelial cells (21). These alterations may result in the increase of vascular permeability and may ultimately lead to PTBE. The correlation among PTBE, VEGF expression, and tumor neovascularization has already been extensively confirmed (22) and may also exist in VS, which was supported by our study. PTBE is probably a complex multifactorial process and VEGF is supposed to play a crucial role during the process. Since VEGF expression is potentiated by hypoxia and ischemia and PTBE can in turn lead to secondary ischemia, these factors are closely interrelated to each other. Additionally, many cofactors and biochemical vasoactive agents, including histamines, oxygen free radicals, leukokinins, bradykinins, and prostaglandins, may act in synergy with VEGF to promote PTBE formation. As part of the complex network, VEGF interacts with many pathways, including hypoxia-inducible factor, Notch, and aquaporin 4, to modulate angiogenesis and PTBE (23), all of which may be involved in the mechanism of PTBE formation (**Figure 5**).

Therefore, new treatment approaches of VS with severe PTBE may lie in the reduction of VEGF secretion or the blockage of its receptors (e.g., flk1 and KDR), as they may reduce tumor neovascularization, tumor growth capacity, and tumor invasion capacity. Anti-VEGF monoclonal antibodies may be the most promising therapy, as it could directly target VEGF-expressing tumor cells and may result in tumor cell elimination and PTBE alleviation.

There were also some limitations in our study. First, the number of examined patients was too small due to low incidence of VS with PTBE. Further study with a larger sample size is warranted to overcome this drawback. Second, we did not detect the expression of other cofactors and biochemical vasoactive agents in tumor, which may act in synergy with VEGF to promote PTBE formation. Future work will be dedicated to solve these problems for further exploring the mechanism of PTBE formation in VS.

CONCLUSION

Our study confirmed the close relationship among VEGF expression, tumor angiogenesis, and formation of PTBE in VS patients. VEGF could promote angiogenesis of VS, and both of them contributed to the formation of PTBE in VS. Therefore, based on these findings, it may be possible to develop new effective therapies to attenuate PTBE in VS for alleviation of symptoms and reduction of postoperative complication.

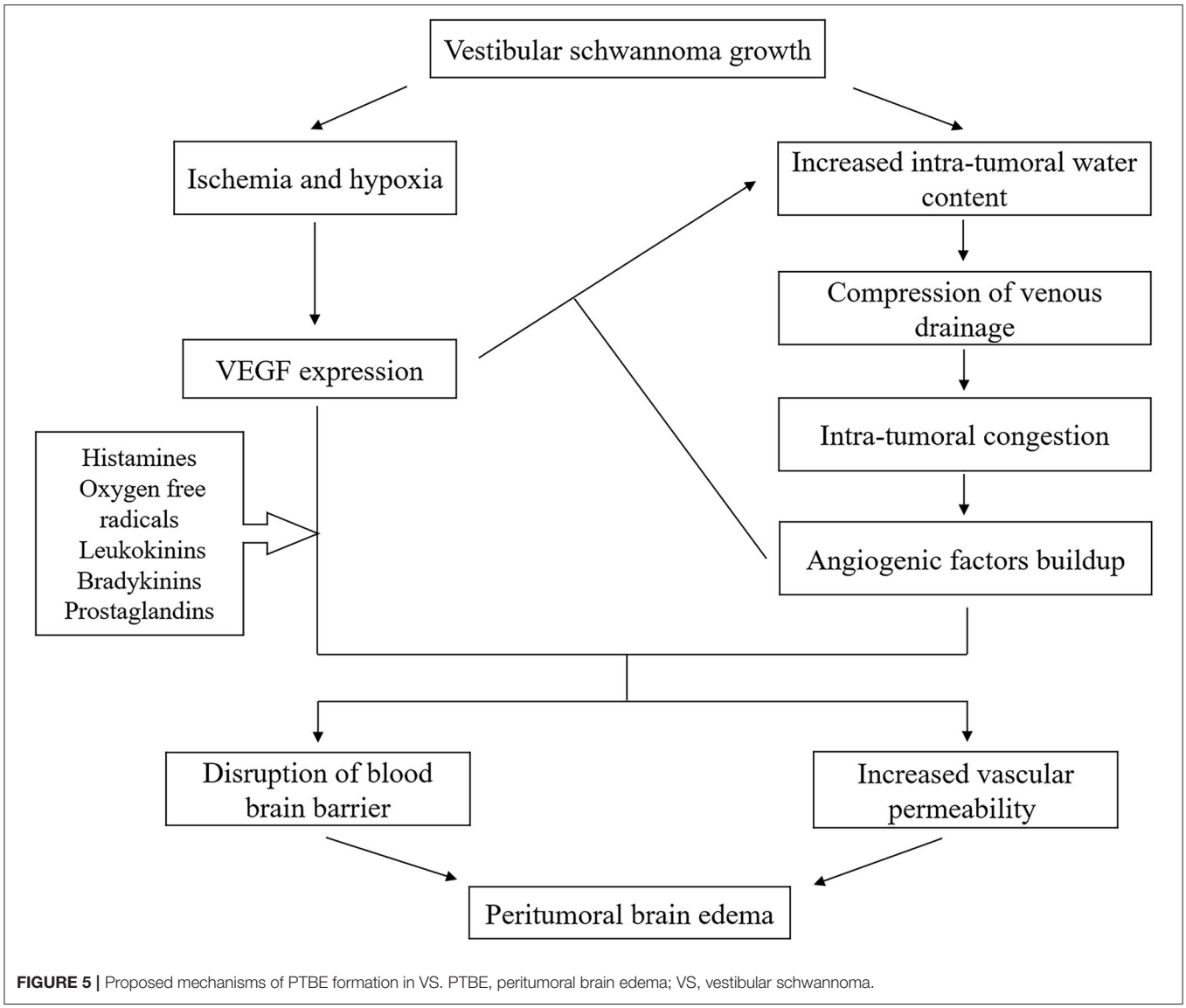

FIGURE 5 | Proposed mechanisms of PTBE formation in VS. PTBE, peritumoral brain edema; VS, vestibular schwannoma.

DATA AVAILABILITY STATEMENT

The raw data supporting the conclusions of this article will be made available by the authors, without undue reservation.

ETHICS STATEMENT

The studies involving human participants were reviewed and approved by the Ethics Committee of the First Affiliated Hospital of Fujian Medical University. Written informed consent to participate in this study was provided by the participants' legal guardian/next of kin.

AUTHOR CONTRIBUTIONS

H-HY, X-YC, and J-YC were major contributors in concept, design, definition of intellectual content, literature search, experimental studies, data acquisition, data analysis, statistical analysis, manuscript preparation, manuscript editing, and manuscript review of the manuscript. YB and F-XC analyzed and interpreted the data and take responsibility for the integrity of the work as a whole from inception to published article. This work was done in the Department of Neurosurgery, The First Affiliated Hospital of Fujian Medical University, Fuzhou, China. All authors contributed to the article and approved the submitted version.

FUNDING

This study was supported by grants from the Startup Fund for Scientific Research, Fujian Medical University (Grant Numbers: 2018QH1060 and 2020QH1051), the Joint Funds for the innovation of science and Technology, Fujian province (Grant Number: 2018Y9085).

REFERENCES

1. Samii M, Giordano M, Metwali H, Almarzooq O, Samii A, Gerganov VM. Prognostic significance of peritumoral edema in patients with vestibular schwannomas. *Neurosurgery*. (2015) 77:81–5; discussion: 5–6. doi: 10.1227/NEU.0000000000000748
2. Giordano M, Gerganov V, Metwali H, Gallieni M, Samii M, Samii A. Imaging features and classification of peritumoral edema in vestibular schwannoma. *Neuroradiol J*. (2020) 33:169–73. doi: 10.1177/1971400919896253
3. Louis DN, Ohgaki H, Wiestler OD, Cavenee WK, Burger PC, Jouvet A, et al. The 2007 WHO classification of tumours of the central nervous system. *Acta Neuropathol*. (2007) 114:97–109. doi: 10.1007/s00401-007-0243-4
4. Schmid S, Aboul-Enein F, Pfisterer W, Birkner T, Stadek C, Knosp E. Vascular endothelial growth factor: the major factor for tumor neovascularization and edema formation in meningioma patients. *Neurosurgery*. (2010) 67:1703–8; discussion: 8. doi: 10.1227/NEU.0b013e3181fb801b
5. Wang W, Da R, Wang M, Wang T, Qi L, Jiang H, et al. Expression of brain-specific angiogenesis inhibitor 1 is inversely correlated with pathological grade, angiogenesis and peritumoral brain edema in human astrocytomas. *Oncol Lett*. (2013) 5:1513–8. doi: 10.3892/ol.2013.1250
6. Weidner N, Semple JP, Welch WR, Folkman J. Tumor angiogenesis and metastasis–correlation in invasive breast carcinoma. *N Engl J Med*. (1991) 324:1–8. doi: 10.1056/NEJM199101033240101
7. Kim YE, Lim JS, Choi J, Kim D, Myoung S, Kim MJ, et al. Perfusion parameters of dynamic contrast-enhanced magnetic resonance imaging in patients with rectal cancer: correlation with microvascular density and vascular endothelial growth factor expression. *Korean J Radiol*. (2013) 14:878–85. doi: 10.3348/kjr.2013.14.6.878
8. Mulkens TH, Parizel PM, Martin JJ, Degryse HR, Van de Heyning PH, Forton GE, et al. Acoustic schwannoma: MR findings in 84 tumors. *AJR Am J Roentgenol*. (1993) 160:395–8. doi: 10.2214/ajr.160.2.8424360
9. Park KJ, Kang SH, Chae Y-S, Yu M-O, Cho T-H, Suh J-K, et al. Influence of interleukin-6 on the development of peritumoral brain edema in meningiomas. *J Neurosurg*. (2020) 112:73–80. doi: 10.3171/2009.4.JNS09158
10. Otsuka S, Tamiya T, Ono Y, Michiue H, Kurozumi K, Daido S, et al. The relationship between peritumoral brain edema and the expression of vascular endothelial growth factor and its receptors in intracranial meningiomas. *J Neurooncol*. (2004) 70:349–57. doi: 10.1007/s11060-004-9164-4
11. Lee SH, Lee YS, Hong YG, Kang CS. Significance of COX-2 and VEGF expression in histopathologic grading and invasiveness of meningiomas. *APMIS*. (2014) 122:16–24. doi: 10.1111/apm.12079
12. Yao Y, Kubota T, Sato K, Kitai R, Takeuchi H, Arishima H, et al. Prognostic value of vascular endothelial growth factor and its receptors Flt-1 and Flk-1 in astrocytic tumours. *Acta Neurochir*. (2001) 143:159–66. doi: 10.1007/s007010170122
13. Nassehi D, Sørensen LP, Dyrbye H, Thomsen C, Juhler M, Laursen H, et al. Peritumoral brain edema in angiomatous supratentorial meningiomas: an investigation of the vascular endothelial growth factor A pathway. *APMIS*. (2013) 121:1025–36. doi: 10.1111/apm.12052
14. Fan C, Zhang J, Liu Z, He M, Kang T, Du T, et al. Prognostic role of microvessel density in patients with glioma. *Medicine*. (2019) 98:e14695. doi: 10.1097/MD.0000000000014695
15. Yao Y, Kubota T, Sato K, Kitai R. Macrophage infiltration-associated thymidine phosphorylase expression correlates with increased microvessel density and poor prognosis in astrocytic tumors. *Clin Cancer Res*. (2001) 7:4021–6.
16. Barresi V, Cerasoli S, Vitarelli E, Tuccari G. Density of microvessels positive for CD105 (endoglin) is related to prognosis in meningiomas. *Acta Neuropathol*. (2007) 114:147–56. doi: 10.1007/s00401-007-0251-4
17. Senger DR, Galli SJ, Dvorak AM, Perruzzi CA, Harvey VS, Dvorak HF. Tumor cells secrete a vascular permeability factor that promotes accumulation of ascites fluid. *Science*. (1983) 219:983–5. doi: 10.1126/science.6823562
18. Ferrara N, Henzel WJ. Pituitary follicular cells secrete a novel heparin-binding growth factor specific for vascular endothelial cells. *Biochem Biophys Res Commun*. (1989) 161:851–8. doi: 10.1016/0006-291X(89)92678-8
19. Connolly DT. Vascular permeability factor: a unique regulator of blood vessel function. *J Cell Biochem*. (1991) 47:219–23. doi: 10.1002/jcb.240470306
20. Noell S, Ritz R, Wolburg-Buchholz K, Wolburg H, Fallier-Becker P. An allograft glioma model reveals the dependence of aquaporin-4 expression on the brain microenvironment. *PLoS ONE*. (2012) 7:e36555. doi: 10.1371/journal.pone.0036555
21. Yang L, Lin Z, Huang Q, Lin J, Chen Z, Zhou L, et al. Effect of vascular endothelial growth factor on remodeling of C6 glioma tissue in vivo. *J Neurooncol*. (2011) 103:33–41. doi: 10.1007/s11060-010-0356-9
22. Salokorpi N, Yrjana S, Tuominen H, Karttunen A, Heljasvaara R, Pihlajaniemi T, et al. Expression of VEGF and collagen XVIII in meningiomas: correlations with histopathological and MRI characteristics. *Acta Neurochir*. (2013) 155:989–96; discussion: 96. doi: 10.1007/s00701-013-1699-8
23. Qiu XX, Wang CH, Lin ZX, You N, Wang XF, Chen YP, et al. Correlation of high delta-like ligand 4 expression with peritumoral brain edema and its prediction of poor prognosis in patients with primary high-grade gliomas. *J Neurosurg*. (2015) 123:1578–85. doi: 10.3171/2014.12.JNS14768

Conflict of Interest: The authors declare that the research was conducted in the absence of any commercial or financial relationships that could be construed as a potential conflict of interest.

Publisher's Note: All claims expressed in this article are solely those of the authors and do not necessarily represent those of their affiliated organizations, or those of the publisher, the editors and the reviewers. Any product that may be evaluated in this article, or claim that may be made by its manufacturer, is not guaranteed or endorsed by the publisher.

Copyright © 2021 You, Chen, Chen, Bai and Chen. This is an open-access article distributed under the terms of the Creative Commons Attribution License (CC BY). The use, distribution or reproduction in other forums is permitted, provided the original author(s) and the copyright owner(s) are credited and that the original publication in this journal is cited, in accordance with accepted academic practice. No use, distribution or reproduction is permitted which does not comply with these terms.

frontiers in Oncology

ORIGINAL RESEARCH
published: 17 August 2021
doi: 10.3389/fonc.2021.633430

HOXA5 Is Recognized as a Prognostic-Related Biomarker and Promotes Glioma Progression Through Affecting Cell Cycle

Fengqin Ding[1‡], *Ping Chen*[2‡], *Pengfei Bie*[3], *Wenhua Piao*[1*] *and Quan Cheng*[4,5,6,7*†]

[1] Department of Clinical Laboratory, People's Hospital of Ningxia Hui Autonomous Region, First Affiliated Hospital of Northwest Minzu University, Yinchuan, China, [2] Medical Experiment Center, General Hospital of Ningxia Medical University, Yinchuan, China, [3] Department of Neurosurgery, People's Hospital of Ningxia Hui Autonomous Region, First Affiliated Hospital of Northwest Minzu University, Yinchuan, China, [4] Department of Neurosurgery, Xiangya Hospital, Central South University, Changsha, China, [5] National Clinical Research Center for Geriatric Disorders, Xiangya Hospital, Central South University, Changsha, China, [6] Clinical Diagnosis and Therapy Center for Glioma of Xiangya Hospital, Central South University, Changsha, China, [7] Department of Clinical Pharmacology, Xiangya Hospital, Central South University, Changsha, China

OPEN ACCESS

Edited by:
Terrance Johns, University of Western Australia, Australia

Reviewed by:
Zhiming Zheng, Shandong Provincial Hospital, China
Yutao Wang, China Medical University, China

***Correspondence:**
Quan Cheng
chengquan@csu.edu.cn
Wenhua Piao
wenhuapiao@163.com

†ORCID:
Quan Cheng
orcid.org/0000-0003-2401-5349

‡These authors have contributed equally to this work

Specialty section:
This article was submitted to Neuro-Oncology and Neurosurgical Oncology, a section of the journal Frontiers in Oncology

Received: 25 November 2020
Accepted: 19 July 2021
Published: 17 August 2021

Citation:
Ding F, Chen P, Bie P, Piao W and Cheng Q (2021) HOXA5 Is Recognized as a Prognostic-Related Biomarker and Promotes Glioma Progression Through Affecting Cell Cycle. Front. Oncol. 11:633430. doi: 10.3389/fonc.2021.633430

Glioma is malignant tumor derives from glial cells in the central nervous system. High-grade glioma shows aggressive growth pattern, and conventional treatments, such as surgical removal and chemo-radiotherapy, archive limitation in the interference of this process. In this work, HOXA5, from the HOX family, was identified as a glioma cell proliferation-associated factor by investigating its feature in the TCGA and CGGA data set. High HOXA5 expression samples contain unfavorable clinical features of glioma, including IDH wild type, un-methylated MGMT status, non-codeletion 1p19q status, malignant molecular subtype. Survival analysis indicates that high HOXA5 expression samples are associated with worse clinical outcome. The CNVs and SNPs profile difference further confirmed the enrichment of glioma aggressive related biomarkers. In the meantime, the activation of DNA damage repair-related pathways and TP53-related pathways is also related to HOXA5 expression. In cell lines, U87MG and U251, by interfering HOXA5 expression significantly inhibit glioma progression and apoptosis, and cell cycle is arrested at the G2/M phase. Collectively, increased HOXA5 expression can promote glioma progression *via* affecting glioma cell proliferation.

Keywords: homeobox A5, glioma, cell cycle, cell proliferation, prognosis

INTRODUCTION

Glioma is a malignant tumor that derived from the central nervous system. Four grades were proposed for evaluating its malignancy according to its pathological features, including grades I, II, II, and IV. Grade IV glioma, also called as glioblastoma or glioblastoma multiforme (GBM), is the worst subtype of glioma with median survival time less than 14.6 months (1). High proliferative ability, disordered tumor angiogenesis, and massive tumor necrotic area were recognized as its feature in GBM (2). Recent study proposed different classification of GBM based on its transcriptomic signatures (3, 4). Treatment like the STUPP protocol is able to prolong patient's

survival time but cannot inhibit glioma progression. Therefore, identification of potential target to glioma may assist in improving its prognosis.

HOXA5 belongs to the gene family encoding transcription factors, which contained homeobox. This gene family expressed subsequently and affected tissue developmental and organogenesis (5). HOXA5 is located on chromosome 7 in human and encodes ANTP-class homeodomain protein consisting of 270 amino acids (5). HOXA5 widely participated in the development of organs such as the respiratory system, digestive system, lipid tissue, mammary gland, and so on (5, 6). Therefore, HOXA5 acts a critical role in human development.

Multiple studies reported that HOXA5 was associated with tumor progression, including leukemia, breast cancer, lung cancer, glioblastoma, colorectal cancer, laryngeal squamous cell cancer, and liver cancer (7–9). In breast cancer, HOXA5 affects the expression of TP53 in tumor cells (10), epithelial-mesenchymal transition (11, 12) and apoptosis (13) to affect tumor progression. HOXA5 inhibits non-small lung cancer metastasis through modulating cytoskeletal remodeling (14). HOXA5 also affects tumor cell proliferation and invasion in cervical cancer (15, 16) and lung cancer (17, 18). TP53, a tumor suppressor gene, highly associates with tumorigenesis and cellular response to DNA damage. It was previously reported that HOXA5 can affect tumor progression through regulating TP53 expression (18–20). Therefore, HOXA5 widely affected tumor progression, but its role in glioma is still unknown.

In this work, the expression profile of the HOXA5 in multiple tumor types was mapped. Its association with glioma progression and potential mechanisms were analyzed by using the GO/KEGG enrichment analysis. We identified that HOXA5 as an unfavorable factor for glioma and its expression are highly connected with the activation of p53-related pathways. We also confirmed that HOXA5 affected tumor cells progression through regulating tumor cell proliferation.

MATERIALS AND METHODS

Sample and Data Collection

From the The Cancer Genome Atlas (TCGA) (https://xenabrowser.net/), Chinese Glioma Genome Atlas (CGGA) (http://www.cgga.org.cn/), and Gene Expression Omnibus (GEO) (https://www.ncbi.nlm.nih.gov/) data sets, we collected HOXA5 data from LGG and GBM samples. RNA-seq data for specific tumor anatomic structure in GBM was from Ivy Glioblastoma Atlas Project (http://glioblastoma.alleninstitute.org/).

Biological Function and Gene Set Enrichment Analyses

Correlation analysis of HOXA5 regarding different pathological features was performed in the TCGA and CGGA data sets with R language (https://www.r-project.org/). Differentially expressed genes between HOXA5 high and HOXA5 low groups with the adjusted p-value <0.05. and the absolute FC larger than 2.0 were considered to be statistically significant. Association between HOXA5 expression and gene sets from the Molecular Signatures Database (MSigDB) were analyzed using gene set enrichment analysis (GSEA). Gene ontology (GO), KEGG (Kyoto Encyclopedia of Genes and Genomes), and HALLMARK analysis was performed using the R package GSVA. Somatic mutations and somatic copy number alternations (CNAs) were downloaded from the TCGA database. Copy number alternations associated with HOXA5 expression were analyzed using GISTIC 2.0.

Survival Analysis

Patients were subdivided into high and low groups according to HOXA5 expression. The overall survival (OS), progression-free interval (PFI), and disease-specific survival (DSS) rates of patients in low and high groups were compared by the Kaplan–Meier method with log-rank test. ROC was performed to evaluate the prediction performance of HOXA5 expression in various aspects, including 3-year, 5-year OS, and subtype of GBM (classical, mesenchymal, neural, proneural).

Cell Culture

U87-MG cells and U251 cells, purchased from the Chinese Academy of Sciences, were cultured in DMEM medium with 10% Gibico FBS+1% penicillin-streptomycin, and the medium was changed every 2 to 3 days.

The siRNA of HOXA5, siRNA-112 (sense 5′-3′: GGACUACCAGUUGCAUAAUTT; antisense 5′-3′: AUUAUGCAACUGGUAGUCCTT), siRNA-610 (sense 5′-3′: GCACAUAAGUCAUGACAACTT; antisense 5′-3′: GUUGUCAUGACUUAUGUGCTT) and siRNA-726 (sense 5′-3′: GCAGAAGGAGGAUUGAAAUTT; antisense 5′-3′: AUUUCAAUCCUCCUUCUGCTT) were purchased from HonorGene (Changsha, China). 95 μl serum-free DMEM medium, 5 μl HOXA5 siRNA, and 5 μl Lip2000 were added into the centrifuge tubes in turns. HOXA5 siRNA-112 was discarded because of its low efficiency according to the Western blot assay.

Western Blotting Assay

HOXA5 primary antibody (Abcam, Cat# ab140636, RRID: AB_2877721) was diluted to 1:1000. β-actin (Proteintech Cat# 66009-1-Ig, RRID: AB_2687938) was diluted to 1:5000 and utilized as the loading control and internal standard. Secondary antibody (Proteintech Cat# SA00001-2, RRID: AB_2722564; Proteintech Cat# SA00001-1, RRID: AB_2722565) was diluted to 1:5000. The total protein concentration was determined using the BCA Protein Assay Kit (Solarbio, China), according to the manufacturer's instructions. The blots were subjected to three 5-min washes with TBST prior to 1-h incubation with the secondary antibody, repeated washing, and signal development with Western Lightning Plus-ECL.

CCK8 Assay

The logarithmic growth phase transfected U251-MG and U87-MG GBM cells were obtained and digested for CCK8 assay. 1×10^3 glioma cells and 100 μl of medium were placed into 96-well

plates. The absorbance at 450 nm was measured after hatched for 1 h under the condition of 37°C and 5 % CO_2.

Colony-Forming Assay

U87-MG cells and U251 cells were digested and plated in six-well plates (300 cells per well) and cultured with 5% CO_2 at 37°C for 2 weeks. The colonies were then fixed with 4% methanol (1 ml per well) for 15 min and stained with crystal violet for 30 min at room temperature. After photograph, discoloration was performed with 10% acetic acid, and cells were measured absorbance at 550 nm.

Cell Cycle Assay

Transfected cells were digested, and cell suspension was obtained after centrifuging. Then, cells were washed two to three times with PBS, and we adjusted the number of cells to 1×10^6 cells/ml, 400 μl PBS was added, the cells were gently resuspended to separate as individual cells, 1.2 ml of pre-cooled 100% ethanol was added, and the cells were placed overnight at 4°C for fixation. PI was excited by a 488-nm argon ion laser and was received by a 630-nm pass filter. The percentage of each cell cycle was analyzed using the PI fluorescence histogram.

Cell Apoptosis Assay

Transfected cells were digested, and cell suspension was obtained after centrifuging. Then, cells were washed two to three times with PBS, 500-μl binding buffer was added, then the cells were gently resuspended to separate into individual cells, followed by staining with 5-μl Annexin V-APC and 5-μl PI solution for 10 min at room temperature and in dark place. The apoptotic cells were measured by the flow cytometer.

Statistical Analysis

Kaplan-Meier survival curves were generated and compared using the log-rank test. Wilcoxon rank test (nonnormally distributed variables), t test (normally distributed variables), and one-way analysis of variance were used to analyze the expression difference of HOXA5 in different clinical factors, including WHO grades, GBM subtypes, and treatment outcome. The Pearson correlation was applied to evaluate the linear relationship between gene expression levels. Statistical analyses of the colony-forming assay and the CCK8 assay were carried out by GraphPad Prism (version 8.0). The Kolmogorov–Smirnov test was used to assess the normal distribution of data. All tests were two-sided, and P values <0.05 were considered to be statistically significant.

RESULTS

HOXA5 Expression Is Elevated in Aggressive Gliomas

The mRNA expression levels of HOXA5 in different WHO grade gliomas were evaluated using expression data from publicly available databases: TCGA, n = 672; CGGA, n = 1013. HOXA5 was observed to be significantly up-regulated in GBM (WHO grade IV) compared with low-grade glioma (LGG) samples (WHO grade III and WHO grade II) in the TCGA and CGGA cohorts (P <0.001, respectively; **Figure 1A**). The expression of HOXA5 was also higher in WHO grade III than WHO grade II cases in the TCGA and CGGA cohorts (P <0.001, respectively; **Figure 1A**). The HOXA5 levels in common cancer types other than gliomas were further evaluated (P <0.001, respectively; **Figure 1B**). We also evaluated the expression levels of HOXA5 in different age groups in pan-glioma analysis in TCGA and CGGA data sets, and in GBM patients in TCGA microarray data set, where patients older than 45 years have higher expression of HOXA5 (P <0.001, respectively; **Figure 1C**). HOXA5 was upregulated in the IDH mutant gliomas in TCGA data set, in the IDH mutant GBM in TCGA microarray data set, and in both the IDH mutant gliomas and GBM alone in CGGA data set (P <0.001, respectively; **Figure 1D**). Furthermore, HOXA5 was upregulated in the 1p19q codeletion in pan-glioma analysis in both TCGA and CGGA data sets (P <0.001, respectively; **Figure 1E**). Additionally, HOXA5 was upregulated in the unmethylated gliomas in TCGA data set (P <0.001; **Figure 1F**).

Inter-Tumor and Intra-Tumor Heterogeneous Characteristics of HOXA5 in Gliomas

Human gliomas have been molecularly categorized into distinct sub-classes: classical (CL), mesenchymal (MES), proneural (PN), and neural (NE). CL and MES subtypes showed more aggressive growth pattern than PN or NE subtypes (21). We subsequently investigated the inter-tumor heterogeneity of HOXA5 among different molecular subtypes based on the VERHAAK 2010 classification scheme (22). HOXA5 was upregulated in CL and ME subtypes by comparing with NE and PN subtypes in pan-glioma analysis in TCGA data set, where CL subtype had the highest expression of HOXA5 (P <0.001; **Figure 2A**). Receiver operating characteristic (ROC) curve further indicated that HOXA5 might serve as a predictor for CL and MES subtypes in pan-gliomas analysis (AUC value = 0.898, P <0.001; **Figure 2B**). Based on the Ivy Glioblastoma Atlas Project data, HOXA5 was found to be abundant in peri-necrotic zones, pseudopalisading cells around necrosis and cellular tumor compared with other pathological areas (P <0.001; **Figure 2C**). Furthermore, the different expression level of HOXA5 in glioma in regard to histology was shown in **Figure 2D**. HOXA5 was also highly expressed in primary glioma (P <0.001, respectively; **Figure 2E**), whereas the analysis for first-course treatment outcome showed that progressive disease was correlated with higher expression of HOXA5 (P <0.001, respectively; **Figure 2F**).

HOXA5 Expression Is Associated With Poor Survival in Glioma Patients

We next assessed the prognostic value of HOXA5 expression in human gliomas using ROC curve analysis and Kaplan-Meier analysis. The ROC curve analysis showed the prognostic value of HOXA5 in survival in TCGA and CGGA cohorts (3-year AUC value = 0.848, 5-year AUC value = 0.813; 3-year AUC value = 0.774, 5-year AUC value = 0.778, respectively; **Figure 2G**). Kaplan-Meier survival curves were generated based on median

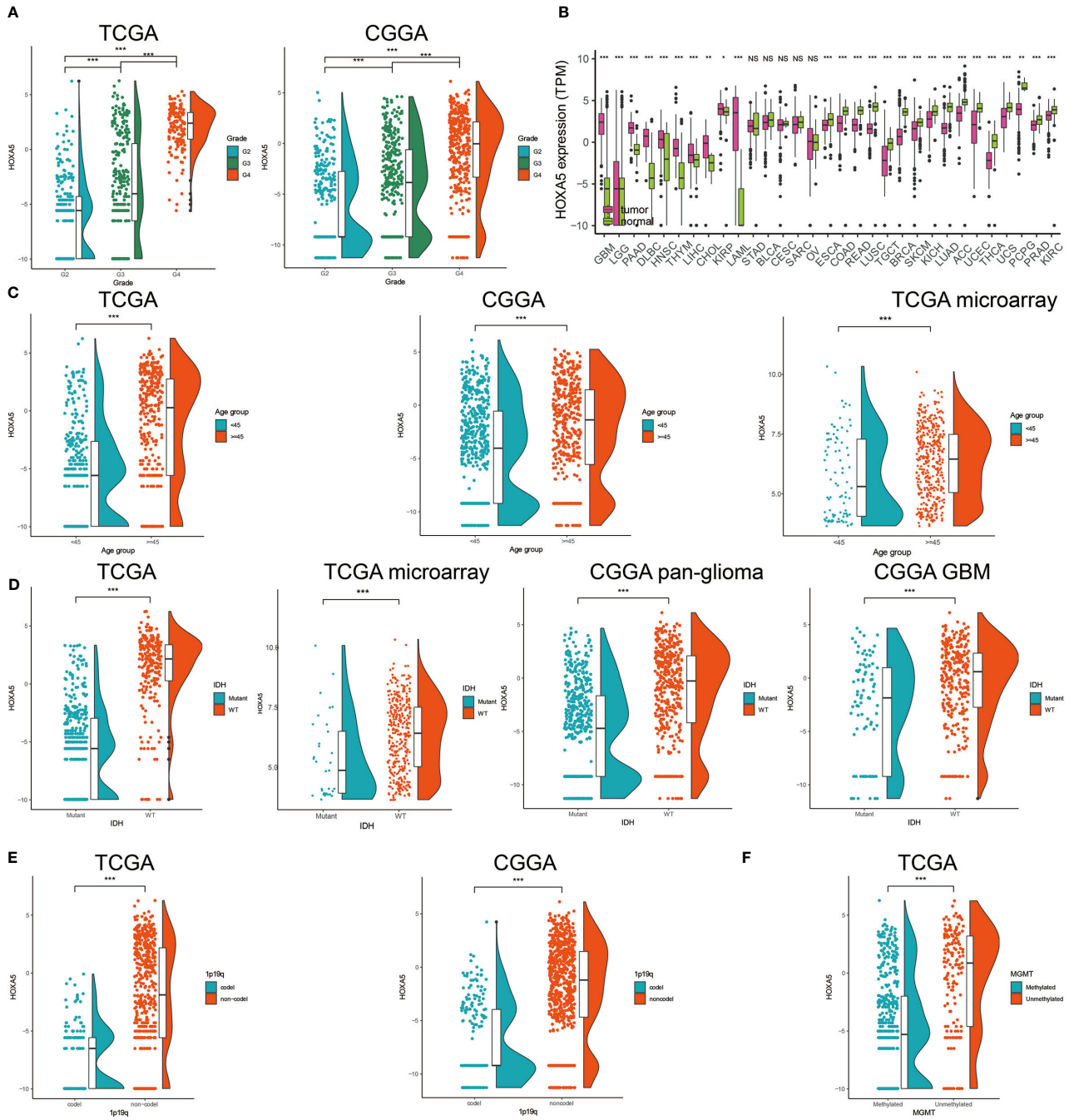

FIGURE 1 | **(A)** Analysis of HOXA5 mRNA levels (log2) in WHO grades II to IV gliomas from TCGA and CGGA. **(B)** Analysis of HOXA5 mRNA levels (log2) in various cancer types. **(C)** The expression level of HOXA5 in different age groups in pan-glioma analysis in TCGA and CGGA data sets, and in GBM patients in TCGA microarray data set. **(D)** HOXA5 was upregulated in the IDH mutant gliomas in TCGA data set, in the IDH mutant GBM in TCGA microarray data set and in both the IDH mutant gliomas and GBM alone in CGGA data set. **(E)** HOXA5 was upregulated in the 1p19q codeletion in pan-glioma analysis in both TCGA and CGGA data sets. **(F)** HOXA5 was upregulated in the methylated gliomas in TCGA data set. NS, Not Statistically Significant; *P < 0.05; **P < 0.01; ***P < 0.001.

values of HOXA5 expression in gliomas. In both TCGA and CGGA data sets, $HOXA5^{high}$ patients exhibited significantly shorter overall survival (OS), disease-specific survival (DSS), progression free interval (PFI) than $HOXA5^{low}$ patients in pan-glioma analysis, (P <0.001, respectively; **Figure 3A**, **Figure S1A**). In addition, $HOXA5^{high}$ patients exhibited significantly shorter OS, DSS, PFI compared with $HOXA5^{low}$ patients in LGG alone in TCGA data set (P <0.001, respectively; **Figure 3B**). Poor

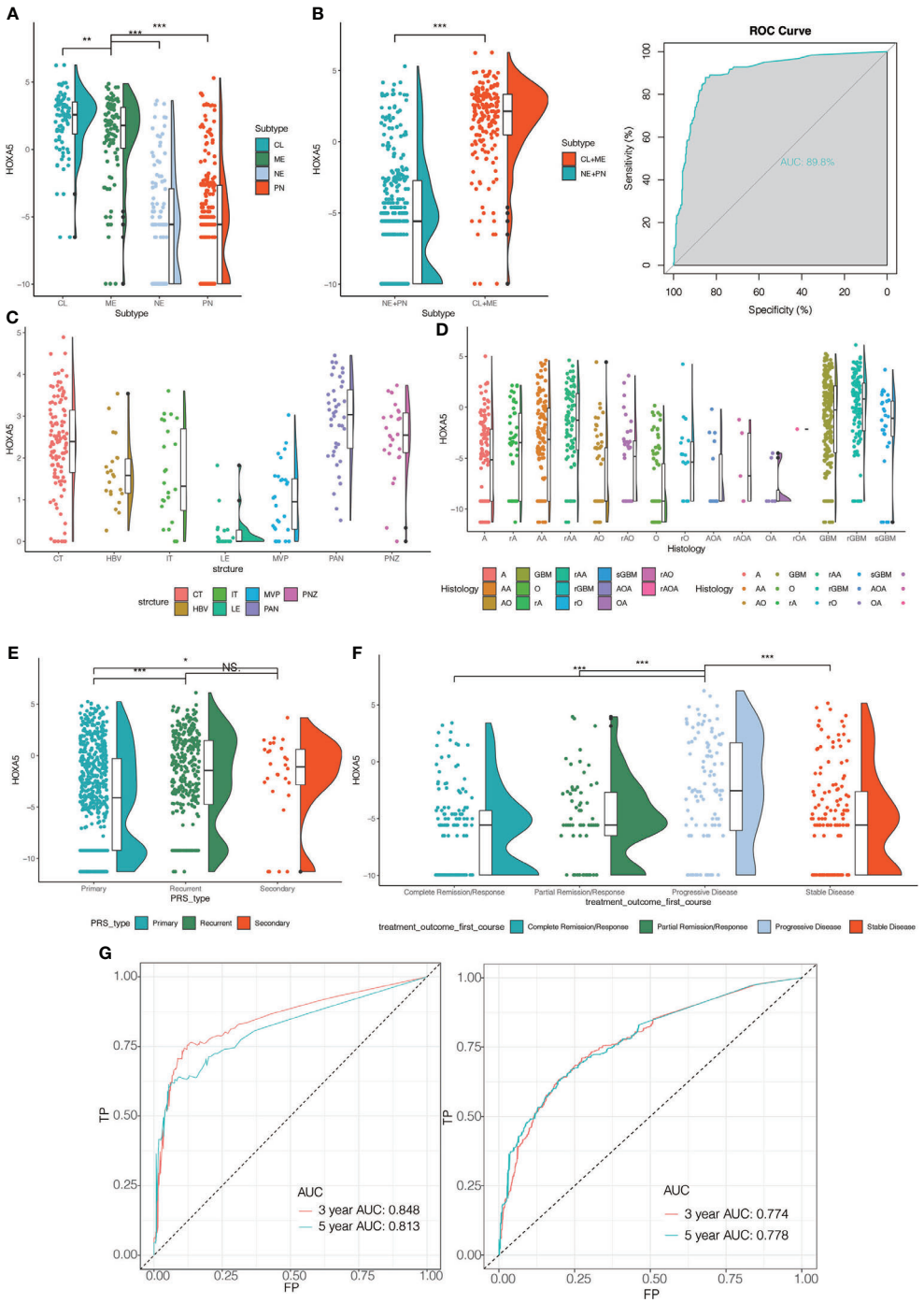

FIGURE 2 | **(A)** The HOXA5 expression pattern in the TCGA molecular subtype in pan-glioma analysis. **(B)** HOXA5 was upregulated in CL and ME subtypes by comparing to NE and PN subtypes in pan-glioma analysis in TCGA data set. Receiver operating characteristic (ROC) curve to assess sensitivity and specificity of HOXA5 expression as a diagnostic biomarker for the ME and CL molecular subtypes in gliomas. **(C)** Intra-tumor analysis of HOXA5 expression using IVY GBM RNA-seq data. Anatomic structures analyzed are the following: LE (leading edge), IT (infiltrating tumor), CT (cellular tumor), PAN (pseudopalisading cells around necrosis), PNZ (perinecrotic zone), MVP (microvascular proliferation), and HBV (hyperplastic blood vessels). **(D)** The expression levels of HOXA5 based on the histopathologic classification. **(E)** The expression level of HOXA5 in primary, recurrent, secondary glioma types. **(F)** The expression level of HOXA5 in different first-course treatment outcomes. **(G)** ROC curve indicating sensitivity and specificity of HOXA5 expression as a diagnostic biomarker for 3- and 5-year survivals in pan-glioma analysis in TCGA and CGGA data sets. A, low-grade astrocytoma; AA, anaplastic astrocytoma; AO, anaplastic oligodendroglioma; GBM, glioblastoma; O, oligodendroglioma; rA, recurrent low-grade astrocytoma; rAA, recurrent anaplastic astrocytoma; rGBM, recurrent glioblastoma; rO, recurrent oligodendroglioma; sGBM, secondary glioblastoma; AOA, anaplastic oligoastrocytoma; OA, oligoastrocytoma. NS, Not Statistically Significant; *P < 0.05; **P < 0.01; ***P < 0.001.

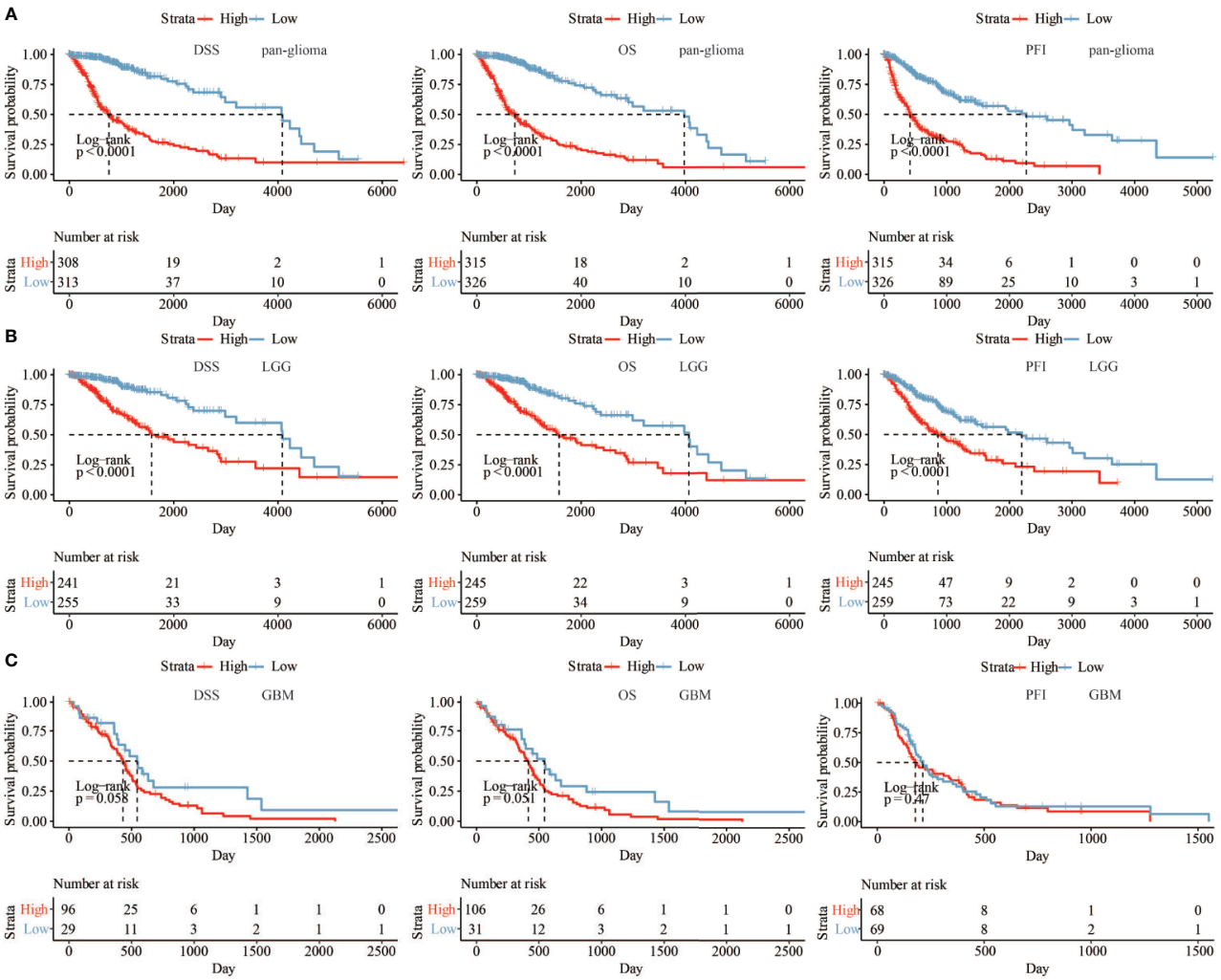

FIGURE 3 | **(A)** The DSS, OS, and PFI survival probabilities of patients in pan-glioma analysis in TCGA data set. **(B)** The DSS, OS, and PFI survival probabilities of LGG patients in TCGA data set. **(C)** The DSS, OS, and PFI survival probabilities of GBM patients in TCGA data set.

OS, DSS, PFI was also associated with high expression of HOXA5 in GBM alone in TCGA data set (P <0.001, respectively; **Figure 3C**). The DSS, OS, and PFI survival probabilities of GBM patients were further testified in the TCGA microarray data set (P <0.001, respectively; **Figure 4A**), in which HOXA5 was correlated with poor survival. Further, HOXA5 predicted worse OS in GSE108474 data set (**Figure 4B**). In TCGA microarray data set, HOXA5 had the highest expression in GBM patients without IDH mutation (P <0.001, respectively; **Figure 4C**), in GBM patients without radiotherapy (P <0.001, respectively; **Figure 4D**), and in GBM patients without chemotherapy (P <0.001, respectively; **Figure 4E**). Similar results were obtained in CGGA data set (P <0.001, respectively; **Figures S1F, S1G, S1H**). In addition, in pan-glioma analysis in TCGA microarray data set, HOXA5 also had the highest expression in patients without IDH mutation (P <0.001, respectively; **Figure 4F**), in patients without radiotherapy (P <0.001, respectively; **Figure 4G**). The results were further confirmed in CGGA data set (P <0.001, respectively; **Figures S1B–D**). Patients without 1p19q codeletion also had the highest expression of HOXA5 in pan-glioma analysis and LGG alone in TCGA microarray data set (P <0.001, respectively; **Figures 4H, I**). Similar results were obtained in pan-glioma analysis and LGG alone in CGGA data set (P <0.001, respectively; **Figures S1E, I**).

HOXA5 Expression Levels Are Associated With Distinct Genomic Alterations

As for the 15 methylation probes designed for HOXA5 from Infinium Human Methylation450 BeadChip, the mean value of methylation probes exhibited negative association with expression of HOXA5 (Pearson test, R = −0.61, P < 2.2 × 10−16). As the IDH mutation exerted great influence on the methylation of the whole genome, we separately analyzed the relationship between HOXA5 and methylation status for IDH-wild and IDH-mutant gliomas.

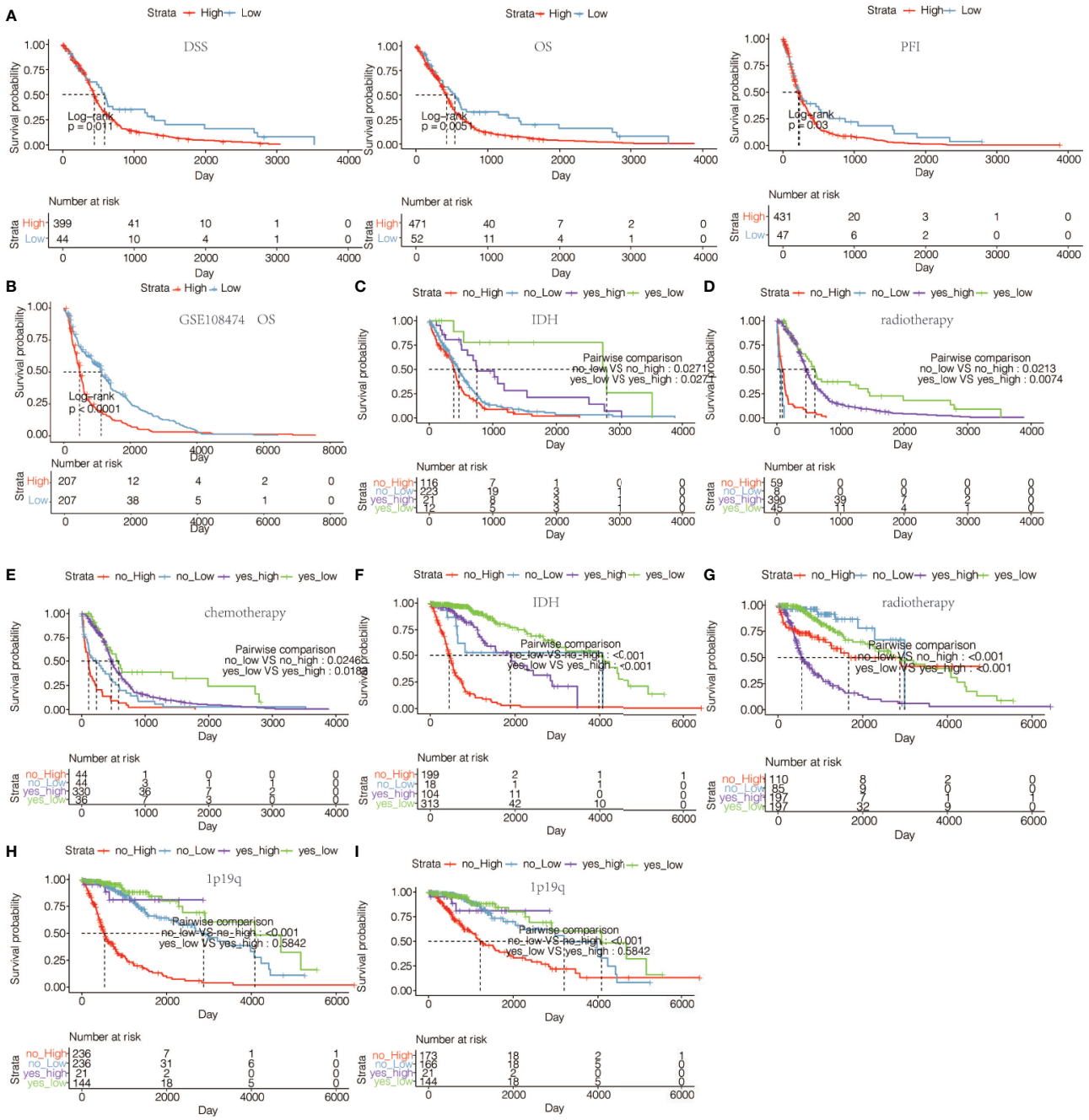

FIGURE 4 | **(A)** The DSS, OS, and PFI survival probabilities of GBM patients in TCGA microarray data set. **(B)** The OS survival probability of glioma patients from GSE108474 data set. **(C)** The OS survival probability of GBM patients without or with IDH mutation with high or low expression of HOXA5 in TCGA microarray data set. **(D)** The OS survival probability of GBM patients without or with radiotherapy with high or low expression of HOXA5 in TCGA microarray data set. **(E)** The OS in GBM patients without or with chemotherapy with high or low expression of HOXA5 in TCGA microarray data set. **(F)** The OS survival probability of patients without or with IDH mutation with high or low expression of HOXA5 in pan-glioma analysis in TCGA data set. **(G)** The OS survival probability of patients without or with radiotherapy with high or low expression of HOXA5 in pan-glioma analysis in TCGA data set. **(H)** The OS survival probability of patients without or with 1p19q codeletion with high or low expression of HOXA5 in pan-glioma analysis in TCGA data set. **(I)** The OS in LGG patients without or with 1p19q codeletion with high or low expression of HOXA5 in TCGA data set.

As shown in **Figure 5A**, in IDH-wild gliomas, methylation was much lower than that of IDH-mutant tumors, as expected (Student's t test, $P = 1.8 \times 10^{-6}$).

To determine whether HOXA5 expression levels were associated with specific genomic characteristics in gliomas, we performed copy number variation (CNV) and somatic mutation

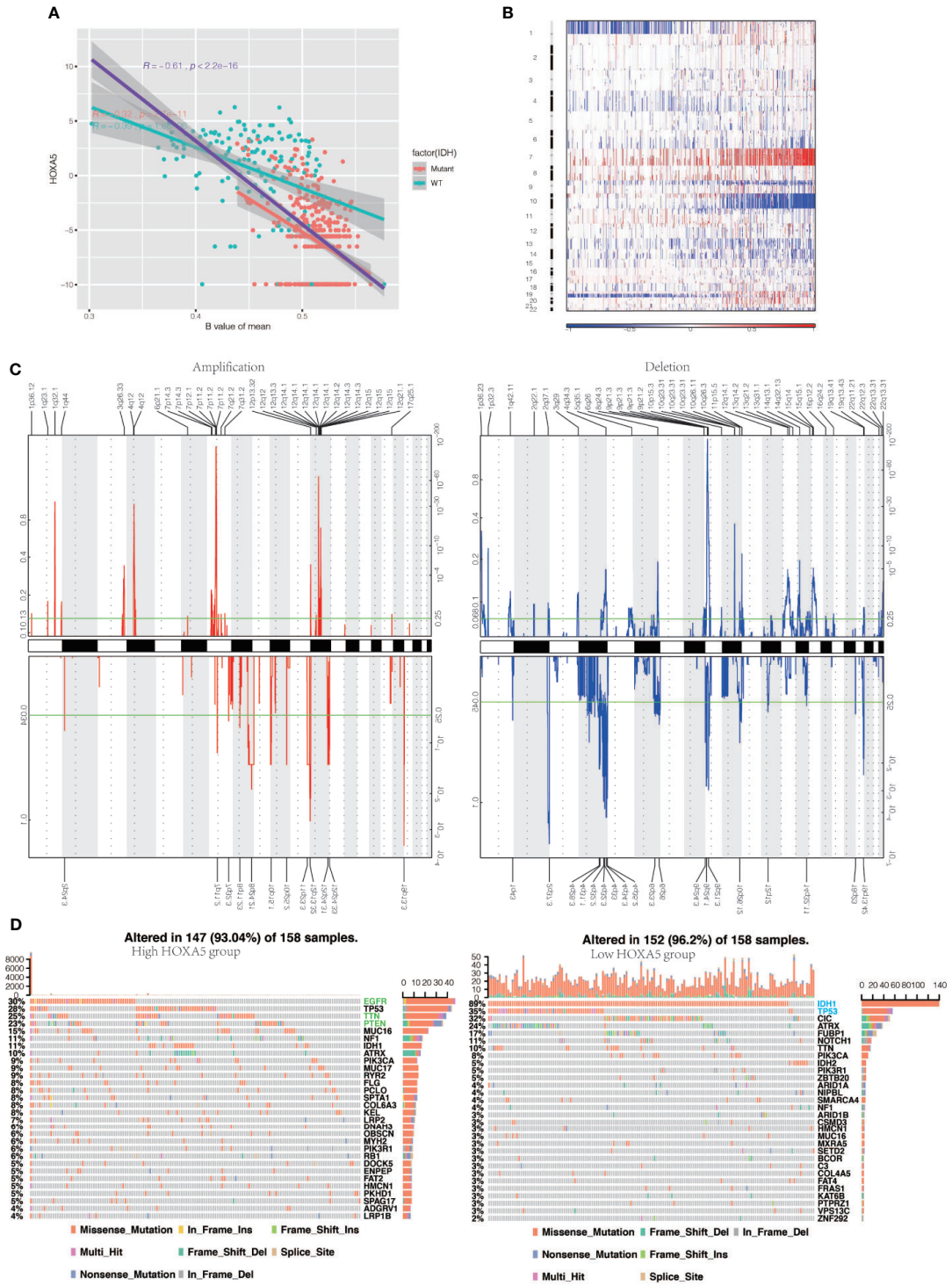

FIGURE 5 | HOXA5 high or low expression is associated with distinct genomic alterations. **(A)** Relationship between HOXA5 and methylation status at promoter region in the cancer genome atlas (TCGA) gliomas samples. The orange dots indicate IDH-mutant samples, and cyan dots indicate IDH wild-type samples, respectively. The purple line indicates linear regression between HOXA5 expression and methylation. The orange line and cyan line indicate linear regression between HOXA5 expression and methylation in IDH-mutant samples and IDH wild-type samples, respectively. **(B)** Overall copy number variation (CNV) profile according to high *vs* low HOXA5 expression. Blue (deletion); red (amplification). **(C)** Frequency of specific changes based on HOXA5low (lower row) and HOXA5high (upper row) groups. The Y-axis represents the frequency of chromosomal deletion (blue) or amplification (red). **(D)** Spectrum of somatic mutations in gliomas from HOXA5low and HOXA5high groups.

analysis using the TCGA data set. A distinct overall CNV profile emerged from the comparison of the HOXA5^{low} (n = 158) *versus* the HOXA5^{high} (n = 158) cluster (**Figures 5B, C**). Amplification of chr7 and deletion of chr10, which are both common genomic events in GBM, frequently occurred in the HOXA5^{high} cluster (**Figure 5B**). Non-deletion of 1p and 19q, a genomic hallmark of oligodendroglioma, also more frequently appeared to be associated with the HOXA5^{high} cluster (**Figure 5C**). In HOXA5^{high} samples, frequently amplified genomic regions included oncogenic driver genes, such as EGFR (7p11.2), IK3C2B (1q32.1), PDGFRA (4q12), and CDK4 (12q14.1), whereas deleted regions contained tumor suppressor genes, including CDKN2A/CDKN2B (9p21.3), PARK7 (1p36.23), and PTEN (10q23.3). In HOXA5^{low} samples, significant amplifications showed peaks in 8q24.21, 12p32.32, and 19p13.3, whereas the frequently deleted genomic regions were 2q37.3, 4q32.3, 9p21.3, and 19q13.43.

Analysis of somatic mutation profiles based on HOXA5 expression levels revealed a high frequency of mutations in EGFR (30%), TP53 (28%), TTN (25%), and PTEN (23%) in the HOXA5^{high} group (n = 158), whereas IDH1 (89%), TP53 (35%), CIC (32%), and ATRX (24%) were more frequently mutated in the HOXA5^{low} group (n = 158; **Figure 5D**).

Potential Mechanism of HOXA5 in Regulating the Progression of Gliomas

To elucidate whether HOXA5 could play a role in promoting gliomas occurrence, GSVA analysis was performed. HOXA5 was found to be associated with regulation of DNA damage response signal transduction by p53 class mediator, signal transduction by p53 class mediator, nucleotide excision repair DNA gap filling, DNA synthesis involved in DNA repair, DNA damage response detection of DNA damage, signal transduction in response to DNA damage, mismatch repair, and base excision repair in TCGA and CGGA data sets (**Figure 6A**, **Figure S2A**). The correlation analysis between HOXA5 and these GO pathways is shown in **Figure 6B**. As the threshold was set as logFC > 2 and adjust P <0.01, a total number of 3,446 differentially expressed genes (DEGs) were detected between high expression of HOXA5 sample and low expression of HOXA5 sample (**Figure 6C**). We paid special attention to two pathways, DNA damage response signal transduction by p53 class mediator and signal transduction by p53 class mediator, in which the GO analysis revealed changes in gene sets related to these two pathways in patients with a higher expression of HOXA5 (**Figures 6D, E**). We further investigated whether HOXA5 might have a role in DNA damage response and p53 signal transduction in gliomas using GSEA analysis in TCGA and CGGA data sets (**Figure 6F**, **Figure S2B**). In KEGG pathway analysis, HOXA5 was found to be associated with mismatch repair, DNA replication, p53 signaling pathway, and base excision repair in TCGA and CGGA data sets (**Figures 7A, B**). The correlation analysis between HOXA5 and KEGG pathways in TCGA and CGGA data sets is shown in **Figure S2C** and **Figure S2D**, respectively. We also investigated the role that HOXA5 might play in mismatch repair and p53 signal transduction in gliomas using GSEA analysis in TCGA and CGGA data sets (**Figures 7C, D**). In HALLMARK pathway analysis, HOXA5 was found to be associated with g2m checkpoint and p53 pathway in TCGA and CGGA data sets (**Figures 7E, F**), in which the correlation analysis is shown in **Figure S2E** and **Figure S2F**, respectively. These results all suggested that HOXA5 was associated with oncogenic processes.

HOXA5 Affect Glioblastoma Cell Proliferation, Viability, and Apoptosis

To further investigate the role that HOXA5 plays in the proliferation of GBM, colony-forming assay, CCK8 assay, and cell cycle analyses were performed. Western blot results verified the silence of HOXA5 by siRNA (**Figures 8A, B**). The cell colony forming assay (**Figures 8C, D**) revealed the remarkable suppression of cell clonality of GBM after silencing HOXA5 in U87 cell line and in U251 cell line (**Figure 8E**). The CCK8 assay revealed that the cells proliferation ability is inhibited by silencing HOXA5 (**Figure 8F**). Cell cycle analysis suggested that cells were blocked at the G2/M phase after silencing HOXA5 (**Figures 8G, H**).

The potential role of HOXA5 in the apoptosis of GBM was also explored. The analysis of flow cytometry described that down-regulation of HOXA5 remarkably enhanced apoptosis in U87 cell line and U251 cell line (**Figures 9A, B**).

DISCUSSION

Glioma is a central nervous system–derived tumor with highly aggressive growth pattern, treatment resistance, and poor prognosis. Nowadays, strategies show their limitations on improving patient's survival outcome, including surgery, chemotherapy, and radiotherapy (23). To reveal the mechanism concealed behind its aggressive growth pattern, we identify HOXA5 as prognostic-related genes through regulating cell proliferation. HOXA5, locate on chromosome 7, is involved in tissue development and organogenesis. Multiple studies reported that high HOXA5 expression was a promotor in tumor progression, including esophageal cancer (24), breast cancer (12), gastric cancer (25), and renal cancer (26). In this study, high HOXA5 expression is associated with malignant clinical features like high-grade glioma or IDH wildtype glioma, worse clinical treatment outcome, and strong cells proliferative ability. We also noticed genes like EGFR, PDGFRA were amplified in HOXA5^{high} samples; and genes like CDKN2A/CDKN2B, PARK7 were down-regulated. Those genes were also identified as glioma promotor-related factors (27–33). Besides, tumor cells cycle was arrested at G2/M phase when inhibited HOXA5 expression implying its role in mediating cell cycle. Along with results from other studies that HOXA5 modulated cell cycle in Jurkat cells and hematopoietic stem cells (34), cervical cancer, mesenchymal stem cells (35), and leukemia cells (36). Further, HOXA5 was found to decrease the apoptosis rates of GBM cells. Together, those evidences supported that HOXA5 promoted glioma progression through affecting cell cycle, cell proliferation, and cell apoptosis.

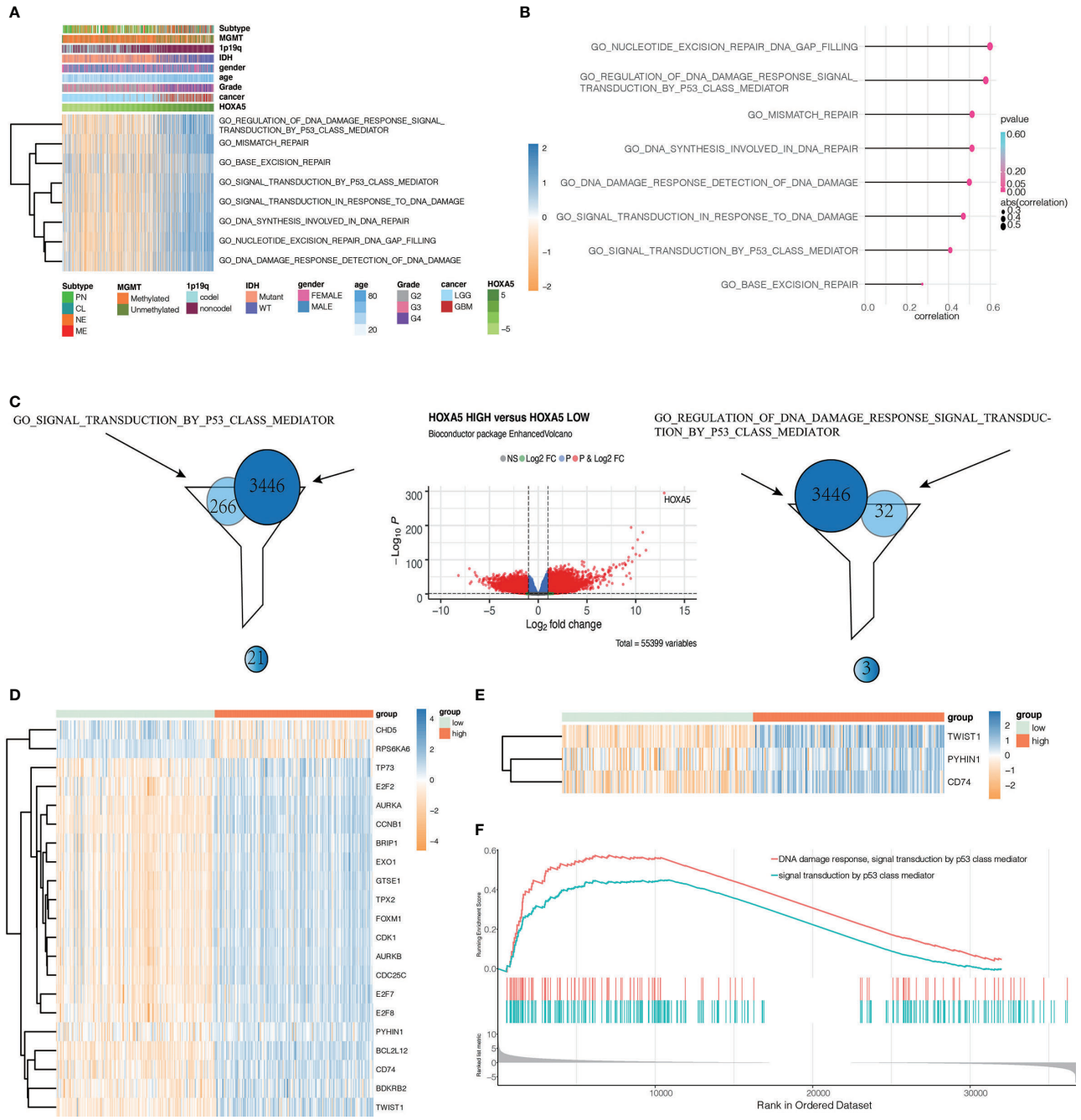

FIGURE 6 | Identifying differentially expressed genes between HOXA5 high and HOXA5 low patients. **(A)** Heatmap of HOXA5-related oncogenic process in pan-glioma analysis in TCGA data set. **(B)** Correlation analysis between HOXA5 and GO pathways. **(C)** Volcano plot of differential gene profiles between HOXA5 high and HOXA5 low groups. **(D)** Genes involved in both regulation of DNA damage response signal transduction by p53 class mediator gene set and DEGs. **(E)** Genes involved in both signal transduction by p53 class mediator gene set and DEGs. **(F)** GSEA plots for enrichment of DNA damage response and p53 signal transduction in HOXA5 high and HOXA5 low samples in the TCGA data set.

The product of HOXA5 is a DNA-binding transcription factor and able to regulate multiple gene expression, including TP53. Previous study reported that HOXA5 can bind to the promoter of TP53 to activate its transcription and affect corresponded pathways (16, 37). HOXA5 affected tumor progression through influencing TP53 homeostasis in breast cancer (10, 38), TP53-dependent apoptosis in liposarcomas (39), and TP53-mediated cell proliferation in cervical cancer

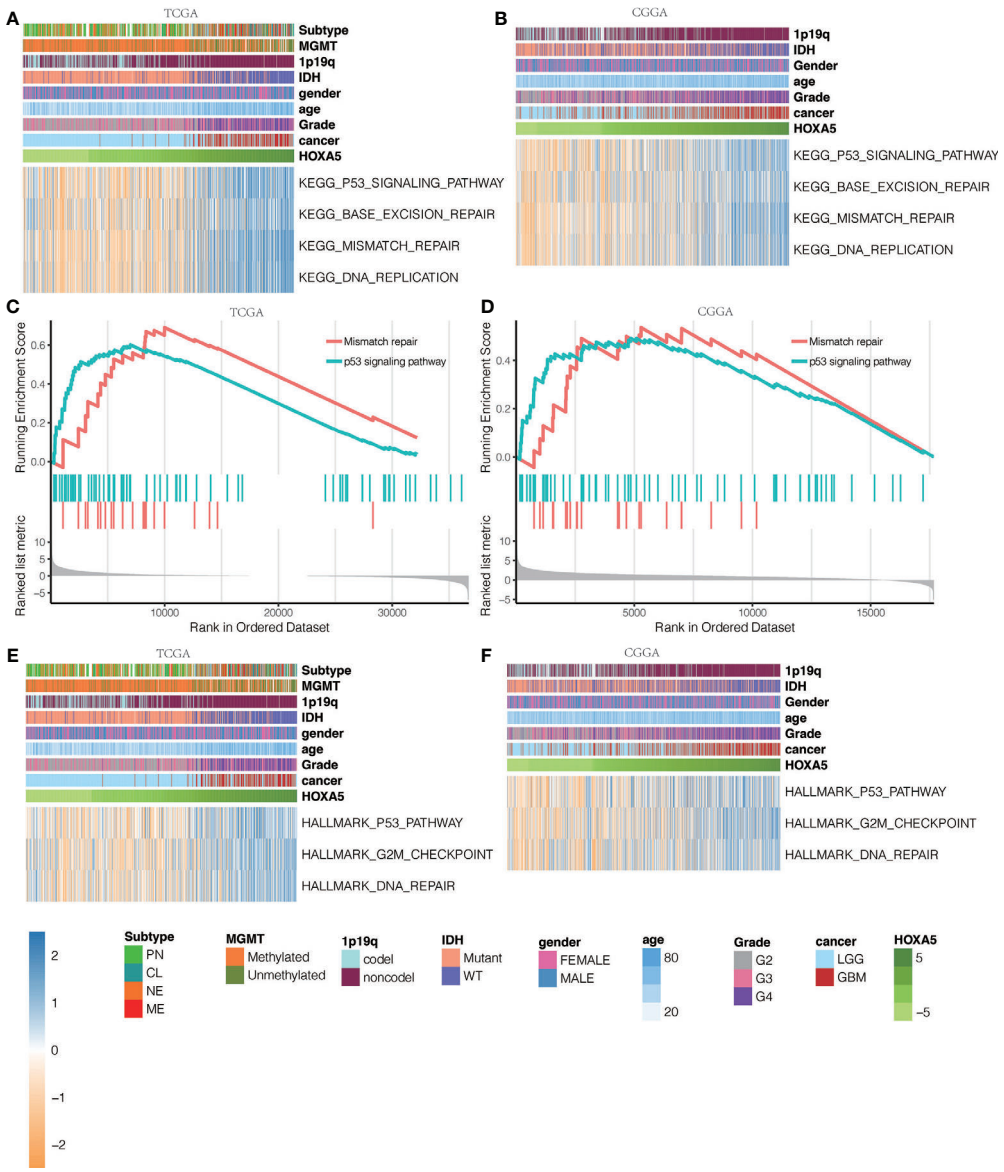

FIGURE 7 | KEGG pathway analysis for mutations based on HOXA5 expression levels in **(A)** TCGA data set and **(B)** CGGA data set. GSEA plots for enrichment of mismatch repair and p53 signaling pathway in HOXA5 high and HOXA5 low samples in **(C)** TCGA data set and **(D)** CGGA data set. HALLMARK pathway analysis for mutations based on HOXA5 expression levels in **(E)** TCGA data set and **(F)** CGGA data set.

(16). Therefore, HOXA5 can affect TP53-mediated pathway by regulating TP53 expression.

Next, we investigated biofunction difference between $HOXA5^{high}$ and $HOXA5^{low}$ samples. Results suggested that DNA repair-related pathways were activated in $HOXA5^{high}$ samples. Because DNA damage repair is also associated tumor resistance to treatment, such as chemo- or radio-therapy, HOXA5 might also contribute to tumor resistance to treatments (40, 41). In this work, survival analysis based on radio- and chemo-therapy suggested that high HOXA5 samples showed worse clinical outcome than low HOXA5 samples in this study. Besides, previous study confirmed that HOXA5 can affect glioblastoma cells sensitivity to radiation therapy (9). Collectively, HOXA5 may target TP53-mediated DNA damage repair to modulate tumor resistance to treatments (42–44). Taken together, HOXA5 may affect glioma response to chemo- or radio-therapy by targeting TP53.

Other family members in the HOX family are also involved in tumor progression, including leukemia, breast cancer, lung cancer and so on (45, 46). For instance, abnormal expressions of HOXA6, HOXA7, HOXA9, HOXA13, HOXB13, HOXD4, HOXD9, HOXD10, and HOXD13 were noticed in tumor tissue

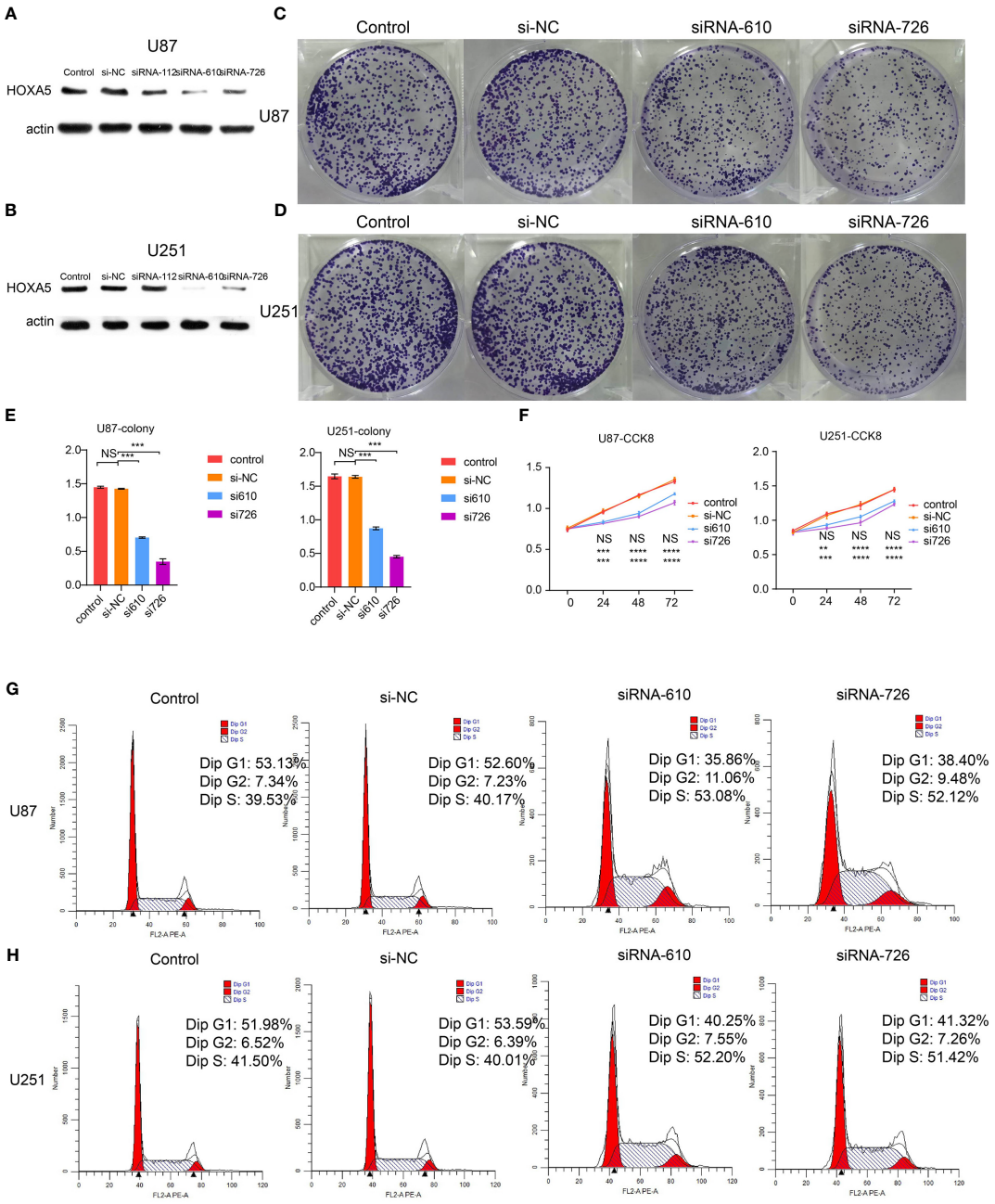

FIGURE 8 | **(A)** The Western blotting results of HOXA5 expression in U87 cell line. **(B)** The Western blotting results of HOXA5 expression in U251 cell line. **(C)** The colony-forming assay, which supports cell viability, is inhibited by silencing HOXA5 expression in U87 cell line. **(D)** The colony-forming assay, which supports cell viability, is inhibited by silencing HOXA5 expression in U251 cell line. **(E)** Statistical analysis for colony-forming assay. NS, not statistically significant; ***P < 0.001. **(F)** Statistical analysis for CCK8 assay. NS, not statistically significant; **P < 0.01; ***P < 0.001; ****P < 0.0001. **(G)** Cell cycle analysis was performed with PI staining by flow cytometry. Representative flow cytometric profiles (left panel) and percentages of cells at the S phase, G1 phase, and G2 phase in U87 cell line are shown. **(H)** Cell cycle analysis was performed with PI staining by flow cytometry. Representative flow cytometric profiles (left panel) and percentages of cells at the S phase, G1 phase, and G2 phase in U251 cell line are shown.

by comparing with normal tissue (47). Those family members can affect glioma cells viability (48, 49), the stemness of glioma stem cells (50), autophagy (51), invasion ability (52), and tumor sensitivity to therapeutic drugs (53). Collectively, this family showed a close association with glioma progression, which deserves further exploration.

In conclusion, this work proved that high HOXA5 expression positively correlated with glioma malignancy's clinical features

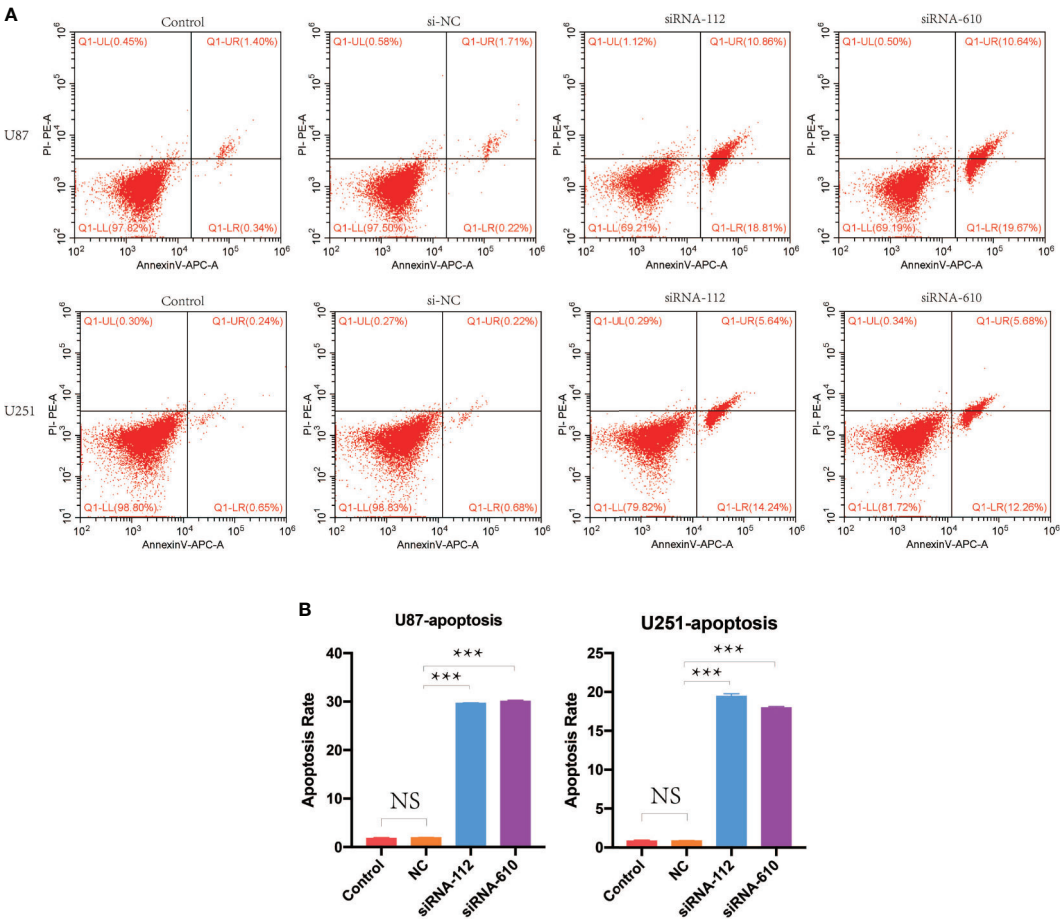

FIGURE 9 | **(A)** Cell apoptosis analysis was performed by flow cytometry. Shown are representative flow cytometric profiles of cells in control group, si-NC group, siRNA-112 group, and siRNA-610 group in U87 and U251 cell lines. **(B)** Statistical analysis for cell apoptosis assay in U87 and U251 cell lines. NS, not statistically significant; ***P < 0.001.

and was associated with an unfavorable survival outcome. Moreover, HOXA5 may affect glioma progression and apoptosis by modulating TP53 expression and corresponding pathways. Critically, HOXA5 can arrest cell cycle at G2/M phase to inhibit tumor cell proliferation.

DATA AVAILABILITY STATEMENT

The original contributions presented in the study are included in the article/**Supplementary Material**. Further inquiries can be directed to the corresponding authors.

AUTHOR CONTRIBUTIONS

FD and PC analyzed the data and performed *in vitro* environments. PB assisted in manuscript writing and revising. WP and QC. designed and supervised the study, and offered funding. All authors contributed to the article and approved the submitted version.

FUNDING

This study was supported by grants from the research projects Hunan Provincial Natural Science Foundation of China (NO. 2018JJ3838), China Postdoctoral Science Foundation (NO. 2018M633002), Hunan Provincial Health Committee Foundation of China (C2019186). Xiangya Hospital Central South University postdoctoral foundation.

SUPPLEMENTARY MATERIAL

The Supplementary Material for this article can be found online at: https://www.frontiersin.org/articles/10.3389/fonc.2021.633430/full#supplementary-material

REFERENCES

1. Zhang H, Wang R, Yu Y, Liu J, Luo T, Fan F. Glioblastoma Treatment Modalities Besides Surgery. *J Cancer* (2019) 10:4793–806. doi: 10.7150/jca.32475
2. Zhang H, Zhou Y, Cui B, Liu Z, Shen H. Novel Insights Into Astrocyte-Mediated Signaling of Proliferation, Invasion and Tumor Immune Microenvironment in Glioblastoma. *BioMed Pharmacother* (2020) 126:110086. doi: 10.1016/j.biopha.2020.110086
3. Zhang H, Chen Z, Wang Z, Dai Z, Hu Z, Zhang X, et al. Correlation Between APOBEC3B Expression and Clinical Characterization in Lower-Grade Gliomas. *Front Oncol* (2021) 11:625838. doi: 10.3389/fonc.2021.625838
4. Zhang N, Dai Z, Wu W, Wang Z, Cao H, Zhang Y, et al. The Predictive Value of Monocytes in Immune Microenvironment and Prognosis of Glioma Patients Based on Machine Learning. *Front Immunol* (2021) 12:656541. doi: 10.3389/fimmu.2021.656541
5. Jeannotte L, Gotti F, Landry-Truchon K. Hoxa5: A Key Player in Development and Disease. *J Dev Biol* (2016) 4(2):13. doi: 10.3390/jdb4020013
6. Cao W, Huang H, Xia T, Liu C, Muhammad S, Sun C. Homeobox A5 Promotes White Adipose Tissue Browning Through Inhibition of the Tenascin C/Toll-Like Receptor 4/Nuclear Factor Kappa B Inflammatory Signaling in Mice. *Front Immunol* (2018) 9:647. doi: 10.3389/fimmu.2018.00647
7. Li J, Ye M, Zhou C. Expression Profile and Prognostic Values of HOXA Family Members in Laryngeal Squamous Cell Cancer. *Front Oncol* (2020) 10:368. doi: 10.3389/fonc.2020.00368
8. Li D, Bai Y, Feng Z, Li W, Yang C, Guo Y, et al. Study of Promoter Methylation Patterns of HOXA2, HOXA5, and HOXA6 and Its Clinicopathological Characteristics in Colorectal Cancer. *Front Oncol* (2019) 9:394. doi: 10.3389/fonc.2019.00394
9. Cimino PJ, Kim Y, Wu HJ, Alexander J, Wirsching HG, Szulzewsky F, et al. Increased HOXA5 Expression Provides a Selective Advantage for Gain of Whole Chromosome 7 in IDH Wild-Type Glioblastoma. *Genes Dev* (2018) 32:512–23. doi: 10.1101/gad.312157.118
10. Stasinopoulos IA, Mironchik Y, Raman A, Wildes F, Winnard P Jr., Raman V. HOXA5-Twist Interaction Alters P53 Homeostasis in Breast Cancer Cells. *J Biol Chem* (2005) 280:2294–9. doi: 10.1074/jbc.M411018200
11. Wang H, Wei H, Wang J, Li L, Chen A, Li Z. MicroRNA-181d-5p-Containing Exosomes Derived From CAFs Promote EMT by Regulating CDX2/HOXA5 in Breast Cancer. *Mol Ther Nucleic Acids* (2020) 19:654–67. doi: 10.1016/j.omtn.2019.11.024
12. Teo WW, Merino VF, Cho S, Korangath P, Liang X, Wu RC, et al. HOXA5 Determines Cell Fate Transition and Impedes Tumor Initiation and Progression in Breast Cancer Through Regulation of E-Cadherin and CD24. *Oncogene* (2016) 35:5539–51. doi: 10.1038/onc.2016.95
13. Chen H, Chung S, Sukumar S. HOXA5-Induced Apoptosis in Breast Cancer Cells is Mediated by Caspases 2 and 8. *Mol Cell Biol* (2004) 24:924–35. doi: 10.1128/MCB.24.2.924-935.2004
14. Wang CC, Su KY, Chen HY, Chang SY, Shen CF, Hsieh CH, et al. HOXA5 Inhibits Metastasis *via* Regulating Cytoskeletal Remodelling and Associates With Prolonged Survival in Non-Small-Cell Lung Carcinoma. *PLoS One* (2015) 10:e0124191. doi: 10.1371/journal.pone.0124191
15. Wang Z, Yu C, Wang H. HOXA5 Inhibits the Proliferation and Induces the Apoptosis of Cervical Cancer Cells *via* Regulation of Protein Kinase B and P27. *Oncol Rep* (2019) 41:1122–30. doi: 10.3892/or.2018.6874
16. Ma HM, Cui N, Zheng PS. HOXA5 Inhibits the Proliferation and Neoplasia of Cervical Cancer Cells *via* Downregulating the Activity of the Wnt/beta-Catenin Pathway and Transactivating TP53. *Cell Death Dis* (2020) 11:420. doi: 10.1038/s41419-020-2629-3
17. Gao XY, Qiao YL, Zhang Y, Wang J, Shen X, Xu CW. Knockdown of MPP8 Suppresses Cell Proliferation *via* Regulation of HOXA5 in Non-Small Cell Lung Cancer Cells. *Cell Mol Biol (Noisy-le-grand)* (2018) 64:27–31. doi: 10.14715/cmb/2018.64.1.6
18. Chang CJ, Chen YL, Hsieh CH, Liu YJ, Yu SL, Chen JJW, et al. HOXA5 and P53 Cooperate to Suppress Lung Cancer Cell Invasion and Serve as Good Prognostic Factors in Non-Small Cell Lung Cancer. *J Cancer* (2017) 8:1071–81. doi: 10.7150/jca.17295
19. Gendronneau G, Lemieux M, Morneau M, Paradis J, Tetu B, Frenette N, et al. Influence of Hoxa5 on P53 Tumorigenic Outcome in Mice. *Am J Pathol* (2010) 176:995–1005. doi: 10.2353/ajpath.2010.090499
20. Chen YQ, Yang TQ, Zhou B, Yang MX, Feng HJ, Wang YL. HOXA5 Overexpression Promotes Osteosarcoma Cell Apoptosis Through the P53 and P38alpha MAPK Pathway. *Gene* (2019) 689:18–23. doi: 10.1016/j.gene.2018.11.081
21. Phillips HS, Kharbanda S, Chen R, Forrest WF, Soriano RH, Wu TD, et al. Molecular Subclasses of High-Grade Glioma Predict Prognosis, Delineate a Pattern of Disease Progression, and Resemble Stages in Neurogenesis. *Cancer Cell* (2006) 9:157–73. doi: 10.1016/j.ccr.2006.02.019
22. Verhaak RG, Hoadley KA, Purdom E, Wang V, Qi Y, Wilkerson MD, et al. Integrated Genomic Analysis Identifies Clinically Relevant Subtypes of Glioblastoma Characterized by Abnormalities in PDGFRA, IDH1, EGFR, and NF1. *Cancer Cell* (2010) 17:98–110. doi: 10.1016/j.ccr.2009.12.020
23. Zhang H, Dai Z, Wu W, Wang Z, Zhang N, Zhang L, et al. Regulatory Mechanisms of Immune Checkpoints PD-L1 and CTLA-4 in Cancer. *J Exp Clin Cancer Res* (2021) 40:184. doi: 10.1186/s13046-021-01987-7
24. Zhang H, Zhao JH, Suo ZM. Knockdown of HOXA5 Inhibits the Tumorigenesis in Esophageal Squamous Cell Cancer. *BioMed Pharmacother* (2017) 86:149–54. doi: 10.1016/j.biopha.2016.12.012
25. Peng X, Zha L, Chen A, Wang Z. HOXA5 Is a Tumor Suppressor Gene That Is Decreased in Gastric Cancer. *Oncol Rep* (2018) 40:1317–29. doi: 10.3892/or.2018.6537
26. Yoo KH, Park YK, Kim HS, Jung WW, Chang SG. Epigenetic Inactivation of HOXA5 and MSH2 Gene in Clear Cell Renal Cell Carcinoma. *Pathol Int* (2010) 60:661–6. doi: 10.1111/j.1440-1827.2010.02578.x
27. Xu H, Zong H, Ma C, Ming X, Shang M, Li K, et al. Epidermal Growth Factor Receptor in Glioblastoma. *Oncol Lett* (2017) 14:512–6. doi: 10.3892/ol.2017.6221
28. Ellis JA, Canoll P, McCormick PC2nd, Feldstein NA, Anderson RC, Angevine PD, et al. Platelet-Derived Growth Factor Receptor (PDGFR) Expression in Primary Spinal Cord Gliomas. *J Neurooncol* (2012) 106:235–42. doi: 10.1007/s11060-011-0666-6
29. Appay R, Dehais C, Maurage CA, Alentorn A, Carpentier C, Colin C, et al. CDKN2A Homozygous Deletion Is a Strong Adverse Prognosis Factor in Diffuse Malignant IDH-Mutant Gliomas. *Neuro Oncol* (2019) 21:1519–28. doi: 10.1093/neuonc/noz124
30. Jin W. Novel Insights Into PARK7 (DJ-1), A Potential Anti-Cancer Therapeutic Target, and Implications for Cancer Progression. *J Clin Med* (2020) 9(5):1256. doi: 10.3390/jcm9051256
31. Zhang H, Fan F, Yu Y, Wang Z, Liu F, Dai Z, et al. Clinical Characterization, Genetic Profiling, and Immune Infiltration of TOX in Diffuse Gliomas. *J Transl Med* (2020) 18:305. doi: 10.1186/s12967-020-02514-6
32. Zhang H, Zhou Y, Cheng Q, Dai Z, Wang Z, Liu F, et al. PDIA3 Correlates With Clinical Malignant Features and Immune Signature in Human Gliomas. *Aging (Albany NY)* (2020) 12:15392–413. doi: 10.18632/aging.103601
33. Zhang H, He J, Dai Z, Wang Z, Liang X, He F, et al. PDIA5 Is Correlated With Immune Infiltration and Predicts Poor Prognosis in Gliomas. *Front Immunol* (2021) 12:628966. doi: 10.3389/fimmu.2021.628966
34. Huang HP, Liu WJ, Guo QL, Bai YQ. Effect of Silencing HOXA5 Gene Expression Using RNA Interference on Cell Cycle and Apoptosis in Jurkat Cells. *Int J Mol Med* (2016) 37:669–78. doi: 10.3892/ijmm.2016.2480
35. Li W, Lin X, Yang H, Cao Y, Zhang C, Fan Z. Depletion of HOXA5 Inhibits the Osteogenic Differentiation and Proliferation Potential of Stem Cells From the Apical Papilla. *Cell Biol Int* (2018) 42:45–52. doi: 10.1002/cbin.10860
36. Gao F, Liu W, Guo Q, Bai Y, Yang H, Chen H. Physcion Blocks Cell Cycle and Induces Apoptosis in Human B Cell Precursor Acute Lymphoblastic Leukemia Cells by Downregulating HOXA5. *BioMed Pharmacother* (2017) 94:850–7. doi: 10.1016/j.biopha.2017.07.149
37. Hou X, Snarski P, Higashi Y, Yoshida T, Jurkevich A, Delafontaine P, et al. Nuclear Complex of Glyceraldehyde-3-Phosphate Dehydrogenase and DNA Repair Enzyme Apurinic/Apyrimidinic Endonuclease I Protect Smooth Muscle Cells Against Oxidant-Induced Cell Death. *FASEB J* (2017) 31:3179–92. doi: 10.1096/fj.201601082R
38. Raman V, Martensen SA, Reisman D, Evron E, Odenwald WF, Jaffee E, et al. Compromised HOXA5 Function Can Limit P53 Expression in Human Breast Tumours. *Nature* (2000) 405:974–8. doi: 10.1038/35016125
39. Lee DH, Forscher C, Di Vizio D, Koeffler HP. Induction of P53-Independent Apoptosis by Ectopic Expression of HOXA5 in Human Liposarcomas. *Sci Rep* (2015) 5:12580. doi: 10.1038/srep12580
40. Yamashiro K, Nakao K, Ohba S, Hirose Y. Human Glioma Cells Acquire Temozolomide Resistance After Repeated Drug Exposure *Via* DNA

Mismatch Repair Dysfunction. *Anticancer Res* (2020) 40:1315–23. doi: 10.21873/anticanres.14073
41. Nunez FJ, Mendez FM, Kadiyala P, Alghamri MS, Savelieff MG, Garcia-Fabiani MB, et al. IDH1-R132H Acts as a Tumor Suppressor in Glioma *via* Epigenetic Up-Regulation of the DNA Damage Response. *Sci Transl Med* (2019) 11(479):eaaq1427. doi: 10.1126/scitranslmed.aaq1427
42. Wang X, Chen JX, Liu JP, You C, Liu YH, Mao Q. Gain of Function of Mutant TP53 in Glioblastoma: Prognosis and Response to Temozolomide. *Ann Surg Oncol* (2014) 21:1337–44. doi: 10.1245/s10434-013-3380-0
43. Boyarskikh UA, Gulyaeva LF, Avdalyan AM, Kechin AA, Khrapov EA, Lazareva DG, et al. Spectrum of TP53 Mutations in BRCA1/2 Associated High-Grade Serous Ovarian Cancer. *Front Oncol* (2020) 10:1103. doi: 10.3389/fonc.2020.01103
44. Jovanovic KK, Escure G, Demonchy J, Willaume A, Van de Wyngaert Z, Farhat M, et al. Deregulation and Targeting of TP53 Pathway in Multiple Myeloma. *Front Oncol* (2018) 8:665. doi: 10.3389/fonc.2018.00665
45. Goncalves CS, Le Boiteux E, Arnaud P, Costa BM. HOX Gene Cluster (De) Regulation in Brain: From Neurodevelopment to Malignant Glial Tumours. *Cell Mol Life Sci* (2020) 77:3797–821. doi: 10.1007/s00018-020-03508-9
46. Li B, Huang Q, Wei GH. The Role of HOX Transcription Factors in Cancer Predisposition and Progression. *Cancers (Basel)* (2019) 11(4):528. doi: 10.3390/cancers11040528
47. Abdel-Fattah R, Xiao A, Bomgardner D, Pease CS, Lopes MB, Hussaini IM. Differential Expression of HOX Genes in Neoplastic and Non-Neoplastic Human Astrocytes. *J Pathol* (2006) 209:15–24. doi: 10.1002/path.1939
48. Duan X, Liu D, Wang Y, Chen Z. Circular RNA hsa_circ_0074362 Promotes Glioma Cell Proliferation, Migration, and Invasion by Attenuating the Inhibition of miR-1236-3p on HOXB7 Expression. *DNA Cell Biol* (2018) 37:917–24. doi: 10.1089/dna.2018.4311
49. Xu K, Qiu C, Pei H, Mehmood MA, Wang H, Li L, et al. Homeobox B3 Promotes Tumor Cell Proliferation and Invasion in Glioblastoma. *Oncol Lett* (2018) 15:3712–8. doi: 10.3892/ol.2018.7750
50. Tabuse M, Ohta S, Ohashi Y, Fukaya R, Misawa A, Yoshida K, et al. Functional Analysis of HOXD9 in Human Gliomas and Glioma Cancer Stem Cells. *Mol Cancer* (2011) 10:60. doi: 10.1186/1476-4598-10-60
51. Xuan F, Huang M, Liu W, Ding H, Yang L, Cui H. Homeobox C9 Suppresses Beclin1-Mediated Autophagy in Glioblastoma by Directly Inhibiting the Transcription of Death-Associated Protein Kinase 1. *Neuro Oncol* (2016) 18:819–29. doi: 10.1093/neuonc/nov281
52. Tan Z, Chen K, Wu W, Zhou Y, Zhu J, Wu G, et al. Overexpression of HOXC10 Promotes Angiogenesis in Human Glioma *via* Interaction With PRMT5 and Upregulation of VEGFA Expression. *Theranostics* (2018) 8:5143–58. doi: 10.7150/thno.27310
53. Pojo M, Goncalves CS, Xavier-Magalhaes A, Oliveira AI, Goncalves T, Correia S, et al. A Transcriptomic Signature Mediated by HOXA9 Promotes Human Glioblastoma Initiation, Aggressiveness and Resistance to Temozolomide. *Oncotarget* (2015) 6:7657–74. doi: 10.18632/oncotarget.3150

Conflict of Interest: The authors declare that the research was conducted in the absence of any commercial or financial relationships that could be construed as a potential conflict of interest.

Publisher's Note: All claims expressed in this article are solely those of the authors and do not necessarily represent those of their affiliated organizations, or those of the publisher, the editors and the reviewers. Any product that may be evaluated in this article, or claim that may be made by its manufacturer, is not guaranteed or endorsed by the publisher.

Copyright © 2021 Ding, Chen, Bie, Piao and Cheng. This is an open-access article distributed under the terms of the Creative Commons Attribution License (CC BY). The use, distribution or reproduction in other forums is permitted, provided the original author(s) and the copyright owner(s) are credited and that the original publication in this journal is cited, in accordance with accepted academic practice. No use, distribution or reproduction is permitted which does not comply with these terms.

frontiers in Oncology

ORIGINAL RESEARCH
published: 27 August 2021
doi: 10.3389/fonc.2021.667847

A Retrospective Study of Brain Metastases From Solid Malignancies: The Effect of Immune Checkpoint Inhibitors

Wei Du[1], *Cristian Sirbu*[1], *B. Daniel Lucas Jr.*[1], *Steven J. Jubelirer*[2], *Ahmed Khalid*[2] *and Lin Mei*[2*]

[1] Charleston Area Medical Center (CAMC) Health Education and Research Institute, Charleston, WV, United States,
[2] CAMC Cancer Center, Charleston, WV, United States

OPEN ACCESS

Edited by:
Terrance Johns,
University of Western Australia, Australia

Reviewed by:
Alessia Pellerino,
University Hospital of the City of Health and Science of Turin, Italy
Zhijian Chen,
Virginia Commonwealth University, United States
Sen Sheng,
University of Arkansas for Medical Sciences, United States

***Correspondence:**
Lin Mei
lin.mei@camc.org

Specialty section:
This article was submitted to Neuro-Oncology and Neurosurgical Oncology, a section of the journal Frontiers in Oncology

Received: 14 February 2021
Accepted: 06 August 2021
Published: 27 August 2021

Citation:
Du W, Sirbu C, Lucas BD Jr., Jubelirer SJ, Khalid A and Mei L (2021) A Retrospective Study of Brain Metastases From Solid Malignancies: The Effect of Immune Checkpoint Inhibitors. Front. Oncol. 11:667847. doi: 10.3389/fonc.2021.667847

Introduction: Brain metastases (BM) are associated with dismal prognosis, and there is a dearth of effective systemic therapy. In this study, patients with BM from multiple solid tumors were identified from TriNetX databases, their clinicopathological features were evaluated, and the effects of immune checkpoint inhibitor (ICI) therapy were assessed.

Methods: Variables, including median overall survival (OS), Eastern Cooperative Oncology Group (ECOG) performance status, primary diagnosis, and date of diagnosis, were retrieved from TriNetX, a real-world database. Kaplan-Meier plots and log-rank tests were applied to assess significance of differences in survival. Hazard ratio (HR) and 95% confidence interval (CI) values were calculated. All patient data were deidentified.

Results: A total of 227,255 patients with BM were identified in the TriNetX database; median OS was 12.3 months from initial cancer diagnosis and 7.1 months from development of BM. OS of BM from nonsmall-cell lung cancer (NSCLC), triple-negative breast cancer (TNBC), melanoma, and renal cell carcinoma (RCC) were 8.7, 14.7, 17.8, and 15.6 months, respectively. After matching patient baseline characteristics, OS of cohorts with or without exposure to ICIs was evaluated. For all types of cancer, median OS durations for the ICI and no-ICI cohorts were 14.0 and 7.9 months, respectively (HR: 0.88; 95% CI: 0.85–0.91). More specifically, OS was remarkably prolonged in patients with NSCLC (14.4 *vs*. 8.2 months; HR: 0.86; 95% CI: 0.82–0.90), TNBC (23.9 *vs*. 11.6 months; HR: 0.87; 95% CI: 0.82–0.92), and melanoma (27.6 *vs*. 16.8 months; HR: 0.80; 95% CI: 0.73–0.88) if patients had exposure to ICIs. In contrast, there was no significant difference in OS of patients with RCC treated with and without ICIs (16.7 *vs*. 14.0 months; HR: 0.96; 95% CI: 0.86–1.10).

Conclusions: Overall, BM indicates poor patient outcome. Treatment with ICIs improves survival of patients with NSCLC, TNBC, and melanoma and BM; however, no significant improvement was observed in RCC. Investigations to identify prognostic features, oncogenomic profiles, and predictive biomarkers are warranted.

Keywords: brain metastases, TriNetX database, immune check point inhibitor, immunotherapy, PD-1 inhibitor, PD-L1 inhibitor, CTLA-4 inhibitor

INTRODUCTION

Brain metastases (BM) are estimated to occur in approximately 20% of patients with all types of cancer and are generally associated with poor outcomes (1); however, population-based analysis of prognosis is lacking. A historical cohort study, conducted from 1973 to 2001 in the Detroit metropolitan area, showed that the incidence of all types of cancer was 9.6% (2). According to data from the Surveillance, Epidemiology and End Results (SEER) database, BM was present in 1.7% of cases at diagnosis of cancer from 2010 to 2013 (3). Lung, breast, melanoma, and renal cell carcinoma are the most common types of cancer associated with BM (2, 4). In stage IV nonsmall-cell lung cancer (NSCLC), approximately 10%–25% of cases present with BM at diagnosis and another 10%–30% subsequently develop BM (5, 6). Hence, patients with BM represent a substantial population with unmet needs.

For many years, therapeutic strategies for patients with BM were mainly palliative in nature and failed to improve survival in the majority of cases. For example, in the population with BM when newly diagnosed with cancer after 2010, the median overall survival (OS) durations were only 4.0 and 6.0 months for patients with squamous cell and NSCLC adenocarcinoma, respectively (4), with 6.0 months recorded for those with triple-negative breast cancer (TNBC) (7); there was no significant improvement in outcomes compared with the historical cohort (1973–1993) (8), indicating an urgent need for effective treatments. Although radiotherapy and surgery remain the cornerstones of treatment regimens, emerging new modalities, such as immunotherapy (9, 10) and targeted therapy (11), have slowly improved survival outcomes for patients with several cancer subtypes. In addition, unraveling the biological profiles and driver mutations in BM is crucial to facilitate identification of therapeutic targets. An increasing number of systemic treatment options are becoming available, including human epidermal growth factor receptor 2 (HER2)-targeted therapies and tyrosine kinase inhibitors for NSCLC with driver mutations; however, tumors without druggable mutations lack effective approaches, partially given the molecular divergence of primary tumors and BM, as well as the limitations caused by the blood-brain barrier (6). Immune checkpoint inhibitors (ICIs) have great promise for treatment of all types of cancer, including BM. Therefore, a better understanding of the epidemiology of BM, and particularly comparison of the survival benefit of treatment with or without ICIs, are important to inform tailored therapeutic approaches. Accordingly, the objective of this study was to investigate survival differences of patients with BM treated with and without ICIs and explore the efficacy of immunotherapy using real-world data.

MATERIALS AND METHODS

Ethics Approval

This study was a retrospective analysis of patient data obtained from deidentified databases. The research was conducted in accordance with the Declaration of Helsinki. The protocol was approved by the Institutional Review Board at CAMC (IRB Number: 20-662). For this type of study, formal patient consent was not required.

Data Source

The TriNetX Research Network (TriNetX Inc., Cambridge, MA) is a real-world and in-house database; it is a global-federated health research network, combining real-time access to longitudinal electronic medical records and administrative claims data. Participating healthcare organizations (HCOs) span patients from a wide range of geographic locations, age groups, and income levels. Details of and use of the network by our team has been described previously (12). The TriNetX platform is Health Insurance Portability and Accountability Act (HIPPA) and General Data Protection Regulation (GDPR) compliant. The majority of contributing HCOs are located in the USA and the European Union.

Data Collection

Data were retrieved from the Diamond Network subnet, which comprises HCOs contributing online patient information from >200 million individuals. The study period for patients with diagnosis of BM was between January 1st, 2015 and June 30th, 2020, with follow-up until December 31st, 2020 for the primary end point (death). Patients were identified using the ICD-10 code for brain metastasis (C79.3), and primary cancers were also identified using the relevant ICD-10 codes. Only patients ≥18 years old were enrolled. Benign tumors and primary brain tumors were excluded from our study. Baseline demographic characteristics, comorbidities, treatment history, and Eastern Cooperative Oncology Group (ECOG) performance status data were collected. Patients with primary NSCLC, TNBC, melanoma, and RCC were included, which were the tumors most commonly treated with ICIs during the period of the study. Exposure to ICIs was defined as treatment with at least one dose with inhibitors of programmed cell death 1 (PD-1) or its ligand (PD-L1) (nivolumab, pembrolizumab, atezolizumab, avelumab, and durvalumab) or the cytotoxic T-lymphocyte antigen 4 (CTLA-4) inhibitor, ipilimumab. In patients with NSCLC, tumors with driver mutations (of EGFR, ALK, or ROS) were excluded. In the breast cancer cohort, only patients with TNBC for which ICI treatment was indicated were included. In the melanoma cohort, tumors with the BRAF V600E mutation were excluded. For all cohort and patient data, results and patient information were extracted from TriNetX by constructing queries including appropriate ICD-10 codes and procedure codes.

Data Analysis

Analyses were conducted by the authors. Categorical and continuous parameters were analyzed using Chi-square and analysis of variance (ANOVA), respectively, to determine the statistical significance of differences. Kaplan-Meier plots were generated for univariate analysis comparisons and the log-rank test used to evaluate the significance of differences in OS.

For multivariate analysis, Cox proportional hazard regression modeling was employed, based on the results of univariate analyses. Hazard ratio (HR) and 95% confidence interval (CI) values were calculated. To account for differences in baseline characteristics between groups, a propensity score matching (PSM) model was developed using logistic regression to derive well-matched groups for comparative outcomes analysis. Verification was conducted using the nearest-neighbor matching algorithm, with a tolerance level of 0.01 and difference between a propensity score of ≤0.1. GraphPad Prism 6 was used to conduct statistical analysis and generate figures. All tests were two sided, and statistical significance was defined as $p < 0.05$.

RESULTS

Overall Survival in Patients With Brain Metastasis

A total of 227,255 patients diagnosed with BM between January 1st, 2015 and June 30th, 2020 were identified in the TriNetX database. Of identified cases, 103,248 died before December 31st, 2020, with a median OS of 12.3 months from initial diagnosis of primary cancer and 7.1 months from the development of BM (**Figure 1A**). Furthermore, we analyzed the survival times of patients with different types of cancer. Specifically, patients with NSCLC, TNBC, melanoma, and RCC were investigated, since ICIs were more commonly used to treat these types of tumor. A total of 104,765 patients were diagnosed with NSCLC, and 48,894 reached the primary end point (death). Median OS in patients with NSCLC was significantly shorter than that in patients with malignancies in all sites (8.7 *vs.* 12.3 months; HR: 1.30; 95% CI: 1.28–1.32). A total of 30,820 patients diagnosed with TNBC with BM were identified, with a median OS of 14.7 months. The median OS durations of patients with melanoma (n = 11,338) and RCC (n = 6,973) were 17.8 and 15.6 months, respectively (**Figure 1B**); all of which represented better than average prognosis.

Influence of Immune Checkpoint Inhibitors on Overall Survival of Patients With Brain Metastasis

To further investigate the influence of ICIs on patient outcome, we matched patients according to baseline demographic characteristics, comorbidities, prior radiotherapy, and surgery, as well as ECOG performance status using a PSM model (**Table 1**). For all types of cancer, the cohort with ICI exposure included 25,220 patients and the non-ICI-exposed group included 25,243 patients. A total of 37,169 events reached the primary end point. The OS durations of patients in the ICI and no-ICI cohorts were 14.0 *vs.* 7.9 months (HR: 0.88; 95% CI: 0.85–0.91), indicating a significant improvement in survival of patients exposed to ICIs (**Figure 1C**). In the NSCLC group, 13,401 cases were included in each of the ICI and no-ICI cohorts and median OS durations were 14.4 *vs.* 8.2 months, respectively (HR: 0.86; 95% CI: 0.82–0.90). In the TNBC group, 3,449 and 3,461 cases were included in the ICI and no-ICI cohorts, with respective

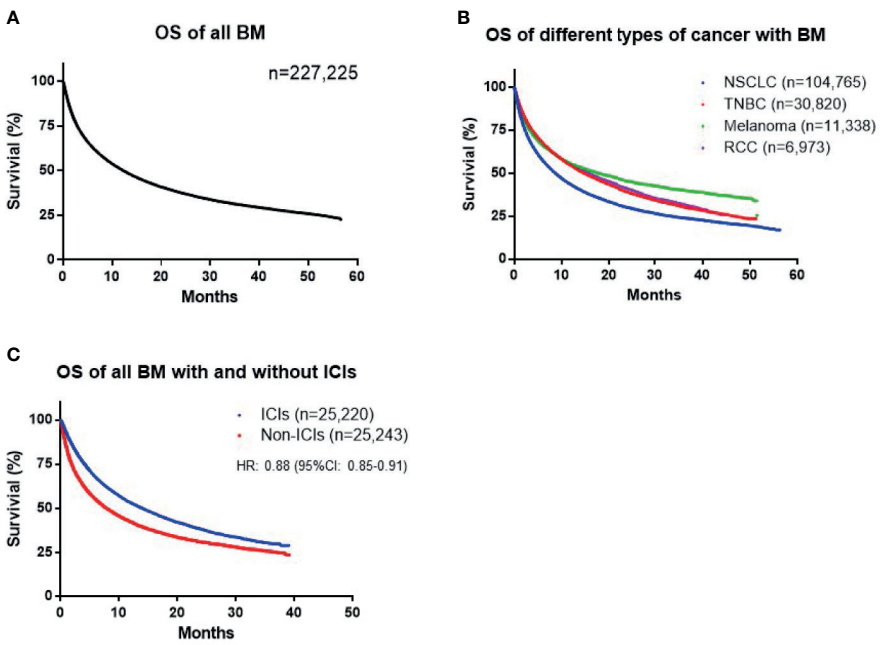

FIGURE 1 | **(A)** Overall survival (OS) of all patients with brain metastases (BM). **(B)** OS of patients with nonsmall-cell lung cancer (NSCLC), triple-negative breast cancer (TNBC), melanoma, and renal cell carcinoma (RCC). **(C)** Difference in survival between cohorts treated with and without immune checkpoint inhibitors (ICIs) among all patients with BM.

TABLE 1 | Demographic and clinical characteristics of patients with brain metastases.

Demographic	NSCLC (nondriven mutation)			Melanoma (non-BRAF mutated)			RCC			TNBC		
	ICIs	Non-ICIs	*p*-Value	ICIs	Non-ICIs	*p*-Value	ICIs	Non-ICIs	*p*-Value	ICIs	Non-ICIs	*p*-Value
Number	13,401	13,429		3,617	3,702		1,333	5,624		3,449	3,461	
Age	65.0 ± 10.1	64.8 ± 11	0.18	63.5 ± 13.7	62.6 ± 14.3	0.07	63.7 ± 10.3	63.3 ± 10.8	0.26	59.0 ± 12.4	61.8 ± 12.7	0.33
Sex												
Female	51.6%	52.6%	0.10	32.8%	33.3%	0.74	27.1%	28.5%	0.41	99.8%	99.8%	0.97
Male	48.3%	47.4%	0.10	67.1%	66.6%	0.74	72.8%	71.4%	0.43	0.2%	0.2%	0.83
Race												
White	75.1%	76.0%	0.67	78.7%	78.2%	0.68	71.0%	75.0%	0.36	77.3%	77.1%	0.88
Non-White	24.9%	24.0%	0.65	21.3%	21.7%	0.69	29.0%	25.0%	0.40	22.7%	22.9%	0.61
Smoking	93.2%	94.1%	0.53	46.9%	51.2%	0.08	31.8%	40.3%	0.19	13.2%	12.9%	0.30
Cardiovascular	52.3%	55.6%	0.73	56.2%	55.5%	0.62	67.8%	66.4%	0.23	51.5%	55.4%	0.25
COPD	41.4%	42.6%	0.92	19.4%	19.2%	0.90	10.7%	8.9%	0.08	14.3%	13.6%	0.41
Liver disease	9.9%	9.2%	0.33	21.4%	21.5%	0.97	18.8%	19.0%	0.88	13.4%	12.0%	0.13
ECOG ≥2	15.0%	16.2%	0.17	26.7%	28.9%	0.50	13.1%	11.3%	0.11	32.1%	26.5%	0.21
Brain radiation	62.5%	64.1%	0.26	40.7%	40.5%	0.85	28.1%	27.9%	0.89	37.2%	43.5%	0.19
Brain surgery	10.1%	9.7%	0.21	9.3%	8.7%	0.56	6.2%	5.3%	0.27	6.3%	3.5%	0.46
Chemo/targeted therapy	38.0%	35.2%	0.19	3.5%	2.6%	0.09	33.0%	30.8%	0.33	80.6%	81.4%	0.53

median OS of 23.9 *vs*. 11.6 months (HR: 0.87; 95% CI: 0.82–0.92). Similarly, 3,617 cases with melanoma and BM were included in the ICI and no-ICI cohorts, with median OS of 27.6 *vs*. 16.8 months, respectively (HR: 0.80; 95% CI: 0.73–0.88). These data reveal significant benefits of ICI exposure in these cancer types; however, analysis of patients with RCC with BM, including 1,333 and 5,624 cases in the ICI and no-ICI cohorts, respectively, failed to demonstrate a significant benefit of ICI treatment, with median OS duration of 16.7 *vs*. 14.0 months (HR: 0.96; 95% CI: 0.86–1.10) (**Figures 2A–D**).

DISCUSSION

Development of BM usually indicates poor prognosis, with 2- and 5-year OS rates of only 8.1% and 2.4%, respectively, across all types of cancer (13). Patients who present with BM at initial diagnosis have even worse outcomes (3). In this study, we found that median OS of patients with BM was 12.3 months from initial cancer diagnosis and 7.1 months from the development of BM. Compared with a single-center report from the University of Minnesota of a study conducted between 1973 and 1993, which revealed a median OS of approximately 4 months from the development of BM (14), our data indicate very limited improvement in patient outcomes, even with the tremendous changes in antitumor therapies over the intervening period.

Lung cancer, including NSCLC and SCLC, remains the most common type of cancer presenting with BM and accounts for >60% of BM cases (5). Similarly, in our study, NSCLC accounted for 46.1% of total BM cases in the TriNetX database. In addition, 10%–25% of patients with NSCLC may present with BM at initial diagnosis (6) and up to 50% of patients with NSCLC develop BM during the course of their illness (15). This number may continue to rise, due to early screening for BM using brain magnetic resonance imaging. We found that the median OS of patients with NSCLC with BM was only 8.7 months, which was similar to a previous report of approximately 7.0 months, based on analysis of multi-institutional retrospective database between 2006 and 2014 (16). Breast cancer is the second most common type of cancer from which BM develops. A recent report from Martin et al. demonstrated that the median OS of patients with TNBC was approximately 6 months from diagnosis of BM (7) with an OS of 12.5 months for patients with hormone receptor-positive breast cancer (17). With the development of anti-HER2 treatment, patients with HER2-positive breast cancer also achieve significantly superior outcomes compared with their counterparts with TNBC (12 *vs*. 5 months) (6, 7). Melanoma and RCC are also common types of cancer which can develop BM and for which there were no major therapeutic advances in the preimmunotherapy era (18, 19).

A revolution in anti-cancer treatment has occurred since the approval of ipilimumab in 2011. Notably, nivolumab and pembrolizumab have been available since late 2014 and were widely accessible from 2015. Since then, the development of ICIs represents a paradigm shift in oncology therapy and prompted us to further study the role of ICIs in treatment of patients with BM. The Checkmate 204 trial of dual ICI therapy showed a dramatic intracranial response rate of 57% of BM from melanoma (10), as did the randomized phase II ABC trial (20). Hence, dual ICI therapy is established as a cornerstone regimen for patients with small asymptomatic BM from melanoma. In contrast, there is limited evidence supporting the efficacy of PD-1/PD-L1 inhibitor treatment for NSCLC. Goldberg et al. reported an approximately 30% intracranial response rate of treatment with pembrolizumab; however, only in the PD-L1-positive patient cohort (9). In contrast, a population study from Italy reported an intracranial response rate of only 17% (21). Unfortunately, untreated BM from RCC failed to show any response to

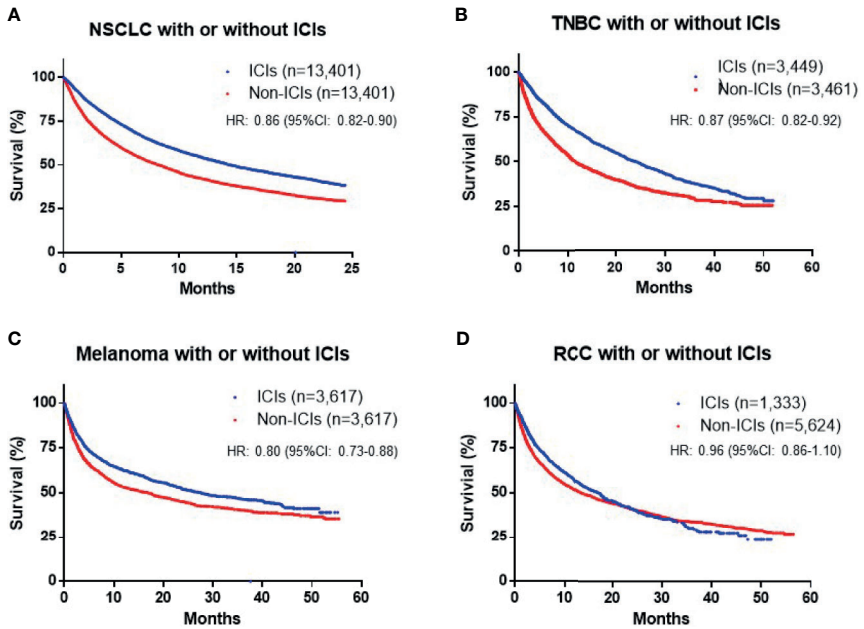

FIGURE 2 | Overall survival (OS) in patients with different cancer subtypes [**(A)** nonsmall-cell lung cancer (NSCLC), **(B)** triple-negative breast cancer (TNBC), **(C)** melanoma and **(D)** renal cell carcinoma (RCC)], with and without immune checkpoint inhibitor (ICI) treatment.

nivolumab in a phase II trial (22). In addition, there is a lack of evidence for the effectiveness of ICIs for treating BM from TNBC, since approval for their use in this context was only obtained relatively recently (23). The efficacy or benefit of ICIs for BM remains controversial to date. Hence, in our study, we sought to validate previously reported results using real-world data.

Using the TriNetX database, we identified patient cohorts with NSCLC, TNBC, melanoma, and RCC, four types of cancer commonly treated with ICIs during 2015–2020. The cohorts were matched for baseline characteristics, including age, sex, race, cardiovascular disease, lung and liver disease, ECOG performance status, prior brain radiotherapy, brain surgery, chemotherapy, and target therapy, which are important prognostic factors. First, our analysis revealed that exposure to ICIs led to improvement of OS by approximately 6 months for all patients with BM. In subtype studies, we specifically excluded NSCLC with driver mutations and melanoma with BRAF V600E mutation, to avoid bias. The results showed that exposure to ICIs significantly prolonged survival of patients with NSCLC, TNBC, and melanoma (HR: 0.80–0.87); however, no significant therapeutic effect was observed for patients with RCC (HR: 0.96). Amin et al. reported an association between immunotherapy and BM after definitive surgery using data from the National Cancer Database from 2010 to 2016 (24). Similarly, they found that exposure to ICIs was associated with improved OS (HR: 0.62), with variable outcomes for patients with different types of tumor, although the number of cases who received immunotherapy was small ($n = 183$). Thus, we conclude that exposure to ICIs prolongs OS for patients with BM overall; however, the efficacy of this type of therapy may be cancer specific.

LIMITATIONS OF THE STUDY

This study has several limitations, due to its retrospective design. First, our dataset has a lack of detailed tumor burden information, particularly intracranial tumor burden, which is an important prognostic factor contributing to patient survival. Second, several other important clinical information is absent. For example, percentage of symptomatic BM, extracranial tumor status, number of resection, and use of steroid could all be important prognostic factors. Third, although the database includes information on patient history of radiotherapy, it does not include the types and timing of radiotherapy. In addition, the sequence of radiotherapy and administration of ICIs is deficient. Especially, several studies have reported significant impacts on survival outcomes of different sequences of ICIs and radiotherapy (25, 26). Fourth, several newer PD-1/PD-L1 inhibitors were not included in this study, including cemiplimab, due to their relatively late approval. Finally, oncogenomic profiles were not included in this database, such as intra- and extracranial PD-1/PD-L1 expression. Although PD-L1 expression has been validated as a predictor of response in patients with NSCLC, its role in other types of cancer is still very controversial (27). Report from Goldberg et al. (9) showed the intracranial response was only observed in PD-L1-positive cohort. However, the sample was obtained from extracranial lesion that is generally not concordant with intracranial tissue (28). Furthermore, systemic and CNS response can be very discordant as well (29). Currently, it is unknown yet about the association of PD-L1 expression and predictive response rate of BM. Other valuable predictive or prognostic biomarkers are also

lacking, despite tremendous efforts to identify such factors. The difficulty involved in accessing human BM samples is invariably a major barrier to many neuro-oncology studies. Retrospective study may not be able to fully address these questions. In the future, there is continuous need of prospective, biomarker driven, multidisciplinary, and innovative clinical trial design to overcome these barriers.

CONCLUSIONS

In conclusion, large-scale data from TriNetX demonstrated a median OS of 12.3 months for patients with all types of cancer with BM, and of 7.1 months from development of BM. More specifically, median OS for patients with NSCLC, TNBC, melanoma, and RCC with BM were 8.7, 14.7, 17.8, and 15.6 months, respectively. We further investigated the efficacy of ICIs in patients with these malignancies, using cohorts matched for baseline characteristics. The results suggest that ICIs are effective for prolonging OS of patients with NSCLC, TNBC, and melanoma; however, this may not be the case in RCC, indicating that the antitumor immune effects of ICIs may be cancer specific. Further studies of underlying molecular mechanisms, better understanding of the intracranial immune microenvironment, and innovative clinical trial design are warranted to further improve BM management.

DATA AVAILABILITY STATEMENT

The raw data supporting the conclusions of this article will be made available by the authors, without undue reservation.

ETHICS STATEMENT

This study was a retrospective study of patients from de-identified databases. It was conducted in accordance with the Declaration of Helsinki. The protocol was approved by Institutional Review Board at CAMC (IRB Number: 20-662). For this type of study, formal consent was not required.

AUTHOR CONTRIBUTIONS

WD, CS, and LM designed and conceptualized this study. WD, CS, and LM conducted the literature research and wrote the manuscript. All authors contributed to the article and approved the submitted version.

FUNDING

The research was supported by the NIGMS of the National Institutes of Health under award number 2U54GM104942-02.

REFERENCES

1. Achrol AS, Rennert RC, Anders C, Soffietti R, Ahluwalia MS, Nayak L, et al. Brain Metastases. *Nat Rev Dis Primers* (2019) 5(1):5. doi: 10.1038/s41572-018-0055-y
2. Barnholtz-Sloan JS, Sloan AE, Davis FG, Vigneau FD, Lai P, Sawaya RE. Incidence Proportions of Brain Metastases in Patients Diagnosed (1973 to 2001) in the Metropolitan Detroit Cancer Surveillance System. *J Clin Oncol Off J Am Soc Clin Oncol* (2004) 22(14):2865–72. doi: 10.1200/jco.2004.12.149
3. Kromer C, Xu J, Ostrom QT, Gittleman H, Kruchko C, Sawaya R, et al. Estimating the Annual Frequency of Synchronous Brain Metastasis in the United States 2010-2013: A Population-Based Study. *J Neurooncol* (2017) 134 (1):55–64. doi: 10.1007/s11060-017-2516-7
4. Cagney DN, Martin AM, Catalano PJ, Redig AJ, Lin NU, Lee EQ, et al. Incidence and Prognosis of Patients With Brain Metastases at Diagnosis of Systemic Malignancy: A Population-Based Study. *Neuro Oncol* (2017) 19 (11):1511–21. doi: 10.1093/neuonc/nox077
5. Siegel RL, Miller KD, Jemal A. Cancer Statistics, 2020. *CA Cancer J Clin* (2020) 70(1):7–30. doi: 10.3322/caac.21590
6. Soffietti R, Ahluwalia M, Lin N, Ruda R. Management of Brain Metastases According to Molecular Subtypes. *Nat Rev Neurol* (2020) 16(10):557–74. doi: 10.1038/s41582-020-0391-x
7. Martin AM, Cagney DN, Catalano PJ, Warren LE, Bellon JR, Punglia RS, et al. Brain Metastases in Newly Diagnosed Breast Cancer: A Population-Based Study. *JAMA Oncol* (2017) 3(8):1069–77. doi: 10.1001/jamaoncol.2017.0001
8. Nussbaum ES, Djalilian HR, Cho KH, Hall WA. Brain Metastases. Histology, Multiplicity, Surgery, and Survival. *Cancer* (1996) 78(8):1781–8. doi: 10.1002/(SICI)1097-0142(19961015)78:8<1781::AID-CNCR19>3.0.CO;2-U
9. Goldberg SB, Schalper KA, Gettinger SN, Mahajan A, Herbst RS, Chiang AC, et al. Pembrolizumab for Management of Patients With NSCLC and Brain Metastases: Long-Term Results and Biomarker Analysis From a Non-Randomised, Open-Label, Phase 2 Trial. *Lancet Oncol* (2020) 21(5):655–63. doi: 10.1016/S1470-2045(20)30111-X
10. Tawbi HA, Forsyth PA, Algazi A, Hamid O, Hodi FS, Moschos SJ, et al. Combined Nivolumab and Ipilimumab in Melanoma Metastatic to the Brain. *New Engl J Med* (2018) 379(8):722–30. doi: 10.1056/NEJMoa1805453
11. Erickson AW, Das S. The Impact of Targeted Therapy on Intracranial Metastatic Disease Incidence and Survival. *Front Oncol* (2019) 9:797. doi: 10.3389/fonc.2019.00797
12. Annie FH, Sirbu C, Frazier KR, Broce M, Lucas BD. Hydroxychloroquine in Hospitalized COVID-19 Patients: Real World Experience Assessing Mortality. *Pharmacotherapy* (2020) 40(11):1072–81. doi: 10.1002/phar.2467
13. Lauko A, Rauf Y, Ahluwalia MS. Medical Management of Brain Metastases. *Neurooncol Adv* (2020) 2(1):vdaa015. doi: 10.1093/noajnl/vdaa015
14. Hall WA, Djalilian HR, Nussbaum ES, Cho KH. Long-Term Survival With Metastatic Cancer to the Brain. *Med Oncol* (2000) 17(4):279–86. doi: 10.1007/BF02782192
15. Page S, Milner-Watts C, Perna M, Janzic U, Vidal N, Kaudeer N, et al. Systemic Treatment of Brain Metastases in non-Small Cell Lung Cancer. *Eur J Cancer* (2020) 132:187–98. doi: 10.1016/j.ejca.2020.03.006
16. Sperduto PW, Yang TJ, Beal K, Pan H, Brown PD, Bangdiwala A, et al. Estimating Survival in Patients With Lung Cancer and Brain Metastases: An Update of the Graded Prognostic Assessment for Lung Cancer Using Molecular Markers (Lung-molGPA). *JAMA Oncol* (2017) 3(6):827–31. doi: 10.1001/jamaoncol.2016.3834
17. Tolaney SM, Sahebjam S, Le Rhun E, Bachelot T, Kabos P, Awada A, et al. A Phase II Study of Abemaciclib in Patients With Brain Metastases Secondary to Hormone Receptor-Positive Breast Cancer. *Clin Cancer Res* (2020) 26 (20):5310–9. doi: 10.1158/1078-0432.ccr-20-1764
18. Suh JH, Kotecha R, Chao ST, Ahluwalia MS, Sahgal A, Chang EL. Current Approaches to the Management of Brain Metastases. *Nat Rev Clin Oncol* (2020) 17(5):279–99. doi: 10.1038/s41571-019-0320-3
19. Valiente M, Ahluwalia MS, Boire A, Brastianos PK, Goldberg SB, Lee EQ, et al. The Evolving Landscape of Brain Metastasis. *Trends Cancer* (2018) 4(3):176–96. doi: 10.1016/j.trecan.2018.01.003
20. Long GV, Atkinson V, Lo S, Sandhu S, Guminski AD, Brown MP, et al. Combination Nivolumab and Ipilimumab or Nivolumab Alone in Melanoma

Brain Metastases: A Multicentre Randomised Phase 2 Study. *Lancet Oncol* (2018) 19(5):672–81. doi: 10.1016/S1470-2045(18)30139-6
21. Crino L, Bronte G, Bidoli P, Cravero P, Minenza E, Cortesi E, et al. Nivolumab and Brain Metastases in Patients With Advanced Non-Squamous Non-Small Cell Lung Cancer. *Lung Cancer (Amsterdam Netherlands)* (2019) 129:35–40. doi: 10.1016/j.lungcan.2018.12.025
22. Flippot R, Dalban C, Laguerre B, Borchiellini D, Gravis G, Negrier S, et al. Safety and Efficacy of Nivolumab in Brain Metastases From Renal Cell Carcinoma: Results of the GETUG-AFU 26 NIVOREN Multicenter Phase II Study. *J Clin Oncol Off J Am Soc Clin Oncol* (2019) 37(23):2008–16. doi: 10.1200/JCO.18.02218
23. Schmid P, Adams S, Rugo HS, Schneeweiss A, Barrios CH, Iwata H, et al. Atezolizumab and Nab-Paclitaxel in Advanced Triple-Negative Breast Cancer. *New Engl J Med* (2018) 379(22):2108–21. doi: 10.1056/NEJMoa 1809615
24. Amin S, Baine MJ, Meza JL, Lin C. Association of Immunotherapy With Survival Among Patients With Brain Metastases Whose Cancer Was Managed With Definitive Surgery of the Primary Tumor. *JAMA Netw Open* (2020) 3(9):e2015444. doi: 10.1001/jamanetworkopen.2020.15444
25. Martins F, Schiappacasse L, Levivier M, Tuleasca C, Cuendet MA, Aedo-Lopez V, et al. The Combination of Stereotactic Radiosurgery With Immune Checkpoint Inhibition or Targeted Therapy in Melanoma Patients With Brain Metastases: A Retrospective Study. *J Neurooncol* (2020) 146(1):181–93. doi: 10.1007/s11060-019-03363-0
26. Kotecha R, Kim JM, Miller JA, Juloori A, Chao ST, Murphy ES, et al. The Impact of Sequencing PD-1/PD-L1 Inhibitors and Stereotactic Radiosurgery for Patients With Brain Metastasis. *Neuro Oncol* (2019) 21(8):1060–8. doi: 10.1093/neuonc/noz046
27. Memmott RM, Wolfe AR, Carbone DP, Williams TM. Predictors of Response, Progression-Free Survival, and Overall Survival in Patients With Lung Cancer Treated With Immune Checkpoint Inhibitors. *J Thorac Oncol* (2021) 16 (7):1086–98. doi: 10.1016/j.jtho.2021.03.017
28. Mansfield AS, Aubry MC, Moser JC, Harrington SM, Dronca RS, Park SS, et al. Temporal and Spatial Discordance of Programmed Cell Death-Ligand 1 Expression and Lymphocyte Tumor Infiltration Between Paired Primary Lesions and Brain Metastases in Lung Cancer. *Ann Oncol* (2016) 27 (10):1953–8. doi: 10.1093/annonc/mdw289
29. Vilariño N, Bruna J, Bosch-Barrera J, Valiente M, Nadal E. Immunotherapy in NSCLC Patients With Brain Metastases. Understanding Brain Tumor Microenvironment and Dissecting Outcomes From Immune Checkpoint Blockade in the Clinic. *Cancer Treat Rev* (2020) 89:102067. doi: 10.1016/ j.ctrv.2020.102067

Author Disclaimer: The content is solely the responsibility of the authors and does not necessarily represent the official views of the National Institutes of Health.

Conflict of Interest: The authors declare that the research was conducted in the absence of any commercial or financial relationships that could be construed as a potential conflict of interest.

Publisher's Note: All claims expressed in this article are solely those of the authors and do not necessarily represent those of their affiliated organizations, or those of the publisher, the editors and the reviewers. Any product that may be evaluated in this article, or claim that may be made by its manufacturer, is not guaranteed or endorsed by the publisher.

Copyright © 2021 Du, Sirbu, Lucas, Jubelirer, Khalid and Mei. This is an open-access article distributed under the terms of the Creative Commons Attribution License (CC BY). The use, distribution or reproduction in other forums is permitted, provided the original author(s) and the copyright owner(s) are credited and that the original publication in this journal is cited, in accordance with accepted academic practice. No use, distribution or reproduction is permitted which does not comply with these terms.

frontiers in Oncology

REVIEW
published: 25 October 2021
doi: 10.3389/fonc.2021.718030

T-Cell Immunotherapy for Pediatric High-Grade Gliomas: New Insights to Overcoming Therapeutic Challenges

Dalia Haydar, Jorge Ibañez-Vega and Giedre Krenciute *

Department of Bone Marrow Transplantation & Cellular Therapy, St. Jude Children's Research Hospital, Memphis, TN, United States

Despite decades of research, pediatric central nervous system (CNS) tumors remain the most debilitating, difficult to treat, and deadliest cancers. Current therapies, including radiation, chemotherapy, and/or surgery, are unable to cure these diseases and are associated with serious adverse effects and long-term impairments. Immunotherapy using chimeric antigen receptor (CAR) T cells has the potential to elucidate therapeutic antitumor immune responses that improve survival without the devastating adverse effects associated with other therapies. Yet, despite the outstanding performance of CAR T cells against hematologic malignancies, they have shown little success targeting brain tumors. This lack of efficacy is due to a scarcity of targetable antigens, interactions with the immune microenvironment, and physical and biological barriers limiting the homing and trafficking of CAR T cells to brain tumors. In this review, we summarize experiences with CAR T–cell therapy for pediatric CNS tumors in preclinical and clinical settings and focus on the current roadblocks and novel strategies to potentially overcome those therapeutic challenges.

Keywords: CAR T cells therapy, immunotherapy, tumor antigen, immune tumor microenvironment, pediatric-type diffuse high-grade glioma, childhood CNS tumors

OPEN ACCESS

Edited by:
Terrance Johns, University of Western Australia, Australia

Reviewed by:
Elizabeth Louise Siegler, Mayo Clinic, United States
Nicholas Vitanza, Seattle Children's Hospital, United States

***Correspondence:**
Giedre Krenciute
giedre.krenciute@stjude.org

Specialty section:
This article was submitted to Neuro-Oncology and Neurosurgical Oncology, a section of the journal Frontiers in Oncology

Received: *31 May 2021*
Accepted: *08 October 2021*
Published: *25 October 2021*

Citation:
Haydar D, Ibañez-Vega J and Krenciute G (2021) T-Cell Immunotherapy for Pediatric High-Grade Gliomas: New Insights to Overcoming Therapeutic Challenges. Front. Oncol. 11:718030. doi: 10.3389/fonc.2021.718030

INTRODUCTION

Central nervous system (CNS) tumors are second only to leukemias, in terms of being the most common pediatric malignancies, and gliomas account for a quarter of all childhood cancers in the U.S (1). Although the prognosis for pediatric low-grade diffuse gliomas (pLGGs) remains promising, with a probability of 5-year survival above 95%, pediatric high-grade diffuse gliomas (pHGGs) are the deadliest childhood cancers (2). Indeed, 5-year survival drops to less than 10% for patients with pHGGs and 1% for those with diffuse midline glioma, *H3 K27-altered* (DMG; previously known as DIPG) (2). Most advances in therapies for pediatric CNS tumors have relied on experiences from adult brain tumor trials. However, given the developmental and histopathological differences in adult and pediatric diseases, such approaches might not provide the most optimal outcome. Specifically, pHGGs present unique molecular heterogeneity and epigenetic characteristics that render the application of results from adult trials ineffective. Moreover, pHGGs form a niche of tumor cells in distinct brain locations surrounded by tight junctions of the blood brain barrier (BBB) and a complex immune tumor microenvironment (TME) (3). These

features affect tumor behavior and the efficacy of new therapeutics. Importantly, the 2021 World Health Organization (WHO) Classification of CNS Tumors (CNS5) recognized two new families of tumor types, "p"LGG and "p"HGG, to reflect on the importance of separating pediatric-type and adult-type gliomas (4). Therefore, when developing new therapies that target pHGGs, we need to consider the distinct characteristic of childhood CNS cancers. In this review, we focus on non-spinal tumors and therefore the term pediatric brain tumors (PBTs) will refer to childhood brain tumors exclusively.

Successful therapies for PBTs need to overcome surgical inaccessibility, limited penetration of chemotherapy drugs, inherent resistance to conventional therapies, and long-term adverse effects. Thus, cell-based immunotherapy using chimeric antigen receptor (CAR)–engineered T cells is an exciting alternative for treating debilitating PBTs. The use of CAR T cells to target a tumor relies on engineering and re-directing a patient's own immune cells (**Figure 1**) to attack tumor cells through selective target recognition and activation of cytotoxic machineries. Activated CAR T cells lyse the tumor expressing the recognized target while sparing normal cells in the absence of target expression. Yet, despite defining several potentially effective targets in adult brain tumors (e.g., IL13Rα2, HER2, and EGFRvIII), clinical testing of CAR T cells in brain tumors failed to produce complete and sustainable antitumor responses (5–8). Challenges included antigen heterogeneity and emergence of antigen-loss variants, limited T-cell persistence, and recruitment of suppressive immune cells in patients (9). Here, we review the lessons learned from preclinical and clinical testing of CAR T cells, with a specific reflection on the unique features of pHGGs that need to be addressed in future efforts to develop effective and safe CAR T–cell immunotherapies for PBTs.

PEDIATRIC-TYPE DIFFUSE HIGH-GRADE GLIOMA

Pediatric gliomas include heterogenous groups of brain malignancies that are histologically similar to adult tumors but with distinct molecular and genetic alterations that dictate clinical behavior and therapeutic considerations (10). Gliomas arise from glial cells, including astrocytes, oligodendrocytes, microglia, or ependymal cells, that normally support neuronal functions. According to the new WHO CNS5 classification, gliomas are classified into two tumor types, pLGG and pHGG, depending on histologic, genetic, and other molecular biomarkers (4). Furthermore, the new classification allows tumor grading within each tumor types (grades 1-4) depending on clinicopathlogical and combined histological and molecular characteristics (4).

The pHGGs are highly aggressive brain tumors with minimal response to standard therapies, including surgery, radiation, and/or chemotherapy. Although less common than pLGGs, pHGGs are the leading cause of death from childhood CNS tumors in the U.S. The pHGGs include four tumor types: Diffuse midline glioma, *H3 K27-altered*; Diffuse hemispheric glioma, *H3 G34-mutant*; Diffuse pediatric-type high-grade glioma, *H3-wildtype* and *IDH-wildtype*; and Infant-type hemispheric glioma (4). Sharing some morphologic features with pLGGs, high-grade tumors are characterized by amplified cell division, increased invasiveness, and augmented neovascularization (10). Additionally, the new CNS5 classification stratifies tumors according to unique genetic and epigenetic alterations which define tumor behavior and response to therapy. For example, patients with isocitrate dehydrogenase (*IDH1* and *IDH2*) mutations tend to have a better prognosis compared to those with *IDH* wild-type tumors (11). Moreover, patients with histone *H3.1* mutations tend to have better overall survival (15 months), while patients with *H3.3* mutations have reduced overall survival (9 months) and enhanced resistance to radiotherapy (12). Therefore, understanding the effects of specific molecular alterations on disease severity and tumor behavior is essential to help select individualized immunotherapeutic targets.

Identifying a patient's histologic tumor diagnosis is essential to guiding therapeutic approaches; yet, it is not sufficient to guide the development of novel directed therapies. For instance, patients with brain stem tumors may require additional modification of adoptive therapies to enhance the accessibility of the infused products to the tumor, compared to those not located in the brain stem. Alternatively, patients with specific genetic or epigenetic alterations may express unique targets or pose specific treatment challenges that require arming new therapies against such stresses. Therefore, understanding the genetic/epigenetic heterogeneity of pHGGs is also key to stratifying patients into subgroups that will benefit most from specific therapies, rather than into groups that require unique modifications to render cellular therapies more effective and safer.

Of note, while the new CNS5 classification regroups the tumor type previously known as diffuse intrinsic pontine glioma (DIPG) into the diffuse midline glioma, H3 K27-altered (DMG) tumor type; we still refer to DIPGs later in our review when citing previous preclinical studies and clinical literature that did not specify the status of the molecular alterations.

ESTABLISHING SUCCESSFUL CAR T–CELL THERAPY FOR PBTS

Standard therapies have failed to improve the outcome of pHGG and have been associated with long-term debilitating adverse effects. Therefore, adoptive immunotherapy using T cells expressing CARs could offer potentially safer, more specific targeting of PBTs by eliciting directed immune responses against tumor cells, while sparing normal cells that do not express the targeted antigen (13). CARs are synthetic receptors composed of an extracellular tumor-specific antigen-recognition domain (usually a single-chain variable fragment of a monoclonal antibody) connected to a hinge, a transmembrane domain, and intracellular signaling domains (14). Upon recognition of tumor antigens, signaling through CAR domains activates T-cell functions, resulting in tumor cell lysis (14). CAR T cells show potent and sustained antitumor activity in patients with hematologic malignancies, as evidenced by

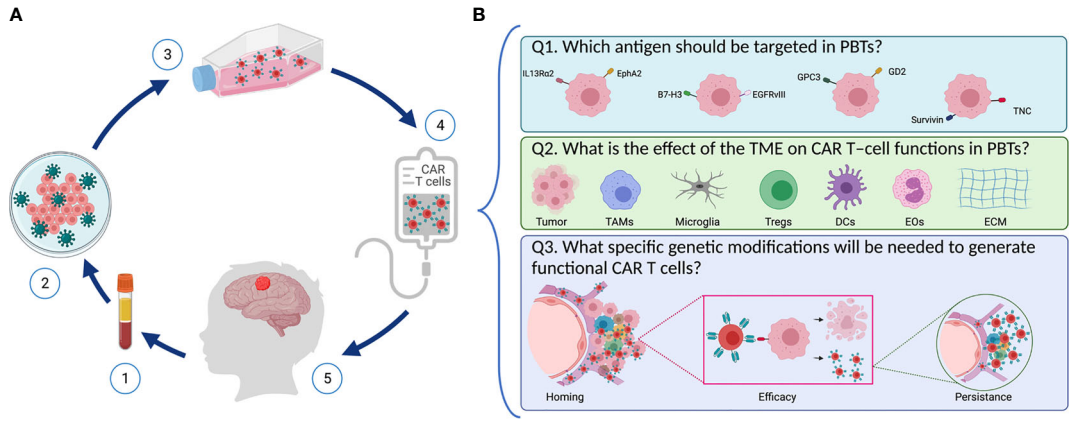

FIGURE 1 | Designing safe, effective, and long-lasting T-cell therapies for PBTs. **(A)** Scheme representing CAR T–cell treatment *via* adoptive T cell transfer in pediatric patients with brain tumors. (1) T cells are isolated from patient's blood followed by (2) T cell activation and reprograming in the lab to express the chimeric antigen receptor (CAR) using viral vectors. (3) CAR T–cells are then expanded, and they undergo quality control testing (4) prior to infusion into the patient (5). **(B)** Key questions to address when designing CAR T–cells for PBTs. (1) Selecting an appropriate target: Several TAAs (including IL13Rα2, EphA2, B7-H3, GD2, EGFRvIII, and TNC) are expressed in PBTs with heterogenous expression patterns. (2) Overcoming the suppressive immune TME: Immune cells (like TAMs, DCs, Tregs, and EOs) infiltrate PBTs and they induce different immune interactions that affect the CAR T–cells' ability to perform their cytotoxic properties. (3) Once infused, CAR T–cells need to home to the patient's tumor and exert their cytolytic activity while expanding and persisting to create long-lasting effects.

continuous FDA approvals of CD19-CAR T cells for different pediatric and adult B-cell leukemias (15). However, early clinical studies with CAR T cells for adult brain tumors failed to recapitulate the potent anti–brain tumor activity of CAR T cells seen in preclinical testing (14). Thus, the development of CAR T–cell therapies for PBTs will be even more complicated, given the unique patient population.

The following questions must be kept in mind as we design and create safer, effective, and long-lasting T-cell therapies for PBTs (**Figure 1**): First (Q1), which antigen should be targeted in PBTs, and will one target be sufficient for a broad group of pHGGs? Second (Q2), what is the effect of the TME on CAR T–cell functions in PBTs? For instance, tumor cells can exert environmental stress (e.g., hypoxia, inhibitory checkpoint ligands, release of suppressive mediators) on CAR T cells, thereby preventing their activation and cytotoxic functions (16, 17). Moreover, suppression of CAR T cells by infiltrating immune cells within the complex tumor niche represents a hurdle to overcome (18, 19). Lastly (Q3), what specific modifications will be needed to generate functional CAR T cells in PBTs? To generate the desired therapeutic efficacy, CAR T cells need to home to the tumors, eradicate tumor cells without on-target off-tumor toxicities, and persist to resolve any recurrent tumors? In the following sections, we will define some aspects of pHGGs that are essential for developing effective adoptive T-cell therapies for children.

Q1. Which Antigen Should Be Targeted in PBTs?

CAR T cells are engineered to selectively recognize and target tumor-associated antigens (TAAs) expressed on tumor cells (20). Targetable TAAs are characterized by exclusive expression on tumor cells, with minimal expression on normal tissues to prevent on-target off-tumor toxicities (21). However, with a limited number of tumor-specific antigens exclusively expressed on tumor cells, targeting TAA that are present on normal cells must consider strategies to prevent, reverse, or manage any potential toxicities that result from lysing normal cells expressing the selected target (discussed in later sections). Traditional targets focus on surface proteins, but novel strategies for target discovery expand to include posttranslationally modified proteins, carbohydrate repeats, lipids, glycoproteins, and alternative splice variants (21). Brain tumor–specific CAR T–cell targets have been identified, mostly based on samples from adult brain tumors; however, a limited number of studies have evaluated their validity in pediatric populations (22–24). Some studies have shown that antigen expression in PBTs does not recapitulate the exact patterns seen in adult brain tumors. Moreover, a study by our group using PBT xenografts revealed a unique inter- and intra-patient variability when TAA expression was compared across tumor subtypes (22). Additionally, experiences from preclinical and clinical studies in adults suggest that it is unlikely that one target will be sufficient to cure heterogenous brain tumors (21). Thus, identifying selective targets that are effective and safe for patients with heterogenous PBTs is a key question for the development of successful CAR T–cell therapies in pHGGs. Here we summarize and review the current knowledge on potential CAR targets in pHGGs.

Disialoganglioside

Disialoganglioside (GD2) belongs to the glycosphingolipid family of gangliosides expressed on outer plasma membranes of various cell types (25). Gangliosides regulate cell interaction, adhesion, and signal transduction (25). GD2 is widely expressed on different solid tumors (neuroblastoma, melanoma,

osteosarcoma) but has limited expression on normal cells, including nerves, lymphocytes, and melanocytes (25). Xenografts of pHGGs robustly express GD2 (~84%) (22). Moreover, GD2 is uniformly expressed in DMGs (24). The use of GD2 as immunotherapeutic target showed potent antitumor effects but was associated with unwanted adverse effects (including neuropathic pain and headaches) due to limited expression in normal tissues (26). Similarly, anti-GD2 CAR T cells have shown potent antiglioma efficacy in preclinical DMG models but resulted in hydrocephalous (24). Nevertheless. Currently, two ongoing clinical trials are evaluating GD2-CAR T cells in pediatric patients with DMG or other pHGGs (NCT04196413 and NCT04099797, **Table 1**) (31). Early results from patients with DMGs treated with GD2 CAR T cells suggest promising clinical responses along with tolerable safety profiles (including incidences of manageable cytokine release syndrome and neurotoxicity) (28). Therefore, data from these clinical studies will define the strategies for GD2-directed CAR T–cell therapy and provide general insights on CAR T–cell therapy efficacy and safety in pHGGs.

B7 Homolog 3

B7 homolog 3 (B7-H3), also known as cluster of differentiation 276 (CD276), is a member of the B7 and CD28 immune checkpoint family (32). B7-H3 is expressed on peripheral lymphoid tissues and antigen-presenting cells and has a controversial role in immune stimulation and inhibition (including promoting T-cell cytotoxicity *vs* inhibiting T-cell proliferation and activation) (33). B7-H3 expression on solid or hematologic malignancies is associated with reduced survival and enhanced cancer progression through mechanisms dependent on immune evasion, enhanced macrophage recruitment, and elevated levels of suppressive cytokines (32, 33). B7-H3 is highly expressed in pHGG (~100%), with its highest expression intensities in more aggressive tumors, like DMG (22, 23, 34). B7-H3–directed CAR T cells showed potent antiglioma efficacy in preclinical xenograft and syngeneic models (22, 35, 36). Although B7-H3 is expressed at some level on normal tissues, including the adrenal gland, salivary gland, and gastric epithelial cells (37–39), preclinical studies show a favorable B7-H3–CAR T–cell safety profile (22, 38). Ongoing clinical trials that are evaluating anti–B7-H3 CAR T cells in adult GBM (NCT04077866) and in pHGG and DMG (NCT04185038, **Table 1**). Preliminary results from pediatric patients with CNS tumors show that serial doses of B7-H3 CAR T cells result in clinically stable disease in the absence of any dose limiting toxicities (27). Thus, data from ongoing clinical studies will further characterize the safety and efficacy of this CAR target.

Interleukin-13 Receptor Alpha 2

Interleukin-13 receptor alpha 2 (IL13Rα2) is a subunit of the IL13 receptor complex. Closely related to the α1 subunit, IL13Rα2 is thought to function as a decoy receptor, reversing IL13-mediated JAK/STAT signaling transduction (40). IL13Rα2 is overexpressed in various solid tumors, including breast, prostate, and pancreatic cancer, with minimal expression on normal tissues (e.g., spermatocytes) (41). IL13Rα2 expression is associated with enhanced metastasis, invasiveness, and reduced survival (41). In gliomas, the level of IL13Rα2 expression increases with malignancy grade, with higher expression in grades III and IV (53%-73%) (42). IL13Rα2 is overexpressed in PBTs (~68%), including pHGGs (22). CAR T cells targeting IL13Rα2 have shown potent antiglioma activity and enhanced survival in preclinical and clinical studies. An ongoing trial is assessing the efficacy of IL3Rα2-CAR T cells in children with refractory glioma (NCT04510051, **Table 1**) (8, 43). Given its favorable safety profile but highly heterogenous expression profile in PBTs, IL13Rα2 will most likely be a promising target for dual-targeting regimens or for specific populations that are resistant to other robustly expressed TAAs.

Human Epidermal Growth Factor Receptor 2

Human epidermal growth factor receptor 2 (HER2; also known as ErbB2), is a transmembrane receptor tyrosine kinase (44). The role of HER2 in tumorigenesis was first defined in breast cancer, where HER2-mediated signaling transduction drives cell proliferation, invasion, survival, and metastasis (45). HER2 expression is inversely correlated with survival and mediates

TABLE 1 | Summary of ongoing clinical studies with CAR T cells for PBTs.

NCT Number	Target	Delivery	Age	Study Results	Toxicity
NCT04510051	IL13Rα2	IT	4 Years to 25 Years	No Results Available	No Results Available
NCT04185038	B7-H3	IT, IC	1 Year to 26 Years	Stable clinical disease with detectable CAR T cells in CSF (27)	No DLTs (27)
NCT03638167	EGFR	IT, IC	1 Year to 26 Years	No Results Available	No Results Available
NCT04099797	GD2	IV	12 Months to 18 Years	No Results Available	No Results Available
NCT04196413	GD2	IV	2 Years to 30 Years	Durable clinical responses and marked CAR T cell expansion (28)	CRS (Grade 1-3) ICANS (Grade 1-2) TIAN No other DLTs (28)
NCT03500991	HER2	IT, IC	1 Year to 26 Years	Clinical and laboratory evidence of local CNS immune activation (29)	No DLTs (29)
NCT02442297	HER2	IT, IC	3 Years and older	No Results Available	No Results Available
NCT01109095	HER2	IV	Child, Adult, Older Adult	1/16 partial response, 7/16 stable disease (6, 30)	No DLTs (6, 30)

(IV, Intravenous; IT, Intrathecal/ventricular; IC, Intratumor/cavity; DLT, Dose limiting toxicity; CRS, Cytokine release syndrome; TIAN, Tumor Inflammation-Associated Neurotoxicity; ICANS, Immune effector cell-associated neurotoxicity syndrome).

faster tumor growth, increased metastatic potential, increased disease grade, and enhanced resistance to endocrine therapies (45). HER2 is robustly expressed in gastric, ovarian, prostate, and CNS tumors (44). Specifically, HER2 is highly expressed in adult HGG (~42%) and pediatric medulloblastomas (~40%), along with less robust expression in pHGGs (~37%) (22, 46). HER-2–directed CAR T cells have shown potent antiglioma efficacy in preclinical and clinical studies (6, 47). Although HER2-CAR T cells have been well tolerated so far, toxic side effects associated with HER2-directed therapies (trastuzumab) have been observed (30, 48, 49). Additionally, ongoing trials in pHGGs are evaluating HER2-CAR T cells in refractory disease (NCT03500991, **Table 1**) and early results suggest that repeated locoregional delivery of HER2 CAR T cells are well tolerated in these young patients (29). Collectively, heterogenous expression of HER2 in normal tissues and in pHGGs necessitates close evaluation of HER2 as a CAR target for PBTs. If selected as a target, the incorporation of a safety switch in the CAR design needs to be considered to avoid any unintended adverse events.

Ephrin Type-A Receptor 2

Ephrin type-A receptor 2 (EphA2) belongs to the ephrin class of receptor tyrosine kinases (50). Upon interaction with its ligand, ephrin A1, EphA2 engages in bidirectional signaling that controls cell adhesion, motility, and tissue development (51). In normal tissues, EphA2 is upregulated and expressed only in rapidly proliferating cells (50). However, in several cancers (i.e., lung, prostate, breast, and brain tumors), EphA2 is robustly and highly expressed (51). A recent study by our group shows that EphA2 is expressed in about 28% of patient-derived xenografts of pHGGs (22). EphA2 overexpression results in extracellular matrix deposition, enhanced proliferation, invasiveness, and angiogenesis (52), thus resulting in reduced survival, increased metastasis, and enhanced malignant progression (51). EphA2-directed CAR T cells have shown promising antiglioma activity in preclinical brain tumor models (53, 54), and at least one clinical trial is accruing patients with recurrent gliomas to evaluate the safety and efficacy of EphA2-CAR T cells (NCT03423992). Due to its role in tumor progression and invasiveness and its potentially safe profile with limited expression on normal tissue, EphA2 is a promising target for CAR T–cell immunotherapy of PBTs that demands further clinical and preclinical investigation.

Epidermal Growth Factor Receptor Splice Variant III

Epidermal growth factor receptors comprise a family of receptor tyrosine kinases (55). Overexpression or mutation of these receptors is a negative prognostic factor in several solid tumors, including lung, breast, ovarian, and CNS cancers (56). Epidermal growth factor receptor splice variant III (EGFRvIII) is the most common EGFR mutation in pHGG resulting from a fusion of exon 1 to exon 8, thereby triggering aberrant ligand-independent receptor activation (57, 58). In PBTs, EGFRvIII is overexpressed in pHGGs (14%-40%) (58, 59). Due to its lack of expression in normal tissues, EGFRvIII is considered an ideal CAR target (60). However, EGFRvIII-directed CAR T cells showed minimal antitumor activity in adults with glioma (NCT02209376) (7). Interestingly, a recent study demonstrated that EGFRvIII, due to its tumor-specific expression, can be successfully used in a SynNotch-CAR system, where it is responsible for turning on the expression of a dual-antigen–targeting CAR (IL13Rα2 and EphA2) at a tumor site. This approach led to a less exhausted CAR T–cell phenotype and improved anti-GBM activity *in vitro* and *in vivo* (61). This study emphasizes the need to incorporate novel methods to target antigens expressed at lower intensities on tumor cells. Moreover, targeting EGFRvIII also shows promising results in vaccine trials in DMG (NCT01058850) (62) while a new trial will be evaluating EGFR CAR T cells in pediatric patients with refractory CNS tumors (NCT03638167, **Table 1**). Therefore, given all the clinical and preclinical data, EGFRvIII is most likely a promising target for immunotherapy of PBTs that may require additional CAR modifications or dual targeting approaches (62).

Tenascin-C

Tenascin-C (TNC) is an embryonic glycoprotein expressed on neurons and astrocytes that functions as an adhesion-modulating protein (63). TNC undergoes posttranslational modification (alternative splicing), which allows the protein to interact with fibronectin and several other growth factors, thus inducing a wide range of functions related to focal adhesion, matrix formation, and cell motility (64). Alternatively spliced TNC is minimally expressed in normal tissues but robustly upregulated in tumors and extracellular matrices of breast, lung, kidney, prostate, and CNS tumors (64). Expression of TNC splice variants is associated with poor prognosis and enhanced tumor invasiveness and metastatic potential (64, 65). TNC is highly expressed in adult HGGs (85%-96%) and pHGGs (>42%) (66, 67). TNC expression in DIPGs correlates with higher tumor grade and more frequent *H3K27M* mutation (67). TNC-targeting immunotherapy, including monoclonal antibodies, therapeutic vaccines, and antibody–drug conjugates, have shown promise in preclinical and clinical studies in CNS tumors and other tumor models (NCT01131364, NCT01134250) (68). Thus, TNC-targeting T-cell therapies are promising not only as a tumor-targeting approach but also as a target that can potentially enhance CAR T–cell permeability and delivery to brain tumors, with potential targeting of the extracellular matrix and TME.

Other Potential Targets

Survivin

As an inhibitor-of-apoptosis protein, survivin regulates programmed cell death and cell cycle progression (69). Survivin is expressed during embryonic development but is absent in normal terminally differentiated tissues (70). It is highly expressed in primary and secondary adult GBMs (83% and 46%, respectively) and in pHGGs and medulloblastoma (71–74). Survivin-targeted adoptive T-cell products have potent anti–acute myeloid leukemia activity, and other survivin-based vaccines, cellular therapies, and gene therapies have shown potent antitumor efficacy and favorable safety (71, 75, 76). Therefore, survivin is an ideal target for cancer immunotherapy due to its limited expression on normal cells and wide expression on PBTs (69, 70).

Glycoprotein 100

Also known as PMEL17, glycoprotein 100 (Gp100) is a premelanosomal protein expressed in melanocytes (77). It is involved in melanosome development, including vesicular formation, structural maturation, and pigmentation (78). Gp100 is more robustly expressed in adult HGGs (>80%) than in pHGGs (~46%) (79). The combination of a Gp100-directed vaccine and IL2 showed promising enhanced survival in patients with melanoma (80). Additionally, dual-specific T cells engineered with Her2-directed CAR and Gp100-specific T-cell receptor repertoire showed durable responses in murine solid tumor models, and transgenic T cells directed against Gp100 showed significant survival advantage in preclinical DIPG models (81, 82). Thus, Gp100 is another target that should be considered for dual-targeting products in specific PBT populations.

Glypican-3

A heparan sulfate proteoglycan, glypican-3 (GPC-3) is attached to the cell surface by a glycosyl–phosphatidylinositol anchor (83). GPC-3 is expressed in fetal lung, liver, and kidney tissues during embryonal development and is very minimally expressed in normal adult cells (84). It is also involved in tumorigenesis of embryonal and pediatric tumors due to its role in malignant transformation *via* Wnt/β-catenin–, Hedgehog-, and FGF-signaling alterations (84). GPC-3 is overexpressed in pHGGs and pLGGs (85). GPC-3–targeted CAR T cells in murine models of hepatocellular carcinoma showed potent antitumor activity without any significant toxicities, while also targeting soluble GPC-3 antigens (86, 87). Thus, anti-GPC-3 CAR T cells could potentially recognize GPC-3–expressing gliomas and GPC-3 antigens shed in the TME, which poses another target for glioma extracellular matrices that could be useful for dual CAR-targeting strategies.

Neogenin

As part of the immunoglobulin superfamily of receptors involved in cell–cell interactions neogenin is normally expressed during embryogenesis and is essential for axonal navigation and adult neurogenesis (88). Neogenin and its ligand, netrin-1, are highly expressed in solid and CNS tumors, including medulloblastoma and glioma (89, 90). In pHGGs, netrin-1 overexpression mediates enhanced oncogenic astrocyte migration, tumor invasion, and metastasis (91). Neogenin is also highly expressed in DMG, where it drives tumor invasiveness and worsens prognosis (92). Neogenin-targeting monoclonal antibodies reverse its tumorigenic effects in DMG models (92). Therefore, neogenin holds great promise as a novel CAR target to reduce tumor burden and invasive tumor phenotypes.

In summary, the TAAs described above have been extensively studied as targets for immunotherapy and have unique characteristics that could serve as successful targets for CAR T–cell therapy in PBTs. Expression patterns in PBTs are mostly heterogenous with some TAAs more robustly expressed across tumor subtypes (GD2, B7-H3, IL13Rα2), while other targets have variable expression frequencies and intensities (HER2, EphA2, EGFRvIII). Here we described the most common, well-studied TAAs, though other potential PBT-specific molecules, such as survivin (75), Gp100 (93), GPC-3 (83), and neogenin (92), should also be considered as CAR T–cell targets for PBTs. Moreover, TAAs like GPC-3 and neogenin have the potential to target the TME and extracellular matrices; this property could be exploited to enhance delivery and accessibility of infused CAR T–cell products. Other unique targets, like Gp100 and survivin, have potential use in multiantigen CAR-targeting approaches. Although expression profiles for most of these TAAs are well defined in PBTs, their validation as targets for CAR T–cell therapy is warranted. **Table 1** provides a summary for ongoing CAR T cell clinical trials in PBT patients (extended details on each trial are available in **Supplemental Table 1**). Preclinical testing in representative PBT models and clinical testing in specific pediatric patient populations should guide target selection and CAR designs to achieve the desired therapeutic benefits. Moreover, development of effective CAR T–cell therapies require additional screening and novel target discovery and validation in PBTs.

Q2. What Is the Effect of the TME on CAR T–Cell Functions in PBTs?

During the past decade, it has been well established that the TME limits CAR T–cell trafficking to tumors and suppresses their effector functions through direct physical contact or molecular interactions (**Figure 2**). Complex tumor vasculature, tumor-induced suppression of chemokine ligands, and reduced expression of chemokine receptors on CAR T cells limit their migration to the tumor (94, 95). Additionally, the deposition of extracellular matrix and accumulation of cancer-associated fibroblasts hinder CAR T–cell penetration and mediate immunosuppression (19, 94). Finally, disrupted BBB permeability and altered endothelial cell functions in pHGGs can affect the accessibility and trafficking of adoptive cell products to the targeted tumor cells (96).

In the brain, the TME includes a highly specialized immunologic niche called the immune TME. In pHGGs, the immune TME contains suppressive immune cells, like tumor-associated neutrophils, myeloid-derived suppressor cells, dendritic cells (DCs), and regulatory T cells (Tregs) (18). Expression of inhibitory checkpoint ligands (TIM3, PD1) on these cells suppresses T-cell proliferation and cytokine release (97). Additionally, the release of inhibitory mediators and metabolites (TGFβ, IL-10, IDO-1) blocks T-cell functions and further recruits other suppressive immune cells (18, 19). In this section of the review, we highlight the specific features of the immune TME in pHGGs and some unique features of DMG that are key to developing successful CAR T–cell therapies in PBTs.

The Immune TME in pHGGs

The TME in pHGGs is heterogenous, with different immune cell compositions at each tumor grade or genetic classification (98). Immune TME heterogeneity depends on the plasticity and distinct immunomodulatory functions of tumor-associated macrophages (TAMs), Tregs, DCs, eosinophils (EOs), and other suppressive immune cells and mediators.

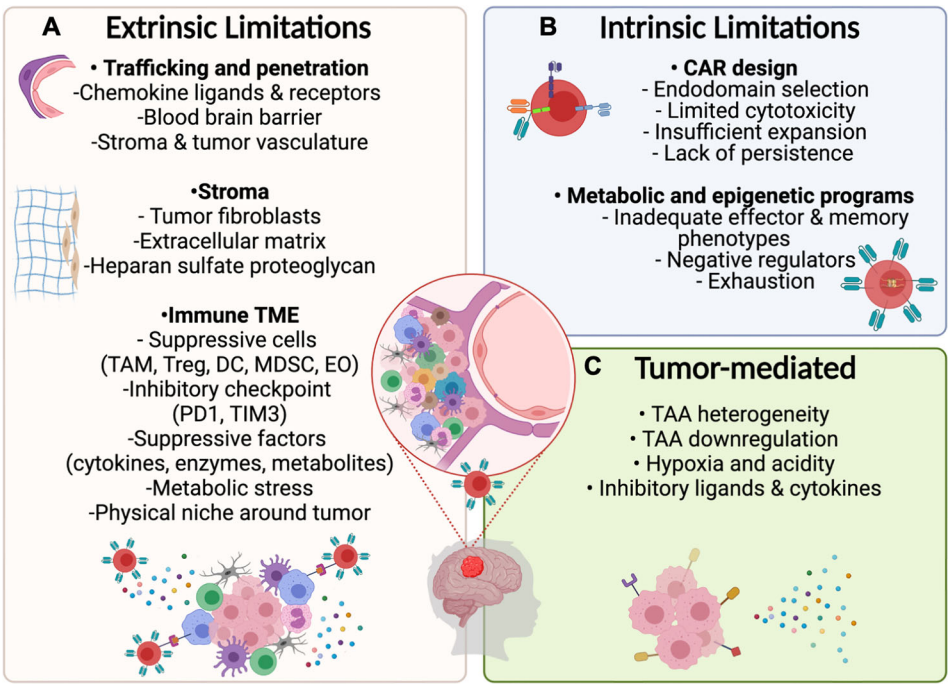

FIGURE 2 | Potential limitations for CAR T–cell therapy in PBTs. **(A)** Extrinsic Challenges for CAR T–cell immunotherapy will depend on the ability of designed products to home to the tumor by overcoming the physical limitations induced by the BBB and stroma surrounding the tumor followed by surviving the suppressive immune TME including inhibitory cytokines and ligands. **(B)** Intrinsic limitations depend on optimizing the CAR design and programs that control metabolic and epigenetic functions to mediate necessary cytotoxic mechanisms while preventing exhaustion. **(C)** Tumor cells may resist CAR T cell therapies by downregulating targeted antigens and by exerting environmental stress on CAR T–cells through the release of suppressive cytokines and expression of inhibitory ligands.

Tumor-Associated Macrophages

Macrophages are key components of the immune TME. TAMs represent more than 30% of nonmalignant cells in adult HGGs, and they are negatively correlated with immune escape, resistance to immune checkpoint blockade, and disease progression (99). However, increased TAM frequencies in pHGGs does not directly correlate with poor outcomes (100). Specifically, two subsets of TAMs are present in pHGGs and are derived from either embryonic microglia or tumor-infiltrating monocytes with distinct functions and effects on antitumor immune responses (98, 101). Microglia-derived TAMs are located around the tumor edges and upregulate inflammatory, metabolic, and suppressive cascades, while monocyte-derived TAMs are generally located within the tumor; they upregulate genes associated with cell proliferation, motility, and migration (102). Distinct TAM subsets in pHGGs play different roles in promoting tumor growth and mediating an immunosuppressive state. Thus, enrichment of monocyte-derived TAMs in pHGGs is associated with poor prognosis and reduced survival (100). Abundance of suppressive monocyte-derived TAMs in pHGGs can potentially limit CAR T–cell therapy by suppressing effector functions (Treg polarization, inducing metabolic T-cell hyporesponsiveness, and direct suppression *via* PD1/PDL1 interaction) and reducing T-cell penetration and chemotaxis to the tumors by forming a chemically and physically suppressive niche around the tumor (103–105). Alternatively, microglia-derived TAMs are most likely essential to promote CAR T–cell effector functions and support their persistence.

Regulatory T Cells

The pHGGs are heavily infiltrated with Tregs, constituting almost 15% of non-neoplastic cells (106). Higher frequencies of Treg infiltration in pHGGs correlate with poor overall survival and greater WHO disease grade (106). Besides suppressing endogenous antiglioma T-cell responses, Tregs also promote tumor growth by inducing STAT3-mediated hypoxia (107). Tregs in pHGGs are heterogenous, with most cells being thymus-derived *versus* another native population induced and maintained by suppressive factors within the glioma TME (98). Tregs in pHGGs also upregulate proapoptotic genes (*Bax*, *Bak*, *Bim*), thus promoting their fitness and survival within the glioma TME, augmenting tumor growth, and suppressing T-cell effector molecules (e.g., granzyme B) (108). Therefore, Tregs are most likely detrimental for CAR T–cell functions in PBTs, and suppressive mediators may polarize infused CAR T cells into Treg-like phenotypes, thus limiting their cytotoxic functions.

Other Immune Cell Populations

Dendritic Cells

Multiple DC populations infiltrate solid tumors and influence antitumor immunity and response to therapy (98). Increased DC recruitment in preclinical glioma models potentiates CD8+

T–cell responses, as well as response to immune checkpoint blockade (109). Moreover, recent studies suggest that increased DCs in adult HGGs is correlated with worse clinical manifestations without significant contribution to disease grade (110). Although limited data are available on the specific role of DCs in pHGGs, reports suggest that their functions are impaired by tumor-mediated immunosuppression (110). Thus, specific interactions of DCs within the TME in pHGGs need to be further investigated, especially in the context of CAR T–cell therapies, which do not require antigen presentation by DCs but could be suppressed by altered DC functions.

Eosinophils

Recruitment of EOs into the glioma TME has been implicated in tumorigenesis and suppression of antitumor immune responses (111). Marked eosinophilia has been observed in patients with HGG, and it correlates with worse prognosis and decreased response to therapy (111). Conversely, correlation analysis in patients with HGGs has shown that lower EO counts are inversely correlated with disease grade and pathology (112). In pHGGs, EOs represent about 13% of noncancer cells, and they tend to cluster with PBTs that are rich in Tregs and natural killer cells (106). Given the plasticity and abundance of EOs, investigating their interaction with CAR T–cell therapies in PBTs is warranted, especially in the context of preconditioning therapies and/or radiation and chemotherapy, which could drastically affect these cells.

The Immune TME in DMGs

A limited number of studies have characterized the TME of DMGs, because deciphering this TME is challenging due to the location and diffuse, infiltrative nature of DMGs. Two recent studies of samples obtained at diagnosis or autopsy have reported some preliminary findings on the immune profile of DMGs (113, 114). Both studies reported a CD45+ leucocyte compartment consisting primarily of CD11b+ macrophages with very few CD3+ T cells in primary DMG tissue samples. In addition, a study by Lieberman et al. showed no increase in immunosuppressive CD163+ tumor-associated macrophages in DMG samples when compared to nontumor controls (114). Finally, DMG-derived cell cultures produce markedly fewer cytokines and chemokines than do adult glioblastomas, indicating that DMGs have a noninflammatory phenotype (113). Thus, both studies concluded that DMGs are immunologically "cold" tumors. In addition, a very recent study using a deconvolution approach (methylCIBERSORT) to assess genome-wide DNA-methylation data from pediatric CNS tumors reported that Tregs, EOs, and monocytes infiltrate DMGs (106). Although limited studies are available, they are admirable first approaches trying to illuminate the DMG TME and then apply this knowledge to cellular therapies. More studies are urgently needed to answer the remaining questions, such as how the quiescent DMG immune TME affects CAR T–cell therapy, and if and how do CAR T cells re-shape the immune landscape of DMGs? Given the recent increase in the generation and availability of syngeneic DMG mouse models, the hope is that more studies will be published in the upcoming years, as researchers will be less dependent on patient sample availability. However, some key finding will have to be validated in the clinical setting.

Q3. What Specific Modifications Will Be Needed to Generate Functional CAR T Cells in PBTs?

Besides selecting targetable TAAs and armoring CAR T cells against the suppressive immune TME, three other T cells-specific functional limitation will determine whether CAR T–cell therapies in PBTs are successful: the ability of infused CAR T–cell products to 1) home to the tumor, 2) exert potent but safe antitumor responses, and 3) establish persistent memory T cells for efficient tumor control. These limitations can be addressed by engineering CAR T cells with additional genetic modifications. In this section, we review CAR-specific modifications and their potential for successful CAR T–cell immunotherapy in pHGGs.

Homing

Homing of CAR T cells to CNS tumors depends on their ability to cross the brain parenchyma and utilize chemotactic factors to migrate to the tumor. For a long time, the brain was considered an immune-privileged organ, with tight junctions of the BBB limiting access of immune cells and mediators (115). However, pHGGs are characterized by leaky and fragile vasculature, altered BBB integrity, and reduced expression of essential chemokine ligands and receptors, including CXCL9, CXCL10, CCL2, and CCL12 (116, 117). Thus, during the development of effective CAR T–cell therapies for PBTs, we must consider the need for chemokine ligands and adhesion receptors essential for T-cell trafficking to the brain as well as considering strategies to bypass the physical barriers for delivery of adoptive cell therapy products.

Routes of CAR T cell administration must be carefully considered to ensure appropriate homing of infused cells to the tumors without unwanted adverse effects. CAR T cells can be administered (i) *via* the blood through intravenous (IV) delivery, (ii) *via* the CSF through intrathecal/ventricular (IT) delivery, or (iii) *via* direct delivery to the tumor through intratumor/cavity (IC) injections (118). While preclinical studies comparing different routes of administration suggest that superior anti-tumor efficacy is observed with locoregional delivery (22, 119, 120), clinical experiences show that the three routes of administration can produce desirable therapeutic efficacy (6, 8, 24, 28). With the lack of clinical studies directly comparing different routes of administration in pediatric patients, selecting the most optimal delivery method will depend on feasibility as well as safety considerations. IV administration would be best for targeting tumors that are anatomically challenging (tumor location complicating catheter implantation for IT or IC delivery) or in instances of abnormal CSF flow (inadequate delivery to bulky or parenchymal tumors with IT administration) (118, 121). Alternatively, IT and IC delivery would be best for CAR T cells with limited peripheral activation or trafficking potential where evidence suggests that T cell activation enhances T cell migration to the CNS (14, 122). Additionally, locoregional delivery (IC) should be considered for targeting antigens that are more readily expressed on normal

cells to avoid the potential for on-target off-tumor toxicities that may otherwise be pronounced with systemic IV delivery. Lastly, while IV routes of administration may result in systemic toxicities (cytokine release syndrome (CRS) or immune effector cell-associated neurotoxicity syndrome (ICANS)), safety concerns with locoregional delivery necessitate careful considerations for potential inflammation and swelling at the tumor site that may complicate catheter functionality as well as increased risks of infections with these devices (118, 123–126). Therefore, locoregional delivery may be a strategy to enhance homing of CAR T cells through bypassing the BBB; yet, it should be carefully evaluated for specific targets in pediatric patients where CNS tumors may have different anatomical locations and distribution compared to adult tumors (127).

Alternatively, strategies to enhance CAR T cell homing to the tumors in PBT patients may include combination therapies or specific genetic modifications of CAR T cells. For example, using MRI-guided focused ultrasound can potentiate CAR T–cell efficacy and homing by transiently disrupting the BBB and blood–tumor barrier (128–130). Additionally, engineering CAR T cells to express chemokine receptors or utilizing receptors that are endogenously expressed in pHGGs could enhance delivery and penetration of adoptive products. For example, anti-CD70 CAR T cells expressing CXCR1 and CXCR2 traffic better to the brain (95). Such strategies have not been tested in pHGGs, thus determining whether these modifications will be beneficial in PBTs necessitates further preclinical and clinical evaluation.

Efficacy and Safety

Promoting the efficacy of CAR T cells, while ensuring the safety of this approach is a key aspect of a successful CAR T–cell therapy. It is now well established that T cells engineered only with a CAR do not produce a sustained antitumor response. Thus, additional genetic modifications must be considered. So far, only a handful of genetic modifications have been tested in adult brain tumor models, let alone PBT models. For example, CARs engineered to express transgenic cytokines, such as IL12, IL15, IL18, have enhanced efficacy in preclinical glioma models (43, 131). Additionally, EphA2-CAR T cells expressing constitutively active IL-7 cytokine receptor (C7R) have enhanced antiglioma efficacy in preclinical models (132).

Engineering tools can also be used to convert tumor-induced suppression of CAR T cells into a beneficial stimulus. For example, engineering CAR T cells to express costimulatory PD1 receptors modified to fuse the extracellular domain of PD1 with an intracellular CD28-activation domain can hijack the system and protect CAR T cells against PD1/PDL1-mediated exhaustion and suppression (133). Other switch receptors, like dominant-negative TGFβ receptor, prevents the otherwise suppressive effects of TGFβ, thus enhancing CAR T–cell cytotoxicity and promoting persistence (134). However, none of these strategies have been evaluated in adult brain tumors or PBTs. Regarding the safety of CAR T cells, every genetic modification has the potential to induce unintended adverse events or uncontrollable T-cell proliferation. Therefore, safety switches, such as CD20, iCas9, tNGFR (135–138), must be considered when designing effective T-cell therapies for PBTs.

Targeting multiple antigens and arming CAR T cells against inhibitory ligands in the TME can also improve their efficacy. Targeting more than one TAA can help overcome the limitations of heterogenous antigen expression and tumor-induced downregulation of targeted antigens (139). Several CAR regimens to target multiple TAAs are available, including the use of pooled products (e.g., combining single-antigen targeting CAR T–cell products), the use of bispecific and trivalent CARs (one T cell expresses several CARs), or the use of tandem CARs (expressing one CAR construct that merges several antigen-recognition domains into one backbone sharing one activation domain) (139, 140). Preclinical studies using CAR T cells against HER2, IL13Rα2, and EphA2 in pooled, bispecific, trivalent, and tandem designs have shown superior antiglioma efficacy (47, 141, 142). Finally, engineering logic-gated (AND, OR, NOT) CAR T cells may offer enhanced specificity and efficacy along with reduced on-target off-tumor toxicities (139). While "OR" logic-gated CAR T cells contain tandem or multiple CAR constructs, a single TAA-CAR interaction is sufficient to activate tumor killing mechanisms which is particularly useful for TAAs with heterogenous expression and to protect against antigen escape (143). Alternatively, "AND" or "NOT" logic-gated CAR T cells protect against on-target off-tumor toxicities by restricting T cell activation to instances where two cognate TAAs are co-expressed (AND); by conditional expression of a second CAR through a SynNotch receptor regulated transcriptional manner (AND); or by selectively killing tumor cells that lack a specific inhibitory ligand which would otherwise suppress the T cells when expressed on normal cells (NOT) (139, 142). However, none of these designs have been evaluated in clinical studies for brain tumors. Although they have the potential for potent synergism and can protect against antigen escape and emergence of antigen-negative tumors, their efficacy and safety in PBTs will depend on how they interact and function in the complex inflammatory pHGGs. If clinical experiences show that pHGGs induce CAR T–cell exhaustion through TME-induced stress, then using pooled products will probably function best to prevent continuous activation of one T cell expressing CARs that target several TAAs at once.

Persistence

Lastly, ensuring that CAR T cells persist in patients long enough to control the primary and any recurrent tumors should be carefully considered when designing CAR T–cell therapies for PBTs. T cells exist in multiple differentiated phenotypes (naïve (T_N), effector (T_{EFF}), central memory (T_{CM}), stem-like memory (T_{SCM}), or tissue resident memory (T_{RM})) (144). Generating CAR T cell products using different pools of T cell differentiation states may be a powerful tool for enhancing self-renewal and persistence. While T_{EFF} cells produce potent cytotoxic responses, they are short-lived compared to T_N, T_{CM}, and T_{SCM} cells (144, 145). The T_N cells circulate without being committed to an effector or memory phenotype while T_{CM} and T_{SCM} cells are long-lived and exhibit self-renewal and multipotent differentiation properties (144, 145). Therefore, generating CAR T cell products using less differentiated pools of T_N, T_{CM}, or T_{SCM} cells may be a preferred strategy to enhance persistence

and long-lived immunological memory. For instance, a Phase I clinical study using T_{CM}-derived CD19 CAR T cells showed improved expansion in leukemia patients (146). However, T_{CM} and T_{SCM} cells express adhesion molecules which favor their homing to lymphoid organs instead of peripheral tissues (147). Since CAR T cells for PBTs need to home to the brain, thorough preclinical and clinical studies need to closely evaluate the use of less differentiated T cells and their potential impact on homing and anti-brain tumor activity. Importantly, T_{RM} cells are tissue-specific memory cells with pluripotent and self-renewal properties similar to T_{CM} and T_{SCM} cells (144, 148). However, isolating these cells for brain tumor patients may not be practical. Moreover, T_{CM} and T_{SCM} cells constitute less than 5% of peripherally circulating cells which would not be sufficient for generating CAR T cell products. Therefore, strategies to enrich for less differentiated T cell phenotypes include using small molecules (Wnt signaling agonists or Akt signaling inhibitors) (149–151), cytokines (IL-21, IL-7 and IL-15) (152, 153), or through transgenic expression of homing ligands and cytokines (154). While some of these modifications have been tested in preclinical models of brain tumors, further clinical evaluation of less differentiated CAR T cell products for patients with brain tumors are needed.

Lastly, enhancing CAR T cell persistence can be achieved through genetic modifications and/or combination therapies. The use of CRISPR/Cas9 technology can help knockout negative T-cell regulators. For instance, silencing PD1 enhances EGFRvIII CAR T–cell activity in preclinical glioma models (155). In addition, knocking-out epigenetic modifier DNMT3A improved IL13Ra2-CAR T cell effector functions in preclinical brain tumor models while antigen negative relapsed have been observed (156). Similarly, using small-molecule inhibitors that can reshape the TME could arm CAR T cells against immune suppression. For example, using an inhibitor of glycogen synthase kinase 3 promotes a memory phenotype in IL13Rα2-CAR T cells and enhances their antitumor efficacy in preclinical HGG models (157). Several small molecule inhibitors have already been evaluated in humans and are effective and well tolerated (NCT00948259 and NCT02718911). Thus, utilizing these novel approaches to enhance long-term effector memory in CAR T–cell regimens for PBTs requires verification in the preclinical and clinical settings.

LEVERAGING THE POWER OF PBT MODELS TO IMPROVE CAR T–CELL EFFICACY

Advancing CAR T–cell therapies for PBTs necessitates the use of adequate brain tumor models that that closely recapitulate human disease. Ideal models should be reproducible and easy to use, manipulate, and most importantly mimic the genetic, epigenetic, and phenotypic tumor heterogeneity and the TME of the human disease (158). Similar to the liquid and solid tumor animal models, brain tumor models are divided into patient derived orthotopic xenografts (PDOXs) and syngeneic models. Below we describe key characteristics and benefits of each model. Although humanized mouse models are gaining momentum and might be instrumental in future cell therapy studies, they are not discussed in this review.

Patient-Derived Orthotopic Xenografts

PDOX models are generated by implanting cell suspensions of freshly isolated patient tumor tissues into the comparable tissue of origin in immunodeficient mice. The resultant tumors are closely representative of the original tumor heterogeneity in patients, including the stromal components, architecture, and biochemical interactions (159–162). Multiple studies have demonstrated that brain tumor PDOX models are transplantable and can be implanted into different brain locations (brain stem, cortex, thalamus, or cerebellum) (161, 163). After multiple passages of PDOX lines in immunocompromised mice, DNA and RNA sequencing of the resultant tumor xenografts revealed that most retain the heterogeneity of their matched patient sample (162). In addition, comparing surface-antigen profiling of PBT PDOX samples and matched patient samples showed that TAA expression is preserved in these models. In addition, the TAA expression is sustained throughout multiple passages (22). Therefore, PDOX models are ideal for target identification and validation and for evaluating the efficacy of novel cancer-directed therapies *in vivo*, especially since they retain their original TAA expression, chemical sensitivity, and drug resistance. However, PDOXs require the use of immunocompromised mice; this system constitutes a major limitation to evaluating the effects of immune contribution to treatment efficacy, resistance, and/or safety. Other disadvantages lie in the tumor latency; many PDOXs require a lengthy period (up to12 months) between implantation and development of tumors (164). This long latency makes it challenging to assess CAR T–cell therapy. In summary, PDOX models are an extremely valuable resource for evaluating CAR T–cell efficacy; however, additional models for validating key findings should be considered.

Syngeneic pHGG Models

Syngeneic brain tumors can be implanted in immunocompetent mice to study the tumor's biological interactions with the host's immune system. Most syngeneic pHGGs are generated through platelet-derived growth factor (PDGF)-driven alterations (PDGFRA mutations or amplifications and/or PDGFB amplifications). These mutations are artificially introduced into neural stem cells (NSCs) (165). Implanting modified NSCs into neonatal mice forms supratentorial tumors that reproduce several features of pHGGs, including transcriptional and biological characteristics (165). Additionally, syngeneic DIPG models have been generated using combinations of mutations in *H3.3K27M* and *Pdgfra* and *p53* knockout in NSCs, which drive hindbrain tumorigenesis resulting in spontaneous DIPGs (166). These tumors recapitulate tumoral heterogeneity, the spontaneous nature of DIPGs, and the immune TME in DIPGs (166). Alternatively, introducing *H3K27M* mutations into human or murine embryonic stem cell–derived neural precursors, along with *PDGFRA*- and *TP53*-targeting mutations, produces transplantable and fast-growing DIPGs when implanted into SCID (severe combined

immunodeficiency) mice (167, 168). Moreover, *in utero* electroporation into the brain stem of embryonic mice to insert the dominant-negative mutation of *p53*, *H3K27M*, and different combinations of *Pdgfb* amplification or *Pdgfra* mutation generates tumors with unique histopathologic and molecular features seen in human DMGs such as minimally disrupted BBBs (169). These models recapitulate the immune interactions and key features of the immune TME in pHGGs and will be very useful for studying CAR T–cell efficacy and safety.

The use of available animal models of PBTs will undoubtedly improve CAR T–cell evaluation and hasten the transition from preclinical to clinical testing. The challenge, however, is the availability of these models; not all investigators have access to them. In addition, some of the models require special handling, which will require additional training for CAR T–cell-focused laboratories. Adapting these models to the CAR T–cell testing pipeline will also pose some challenges. For example, some models can only be passaged *in vivo*, which complicates initial *in vitro* studies. Others might require special growth conditions for *in vitro* co-culture experiments that might not be compatible with T cells. On a positive note, these challenges might motivate productive collaborations between translational immunologists and brain tumor biologists that may result in more efficient efforts to generate safer, effective CAR T–cell therapies for PBTs.

CONCLUSIONS AND FUTURE PERSPECTIVES

CAR T–cell therapy is a promising approach to treat PBTs. However, very few CAR T–cell studies have been done in a PBT setting. To advance the field and establish effective CAR T cells for PBTs, more studies are needed. Most importantly, studies must be done in PBT models, targeting PBT-specific antigens, and taking into account the tumor heterogeneity and unique features of the PBT TME. Although achieving this will be quite challenging, given the recent rapid advances in single-cell molecular approaches, preclinical model systems, and CAR design, it is not unreasonable to hope that it will be achievable in the near future.

AUTHOR CONTRIBUTIONS

DH, JI, and GK conceived, interpreted, and reviewed the literature. DH and GK conceptualized the research review, designed the figures, and wrote the manuscript. All authors contributed to the article and approved the submitted version.

FUNDING

Funding was provided by NCI award K99CA256262 to DH and NIH/NINDS award R01NS121249 to GK.

ACKNOWLEDGMENTS

We thank Dr. Angela J. McArthur for reviewing and editing our manuscript. **Figures 1** and **2** were created with BioRender.com.

SUPPLEMENTARY MATERIAL

The Supplementary Material for this article can be found online at: https://www.frontiersin.org/articles/10.3389/fonc.2021.718030/full#supplementary-material

REFERENCES

1. N. R. Council. *Childhood Cancer Survivorship: Improving Care and Quality of Life*. (2003). Washington, DC: The National Academies Press. doi: 10.17226/10767
2. Blionas A, Giakoumettis D, Klonou A, Neromyliotis E, Karydakis P, Themistocleous MS. Paediatric Gliomas: Diagnosis, Molecular Biology and Management. *Ann Trans Med* (2018) 6(12):251. doi: 10.21037/atm.2018.05.11
3. Aldape K, Brindle KM, Chesler L, Chopra R, Gajjar A, Gilbert MR, et al. Challenges to Curing Primary Brain Tumours. *Nat Rev Clin Oncol* (2019) 16 (8):509–20. doi: 10.1038/s41571-019-0177-5
4. Louis DN, Perry A, Wesseling P, Brat DJ, Cree IA, Figarella-Branger D, et al. The 2021 WHO Classification of Tumors of the Central Nervous System: A Summary. *Neuro-Oncology* (2021) 23(8):1231–51. doi: 10.1093/neuonc/noab106
5. Lee DW, Stetler-Stevenson M, Yuan CM, Shah NN, Delbrook C, Yates B, et al. Long-Term Outcomes Following CD19 CAR T Cell Therapy for B-ALL Are Superior in Patients Receiving a Fludarabine/Cyclophosphamide Preparative Regimen and Post-CAR Hematopoietic Stem Cell Transplantation. *Am Soc Hematol* (2016) 128(22):218. doi: 10.1182/blood.V128.22.218.218
6. Ahmed N, Brawley V, Hegde M, Bielamowicz K, Kalra M, Landi D, et al. Her2-Specific Chimeric Antigen Receptor–Modified Virus-Specific T Cells for Progressive Glioblastoma: A Phase 1 Dose-Escalation Trial. *JAMA Oncol* (2017) 3(8):1094–101. doi: 10.1001/jamaoncol.2017.0184
7. O'Rourke DM, Nasrallah MP, Desai A, Melenhorst JJ, Mansfield K, Morrissette JJ, et al. A Single Dose of Peripherally Infused Egfrviii-Directed CAR T Cells Mediates Antigen Loss and Induces Adaptive Resistance in Patients With Recurrent Glioblastoma. *Sci Trans Med* (2017) 9(399). doi: 10.1126/scitranslmed.aaa0984
8. Brown CE, Starr R, Aguilar B, Brito A, Chang B, Sarkissian A, et al. Clinical Development of IL13Rα2-Targeting CAR T Cells for the Treatment of Glioblastoma. *J ImmunoTherapy Cancer* (2015) 3(2):1–1. doi: 10.1186/2051-1426-3-S2-P114
9. Yeku OO, Brentjens RJ. Armored CAR T-Cells: Utilizing Cytokines and Pro-Inflammatory Ligands to Enhance CAR T-Cell Anti-Tumour Efficacy. *Biochem Soc Trans* (2016) 44(2):412–8. doi: 10.1042/BST20150291
10. Cacciotti C, Fleming A, Ramaswamy V. Advances in the Molecular Classification of Pediatric Brain Tumors: A Guide to the Galaxy. *J Pathol* (2020) 251(3):249–61. doi: 10.1002/path.5457
11. Grimm SA, Chamberlain MC. Anaplastic Astrocytoma. *CNS Oncol* (2016) 5 (3):145–57. doi: 10.2217/cns-2016-0002
12. Jones C, Baker SJ. Unique Genetic and Epigenetic Mechanisms Driving Paediatric Diffuse High-Grade Glioma. *Nat Rev Cancer* (2014) 14(10):651–61. doi: 10.1038/nrc3811
13. Brown CE, Mackall CL. CAR T Cell Therapy: Inroads to Response and Resistance. *Nat Rev Immunol* (2019) 19(2):73. doi: 10.1038/s41577-018-0119-y
14. Akhavan D, Alizadeh D, Wang D, Weist MR, Shepphird JK, Brown CE. CAR T Cells for Brain Tumors: Lessons Learned and Road Ahead. *Immunol Rev* (2019) 290(1):60–84. doi: 10.1111/imr.12773

15. Bao F, Wan W, He T, Qi F, Liu G, Hu K, et al. Wang: Autologous CD19-Directed Chimeric Antigen Receptor-T Cell Is an Effective and Safe Treatment to Refractory or Relapsed Diffuse Large B-Cell Lymphoma. *Cancer Gene Ther* (2019) 1:248–55. doi: 10.1038/s41417-018-0073-7
16. Reardon DA, Freeman G, Wu C, Chiocca EA, Wucherpfennig KW, Wen PY, et al. Immunotherapy Advances for Glioblastoma. *Neuro-Oncology* (2014) 16(11):1441–58. doi: 10.1093/neuonc/nou212
17. Chen N, Li X, Chintala NK, Tano ZE, Adusumilli PS. Driving Cars on the Uneven Road of Antigen Heterogeneity in Solid Tumors. *Curr Opin Immunol* (2018) 51:103–10. doi: 10.1016/j.coi.2018.03.002
18. Morgan MA, Schambach A. Engineering CAR-T Cells for Improved Function Against Solid Tumors. *Front Immunol* (2018) 9:2493. doi: 10.3389/fimmu.2018.02493
19. Srivastava S, Riddell SR. Chimeric Antigen Receptor T Cell Therapy: Challenges to Bench-to-Bedside Efficacy. *J Immunol* (2018) 200(2):459–68. doi: 10.4049/jimmunol.1701155
20. Liu B, Yan L, Zhou M. Target Selection of CAR T Cell Therapy in Accordance With the TME for Solid Tumors. *Am J Cancer Res* (2019) 9 (2):228.
21. Abbott RC, Cross RS, Jenkins MR. Finding the Keys to the CAR: Identifying Novel Target Antigens for T Cell Redirection Immunotherapies. *Int J Mol Sci* (2020) 21(2):515. doi: 10.3390/ijms21020515
22. Haydar D, Houke H, Chiang J, Yi Z, Odé Z, Caldwell K, et al. Cell Surface Antigen Profiling of Pediatric Brain Tumors: B7-H3 Is Consistently Expressed and Can Be Targeted *via* Local or Systemic CAR T-Cell Delivery. *Neuro-Oncology* (2020) 23(6):999-1011. doi: 10.1093/neuonc/noaa278
23. Majzner RG, Theruvath JL, Nellan A, Heitzeneder S, Cui Y, Mount CW, et al. CAR T Cells Targeting B7-H3, A Pan-Cancer Antigen, Demonstrate Potent Preclinical Activity Against Pediatric Solid Tumors and Brain Tumors. *Clin Cancer Res* (2019) 25(8):2560–74. doi: 10.1158/1078-0432.CCR-18-0432
24. Mount CW, Majzner RG, Sundaresh S, Arnold EP, Kadapakkam M, Haile S, et al. Potent Antitumor Efficacy of Anti-GD2 CAR T Cells in H3-K27M+ Diffuse Midline Gliomas. *Nat Med* (2018) 24(5):572–9. doi: 10.1038/s41591-018-0006-x
25. Nazha B, Inal C, Owonikoko TK. Disialoganglioside GD2 Expression in Solid Tumors and Role as a Target for Cancer Therapy. *Front Oncol* (2020) 10. doi: 10.3389/fonc.2020.01000
26. Voeller J, Sondel PM. Advances in Anti-GD2 Immunotherapy for Treatment of High-Risk Neuroblastoma. *J Pediatr Hematol/Oncol* (2019) 41(3):163. doi: 10.1097/MPH.0000000000001369
27. Vitanza N, Wilson A, Gust J, Huang W, Perez F, Albert C, et al. Immu-11. Clinical Updates and Correlative Findings From the First Patient With Dipg Treated With Intracranial Car T Cells. *Neuro-Oncology* (2021) 23 (Supplement_1):i29–9. doi: 10.1093/neuonc/noab090.119
28. Majzner RG, Ramakrishna S, Mochizuki A, Patel S, Chinnasamy H, Yeom K, et al. Abstract CT031: GD2 CAR T Cells Mediate Clinical Activity and Manageable Toxicity in Children and Young Adults With DIPG and H3K27M-Mutated Diffuse Midline Gliomas. *AACR* (2021) CT031. doi: 10.1158/1538-7445.AM2021-CT031
29. Vitanza NA, Johnson AJ, Wilson AL, Brown C, Yokoyama JK, Künkele A, et al. Locoregional Infusion of HER2-Specific CAR T Cells in Children and Young Adults With Recurrent or Refractory CNS Tumors: An Interim Analysis. *Nat Med* (2021) 27:1–9. doi: 10.1038/s41591-021-01404-8
30. Ahmed N, Brawley V, Hegde M, Bielamowicz K, Wakefield A, Ghazi A, et al. Autologous HER2 CMV Bispecific CAR T Cells Are Safe and Demonstrate Clinical Benefit for Glioblastoma in a Phase I Trial. *J ImmunoTherapy Cancer* (2015) 3(2):1–1. doi: 10.1186/2051-1426-3-S2-O11
31. Brown MP, Ebert LM, Gargett T. Clinical Chimeric Antigen Receptor-T Cell Therapy: A New and Promising Treatment Modality for Glioblastoma. *Clin Trans Immunol* (2019) 8(5):e1050. doi: 10.1002/cti2.1050
32. Yang S, Wei W, Zhao Q. B7-H3, a Checkpoint Molecule, as a Target for Cancer Immunotherapy. *Int J Biol Sci* (2020) 16(11):1767. doi: 10.7150/ijbs.41105
33. Son Y, Kwon SM, Cho JY. CD276 (B7-H3) Maintains Proliferation and Regulates Differentiation in Angiogenic Function in Late Endothelial Progenitor Cells. *Stem Cells* (2019) 37(3):382–94. doi: 10.1002/stem.2944
34. Maachani UB, Tosi U, Pisapia DJ, Mukherjee S, Marnell CS, Voronina J, et al. B7–H3 as a Prognostic Biomarker and Therapeutic Target in Pediatric Central Nervous System Tumors. *Trans Oncol* (2020) 13(2):365–71. doi: 10.1016/j.tranon.2019.11.006
35. Tang X, Zhao S, Zhang Y, Wang Y, Zhang Z, Yang M, et al. B7-H3 as a Novel CAR-T Therapeutic Target for Glioblastoma. *Mol Therapy-Oncolytics* (2019) 14:279–87. doi: 10.1016/j.omto.2019.07.002
36. Nehama D, Di Ianni N, Musio S, Du H, Patané M, Pollo B, et al. B7-H3-Redirected Chimeric Antigen Receptor T Cells Target Glioblastoma and Neurospheres. *EBioMedicine* (2019) 47:33–43. doi: 10.1016/j.ebiom.2019.08.030
37. Nguyen P, Okeke E, Clay M, Haydar D, Justice J, O'Reilly C, et al. Route of 41BB/41BBL Costimulation Determines Effector Function of B7-H3-CAR. CD28ζ T Cells. *Mol Therapy-Oncolytics* (2020) 18:202–14. doi: 10.1016/j.omto.2020.06.018
38. Du H, Hirabayashi K, Ahn S, Kren NP, Montgomery SA, Wang X, et al. Antitumor Responses in the Absence of Toxicity in Solid Tumors by Targeting B7-H3 Via Chimeric Antigen Receptor T Cells. *Cancer Cell* (2019) 35(2):221–37.e8. doi: 10.1016/j.ccell.2019.01.002
39. Seaman S, Zhu Z, Saha S, Zhang XM, Yang MY, Hilton MB, et al. Eradication of Tumors Through Simultaneous Ablation of CD276/B7-H3-Positive Tumor Cells and Tumor Vasculature. *Cancer Cell* (2017) 31(4):501–515. e8. doi: 10.1016/j.ccell.2017.03.005
40. Rahaman SO, Sharma P, Harbor PC, Aman MJ, Vogelbaum MA, Haque SJ. Il-13rα2, a Decoy Receptor for IL-13 Acts as an Inhibitor of IL-4-Dependent Signal Transduction in Glioblastoma Cells. *Cancer Res* (2002) 62(4):1103–9.
41. Okamoto H, Yoshimatsu Y, Tomizawa T, Kunita A, Takayama R, Morikawa T, et al. Interleukin-13 Receptor α2 Is a Novel Marker and Potential Therapeutic Target for Human Melanoma. *Sci Rep* (2019) 9(1):1–13. doi: 10.1038/s41598-019-39018-3
42. Brown CE, Warden CD, Starr R, Deng X, Badie B, Yuan Y-C, et al. Glioma Il13rα2 Is Associated With Mesenchymal Signature Gene Expression and Poor Patient Prognosis. *PloS One* (2013) 8(10):e77769. doi: 10.1371/journal.pone.0077769
43. Krenciute G, Prinzing BL, Yi Z, Wu M-F, Liu H, Dotti G, et al. Transgenic Expression of IL15 Improves Antiglioma Activity of IL13Rα2-CAR T Cells But Results in Antigen Loss Variants. *Cancer Immunol Res* (2017) 5(7):571–81. doi: 10.1158/2326-6066.CIR-16-0376
44. Tai W, Mahato R, Cheng K. The Role of HER2 in Cancer Therapy and Targeted Drug Delivery. *J Control Release* (2010) 146(3):264–75. doi: 10.1016/j.jconrel.2010.04.009
45. Gutierrez C, Schiff R. HER2: Biology, Detection, and Clinical Implications. *Arch Pathol Lab Med* (2011) 135(1):55–62. doi: 10.5858/2010-0454-RAR.1
46. Ahmed N, Ratnayake M, Savoldo B, Perlaky L, Dotti G, Wels WS, et al. Regression of Experimental Medulloblastoma Following Transfer of HER2-Specific T Cells. *Cancer Res* (2007) 67(12):5957–64. doi: 10.1158/0008-5472.CAN-06-4309
47. Bielamowicz K, Fousek K, Byrd TT, Samaha H, Mukherjee M, Aware N, et al. Trivalent CAR T Cells Overcome Interpatient Antigenic Variability in Glioblastoma. *Neuro-Oncology* (2018) 20(4):506–18. doi: 10.1093/neuonc/nox182
48. Ewer MS, O'Shaughnessy JA. Cardiac Toxicity of Trastuzumab-Related Regimens in HER2-Overexpressing Breast Cancer. *Clin Breast Cancer* (2007) 7(8):22–9. doi: 10.3816/CBC.2007.n.017
49. Buono G, Fabi A, Del Mastro L, Cannita K, La Verde NM, Ardito R, et al. Long-Term Toxicity Profile of Trastuzumab Emtansine (T-DM1): A Multicenter Real-Life Study. *In: Am Soc Clin Oncol* (2019) e12507. doi: 10.1200/JCO.2019.37.15_suppl.e12507
50. Ireton RC, Chen J. Epha2 Receptor Tyrosine Kinase as a Promising Target for Cancer Therapeutics. *Curr Cancer Drug Targets* (2005) 5(3):149–57. doi: 10.2174/1568009053765780
51. Xiao T, Xiao Y, Wang W, Tang YY, Xiao Z, Su M. Targeting Epha2 in Cancer. *J Hematol Oncol* (2020) 13(1):1–17. doi: 10.1186/s13045-020-00944-9
52. Zhou Y, Sakurai H. Emerging and Diverse Functions of the Epha2 Noncanonical Pathway in Cancer Progression. *Biol Pharm Bull* (2017) 40 (10):1616–24. doi: 10.1248/bpb.b17-00446
53. Chow KK, Naik S, Kakarla S, Brawley VS, Shaffer DR, Yi Z, et al. T Cells Redirected to Epha2 for the Immunotherapy of Glioblastoma. *Mol Ther* (2013) 21(3):629–37. doi: 10.1038/mt.2012.210

54. Yi Z, Prinzing BL, Cao F, Gottschalk S, Krenciute G. Optimizing Epha2-CAR T Cells for the Adoptive Immunotherapy of Glioma. *Mol Therapy-Methods Clin Dev* (2018) 9:70–80. doi: 10.1016/j.omtm.2018.01.009
55. Wieduwilt M, Moasser M. The Epidermal Growth Factor Receptor Family: Biology Driving Targeted Therapeutics. *Cell Mol Life Sci* (2008) 65 (10):1566–84. doi: 10.1007/s00018-008-7440-8
56. Nicholson RI, Gee JMW, Harper ME. EGFR and Cancer Prognosis. *Eur J Cancer* (2001) 37:9–15. doi: 10.1016/S0959-8049(01)00231-3
57. Sigismund S, Avanzato D, Lanzetti L. Emerging Functions of the EGFR in Cancer. *Mol Oncol* (2018) 12(1):3–20. doi: 10.1002/1878-0261.12155
58. Li G, Mitra SS, Monje M, Henrich KN, Bangs CD, Nitta RT, et al. Expression of Epidermal Growth Factor Variant III (Egfrviii) in Pediatric Diffuse Intrinsic Pontine Gliomas. *J Neuro-Oncol* (2012) 108(3):395–402. doi: 10.1007/s11060-012-0842-3
59. Bax DA, Gaspar N, Little SE, Marshall L, Perryman L, Regairaz M, et al. Egfrviii Deletion Mutations in Pediatric High-Grade Glioma and Response to Targeted Therapy in Pediatric Glioma Cell Lines. *Clin Cancer Res* (2009) 15(18):5753–61. doi: 10.1158/1078-0432.CCR-08-3210
60. Ge H, Gong X, Tang CK. Evidence of High Incidence of Egfrviii Expression and Coexpression With EGFR in Human Invasive Breast Cancer by Laser Capture Microdissection and Immunohistochemical Analysis. *Int J Cancer* (2002) 98(3):357–61. doi: 10.1002/ijc.10224
61. Choe JH, Watchmaker PB, Simic MS, Gilbert RD, Li AW, Krasnow NA, et al. Synnotch-CAR T Cells Overcome Challenges of Specificity, Heterogeneity, and Persistence in Treating Glioblastoma. *Sci Trans Med* (2021) 13(591). doi: 10.1126/scitranslmed.abe7378
62. Xu LW, Chow KK, Lim M, Li G. Current Vaccine Trials in Glioblastoma: A Review. *J Immunol Res* (2014) 2014. doi: 10.1155/2014/796856
63. Miyake JA, Vooijs M. Tenascin-C a Novel Regulator of Brain Tumor-Initiating Cells (BTIC) in Glioma Acts Through NOTCH. *Trans Cancer Res* (2017) 6:S1055. doi: 10.21037/tcr.2017.07.10
64. Giblin SP, Midwood KS. Tenascin-C: Form *Versus* Function. *Cell Adhesion Migration* (2015) 9(1-2):48–82. doi: 10.4161/19336918.2014.987587
65. Ikeda Y, Mori M, Kajiyama K, Haraguchi Y, Sasaki O, Sugimachi K. Immunohistochemical Expression of Tenascin in Normal Stomach Tissue, Gastric Carcinomas and Gastric Carcinoma in Lymph Nodes. *Br J Cancer* (1995) 72(1):189–92. doi: 10.1038/bjc.1995.301
66. Leins A, Riva P, Lindstedt R, Davidoff MS, Mehraein P, Weis S. Expression of Tenascin-C in Various Human Brain Tumors and Its Relevance for Survival in Patients With Astrocytoma. *Cancer* (2003) 98(11):2430–9. doi: 10.1002/cncr.11796
67. Qi J, Esfahani D, Huang T, Ozark P, Bartom E, Hashizume R, et al. Tenascin-C Expression Contributes to Pediatric Brainstem Glioma Tumor Phenotype and Represents a Novel Biomarker of Disease. *Acta Neuropathologica Commun* (2019) 7(1):1–19. doi: 10.1186/s40478-019-0727-1
68. Spenlé C, Saupe F, Midwood K, Burckel H, Noel G, Orend G. Tenascin-C: Exploitation and Collateral Damage in Cancer Management. *Cell Adhesion Migration* (2015) 9(1-2):141–53. doi: 10.1080/19336918.2014.1000074
69. Jaiswal PK, Goel A, Mittal R. Survivin: A Molecular Biomarker in Cancer. *Indian J Med Res* (2015) 141(4):389. doi: 10.4103/0971-5916.159250
70. Garg H, Suri P, Gupta JC, Talwar G, Dubey S. Survivin: A Unique Target for Tumor Therapy. *Cancer Cell Int* (2016) 16(1):1–14. doi: 10.1186/s12935-016-0326-1
71. Xie D, Zeng Y, Wang H, Wen J, Tao Y, Sham J, et al. Expression of Cytoplasmic and Nuclear Survivin in Primary and Secondary Human Glioblastoma. *Br J Cancer* (2006) 94(1):108–14. doi: 10.1038/sj.bjc.6602904
72. Brun SN, Markant SL, Esparza LA, Garcia G, Terry D, Huang J-M, et al. Survivin as a Therapeutic Target in Sonic Hedgehog-Driven Medulloblastoma. *Oncogene* (2015) 34(29):3770–9. doi: 10.1038/onc.2014.304
73. Okada H, Low KL, Kohanbash G, McDonald HA, Hamilton RL, Pollack IF. Expression of Glioma-Associated Antigens in Pediatric Brain Stem and Non-Brain Stem Gliomas. *J Neuro-Oncol* (2008) 88(3):245–50. doi: 10.1007/s11060-008-9566-9
74. Li M, Wang J, Sui Y, Li T, Liu F, Zhang L, et al. Dipg-41. Identification of Birc5 as a Novel Therapeutic Target for Diffuse Intrinsic Pontine Glioma. *Neuro-Oncology* (2018) 20(Suppl 2):i57. doi: 10.1093/neuonc/noy059.134
75. Liu R, Mitchell DA. Survivin as an Immunotherapeutic Target for Adult and Pediatric Malignant Brain Tumors. *Cancer Immunol Immunother* (2010) 59 (2):183–93. doi: 10.1007/s00262-009-0757-9
76. Arber C, Feng X, Abhyankar H, Romero E, Wu M-F, Heslop HE, et al. Survivin-Specific T Cell Receptor Targets Tumor But Not T Cells. *J Clin Invest* (2015) 125(1):157–68. doi: 10.1172/JCI75876
77. Bianchi V, Bulek A, Fuller A, Lloyd A, Attaf M, Rizkallah PJ, et al. A Molecular Switch Abrogates Glycoprotein 100 (Gp100) T-Cell Receptor (TCR) Targeting of a Human Melanoma Antigen. *J Biol Chem* (2016) 291 (17):8951–9. doi: 10.1074/jbc.M115.707414
78. Raposo G, Marks MS. Melanosomes—Dark Organelles Enlighten Endosomal Membrane Transport. *Nat Rev Mol Cell Biol* (2007) 8 (10):786–97. doi: 10.1038/nrm2258
79. Zhang JG, Kruse CA, Driggers L, Hoa N, Wisoff J, Allen JC, et al. Tumor Antigen Precursor Protein Profiles of Adult and Pediatric Brain Tumors Identify Potential Targets for Immunotherapy. *J Neuro-Oncol* (2008) 88 (1):65–76. doi: 10.1007/s11060-008-9534-4
80. Rodríguez-Cerdeira C, Carnero Gregorio M, López-Barcenas A, Sánchez-Blanco E, Sánchez-Blanco B, Fabbrocini G, et al. Advances in Immunotherapy for Melanoma: A Comprehensive Review. *Mediators Inflammation* (2017) 2017. doi: 10.1155/2017/3264217
81. Slaney CY, Von Scheidt B, Davenport AJ, Beavis PA, Westwood JA, Mardiana S, et al. Dual-Specific Chimeric Antigen Receptor T Cells and an Indirect Vaccine Eradicate a Variety of Large Solid Tumors in an Immunocompetent, Self-Antigen Setting. *Clin Cancer Res* (2017) 23 (10):2478–90. doi: 10.1158/1078-0432.CCR-16-1860
82. Schuelke M, Evgin L, Wongthida P, Thompson J, Kottke T, Sanchez-Perez L, et al. Immu-12. T-Cell Therapies Demonstrate Efficacy Without Toxicity in Immunocompetent Models of Brainstem Tumors. *Neuro-Oncology* (2018) 20(Suppl 2):i101. doi: 10.1093/neuonc/noy059.328
83. Ho M, Kim H. Glypican-3: A New Target for Cancer Immunotherapy. *Eur J Cancer* (2011) 47(3):333–8. doi: 10.1016/j.ejca.2010.10.024
84. Ortiz MV, Roberts SS, Glade Bender J, Shukla N, Wexler LH. Immunotherapeutic Targeting of GPC3 in Pediatric Solid Embryonal Tumors. *Front Oncol* (2019) 9:108. doi: 10.3389/fonc.2019.00108
85. Yu K, Lin CJ, Hatcher A, Lozzi B, Kong K, Huang-Hobbs E, et al. PIK3CA Variants Selectively Initiate Brain Hyperactivity During Gliomagenesis. *Nature* (2020) 578(7793):166–71. doi: 10.1038/s41586-020-1952-2
86. Sun L, Gao F, Gao Z, Ao L, Li N, Ma S, et al. Shed Antigen-Induced Blocking Effect on CAR-T Cells Targeting Glypican-3 in Hepatocellular Carcinoma. *J Immunother Cancer* (2021) 9(4). doi: 10.1136/jitc-2020-001875
87. Kang CH, Kim Y, Lee SM, Choi SU, Park CH. Development of Antigen-Specific Chimeric Antigen Receptor KHYG-1 Cells for Glioblastoma. *Anticancer Res* (2021) 41(4):1811–9. doi: 10.21873/anticanres.14947
88. Sun X-D, Chen W-B, Sun D, Huang J, Li Y-Q, Pan J-X, et al. Neogenin in Amygdala for Neuronal Activity and Information Processing. *J Neurosci* (2018) 38(44):9600–13. doi: 10.1523/JNEUROSCI.0433-18.2018
89. Ylivinkka I, Hu Y, Chen P, Rantanen V, Hautaniemi S, Nyman TA, et al. Netrin-1-Induced Activation of Notch Signaling Mediates Glioblastoma Cell Invasion. *J Cell Sci* (2013) 126(11):2459–69. doi: 10.1242/jcs.120022
90. Akino T, Han X, Nakayama H, McNeish B, Zurakowski D, Mammoto A, et al. Netrin-1 Promotes Medulloblastoma Cell Invasiveness and Angiogenesis, and Demonstrates Elevated Expression in Tumor Tissue and Urine of Patients With Pediatric Medulloblastoma. *Cancer Res* (2014) 74(14):3716–26. doi: 10.1158/0008-5472.CAN-13-3116
91. Shimizu A, Nakayama H, Wang P, König C, Akino T, Sandlund J, et al. Netrin-1 Promotes Glioblastoma Cell Invasiveness and Angiogenesis by Multiple Pathways Including Activation of Rhoa, Cathepsin B, and Camp-Response Element-Binding Protein. *J Biol Chem* (2013) 288(4):2210–22. doi: 10.1074/jbc.M112.397398
92. Sesen J, Driscoll J, Shah N, Moses-Gardner A, Luiselli G, Alexandrescu S, et al. Neogenin Is Highly Expressed in Diffuse Intrinsic Pontine Glioma and Influences Tumor Invasion. *Brain Res* (2021) 1762:147348. doi: 10.1016/j.brainres.2021.147348
93. Saikali S, Avril T, Collet B, Hamlat A, Bansard J-Y, Drenou B, et al. Expression of Nine Tumour Antigens in a Series of Human Glioblastoma Multiforme: Interest of Egfrviii, IL-13Rα2, Gp100 and TRP-2 for

Immunotherapy. *J Neuro-Oncol* (2007) 81(2):139–48. doi: 10.1007/s11060-006-9220-3
94. Wang Z, Chen W, Zhang X, Cai Z, Huang W. A Long Way to the Battlefront: CAR T Cell Therapy Against Solid Cancers. *J Cancer* (2019) 10(14):3112. doi: 10.7150/jca.30406
95. Jin L, Tao H, Karachi A, Long Y, Hou AY, Na M, et al. CXCR1-or CXCR2-Modified CAR T Cells Co-Opt IL-8 for Maximal Antitumor Efficacy in Solid Tumors. *Nat Commun* (2019) 10(1):1–13. doi: 10.1038/s41467-019-11869-4
96. Dubois LG, Campanati L, Righy C, D'Andrea-Meira I, Porto-Carreiro I, Pereira CM, et al. R. Oliveira: Gliomas and the Vascular Fragility of the Blood Brain Barrier. *Front Cell Neurosci* (2014) 8:418. doi: 10.3389/fncel.2014.00418
97. Wherry EJ, Kurachi M. Molecular and Cellular Insights Into T Cell Exhaustion. *Nat Rev Immunol* (2015) 15(8):486–99. doi: 10.1038/nri3862
98. Antunes ARP, Scheyltjens I, Duerinck J, Neyns B, Movahedi K, Van Ginderachter JA. Understanding the Glioblastoma Immune Microenvironment as Basis for the Development of New Immunotherapeutic Strategies. *Elife* (2020) 9:e52176. doi: 10.7554/eLife.52176
99. Yang L, Zhang Y. Tumor-Associated Macrophages: From Basic Research to Clinical Application. *J Hematol Oncol* (2017) 10(1):58. doi: 10.1186/s13045-017-0430-2
100. Engler JR, Robinson AE, Smirnov I, Hodgson JG, Berger MS, Gupta N, et al. Increased Microglia/Macrophage Gene Expression in a Subset of Adult and Pediatric Astrocytomas. *PloS One* (2012) 7(8):e43339. doi: 10.1371/journal.pone.0043339
101. Bowman RL, Klemm F, Akkari L, Pyonteck SM, Sevenich L, Quail DF, et al. Macrophage Ontogeny Underlies Differences in Tumor-Specific Education in Brain Malignancies. *Cell Rep* (2016) 17(9):2445–59. doi: 10.1016/j.celrep.2016.10.052
102. Chen Z, Feng X, Herting CJ, Garcia VA, Nie K, Pong WW, et al. Cellular and Molecular Identity of Tumor-Associated Macrophages in Glioblastoma. *Cancer Res* (2017) 77(9):2266–78. doi: 10.1158/0008-5472.CAN-16-2310
103. Peranzoni E, Lemoine J, Vimeux L, Feuillet V, Barrin S, Kantari-Mimoun C, et al. Macrophages Impede CD8 T Cells From Reaching Tumor Cells and Limit the Efficacy of Anti–PD-1 Treatment. *Proc Natl Acad Sci* (2018) 115(17):E4041–50. doi: 10.1073/pnas.1720948115
104. Spear P, Barber A, Rynda-Apple A, Sentman CL. Chimeric Antigen Receptor T Cells Shape Myeloid Cell Function Within the Tumor Microenvironment Through IFN-γ and GM-CSF. *J Immunol* (2012) 188(12):6389–98. doi: 10.4049/jimmunol.1103019
105. Ruella M, Klichinsky M, Kenderian SS, Shestova O, Ziober A, Kraft DO, et al. Overcoming the Immunosuppressive Tumor Microenvironment of Hodgkin Lymphoma Using Chimeric Antigen Receptor T Cells. *Cancer Discov* (2017) 7(10):1154–67. doi: 10.1158/2159-8290.CD-16-0850
106. Grabovska Y, Mackay A, O'Hare P, Crosier S, Finetti M, Schwalbe EC, et al. Pediatric Pan-Central Nervous System Tumor Analysis of Immune-Cell Infiltration Identifies Correlates of Antitumor Immunity. *Nat Commun* (2020) 11(1):1–15. doi: 10.1038/s41467-020-18070-y
107. Ooi YC, Tran P, Ung N, Thill K, Trang A, Fong BM, et al. The Role of Regulatory T-Cells in Glioma Immunology. *Clin Neurol Neurosurg* (2014) 119:125–32. doi: 10.1016/j.clineuro.2013.12.004
108. Barsheshet Y, Wildbaum G, Levy E, Vitenshtein A, Akinseye C, Griggs J, et al. CCR8+ Foxp3+ Treg Cells as Master Drivers of Immune Regulation. *Proc Natl Acad Sci* (2017) 114(23):6086–91. doi: 10.1073/pnas.1621280114
109. Yan J, Zhao Q, Gabrusiewicz K, Kong L-Y, Xia X, Wang J, et al. FGL2 Promotes Tumor Progression in the CNS by Suppressing CD103+ Dendritic Cell Differentiation. *Nat Commun* (2019) 10(1):1–15. doi: 10.1038/s41467-019-08770-5
110. Wang R, Zhang J-L, Wei B, Tian Y, Li Z-H, Wang L, et al. Upregulation of Plasmacytoid Dendritic Cells in Glioma. *Tumor Biol* (2014) 35(10):9661–6. doi: 10.1007/s13277-014-2211-7
111. Curran CS, Bertics PJ. Eosinophils in Glioblastoma Biology. *J Neuroinflamm* (2012) 9(1):1–14. doi: 10.1186/1742-2094-9-11
112. Huang Z, Wu L, Hou Z, Zhang P, Li G, Xie J. Eosinophils and Other Peripheral Blood Biomarkers in Glioma Grading: A Preliminary Study. *BMC Neurol* (2019) 19(1):1–11. doi: 10.1186/s12883-019-1549-2
113. Lin GL, Nagaraja S, Filbin MG, Suvà ML, Vogel H, Monje M. Non-Inflammatory Tumor Microenvironment of Diffuse Intrinsic Pontine Glioma. *Acta Neuropathologica Commun* (2018) 6(1):1–12. doi: 10.1186/s40478-018-0553-x
114. Lieberman NA, DeGolier K, Kovar HM, Davis A, Hoglund V, Stevens J, et al. Characterization of the Immune Microenvironment of Diffuse Intrinsic Pontine Glioma: Implications for Development of Immunotherapy. *Neuro-Oncology* (2019) 21(1):83–94. doi: 10.1093/neuonc/noy145
115. Engelhardt B, Ransohoff RM. Capture, Crawl, Cross: The T Cell Code to Breach the Blood–Brain Barriers. *Trends Immunol* (2012) 33(12):579–89. doi: 10.1016/j.it.2012.07.004
116. Amankulor NM, Kim Y, Arora S, Kargl J, Szulzewsky F, Hanke M, et al. Mutant IDH1 Regulates the Tumor-Associated Immune System in Gliomas. *Genes Dev* (2017) 31(8):774–86. doi: 10.1101/gad.294991.116
117. Wu L, Li X, Janagam DR, Lowe TL. Overcoming the Blood-Brain Barrier in Chemotherapy Treatment of Pediatric Brain Tumors. *Pharm Res* (2014) 31(3):531–40. doi: 10.1007/s11095-013-1196-z
118. Patterson JD, Henson JC, Breese RO, Bielamowicz KJ, Rodriguez A. Car T Cell Therapy for Pediatric Brain Tumors. *Front Oncol* (2020) 10:1582. doi: 10.3389/fonc.2020.01582
119. Donovan LK, Delaidelli A, Joseph SK, Bielamowicz K, Fousek K, Holgado BL, et al. Locoregional Delivery of CAR T Cells to the Cerebrospinal Fluid for Treatment of Metastatic Medulloblastoma and Ependymoma. *Nat Med* (2020) 26(5):720–31. doi: 10.1038/s41591-020-0827-2
120. Theruvath J, Sotillo E, Mount CW, Graef CM, Delaidelli A, Heitzeneder S, et al. Locoregionally Administered B7-H3-Targeted CAR T Cells for Treatment of Atypical Teratoid/Rhabdoid Tumors. *Nat Med* (2020) 26(5):712–9. doi: 10.1038/s41591-020-0821-8
121. Graber JJ, Kesari S. Leptomeningeal Metastases. *Curr Treat Options Oncol* (2018) 19(1):1–14. doi: 10.1007/s11864-018-0518-0
122. Hong JJ, Rosenberg SA, Dudley ME, Yang JC, White DE, Butman JA, et al. Successful Treatment of Melanoma Brain Metastases With Adoptive Cell Therapy. *Clin Cancer Res* (2010) 16(19):4892–8. doi: 10.1158/1078-0432.CCR-10-1507
123. Cohen-Pfeffer JL, Gururangan S, Lester T, Lim DA, Shaywitz AJ, Westphal M, et al. Intracerebroventricular Delivery as a Safe, Long-Term Route of Drug Administration. *Pediatr Neurol* (2017) 67:23–35. doi: 10.1016/j.pediatrneurol.2016.10.022
124. Yakoub-Agha I, Chabannon C, Bader P, Basak GW, Bonig H, Ciceri F, et al. Management of Adults and Children Undergoing Chimeric Antigen Receptor T-Cell Therapy: Best Practice Recommendations of the European Society for Blood and Marrow Transplantation (EBMT) and the Joint Accreditation Committee of ISCT and EBMT (JACIE). *Haematologica* (2020) 105(2):297. doi: 10.3324/haematol.2019.229781
125. Zhou Z, Luther N, Ibrahim GM, Hawkins C, Vibhakar R, Handler MH, et al. B7-H3, a Potential Therapeutic Target, Is Expressed in Diffuse Intrinsic Pontine Glioma. *J Neuro-Oncol* (2013) 111(3):257–64. doi: 10.1007/s11060-012-1021-2
126. Holtzman NG, Xie H, Bentzen S, Kesari V, Bukhari A, El Chaer F, et al. Immune Effector Cell–Associated Neurotoxicity Syndrome After Chimeric Antigen Receptor T-Cell Therapy for Lymphoma: Predictive Biomarkers and Clinical Outcomes. *Neuro-Oncology* (2021) 23(1):112–21. doi: 10.1093/neuonc/noaa183
127. AlRayahi J, Zapotocky M, Ramaswamy V, Hanagandi P, Branson H, Mubarak W, et al. Pediatric Brain Tumor Genetics: What Radiologists Need to Know. *Radiographics* (2018) 38(7):2102–22. doi: 10.1148/rg.2018180109
128. Curley CT, Mead BP, Negron K, Kim N, Garrison WJ, Miller GW, et al. Augmentation of Brain Tumor Interstitial Flow *via* Focused Ultrasound Promotes Brain-Penetrating Nanoparticle Dispersion and Transfection. *Sci Adv* (2020) 6(18):eaay1344. doi: 10.1126/sciadv.aay1344
129. Mesiwala AH, Farrell L, Wenzel HJ, Silbergeld DL, Crum LA, Winn HR, et al. High-Intensity Focused Ultrasound Selectively Disrupts the Blood-Brain Barrier *In Vivo*. *Ultrasound Med Biol* (2002) 28(3):389–400. doi: 10.1016/S0301-5629(01)00521-X
130. Chen P-Y, Hsieh H-Y, Huang C-Y, Lin C-Y, Wei K-C, Liu H-L. Focused Ultrasound-Induced Blood–Brain Barrier Opening to Enhance Interleukin-12 Delivery for Brain Tumor Immunotherapy: A Preclinical Feasibility Study. *J Trans Med* (2015) 13(1):1–12. doi: 10.1186/s12967-015-0451-y

131. Zimmermann K, Kuehle J, Dragon AC, Galla M, Kloth C, Rudek LS, et al. Design and Characterization of an "All-in-One" Lentiviral Vector System Combining Constitutive Anti-GD2 CAR Expression and Inducible Cytokines. *Cancers* (2020) 12(2):375. doi: 10.3390/cancers12020375
132. Shum T, Omer B, Tashiro H, Kruse RL, Wagner DL, Parikh K, et al. Constitutive Signaling From an Engineered IL7 Receptor Promotes Durable Tumor Elimination by Tumor-Redirected T Cells. *Cancer Discov* (2017) 7 (11):1238–47. doi: 10.1158/2159-8290.CD-17-0538
133. Martínez Bedoya D, Dutoit V, Migliorini D. Allogeneic CAR T Cells: An Alternative to Overcome Challenges of CAR T Cell Therapy in Glioblastoma. *Front Immunol* (2021) 12:506. doi: 10.3389/fimmu.2021.640082
134. Kloss CC, Lee J, Zhang A, Chen F, Melenhorst JJ, Lacey SF, et al. Dominant-Negative TGF-β Receptor Enhances PSMA-Targeted Human CAR T Cell Proliferation and Augments Prostate Cancer Eradication. *Mol Ther* (2018) 26(7):1855–66. doi: 10.1016/j.ymthe.2018.05.003
135. Gargett T, Brown MP. The Inducible Caspase-9 Suicide Gene System as a "Safety Switch" to Limit on-Target, Off-Tumor Toxicities of Chimeric Antigen Receptor T Cells. *Front Pharmacol* (2014) 5:235. doi: 10.3389/fphar.2014.00235
136. Budde LE, Berger C, Lin Y, Wang J, Lin X, Frayo SE, et al. Combining a CD20 Chimeric Antigen Receptor and an Inducible Caspase 9 Suicide Switch to Improve the Efficacy and Safety of T Cell Adoptive Immunotherapy for Lymphoma. *PloS One* (2013) 8(12):e82742. doi: 10.1371/journal.pone.0082742
137. Paszkiewicz PJ, Fräßle SP, Srivastava S, Sommermeyer D, Hudecek M, Drexler I, et al. Targeted Antibody-Mediated Depletion of Murine CD19 CAR T Cells Permanently Reverses B Cell Aplasia. *J Clin Invest* (2016) 126 (11):4262–72. doi: 10.1172/JCI84813
138. Serafini M, Manganini M, Borleri G, Bonamino M, Imberti L, Biondi A, et al. Characterization of CD20-Transduced T Lymphocytes as an Alternative Suicide Gene Therapy Approach for the Treatment of Graft-*Versus*-Host Disease. *Hum Gene Ther* (2004) 15(1):63–76. doi: 10.1089/10430340460732463
139. Han X, Wang Y, Wei J, Han W. Multi-Antigen-Targeted Chimeric Antigen Receptor T Cells for Cancer Therapy. *J Hematol Oncol* (2019) 12(1):1–10. doi: 10.1186/s13045-019-0813-7
140. Land CA, Musich PR, Haydar D, Krenciute G, Xie Q. Chimeric Antigen Receptor T-Cell Therapy in Glioblastoma: Charging the T Cells to Fight. *J Trans Med* (2020) 18(1):1–13. doi: 10.1186/s12967-020-02598-0
141. Hegde M, Mukherjee M, Grada Z, Pignata A, Landi D, Navai SA, et al. Tandem CAR T Cells Targeting HER2 and IL13Rα2 Mitigate Tumor Antigen Escape. *J Clin Invest* (2016) 126(8):3036–52. doi: 10.1172/JCI83416
142. Hegde M, Corder A, Chow KK, Mukherjee M, Ashoori A, Kew Y, et al. Combinational Targeting Offsets Antigen Escape and Enhances Effector Functions of Adoptively Transferred T Cells in Glioblastoma. *Mol Ther* (2013) 21(11):2087–101. doi: 10.1038/mt.2013.185
143. Davies DM, Maher J. Gated Chimeric Antigen Receptor T-Cells: The Next Logical Step in Reducing Toxicity? *Trans Lung Cancer Res* (2016) 5(S1):S61–5. doi: 10.21037/tcr.2016.06.04
144. Tantalo DG, Oliver AJ, von Scheidt B, Harrison AJ, Mueller SN, Kershaw MH, et al. Understanding T Cell Phenotype for the Design of Effective Chimeric Antigen Receptor T Cell Therapies. *J Immunotherapy Cancer* (2021) 9(5). doi: 10.1136/jitc-2021-002555
145. Gattinoni L, Lugli E, Ji Y, Pos Z, Paulos CM, Quigley MF, et al. A Human Memory T Cell Subset With Stem Cell–Like Properties. *Nat Med* (2011) 17 (10):1290–7. doi: 10.1038/nm.2446
146. Wang X, Popplewell LL, Wagner JR, Naranjo A, Blanchard MS, Mott MR, et al. Phase 1 Studies of Central Memory–Derived CD19 CAR T–Cell Therapy Following Autologous HSCT in Patients With B-Cell NHL. *Blood J Am Soc Hematol* (2016) 127(24):2980–90. doi: 10.1182/blood-2015-12-686725
147. Zhou X, Yu S, Zhao D-M, Harty JT, Badovinac VP, Xue H-H. Differentiation and Persistence of Memory CD8+ T Cells Depend on T Cell Factor 1. *Immunity* (2010) 33(2):229–40. doi: 10.1016/j.immuni.2010.08.002
148. Amsen D, van Gisbergen KP, Hombrink P, van Lier RA. Tissue-Resident Memory T Cells at the Center of Immunity to Solid Tumors. *Nat Immunol* (2018) 19(6):538–46. doi: 10.1038/s41590-018-0114-2
149. Gattinoni L, Zhong X-S, Palmer DC, Ji Y, Hinrichs CS, Yu Z, et al. Wnt Signaling Arrests Effector T Cell Differentiation and Generates CD8+ Memory Stem Cells. *Nat Med* (2009) 15(7):808–13. doi: 10.1038/nm.1982
150. Macintyre AN, Finlay D, Preston G, Sinclair LV, Waugh CM, Tamas P, et al. Protein Kinase B Controls Transcriptional Programs That Direct Cytotoxic T Cell Fate But Is Dispensable for T Cell Metabolism. *Immunity* (2011) 34 (2):224–36. doi: 10.1016/j.immuni.2011.01.012
151. Mousset CM, Hobo W, Ji Y, Fredrix H, De Giorgi V, Allison RD, et al. *Ex Vivo* AKT-Inhibition Facilitates Generation of Polyfunctional Stem Cell Memory-Like CD8+ T Cells for Adoptive Immunotherapy. *Oncoimmunology* (2018) 7 (10):e1488565. doi: 10.1080/2162402X.2018.1488565
152. Singh H, Figliola MJ, Dawson MJ, Huls H, Olivares S, Switzer K, et al. Reprogramming CD19-Specific T Cells With IL-21 Signaling Can Improve Adoptive Immunotherapy of B-Lineage Malignancies. *Cancer Res* (2011) 71 (10):3516–27. doi: 10.1158/0008-5472.CAN-10-3843
153. McLellan AD, Ali Hosseini Rad SM. Chimeric Antigen Receptor T Cell Persistence and Memory Cell Formation. *Immunol Cell Biol* (2019) 97 (7):664–74. doi: 10.1111/imcb.12254
154. Hurton LV, Singh H, Najjar AM, Switzer KC, Mi T, Maiti S, et al. Tethered IL-15 Augments Antitumor Activity and Promotes a Stem-Cell Memory Subset in Tumor-Specific T Cells. *Proc Natl Acad Sci* (2016) 113(48):E7788–97. doi: 10.1073/pnas.1610544113
155. Choi BD, Yu X, Castano AP, Darr H, Henderson DB, Bouffard AA, et al. CRISPR-Cas9 Disruption of PD-1 Enhances Activity of Universal Egfrviii CAR T Cells in a Preclinical Model of Human Glioblastoma. *J Immunother Cancer* (2019) 7(1):1–8. doi: 10.1186/s40425-019-0806-7
156. Prinzing B, Zebley CC, Petersen CT, Bell M, Fan Y, Crawford JC, et al. DNMT3A-Dependent Epigenetic Programs Constrain CAR T Cell Survival and Effector Function. In: *Molecular Therapy*. 50 HAMPSHIRE ST, FLOOR 5, CAMBRIDGE, MA 02139 USA: CELL PRESS (2020).
157. Sengupta S, Katz SC, Sengupta S, Sampath P. Glycogen Synthase Kinase 3 Inhibition Lowers PD-1 Expression, Promotes Long-Term Survival and Memory Generation in Antigen-Specific CAR-T Cells. *Cancer Lett* (2018) 433:131–9. doi: 10.1016/j.canlet.2018.06.035
158. Lenting K, Verhaak R, ter Laan M, Wesseling P, Leenders W. Glioma: Experimental Models and Reality. *Acta Neuropathologica* (2017) 133:263–82. doi: 10.1007/s00401-017-1671-4
159. Lwin TM, Hoffman RM, Bouvet M. Advantages of Patient-Derived Orthotopic Mouse Models and Genetic Reporters for Developing Fluorescence-Guided Surgery. *J Surg Oncol* (2018) 118(2):253–64. doi: 10.1002/jso.25150
160. Biery MC, Noll A, Myers C, Morris SM, Winter CA, Pakiam F, et al. A Protocol for the Generation of Treatment-Naïve Biopsy-Derived Diffuse Intrinsic Pontine Glioma and Diffuse Midline Glioma Models. *J Exp Neurol* (2020) 1(4):158. doi: 10.33696/Neurol.1.025
161. Smith KS, Xu K, Mercer KS, Boop F, Klimo P, DeCupyere M, et al. Patient-Derived Orthotopic Xenografts of Pediatric Brain Tumors: A St. Jude Resource. *Acta Neuropathologica* (2020) 140(2):209–25. doi: 10.1007/s00401-020-02171-5
162. He C, Xu K, Zhu X, Dunphy PS, Gudenas B, Lin W, et al. Patient-Derived Models Recapitulate Heterogeneity of Molecular Signatures and Drug Response in Pediatric High-Grade Glioma. *Nat Commun* (2021) 12(1):1–17. doi: 10.1038/s41467-021-24168-8
163. SJCRH. *Pediatric Brain Tumor Portal*. St. Jude Children's Research Hospital Memphis (2021).
164. Pompili L, Porru M, Caruso C, Biroccio A, Leonetti C. Patient-Derived Xenografts: A Relevant Preclinical Model for Drug Development. *J Exp Clin Cancer Res* (2016) 35(1):1–8. doi: 10.1186/s13046-016-0462-4
165. Sreedharan S, Maturi NP, Xie Y, Sundström A, Jarvius M, Libard S, et al. Mouse Models of Pediatric Supratentorial High-Grade Glioma Reveal How Cell-of-Origin Influences Tumor Development and Phenotype. *Cancer Res* (2017) 77(3):802–12. doi: 10.1158/0008-5472.CAN-16-2482
166. Larson JD, Kasper LH, Paugh BS, Jin H, Wu G, Kwon C-H, et al. Histone H3.3 K27M Accelerates Spontaneous Brainstem Glioma and Drives Restricted Changes in Bivalent Gene Expression. *Cancer Cell* (2019) 35(1):140–155. e7. doi: 10.1016/j.ccell.2018.11.015
167. Funato K, Major T, Lewis PW, Allis CD, Tabar V. Use of Human Embryonic Stem Cells to Model Pediatric Gliomas With H3. 3K27M Histone Mutation. *Science* (2014) 346(6216):1529–33. doi: 10.1126/science.1253799

168. Mohammad F, Weissmann S, Leblanc B, Pandey DP, Højfeldt JW, Comet I, et al. EZH2 Is a Potential Therapeutic Target for H3K27M-Mutant Pediatric Gliomas. *Nat Med* (2017) 23(4):483–92. doi: 10.1038/nm.4293
169. Patel SK, Hartley RM, Wei X, Furnish R, Escobar-Riquelme F, Bear H, et al. Generation of Diffuse Intrinsic Pontine Glioma Mouse Models by Brainstem-Targeted *In Utero* Electroporation. *Neuro Oncol* (2020) 22 (3):381–92. doi: 10.1093/neuonc/noz197

Conflict of Interest: GK has patent applications in the field of immunotherapy.

The remaining authors declare that the research was conducted in the absence of any commercial or financial relationships that could be construed as a potential conflict of interest.

Publisher's Note: All claims expressed in this article are solely those of the authors and do not necessarily represent those of their affiliated organizations, or those of the publisher, the editors and the reviewers. Any product that may be evaluated in this article, or claim that may be made by its manufacturer, is not guaranteed or endorsed by the publisher.

Copyright © 2021 Haydar, Ibañez-Vega and Krenciute. This is an open-access article distributed under the terms of the Creative Commons Attribution License (CC BY). The use, distribution or reproduction in other forums is permitted, provided the original author(s) and the copyright owner(s) are credited and that the original publication in this journal is cited, in accordance with accepted academic practice. No use, distribution or reproduction is permitted which does not comply with these terms.

frontiers in Oncology

REVIEW
published: 03 December 2021
doi: 10.3389/fonc.2021.718590

Antibody Drug Conjugates in Glioblastoma – Is There a Future for Them?

Sagun Parakh[1,2,3], *Joseph Nicolazzo*[4], *Andrew M Scott*[2,3,5,6] *and Hui Kong Gan*[1,2,3,5*]

[1] Department of Medical Oncology, Austin Hospital, Heidelberg, VIC, Australia, [2] Tumour Targeting Laboratory, Olivia Newton-John Cancer Research Institute, Heidelberg, VIC, Australia, [3] School of Cancer Medicine, La Trobe University, Heidelberg, VIC, Australia, [4] Drug Delivery, Disposition and Dynamics, Monash Institute of Pharmaceutical Sciences, Monash University, Parkville, VIC, Australia, [5] Department of Medicine, University of Melbourne, Heidelberg, VIC, Australia, [6] Department of Molecular Imaging and Therapy, Austin Health, Heidelberg, VIC, Australia

Glioblastoma (GBM) is an aggressive and fatal malignancy that despite decades of trials has limited therapeutic options. Antibody drug conjugates (ADCs) are composed of a monoclonal antibody which specifically recognizes a cellular surface antigen linked to a cytotoxic payload. ADCs have demonstrated superior efficacy and/or reduced toxicity in a range of haematological and solid tumors resulting in nine ADCs receiving regulatory approval. ADCs have also been explored in patients with brain tumours but with limited success to date. While earlier generations ADCs in glioma patients have had limited success and high toxicity, newer and improved ADCs characterised by low immunogenicity and more effective payloads have shown promise in a range of tumour types. These newer ADCs have also been tested in glioma patients, however, with mixed results. Factors affecting the effectiveness of ADCs to target the CNS include the blood brain barrier which acts as a physical and biochemical barrier, the pro-cancerogenic and immunosuppressive tumor microenvironment and tumour characteristics like tumour volume and antigen expression. In this paper we review the data regarding the ongoing the development of ADCs in glioma patients as well as potential strategies to overcome these barriers to maximise their therapeutic potential.

Keywords: antibody drug conjugates (ADC), glioma, glioblastoma, blood brain barrier, tumour microenvironment, biomarkers, molecular imaging

OPEN ACCESS

Edited by:
David Nathanson, UCLA David Geffen School of Medicine, United States

Reviewed by:
Terry Calvin Burns, Mayo Clinic, United States
Gerardo Caruso, University Hospital of Policlinico G. Martino, Italy

***Correspondence:**
Hui Kong Gan
hui.gan@onjcri.org.au

Specialty section:
This article was submitted to Neuro-Oncology and Neurosurgical Oncology, a section of the journal Frontiers in Oncology

Received: *01 June 2021*
Accepted: *15 November 2021*
Published: *03 December 2021*

Citation:
Parakh S, Nicolazzo J, Scott AM and Gan HK (2021) Antibody Drug Conjugates in Glioblastoma – Is There a Future for Them? Front. Oncol. 11:718590. doi: 10.3389/fonc.2021.718590

INTRODUCTION

Glioblastoma (GBM) is an aggressive fatal disease characterised by complex molecular heterogeneity and aggressive infiltrative growth. Despite s decades of trials testing novel agents, the median survival remains unchanged at 14 - 17 months only (1–4). Multiple strategies have been explored with limited success to improve the efficacy of chemotherapy in GBM, including novel formulations, direct administration into the central nervous system (CNS) and targeted vascular disruption; unfortunately, these have often resulted in higher toxicity rates without significantly improving patient outcomes (5–7).

Antibody drug conjugates (ADCs) are a new but proven class of highly potent therapeutics, composed of a monoclonal antibody which specifically recognizes a cellular surface antigen linked to a cytotoxic payload (8). This results in a number of advantages: reduced toxicity due to more targeted delivery of cytotoxic therapy directly into the tumours; enhanced cell kill from the ability of use more toxic drugs that cannot be safely administered systemically; and the additive/synergistic benefit of combined tumour kill from the antibody and the payload respectively (9, 10). The ultimate efficacy of ADCs though relies on the complex interplay between three vital components: antibody, linker and payload. Early failures in the development of ADCs were due in part to challenges associated with these components, however recent advances have resulted in notable successes, resulting in nine ADCs receiving regulatory approval by the Food and Drug Administration in the USA and four ADCs by the European Medicines Agency (8, 11).

ADCs have also been explored for patients with brain tumours but with limited success to date. In particular, the apparent failure of two recent high-profile ADCs has resulted in a lessening of interest to this approach in glioma patients currently (12, 13). In this article, we will review the development of ADCs in glioma patients and summarise the data supporting their on-going development. We will discuss potential strategies to maximise their therapeutic potential by increasing their penetration through the blood-brain barrier (BBB), selection of more biologically relevant targets in the brain and its microenvironment, novel methods of drug targeting, newer payloads and better patient selection.

EARLY ADCs IN GLIOMA THERAPY

The first generation of ADCs tested in glioma patients comprised mainly immunotoxins and radioimmunotherapy (**Table 1**). Immunotoxins are antibodies conjugated to naturally occurring bacterial toxins, such as *Pseudomonas aeruginosa* exotoxin A and diphtheria toxin. Radioimmunoconjugates utilise isotopes such as iodine-125 or iodine-131 as payloads. These commonly targeted the EGFR axis (either the receptor itself or its mutants and ligands) due the relatively high prevalence of these targets in gliomas and their likely role as an oncogenic pathway in glioma. Targeting the EGFRvIII mutation was particularly attractive. This is comprised of an in-frame deletion of exons 2-7 that results in a truncated by constitutively active receptor (24). Furthermore, the EGFRvIII mutation is relatively frequent (in 20-40% of GBM tumours) but shows a tumour restricted expression pattern compared to wildtype EGFR (24). However,

TABLE 1 | Selected ADCs, immunotoxins and radioimmunoconjugates in high grade gliomas.

Drug	Class	Phase	Date	Toxicities	Efficacy	Comments
ADCs i						
ABT-414 (14)	Anti-EGFR ADC with MMAF	I	2015	Lymphopenia, ocular toxicity, brain oedema, increased transaminases	Monotherapy: RR 8%, mOS N/A, PFS-6 24% With TMZ: RR 17%, mOS N/A, PFS-6 25%	Data in EGFR amplified. Phase 2 and 3 studies in progress
AMG-595 (15)	Anti-EGFR ADC with DM1	I	2014	Thrombocytopenia, LFT abnormalities	RR 8%; mOS N/A; PFS-6 N/A	
Immunotoxins						
Cintredexin Besudotoxin (16)	IL13–PE38QQR	III	2010	Pulmonary embolism (8% including one fatal)	RR N/A; mOS 11.3 months; PFS-6 N/A	
NBI-3001 (17)	Circularized IL4–PE38KDEL	I/II	2003	Neurological deficits (Weakness, aphasia, confusion, coma), seizures, headaches, cerebral oedema, nausea, meningitis)	RR N/A; mOS 5.8months*; PFS-6 48%	
TP-38 (IVAX) (18)	TGFα + PE38	I	2008	Fatigue, neurological deterioration (seizures, hemiparesis)	RR 13%; mOS 5 months*; PFS-6 N/A	
Tf-CRM107 (19)	Transferrin-DT	II	2003	Cerebral oedema, seizures	RR 35%; mOS 9 months; PFS-6 N/A	Phase 3 studies were aborted or remain unreported (20)
Radioimmunoconjugates						
^{125}I-Mab 425 (21)	**IV** murine anti-EGFR (with RT-TMZ)	II	2010	Occasional nausea, flushing, hypotension, skin irritation. Only 4 pts had HAMA	RR N/A; mOS 20.4 months	A sequential cohort with RT alone had mOS 10.2 months
^{131}I-81C6 (22)	**LR** murine anti-tenascin (with RT-chemo)	Pilot	2008	Seizures (including status epilepticus), haematological, neurological, infective, thrombotic	RR N/A; mOS 22.6 months	
^{131}I-BC2/ BC4 (23)	**LR** murine anti-tenascin (with conventional surgery and post-operative treatment)	I/II	1999	Headaches, HAMA reactions	RR N/A; mOS 19 months	Data shown for GBM patients; mOS was 25 months in small volume disease

ADC, Antibody drug conjugate; EGFR, Epidermal growth factor receptor; HAMA, human anti–mouse antibody; LFTs, liver function tests; mOS, median overall survival; mPFS, median progression free survival; N/A; Not Available, RR, Response rate; RT, Radiotherapy; TMZ, temozolomide.

TABLE 2 | Common toxicities associated with antibody drug conjugates.

Payload type	Mechanism of action	Common toxicities
DM1	Inhibits tubulin polymerization and causes destabilization of microtubule structures	Thrombocytopenia, fatigue, increased levels of transaminases, anemia, nausea, hemorrhage, abdominal pain, pyrexia, musculoskeletal pain, vomiting, and dyspnea (28, 29)
DM4		Elevated transaminases; ocular toxicity (including decreased visual acuity, corneal deposits, keratitis); generalized symptoms (including headache, confusion, fatigue), mucositis (30)
MMAE		Infections, nausea, fatigue, diarrhea, peripheral sensory neuropathy, neutropenia, peripheral motor neuropathy, rash, cough, vomiting, myalgia, pyrexia, abdominal pain, arthralgia, pruritus, constipation, dyspnea, loss of weight, and upper respiratory tract infection (31)
MMAF		Neutropenia, thrombocytopenia, ocular toxicity (including corneal deposits, keratopathy) (30)
Calicheamicin	Binds to the DNA minor groove cleaving the double-stranded DNA	Lymphopenia, skin toxicity, neutropenia, thrombocytopenia; pyrexia, chills, nausea, infection, hemorrhage, fatigue, headache, increased transaminases and hyperbilirubinemia, vomiting, abdominal pain, stomatitis, veno-occlusive disease/sinusoidal obstruction syndrome and diarrhea (32, 33)
Duocarmycin derivative		Hypersensitivity, hyperpigmentation (34)
PBD		Hypocellular marrow, epistaxis, fatigue, thrombocytopenia, transaminitis, oedema, hypoalbuminemia, dyspnoea (35)
SN-38	Prevents DNA unwinding by inhibition of DNA topoisomerase I resulting in irreversible double strand breaks	Thyphilitis, neutropenia, nausea, vomiting (36)

DM1, Mertansine/emtansine; DM4, Ravtansine/soravtansine; MMAE, Monomethyl auristatin E; MMAF, Monomethyl auristatin F; PBD, Pyrrolobenzodiazepine; SN38, Irinotecan metabolite.

other targets of these early ADCs included IL-13Rα2 receptor, IL4 and transferrin. Unfortunately, these early ADCs were found to be ineffective due to a number of problems including high immunogenicity, unstable linkers, inefficient deliver due *via* early convection delivery systems, biomarker limitations to address tumour heterogeneity and toxicity (25–27).

NEWER ADCs IN NON-GLIOMA THERAPY

Subsequently, improved ADCs were generated which were characterised by low immunogenicity (usually with chimeric, humanised or fully human antibodies) and more effective payloads (**Table 2**). The success of these newer generation ADCs has been shown in haematological as well as in triple negative breast cancer (TNBC). These include brentuximab vedotin, an anti-CD30, antibody conjugated with monomethyl auristatin E (MMAE), an auristatin payload which disrupts microtubules. This has been shown to improve patient outcomes as consolidation after autologous stem cell transplant in patients with Hodgkin's lymphoma (37), and the subsequently in combination therapy with chemotherapy in newly diagnosed patients (38). It has also been shown to be effective in patients with CD30-positive T-cell lymphoma (39, 40) and anaplastic large cell lymphoma (41). Trastuzumab emtansine, which carries also carries a microtubule targeting payload, DM1, has shown efficacy in patients with HER2-positive breast cancer and is the first ADC to be approved in solid tumors (42, 43). Other examples of successful ADCs utilising DNA-damaging payloads include inotuzumab ozogamicin with a caliceamicin payload in CD-22 positive ALL (44) and gemtuzumab ozogamicin with a caliceamicin payload in AML (45). Another highly promising class of payloads are is those targeting topoisomerase, such as Sacituzumab govitecan (SG) against Trop 2 and bearing the SN38 payload. SG has shown significant activity in TNBC with improvements in PFS and OS compared to chemotherapy alone (46). In addition, SG has demonstrated activity in intracranial xenograft models and demonstrated activity in patients with recurrent GBM in a single centre pilot study (47).

NEWER ADCs IN GLIOMA THERAPY

In addition to their use in extra-cranial malignancies as described above, these newer ADCs have also been tested in glioma patients with mixed results. As before, targeting EGFR remained highly attractive due to the high frequency of abnormalities in this pathway in high grade gliomas. Furthermore, several highly specific and novel antibodies against EGFR and EGFRvIII had been developed which promised more selective targeting. The monoclonal antibody 806 (mAb806) is a murine anti-EGFR antibody that selectively targets a cryptic epitope of the EGFR which is only exposed under certain conditions, including where wild-type EGFR is highly over-expressed, where there are autocrine loops and/or harbor there are specific mutations which expose the epitope e.g. the EGFRvIII deletion variant. As these conditions are essential tumour restricted, mAb806 and derivative constructs are also tumour restricted with no normal tissue binding. This in this way, there avoid the toxicity typically associated with other systemic EGFR drugs inhibitors (48, 49). ABT-806, the humanized form of mAb806, has shown to be well tolerated and devoid of conventional anti-EGFR toxicities like rash and diarrhoea. Furthermore, biodistribution studies of ^{111}In-ABT-806 showed no normal tissue uptake highlighting the tumor-specific nature of mAb806 (49–52). Depatuxizumab mafodotin (Depatux-M) is an EGFR targeting ADC comprising of mAb806

linked to the anti-microtubule toxin monomethyl auristatin F (MMAF). Depatux-M has shown promising *in-vivo* activity in tumor models overexpressing wild type EGFR, *EGFR* amplification, or EGFRvIII mutation (53). Depatuxizumab mafodotin was also found to improve anti-tumour efficacy when combined with radiotherapy and temozolomide in preclinical models (53). The combination was also subsequently confirmed to be safe when tested in a Phase 1 study with newly diagnosed GBM with patients (54), and hence proceed to Phase 3 testing in the INTELLANCE I trial. Unfortunately, the addition of Depatux-M to standard chemo-irradiation with TMZ in newly diagnosed EGFR amplified glioblastoma patients was eventually discontinued for futility (12).

In contrast to the negative results in newly diagnosed patients, anti-EGFR ADCs targeting glioma with EGFR over-expression or EGFRvIII showed clear signals of efficacy in patients with relapsed glioma after chemo-radiation. Depatux-M was evaluated in the randomised phase II INTELLANCE 2 study in patients with EGFR amplified recurrent GBM (55, 56). In this study, the combination of Depatux-M with temozolomide (TMZ) demonstrated a strong trend towards substantial benefit in overall survival compared to the chemotherapy arm (HR 0.71, p=0.062) (57). The benefit of Depatux-M was highest in patients relapsing more than 16 weeks after the start of the last TMZ cycle. No evidence of efficacy in the monotherapy arm was observed in the subgroup with the MGMT promoter unmethylated tumors. These results are given added weight by the results of a Phase I/II study with AMG 595, an ADC comprising a fully human, anti-EGFRvIII monoclonal antibody linked *via* a non-cleavable linker to the maytansinoid DM1. AMG 595 has shown promising preclinical activity in assays including orthotopic murine models (58). In a phase I/II study of AMG 595 in patients with recurrent glioma expressing EGFRvIII (NCT01475006), the most common adverse events were thrombocytopenia (50%) and fatigue (25%); grade ≥ 3 treatment-related AEs occurred in 17 patients (53%). However, it is important to note that two patients had partial responses; 15 (47%) had stable disease, including one patient who was on treatment for 15 months (59). Unfortunately, development of this drug has also been discontinued.

FUTURE DIRECTIONS FOR THE DEVELOPMENT OF ADCs IN GLIOMA

The disappointing results of INTELLANCE 1 has rightly given pause and reconsideration to the role of ADCs in patients with gliomas. It has prompted reconsideration of reason why ADCs may not be suitable for use in patients with gliomas, including the relatively high toxicity when targeting the EGFR family with certain payloads, and the concern that these drugs are unable to penetrate the blood brain barrier to reach glioma tumour cells. One key concern is whether the results of INTELLANCE 1 should be allowed to overshadow the results of INTELLANCE 2 and the AMG-595 study. Much data suggest that recurrent gliomas are different disease from newly diagnosed GBM with changes in its genetic and molecular phenotype (60–66). While the further development of Depatux-M has been terminated by the company, the results of the INTELLANCE 2 study are intriguing about the possible use of this class of ADCs based on the mAb806 antibody particularly when compared to other drugs tested in GBM, such as immunotherapy, which have been universally disappointing in their lack of efficacy (**Table 3**). Formal testing in a phase III would be reasonable but understandably, improved ADCs with a better toxicity profile would be selected if possible. Also, better patient selection is clearly required to identify the subset of patients who clearly have exceptional sensitivity of these ADCs as has been seen with in trials with Depatux-M to date (unpublished data). In a preclinical study, disruption of BBB through the over-expression of vascular endothelial growth factor or avoiding the BBB entirely by direct intra-tumoral injection resulted in improved efficacy of Deptux-M (77). In addition, suppression of EGFR or expression of an EGFR variant lacking the binding epitope and upregulation of compensatory signaling pathways associated with altered EGFR expression and known to function in parallel or downstream from EGFR were identified as potential mechanisms of resistance to Depatux-M.

Improved Drug Delivery Through BBB

One of the main reasons for the ineffectiveness of therapeutic agents intended to target the CNS following peripheral administration is the restrictive nature of the BBB. The BBB is formed by endothelial cells, connected by tight junctions, which continuously interact with surrounding cells like astrocytes, pericytes, and perivascular macrophages, forming the so-called neurovascular unit (78). Primary brain tumors, in particular glioblastoma, cause disruption in the integrity of the BBB as evidenced by the accumulation of gadolinium-based magnetic resonance imaging (MRI) contrast agents within tumor regions. However this disruption is heterogeneous and there is also a clinically significant portion of the tumor with an intact BBB which affects the distribution and efficacy of drugs exposed to this region of the tumor (79). Disrupting the BBB more completely would clearly be useful for treating gliomas with ADCs, amongst other drugs. There has also been recent interest in chemical-induced BBB disruption which has led to increased CNS exposure of ADCs. For example, NEO110, which is a high purity version of the natural monoterpene perillyl alcohol, has been shown to increase the brain delivery of T-DM1 in a mouse model harbouring intracranial HER2+ breast cancer, leading to a significantly greater survival (80). The clinical translation of BBB-disruptors such as NEO110 requires evaluation before such an approach may be considered appropriate for enhancing ADC penetration into the human brain.

In addition to being a physical barrier, the BBB also acts as a biochemical barrier through the function of efflux transporters, such as P-glycoprotein (P-gp) (81) and breast cancer resistance protein (BCRP) (82). While these efflux transporters protect the brain from potentially harmful xenobiotics, they recognise many therapeutics, including a large number of anti-cancer drugs, therefore, limiting their access to the CNS (83). In addition,

TABLE 3 | Selected trials of therapeutic agents tested in glioma.

Class of drugs	Setting	Trial Description	Target	Phase	NCT	Response rate	OS (months)	Toxicity
Immunotherapy								
Nivolumab (67) (68)	Neoadjuvant (n = 30)	Neoadjuvant Nivolumab in Glioblastoma	PD-1	II	NCT02550249	No clinical benefit was substantiated following salvage surgery		NR
Pembrolizumab (69)	Neoadjuvant (n= 35)	Neoadjuvant anti-PD-1 immunotherapy in recurrent glioblastoma	PD-1	Pilot	–		13.7	10 patients (67%) in the neoadjuvant group experienced grade 3-4 adverse events likely attributable pembrolizumab
Autologous lymphoid effector cells specific against tumor cells (ALECSAT) (70)	Recurrent (n = 25)	Assess the tolerability and efficacy of ALECSAT in GBM patients (ALECSAT-GBM)		I	NCT01588769	DCR 50%*	NR	5/23 (22%) experienced grade 4/5 toxicity including: pneumonia, respiratory insufficiency, cerebral vascular lesion and general physical health deterioration
CART-cell therapy (71)	Recurrent (NR)	Anti- interleukin-13 receptor alpha 2 chimeric antigen receptor (CAR) T-cells	IL13Rα2	I	NCT00730613	NR		
CART-cell therapy (72)	Recurrent (n = 17)±	CMV-specific cytotoxic T lymphocytes expressing CAR targeting HER2 (HERT-GBM)	HER2	I	NCT01109095	DCR 50%	11.1	TRAEs were grade 1-2 and included 3 patients with headache and seizures. No ≥ grade 3 TRAEs reported. No DLT observed
IMA950 multi-peptide vaccine + poly-ICLC (73)	New diagnosis (n = 19 16 GBM and 3 grade III astrocytoma)	Trial of IMA950 Multi-peptide Vaccine Plus Poly-ICLC	Human leukocyte antigen (HLA)-A2 restricted peptides	I/II	NCT01920191	DCR 42%	19	Grade 1-2 TRAEs: inflammatory reactions at injection sites (53%), headache (37%), fatigue (63%), and flu-like syndrome (21%) 1 x Grade 4 - interstitial pneumonia due to pneumocystic infection
Monoclonal antibodies								
Onartuzumab (74)	Recurrent (n = 129)	Onartuzumab in Combination With Bevacizumab Compared to Bevacizumab Alone or Onartuzumab Monotherapy	c-MET	II	NCT01632228	8.8 (Onartuzumab + Bevacizumab) vs 12.6 (Bevacizumab)		Grade ≥ 3 TRAEs: 38.5% (experimental arm) vs 35.9% (bevacizumab) Experimental arm had higher rates of drug withdrawal + drug interruptions
Tanibirumab (75)	Recurrent (n = 10)	Trial to Evaluate the Safety of TTAC-0001 (Tanibirumab)	VEGFR-2	II	NCT03033524	NR	NR	No dose limiting toxicities Cutaneous hemangiomas (83%) - ≤ grade 2 No drug-related G3 or 4 AEs
Nanoparticles								
DNX-2401 (tasadenoturev) (76)	Recurrent (n = 37)	DNX-2401 for Recurrent Malignant Gliomas Group A (n = 25) - single intratumoral injection of DNX-2401 into biopsy of confirmed recurrent tumor Group B (n = 12) - intratumoral injection post resection	Oncolytic adenovirus	I	NCT00805376	Group A (n = 25): 20% of patients survived > 3 years Group B (n = 12) – NR		NR

*****10 of the 25 recruited patients were evaluable.*

±17 patients included 10 adults and 7 children.

CAR-T cells, Chimeric Antigen Receptor (CAR) T-Cell Therapy; DLT, Dose limiting toxicity; GSC, glioma stem cells; NR, not reported; ORR, Overall response rate; TRAE, treatment related adverse event; VEGFR, vascular endothelial growth factor receptor.

elimination of the cytotoxic payloads from the cellular cytoplasm by the ATP-binding cassette (ABC) transporters contribute to lower efficacy and resistance to ADCs (26). Increased MDR1 expression has shown to contribute to resistance to auristatin and maytansinoids based ADC analogues, leading to poorer patient outcomes (84, 85). Strategies to overcome drug efflux from cells include using agents that are poor efflux substrates such as hydrophilic compounds or switching from a non-

cleavable linker to a protease cleavable and using newer design drugs such as bispecific and biparatopic antibodies can increase cellular internalization (26). Another mechanism that affects the therapeutic effectiveness of ADCs involves defects in the internalization pathway and reduced cell surface trafficking (86). Following internalisation, degradation of ADCs in lysosomes may be impaired by reduced lysosomal proteolytic or acidification function and/or loss of lysosomal transporter expression, resulting in failure of cleavage of cytotoxic payload from ADCs (87). Loss of lysosomal transporter expression, e.g., SLC46A3 has also been reported as a mechanism of innate and acquired resistance to PBD and DM1 bearing ADCs (88). Other potential mechanisms of escape include selection pressure and downregulation of antigens, loss of antigen expression or mutations in antigen as well as presence of ligands for antigens and resistance to ADC and acquired or innate insensitivity to the payload.

With increasing insight into the biology of the BBB and the discovery of novel transporters for trafficking of endogenous compounds, there has been significant interest in attaching natural ligands of these transporter systems to chemotherapeutics to increase their CNS access. One such ligand is angiopep-2, a 19 amino acid peptide targeting the low-density lipoprotein receptor-related protein 1 (LRP1). This has been conjugated to paclitaxel, amongst other anticancer agents. This construct of angiopep-2 and paclitaxel (GRN1005) was shown to be safe and somewhat effective in patients with advanced solid tumours (89), and a subsequent Phase I study showed that GRN1005 had similar toxicity to paclitaxel and some activity in recurrent glioma (90). These techniques were then applied to antibodies, albeit with a modified version of angiopep-2 that also is considered to exploit LRP1 to traverse the BBB i.e. melanotransferrin. Administration of melanotransferrin-trastuzumab conjugate (BT2111) reduced the number of HER2+ breast cancer metastases in the brain (by 68%) with tumours being 46% smaller in BT2111 treated mice relative to control mice (91). To the authors knowledge, there have been no studies where either Angiopep-2 or melanotransferrin have been conjugated to ADCs for the purposes of increasing CNS access, however, based on the results with trastuzumab, it is expected that utilising these shuttle protein approaches should result in increased ADC brain uptake and efficacy.

Lastly, drug penetration into tumours is not just impacted by the BBB. Physico-chemical properties such as tumour volume could be modulated to increase ADC penetration. Larger tumours have increased interstitial pressures, more impaired circulation/lymphatics and increased necrotic areas that limit the ability of ADCs to penetrate the tumours (92–94). Data from the M12-356 Phase 1 study of Depatux-M provides evidence of this problem in glioma patients (95). Preclinical imaging and biodistribution studies showed specific and significantly higher tumor uptake of zirconium-89 labelled Depatux-M (^{89}Zr-Depatux-M) in mice with smaller tumor volume *versus* those with larger volumes. Concordantly, mice with smaller tumor volumes at treatment commencement had significantly better growth inhibition and significantly longer overall survival compared to mice with large tumors at treatment commencement. These findings were supported by an analysis of tumor volumes on outcomes in the M12-356 study; patients with large tumors had significantly worse response rates and overall survival. These findings strongly support strategies that would reduce tumor size and/or interstitial pressure to increase efficacy of ADCs in brain tumors (96–98). The tumour microenvironment (TME) in GBM is complex; it is characteristically immunosuppressive and made up of numerous cell types surrounded by a distinctive extracellular matrix (99). Dynamic changes in the cellular and metabolic composition within the TME can result in treatment resistant and tumor recurrence (100). Given the role of TME in tumor growth and blood vessel formation, strategies being investigated include targeting antigens of the TME instead of tumor specific antigens as well as overcoming the inherent immunosuppressive effects and making tumors more immune competent (99, 101, 102). Antigens of the TME are likely more accessible and targeting them allows ADCs to accumulate within tumors and release their payload based on TME-specific factors (103, 104). For example, CD25, CD205, B7-H3 are targets found in the TME for which specific ADCs are in clinical development in a number of non-CNS tumour types (105).

Approaches to Reduce ADC Size/Polarity

The antibody component of an ADC is vital for binding to the desired antigen with high affinity and specificity, maintaining a long half-life and releasing the toxic payload into tumor cells; however its large size presents a physical barrier to efficient extravasation across blood vessel walls and diffusion through tumors (106). This has led to the development of smaller formats as carriers of toxic payloads and include: antibody fragments, peptides, natural ligands, and small molecules (107). Several drug conjugates using smaller targeting domains are being evaluated in clinical trials (NCT02936323, NCT03221400, NCT03486730).

Aptamers are short single-stranded nucleic acids (RNA or ssDNA) that represent a novel imaging and drug-delivery strategy based on their sensitivity and specificity, ease of modification and low immunogenicity (108). Aptamers can be physically conjugated either by intercalating or covalent linking to novel therapeutics such as noncoding RNA or cytotoxic payloads like doxorubicin (109). Recent studies demonstrating the ability of aptamers to cross the BBB and deliver payloads to tumors (110) has resulted in considered interest in the potential role of aptamers in the management of gliomas. To date, several studies have evaluated the role of aptamer-based therapies as well as aptamer-based conjugates (non-coding RNA, nanoparticles, chemotherapeutics) in a number preclinical glioma models (111). The majority of studies targeted EGFR/EGFRvIII while others looked at other GBM-associated proteins including Tenascin-C, EphB2/3 receptors, nucleolin, vascular endothelial growth factor receptor (VEGF), and integrin $\alpha5\beta1$ (108, 111). While the results in early preclinical studies are encouraging, further optimization of aptamers with regards to their sensitivity to body-fluid nucleases, CpG toxicity, and stability remain to be optimized.

Nanoparticles are promising carriers for drug delivery to the brain due to their unique characteristics which include their small size and specific and homogenous tumor targeting. Various

classes of nanoparticles, including metallic, polymeric and lipid nanoparticles can be readily modified to effectively carry drugs across the BBB. By attaching toxic payloads to nanoparticles, tumour-specific targets expressed in GBM cells and responsible for tumorigenesis can be targeted; examples of these include antigens (i.e., A2B5), differentiation clusters (i.e., CD15, CD33, CD44, or CD133), receptors of cytokines (i.e., interleukin13 receptor), and several proteins (i.e., EGFR, Integrin-a6, $\alpha5\beta3$, $\alpha v\beta3$ or L1CAM). An alternative to the classical antibody-drug conjugate is the antibody-mediated delivery of a drug containing nanoparticles. In a recent example, panitumumab/Vectibix was attached to a 400nm nanoparticle (minicell) derived from Salmonella typhimurium in the attempt to deliver an effective dose of doxorubicin to 14 patients with recurrent GBM (112). This study showed that EGFR targeting antibody-coated nanoparticles containing chemotherapeutic drugs could be delivered in recurrent GBM patients.

ADCs Against Novel Targets

Selecting an appropriate target antigen is a critical step for the success of an ADC. Ideally, the appropriate target antigen should tumor-specific and homogenous in expression. The ideal target is one which is strongly and homogenous expressed on tumor cells, absent on normal tissue and efficient internalisation when bound (113–115). The potency of ADCs is dependent on the ability of the antibody-antigen complex to internalize, release the payload within the target cells and exert the cytotoxic effect. This dependency on antigen expression levels and finite internalization limits the therapeutic potential of ADCs as well as contributes to off-target toxicities (27).Some strategies to overcome the requirement of internalisation include the targeting of non-internalising receptors and extracellular matrix targets. Furthermore, the identification of tumour microenvironment targets also raises the possibility of therapeutic approaches with ADCs which do not target tumor cells alone (8, 26, 115). Novel approaches to developing non-internalization ADCs include diabody-based ADCs against non-internalizing targets and anti-tumor angiogenesis ADC which have shown promise in preclinical studies (116, 117).

The cell surface Notch ligand delta-like 3 (DLL3) inhibits Notch pathway activation and has shown to be expressed on the cell surface of several tumor types including gliomas where DLL3 expression inversely correlated with outcome (118, 119). In brain tumors, DLL3 has been shown to be most intensely and homogeneously overexpressed in *IDH*-mutant gliomas compared to other glioma subtypes (120). Interestingly, in gliomas DLL3 overexpression is not a consequence of *DLL3* mutations or gene amplification (120). DLL3 is not expressed in adult normal tissues (119), making it an attractive therapeutic target. Rovalpituzumab teserine (Rova-T; SC16LD6.5) is an ADC consisting of a monoclonal antibody targeting DLL3, a cathepsin-cleavable linker, and a PBD payload (119). The first-in-human clinical trial of Rova-T in small cell lung cancer (SCLC) demonstrated encouraging activity albeit significant toxicity related to the payload (121). The phase 3 study (TAHOE) in recurrent SCLC however was halted early due futility (122). An active phase 3 trial of Rova-T in the maintenance setting (MERU) is ongoing (NCT03033511). In a phase 1/2 study (NCT02709889) patients with relapsed DLL3-positive (>1% by IHC) advanced solid tumors received Rova-T at 0.2, 0.3, or 0.4 mg/kg every 6-weeks for dose escalation in disease specific cohorts (123). The study enrolled 200 patients including 23 patients with GBM. The recommended phase 2 dose was 0.3 mg/kg q6wk for 2 cycles in all cohorts. The most common adverse events were fatigue, nausea, thrombocytopenia, pleural effusion and peripheral oedema. The objective response rate (ORR) was 11% including one complete response in the GBM cohort.

Increasingly, it is also becoming apparent that targeting the tumour microenvironment may be feasible in glioma and may have advantages over targeting tumours directly. Leucine-rich repeat containing 15 (LRRC15) is a type I membrane protein with low expression in normal tissue but is highly expressed on cancer associated fibroblasts within the tumor stroma as well as directly on cancer cells including GBM (124). ABBV-085 is an ADC composed of an anti-LRRC15 humanized monoclonal antibody conjugated to MMAE *via* a protease cleavable valine–citrulline linker. ABBV-085 has demonstrated significant antitumor activity in multiple LRRC15 cancer-positive models, including GBM. ABBV-085 also showed enhanced activity in combination with other therapies including cytotoxic chemotherapy, radiation, immunotherapy and targeted therapies (124).

Another promising target in the tumour microenvironment is the Eph family. Eph receptor tyrosine kinases and their cell-associated ephrin ligands have been implicated in the growth and progression of a large range of cancers and are increasingly recognized as important therapeutic anti-cancer targets (125). EphA2 and EphA3 are commonly expressed in GBM, including in regions of tumor neovasculature, tumor-associated immune cells, and tumor-infiltrating cells (126), and associated with poorer outcomes in GBM patients (127). MEDI-547 is an ADC comprising an EphA2 targeted monoclonal antibody (1C1) conjugated *via* a non-cleavable linker to the auristatin derivative maleimidocaproyl-monomethyl auristatin phenylalanine (mcMMAF). MEDI-547 displayed encouraging antitumor activity in preclinical models (128) however clinical development was halted due to due to treatment-related adverse events during the early phase studies (129). Despite these results, given the overexpression of EphA2 in many tumor types targeting EphA2 for toxin delivery remains a promising therapeutic strategy. MM-310, an anti-EphA2 immuno-liposome containing docetaxel prodrug has shown superior tumor penetration and anti-tumor activity in a range of xenograft models compared to free docetaxel and significantly with lower toxicity (130). An ADC directed against EphA3, another member of this family, is also being pursued. An ADC based on the IIIA4 mAb, and utilizing the microtubule inhibitor maytansine (IIIA4-USAN), has highly effective in killing preclinical GBM models compared to the naked antibody (131). Similarly, anti-EphA3 bound nanoparticles loaded with the DNA alkylation agent temozolomide showed specific tumor targeting and potent anti-tumor effects in a rat glioma model (132). A phase 1 study of the Ifabotuzumab, the humaneered version of IIIA4, has shown the drug is safe, is able to successfully target the tumour

microenvironment in all patients tested but without normal tissue binding (133); an ADC based on Ifabotuzumab is therefore an attractive prospect.

Novel ADCs With Improved Payloads

Coupled with the above strategies are strategies to utilise newer payloads with increased therapeutic ratios. A number of known issues can adverse impact ADCs. Linkers are an essential interface between antibody and drug payload and are critical in stability, site of conjugation and final drug/antibody ratio (DAR): parameters that impact on toxicity, efficacy and pharmacokinetic properties of ADCs (8, 30). Current linkers may release payloads in the circulation which can lead to off-target toxicity. The development of novel linkers and advances in linker technology is beyond the scope of this review but has been discussed elsewhere in detail (134, 135). In addition, the IgG1 isotype of some of these ADCs can engage the Fc-gamma receptors (FcγR), which can trigger a target-independent, FcγR–dependent internalization in FcγR-positive cells resulting in toxic effects on these untargeted healthy cells (136). In addition, each class of payload often has characteristics toxicities (**Table 2**). A number of newer payloads are being tested. Pyrrolobenzodiazepines (PBDs) are DNA−crosslinking agents that exert their biological activity by binding in the minor groove of DNA with enhanced potent anti-cancer activity compared to auristatins or maytansinoids (137, 138). PBD dimers exhibit significant cell permeability, potentially enabling bystander killing of neighboring tumor cells (139). A number of PBD-conjugated ADCs are being developed and in clinical trials for both solid and hematological tumors (140). For example, ABBV-321 (serclutamab talirine) is a highly selective next-generation EGFR-targeting ADC which incorporates a PBD dimer toxin conjugated to the EGFR-targeting ABT-806 affinity-matured AM1 antibody (10). It is expected that the highly selective nature of ABBV-321 would differentiate it from previously developed antibody PBD conjugates that lack a therapeutic window. In a number of xenograft cell line and patient-derived xenograft tumour models including in GBM, ABBV-321 exhibited potent anti-tumor activity (10). ABBV-321 is currently under clinical investigation in patients with advanced solid tumors (141).

Deruxtecan (DXd) is a potent topoisomerase I inhibitor with a short half-life and ability to elicit a bystander killing effect on neighboring tumour cells indicating low concern in terms of systemic toxicity and importantly may assist in overcoming intratumoral heterogeneity of cancer cells (142, 143). In addition to its by stander effect, DXd is cell membrane permeable and therefore may enter nearby cells, even those without strong HER2 expression, making it effective in low HER2-expressing cancer cells and overcome tumour heterogeneity. Bioconjugation of DXd to a humanized monoclonal antibody specifically targeting HER2 *via* a cleavable tetrapeptide-based linker, made it possible to obtain the conjugate Trastuzumab Deruxtecan (DS-8201a, T-DXd) with a homogeneous DAR of 7.7. Trastuzumab deruxtecan has shown impressive response rates in early phase studies in tumours with high and low HER2 expression as well as HER2 mutant cancers (144, 145). The most common side effects were gastrointestinal and haematological, however potentially fatal adverse event of interstitial lung disease (ILD) was reported in 13.6% of patients in the phase II trial, including four patients who died due to lung injury (146). The mechanism of lung injury is not well understood and predictive biomarkers for response as well as identifying patients at risk of developing toxicity lung injury are required. Another ADC carrying the DXd payload is patritumab deruxtecan which uses the same linker-payload system as trastuzumab deruxtecan and is conjugated to the anti-HER3 monoclonal antibody patritumab. In a phase I study, patritumab deruxtecan demonstrated impressive responses in patients who were heavily pretreated with a median number of four regimens, including EGFR targeting tyrosine kinase inhibitors (147). Notably, its efficacy is observed regardless of the resistance mechanisms for EGFR-TKIs, including C797S secondary EGFR mutation, MET amplification, HER2 mutation, BRAF fusion, and PIK3CA mutation (147).

Lastly, there is on-going interest in utilising new radioisotopes in antibody payload delivery. Both the EphA2 mAb IF7 coupled to Lutetium-177 and then anti-EphA3 antibody IIIA4 linked to an α-particle-emitting Bismuth-213 payload showed therapeutic effect in EphA2 and EphA3 expressing leukemia models (148, 149). In GBM models, treatment with IIIA4 labelled with the β-particle-emitting Lutetium-177 showed dose-dependent tumor cell killing and tumor growth inhibition *in vivo*, compared to unlabelled antibody (150).

Combinatorial Treatment Approaches to Address Heterogeneity and Resistance

Cancer cells are constantly under strong selection and evolutionary pressures, resulting in the emergence of subclones and heterogeneity in gene expression and antigen expression (151). This in turn can affect ADC efficacy which is correlated with the level of target antigen expression (114). In a phase II study, patients with early-stage HER2-positive breast cancer received six cycles of trastuzumab emtansine (T-DM1), in combination with pertuzumab in the neoadjuvant setting (152). In this study complete pathological response (pCR) was higher in those with HER2 scores of 3+ *versus* 2+ and no pCR was seen among the patients classified as having HER2 heterogeneity, indicating that heterogeneity of target antigen expression is an important factor in patient selection. GBM is characterised by significant heterogeneity even at the single cell level (153). Studies have reported substantial inter- and intra-tumoral variation in the levels of EGFR expression and mutation. Furthermore, EGFR mutations are frequently lost or gained between the initial tumor and recurrence while molecular alterations, such as EGFR amplification, remain persistent unchanged (60). Recently studies have also shown that EGFRvIII can be eliminated from extrachromosomal DNA of tumor cells as a resistance mechanism when tumor cells are treated with EGFR TKIs. However, upon drug removal, EGFRvIII reappears (154). Data from clinical studies suggest that substantial inter - and intra-tumoral variation in the levels of EGFR and EGFRvIII expression and mutation contribute to therapeutic resistance (155, 156).

Combinatorial approaches is one approach to address tumour heterogeneity and resistance in gliomas, and as already demonstrated improved responses and survival rates in other tumor types (157). Dual targeting of both wildtype EGFR and

EGFRvIII has been shown to have more effective anti-tumor activity in intracranial murine glioma models than single targeting of either variant alone (158). The anti-EGFR TKI AG1478 has shown to increase mAb 806-reactive dimers on the surface of cells overexpressing EGFR, and the combination has of mAb806 and AG1478 resulted in enhanced anti-tumour activity in xenograft models (159). Furthermore, Orellana et al. demonstrated that stabilizing the inactive kinase conformation with lapatinib correlated convincingly with increased binding of ABT-806 (160), further supporting the approach of targeting both EGFR and its variants.

Combinatorial strategies with ADCs may also effectively address the issue of tumour heterogeneity. Combining ABBV-321 and Depatux-M resulted in greater tumor growth inhibition in an EGFR-overexpressing GBM PDX model compared to either monotherapy treatment (161). It is also possible to incorporate two payloads into an ADC using multi-loading linkers, with improvements in conjugation efficiency and ADC homogeneity. Levengood et al. developed a dual-auristatin ADCs containing both monomethyl auristatin E (MMAE) and monomethyl auristatin F (MMAF) and showed superior therapeutic benefit in preclinical anaplastic large cell lymphoma models refractory to ADCs comprised of the individual auristatin components (162). Anami et al. developed an ADC composed of anti-HER2 antibody conjugated to the MMAF payload *via* branched linkers and compared with the ADC composed of linear linkers. Their results demonstrated compared to linear linkers, branched linkers were highly stable in the human plasma, having high cell specificity and antigen-binding efficiency, and more significant *in vitro* cell killing potency (163).

Immunogenic cell death of tumor cells induced by cytotoxic compounds used as payloads in ADCs can be potent stimulators of effector T-cell recruitment to tumors and can directly result in dendritic cell activation and maturation (164). Indeed, infiltration of T cells has been observed in tumor biopsy specimens from patients after treatment with ado-trastuzumab emtansine (T-DM1) (165). Based on the induction of antibody dependent cellular cytotoxicity (ADCC) by anti-HER2 therapies, preclinical studies addressed the potential synergistic effect of ado-trastuzumab emtansine (T-DM1) and ICIs. Preclinical studies have shown the combination of HER2-targeting ADCs with ICI resulted in curative responses despite primary resistance to immunotherapy model (166–168). Exploration of tumor specimens from patients enrolled on phase 1 study (M12-356, NCT01800695) (169) has revealed a significant association between T-cell activity and response to ABT-414 treatment (170). This raises the possibility that combination of ADCs with currently approved immunotherapy are very likely to be effective.

Improved Patient Selection

In order to maximize the therapeutic potential of ADCs and limit exposure of ADCs to patients unlikely to benefit, more sophisticated biomarkers to select patients are needed. The current strategy of identifying patients is based on tumor target expression, which can be challenging due to multiple factors including: tumor heterogeneity, assay sensitivity, and accuracy, potential changes in target expression after multiple therapies, and difficulties in determining threshold levels for target expression that correlate with efficacy (171). In most trials, patients are preselected based target expression on archival tumor tissue. The most commonly employed methodology to determine target expression is by immunohistochemistry (IHC) which does possess limitations including lacks standardisation, reproducibility and, most importantly, correlation with clinical outcome. For example, while antigen expression levels have shown to correlate with response, ADCs have also shown clinical activity in patients with low levels of target antigen expression cancers due to imperfect assays (144, 145). Furthermore, emerging data suggest that selection based on payload sensitivity may add additional value above simply target expression. In the phase 1 study (M12-356, NCT01800695) of Depatux-M in patients with newly diagnosed GBM and recurrent GBM with EGFR amplification, responses in patients with recurrent GBM correlated with EGFR amplification however not all patients with *EGFR* amplification responded (169). Detailed examination of tumors [RNASeq, WES, immunohistochemistry (IHC)] from patients enrolled in the M12-356 trial revealed that mutations for tubulin genes were differentially expressed in responders vs non-responders, with TTLL2, TTLL4, TUBB2A, TUBB2B, TUBG1 and TUBGCP2 mutations (1-3 per tumor) overexpressed in non-responders (172). Preliminary synthetic lethality siRNA experiments have shown that mutations of these genes render sensitive GBM lines resistant to ABT-414 treatment. Furthermore, preliminary analysis of pre-treatment tumor samples with RNASeq has also revealed that responding patients had a higher number of tumor infiltrating lymphocytes (TIL) compared to non-responders, and CD3E expression. This was confirmed by immunohistochemistry analysis of CD3+ cells, with higher CD3+ cells in responding tumors. Preliminary T cell subset IHC analysis has also shown that CD8 cells are more frequently observed in responders, and that CD4 T cells are more abundant in non-responders. These data are highly suggestive of the immune microenvironment of GBM tumors playing a role in the responsiveness of GBM to ABT-414 treatment.

Lastly, molecular imaging by single photon computed tomography (SPECT) or positron emission tomography (PET), or immuno-PET, has been successfully employed to identify target expression, drug distribution and *in-vivo* target delivery and interlesional target heterogeneity (26). The humanized EphA2 mAb 1C1, libelled with ^{64}Cu, was used for positron emission tomography (PET) imaging of eight tumor models with different EphA2 expression levels, showing good correlation between tumor uptake and EphA2 expression (125). Imaging of the conformational form of EGFR expressed only on tumors has also been demonstrated in GBM patients with ^{111}In-ch806 and ABT-806 (173, 174). The ability to image the target of ADCs has the potential to improve selection of patients and increase therapeutic outcomes in patients with gliomas.

CONCLUSION

ADCs have shown to be effective and safe therapies, expanding the armamentarium in several haematological and solid tumors and in many cases transforming treatment paradigms. To date,

their potential in glioma patients has not been established. Early ADCs were clearly ineffective due to limitations of early ADCs in general which affected their efficacy in all tumours. More recent ADCs like ABT-414 and AMG-595 clearly show the potential of these drugs in glioma, especially in recurrent gliomas. Clearly, more sophisticated strategies in their use will be needed if we are to make ADCs therapeutically useful for most glioma patients and to improve their therapeutic ratio. A number of such strategies are already available. Improvements in the ADC technology, building on the results of results to date, is clearly needed. These should focus on improvements in selecting targets and payloads. The use of adjunctive strategies is also appealing, seeking to improve drug access to tumours across the BBB and to better select patients. Lastly, combinatorial strategies are likely if we are to substantially improve outcomes in these patients and ADCs could have a major contribution to make in such strategies.

AUTHOR CONTRIBUTIONS

All authors contributed to conception and design of the review. All authors contributed to manuscript revision, read, and approved the submitted version.

FUNDING

We would like to acknowledge our funding sources including: the Cancer Council Victoria (grant No 1164229), the Victorian Cancer Agency (CRE in Brain Cancer and ECF Fellowship for SP), the Operational Infrastructure Support from the Victorian Government. The support of AMS (National Health and Medical Research Council Investigator Fellowship No 1177837) is also acknowledged.

REFERENCES

1. Stupp R, Mason WP, van den Bent MJ, Weller M, Fisher B, Taphoorn MJ, et al. Radiotherapy Plus Concomitant and Adjuvant Temozolomide for Glioblastoma. *N Engl J Med* (2005) 352(10):987–96. doi: 10.1056/NEJMoa043330
2. Stupp R, Hegi ME, Mason WP, van den Bent MJ, Taphoorn MJB, Janzer RC, et al. Effects of Radiotherapy With Concomitant and Adjuvant Temozolomide Versus Radiotherapy Alone on Survival in Glioblastoma in a Randomised Phase III Study: 5-Year Analysis of the EORTC-NCIC Trial. *Lancet Oncol* (2009) 10(5):459–66. doi: 10.1016/S1470-2045(09)70025-7
3. Chinot OL, Wick W, Mason W, Henriksson R, Saran F, Nishikawa R, et al. Bevacizumab Plus Radiotherapy-Temozolomide for Newly Diagnosed Glioblastoma. *N Engl J Med* (2014) 370(8):709–22. doi: 10.1056/NEJMoa1308345
4. Gilbert MR, Dignam JJ, Armstrong TS, Wefel JS, Blumenthal DT, Vogelbaum MA, et al. A Randomized Trial of Bevacizumab for Newly Diagnosed Glioblastoma. *N Engl J Med* (2014) 370(8):699–708. doi: 10.1056/NEJMoa1308573
5. Muldoon LL, Pagel MA, Netto JP, Neuwelt EA. Intra-Arterial Administration Improves Temozolomide Delivery and Efficacy in a Model of Intracerebral Metastasis, But Has Unexpected Brain Toxicity. *J Neurooncol* (2016) 126(3):447–54. doi: 10.1007/s11060-015-2000-1
6. Chowdhary SA, Ryken T, Newton HB. Survival Outcomes and Safety of Carmustine Wafers in the Treatment of High-Grade Gliomas: A Meta-Analysis. *J Neurooncol* (2015) 122(2):367–82. doi: 10.1007/s11060-015-1724-2
7. Brastianos PK, Batchelor TT. VEGF Inhibitors in Brain Tumors. *Clin Adv Hematol Oncol* (2009) 7(753-760):768.
8. Parakh S, Parslow AC, Gan HK, Scott AM. Antibody-Mediated Delivery of Therapeutics for Cancer Therapy. *Expert Opin Drug Deliv* (2016) 13(3):401–19. doi: 10.1517/17425247.2016.1124854
9. Sievers EL, Senter PD. Antibody-Drug Conjugates in Cancer Therapy. *Annu Rev Med* (2013) 64:15–29. doi: 10.1146/annurev-med-050311-201823
10. Anderson MG, Falls HD, Mitten MJ, Oleksijew A, Vaidya KS, Boghaert ER, et al. Targeting Multiple EGFR-Expressing Tumors With a Highly Potent Tumor-Selective Antibody–Drug Conjugate. *Mol Cancer Ther* (2020) 19 (10):2117–25. doi: 10.1158/1535-7163.MCT-20-0149
11. Hafeez U, Parakh S, Gan HK, Scott AM. Antibody–Drug Conjugates for Cancer Therapy. *Molecules* (2020) 25(20):4764. doi: 10.3390/molecules25204764
12. Lassman AB, Pugh SL, Wang TJC, Aldape K, Gan HK, Preusser M, et al. (2019). Depatuxizumab Mafodotin (ABT-414) in EGFR-Amplified Newly Diagnosed GBM: A Randomized, Double-Blind, Phase III, International Clinical Trial, in: *Annual Meeting of the Society for Neuro-Oncology*, . AZ, USA: Phoenix.
13. Rosenthal M, Curry R, Reardon DA, Rasmussen E, Upreti VV, Damore MA, et al. Safety, Tolerability, and Pharmacokinetics of Anti-EGFRvIII Antibody-Drug Conjugate AMG 595 in Patients With Recurrent Malignant Glioma Expressing EGFRvIII. *Cancer Chemother Pharmacol* (2019) 84(2):327–36. doi: 10.1007/s00280-019-03879-2
14. Lassman A, Gan H, Fichtel L, Merrell R, Van Den Bent M, Kumthekar P, et al. A Phase 1 Study Evaluating ABT-414 With Temozolomide (TMZ) or Concurrent Radiotherapy (RT) and TMZ in Glioblastoma (GBM)(S43. 006). *Neurology* (2015) 84(14 Supplement):S43. 006.
15. Rosenthal M, Curry R, Reardon DA, Rasmussen E, Upreti VV, Damore MA, et al. Safety, Tolerability, and Pharmacokinetics of Anti-EGFRvIII Antibody-Drug Conjugate AMG 595 in Patients With Recurrent Malignant Glioma Expressing EGFRvIII. *Mol Cancer Ther* (2015) 14(7):1614–24. doi: 10.1007/s00280-019-03879-2
16. Kunwar S, Chang S, Westphal M, Vogelbaum M, Sampson J, Barnett G, et al. Phase III Randomized Trial of CED of IL13-PE38QQR vs Gliadel Wafers for Recurrent Glioblastoma. *Neuro-Oncol* (2010) 12(8):871–81. doi: 10.1093/neuonc/nop054
17. Weber F, Asher A, Bucholz R, Berger M, Prados M, Chang S, et al. Safety, Tolerability, and Tumor Response of IL4-Pseudomonas Exotoxin (NBI-3001) in Patients With Recurrent Malignant Glioma. *J Neurooncol* (2003) 64 (1-2):125–37. doi: 10.1007/BF02700027
18. Sampson JH, Akabani G, Archer GE, Berger MS, Coleman RE, Friedman AH, et al. Intracerebral Infusion of an EGFR-Targeted Toxin in Recurrent Malignant Brain Tumors. *Neuro-Oncol* (2008) 10(3):320–9. doi: 10.1215/15228517-2008-012
19. Weaver M, Laske DW. Transferrin Receptor Ligand-Targeted Toxin Conjugate (Tf-CRM107) for Therapy of Malignant Gliomas. *J Neurooncol* (2003) 65(1):3–13. doi: 10.1023/A:1026246500788
20. Tortorella S, Karagiannis TC. Transferrin Receptor-Mediated Endocytosis: A Useful Target for Cancer Therapy. *J Membr Biol* (2014) 247(4):291–307. doi: 10.1007/s00232-014-9637-0
21. Li L, Quang TS, Gracely EJ, Kim JH, Emrich JG, Yaeger TE, et al. A Phase II Study of Anti-Epidermal Growth Factor Receptor Radioimmunotherapy in the Treatment of Glioblastoma Multiforme. *J Neurosurg* (2010) 113(2):192–8. doi: 10.3171/2010.2.JNS091211
22. Reardon DA, Zalutsky MR, Akabani G, Coleman RE, Friedman AH, Herndon JE 2nd, et al. A Pilot Study: 131I-Antitenascin Monoclonal Antibody 81c6 to Deliver a 44-Gy Resection Cavity Boost. *Neuro-Oncol* (2008) 10(2):182–9. doi: 10.1215/15228517-2007-053
23. Riva P, Franceschi G, Frattarelli M, Riva N, Guiducci G, Cremonini AM, et al. 131I Radioconjugated Antibodies for the Locoregional Radioimmunotherapy of High-Grade Malignant Glioma–Phase I and II Study. *Acta Oncol* (1999) 38(3):351–9. doi: 10.1080/028418699431438
24. Gan HK, Cvrljevic AN, Johns TG. The Epidermal Growth Factor Receptor Variant III (EGFRvIII): Where Wild Things Are Altered. *FEBS J* (2013) 280 (21):5350–70. doi: 10.1111/febs.12393

25. Gan HK, van den Bent M, Lassman AB, Reardon DA, Scott AM. Antibody-Drug Conjugates in Glioblastoma Therapy: The Right Drugs to the Right Cells. *Nat Rev Clin Oncol* (2017) 14(11):695–707. doi: 10.1038/nrclinonc.2017.95
26. Hafeez U, Parakh S, Gan HK, Scott AM. Antibody–Drug Conjugates for Cancer Therapy. *Molecules* (2020) 25(20):4764. doi: 10.3390/molecules25204764
27. Tang H, Liu Y, Yu Z, Sun M, Lin L, Liu W, et al. The Analysis of Key Factors Related to Adcs Structural Design. *Front Pharmacol* (2019) 10:373. doi: 10.3389/fphar.2019.00373
28. Krop IE, Beeram M, Modi S, Jones SF, Holden SN, Yu W, et al. Phase I Study of Trastuzumab-DM1, an HER2 Antibody-Drug Conjugate, Given Every 3 Weeks to Patients With HER2-Positive Metastatic Breast Cancer. *J Clin Oncol* (2010) 28(16):2698–704. doi: 10.1200/JCO.2009.26.2071
29. Shen K, Ma X, Zhu C, Wu X, Jia H. Safety and Efficacy of Trastuzumab Emtansine in Advanced Human Epidermal Growth Factor Receptor 2–Positive Breast Cancer: A Meta-Analysis. *Sci* (2016) 6(1):1–8. doi: 10.1038/srep23262
30. Donaghy H. Effects of Antibody, Drug and Linker on the Preclinical and Clinical Toxicities of Antibody-Drug Conjugates. *MAbs* (2016) 8(4):659–71. Taylor & Francis. doi: 10.1080/19420862.2016.1156829
31. Oak E, Bartlett NL. A Safety Evaluation of Brentuximab Vedotin for the Treatment of Hodgkin Lymphoma. *Expert Opin Drug Saf* (2016) 15(6):875–82. doi: 10.1080/14740338.2016.1179277
32. Sievers EL, Larson RA, Stadtmauer EA, Estey E, Löwenberg B, Dombret H, et al. Efficacy and Safety of Gemtuzumab Ozogamicin in Patients With CD33-Positive Acute Myeloid Leukemia in First Relapse. *J Clin Oncol* (2001) 19(13):3244–54. doi: 10.1200/JCO.2001.19.13.3244
33. Kantarjian HM, DeAngelo DJ, Stelljes M, Martinelli G, Liedtke M, Stock W, et al. Inotuzumab Ozogamicin Versus Standard Therapy for Acute Lymphoblastic Leukemia. *N Engl J Med* (2016) 375(8):740–53. doi: 10.1056/NEJMoa1509277
34. Owonikoko TK, Hussain A, Stadler WM, Smith DC, Sznol M, Molina AM, et al. A Phase 1 Multicenter Open-Label Dose-Escalation Study of BMS-936561 (MDX-1203) in Clear Cell Renal Cell Carcinoma (ccRCC) and B-Cell Non Hodgkin Lymphoma (B-NHL). *J Clin Oncol* (2014) 32 (15_suppl):2558. doi: 10.1200/jco.2014.32.15_suppl.2558
35. Mantaj J, Jackson PJ, Rahman KM, Thurston DE. From Anthramycin to Pyrrolobenzodiazepine (PBD)-Containing Antibody–Drug Conjugates (ADCs). *Angew Chem Int Edition* (2017) 56(2):462–88. doi: 10.1002/anie.201510610
36. Dotan E, Starodub A, Berlin J, Lieu CH, Guarino MJ, Marshall J, et al. A New Anti-CEA-SN-38 Antibody-Drug Conjugate (ADC), IMMU-130, Is Active in Controlling Metastatic Colorectal Cancer (mCRC) in Patients (Pts) Refractory or Relapsing After Irinotecan-Containing Chemotherapies: Initial Results of a Phase I/II Study. *J Clin Oncol* (2015) 35(29):3338–46. doi: 10.1200/jco.2015.33.15_suppl.2505
37. Moskowitz CH, Nademanee A, Masszi T, Agura E, Holowiecki J, Abidi MH, et al. Brentuximab Vedotin as Consolidation Therapy After Autologous Stem-Cell Transplantation in Patients With Hodgkin's Lymphoma at Risk of Relapse or Progression (AETHERA): A Randomised, Double-Blind, Placebo-Controlled, Phase 3 Trial. *Lancet* (2015) 385(9980):1853–62. doi: 10.1016/S0140-6736(15)60165-9
38. Connors JM, Jurczak W, Straus DJ, Ansell SM, Kim WS, Gallamini A, et al. Brentuximab Vedotin With Chemotherapy for Stage III or IV Hodgkin's Lymphoma. *New Engl J Med* (2018) 378(4):331–44. doi: 10.1056/NEJMoa1708984
39. Horwitz S, O'Connor OA, Pro B, Illidge T, Fanale M, Advani R, et al. Brentuximab Vedotin With Chemotherapy for CD30-Positive Peripheral T-Cell Lymphoma (ECHELON-2): A Global, Double-Blind, Randomised, Phase 3 Trial. *Lancet (London England)* (2019) 393(10168):229–40. doi: 10.1016/S0140-6736(18)32984-2
40. Prince HM, Kim YH, Horwitz SM, Dummer R, Scarisbrick J, Quaglino P, et al. Brentuximab Vedotin or Physician's Choice in CD30-Positive Cutaneous T-Cell Lymphoma (ALCANZA): An International, Open-Label, Randomised, Phase 3, Multicentre Trial. *Lancet* (2017) 390 (10094):555–66. doi: 10.1016/S0140-6736(17)31266-7
41. Pro B, Advani R, Brice P, Bartlett NL, Rosenblatt JD, Illidge T, et al. Five-Year Results of Brentuximab Vedotin in Patients With Relapsed or Refractory Systemic Anaplastic Large Cell Lymphoma. *Blood* (2017) 130 (25):2709–17. doi: 10.1182/blood-2017-05-780049
42. Krop IE, Kim S-B, Martin AG, Lorusso PM, Ferrero J-M, Badovinac-Crnjevic T, et al. Trastuzumab Emtansine Versus Treatment of Physician's Choice in Patients With Previously Treated HER2-Positive Metastatic Breast Cancer (TH3RESA): Final Overall Survival Results From a Randomised Open-Label Phase 3 Trial. *Lancet Oncol* (2017) 18(6):743–54. doi: 10.1016/S1470-2045(17)30313-3
43. Verma S, Miles D, Gianni L, Krop IE, Welslau M, Baselga J, et al. Trastuzumab Emtansine for HER2-Positive Advanced Breast Cancer. *N Engl J Med* (2012) 367(19):1783–91. doi: 10.1056/NEJMoa1209124
44. Kantarjian HM, DeAngelo DJ, Stelljes M, Martinelli G, Liedtke M, Stock W, et al. Inotuzumab Ozogamicin Versus Standard Therapy for Acute Lymphoblastic Leukemia. *New Engl J Med* (2016) 375(8):740–53. doi: 10.1056/NEJMoa1509277
45. Castaigne S, Pautas C, Terré C, Raffoux E, Bordessoule D, Bastie J-N, et al. Effect of Gemtuzumab Ozogamicin on Survival of Adult Patients With De-Novo Acute Myeloid Leukaemia (ALFA-0701): A Randomised, Open-Label, Phase 3 Study. *Lancet* (2012) 379(9825):1508–16. doi: 10.1016/S0140-6736(12)60485-1
46. Bardia A, Hurvitz SA, Tolaney SM, Loirat D, Punie K, Oliveira M, et al. Sacituzumab Govitecan in Metastatic Triple-Negative Breast Cancer. *N Engl J Med* (2021) 384(16):1529–41. doi: 10.1056/NEJMoa2028485
47. Brenner A, Floyd J, Pandey R, Chiou J, Surapreneni P, Kaklamani V, et al. Delivery and Activity of Sn-38 by Sacituzumab Govitecan in CNS Tumors. *Ann Oncol* (2020) 31(suppl_4):S396–408. doi: 10.1016/j.annonc.2020.08.482
48. Johns TG, Adams TE, Cochran JR, Hall NE, Hoyne PA, Olsen MJ, et al. Identification of the Epitope for the Epidermal Growth Factor Receptor-Specific Monoclonal Antibody 806 Reveals That It Preferentially Recognizes an Untethered Form of the Receptor. *J Biol Chem* (2004) 279(29):30375–84. doi: 10.1074/jbc.M401218200
49. Gan HK, Burgess AW, Clayton AH, Scott AM. Targeting of a Conformationally Exposed, Tumor-Specific Epitope of EGFR as a Strategy for Cancer Therapy. *Cancer Res* (2012) 72(12):2924–30. doi: 10.1158/0008-5472.CAN-11-3898
50. Cleary JM, Reardon DA, Azad N, Gandhi L, Shapiro GI, Chaves J, et al. A Phase 1 Study of ABT-806 in Subjects With Advanced Solid Tumors. *Invest New Drugs* (2015) 33(3):671–8. doi: 10.1007/s10637-015-0234-6
51. Cleary JM, Yee LK-C, Azad N, Carducci M, Cosgrove D, Limaye S, et al. A Phase 1 Study of ABT-806, a Humanized Recombinant Anti-EGFR Monoclonal Antibody, in Patients With Advanced Solid Tumors. *Cancer Res* (2012) 72(8 Suppl):2506. doi: 10.1158/1538-7445.AM2012-2506
52. Luwor RB, Johns TG, Murone C, Huang HS, Cavenee WK, Ritter G, et al. Monoclonal Antibody 806 Inhibits the Growth of Tumor Xenografts Expressing Either the De2–7 or Amplified Epidermal Growth Factor Receptor (EGFR) But Not Wild-Type EGFR. *Cancer Res* (2001) 61 (14):5355–61.
53. Phillips AC, Boghaert ER, Vaidya KS, Mitten MJ, Norvell S, Falls HD, et al. ABT-414, an Antibody-Drug Conjugate Targeting a Tumor-Selective EGFR Epitope. *Mol Cancer Ther* (2016) 15(4):661–9. doi: 10.1158/1535-7163.MCT-15-0901
54. Reardon DA, Lassman AB, van den Bent M, Kumthekar P, Merrell R, Scott AM, et al. Efficacy and Safety Results of ABT-414 in Combination With Radiation and Temozolomide in Newly Diagnosed Glioblastoma. *Neuro-oncol* (2016) 19:965–75. doi: 10.1093/neuonc/now257
55. Van Den Bent MJ, French P, Eoli M, Sepúlveda JM, Walenkamp AME, Frenel J-S, et al. Updated Results of the INTELLANCE 2/EORTC Trial 1410 Randomized Phase II Study on Depatux–M Alone, Depatux-M in Combination With Temozolomide (TMZ) and Either TMZ or Lomustine (LOM) in Recurrent EGFR Amplified Glioblastoma (NCT02343406). *J Clin Oncol* (2018) 36 (15_suppl):2023. doi: 10.1200/JCO.2018.36.15_suppl.2023
56. van den Bent M, Eoli M, Sepulveda JM, Smits M, Walenkamp A, Frenel J-S, et al. Ltbk-04 First Results of the Randomized Phase Ii Study on Depatux–M Alone, Depatux-M in Combination With Temozolomide and Either Temozolomide or Lomustine in Recurrent Egfr Amplified Glioblastoma: First Report From Intellance 2/Eortc Trial 1410. *Neuro-Oncol* (2017) 19 (suppl_6):vi316–vi. doi: 10.1093/neuonc/nox213

57. Van Den Bent M, Eoli M, Sepulveda JM, Smits M, Walenkamp A, Frenel J-S, et al. INTELLANCE 2/EORTC 1410 Randomized Phase II Study of Depatux-M Alone and With Temozolomide vs Temozolomide or Lomustine in Recurrent EGFR Amplified Glioblastoma. *Neuro-oncol* (2020) 22(5):684–93. doi: 10.1093/neuonc/noz222
58. Hamblett KJ, Kozlosky CJ, Siu S, Chang WS, Liu H, Foltz IN, et al. AMG 595, an Anti-EGFRvIII Antibody Drug Conjugate, Induces Potent Anti-Tumor Activity Against EGFRvIII Expressing Glioblastoma. *Mol Cancer Ther* (2015) 14(7):1614–24. doi: 10.1158/1535-7163
59. Rosenthal M, Curry R, Reardon DA, Rasmussen E, Upreti VV, Damore MA, et al. Safety, Tolerability, and Pharmacokinetics of Anti-EGFRvIII Antibody–Drug Conjugate AMG 595 in Patients With Recurrent Malignant Glioma Expressing EGFRvIII. *Cancer Chemother Pharmacol* (2019) 84(2):327–36. doi: 10.1007/s00280-019-03879-2
60. Barthel FP, Johnson KC, Varn FS, Moskalik AD, Tanner G, Kocakavuk E, et al. Longitudinal Molecular Trajectories of Diffuse Glioma in Adults. *Nature* (2019) 576(7785):112–20. doi: 10.1038/s41586-019-1775-1
61. Eskilsson E, Verhaak RGW. Longitudinal Genomic Characterization of Brain Tumors for Identification of Therapeutic Vulnerabilities. *Neuro-Oncol* (2016) 18(8):1037–9. doi: 10.1093/neuonc/now064
62. Sottoriva A, Spiteri I, Piccirillo SGM, Touloumis A, Collins VP, Marioni JC, et al. Intratumor Heterogeneity in Human Glioblastoma Reflects Cancer Evolutionary Dynamics. *Proc Natl Acad Sci* (2013) 110(10):4009–14. doi: 10.1073/pnas.1219747110
63. Kim J, Lee IH, Cho HJ, Park CK, Jung YS, Kim Y, et al. Spatiotemporal Evolution of the Primary Glioblastoma Genome. *Cancer Cell* (2015) 28 (3):318–28. doi: 10.1016/j.ccell.2015.07.013
64. Johnson BE, Mazor T, Hong C, Barnes M, Aihara K, McLean CY, et al. Mutational Analysis Reveals the Origin and Therapy-Driven Evolution of Recurrent Glioma. *Science* (2014) 343(6167):189–93. doi: 10.1126/science.1239947
65. Wang J, Cazzato E, Ladewig E, Frattini V, Rosenbloom DI, Zairis S, et al. Clonal Evolution of Glioblastoma Under Therapy. *Net Genet* (2016) 48 (7):768–76. doi: 10.1038/ng.3590
66. Weller M, Butowski N, Tran DD, Recht LD, Lim M, Hirte H, et al. Rindopepimut With Temozolomide for Patients With Newly Diagnosed, EGFRvIII-Expressing Glioblastoma (ACT IV): A Randomised, Double-Blind, International Phase 3 Trial. *Lancet Oncol* (2017) 18(10):1373–85. doi: 10.1093/neuonc/now212.068
67. Schalper KA, Rodriguez-Ruiz ME, Diez-Valle R, López-Janeiro A, Porciuncula A, Idoate MA, et al. Neoadjuvant Nivolumab Modifies the Tumor Immune Microenvironment in Resectable Glioblastoma. *Nat Med* (2019) 25(3):470–6. doi: 10.1038/s41591-018-0339-5
68. Reardon DA, Kim T-M, Frenel J-S, Santoro A, Lopez J, Subramaniam DS, et al. ATIM-35. Results of the Phase IB KEYNOTE-028 Multi-Cohort Trial of Pembrolizumab Monotherapy in Patients With Recurrent PD-L1-Positive Glioblastoma Multiforme (GBM). *Neuro-Oncol* (2016) 18(suppl_6):vi25–6. doi: 10.1093/neuonc/now212.100
69. Cloughesy TF, Mochizuki AY, Orpilla JR, Hugo W, Lee AH, Davidson TB, et al. Neoadjuvant Anti-PD-1 Immunotherapy Promotes a Survival Benefit With Intratumoral and Systemic Immune Responses in Recurrent Glioblastoma. *Nat Med* (2019) 25(3):477–86. doi: 10.1038/s41591-018-0337-7
70. Kirkin AF, Dzhandzhugazyan KN, Guldberg P, Fang JJ, Andersen RS, Dahl C, et al. Adoptive Cancer Immunotherapy Using DNA-Demethylated T Helper Cells as Antigen-Presenting Cells. *Nat Commun* (2018) 9(1):1–12. doi: 10.1038/s41467-018-03217-9
71. Brown CE, Alizadeh D, Starr R, Weng L, Wagner JR, Naranjo A, et al. Regression of Glioblastoma After Chimeric Antigen Receptor T-Cell Therapy. *N Engl J Med* (2016) 375(26):2561–9. doi: 10.1056/NEJMoa1610497
72. Ahmed N, Brawley V, Hegde M, Bielamowicz K, Kalra M, Landi D, et al. Her2-Specific Chimeric Antigen Receptor–Modified Virus-Specific T Cells for Progressive Glioblastoma: A Phase 1 Dose-Escalation Trial. *JAMA Oncol* (2017) 3(8):1094–101. doi: 10.1001/jamaoncol.2017.0184
73. Migliorini D, Dutoit V, Allard M, Grandjean Hallez N, Marinari E, Widmer V, et al. Phase I/II Trial Testing Safety and Immunogenicity of the Multipeptide IMA950/poly-ICLC Vaccine in Newly Diagnosed Adult Malignant Astrocytoma Patients. *Neuro-Oncol* (2019) 21(7):923–33. doi: 10.1093/neuonc/noz040
74. Cloughesy T, Finocchiaro G, Belda-Iniesta C, Recht L, Brandes AA, Pineda E, et al. Randomized, Double-Blind, Placebo-Controlled, Multicenter Phase II Study of Onartuzumab Plus Bevacizumab Versus Placebo Plus Bevacizumab in Patients With Recurrent Glioblastoma: Efficacy, Safety, and Hepatocyte Growth Factor and O (6)-Methylguanine-DNA Methyltransferase Biomarker Analyses. *J Clin Oncol* (2017) 35(3):343–51. doi: 10.1200/JCO.2015.64.7685
75. Cher L, Nowak A, Iatropoulos G, Lee WS, Lee SY, Shim SR, et al. ACTR-75. A Multicenter, 3-Arm, Open-Label, Phase IIa Clinical Trial to Evaluate Safety and Efficacy of Tanibirumab (VEGFR2 mAB), in Patients With Recurrent GBM Assessed With K-Trans and Initial Area Under the Gadolinium Concentration-Time Curve (IAUGC). *Neuro Oncol* (2017) 19 (Suppl 6):17. doi: 10.1093/neuonc/nox168.062
76. Lang FF, Conrad C, Gomez-Manzano C, Yung WA, Sawaya R, Weinberg JS, et al. Phase I Study of DNX-2401 (Delta-24-RGD) Oncolytic Adenovirus: Replication and Immunotherapeutic Effects in Recurrent Malignant Glioma. *J Clin Oncol* (2018) 36(14):1419. doi: 10.1200/JCO.2017.75.8219
77. Marin B-M, Porath KA, Jain S, Kim M, Conage-Pough JE, Oh J-H, et al. Heterogeneous Delivery Across the Blood-Brain Barrier Limits the Efficacy of an EGFR-Targeting Antibody Drug Conjugate in Glioblastoma. *Neuro-Oncol* (2021) 29:noab133. doi: 10.1093/neuonc/noab133
78. Abbott NJ, Patabendige AA, Dolman DE, Yusof SR, Begley DJ. Structure and Function of the Blood–Brain Barrier. *Neurobiol Dis* (2010) 37(1):13–25. doi: 10.1016/j.nbd.2009.07.030
79. Sarkaria JN, Hu LS, Parney IF, Pafundi DH, Brinkmann DH, Laack NN, et al. Is the Blood–Brain Barrier Really Disrupted in All Glioblastomas? A Critical Assessment of Existing Clinical Data. *Neuro-Oncol* (2018) 20 (2):184–91. doi: 10.1093/neuonc/nox175
80. Wang W, He H, Marin-Ramos NI, Zeng S, Swenson SD, Cho H-Y, et al. Enhanced Brain Delivery and Therapeutic Activity of Trastuzumab After Blood-Brain Barrier Opening by NEO100 in Mouse Models of Brain-Metastatic Breast Cancer. *Neuro Oncol* (2021) 23(10):1656–67. doi: 10.1093/neuonc/noab204
81. Schinkel AH. P-Glycoprotein, a Gatekeeper in the Blood-Brain Barrier. *Adv Drug Deliv Rev* (1999) 36(2-3):179–94. doi: 10.1016/S0169-409X(98)00085-4
82. Nicolazzo JA, Katneni K. Drug Transport Across the Blood-Brain Barrier and the Impact of Breast Cancer Resistance Protein (ABCG2). *Curr Topics Med Chem* (2009) 9(2):130–47. doi: 10.2174/156802609787521580
83. Kim M, Kizilbash SH, Laramy JK, Gampa G, Parrish KE, Sarkaria JN, et al. Barriers Tor Effective Drug Treatment for Brain Metastases: A Mulltifactorial Problem in the Delivery of Precision Medicine. *Pharm Res* (2018) 35(9):177. doi: 10.1007/s11095-018-2455-9
84. Loganzo F, Tan X, Sung M, Jin G, Myers JS, Melamud E, et al. Tumor Cells Chronically Treated With a Trastuzumab–Maytansinoid Antibody–Drug Conjugate Develop Varied Resistance Mechanisms But Respond to Alternate Treatments. *Mol Cancer Ther* (2015) 14(4):952–63. doi: 10.1158/1535-7163.MCT-14-0862
85. Chen R, Hou J, Newman E, Kim Y, Donohue C, Liu X, et al. CD30 Downregulation, MMAE Resistance, and MDR1 Upregulation Are All Associated With Resistance to Brentuximab Vedotin. *Mol Cancer Ther* (2015) 14(6):1376–84. doi: 10.1158/1535-7163.MCT-15-0036
86. Sung M, Golas J, Wang F, King L, Myers J, Rosfjord E, et al. Caveolae-Mediated Endocytosis as a Novel Mechanism of Resistance to Trastuzumab Emtansine (T-Dm1). *Mol Cancer Ther* (2018) 17(1):243–53. doi: 10.1158/1535-7163.MCT-17-0403
87. Ríos-Luci C, García-Alonso S, Díaz-Rodríguez E, Nadal-Serrano M, Arribas J, Ocaña A, et al. Resistance to the Antibody-Drug Conjugate T-DM1 Is Based in a Reduction in Lysosomal Proteolytic Activity. *Cancer Res* (2017) 77(17):4639. doi: 10.1158/0008-5472.CAN-16-3127
88. Kinneer K, Meekin J, Tiberghien AC, Tai Y-T, Phipps S, Kiefer CM, et al. SLC46A3 as a Potential Predictive Biomarker for Antibody-Drug Conjugates Bearing Noncleavable Linked Maytansinoid and Pyrrolobenzodiazepine Warheads. *Clin Cancer Res Off J Am Assoc Cancer Res* (2018) 24(24):6570. doi: 10.1158/1078-0432.CCR-18-1300
89. Kurzrock R, Gabrail N, Chandhasin C, Moulder S, Smith C, Brenner A, et al. Safety, Pharmacokinetics, and Activity of GRN1005, a Novel Conjugate of Angiopep-2, a Peptide Facilitating Brain Penetration, and Paclitaxel, in

Patients With Advanced Solid Tumors. *Mol Cancer Ther* (2012) 11(2):308–16. doi: 10.1158/1535-7163.MCT-11-0566
90. Drappatz J, Brenner A, Wong ET, Eichler A, Schiff D, Groves MD, et al. Phase I Study of GRN1005 in Recurrent Malignant Glioma. *Clin Cancer Res* (2013) 19(6):1567–76. doi: 10.1158/1078-0432.CCR-12-2481
91. Nounou MI, Adkins CE, Rubinchik S, Terrell-Hall TB, Afroz M, Vitalis T, et al. Anti-Cancer Antibody Trastuzumab-Melanotransferrin Conjugate (BT2111) for the Treatment of Metastatic HER2+ Breast Cancer Tumors in the Brain: An *In-Vivo* Study. *Pharm Res* (2016) 33(12):2930–42. doi: 10.1007/s11095-016-2015-0
92. Leu AJ, Berk DA, Lymboussaki A, Alitalo K, Jain RK. Absence of Functional Lymphatics Within a Murine Sarcoma: A Molecular and Functional Evaluation. *Cancer Res* (2000) 60(16):4324–7.
93. Munson JM, Shieh AC. Interstitial Fluid Flow in Cancer: Implications for Disease Progression and Treatment. *Cancer Manag Res* (2014) 6:317. doi: 10.2147/CMAR.S65444
94. Harder BG, Blomquist MR, Wang J, Kim AJ, Woodworth GF, Winkles JA, et al. Developments in Blood-Brain Barrier Penetrance and Drug Repurposing for Improved Treatment of Glioblastoma. *Front Oncol* (2018) 8:462. doi: 10.3389/fonc.2018.00462
95. Gan H, Seow A, Lau E, Sze-Ting L, Ameratunga M, Perchyonok Y, et al. ACTR-55. Tumour Volume as a Predictor of Response to Ant-EGFR ADC ABT-414. *Neuro-Oncol* (2018) 20(suppl_6):vi24. doi: 10.1093/neuonc/noy148.087
96. Trédan O, Galmarini CM, Patel K, Tannock IF. Drug Resistance and the Solid Tumor Microenvironment. *J Natl Cancer Inst* (2007) 99(19):1441–54. doi: 10.1093/jnci/djm135
97. Böckelmann LC, Schumacher U. Targeting Tumor Interstitial Fluid Pressure: Will It Yield Novel Successful Therapies for Solid Tumors? *Expert Opin Ther Targets* (2019) 23(12):1005–14. doi: 10.1080/14728222.2019.1702974
98. Heldin C-H, Rubin K, Pietras K, Östman A. High Interstitial Fluid Pressure —an Obstacle in Cancer Therapy. *Nat Rev Cancer* (2004) 4(10):806–13. doi: 10.1038/nrc1456
99. Fanelli GN, Grassini D, Ortenzi V, Pasqualetti F, Montemurro N, Perrini P, et al. Decipher the Glioblastoma Microenvironment: The First Milestone for New Groundbreaking Therapeutic Strategies. *Genes* (2021) 12(3):445. doi: 10.3390/genes12030445
100. Abels ER, Maas SL, Tai E, Ting DT, Broekman ML, Breakefield XO, et al. GlioM&M: Web-Based Tool for Studying Circulating and Infiltrating Monocytes and Macrophages in Glioma. *Sci Rep* (2020) 10(1):1–11. doi: 10.1038/s41598-020-66728-w
101. Butler M, Prasad S, Srivastava SK. Targeting Glioblastoma Tumor Microenvironment. In: *Tumor Microenvironments in Organs*. Switzerland: Springer (2020). p. 1–9.
102. Ali S, Borin TF, Piranlioglu R, Ara R, Lebedyeva I, Angara K, et al. Changes in the Tumor Microenvironment and Outcome for TME-Targeting Therapy in Glioblastoma: A Pilot Study. *PloS One* (2021) 16(2):e0246646. doi: 10.1371/journal.pone.0246646
103. Lucas AT, Price LS, Schorzman AN, Storrie M, Piscitelli JA, Razo J, et al. Factors Affecting the Pharmacology of Antibody–Drug Conjugates. *Antibodies* (2018) 7(1):10. doi: 10.3390/antib7010010
104. Mathur R, Weiner GJ. Picking the Optimal Target for Antibody-Drug Conjugates. *Am Soc Clin Oncol Educ Book* (2013) 33(1):e103–7. doi: 10.14694/EdBook_AM.2013.33.e103
105. Boni V, Sharma MR, Patnaik A. The Resurgence of Antibody Drug Conjugates in Cancer Therapeutics: Novel Targets and Payloads. *Am Soc Clin Oncol Educ Book* (2020) 40:e58–74. doi: 10.1200/EDBK_281107
106. Sarkaria JN, Hu LS, Parney IF, Pafundi DH, Brinkmann DH, Laack NN, et al. Is the Blood–Brain Barrier Really Disrupted in All Glioblastomas? A Critical Assessment of Existing Clinical Data. *Neuro-Oncol* (2017) 20(2):184–91. doi: 10.1093/neuonc/nox175
107. Coats S, Williams M, Kebble B, Dixit R, Tseng L, Yao N-S, et al. Antibody–drug Conjugates: Future Directions in Clinical and Translational Strategies to Improve the Therapeutic Index. *Clin Cancer Res* (2019) 25(18):5441–8. doi: 10.1158/1078-0432.CCR-19-0272
108. Amero P, Khatua S, Rodriguez-Aguayo C, Lopez-Berestein G. Aptamers: Novel Therapeutics and Potential Role in Neuro-Oncology. *Cancers* (2020) 12(10):2889. doi: 10.3390/cancers12102889
109. Nimjee SM, White RR, Becker RC, Sullenger BA. Aptamers as Therapeutics. *Annu Rev Pharmacol Toxicol* (2017) 57:61–79. doi: 10.1146/annurev-pharmtox-010716-104558
110. Monaco I, Camorani S, Colecchia D, Locatelli E, Calandro P, Oudin A, et al. Aptamer Functionalization of Nanosystems for Glioblastoma Targeting Through the Blood–Brain Barrier. *J Med Chem* (2017) 60(10):4510–6. doi: 10.1021/acs.jmedchem.7b00527
111. Nuzzo S, Brancato V, Affinito A, Salvatore M, Cavaliere C, Condorelli G. The Role of RNA and DNA Aptamers in Glioblastoma Diagnosis and Therapy: A Systematic Review of the Literature. *Cancers* (2020) 12(8):2173. doi: 10.3390/cancers12082173
112. Whittle JR, Lickliter JD, Gan HK, Scott AM, Simes J, Solomon BJ, et al. First in Human Nanotechnology Doxorubicin Delivery System to Target Epidermal Growth Factor Receptors in Recurrent Glioblastoma. *J Clin Neurosci Off J Neurosurg Soc Australas* (2015) 22(12):1889–94. doi: 10.1016/j.jocn.2015.06.005
113. Lambert JM, Morris CQ. Antibody–drug Conjugates (ADCs) for Personalized Treatment of Solid Tumors: A Review. *Adv Ther* (2017) 34(5):1015–35. doi: 10.1007/s12325-017-0519-6
114. Perez EA, Hurvitz SA, Amler LC, Mundt KE, Ng V, Guardino E, et al. Relationship Between HER2 Expression and Efficacy With First-Line Trastuzumab Emtansine Compared With Trastuzumab Plus Docetaxel in TDM4450g: A Randomized Phase II Study of Patients With Previously Untreated HER2-Positive Metastatic Breast Cancer. *Breast Cancer Res* (2014) 16(3):1–10. doi: 10.1186/bcr3661
115. Scott AM, Wolchok JD, Old LJ. Antibody Therapy of Cancer. *Nat Rev Cancer* (2012) 12(4):278–87. doi: 10.1038/nrc3236
116. Rossin R, Versteegen RM, Wu J, Khasanov A, Wessels HJ, Steenbergen EJ, et al. Chemically Triggered Drug Release From an Antibody-Drug Conjugate Leads to Potent Antitumour Activity in Mice. *Nat Commun* (2018) 9(1):1–11. doi: 10.1038/s41467-018-03880-y
117. Seaman S, Zhu Z, Saha S, Zhang XM, Yang MY, Hilton MB, et al. Eradication of Tumors Through Simultaneous Ablation of CD276/B7-H3-Positive Tumor Cells and Tumor Vasculature. *Cancer Cell* (2017) 31(4):501–15.e8. doi: 10.1016/j.ccell.2017.03.005
118. Peng SL, Saunders L, Bheddah S, Williams S, Aggarwal RR, Shea JE, et al. Metastatic Melanoma, Glioblastoma and High-Grade Extrapulmonary Neuroendocrine Carcinomas (NECs) as Novel Indications for Rovalpituzumab Tesirine: A Delta-Like Protein 3 (DLL3)-Targeted Antibody-Drug Conjugate (ADC). *J Clin Oncol* (2016) 34(15_suppl):11611. doi: 10.1200/JCO.2016.34.15_suppl.11611
119. Saunders LR, Bankovich AJ, Anderson WC, Aujay MA, Bheddah S, Black K, et al. A DLL3-Targeted Antibody-Drug Conjugate Eradicates High-Grade Pulmonary Neuroendocrine Tumor-Initiating Cells In Vivo. *Sci Trans Med* (2015) 7(302):302ra136–302ra136. doi: 10.1126/scitranslmed.aac9459
120. Spino M, Kurz SC, Chiriboga L, Serrano J, Zeck B, Sen N, et al. Cell Surface Notch Ligand DLL3 Is a Therapeutic Target in Isocitrate Dehydrogenase–Mutant Glioma. *Clin Cancer Res* (2019) 25(4):1261–71. doi: 10.1158/1078-0432.CCR-18-2312
121. Rudin CM, Pietanza MC, Bauer TM, Ready N, Morgensztern D, Glisson BS, et al. Rovalpituzumab Tesirine, a DLL3-Targeted Antibody-Drug Conjugate, in Recurrent Small-Cell Lung Cancer: A First-in-Human, First-in-Class, Open-Label, Phase 1 Study. *Lancet Oncol* (2017) 18(1):42–51. doi: 10.1016/S1470-2045(16)30565-4
122. Blackhall F, Jao K, Greillier L, Cho BC, Penkov K, Reguart N, et al. Efficacy and Safety of Rovalpituzumab Tesirine Compared With Topotecan as Second-Line Therapy in DLL3-High SCLC: Results From the Phase 3 TAHOE Study. *J Thorac Oncol* (2021) 16(9):1547–58. doi: 10.1016/j.jtho.2021.02.009
123. Mansfield AS, Hong DS, Hann CL, Farago AF, Beltran H, Waqar SN, et al. A Phase I/II Study of Rovalpituzumab Tesirine in Delta-Like 3-Expressing, Advanced Solid Tumors. *J Clin Oncol* (2020) 38(15_suppl):3552. doi: 10.1038/s41698-021-00214-y
124. Purcell JW, Tanlimco SG, Hickson J, Fox M, Sho M, Durkin L, et al. LRRC15 Is a Novel Mesenchymal Protein and Stromal Target for Antibody–Drug Conjugates. *Cancer Res* (2018) 78(14):4059–72. doi: 10.1158/0008-5472.CAN-18-0327
125. Janes PW, Vail ME, Gan HK, Scott AM. Antibody Targeting of Eph Receptors in Cancer. *Pharmaceuticals* (2020) 13(5):88. doi: 10.3390/ph13050088

126. Wykosky J, Gibo DM, Stanton C, Debinski W. EphA2 as a Novel Molecular Marker and Target in Glioblastoma Multiforme. *Mol Cancer Res* (2005) 3 (10):541–51. doi: 10.1158/1541-7786.MCR-05-0056
127. Liu F, Park PJ, Lai W, Maher E, Chakravarti A, Durso L, et al. A Genome-Wide Screen Reveals Functional Gene Clusters in the Cancer Genome and Identifies EphA2 as a Mitogen in Glioblastoma. *Cancer Res* (2006) 66 (22):10815–23. doi: 10.1158/0008-5472.CAN-06-1408
128. Jackson D, Gooya J, Mao S, Kinneer K, Xu L, Camara M, et al. A Human Antibody–Drug Conjugate Targeting EphA2 Inhibits Tumor Growth In Vivo. *Cancer Res* (2008) 68(22):9367–74. doi: 10.1158/0008-5472.CAN-08-1933
129. Annunziata CM, Kohn EC, LoRusso P, Houston ND, Coleman RL, Buzoianu M, et al. Phase 1, Open-Label Study of MEDI-547 in Patients With Relapsed or Refractory Solid Tumors. *Invest New Drugs* (2013) 31(1):77–84. doi: 10.1007/s10637-012-9801-2
130. Kamoun WS, Kirpotin DB, Huang ZR, Tipparaju SK, Noble CO, Hayes ME, et al. Antitumour Activity and Tolerability of an EphA2-Targeted Nanotherapeutic in Multiple Mouse Models. *Nat Biomed Eng* (2019) 3 (4):264–80. doi: 10.1038/s41551-019-0385-4
131. Offenhäuser C, Al-Ejeh F, Puttick S, Ensbey KS, Bruce ZC, Jamieson PR, et al. EphA3 Pay-Loaded Antibody Therapeutics for the Treatment of Glioblastoma. *Cancers* (2018) 10(12):519. doi: 10.3390/cancers10120519
132. Chu L, Wang A, Ni L, Yan X, Song Y, Zhao M, et al. Nose-To-Brain Delivery of Temozolomide-Loaded PLGA Nanoparticles Functionalized With Anti-EPHA3 for Glioblastoma Targeting. *Drug Deliv* (2018) 25(1):1634–41. doi: 10.1080/10717544.2018.1494226
133. Gan H, Cher L, Inglis P, Lwin Z, Lau E, Wichmann C, et al. Abstract CT063: Preliminary Findings of a Phase I Safety and Bioimaging Trial of KB004 (Ifabotuzumab) in Patients With Glioblastoma. *Cancer Res* (2019) 79(13 Supplement):CT063–CT. doi: 10.1158/1538-7445.AM2019-CT063
134. Su Z, Xiao D, Xie F, Liu L, Wang Y, Fan S, et al. Antibody-drug Conjugates: Recent Advances in Linker Chemistry. *Acta Pharm Sin B* (2021) 12:687926. doi: 10.1016/j.apsb.2021.03.042
135. Su D, Zhang D. Linker Design Impacts Antibody-Drug Conjugate Pharmacokinetics and Efficacy *via* Modulating the Stability and Payload Release Efficiency. *Front Pharmacol* (2021) 12:1558. doi: 10.3389/fphar.2021.687926
136. Joubert N, Beck A, Dumontet C, Denevault-Sabourin C. Antibody–Drug Conjugates: The Last Decade. *Pharmaceuticals* (2020) 13(9):245. doi: 10.3390/ph13090245
137. Jeffrey SC, Burke PJ, Lyon RP, Meyer DW, Sussman D, Anderson M, et al. A Potent Anti-CD70 Antibody-Drug Conjugate Combining a Dimeric Pyrrolobenzodiazepine Drug With Site-Specific Conjugation Technology. *Bioconjug Chem* (2013) 24(7):1256–63. doi: 10.1021/bc400217g
138. Hartley JA, Flynn MJ, Bingham JP, Corbett S, Reinert H, Tiberghien A, et al. Pre-Clinical Pharmacology and Mechanism of Action of SG3199, the Pyrrolobenzodiazepine (PBD) Dimer Warhead Component of Antibody-Drug Conjugate (ADC) Payload Tesirine. *Sci* (2018) 8(1):1–10. doi: 10.1038/s41598-018-28533-4
139. Li F, Emmerton KK, Jonas M, Zhang X, Miyamoto JB, Setter JR, et al. Intracellular Released Payload Influences Potency and Bystander-Killing Effects of Antibody-Drug Conjugates in Preclinical Models. *Cancer Res* (2016) 76(9):2710–9. doi: 10.1158/0008-5472.CAN-15-1795
140. Saber H, Simpson N, Ricks TK, Leighton JK. An FDA Oncology Analysis of Toxicities Associated With PBD-Containing Antibody-Drug Conjugates. *Regul Toxicol Pharmacol* (2019) 107:104429–36. doi: 10.1016/j.yrtph.2019.104429
141. Carneiro BA, Bestvina CM, Shacham-Shmueli E, Gan HK, Beck JT, Robinson R, et al. Phase I Study of the Antibody-Drug Conjugate ABBV-321 in Patients With Non-Small Cell Lung Cancer and Squamous Head and Neck Cancer With Overexpression of the Epidermal Growth Factor Receptor. *J Clin Oncol* (2020) 38(15_suppl):TPS3649. doi: 10.1200/JCO.2020.38.15_suppl.TPS3649
142. Ogitani Y, Hagihara K, Oitate M, Naito H, Agatsuma T. Bystander Killing Effect of DS-8201a, A Novel Anti-Human Epidermal Growth Factor Receptor 2 Antibody–Drug Conjugate, in Tumors With Human Epidermal Growth Factor Receptor 2 Heterogeneity. *Cancer Sci* (2016) 107(7):1039–46. doi: 10.1111/cas.12966
143. Ogitani Y, Aida T, Hagihara K, Yamaguchi J, Ishii C, Harada N, et al. DS-8201a, a Novel HER2-Targeting ADC With a Novel DNA Topoisomerase I Inhibitor, Demonstrates a Promising Antitumor Efficacy With Differentiation From T-Dm1. *Clin Cancer Res* (2016) 22(20):5097–108. doi: 10.1158/1078-0432.CCR-15-2822
144. Linehan AS, Fitzpatrick OM, Morris PG. Profile of Trastuzumab Deruxtecan in the Management of Patients With HER2-Positive Unresectable or Metastatic Breast Cancer: An Evidence-Based Review. *Breast Cancer: Targets Ther* (2021) 13:151. doi: 10.2147/BCTT.S245024
145. Tsurutani J, Iwata H, Krop I, Jänne PA, Doi T, Takahashi S, et al. Targeting HER2 With Trastuzumab Deruxtecan: A Dose-Expansion, Phase I Study in Multiple Advanced Solid Tumors. *Cancer Discov* (2020) 10(5):688–701. doi: 10.1158/2159-8290.CD-19-1014
146. Modi S, Saura C, Yamashita T, Park YH, Kim S-B, Tamura K, et al. Trastuzumab Deruxtecan in Previously Treated HER2-Positive Breast Cancer. *N Engl J Med* (2020) 382(7):610–21. doi: 10.1056/NEJMoa1914510
147. Yu H, Baik C, Gold K, Hayashi H, Johnson M, Koczywas M, et al. LBA62 Efficacy and Safety of Patritumab Deruxtecan (U3-1402), A Novel HER3 Directed Antibody Drug Conjugate, in Patients (Pts) With EGFR-Mutated (EGFRm) NSCLC. *Ann Oncol* (2020) 31:S1189–90. doi: 10.1016/j.annonc.2020.08.2295
148. Charmsaz S, Beckett K, Smith FM, Bruedigam C, Moore AS, Al-Ejeh F, et al. EphA2 Is a Therapy Target in EphA2-Positive Leukemias But Is Not Essential for Normal Hematopoiesis or Leukemia. *PloS One* (2015) 10(6): e0130692. doi: 10.1371/journal.pone.0130692
149. Charmsaz S, Al-Ejeh F, Yeadon T, Miller K, Smith FM, Stringer BW, et al. EphA3 as a Target for Antibody Immunotherapy in Acute Lymphoblastic Leukemia. *Leukemia* (2017) 31(8):1779–87. doi: 10.1038/leu.2016.371
150. Day BW, Stringer BW, Al-Ejeh F, Ting MJ, Wilson J, Ensbey KS, et al. EphA3 Maintains Tumorigenicity and Is a Therapeutic Target in Glioblastoma Multiforme. *Cancer Cell* (2013) 23(2):238–48. doi: 10.1016/j.ccr.2013.01.007
151. McGranahan N, Swanton C. Biological and Therapeutic Impact of Intratumor Heterogeneity in Cancer Evolution. *Cancer Cell* (2015) 27 (1):15–26. doi: 10.1016/j.ccell.2014.12.001
152. Metzger Filho O, Viale G, Trippa L, Li T, Yardley DA, Mayer IA, et al. HER2 Heterogeneity as a Predictor of Response to Neoadjuvant T-DM1 Plus Pertuzumab: Results From a Prospective Clinical Trial. *J Clin Oncol* (2019) 37(15_suppl):502. doi: 10.1200/JCO.2019.37.15_suppl.502
153. Yu K, Hu Y, Wu F, Guo Q, Qian Z, Hu W, et al. Surveying Brain Tumor Heterogeneity by Single-Cell RNA-Sequencing of Multi-Sector Biopsies. *Natl Sci Rev* (2020) 7(8):1306–18. doi: 10.1093/nsr/nwaa099
154. Nathanson DA, Gini B, Mottahedeh J, Visnyei K, Koga T, Gomez G, et al. Targeted Therapy Resistance Mediated by Dynamic Regulation of Extrachromosomal Mutant EGFR DNA. *Science* (2014) 343(6166):72–6. doi: 10.1126/science.1241328
155. Francis JM, Zhang C-Z, Maire CL, Jung J, Manzo VE, Adalsteinsson VA, et al. EGFR Variant Heterogeneity in Glioblastoma Resolved Through Single-Nucleus Sequencing. *Cancer Discov* (2014) 4(8):956–71. doi: 10.1158/2159-8290.CD-13-0879
156. Felsberg J, Hentschel B, Kaulich K, Gramatzki D, Zacher A, Malzkorn B, et al. Epidermal Growth Factor Receptor Variant III (EGFRvIII) Positivity in EGFR-Amplified Glioblastomas: Prognostic Role and Comparison Between Primary and Recurrent Tumors. *Clin Cancer Res* (2017) 23(22):6846–55. doi: 10.1158/1078-0432.CCR-17-0890
157. Gadgeel S, Rodríguez-Abreu D, Speranza G, Esteban E, Felip E, Dómine M, et al. Updated Analysis From KEYNOTE-189: Pembrolizumab or Placebo Plus Pemetrexed and Platinum for Previously Untreated Metastatic Nonsquamous Non-Small-Cell Lung Cancer. *J Clin Oncol* (2020) 38 (14):1505–17. doi: 10.1200/JCO.19.03136
158. Chandramohan V, Bao X, Yu X, Parker S, McDowall C, Yu Y-R, et al. Improved Efficacy Against Malignant Brain Tumors With EGFRwt/EGFRvIII Targeting Immunotoxin and Checkpoint Inhibitor Combinations. *J Immunother Cancer* (2019) 7(1):1–14. doi: 10.1186/s40425-019-0614-0
159. Gan HK, Walker F, Burgess AW, Rigopoulos A, Scott AM, Johns TG. The Epidermal Growth Factor Receptor (EGFR) Tyrosine Kinase Inhibitor AG1478 Increases the Formation of Inactive Untethered EGFR Dimers:

Implications for Combination Therapy With Monoclonal Antibody 806. *J Biol Chem* (2007) 282(5):2840–50. doi: 10.1074/jbc.M605136200
160. Orellana L, Thorne AH, Lema R, Gustavsson J, Parisian AD, Cordeiro TN, et al. Oncogenic Mutations at the EGFR Ectodomain Structurally Converge to Remove a Steric Hindrance on a Kinase-Coupled Cryptic Epitope. *Proc Natl Acad Sci* (2019) 116(20):10009–18. doi: 10.1073/pnas.1821442116
161. Anderson MG, Falls HD, Mitten MJ, Oleksijew A, Vaidya KS, Boghaert ER, et al. Targeting Multiple EGFR-Expressing Tumors With a Highly Potent Tumor-Selective Antibody-Drug Conjugate. *Mol Cancer Ther* (2020) 19 (10):2117–25. doi: 10.1158/1535-7163.MCT-20-0149
162. Levengood MR, Zhang X, Hunter JH, Emmerton KK, Miyamoto JB, Lewis TS, et al. Orthogonal Cysteine Protection Enables Homogeneous Multi-Drug Antibody–Drug Conjugates. *Angew Chem Int Edition* (2017) 56(3):733–7. doi: 10.1002/anie.201608292
163. Anami Y, Xiong W, Gui X, Deng M, Zhang CC, Zhang N, et al. Enzymatic Conjugation Using Branched Linkers for Constructing Homogeneous Antibody–Drug Conjugates With High Potency. *Org Biomol Chem* (2017) 15(26):5635–42. doi: 10.1039/C7OB01027C
164. Gerber H-P, Sapra P, Loganzo F, May C. Combining Antibody–Drug Conjugates and Immune-Mediated Cancer Therapy: What to Expect? *Biochem Pharmacol* (2016) 102:1–6. doi: 10.1016/j.bcp.2015.12.008
165. Griguolo G, Pascual T, Dieci MV, Guarneri V, Prat A. Interaction of Host Immunity With HER2-Targeted Treatment and Tumor Heterogeneity in HER2-Positive Breast Cancer. *J Immunother Cancer* (2019) 7(1):1–14. doi: 10.1186/s40425-019-0548-6
166. Khattar M, Traore T, Horton K, Gallery M, Brauer P, Riceberg J, et al. Synergy of an Anti-HER2 ADC TAK-522 (XMT-1522) in Combination With Anti-PD1 Monoclonal Antibody (mAb) in a Syngeneic Breast Cancer Model Expressing Human HER2. *Cancer Res* (2018) 78(13 Suppl):LB-294. doi: 10.1158/1538-7445.AM2018-LB-294
167. Müller P, Kreuzaler M, Khan T, Thommen DS, Martin K, Glatz K, et al. Trastuzumab Emtansine (T-DM1) Renders HER2+ Breast Cancer Highly Susceptible to CTLA-4/PD-1 Blockade. *Sci Trans Med* (2015) 7 (315):315ra188–315ra188. doi: 10.1126/scitranslmed.aac4925
168. Rios-Doria J, Harper J, Rothstein R, Wetzel L, Chesebrough J, Marrero A, et al. Antibody–Drug Conjugates Bearing Pyrrolobenzodiazepine or Tubulysin Payloads Are Immunomodulatory and Synergize With Multiple Immunotherapies. *Cancer Res* (2017) 77(10):2686–98. doi: 10.1158/0008-5472.CAN-16-2854
169. Reardon DA, Lassman AB, van den Bent M, Kumthekar P, Merrell R, Scott AM, et al. Efficacy and Safety Results of ABT-414 in Combination With Radiation and Temozolomide in Newly Diagnosed Glioblastoma. *Neuro-Oncol* (2017) 19(7):965–75. doi: 10.1093/neuonc/now257
170. Lassman AB, Gan HK, Roberts-Rapp L, Ansell P, Merrell R, Kumthekar P, et al. (2017). Identifying the Correct Patient Population for Depatuxizumab Mafodotin (ABT-414): Biomarker Assays for Epidermal Growth Factor Receptor (EGFR) in Patients With Glioblastoma. In: *World Federation of Neuro-Oncology*. Zurich, 4-7 May, 2017.
171. Ileana Dumbrava E, Meric-Bernstam F, Yap TA. Challenges With Biomarkers in Cancer Drug Discovery and Development. *Expert Opin Drug Discov* (2018) 13(8):685–90. doi: 10.1080/17460441.2018.1479740
172. Lassman A, Roberts-Rapp L, He L, Lu X, van den Bent M, Papadopoulos K, et al. PATH-29. Molecular Determinants Associated With Response and Resistance to Depatuxizumab Mafodotin (ABT-414) In Patients With Recurrent GLIOBLASTOMA. *Neuro-Oncol* (2017) 19(suppl_6):vi176–7. doi: 10.1093/neuonc/nox168.719
173. Scott AM, Lee F-T, Tebbutt N, Herbertson R, Gill SS, Liu Z, et al. A Phase I Clinical Trial With Monoclonal Antibody Ch806 Targeting Transitional State and Mutant Epidermal Growth Factor Receptors. *Proc Natl Acad Sci* (2007) 104(10):4071–6. doi: 10.1073/pnas.0708144104
174. Gan HK, Burge M, Solomon B, Lee S, Holen KD, Zhang Y, et al. A Phase 1 and Biodistribution Study of ABT-806i, An Indium-111 Radiolabeled Conjugate of the Tumor-Specific Anti-EGFR Antibody ABT-806. *J Nucl Med* (2021) 62(11). doi: 10.2967/jnumed.120.253146

Conflict of Interest: The authors declare that the research was conducted in the absence of any commercial or financial relationships that could be construed as a potential conflict of interest.

Publisher's Note: All claims expressed in this article are solely those of the authors and do not necessarily represent those of their affiliated organizations, or those of the publisher, the editors and the reviewers. Any product that may be evaluated in this article, or claim that may be made by its manufacturer, is not guaranteed or endorsed by the publisher.

Copyright © 2021 Parakh, Nicolazzo, Scott and Gan. This is an open-access article distributed under the terms of the Creative Commons Attribution License (CC BY). The use, distribution or reproduction in other forums is permitted, provided the original author(s) and the copyright owner(s) are credited and that the original publication in this journal is cited, in accordance with accepted academic practice. No use, distribution or reproduction is permitted which does not comply with these terms.

frontiers in Oncology

ORIGINAL RESEARCH
published: 15 December 2021
doi: 10.3389/fonc.2021.667884

Novel Biomarker Genes for Prognosis of Survival and Treatment of Glioma

Xiaopeng Zhu[1†], Sian Pan[2†], Rui Li[3], Zebo Chen[1], Xingyun Xie[1], Deqing Han[1], Shengqing Lv[4] and Yongkai Huang[1*]*

[1] Department of Neurosurgery, Zhuzhou Central Hospital, Zhuzhou, China, [2] Department of Rehabilitation Medicine, Zhuzhou Central Hospital, Zhuzhou, China, [3] Department of Operating Theatre, Zhuzhou Central Hospital, Zhuzhou, China, [4] Department of Neurosurgery, Xinqiao Hospital, Third Military Medical University, Chongqing, China

Glioblastoma multiforme (GBM) is the most aggressive malignant primary central nervous system tumor. Although surgery, radiotherapy, and chemotherapy treatments are available, the 5-year survival rate of GBM is only 5.8%. Therefore, it is imperative to find novel biomarker for the prognosis and treatment of GBM. In this study, a total of 141 differentially expressed genes (DEGs) in GBM were identified by analyzing the GSE12657, GSE90886, and GSE90598 datasets. After reducing the data dimensionality, Kaplan-Meier survival analysis indicated that expression of PTPRN and RIM-BP2 were downregulated in GBM tissues when compared with that of normal tissues and that the expression of these genes was a good prognostic biomarker for GBM ($p<0.05$). Then, the GSE46531 dataset and the Genomics of Drug Sensitivity in Cancer (GDSC) database were used to examine the relationship between sensitivity radiotherapy (RT) and chemotherapy for GBM and expression of PTPRN and RIM-BP2. The expression of PTPRN was significantly high in RT-resistant patients ($p<0.05$) but it was not related to temozolomide (TMZ) resistance. The expression level of RIM-BP2 was not associated with RT or TMZ treatment. Among the chemotherapeutic drugs, cisplatin and erlotinib had a significantly good treatment effect for glioma with expression of PTPRN or RIM-BP2 and in lower-grade glioma (LGG) with IDH mutation. ($p < 0.05$). The tumor mutational burden (TMB) score in the low PTPRN expression group was significantly higher than that in the high PTPRN expression group ($p=0.013$), with a large degree of tumor immune cell infiltration. In conclusion, these findings contributed to the discovery process of potential biomarkers and therapeutic targets for glioma patients.

Keywords: glioblastoma, prognosis, GEO, radiotherapy, chemotherapy, immunotherapy, TMB

OPEN ACCESS

Edited by:
David Nathanson, UCLA David Geffen School of Medicine, United States

Reviewed by:
Joshua Pearson, Nottingham Trent University, United Kingdom
Lyndon Kim, Mount Sinai Hospital, United States

****Correspondence:***
Yongkai Huang
605404379@qq.com
Shengqing Lv
lvsq0518@hotmail.com

†These authors share first authorship

Specialty section:
This article was submitted to Neuro-Oncology and Neurosurgical Oncology, a section of the journal Frontiers in Oncology

Received: *15 February 2021*
Accepted: *17 November 2021*
Published: *15 December 2021*

Citation:
Zhu X, Pan S, Li R, Chen Z, Xie X, Han D, Lv S and Huang Y (2021) Novel Biomarker Genes for Prognosis of Survival and Treatment of Glioma. Front. Oncol. 11:667884. doi: 10.3389/fonc.2021.667884

INTRODUCTION

An estimated 86,010 new cases of primary brain and other central nervous system (CNS) tumors were diagnosed in the US in 2019 (1). Glioblastoma multiforme (GBM) is the most common and aggressive primary CNS tumor (2). Despite the availability of several treatment options, including surgery, radiotherapy, and chemotherapy, the median overall survival (OS) of GBM remains

approximately 15 months, and the 5-year survival rate is 5.8% (3). In 2016, the updated World Health Organization (WHO) classification was the first to integrate molecular parameters with histology to define many tumor entities, including GBM (4), thus formulating a new concept for how GBM diagnoses should be structured in the molecular era. Although IDH1/2 mutations, MGMT promoter methylation, and 1p/19q loss have been recognized as appropriate diagnostic and prognostic markers (5, 6), patients with GBM still have poor outcomes, with one of the worst 5-year OS rates among all human cancers (7). Therefore, it is vital to develop appropriate and effective novel molecular signatures to improve survival and treatment response prediction for patients with GBM. With the development of next-generation sequencing (NGS) technologies, a large amount of data on differentially expressed genes (DEGs), non-coding RNAs, and protein modifications have been identified and stored in public databases. Gene Expression Omnibus (GEO, https://www.ncbi. nlm.nih.gov/geo/), The Cancer Genome Atlas (TCGA, https://portal.gdc.cancer.gov), and Chinese Glioma Genome Atlas (CGGA, http://www.cgga.org.cn) provide us with the opportunity and resources to explore, integrate, and reanalyze the existing data for new GBM biomarker discovery.

Although genomic analysis of cancers is at the forefront of drug and molecular pathogenesis discovery (8), much of the research has focused on biomarkers related to GBM prognosis. Only a few studies have explored potential therapeutic options related to novel molecular signatures.

In this study, bioinformatics methods were used, and we found two potential markers, PTPRN and RIM-BP2, associated with OS in patients with GBM. Furthermore, our goal was to provide information for designing radiotherapy and chemotherapy regimens by monitoring these biomarkers.

MATERIALS AND METHODS

Data Source

The Series Matrix Files for gene expression microarray datasets were downloaded from the National Center of Biotechnology Information (NCBI) Gene Expression Omnibus(GEO). GBM tumor samples smaller than 6 and without normal or adjacent tumor tissue in GEO data were considered inappropriate samples in this study. In addition, to rule out interference, samples that had undergone chemotherapy or radiotherapy were also excluded.Among them, 3 independent GEO datasets, GSE12657, GSE90886, and GSE90598, including 7 samples of GBM and 5 samples of normal brain tissue, 9 samples of GBM and 9 samples of normal brain tissue, and 16 samples of GBM and 7 samples of normal brain tissue, respectively, were included. The dataset was based on the GPL8300, GPL15207, and GPL17692 platforms of the Affymetrix Human Genome U133 Plus 2.0 Array (Affymetrix, Santa Clara, CA, United States). Then, gene profiles were standard normalized by spatially variant apodization (SVA) within and among samples. To analyze the sensitivity of radiotherapy based on hub genes, the Gene expression microarray dataset GSE46531, which is only qualified and relevant data, was extracted for subsequent analysis. Glioma stem cell(GSC)culture lines were established from fresh GBM tumors. Treatment-resistant clones, including sensitive clones (n=6), RT-resistant clones (n = 3) and RT+TMZ-resistant clones (n = 3), obtained by irradiating the cultured cells with a certain dose of radiation and adding TMZ to the cell culture, were used for microarray analysis to explore different molecules involved in response therapy (9). The GBM RNA sequencing data (RNA-seq) were downloaded from the TCGA database (https://portal.gdc.cancer.gov). A total of 174 RNA-seq datasets were extracted for subsequent validation.

Gene Ontology (GO) and Kyoto Encyclopedia of Genes and Genomes (KEGG) Annotation

GO and KEGG enrichment analyses were performed on the survival-related genes. The Metascape database (www.metascape.org) was used to annotate and visualize GO terms and KEGG pathways. Min overlap≥3 and $P < 0.01$ were set as threshold values.

Identification of Optimal Diagnostic Gene Biomarkers

The LASSO algorithm was applied with the glmnet package (https://cran.r-project.org/web/packages/glmnet/) (10). The Boruta algorithm (https://cran.r-project.org/web/packages/Boruta/) employs a wrapper approach built around a random forest classifier (11). The DEGs between GBM and normal controls were retained for feature selection, and biomarker genes for GBM were identified with the above algorithms. The optimal biomarker genes for GBM were then identified by overlapping the biomarkers derived from these two algorithms. Based on these optimal gene biomarkers, the Boruta package was used further to evaluate the diagnostic value of these biomarkers in GBM.

Tumor-Infiltrating Immune Cell Analysis

The CIBERSORT package was used to explore the differences in immune cell subtypes including B cells, T cells, natural killer (NK) cells, macrophages, and dendritic cells (DCs), based on the expression data (12). Samples with $P < 0.05$ in CIBERSORT analysis results were used for further analysis. Spearman analysis was used to compare differences in immune cell subtypes in the high hub-gene and low hub-gene groups.

Gene Set Variation Analysis (GSVA)

The gene set variation analysis (GSVA) method is nonparametric and unsupervised and bypasses the conventional approach of explicitly modeling phenotypes within the enrichment scoring algorithm (13). GSVA calculates samples gene set enrichment scores as a function of the genes inside and outside the gene set. Furthermore, it estimates the variation in gene set enrichment over the samples independently of any class label. In this study, gene sets were obtained from the Molecular Signatures Database

v7.0. GSVA was used to compute single-sample enrichment scores to describe the potential changes in biological function.

Drug Sensitivity Analysis

The largest publicly available pharmacogenomics database, Genomics of Drug Sensitivity in Cancer (GDSC, https://www.cancerrxgene.org/) has characterised 1000 human cancer cell lines and screened them 100s of compounds, was used to obtain drug IC50 values and predict the chemotherapeutic response of each sample (14). The prediction procedure was performed by the R software package "prophetic". Tenfold cross-validation was used to assess the prediction accuracy based on the GDSC training set (15).

Tumor Mutational Burden Analysis

The TMB was defined as the number of somatic, coding, base substitution, and indel mutations identified by next-generation sequencing (NGS). Mutations obtained from SNPs in GBM samples were downloaded from the database using VarScan2 and SAMtools (16). To estimate the TMB of the training set, we counted all coding somatic base substitutions and indels in the targeted regions, including "stop/start-loss/frameshift/missense/inframe" alterations.

GeneMANIA Analysis

GeneMANIA (http://genemania.org) is a flexible, user-friendly website for generating hypotheses about gene functions, analyzing gene lists, and prioritizing genes for functional assays (17).Given a query gene list, GeneMANIA finds functionally similar genes using a wealth of genomics and proteomics data. In this mode, it weights each functional genomic dataset according to its predictive value for the query. In this study, GeneMANIA was used to visualize the molecular network analyses to explore possible hub genes and their mechanisms in GBM.

Statistical Analysis

All P-values were two-sided, and values lower than 0.05 were considered significant. Statistical significance is indicated in the figures as follows: * P <0.05, * * P < 0.01. R Studio (version 3.6) and corresponding packages was used for all statistical analyses. The glmnet R package was used for LASSO analysis. Survival curves plotted by the Kaplan–Meier method were compared to the log-rank test. The mutation were analyzed by cBioportal package. The CIBERSORT package was used to explore the differences in immune cell subtypes. The prophetic package was performed to predict the chemotherapeutic response.

RESULTS

Construction of a Prognostic Classifier Based on DEGs in GBM

GBM gene expression microarray data (GSE12657, GSE90886, and GSE90598) with a total of 53 samples (32 GBM and 21 control) were downloaded from the NCBI GEO. The spatial variant apodization (SVA) algorithm was used to normalize the datasets, and the principal component analysis (PCA) plot shows the batch effect before and after normalization (**Figures 1A, B**). The package limma was used to perform the data analysis. Fold change > 1 and $p < 0.05$ were set as the cutoffs to screen for DEGs. Compared with normal brain tissues, the limma package identified 141 DEGs (**Supplementary Table 1**) in GBM, of which 30 were upregulated and 111 were downregulated (**Figure 1C**). GO and KEGG pathway enrichment analyses suggested that these genes mainly participated in the following pathways: chemical synaptic transmission, presynapse, postsynapse, synaptic membrane, and axon (**Figures 1D, E**). Biological processes of DEGs were mainly associated with the chemical synaptic transmission that affects the neuronal activity and neurotransmitters to participate in the onset and progression of GBM (18, 19). Some synapse-related genes, such as RIM-BP2 and CACNG3, have been less studied in tumors.

The results of the GSVA database analysis showed that differential expression of PTPRN and RIM-BP2 was involved in DNA repair and the APICAL_JUNCTION and APICAL_SURFACE ESTROGEN_RESPONSE_EARLY pathways (**Figures 2A, B**). Metascape was used to construct protein-protein interaction (PPI) networks (**Figure 2C**). The coexpression network of the DEGs is shown in **Figure 2D**.

Next, we identified 14 DEGs as GBM survival-related genes to be included in the classifier using the LASSO analysis (**Figures 3A, B**). Boruta algorithm analysis identified 17 DEGs as survival-related genes (**Figure 3C**). Then, we obtained five DEGs, including SLC8A2, PTPRN, F2R, RIM-BP2, and IFI44, by overlapping the two analyses (**Figure 3D**); of these, PTPRN and RIM-BP2 were highly expressed in GBM ($p<0.05$) (**Figures 3E, F**). Kaplan-Meier survival curves from the TCGA database were used to explore the potential roles of individual DEGs in GBM OS. Among the five genes, high expression of PTPRN (p=7.632e-06) or RIM-BP2 (p=1.669e-03) significantly predicted poor overall survival (**Figures 3G, H**). Combined analysis of *PTPRN* and *RIM-BP2* showed no significant advantage for the prediction of GBM prognosis compared with either gene individual analysis. In addition, PTPRN was found to play the dominant role in prognosis prediction in the combined analysis of the two genes (**Figure 4**).

Expression of PTPRN and RIM-BP2 in Response to Radiation Treatment (RT) and Drug Therapy in GBM

To explore the relationship between expression of PTPRN and RIM-BP2 and the sensitivity to RT or TMZ, we first wanted to know whether the PTPRN and RIM-BP2 genes were differentially expressed in RT-resistant and RT+TMZ-resistant patients than RT-sensitive and RT+TMZ- sensitive patients. Six sensitive groups (three patients, two clones per patient), three RT-resistant groups, and three RT+TMZ-resistant groups were used for the analysis. The results showed that expression of PTPRN was significantly higher in the RT-resistant patient group and RT+TMZ-resistant group than in the sensitive

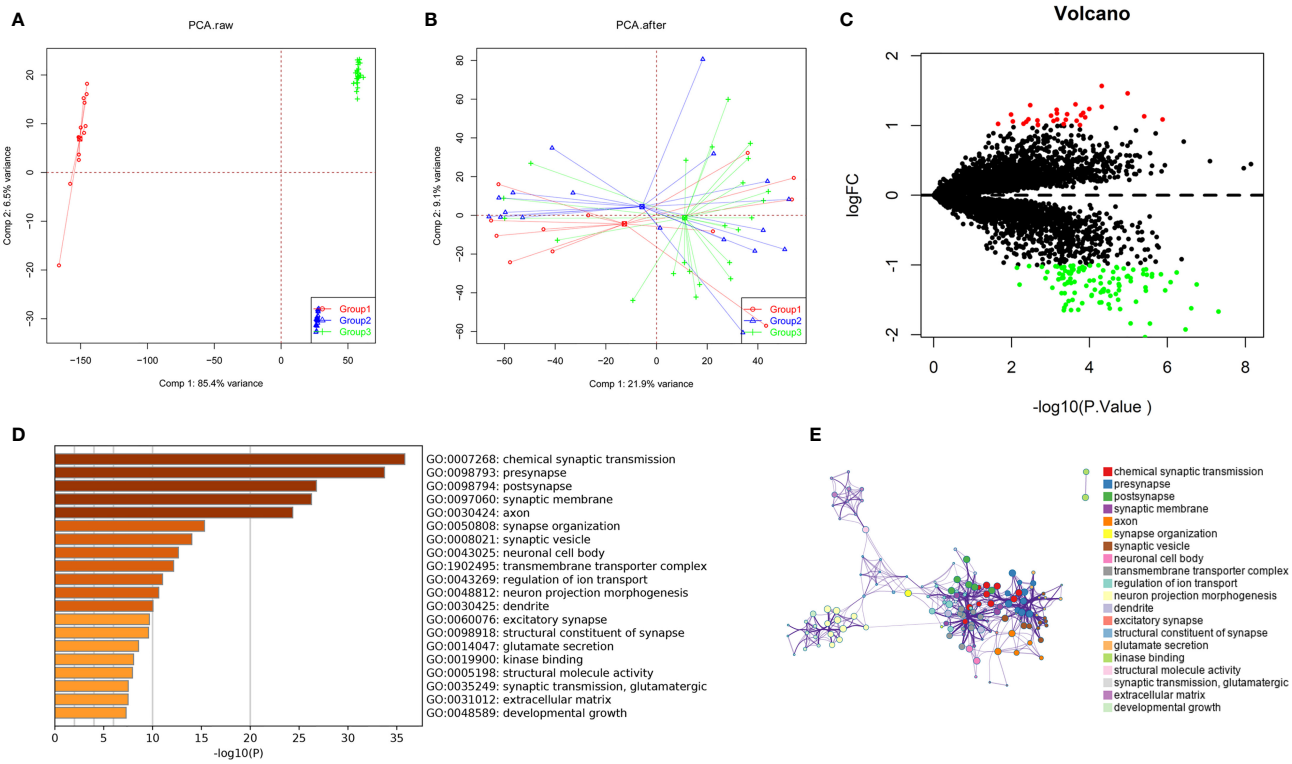

FIGURE 1 | Identification of DEGs among GBM datasets from TCGA and GEO. **(A, B)** The SVA algorithm was used to normalize the datasets, and the PCA plot shows the batch effect. **(C)** Volcano plots of DEGs created by using the limma package. **(D, E)** GO and KEGG pathway enrichment analysis performed by the Metascape database.

groups ($p<0.05$). There were no differences in the expression of PTPRN between the RT-resistant group and the RT+TMZ-resistant group (**Figure 5A**). Moreover, the difference in the expression of RIM-BP2 was also not significant among the three groups (**Figure 5B**). These results suggested that the patients with higher PTPRN expression were more resistant to RT. TMZ treatment did not change the resistance to RT, suggesting that PTPRN expression was not associated with sensitivity to TMZ.

Chemotherapy is a common treatment for GBM. We further analyzed the sensitivity of PTPRN and RIM-BP2 to chemotherapy drugs, including AKT inhibitor VIII, cisplatin, erlotinib, gefitinib, and gemcitabine. The prediction model on the GDSC was used. 10-fold cross-validation for TCGA GBM cohort resulted in satisfactory prediction. The results showed that there were significant differences in PTPRN and RIM-BP2 expression in response to several drugs, suggesting that both PTPRN and RIM-BP2 were sensitive to common chemotherapy drugs ($p < 0.05$). According to the predictive model of chemotherapy drugs in TCGA dataset, the order of sensitivity responses PTPRN to chemotherapy drugs was AKT inhibitor VIII > cisplatin > erlotinib > gefitinib > gemcitabine. In contrast, the order of sensitivity responses of RIM-BP2 to chemotherapy drugs was AKT inhibitor VIII > cisplatin > dasatinib > erlotinib > gefitinib > gemcitabine (**Figures 5C, D**).

Expression of PTPRN and RIM-BP2 in Response to Anticancer Drugs in LGG With IDH Mutation

LGG accounts for approximately 20% of primary malignant tumors of the CNS and occurs most commonly in young adults. According to the RTOG 9802 standard, LGG is clinically divided into a low-risk group and a high-risk group according to patient age, the occurrence of subtotal resection, and histology findings (20). RT is necessary to treat high-risk LGG, and the treatment appears to be effective in patients with IDH mutations. For patients with high-risk LGG, National Comprehensive Cancer Network (NCCN) guidelines recommend postoperative RT + procarbazine, lomustine, and vincristine (PCV) chemotherapy or RT + adjuvant TMZ chemotherapy or RT + synchronous adjuvant TMZ chemotherapy (20, 21). The appropriate postoperative treatment for patients with high-risk LGG remains under debate.

Therefore, we evaluated the relationship between PTPRN and RIM-BP2 expression and chemotherapy in LGG, and the order of sensitivity in cases with high PTPRN and RIM-BP2 was as follows: AKT inhibitor VIII > cisplatin > dasatinib > erlotinib > gefitinib > gemcitabine ($p < 0.05$) (**Figures 6A, B**).

IDH mutations are common in LGG; thus, we analyzed the sensitivity of LGG tumors with IDH mutations to chemotherapy drugs.

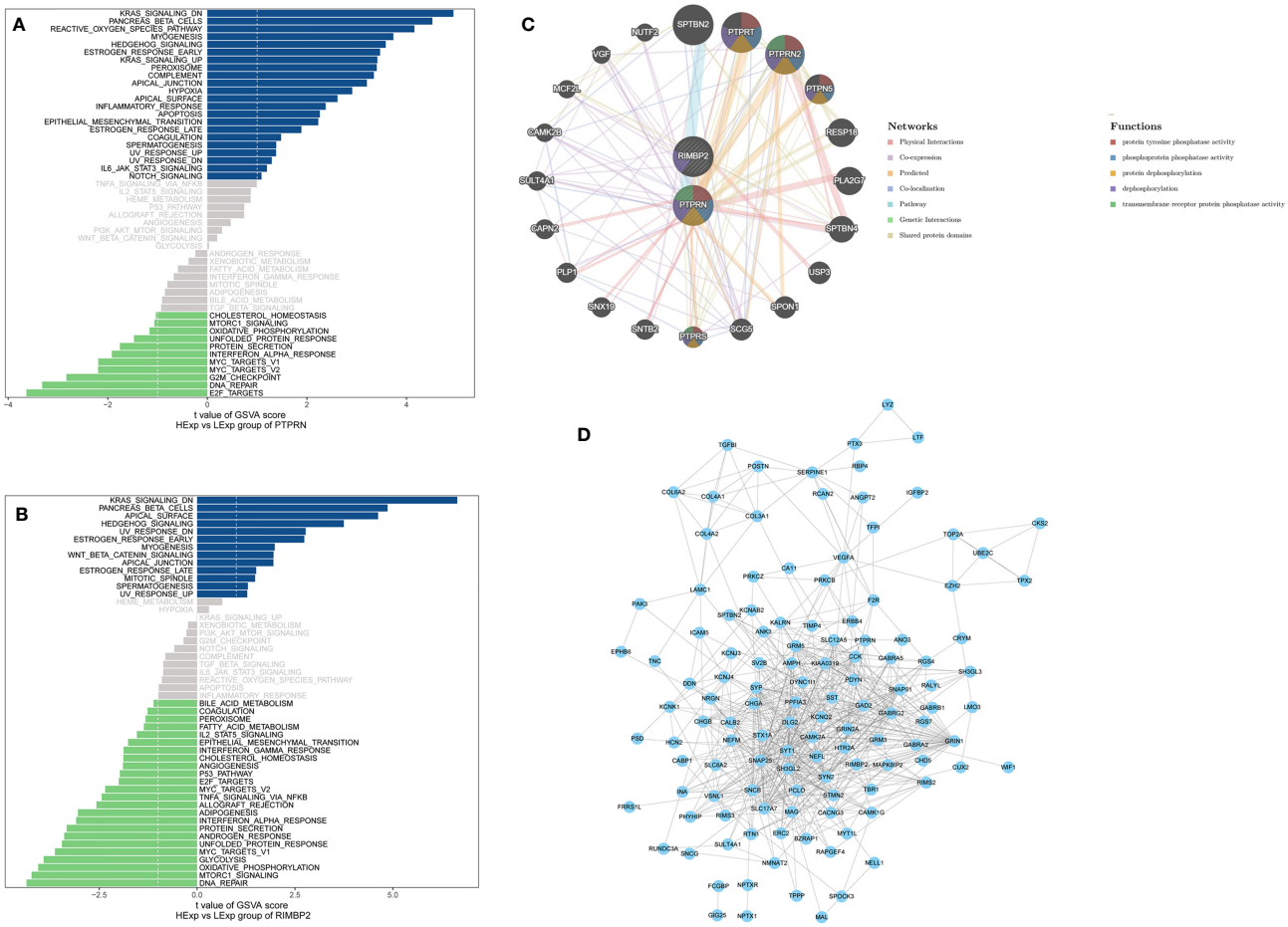

FIGURE 2 | The pathway and coexpression networks of different levels of PTPRN and RIM-BP2 expression. **(A, B)** The GSVA database shows the pathways associated with different expression levels of PTPRN and RIM-BP2. **(C)** The coexpression network of the two-gene signature. **(D)** Visualization of the coexpression network of the DEGs was generated using Cytoscape. Based on weights, not all genes corresponding to each module were represented.

We found that tumors with IDH mutations were more sensitive to cisplatin, dasatinib, and erlotinib than those without IDH mutations (IDH-wt, **Figure 6C**).

Moreover, we found that LGG was most sensitive to cisplatin and erlotinib when high expression of PTPRN or RIM-BP2 was combined with the IDH mutation. Therefore, cisplatin and erlotinib are preferred chemotherapies in LGG with IDH mutations and high PTPRN and RIM-BP2 expression.

Tumor Mutational Burden of PTPRN and RIM-BP2

After demonstrating the effect of PTPRN and RIM-BP2 expression on the response to RT and chemotherapy, we identified the PTPRN and RIM-BP2 mutations in tumors. All GBM data sets were derived from the TCGA-Pancancer database, and TMB of PTPRN and RIM-BP2 was estimated using CIBERSORT (https://cibersort.stanford.edu/). The results showed that PTPRN and RIM-BP2 coding mutations existed in a total of 15 patients with GBM (10%). The mutation frequencies were 8% and 6% for PTPRN and RIM-BP2, respectively, in 15 patients (**Figure 7A**). Subsequently, we analyzed the relationship between PTPRN or RIM-BP2 expression and TMB score. The results showed that the TMB score in patients with GBM and low PTPRN expression was significantly higher than that of patients with high PTPRN expression (**Figure 7B**). The difference in the RIM-BP2 expression group was not statistically significant (**Figure 7C**).

Correlation Between Immune Cell Subtypes and of the Expression of PTPRN and RIM-BP2

The immune microenvironment has been shown to play a critical role in tumor biology. Recently, numerous promising preclinical and clinical immunotherapeutic treatments and gene therapy have been achieved for GBM. However, the role of

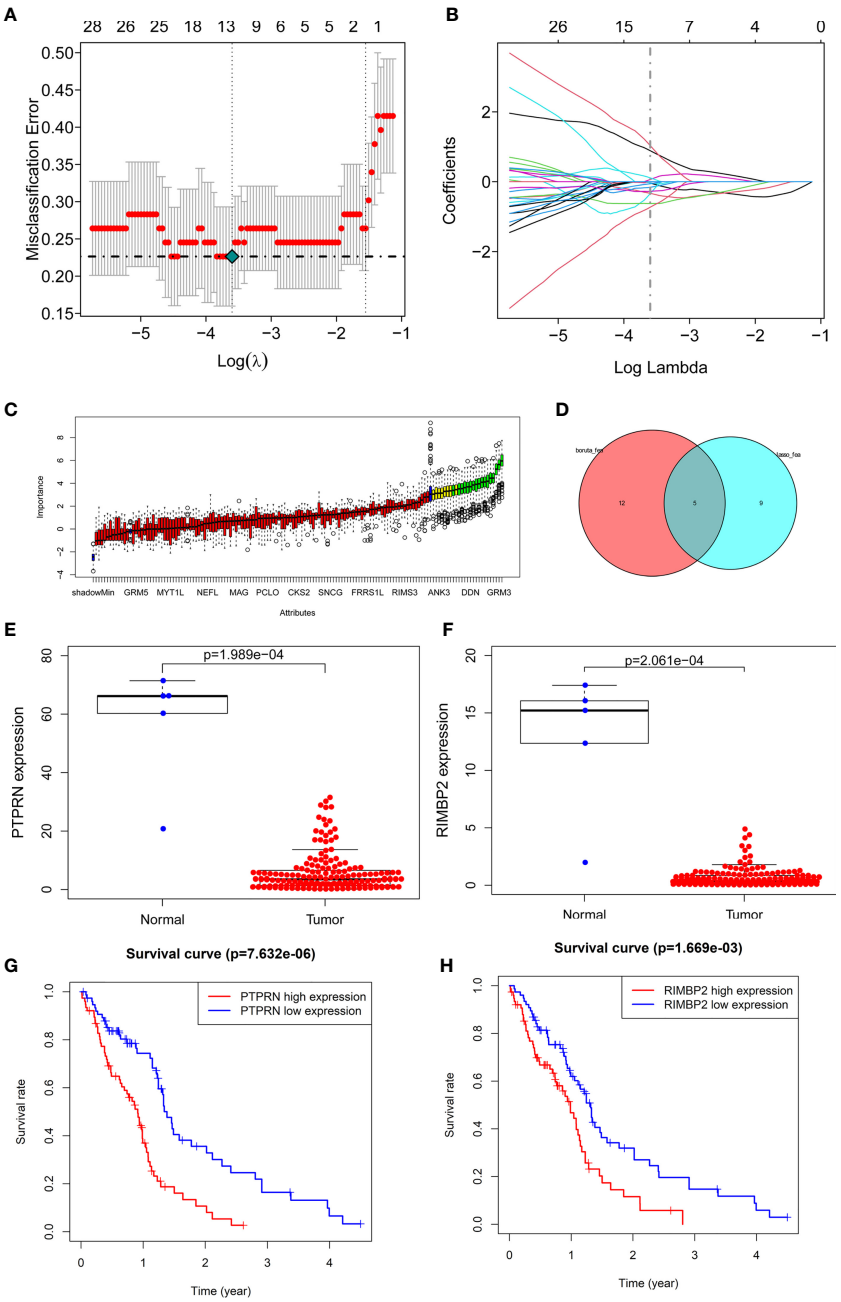

FIGURE 3 | Identification of optimal survival biomarker genes **(A, B).** Determination of the number of factors by LASSO analysis. **(C)** Determination of the number of elements by the Boruta algorithm. **(D)** The Venn diagram of DEGs among the LASSO analysis and Boruta algorithm defined 5 hub genes. Among them, 2 genes (PTPRN and RIM-BP2) were associated with survival. **(E, F)** Expression of PTPRN and RIM-BP2 in normal and GBM tissues. **(G, H)** Kaplan–Meier analysis using the median risk score cutoff to divide patients into low gene expression and high gene expression groups.

immunotherapy in gliomas needs to be further clarified (22, 23). Hence, the molecular profiles within the tumor microenvironment may be valuable predictive biomarkers.

The CIBERSORT algorithm acquired the relative proportions of 22 immune cell subsets in GBM. The correlations between the proportions of the 22 immune cell subtypes and PTPRN and RIM-BP2 expression are shown in **Figure 8A**. There was a large degree of tumor immune cell infiltration, including M0 macrophages, M2 macrophages, activated mast cells, neutrophils, and resting memory CD4 T cells, in patients with GBM and high PTPRN expression. At the same time, there was also massive tumor immune cell infiltration, such as M2

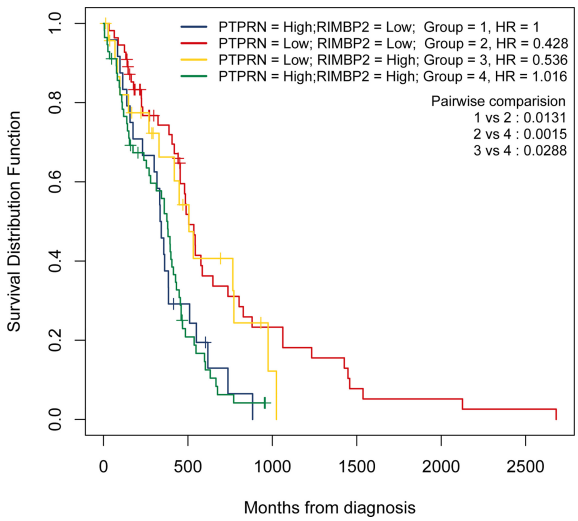

FIGURE 4 | PTPRN and RIM-BP2 predict the prognosis of GBM. Kaplan-Meier curves of overall survival for GBM patients with different PTPRN and RIM-BP2 (combined) expression levels.

macrophages, M0 macrophages, resting memory CD4 T cells, and gamma delta T cells, in patients with GBM and high expression of RIM-BP2 (**Figure 8B**). Combining the prognosis analysis, RT and chemotherapy sensitivity analysis, and tumor infiltrated immune cell subsets analysis, we concluded that patients with higher expression of PTPRN and RIM-BP2 were resistant to RT and chemotherapy, potentially due to poor tumor microenvironment; therefore, their prognosis was very poor.

DISCUSSION

By normalizing and analyzing the GSE12657, GSE90886, and GSE90598 datasets, we identified 141 significantly overlapping DEGs in GBM. By overlapping biomarkers derived from the LASSO algorithm and the Boruta algorithm, we obtained five GBM biomarkers. According to Kaplan-Meier survival curve analysis, high PTPRN or RIM-BP2 expression was shown to predict poor OS.

RIM-binding protein 2 (RIM-BP2), a multidomain cytomatrix protein, is present at the inner hair cell active zones (24). RIM-BP2 has diversified functions in neurotransmitter release at different central murine synapses and thus contributes to synaptic diversity (25). However, little work has been done to elucidate the expression and role of RIM-BP2 in cancer. Our study found for the first time that RIM-BP2 was significantly downregulated in GBM and that high RIM-BP2 expression was strongly associated with poor prognosis in patients with GBM. These results suggested that in the molecular pathogenesis, progression, and prognosis of GBM, RIM-BP2 may play an important role. PTPRN is a gene that encodes the protein tyrosine phosphatase receptor type N, a 105.8-kDa protein from the tyrosine phosphatase (PTP) family responsible for signaling related to cancer initiation and progression (26, 27). PTPRN is abnormally expressed in many tumors, including small cell lung cancer (SCLC), breast cancer, and liver cancer, and affects tumor progression. We found that high PTPRN expression is strongly associated with a poor prognosis in patients with GBM, which was consistent with previous findings (28–30).

Studies to identify and validate protein targets to improve the therapeutic options are underway. We further analyzed whether the current treatment options for GBM, including RT and chemotherapy, are beneficial even when the PTPRN or RIM-BP2 expression in glioma is abnormal.

The RT regimen of 60 Gy for six weeks has long been the standard adjuvant approach for GBM. It remains the primary treatment modality for unresectable GBM and prolongs survival (31, 32). The results showed that the expression of PTPRN was related to the sensitivity of RT. The GSVA database showed that the differential expression of PTPRN is involved in the DNA repair pathway. Moreover, our results also showed that the activation of DNA repair pathways is correlated with low PTPRN expression (p=1.989e-04). An enhanced cellular DNA repair system is recognized as a major cause of RT failure and, accordingly. GBM is often resistant to RT due to enhanced DNA repair activity (33). Our results implied that low PTPRN expression in GBM is associated with the activation of DNA repair systems as defense mechanisms underlying radioadaptive protection.

TMZ is part of the standard chemotherapeutic regimen for GBM (34). As an alternative, targeted therapies can limit harmful toxicity and more effectively block tumor proliferation. The use of existing clinical data to model the tumor dynamic response to antitumor treatments is a promising approach toward improving treatment efficacy and accelerating the development of antitumor drugs. To identify targets for GBM treatment, Andrea Shergalis,

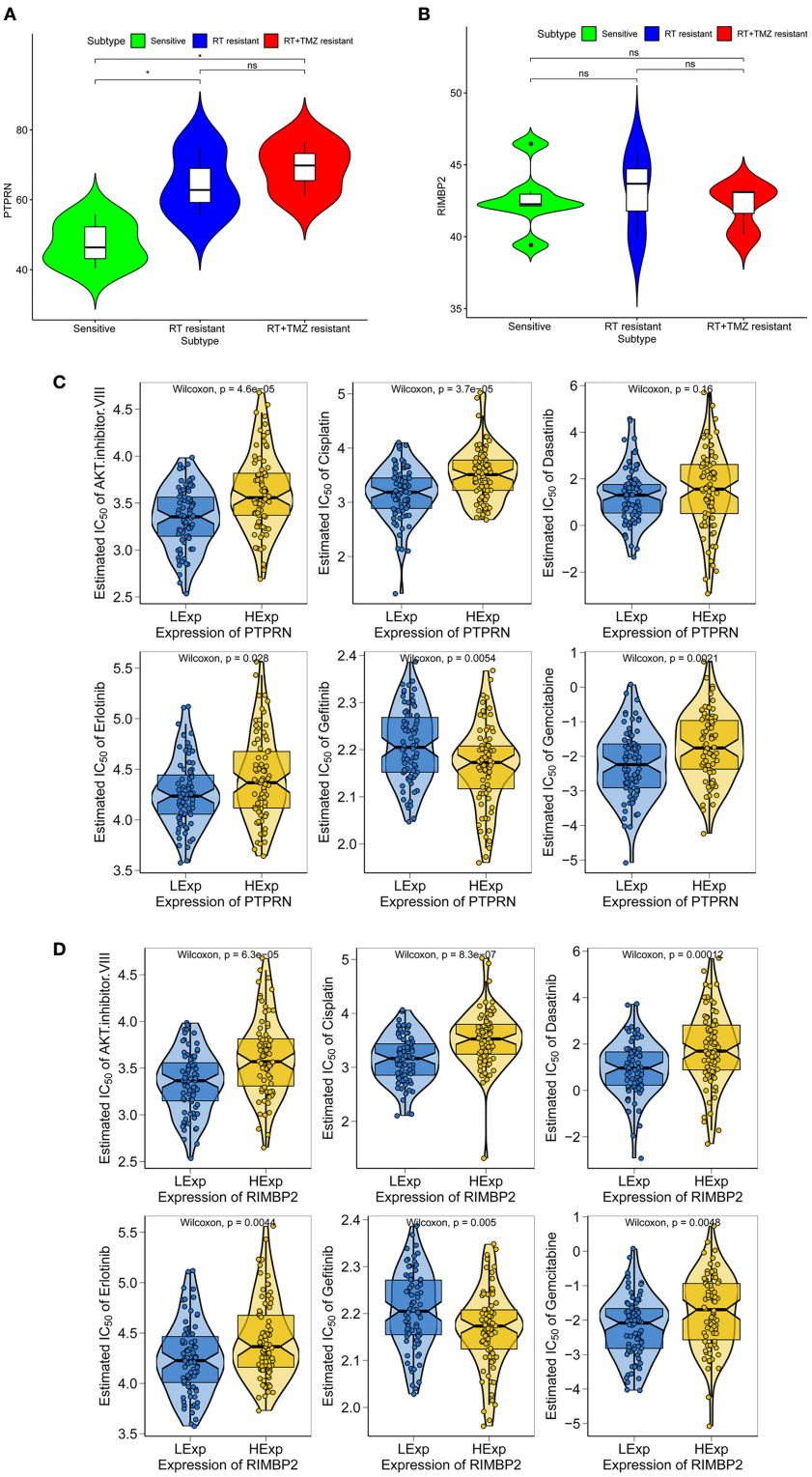

FIGURE 5 | Expression of PTPRN and RIM-BP2 in response to radiation treatment (RT) and anticancer drugs in GBM. **(A, B)** Expression of PTPRN and RIM-BP2 insensitive, RT-resistant and RT+TMZ-resistant groups. **(C, D)** GBM sensitivity to standard chemotherapy drugs with respect to PTPRN and RIM-BP2 expression. *$p < 0.05$; ns, no significant.

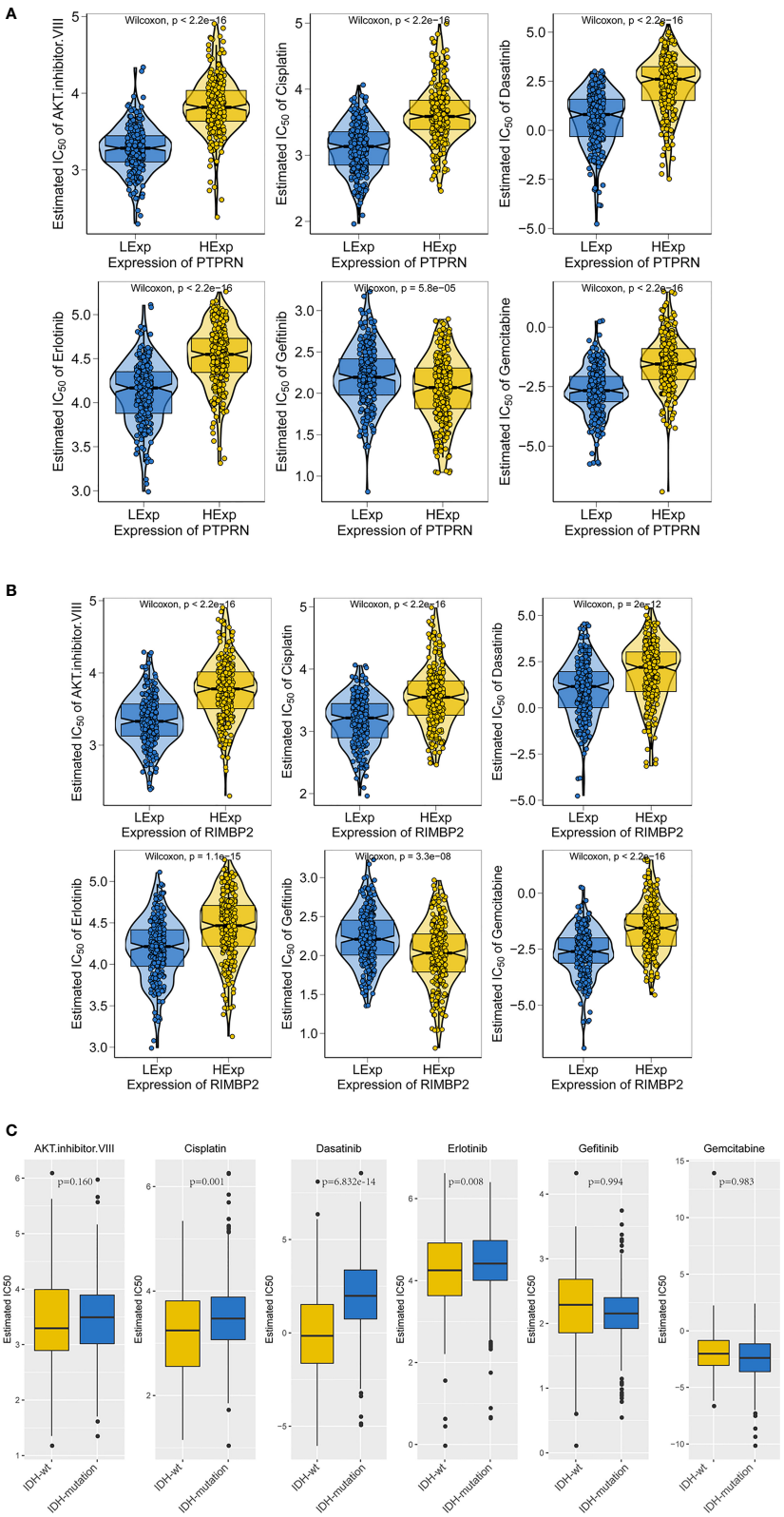

FIGURE 6 | The gene expression and IDH mutation response to anticancer drugs in LGG. **(A, B)** Sensitivity to standard chemotherapy drugs relative to PTPRN and RIM-BP2 in LGG. **(C)** Sensitivity to traditional chemotherapy drugs comparable to IDH mutation in LGG.

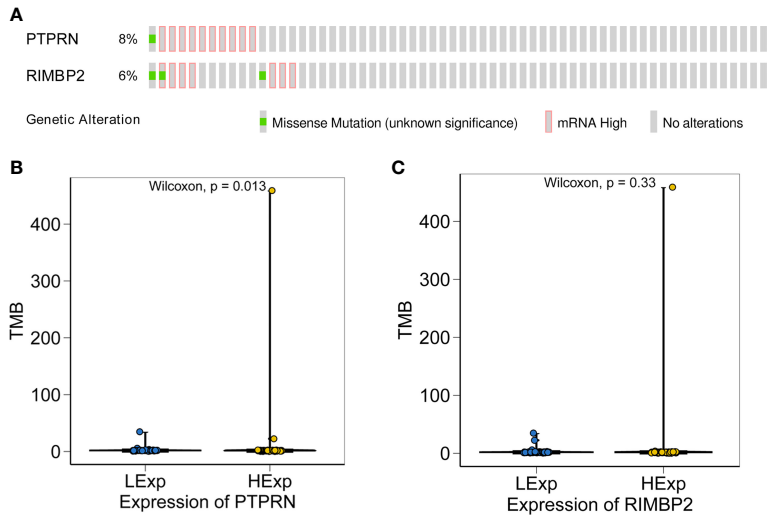

FIGURE 7 | Relationship between the expression of PTPRN and RIM-BP2 and TMB score. **(A)** PTPRN and RIM-BP2 mutations in tumors. **(B, C)** The TMB score of the high PTPRN expression group was significantly higher than that of the low expression group (p=0.013). TMB score was not significantly related to the expression of RIM-BP2.

using data from TCGA, discovered 20 genes, including PTPRN, that correlated with poor survival outcomes, which was consistent with our findings (35). However, the author did not further discuss the possible chemotherapy drugs that might target these genes. In our study, the prediction model of the GDSC was used to evaluate chemotherapy drugs according to the IC50 value. There were significant differences for several drugs according to the *PTPRN* and *RIM-BP2* expression. PTPRN in GBM is more susceptible to AKT inhibitor VIII, cisplatin, erlotinib, gefitinib, and gemcitabine. RIM-BP2 may be more sensitive to AKT inhibitor VIII, cisplatin, dasatinib, erlotinib, gefitinib, and gemcitabine. To explore the chemotherapy drugs targeting IDH mutation in LGG, we identified drugs with different estimated IC50 values for the IDH mutation compared to IDH-wt. Our results showed that the estimated IC50 values of chemotherapeutic drugs (cisplatin, dasatinib, and erlotinib) are different between the IDH-wt and IDH-mutation groups. The chemotherapy drugs cisplatin and erlotinib had significant impact in GBM, LGG, and tumor with IDH mutations. There is no standard approach for the successful treatment of recurrent brain tumors. Cisplatin and erlotinib may provide a new line of chemotherapy for gliomas.

Cisplatin has been approved for use as an antitumor drug for approximately forty years, and the antitumor efficacy of cisplatin is unquestionable (36). The proposed treatment protocol based on a combination of carboplatin and vincristine, first reported in 1993, has achieved high objective response rates of 52% and 62%, respectively, in relapsed and newly diagnosed LGG patients (37). Although cisplatin is used for adjuvant chemotherapy against glioma, intrinsic and acquired resistance restricts cisplatin application (38). Erlotinib, a tyrosine kinase inhibitor, has shown promising response rates in malignant gliomas. Among glioma patients, those with glioblastoma multiforme tumors who have high EGFR expression levels and low levels of phosphorylated PKB/Akt had a better response to erlotinib treatment (39). However, although this targeted compound performed well in preclinical studies, it has failed phase II clinical trials in humans (40, 41). Ultimately, several factors are responsible for drug treatment failure, including toxicity and the failure of the compounds to reach effective concentrations in the brain (40).

TMB is a promising marker of response to immune therapy (IT) that is emerging as a new predictive biomarker to select patients who may benefit from immune checkpoint inhibitor therapy (ICI) (42). High TMB can increase the number of neoantigens that recruit the adaptive immune system and thus provide a potential biomarker for response to IT. In recent years, an association between clinical benefit and high TMB was observed in some human cancers (43, 44). The TMB cutoff points associated with improved survival vary markedly between cancer types, and there may not be one universal definition of high TMB (45). Interestingly, our results showed that the TMB score of the low PTPRN expression group was significantly higher than that of the high expression group (p=0.013). M0 macrophages, M2 macrophages, activated mast cells, neutrophils, and resting memory CD4 T cells comprise a large proportion of PTPRN-related immune cell infiltrates. The difference in the RIM-BP2 expression group was not statistically significant. Whether PTPRN expression, identified in our study as a novel biomarker,is a potential predictor of GBM prognosis related to TMB needs further investigation. PTPRN-related immune cell infiltration is more likely to be a response to immunotherapy, providing us with new insights and opportunities to further investigate its association with disease course and response to therapy.

There are some limitations to our work. First, the sample size included in our analysis was small, which might lead to the

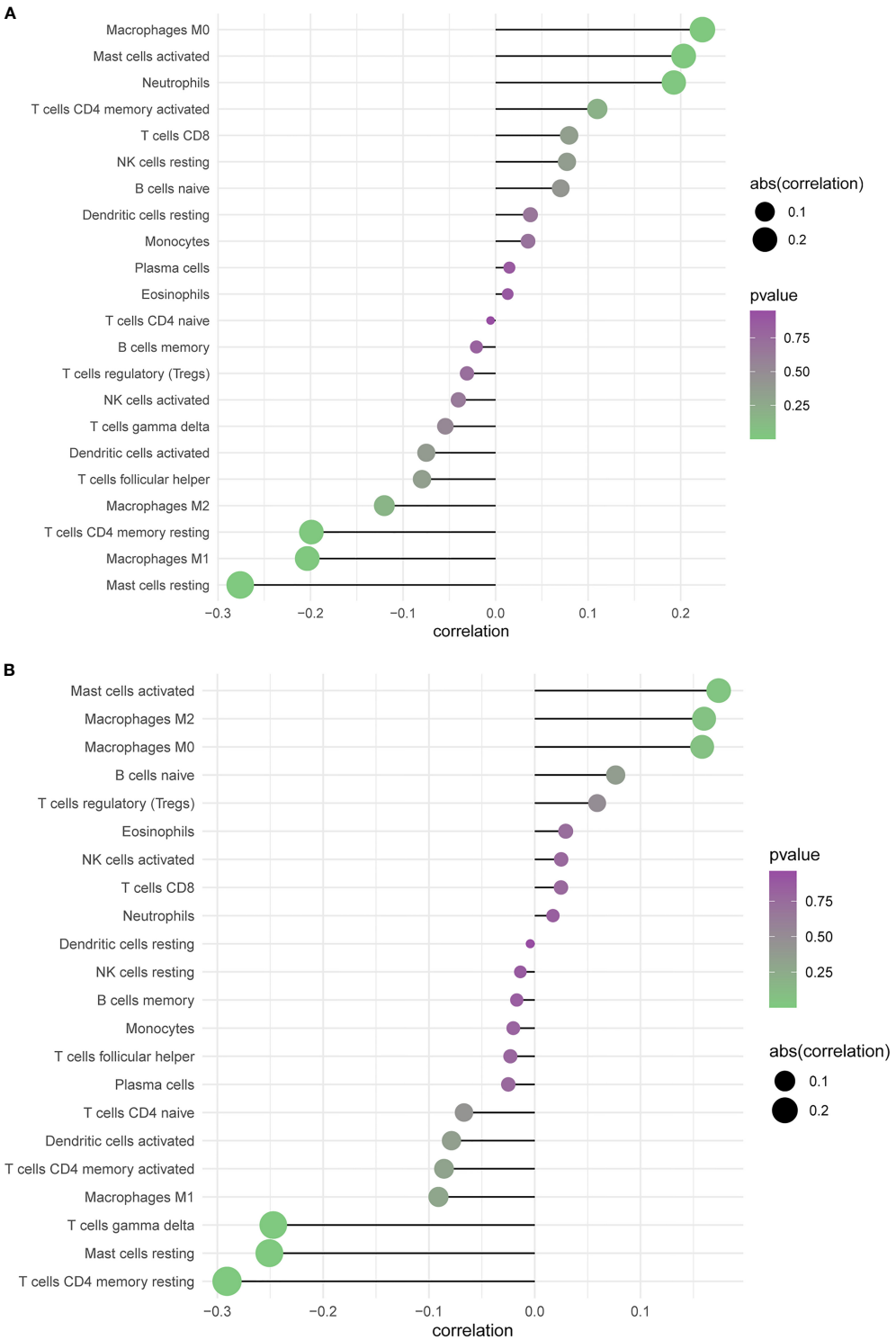

FIGURE 8 | Profiling Tumor-Infiltrating Immune Cells with CIBERSORT. **(A, B)** Summarizing immune cell subset proportions in GBM against the expression of PTPRN and RIM-BP2 status and CIBERSORT p-value.

omission of some potential messenger RNAs (mRNAs). Moreover, the expression of PTPRN and RIM-BP2 was only detected using bioinformatics analysis and require further experimental verification in more patients with GBM. Third, we did not validate the prognostic value of PTPRN and RIM-BP2. Furthermore, we provided some potential treatment options relating to PTPRN, including radiotherapy and chemotherapy. The molecular mechanisms of how the gene signatures and treatment selection affect the prognosis of GBM should be further elucidated.

In conclusion, we identified two novel biomarkers (PTPRN and RIM-BP2) that can potentially be used for prognosis prediction in GBM. These genes have potential clinical implications for radiotherapy and chemotherapy GBM treatment. However, the molecular mechanism and function of these genes need to be confirmed in further experiments.

DATA AVAILABILITY STATEMENT

The original contributions presented in the study are included in the article/**Supplementary Material**. Further inquiries can be directed to the corresponding authors.

AUTHOR CONTRIBUTIONS

SL and YH conceptualized and designed the study. SP participated in the bioinformatics analyses. XZ drafted the manuscript. RL and ZC participated in the design of the study. XX helped to revise the study. All authors contributed to the article and approved the submitted version.

FUNDING

This work was supported by the Scientific research project (2019) of the health commission of Hunan (grants B2019200) and the Science and technology innovation project of Hunan (grants 2018SK52802).

ACKNOWLEDGMENTS

The authors thank Huaming Wu in the key laboratory of carcinogenesis of the Chinese ministry of health, Cancer Research Institute and central south university for ongoing support and discussion.

SUPPLEMENTARY MATERIAL

The Supplementary Material for this article can be found online at: https://www.frontiersin.org/articles/10.3389/fonc.2021.667884/full#supplementary-material

REFERENCES

1. Ostrom QT, Cioffi G, Gittleman H, Patil N, Waite K, Kruchko C, et al. CBTRUS Statistical Report: Primary Brain and Other Central Nervous System Tumors Diagnosed in the United States in 2012-2016. *Neuro Oncol* (2019) 21 (Suppl 5):v1–v100. doi: 10.1093/neuonc/noz150
2. Ma Q, Long W, Xing C, Chu J, Luo M, Wang HY, et al. Cancer Stem Cells and Immunosuppressive Microenvironment in Glioma. *Front Immunol* (2018) 9:2924. doi: 10.3389/fimmu.2018.02924
3. Tan AC, Ashley DM, López GY, Malinzak M, Friedman HS, Khasraw M. Management of Glioblastoma: State of the Art and Future Directions. *CA Cancer J Clin* (2020) 70:299–312. doi: 10.3322/caac.21613
4. Louis DN, Perry A, Reifenberger G, von Deimling A, Figarella-Branger D, Cavenee WK, et al. The 2016 World Health Organization Classification of Tumors of the Central Nervous System: A Summary. *Acta Neuropathol* (2016) 131(6):803–20. doi: 10.1007/s00401-016-1545-1
5. Brandner S, Jaunmuktane Z. Neurological Update: Gliomas and Other Primary Brain Tumours in Adults. *J Neurol* (2018) 265(3):717–27. doi: 10.1007/s00415-017-8652-3
6. Binabaj MM, Bahrami A, ShahidSales S, Joodi M, Joudi Mashhad M, Hassanian SM, et al. The Prognostic Value of MGMT Promoter Methylation in Glioblastoma: A Meta-Analysis of Clinical Trials. *J Cell Physiol* (2018) 233(1):378–86. doi: 10.1002/jcp.25896
7. Tykocki T, Eltayeb M. Ten-Year Survival in Glioblastoma. A Systematic Review. *J Clin Neurosci* (2018) 54:7–13. doi: 10.1016/j.jocn.2018.05.002
8. Aldape K, Zadeh G, Mansouri S, Reifenberger G, von Deimling A. Glioblastoma: Pathology, Molecular Mechanisms and Markers. *Acta Neuropathol* (2015) 129(6):829–48. doi: 10.1007/s00401-015-1432-1
9. Ye F, Zhang Y, Liu Y, Yamada K, Tso JL, Menjivar JC, et al. Protective Properties of Radio-Chemoresistant Glioblastoma Stem Cell Clones Are Associated With Metabolic Adaptation to Reduced Glucose Dependence. *PLoS One* (2013) 8(11):e80397. doi: 10.1371/journal.pone.0080397
10. Friedman J, Hastie T, Tibshirani R. Regularization Paths for Generalized Linear Models *via* Coordinate Descent. *J Stat Softw* (2010) 33(1):1–22. doi: 10.18637/jss.v033.i01
11. Degenhardt F, Seifert S, Szymczak S. Evaluation of Variable Selection Methods for Random Forests and Omics Data Sets. *Brief Bioinform* (2019) 20(2):492–503. doi: 10.1093/bib/bbx124
12. Newman AM, Liu CL, Green MR, Gentles AJ, Feng W, Xu Y, et al. Robust Enumeration of Cell Subsets From Tissue Expression Profiles. *Nat Methods* (2015) 12(5):453–7. doi: 10.1038/nmeth.3337
13. Hänzelmann S, Castelo R, Guinney J. GSVA: Gene Set Variation Analysis for Microarray and RNA-Seq Data. *BMC Bioinf* (2013) 14:7. doi: 10.1186/1471-2105-14-7
14. Yang W, Soares J, Greninger P, Gentles AJ, Feng W, Xu Y, et al. Genomics of Drug Sensitivity in Cancer (GDSC): A Resource for Therapeutic Biomarker Discovery in Cancer Cells. *Nucleic Acids Res* (2013) 41(Database issue):D955–61. doi: 10.1093/nar/gks1111
15. Geeleher P, Cox NJ, Huang RS. Clinical Drug Response can be Predicted Using Baseline Gene Expression Levels and *In Vitro* Drug Sensitivity in Cell Lines. *Genome Biol* (2014) 15(3):R47. doi: 10.1186/gb-2014-15-3-r47
16. Koboldt DC, Zhang Q, Larson DE, Shen D, McLellan MD, Lin L, et al. VarScan 2: Somatic Mutation and Copy Number Alteration Discovery in Cancer by Exome Sequencing. *Genome Res* (2012) 22(3):568–76. doi: 10.1101/gr.129684.111
17. Franz M, Rodriguez H, Lopes C, Zuberi K, Montojo J, Bader GD, et al. GeneMANIA Update 2018. *Nucleic Acids Res* (2018) 46(W1):W60–4. doi: 10.1093/nar/gky311
18. Caragher SP, Hall RR, Ahsan R, Ahmed AU. Monoamines in Glioblastoma: Complex Biology With Therapeutic Potential. *Neuro Oncol* (2018) 20:1014–25. doi: 10.1093/neuonc/nox210
19. Venkatesh HS, Tam LT, Woo PJ, Lennon J, Nagaraja S, Gillespie SM, et al. Targeting Neuronal Activity-Regulated Neuroligin-3 Dependency in High-Grade Glioma. *Nature* (2017) 549:533–7. doi: 10.1038/nature24014

20. Buckner JC, Shaw EG, Pugh SL, Chakravarti A, Gilbert MR, Barger GR, et al. Radiation Plus Procarbazine, CCNU, and Vincristine in Low-Grade Glioma. *N Engl J Med* (2016) 374:1344–55. doi: 10.1056/NEJMoa1500925
21. Fisher BJ, Hu C, Macdonald DR, Lesser GJ, Coons SW, Brachman DG, et al. Phase 2 Study of Temozolomide-Based Chemoradiation Therapy for High-Risk Low-Grade Gliomas: Preliminary Results of Radiation Therapy Oncology Group 0424Phys. *Int J Radiat Oncol Biol* (2015) 91:497–504. doi: 10.1016/j.ijrobp.2014.11.012
22. Simonelli M, Persico P, Perrino M, Zucali PA, Navarria P, Pessina F, et al. Checkpoint Inhibitors as Treatment for Malignant Gliomas: "A Long Way to the Top". *Cancer Treat Rev* (2018) 69:121–31. doi: 10.1016/j.ctrv.2018.06.016
23. Jia D, Li S, Li D, Xue H, Yang D, Liu Y. Mining TCGA Database for Genes of Prognostic Value in Glioblastoma Microenvironment. *Aging (Albany NY)* (2018) 10:592–605. doi: 10.18632/aging.101415
24. Krinner S, Butola T, Jung S, Wichmann C, Moser T. RIM-Binding Protein 2 Promotes a Large Number of CaV1.3 Ca2+-Channels and Contributes to Fast Synaptic Vesicle Replenishment at Hair Cell Active Zones. *Front Cell Neurosci* (2017) 11:334. doi: 10.3389/fncel.2017.00334
25. Brockmann MM, Maglione M, Willmes CG, Stumpf A, Bouazza BA, Velasquez LM, et al. RIM-BP2 Primes Synaptic Vesicles via Recruitment of Munc13-1 at Hippocampal Mossy Fiber Synapses. *Elife* (2019) 8. doi: 10.7554/eLife.43243
26. Zhangyuan G, Yin Y, Zhang W, Yu W, Jin K, Wang F, et al. Prognostic Value of Phosphotyrosine Phosphatases in Hepatocellular Carcinoma. *Cell Physiol Biochem* (2018) 46(6):2335–46. doi: 10.1159/000489625
27. Lan MS, Modi WS, Xie H, Notkins AL. Assignment of the IA-2 Gene Encoding an Autoantigen in IDDM to Chromosome 2q35. *Diabetologia* (1996) 39(8):1001–2. doi: 10.1007/BF00403923
28. Yin W, Tang G, Zhou Q, Cao Y, Li H, Fu X, et al. Expression Profile Analysis Identifies a Novel Five-Gene Signature to Improve Prognosis Prediction of Glioblastoma. *Front Genet* (2019) 10:419. doi: 10.3389/fgene.2019.00419
29. Xu P, Yang J, Liu J, Yang X, Liao J, Yuan F, et al. Identification of Glioblastoma Gene Prognosis Modules Based on Weighted Gene Co-Expression Network Analysis. *BMC Med Genomics* (2018) 11(1):96. doi: 10.1186/s12920-018-0407-1
30. Prasad B, Tian Y, Li X. Large-Scale Analysis Reveals Gene Signature for Survival Prediction in Primary Glioblastoma. *Mol Neurobiol* (2020) 57 (12):5235–46. doi: 10.1007/s12035-020-02088-w
31. Hua L, Wang Z, Zhao L, Mao H, Wang G, Zhang K, et al. Hypoxia-Responsive Lipid-Poly-(Hypoxic Radiosensitized Polyprodrug) Nanoparticles for Glioma Chemo- and Radiotherapy. *Theranostics* (2018) 8(18):5088–105. doi: 10.7150/thno.26225
32. Malmström A, Grønberg BH, Marosi C, Stupp R, Frappaz D, Schultz H, et al. Temozolomide Versus Standard 6-Week Radiotherapy Versus Hypofractionated Radiotherapy in Patients Older Than 60 Years With Glioblastoma: The Nordic Randomised, Phase 3 Trial. *Lancet Oncol* (2012) 13(9):916–26. doi: 10.1016/S1470-2045(12)70265-6
33. Dutreix M, Cosset JM, Sun JS. Molecular Therapy in Support to Radiotherapy. *Mutat Res* (2010) 704(1-3):182–9. doi: 10.1016/j.mrrev.2010.01.001
34. Perry JR, Laperriere N, O'Callaghan CJ, Brandes AA, Menten J, Phillips C, et al. Short-Course Radiation Plus Temozolomide in Elderly Patients With Glioblastoma. *N Engl J Med* (2017) 376(11):1027–37. doi: 10.1056/NEJMoa1611977
35. Shergalis A, Bankhead A3rd, Luesakul U, Muangsin N, Neamati N. Current Challenges and Opportunities in Treating Glioblastoma. *Pharmacol Rev* (2018) 70(3):412–45. doi: 10.1124/pr.117.014944
36. Agudo-López A, Prieto-García E, Alemán J, Pérez C, Díaz-García CV, Parrilla-Rubio L, et al. Mechanistic Added Value of a Trans-Sulfonamide-Platinum-Complex in Human Melanoma Cell Lines and Synergism With Cis-Platin. *Mol Cancer* (2017) 16:45. doi: 10.1186/s12943-017-0618-7
37. Packer RJ, Lange B, Ater J, Nicholson HS, Allen J, Walker R, et al. Carboplatin and Vincristine for Recurrent and Newly Diagnosed Low-Grade Gliomas of Childhood. *J Clin Oncol* (1993) 11:850–6. doi: 10.1200/JCO.1993.11.5.850
38. Yi DY, Su Q, Zhang FC, Fu P, Zhang Q, Cen YC, et al. Effect of microRNA-128 on Cisplatin Resistance of Glioma SHG-44 Cells by Targeting JAG1. *J Cell Biochem* (2018) 119:3162–73. doi: 10.1002/jcb.26469
39. Haas-Kogan DA, Prados MD, Tihan T, Eberhard DA, Jelluma N, Arvold ND, et al. Epidermal Growth Factor Receptor, Protein Kinase B/Akt, and Glioma Response to Erlotinib. *J Natl Cancer Inst* (2005) 97(12):880–7. doi: 10.1093/jnci/dji161
40. Wen PY, Chang SM, Lamborn KR, Kuhn JG, Norden AD, Cloughesy TF, et al. Phase I/II Study of Erlotinib and Temsirolimus for Patients With Recurrent Malignant Gliomas: North American Brain Tumor Consortium Trial 04-02. *Neuro Oncol* (2014) 16(4):567–78. doi: 10.1093/neuonc/not247
41. Raizer JJ, Abrey LE, Lassman AB, Kuhn JG, Norden AD, Cloughesy TF, et al. A Phase II Trial of Erlotinib in Patients With Recurrent Malignant Gliomas and Nonprogressive Glioblastoma Multiforme Postradiation Therapy. *Neuro Oncol* (2010) 12(1):95–103. doi: 10.1093/neuonc/nop015
42. Goodman AM, Kato S, Bazhenova L, Patel SP, Frampton GM, Miller V, et al. Tumor Mutational Burden as an Independent Predictor of Response to Immunotherapy in Diverse Cancers. *Mol Cancer Ther* (2017) 16(11):2598–608. doi: 10.1158/1535-7163.MCT-17-0386
43. Hugo W, Zaretsky JM, Sun L, Song C, Moreno BH, Hu-Lieskovan S, et al. Genomic and Transcriptomic Features of Response to Anti-PD-1 Therapy in Metastatic Melanoma. *Cell* (2016) 165(1):35–44. doi: 10.1016/j.cell.2016.02.065
44. Rizvi NA, Hellmann MD, Snyder A, Kvistborg P, Makarov V, Havel JJ, et al. Cancer Immunology. Mutational Landscape Determines Sensitivity to PD-1 Blockade in non-Small Cell Lung Cancer. *Science* (2015) 348(6230):124–8. doi: 10.1126/science.aaa1348
45. Samstein RM, Lee CH, Shoushtari AN, Hellmann MD, Shen R, Janjigian YY, et al. Tumor Mutational Load Predicts Survival After Immunotherapy Across Multiple Cancer Types. *Nat Genet* (2019) 51(2):202–6. doi: 10.1038/s41588-018-0312-8

Conflict of Interest: The authors declare that the research was conducted in the absence of any commercial or financial relationships that could be construed as a potential conflict of interest.

Publisher's Note: All claims expressed in this article are solely those of the authors and do not necessarily represent those of their affiliated organizations, or those of the publisher, the editors and the reviewers. Any product that may be evaluated in this article, or claim that may be made by its manufacturer, is not guaranteed or endorsed by the publisher.

Copyright © 2021 Zhu, Pan, Li, Chen, Xie, Han, Lv and Huang. This is an open-access article distributed under the terms of the Creative Commons Attribution License (CC BY). The use, distribution or reproduction in other forums is permitted, provided the original author(s) and the copyright owner(s) are credited and that the original publication in this journal is cited, in accordance with accepted academic practice. No use, distribution or reproduction is permitted which does not comply with these terms.

Advantages of publishing in Frontiers

OPEN ACCESS
Articles are free to read for greatest visibility and readership

FAST PUBLICATION
Around 90 days from submission to decision

HIGH QUALITY PEER-REVIEW
Rigorous, collaborative, and constructive peer-review

TRANSPARENT PEER-REVIEW
Editors and reviewers acknowledged by name on published articles

Frontiers
Avenue du Tribunal-Fédéral 34
1005 Lausanne | Switzerland

Visit us: www.frontiersin.org
Contact us: frontiersin.org/about/contact

REPRODUCIBILITY OF RESEARCH
Support open data and methods to enhance research reproducibility

DIGITAL PUBLISHING
Articles designed for optimal readership across devices

FOLLOW US
@frontiersin

IMPACT METRICS
Advanced article metrics track visibility across digital media

EXTENSIVE PROMOTION
Marketing and promotion of impactful research

LOOP RESEARCH NETWORK
Our network increases your article's readership